

MEDICINAL PLANTS AS A SOURCE OF NOVEL AUTOIMMUNE-MODULATING AND ANTI-INFLAMMATORY DRUG PRODUCTS

EDITED BY: Xiao Bin Zeng, Jun Tian, Xiaohong Tian and Yihai Wang
PUBLISHED IN: Frontiers in Pharmacology





frontiers

Frontiers eBook Copyright Statement

The copyright in the text of individual articles in this eBook is the property of their respective authors or their respective institutions or funders. The copyright in graphics and images within each article may be subject to copyright of other parties. In both cases this is subject to a license granted to Frontiers.

The compilation of articles constituting this eBook is the property of Frontiers.

Each article within this eBook, and the eBook itself, are published under the most recent version of the Creative Commons CC-BY licence.

The version current at the date of publication of this eBook is CC-BY 4.0. If the CC-BY licence is updated, the licence granted by Frontiers is automatically updated to the new version.

When exercising any right under the CC-BY licence, Frontiers must be attributed as the original publisher of the article or eBook, as applicable.

Authors have the responsibility of ensuring that any graphics or other materials which are the property of others may be included in the CC-BY licence, but this should be checked before relying on the CC-BY licence to reproduce those materials. Any copyright notices relating to those materials must be complied with.

Copyright and source acknowledgement notices may not be removed and must be displayed in any copy, derivative work or partial copy which includes the elements in question.

All copyright, and all rights therein, are protected by national and international copyright laws. The above represents a summary only. For further information please read Frontiers' Conditions for Website Use and Copyright Statement, and the applicable CC-BY licence.

ISSN 1664-8714

ISBN 978-2-83250-247-1

DOI 10.3389/978-2-83250-247-1

About Frontiers

Frontiers is more than just an open-access publisher of scholarly articles: it is a pioneering approach to the world of academia, radically improving the way scholarly research is managed. The grand vision of Frontiers is a world where all people have an equal opportunity to seek, share and generate knowledge. Frontiers provides immediate and permanent online open access to all its publications, but this alone is not enough to realize our grand goals.

Frontiers Journal Series

The Frontiers Journal Series is a multi-tier and interdisciplinary set of open-access, online journals, promising a paradigm shift from the current review, selection and dissemination processes in academic publishing. All Frontiers journals are driven by researchers for researchers; therefore, they constitute a service to the scholarly community. At the same time, the Frontiers Journal Series operates on a revolutionary invention, the tiered publishing system, initially addressing specific communities of scholars, and gradually climbing up to broader public understanding, thus serving the interests of the lay society, too.

Dedication to Quality

Each Frontiers article is a landmark of the highest quality, thanks to genuinely collaborative interactions between authors and review editors, who include some of the world's best academicians. Research must be certified by peers before entering a stream of knowledge that may eventually reach the public - and shape society; therefore, Frontiers only applies the most rigorous and unbiased reviews.

Frontiers revolutionizes research publishing by freely delivering the most outstanding research, evaluated with no bias from both the academic and social point of view. By applying the most advanced information technologies, Frontiers is catapulting scholarly publishing into a new generation.

What are Frontiers Research Topics?

Frontiers Research Topics are very popular trademarks of the Frontiers Journals Series: they are collections of at least ten articles, all centered on a particular subject. With their unique mix of varied contributions from Original Research to Review Articles, Frontiers Research Topics unify the most influential researchers, the latest key findings and historical advances in a hot research area! Find out more on how to host your own Frontiers Research Topic or contribute to one as an author by contacting the Frontiers Editorial Office: frontiersin.org/about/contact

MEDICINAL PLANTS AS A SOURCE OF NOVEL AUTOIMMUNE-MODULATING AND ANTI-INFLAMMATORY DRUG PRODUCTS

Topic Editors:

Xiao Bin Zeng, Shenzhen People's Hospital, Jinan University, China

Jun Tian, Jiangsu Normal University, China

Xiaohong Tian, McGill University, Canada

Yihai Wang, Guangdong Pharmaceutical University, China

Citation: Zeng, X. B., Tian, J., Tian, X., Wang, Y., eds. (2022). Medicinal Plants as a Source of Novel Autoimmune-Modulating and Anti-Inflammatory Drug Products. Lausanne: Frontiers Media SA. doi: 10.3389/978-2-83250-247-1

Table of Contents

- 05 Editorial: Medicinal Plants as a Source of Novel Autoimmune-Modulating and Anti-Inflammatory Drug Products**
Yang Wang, Ji Chen, Jun Tian, Yihai Wang, Zhengang Zha and Xiaobin Zeng
- 09 Combined *Cornus Officinalis* and *Paeonia Lactiflora* Pall Therapy Alleviates Rheumatoid Arthritis by Regulating Synovial Apoptosis via AMPK-Mediated Mitochondrial Fission**
Lichuang Huang, Shaoqi Hu, Meiyu Shao, Xin Wu, Jida Zhang and Gang Cao
- 23 Development of an Advanced Multicellular Intestinal Model for Assessing Immunomodulatory Properties of Anti-Inflammatory Compounds**
Diego Marescotti, Giuseppe Lo Sasso, Diego Guerrero, Kasper Renggli, Pedro A. Ruiz Castro, Romain Piault, Vincent Jaquet, Fabian Moine, Karsta Luettich, Stefan Frentzel, Manuel C. Peitsch and Julia Hoeng
- 36 Xiao-Yin-Fang Therapy Alleviates Psoriasis-like Skin Inflammation Through Suppressing $\gamma\delta$ T17 Cell Polarization**
Xilin Zhang, Xiaorui Li, Youdong Chen, Bingjie Li, Chunyuan Guo, Peng Xu, Zengyang Yu, Yangfeng Ding, Yuling Shi and Jun Gu
- 51 Pharmacological Benefits of *Triphala*: A Perspective for Allergic Rhinitis**
Salinee Jantrapirom, Pannaphak Hirunsatitpron, Saranyapin Potikanond, Wutigri Nimlamool and Nutthiya Hanprasertpong
- 75 Rhoifolin Ameliorates Osteoarthritis via Regulating Autophagy**
Jiyuan Yan, Bowei Ni, Gaohong Sheng, Yingchi Zhang, Yifan Xiao, Yongzhuang Ma, Hao Li, Hua Wu and Chang Tu
- 83 The Effect of Chinese Medicine Compound in the Treatment of Rheumatoid Arthritis on the Level of Rheumatoid Factor and Anti-Cyclic Citrullinated Peptide Antibodies: A Systematic Review and Meta-Analysis**
Xuan Tang, Zehao Liu, Zhihua Yang, Shengmei Xu, Maojie Wang, Xiumin Chen, Zehuai Wen and Runyue Huang
- 112 Salvianolate Ameliorates Osteopenia and Improves Bone Quality in Prednisone-Treated Rheumatoid Arthritis Rats by Regulating RANKL/RANK/OPG Signaling**
Xiang Gao, Qingyun Wu, Xinle Zhang, Jia Tian, Dahong Liang, Yalin Min, Jiaqi Lu, Xuemei Zhang, Liao Cui, Bilian Xu and Yanzhi Liu
- 126 The Essential Oil of *Artemisia argyi* H.Lév. and Vaniot Attenuates NLRP3 Inflammasome Activation in THP-1 Cells**
Pengxiao Chen, Qi Bai, Yanting Wu, Qiongzheng Zeng, Xiaowei Song, Yuying Guo, Pengjun Zhou, Yao Wang, Xiaofeng Liao, Qiaoli Wang, Zhe Ren and Yifei Wang
- 143 The Mechanism Action of German Chamomile (*Matricaria recutita* L.) in the Treatment of Eczema: Based on Dose–Effect Weight Coefficient Network Pharmacology**
Wenfei Wang, Yichun Wang, Junbo Zou, Yanzhuo Jia, Yao Wang, Jia Li, Changli Wang, Jing Sun, Dongyan Guo, Fang Wang, Zhenfeng Wu, Ming Yang, Lei Wu, Xiaofei Zhang and Yajun Shi

- 156** *Network Pharmacology to Explore the Molecular Mechanisms of Prunella vulgaris for Treating Hashimoto's Thyroiditis*
Xiao-xiong Gan, Lin-kun Zhong, Fei Shen, Jian-hua Feng, Ya-yi Li, Si-jing Li, Wen-song Cai and Bo Xu
- 166** *Prevention of Cyclophosphamide-Induced Immunosuppression in Mice With Traditional Chinese Medicine Xuanfei Baidu Decoction*
Huimin Yan, Jia Lu, Jiabao Wang, Lu Chen, Yu Wang, Lin Li, Lin Miao and Han Zhang
- 175** *Ethyl 2-Succinate-Anthraquinone Attenuates Inflammatory Response and Oxidative Stress via Regulating NLRP3 Signaling Pathway*
Burong Feng, Xiuye Zhao, Wei Zhao, Huiwei Jiang, Zijing Ren, Yingfu Chen, Ye Yuan and Zhimin Du
- 186** *Analgesic and Anti-Arthritic Activities of Polysaccharides in Chaenomeles Speciosa*
Doudou Huang, Shenggui Jiang, Zenan Du, Yanhong Chen, Dan Xue, Xiujuan Wang, Mengshuang Li, Feng Zhang, Wansheng Chen and Lianna Sun



OPEN ACCESS

EDITED BY
Javier Echeverria,
University of Santiago, Chile

REVIEWED BY
Dâmaris Silveira,
University of Brasilia, Brazil
Adolfo Andrade-Cetto,
National Autonomous University of
Mexico, Mexico

*CORRESPONDENCE
Xiaobin Zeng,
zengxiaobin1983@163.com

[†]These authors have contributed equally
to this work

SPECIALTY SECTION
This article was submitted to
Ethnopharmacology,
a section of the journal
Frontiers in Pharmacology

RECEIVED 26 June 2022
ACCEPTED 05 August 2022
PUBLISHED 06 September 2022

CITATION
Wang Y, Chen J, Tian J, Wang Y, Zha Z
and Zeng X (2022), Editorial: Medicinal
plants as a source of novel
autoimmune-modulating and anti-
inflammatory drug products.
Front. Pharmacol. 13:978581.
doi: 10.3389/fphar.2022.978581

COPYRIGHT
© 2022 Wang, Chen, Tian, Wang, Zha
and Zeng. This is an open-access article
distributed under the terms of the
Creative Commons Attribution License
(CC BY). The use, distribution or
reproduction in other forums is
permitted, provided the original
author(s) and the copyright owner(s) are
credited and that the original
publication in this journal is cited, in
accordance with accepted academic
practice. No use, distribution or
reproduction is permitted which does
not comply with these terms.

Editorial: Medicinal plants as a source of novel autoimmune-modulating and anti-inflammatory drug products

Yang Wang^{1,2†}, Ji Chen^{3†}, Jun Tian⁴, Yihai Wang⁵,
Zhengang Zha⁶ and Xiaobin Zeng^{1,7*}

¹Central Laboratory of Longhua Branch and Department of Infectious Disease, Shenzhen People's Hospital (The Second Clinical Medical College, Jinan University, The First Affiliated Hospital, Southern University of Science and Technology), Shenzhen, China, ²School of Pharmaceutical Sciences (Shenzhen), Shenzhen Campus of Sun Yat-sen University, Shenzhen, China, ³Department of Orthopaedics, Shenzhen People's Hospital (The Second Clinical Medical College, Jinan University, The First Affiliated Hospital, Southern University of Science and Technology), Shenzhen, China, ⁴College of Life Science, Jiangsu Normal University, Xuzhou, China, ⁵School of Pharmacy, Guangdong Pharmaceutical University, Guangzhou, China, ⁶Department of Orthopaedics, The First Clinical Medical College, Jinan University, Guangzhou, China, ⁷Guangdong Provincial Key Laboratory of Regional Immunity and Diseases, Medicine School of Shenzhen University, Shenzhen, China

KEYWORDS

functional foods, autoimmune diseases, inflammatory diseases, pathogenesis, drug development, medicinal plants

Editorial on the Research Topic

Medicinal plants as a source of novel autoimmune-modulating and anti-inflammatory drug products

Medicinal plants as a source of novel autoimmune modulating and anti-inflammatory drug products

Inflammation response is activated as the first line of defense against the invasion of foreign pathogens and harmful stimuli, which in turn helps the body repair damaged tissue and remove irritants and damaged cells. Basically, Cytokine mediate the occurrence of an effective immune response, although cytokines are well initiated and coordinated in immune response, but unregulated cytokine signaling inadvertently constitutes the major determinant of immune pathology, leading to autoimmune diseases or chronic inflammation that affects older people around the world (Bello et al., 2018; Galindo et al., 2018). Such as arthritis (osteoarthritis, rheumatoid arthritis), allergies, atopic dermatitis, psoriasis, asthma, chronic obstructive pulmonary disease, inflammatory bowel diseases, steatohepatitis (Placha and Jampilek, 2021). The classic anti-inflammatory drugs are glucocorticoids and cyclooxygenase (COX-1 and 2) inhibitors. However, withdrawn COX-2 inhibitors, such as valdecoxib and rofecoxib, were associated

with a higher risk of stroke, while etoricoxib raised blood pressure (Davies, 1995). Historically, medicinal plants and natural products have been used in anti-inflammatory treatment, and many new medicines have been discovered from herbal sources, most of which are plant-derived secondary metabolites (Akhtar, 2022). Such as quercetin and kaempferol (Hämäläinen et al., 2007) and resveratrol (Kundu et al., 2006). Therefore, it is a very important strategic approach to seek effective anti-inflammatory inhibitors from medicinal plants.

Macrophages play a key role in “inflammatory pathways” that lead to a range of diseases and disorders (Chen et al., 2018). The classical activation of macrophages occurs after injury or infection of microbial products or pro-inflammatory cytokines, including bacterial lipopolysaccharide (LPS), interferon- γ (IFN- γ), or tumor necrosis factor- α (TNF- α), and trigger inflammatory signaling pathways, most commonly, NF-Kb (nuclear factor kappa-light-chain-enhancer of activated B cells), MAPK (mitogen-activated protein kinase) and JAK-STAT (Janus kinases (JAKS)—signal transducer and activator of transcription proteins) (Besednova et al., 2022). Recently, the non-classical Hippo pathway and NLRP3 inflammasome have been highlighted in inflammatory responses of macrophage (Jo et al., 2016; Tsai et al., 2021; Xie et al., 2021). However, the molecular mechanisms underlying autoimmunity regulation or anti-inflammatory potential remain unclear. Therefore, it has become a research hotspot to explore the molecular mechanism of autoimmunity regulation or anti-c and discover new therapeutic schemes.

The 13 articles collected in this Research Topic focus on the most recent advances on medicinal plants as a source of novel autoimmune modulating and anti-inflammatory, mainly on novel molecular targets and on innovative pharmacological approaches. Kangfuxiaoyanshuan (KFXYS) is a traditional Chinese herbal compound that composed of eight classical medicinal herbs. The various chemical components of this Chinese herbal compound, including alkaloids, flavonoids, diterpenoid lactones, bile acids, anthraquinones, naphthoquinones, and organic acids (Xie et al., 2019). Here, Liu et al. demonstrate KFXYS remarkably reduced the levels of proinflammatory factors (IFN- γ , IL-1 β , IL-4) and adhesion related factors (TNF- α) in the acute stage of pelvic inflammatory disease (PID), and had protective effect of ultrastructure of endometrial epithelial cells. In addition, KFXYS had been exerted significant anti-inflammatory effect through inhibiting the activation of the NF- κ B pathway, and decreasing the TGF- β /MMP-2 associated tissue adhesion. Gao et al. reported that salvianolate (total polyphenols), a traditional Chinese medicine extracted from *Salvia miltiorrhiza*, ameliorated osteopenia and bone quality in glucocorticoid treated RA rats. Combined treatment with prednisone and salvianolate for ameliorating joint damage and improved bone quality in collagen-induced arthritis rats via activation of the RANKL/

RANK/OPG signaling pathway and TRAIL-TRAF6-NF κ B signal axis, thus decreasing the risk of fracture. The study by Tu et al. showed that the alleviating inflammatory responses and cartilage degradation of Rhoifolin (a flavanone extracted from *Rhus succedanea*) in rat chondrocytes is mediated by P38/JNK and PI3K/AKT/mTOR signal pathways.

NLRP3, a sensor of innate immunity, mediates the activation of caspase-1 and secretion of pro-inflammatory cytokine IL-1 β /IL-18 through the formation of a complex called inflammasome. Abnormal activation of the NLRP3 inflammasome has been associated with a variety of inflammatory disorders, including metabolic disorders, gout, neurodegenerative diseases and autoimmune diseases. Therefore, suppressing the activity of NLRP3 inflammasome becomes a novel signaling pathway on preventing and treating inflammatory diseases. *Artemisia argyi* H. Lév. and *Vaniot* is a traditional herb medicine that has been widely applied for treating inflammation-related diseases. Chen et al. demonstrated that essential oil of *Artemisia argyi* H. Lév. and *Vaniot* (EOAA) inhibited the activation of NLRP3 inflammasome in THP-1 cells induced by monosodium urate and nigericin. Feng et al. confirmed that ethyl 2-succinate-anthraquinone (LHD) has better anti-inflammatory and antibacterial activity than aloe emodin, a novel compound has been chemically modified. It has been an effect on anti-inflammatory effects through reducing the expression of NLRP3, IL-1 β , and caspase-1 protein thus mediating the NLRP3 inflammasome signaling pathway.

Many plants with autoimmune modulatory or anti-inflammatory potential remain unexplored. It is high time that these medicinal plants and natural products were systematically studied using modern tools. For example, the prediction and putative targets of traditional Chinese medicine prescriptions on the mechanism of autoimmune regulation or anti-inflammatory action were further analyzed based on network pharmacology, and further enrichment analysed by KEGG pathways and GO terms related with biological processes, molecular functions, and cellular components. New autoimmune modulatory or anti-inflammatory plant products can also be discovered through high-throughput and high-content screening. In the meanwhile, to develop an immunocompetent 3D *in vitro* model allows screening of potential plant derived therapeutic agents against inflammation.

Rheumatoid factor (RF) or anti-cyclic citrullinated peptide antibodies (anti-CCP) are serological indicators for the diagnosis of RA. Through meta-analysis and systematic review, Tang et al. found that the treatment of RA by Chinese herbal compound could effectively reduce the level of RF or anti-CCP, and the clinical efficacy might be superior to western single drug therapy. They summarized the active components and pharmacological effects of five high-frequency representative Chinese herbal medicines, including *Angelica sinensis* (Oliv.) Diels, *Glycyrrhiza glabra* L., *Neolitsea cassia* (L.) Kosterm., *Paeonia lactiflora* Pall., and *Angelica dahurica* (Hoffm.) Benth. and Hook.

f. Ex Franch. and Sav., and found that Chinese herbal compound may reduce RF and anti-CCP levels by regulating immune response and inhibiting B lymphocyte proliferation. Through network pharmacology, Huang et al. revealed that *Cornus officinalis* Sieb. And *Paeonia lactiflora* Pall. Have been identified as therapeutic candidates to treat RA, as well as their main active compounds ursolic acid and paeoniflorin could reduce synovial hyperplasia and inflammatory infiltration of joint tissues while promoting synovial apoptosis in the rat model of collagen-induced arthritis (CIA).

The “multi-target” feature of traditional Chinese medicine has a particular advantage in the treatment of inflammatory diseases. The use of specific Chinese herbal medicine or plant compounds can reduce symptoms and pathological damage and play a synergistic healing effects when combined with western medicine. Wang et al. selected five key targets, namely JAK3, RORC, PRKCQ, ZAP70, and IL6, and their corresponding active components and positive drugs as ligands through the network pharmacology method. The interaction between the main active components and potential targets of volatile oil from *Matricaria recutita* L. was verified by molecular docking. *Prunella vulgaris* L. is a traditional Chinese medicine, which has been used to thyroid diseases in China. Xu et al. investigate the bio-active ingredients and mechanisms against hashimoto's thyroiditis via network pharmacology and molecular docking technology. The key targets of *Prunella vulgaris* L. were analyzed, and the main targets were JUN, AKI, MAPK1, TP53. Molecular docking results suggest that luteolin and kaolin may play an important role in the treatment of hashimoto's thyroiditis by regulating multiple signaling pathways. Maescotti et al. focus on the development of an immunocompetent 3D *in vitro* triculture intestinal model contain with a differentiated intestinal epithelial layer and immune-competent macrophages. The model imitated a healthy intestine with stable barrier integrity. They evaluated the model with known anti-inflammatory compounds and natural alkaloids of plant origin. By catching the critical specialty of the intestinal mucosa, the immunocompetent 3D *in vitro* model could select potential plant derived of compounds or extract agents against intestinal inflammation.

The clinical application of Traditional Chinese Medicine (TCM) is one of the most effective complementary drugs for the treatment of autoimmune diseases or inflammatory diseases. However, the molecular therapeutic mechanism of TCM is still unclear, which limits its application worldwide. Xiao-Yin-Fang (XYF) has been used by Shanghai Changhai Hospital to treat patients with psoriasis for more than 30 years, and its efficacy has been proved by clinical studies. Zhang et al. demonstrated that XYF relieved psoriasis-like skin inflammation chiefly by inhibiting polarization of $\gamma\delta$ T17 cells in dermis and draining lymph nodes. In addition, XYF can improve the recurrence of psoriatic dermatitis and inhibit the activation of $\gamma\delta$ T cells. Transcriptional analysis showed that XYF may regulate a

variety of inflammatory signal transduction and metabolic processes. Here, Jantrapirom et al. reviewed phytochemicals constituents of Triphala, a potential herbal candidate for the treatment of allergic rhinitis. Though inhibiting the phosphorylation of p38, c-Jun N-terminal kinase (JNK), and ERK and activating the Akt/AMP-activated protein kinase/nuclear factor erythroid 2-related factor (Akt/AMPK/Nrf) signaling pathway to reduce NF- κ B activation and nuclear translocation. Traditional Chinese Medicine Xuanfei Baidu Decoction (XFBD) has been successfully used in the treatment of COVID-19 in China. Yang et al. evidenced that XFBD has multiple positive effects on enhancing cellular immunity via regulating the immune systems in cyclophosphamide treated mice. Previously, network strategies were used to predict the potential signaling pathways that XFBD may participate in the anti-COVID-19 effect (Wang et al., 2020). XFBD significantly inhibited the expression of IL-6, IP-10, and TNF- α in LPS-induced THP-1 cells, and inhibited the secretion of TNF- α , IL-6, and IL-1 β in RAW 264.7 cells, suggesting that XFBD had bidirectional immune modulatory effects.

In summary, this Research Topic provided a platform for medicinal plants researchers to present novel findings on therapeutic targets for inflammation disease and to learn new insights into modern tools between inflammation therapy and medicinal plants. New therapeutic strategies are needed to reduce the harmful effects of chronic inflammation disease. Further research is necessary to understand autoimmune diseases, or inflammatory diseases potential of medicinal plants.

Author contributions

YW, JC, JT, YHW, ZZ, XZ wrote the editorial. All Authors contributed, revised and approved this article.

Funding

This work was supported by National Natural Science Foundation of China (81503221, 819714703, 81903760, and 81903914), Natural Science Foundation of Guangdong Province (2017A030313659), and Shenzhen Fundamental Research and Discipline Layout Project (JCYJ20170413093108233, JCYJ20180228164437735, JCYJ20190809143803732, JCYJ20190806151816859, and JCYJ20210324113003007).

Conflict of interest

The authors declare that the research was conducted in the absence of any commercial or financial relationships that could be construed as a potential conflict of interest.

Publisher's note

All claims expressed in this article are solely those of the authors and do not necessarily represent those of their affiliated

organizations, or those of the publisher, the editors and the reviewers. Any product that may be evaluated in this article, or claim that may be made by its manufacturer, is not guaranteed or endorsed by the publisher.

References

- Akhtar, M. A. (2022). Anti-inflammatory medicinal plants of Bangladesh—a pharmacological evaluation. *Front. Pharmacol.* 13, 809324. doi:10.3389/fphar.2022.809324
- Bello, R. O., Chin, V. K., Isnadi, M. F. A. R., Majid, R. A., Atmadini Abdullah, M., Lee, T. Y., et al. (2018). The role, involvement and function(s) of interleukin-35 and interleukin-37 in disease pathogenesis. *Int. J. Mol. Sci.* 19 (4), 1149. doi:10.3390/ijms19041149
- Besednova, N. N., Andryukov, B. G., Zaporozhets, T. S., Kuznetsova, T. A., Kryzhanovsky, S. P., Ermakova, S. P., et al. (2022). Molecular targets of Brown algae phlorotannins for the therapy of inflammatory processes of various origins. *Mar. Drugs* 20 (4), 243. doi:10.3390/md20040243
- Chen, L., Deng, H., Cui, H., Fang, J., Zuo, Z., Deng, J., et al. (2018). Inflammatory responses and inflammation-associated diseases in organs. *Oncotarget* 9 (6), 7204–7218. doi:10.18632/oncotarget.23208
- Davies, N. M. (1995). Toxicity of nonsteroidal anti-inflammatory drugs in the large intestine. *Dis. Colon Rectum* 38 (12), 1311–1321. doi:10.1007/BF02049158
- Galindo, T., Reyna, J., and Weyer, A. (2018). Evidence for transient receptor potential (TRP) channel contribution to arthritis pain and pathogenesis. *Pharmaceuticals* 11 (4), 105. doi:10.3390/ph11040105
- Hämäläinen, M., Nieminen, R., Vuorela, P., Heinonen, M., and Moilanen, E. (2007). Anti-inflammatory effects of flavonoids: Genistein, kaempferol, quercetin, and daidzein inhibit STAT-1 and NF-kappaB activations, whereas flavone, isorhamnetin, naringenin, and pelargonidin inhibit only NF-kappaB activation along with their inhibitory effect on iNOS expression and NO production in activated macrophages. *Mediat. Inflamm.* 2007, 45673. doi:10.1155/2007/45673
- Jo, E. K., Kim, J. K., Shin, D. M., and Sasakawa, C. (2016). Molecular mechanisms regulating NLRP3 inflammasome activation. *Cell. Mol. Immunol.* 13 (2), 148–159. doi:10.1038/cmi.2015.95
- Kundu, J. K., Shin, Y. K., and Surh, Y. J. (2006). Resveratrol modulates phorbol ester-induced pro-inflammatory signal transduction pathways in mouse skin *in vivo*: NF-kappaB and AP-1 as prime targets. *Biochem. Pharmacol.* 72 (11), 1506–1515. doi:10.1016/j.bcp.2006.08.005
- Placha, D., and Jampilek, J. (2021). Chronic inflammatory diseases, anti-inflammatory agents and their delivery nanosystems. *Pharmaceutics* 13 (1), 64. doi:10.3390/pharmaceutics13010064
- Tsai, H., Zeng, X. B., Liu, L. S., Xin, S. C., Wu, Y. Y., Xu, Z., et al. (2021). NF45/NF90-mediated rDNA transcription provides a novel target for immunosuppressant development. *EMBO Mol. Med.* 13 (3), e12834. doi:10.15252/emmm.202012834
- Wang, Y., Li, X., Zhang, J. H., Xue, R., Qian, J. Y., Zhang, X. H., et al. (2020). Mechanism of Xuanfei Baidu Tang in treatment of COVID-19 based on network pharmacology. *Zhongguo ZhongYao Za Zhi* 45 (10), 2249–2256. doi:10.19540/j.cnki.cjmm.20200325.401
- Xie, Z., Yu, C., and Gao, X. (2019). A method toward constituents with weak response in mass spectra for comprehensively characterizing constituents in traditional Chinese medicine formula, Kangfuxiaoyanshuan as a case. *J. Sep. Sci.* 42 (19), 3152–3160. doi:10.1002/jssc.201900172
- Xie, Z., Wang, Y., Yang, G., Han, J., Zhu, L., Li, L., et al. (2021). The role of the Hippo pathway in the pathogenesis of inflammatory bowel disease. *Cell Death Dis.* 12 (1), 79. doi:10.1038/s41419-021-03395-3



Combined *Cornus Officinalis* and *Paeonia Lactiflora* Pall Therapy Alleviates Rheumatoid Arthritis by Regulating Synovial Apoptosis via AMPK-Mediated Mitochondrial Fission

Lichuang Huang^{1†}, Shaoqi Hu^{1†}, Meiyu Shao^{1†}, Xin Wu¹, Jida Zhang^{2*} and Gang Cao^{1*}

¹School of Pharmacy, Zhejiang Chinese Medical University, Hangzhou, China, ²College of Basic Medical Science, Institute of Basic Research in Clinical Medicine, Zhejiang Chinese Medical University, Hangzhou, China

OPEN ACCESS

Edited by:

Xiao Bin Zeng,
Jinan University, China

Reviewed by:

Guangrui Huang,
Beijing University of Chinese Medicine,
China
Mohammad Shahid Mansuri,
Yale University, United States

*Correspondence:

Jida Zhang
zhjd82@tom.com
Gang Cao
cgang1126@163.com

[†]These authors have contributed
equally to this work

Specialty section:

This article was submitted to
Inflammation Pharmacology,
a section of the journal
Frontiers in Pharmacology

Received: 08 December 2020

Accepted: 03 March 2021

Published: 09 April 2021

Citation:

Huang L, Hu S, Shao M, Wu X, Zhang J
and Cao G (2021) Combined *Cornus*
Officinalis and *Paeonia Lactiflora* Pall
Therapy Alleviates Rheumatoid
Arthritis by Regulating Synovial
Apoptosis via AMPK-Mediated
Mitochondrial Fission.
Front. Pharmacol. 12:639009.
doi: 10.3389/fphar.2021.639009

Rheumatoid arthritis (RA) is a chronic autoimmune disease that leads to cartilage destruction and bone erosion. In-depth exploration of the pathogenesis of RA and the development of effective therapeutic drugs are of important clinical and social value. Herein, we explored the medicinal value of *Cornus officinalis* Sieb. and *Paeonia lactiflora* Pall. in RA treatment using a rat model of collagen-induced arthritis (CIA). We compared the therapeutic effect of *Cornus officinalis* and *Paeonia lactiflora* with that of their main active compounds, ursolic acid and paeoniflorin, respectively. We demonstrated that the combination of *Cornus officinalis* and *Paeonia lactiflora* effectively inhibited the release of factors associated with oxidative stress and inflammation during RA, therein ameliorating the symptoms and suppressing the progression of RA. We further showed that the underlying mechanisms may be related to the regulation of apoptosis in synovial tissues, and we investigated the potential involvement of AMPK-mediated mitochondrial dynamics in the therapeutic action of the two drugs and their active components.

Keywords: ursolic acid, paeoniflorin, inflammation, oxidative stress, synovial tissue

INTRODUCTION

Rheumatoid arthritis (RA) is a chronic autoimmune disease that leads to cartilage destruction and bone erosion (Gong et al., 2019; Tseng et al., 2020). It usually occurs in individuals aged 30–50, and its incidence rate in women is approximately three times that in men (Intriago et al., 2019; Kohler et al., 2019). RA exhibits an intricate pathological course and is difficult to manage, and the high disability rate severely lowers the quality of life, bringing about heavy socioeconomic burdens. The pathogenesis of RA is not completely clear and may be related to a variety of factors such as genetics, environment, and immunity (Klareskog et al., 2006; Deane et al., 2017). Pathological features of RA include joint inflammation, synovial hyperproliferation, and articular swelling (Guo et al., 2018). RA progression may lead to a number of comorbid conditions such as coronary heart disease, atherosclerosis, and interstitial pneumonia (Kaplan, 2010; Kakuwa et al., 2019), resulting in significant life span shortening in some RA patients. Therefore, in-depth exploration of the

pathogenesis of RA and the development of effective therapeutic drugs are of important clinical and social value.

Oxidative stress has been heavily implicated in the pathophysiology of inflammatory diseases such as RA (da Fonseca et al., 2019). As the main organelle involved in energy metabolism and a main source of intracellular reactive oxygen species (ROS), mitochondria play an indispensable role in homeostatic maintenance. Normal mitochondrial function is critical in upholding redox balance (Ippolito et al., 2020), and overproduction of ROS leads to a disruption in redox equilibrium and mitochondrial dysfunction, which may aggravate arthritic development (Valcarcel-Ares et al., 2014). In addition, excessive ROS is associated with immunopathogenesis and inflammation. For example, macrophages are activated by pro-inflammatory factors such as interleukin (IL)-1 β and tumor necrosis factor (TNF)- α under oxidative stress to produce superoxides (Filippin et al., 2008), in turn accelerating the development of arthritis. The maintenance of proper mitochondrial function is important in the regulation of cell fate. In particular, mitochondrial fission has been shown to be closely linked to cell apoptosis, and the balance between mitochondrial fission and fusion is critical in determining cell health (Wang and Youle, 2009). The involvement of ROS regulation, apoptosis, and AMPK-mediated mitochondrial dynamics in RA pathogenesis and treatment warrants further investigation.

Cornus officinalis Sieb. et Zucc, also known as Corni Fructus, is a plant traditionally used to treat tinnitus, impotence, and excessive urination. It has exhibited anti-oxidant (Lee et al., 2006), anti-diabetic (Yamahara et al., 1981), and anti-tumorigenic (Chang et al., 2004) effects. The active compounds of *Cornus officinalis* include malic acid, ursolic acid, and loganin (Endo and Taguchi, 1973; Czerwinska and Melzig, 2018; Dong et al., 2018). Among these, the relative content of loganin and ursolic acid are often evaluated in assessing the quality of *Cornus officinalis*. In particular, ursolic acid inhibited the release of inflammatory factors, repaired the balance between Th1/Th17, and suppressed matrix metalloproteinase production in an *in vivo* model of type II collagen-induced arthritis (Lee et al., 2017). *Paeonia lactiflora* Pall. has also demonstrated effectiveness in RA treatment. Paeoniflorin is one of the main active components of *Paeonia lactiflora* and has shown a variety of anti-inflammatory and immunomodulatory effects (Zhang and Wei, 2020). Taken together, both *Cornus officinalis* and *Paeonia lactiflora* have shown promising effects in RA treatment, but the specific molecular mechanism behind their therapeutic action have not been studied in-depth.

Herein, we explored the medicinal value of *Cornus officinalis* and *Paeonia lactiflora* in RA treatment using a rat model of collagen-induced arthritis (CIA). We hypothesized that the combination of *Cornus officinalis* and *Paeonia lactiflora* can effectively inhibit the release of oxidative stress-related and inflammatory factors during RA, therein ameliorating the symptoms and suppressing the progression of RA. We further propose that the underlying mechanisms may be related to the regulation of apoptosis in synovial tissues, and we investigated the

potential involvement of AMPK-mediated mitochondrial dynamics in the therapeutic action of the two drugs.

MATERIALS AND METHODS

CIA Induction and Drug Treatment

Commercially available *Cornus officinalis* (200309) and *Paeonia lactiflora* (200101) were purchased from Zhejiang Chinese Medical University Medical Pieces Ltd. (Hangzhou, China), ursolic acid (DX0019) and paeoniflorin (DS0070) were purchased from Desite (Chengdu, China), and dexamethasone (D1756) was purchased from Sigma-Aldrich (St. Louis, MO, United States). To prepare the drugs for gavaging, each compound was dissolved in sterilized water at specified concentrations, given that the drugs were administered at 10ml per kg of animal body weight. All animal experiments were performed at Wuhan Myhalic Biotechnology Co., Ltd. (Wuhan, China). The experimental protocol was approved by the institutional review board of the Model Animal Research Institute at Wuhan Myhalic Biotechnology Co., Ltd. and adhered to the guidelines for animal care and use (approval number: HLK-20190418–01). Male specific-pathogen-free Sprague-Dawley rats weighing 200 ± 20 g were acquired from China Three Gorges University. The rats were housed in a facility with 50–60% relative humidity at 25°C. Before the experiment, the rats adaptively fed for seven days, where they were allowed free access to food and water. The CIA model was established following previously reported methods (Jia et al., 2014; Xu et al., 2018), with three rats in each group. Control rats were not treated in any way. To induce CIA, 10mg of type II collagen (PAB43878, Bioswamp) was mixed with 0.01M acetic acid and emulsified with an equal volume of Freund's complete adjuvant to a final collagen concentration of 2mg/ml. On day 0, experimental rats were intradermally injected with 0.1ml of emulsified collagen II in the right hind toe. Boost immunization was induced after seven days with an additional intradermal injection of 0.1ml of emulsified collagen II in the right hind toe. Drug treatment began after another seven days (14 days of CIA induction) by gavaging the rats daily with the following drug doses: *Cornus officinalis* (COR, low/L dose: 1.68 g of drug per kg of rat body weight per day (g/kg/d); medium/M dose: 3.36 g/kg/d; high/H dose: 6.27 g/kg/d), *Paeonia lactiflora* (PAE, L: 3.36 g/kg/d; M: 6.27 g/kg/d; H: 13.44 g/kg/d), combination of COR and PAE, paeoniflorin (PF, 7.5 mg/kg/d) (Xu et al., 2018), ursolic acid (UA, 25 mg/kg/d) (Lee et al., 2017), or dexamethasone (DEX, 0.5 mg/kg/d) as a positive control. The doses of COR and PAE were determined based on the clinically administered doses of each drug, which range from 15 to 30 g/60 kg/d and 30–60 g/60 kg/d, respectively (60 kg being the normal adult human weight). The lower and higher ends of these ranges were taken to be the low (COR-L and PAE-L) and medium (COR-M and PAE-M) doses, respectively. The highest doses (COR-H and PAE-H) were determined by multiplying the medium dose by 2.5. These doses were then converted into corresponding drug doses for rats based on the literature (from human to rat: multiplied by 6.2) (Nair and Jacob, 2016).

Evaluation of Toe Swelling and Arthritic Score

During the experimentation period, toe volume was measured by water displacement plethysmometry (Obiri et al., 2014; Zhang et al., 2016) on day 0, 4, 7, 12, 14, 24, 32, and 34. The degree of swelling was calculated using the following equation:

$$\% \text{ swelling} = (V_x - V_0) / V_0 \times 100\%$$

Where V_x is the toe volume on day x and V_0 is the initial toe volume measured on day 0 in the same drug treatment group. On the same days, the paw of the rats was observed macroscopically and the severity of arthritis was assessed. An arthritic score was given using the following scale (Wang et al., 2007): 0, no redness or swelling; 1, redness and swelling at the toe joints; 2, redness and swelling at the toes and toe joints; 3, redness and swelling in all areas below the ankle; 4, redness and swelling in all areas below the ankle, including the ankle joint.

Sample Preparation

After 20 days of drug administration (34 days after initial CIA induction), the rats were sacrificed *via* an overdose of sodium pentobarbital. Whole blood was collected from the abdominal aorta of the rats and serum was separated by centrifugation. To isolate synovial tissues, the knee joint was cut open to expose the kneecap and separate the muscles. The synovial and fibrous layers of the joint capsule were separated using surgical scalpels, and synovial tissues were extracted. The right ankle joint was fixed in 4% paraformaldehyde, decalcified, and paraffin-embedded for histological examination.

Hematoxylin and Eosin (HE) Staining

HE staining was performed to observe general joint tissue morphology. Decalcified and paraffin-embedded samples were frozen at -20°C and cut using a microtome at a thickness of $3\text{ }\mu\text{m}$. The sections were fixed on microscope slides and deparaffinized, then washed with water for 2 min. The sections were stained with hematoxylin (G1140, Solarbio) for 5 min and residual dye solution was removed with running water. For differentiation, 1% hydrochloric alcohol was added to the sections for several seconds, and the sections were washed again with water. A bluing solution was added for 10 s and the sections were washed again with water. Next, the sections were stained with 0.5% eosin (E8090, Solarbio) for 3 min and washed briefly with distilled water. The sections were dehydrated in a graded concentration series of ethanol (80% for 30 s, 90% for 30 s, 100% for 2 s) and immersed twice in xylene for several seconds. The sections were then sealed and observed under an upright microscope (DM1000, Leica). Images of joint and bone tissue were acquired using Leica Application Suite. Each joint tissue and bone tissue section was given an inflammation score and bone destruction score, respectively, and the two scores were added to obtain the total pathology score. Inflammation was scored based on the following standards: 0, no inflammatory infiltration; 1, approximately 20 inflammatory infiltrates per field of view ($400\times$); 2, 20 to 50 inflammatory infiltrates per field of view ($400\times$); 3, more than 50 inflammatory infiltrates per field of view ($400\times$). Bone

destruction was scored based on the following standards: 0, normal; 1, small amount of cartilage loss and bone destruction is limited to isolated regions; 2, large areas of cartilage destruction and bone erosion caused by pannus; 3, complete destruction of joint structure.

Terminal Deoxynucleotidyl Transferase dUTP Nick End Labeling (TUNEL) Staining

TUNEL staining was performed to evaluate tissue apoptosis in ankle joint samples using an *In Situ* Cell Death Detection Kit (11684817910, Roche). Decalcified and paraffin-embedded joint tissue samples were frozen at -20°C and cut using a microtome at a thickness of $3\text{ }\mu\text{m}$. The sections were fixed on microscope slides and heated at 65°C for 1 h, then immersed twice in xylene for 15 min each. The deparaffinized sections were rehydrated in a graded concentration series of ethanol (100%, 95% s, 85%, and 75% for 5 min each) and washed with running tap water for 10 min. Then, the sections were incubated with proteinase K solution (P1120, Solarbio) at 37°C for 15 min and washed twice with PBS. TUNEL reaction solution was prepared by mixing $50\text{ }\mu\text{l}$ of enzyme solution with $450\text{ }\mu\text{l}$ of solvent (both included in the assay kit). After the PBS washes, the sections were incubated with $50\text{ }\mu\text{l}$ of TUNEL reaction solution in a humidified box in the dark for 1 h at 37°C . After three washes with PBS, $50\text{ }\mu\text{l}$ of POD solution (included in the assay kit) was added to each section, which were then incubated in a humidified box for 30 min at 37°C . The sections were washed three times with PBS and incubated with $50\text{ }\mu\text{l}$ of diaminobenzidine (DA1010-2, Solarbio) at room temperature for 10 min, after which they were washed again three times with PBS. Counterstaining was performed using hematoxylin, and the sections were dehydrated, transparentized, and sealed. Tissue apoptosis was observed under an upright microscope (DM1000, Leica) and analyzed using Leica Application Suite. Positive TUNEL staining representative of apoptotic cells is shown in dark brown.

Biochemical Assays

The levels of cytokines in the serum of CIA-induced rats were evaluated using enzyme-linked immunosorbent assay. Commercial assay kits for TNF- α (RA30025), IL-1 β (RA20020), IL-6 (RA20607), and IL-10 (RA20090) were obtained from Bioswamp and the assay was carried out by following the protocols specified by the manufacturer. Colorimetric assays were performed to detect the levels of oxidative stress-related factors in the serum and synovial tissues of CIA-induced rats. Commercial assay kits for malondialdehyde (MDA, A003-1), superoxide dismutase (SOD, A001-1), and nitric oxide (NO, A-013-2) were obtained from Nanjing Jiancheng Bioengineering Institute (Nanjing, China) and the assay was carried out by following the protocols specified by the manufacturers. All required reagents were included in the ELISA and colorimetry assay kits. For all biochemical assays, absorbance of the well plates was measured using a microplate reader (MK3, Finnpipette).

Western Blot

Synovial tissues were homogenized and lysed using radioimmunoprecipitation assay buffer (JC9610, Gelatins) containing protease and phosphatase inhibitors. After complete lysis, the samples were centrifuged for 15 min at $12000 \times g$ at 4°C , and the concentration of proteins in the supernatant was measured using a bicinchoninic acid assay kit (PN0120, G-CLONE). For western blot, sodium dodecyl sulfate-polyacrylamide gel electrophoresis was performed using 20 μg of denatured proteins from each sample. After electrophoresis, the proteins were transferred onto polyvinylidene fluoride membranes (16220405, DocLab), which were then blocked in 5% skim milk overnight at 4°C . Primary antibody incubation was performed for 1 h at room temperature with antibodies against the following proteins: Bax (1:1000, PAB32583, Bioswamp), Bcl-2 (1:1000, PAB33482, Bioswamp), cleaved caspase-3 (1:1000, 9661S, Cell Signaling Technology), cytochrome-c (1:1000, PAB30055, Bioswamp), dynamin-related protein 1 (Drp1, 1:1000, PAB33409, Bioswamp), phosphorylated Drp1 at serine 616 (pDrp1-Ser616, 1:1000, 4867S, Cell Signaling Technology), phosphorylated Drp1 at serine 637 (pDrp-Ser637, 1:1000, PA5-64821, eBioscience), mitochondrial fission process protein 1 (MTFP1, 1:1000, PAB42161, Bioswamp), mitofusin 2 (MFN2, 1:1000, PAB37988, Bioswamp), AMPK (1:1000, PAB30970, Bioswamp), and phosphorylated AMPK (pAMPK, 1:1000, ab23875, Abcam), with glyceraldehyde 3-phosphate dehydrogenase (GAPDH, 1:1000, PAB36296, Bioswamp) as a housekeeping control. The membranes were washed three times with PBS/Tween 20 for 5 min each and incubated with horseradish peroxidase-conjugated goat anti-rabbit IgG secondary antibodies (1:20000, SAB43714, Bioswamp) for 1 h at room temperature. After three washes with PBS/Tween 20 for 5 min each, the membranes were immersed in enhanced chemiluminescence solution and the protein bands were exposed using an automatic analyzer (JP-K900, Jiapeng, Shanghai, China). The gray values of the protein bands were measured using Tanon GIS software.

Transmission Electron Microscopy

Synovial tissues were first fixed with 2.5% glutaraldehyde (30092436, Sinopharm) at 4°C for 30 min. After three washes with PBS for 10 min each, the tissues were fixed with 1% osmium acid (18,456, TedPella) for 1 h and washed again three times with PBS for 10 min each. To dehydrate the sample, the synovial tissues were sequentially immersed in ethanol at increasing concentrations (50, 70, 80, and 90%) for 5 min at each concentration, then in 90% acetone for 5 min and twice in 100% acetone for 4 min each. For soaking, the tissues were semi-immersed in a solution of acetone and epoxy resin 812 (1:1 ratio) at 40°C for 6 h and then fully immersed in pure epoxy resin 612 at 40°C for 4 h. After fixation, dehydration, and soaking, the tissues were embedded in a plastic plate and placed in an oven for polymerization for 4 h at 40°C , 2 h at 50°C , and 12 h at 90°C . The embedded samples were sectioned using an ultramicrotome at 60 nm. The sectioned samples were dyed in uranyl acetate (1005–25 g, Merck) in the dark for 20 min and washed three times with double-distilled water. After drying, the samples were

stained with lead citrate (1101125, SPI) in the dark for 15 min. Excess lead residue was washed away with double-distilled water. The samples were blotted dry with filter paper and observed under a transmission electron microscope (HT7700, Hitachi).

Statistical Analysis

Statistical analysis was performed using OriginPro 8.0. All data are presented as the mean \pm standard deviation ($n = 3$). The significance of differences between means among more than two groups was evaluated by the one-way analysis of variance with Tukey's post-hoc test. Statistical significance was defined as $p < 0.05$.

RESULTS

Construction and Validation of CIA Model in Sprague-Dawley Rats

The experimental scheme in **Figure 1A** demonstrates the method of establishing the CIA model in Sprague-Dawley rats. Emulsified type II collagen in Freund's complete adjuvant was injected on days 0 (initiation) and 7 (boost immunization), and drug administration began on day 14 and continued for 20 consecutive days. CIA-induced rats were treated with 3.36 mg/kg/d *Cornus officinalis* (COR) or/and 6.27 mg/kg/d *Paeonia lactiflora* (PAE), 7.5 mg/kg/d paeoniflorin (PF, active compound in PAE), 25 mg/kg/d ursolic acid (UA, active compound in COR), or 0.5 mg/kg/d dexamethasone (DEX, positive control drug). Macroscopic observation of the paws of the rats (**Figure 1B**) demonstrated intense redness and swelling of the toes in all CIA-induced rats on day 14. By day 34, the toes of untreated CIA-induced rats still showed redness and swelling, but those of drug-treated rats recovered to a large extent. In particular, the appearance of the toes of rats treated with paeoniflorin, ursolic acid, and DEX seemed to closely resemble that of Control rats, indicating the therapeutic efficacy of these treatments. An arthritic score was assigned to each rat on specified days during the experimental period as an indication of the severity of arthritis based on the pre-defined criteria (**Table 1**). Consistent with the macroscopic observations, CIA induced severe redness and swelling by day 14, but drug treatment alleviated these symptoms to varying degrees, with paeoniflorin, ursolic acid, and DEX showing the best effect among the tested drugs.

During the experimental period, the rats were monitored and changes in toe volume, which were a sign of swelling, were measured on specified days (**Figure 1C**). Evidently, the peak of CIA induction, indicated by the greatest toe volume, appeared on day 14 (except for the Control group, which did not receive CIA induction), as drug treatment began thereafter. From day 14 to day 34 (end of experimental period), there was a gradual decrease in toe volume in all drug-treated rats. By day 34, the toe volume of all drug-treated rats was significantly lower than that of non-treated CIA-induced rats, almost reaching the level of Control rats. To further analyze the effect of CIA and drug treatment on toe healing in CIA-induced rats, the swelling rate was calculated (**Figure 1D**). All CIA-induced rats have achieved

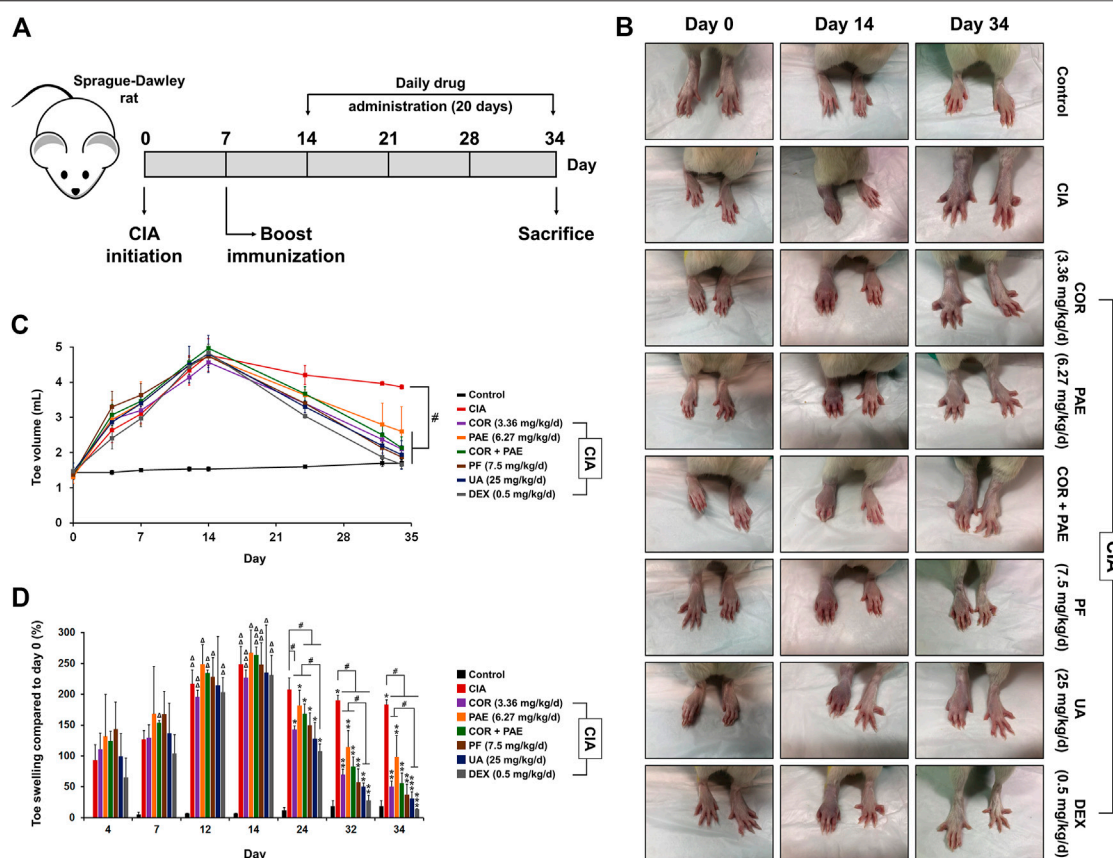


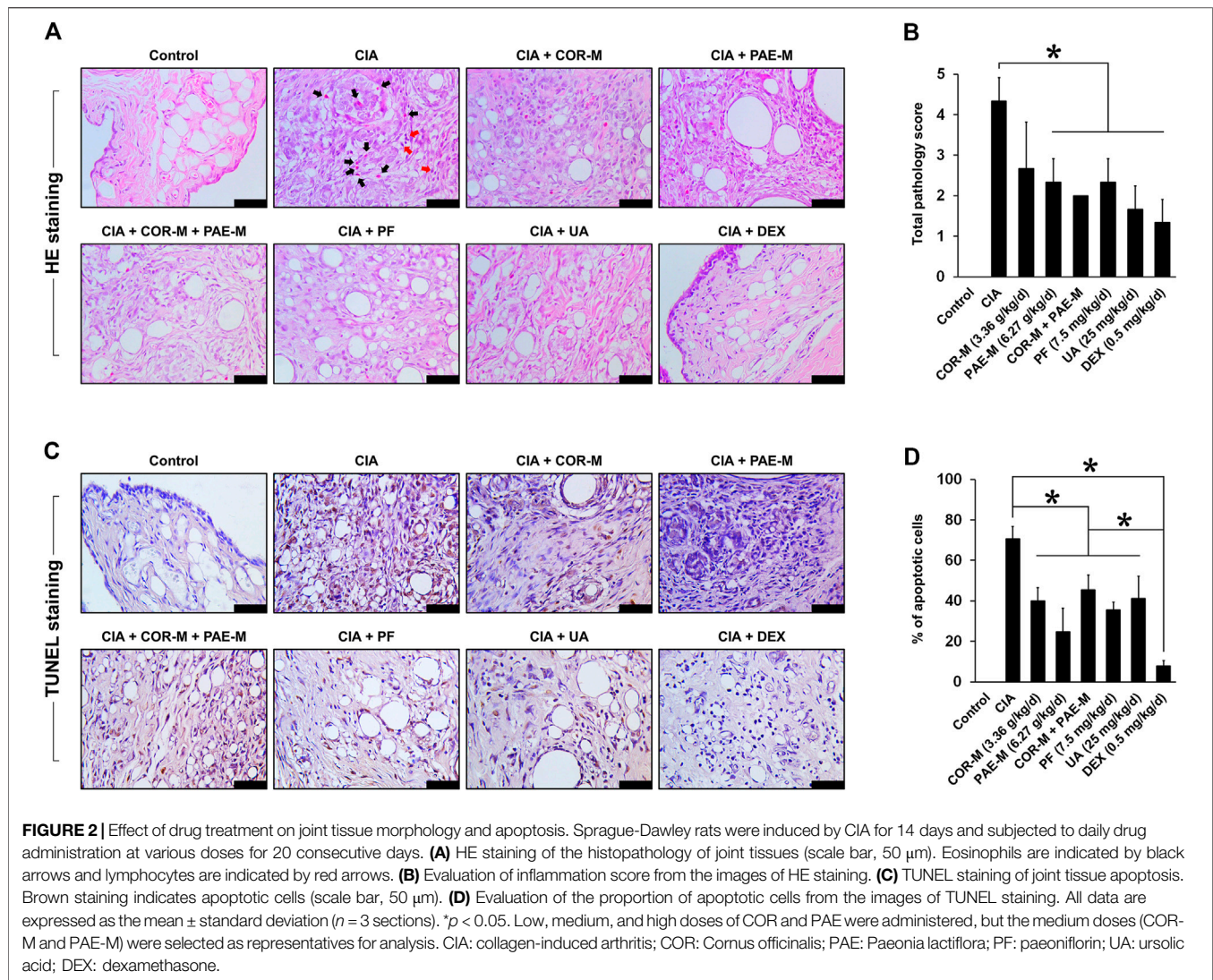
FIGURE 1 | Validation of CIA model establishment. **(A)** To induce CIA, Sprague-Dawley rats were given an initial injection of CFA containing collagen II (day 0). After 7 days, boost immunization was induced via CFA injection. Drug administration began on day 14 and continued daily for 20 days. The rats were sacrificed on day 34. **(B)** Macroscopic observation of toe swelling on day 0 (CIA initiation), day 14 (beginning of drug treatment), and day 34 (end of drug treatment). **(C)** Toe volume was measured on day 0, 4, 7, 12, 14, 24, 32, and 34. **(D)** Relative toe swelling was calculated using the following equation $(V_x - V_0)/V_0 \times 100\%$, where V_x is the toe volume measured on day x and V_0 is the initial toe volume of the respective drug treatment group measured on day 0. All data are expressed as the mean \pm standard deviation ($n = 3$ rats). # $p < 0.05$; Δ , $\Delta\Delta$, and $\Delta\Delta\Delta$ denote $p < 0.05$ compared to day 4, 7, and 12, respectively, in the same drug treatment group; *, **, and *** denote $p < 0.05$ compared to day 14, 24, and 32, respectively, in the same drug treatment group. Low, medium, and high doses of COR and PAE were administered, but the medium doses (COR-M and PAE-M) were selected as representatives for analysis. CIA: collagen-induced arthritis; COR: Cornus officinalis; PAE: Paeonia lactiflora; PF: paeoniflorin; UA: ursolic acid; DEX: dexamethasone.

TABLE 1 | Evaluation of arthritic score in CIA-induced rats ($n = 3$). Arthritic score was assessed using the following scale: 0, no redness or swelling; 1, redness and swelling at the toe joints; 2, redness and swelling at the toes and toe joints; 3, redness and swelling in all areas below the ankle; 4, redness and swelling at in all areas below the ankle, including the ankle joint. COR: Cornus officinalis; PAE: Paeonia lactiflora Pall.; PF: paeoniflorin; UA: ursolic acid; DEX: dexamethasone.

	Day 0	Day 4	Day 7	Day 12	Day 14	Day 24	Day 32	Day 34
Control	0 \pm 0	0 \pm 0	0 \pm 0	0 \pm 0	0 \pm 0	0 \pm 0	0 \pm 0	0 \pm 0
CIA + CIA	0 \pm 0	3 \pm 0	3 \pm 0	4 \pm 0	4 \pm 0	4 \pm 0	4 \pm 0	3 \pm 0
COR (3.36 mg/kg/d)	0 \pm 0	3 \pm 0	3 \pm 0	4 \pm 0	4 \pm 0	3.33 \pm 0.58	2.33 \pm 0.58	2 \pm 0
PAE (6.27 mg/kg/d)	0 \pm 0	2.67 \pm 0.58	3 \pm 0	4 \pm 0	4 \pm 0	3 \pm 0	3 \pm 0	2 \pm 1
COR + PAE	0 \pm 0	2.67 \pm 1.15	3 \pm 0	4 \pm 0	4 \pm 0	3.67 \pm 0.58	2.67 \pm 0.58	1.67 \pm 0.58
PF (7.5 mg/kg/d)	0 \pm 0	3.33 \pm 0.58	3.33 \pm 0.58	4 \pm 0	4 \pm 0	3 \pm 1	2 \pm 1	1.33 \pm 0.58
UA (25 mg/kg/d)	0 \pm 0	2 \pm 0	3 \pm 0	4 \pm 0	4 \pm 0	3.33 \pm 0.58	2 \pm 0	1.33 \pm 1.15
DEX (0.5 mg/kg/d)	0 \pm 0	2.67 \pm 0.58	2.67 \pm 0.58	4 \pm 0	4 \pm 0	2.33 \pm 0.58	2.67 \pm 0.58	0.33 \pm 0.58

significant toe swelling compared to the beginning of the experiment by day 14. Upon drug treatment, toe swelling was gradually alleviated compared to that in non-treated rats (CIA),

and swelling was significantly relieved by all drug treatments by day 34. Individual administration of COR seemed to be more effect than PAE in alleviating toe swelling, while combined



administration of the two did not accentuate the effect of individual drug treatment. In addition, the effect of ursolic acid and DEX was time-dependent up to day 34, whereas that of COR, PAE, and paeoniflorin was time-dependent up to day 32.

Cornus Officinalis and Paeonia Lactiflora Restored Normal Joint Morphology and Inhibited Joint Tissue Apoptosis in CIA-Induced Rats

The morphology of joint tissues was observed by HE staining after the animals were sacrificed on day 34 (Figure 2A). In the control rats, joint tissues exhibited normal morphology and did not show signs of inflammatory infiltration or fibrosis. In the untreated CIA-induced rats, however, hyperproliferation of synovial cells was observed. This was indicated by the filling of voids in the joint tissues, leading to synovial hyperplasia and

thickening. In addition, we noticed areas of fibrous deposition and inflammatory infiltration, pointed out by black and red arrows (eosinophils and lymphocytes, respectively). Upon treatment using COR or/and PAE, these conditions seemed to be suppressed, as demonstrated by the reduction in synovial proliferation and hyperplasia. The effect of the individual active compounds paeoniflorin and ursolic acid appeared to be superior to that of COR and PAE, as joint tissue morphology most closely resembled those of control rats after paeoniflorin and ursolic acid treatment. In particular, inflammatory infiltration was cleared and synovial hyperplasia was remarkably alleviated. The inflammation scores (Figure 2B) are in agreement with the histological observations (results of bone destruction score are not shown), with CIA-induced rats showing the highest score. With each treatment, the inflammation score was significantly decreased (except for COR-M, where the difference was not significant).

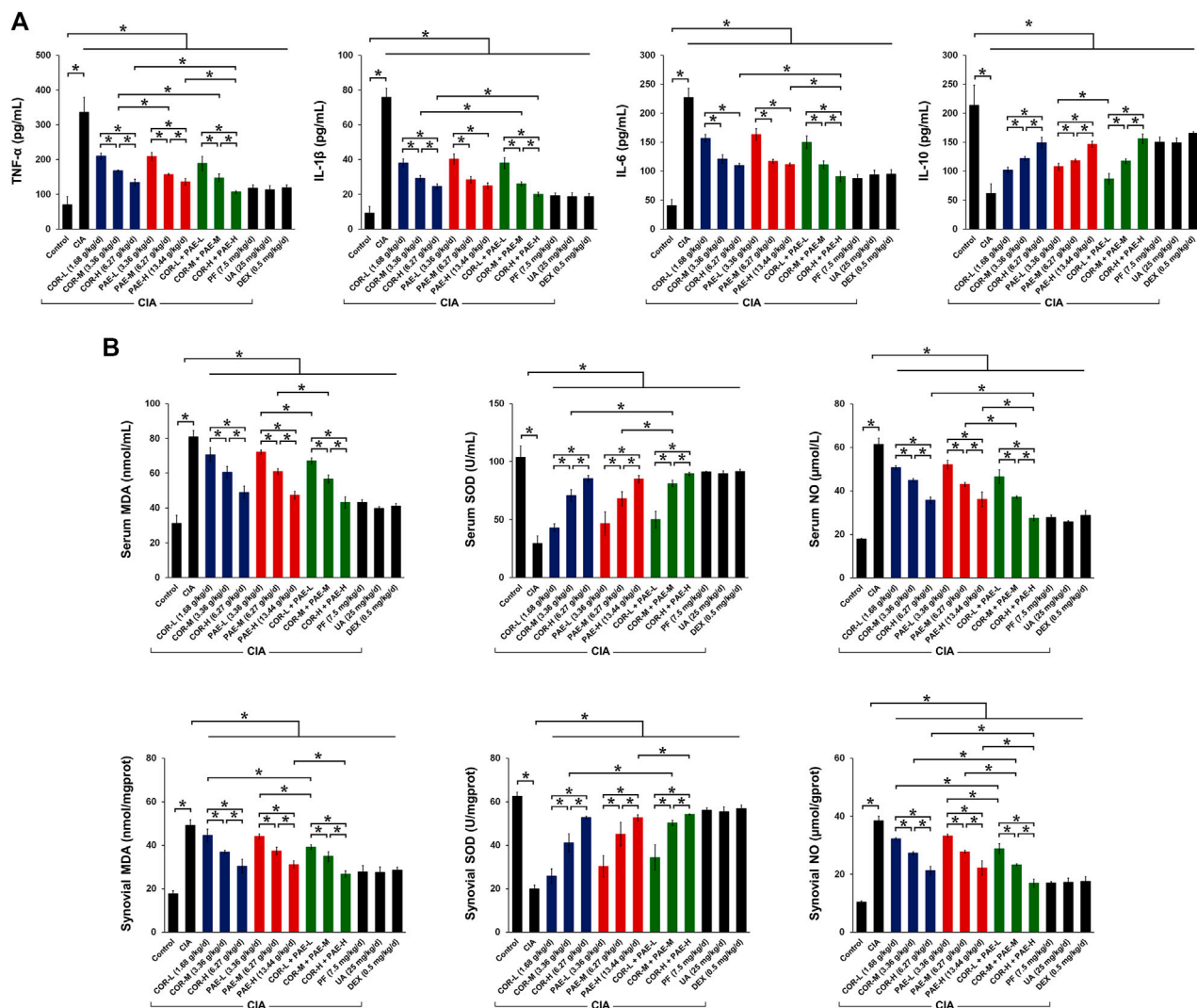
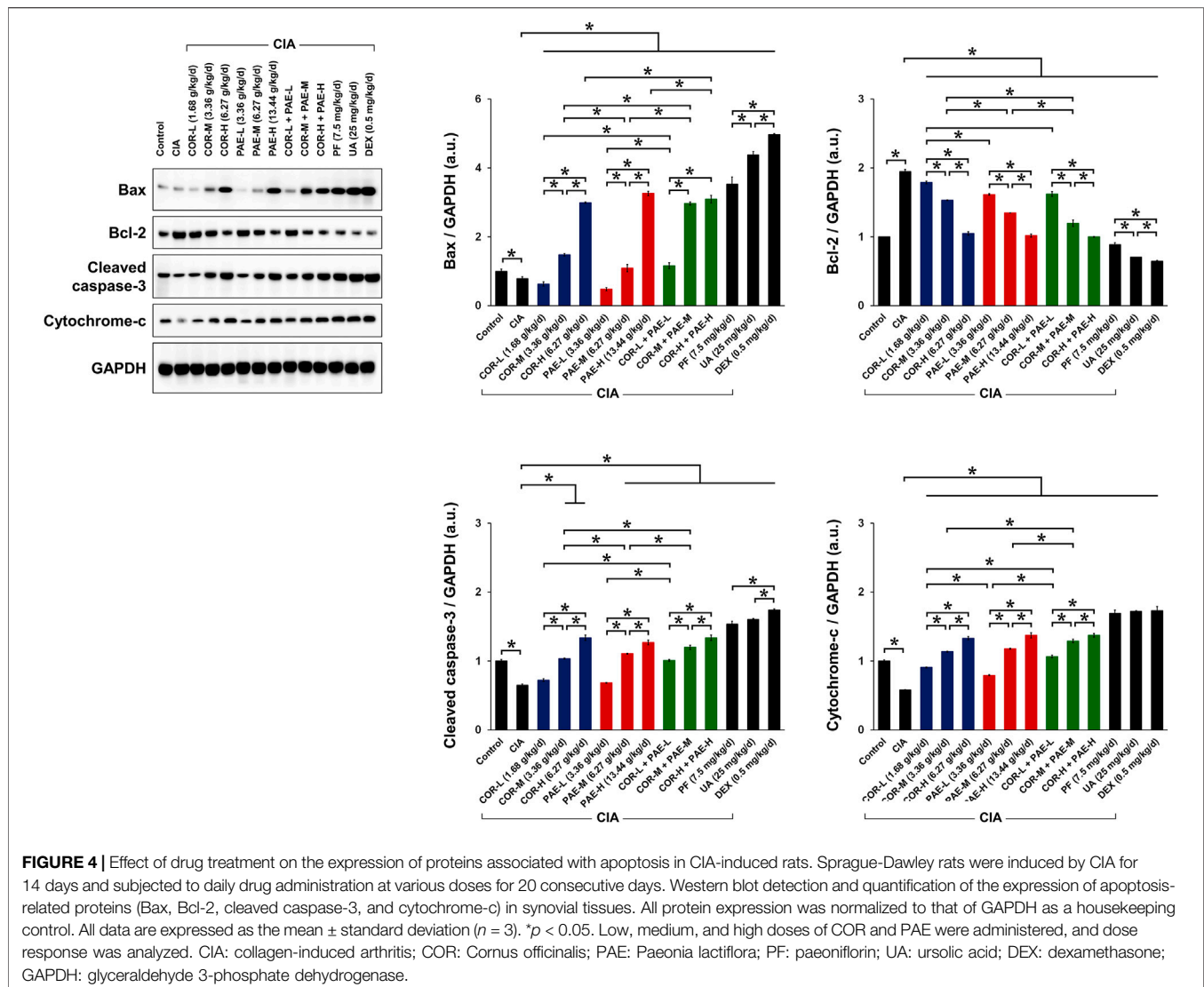


FIGURE 3 | Effect of drug treatment on inflammatory cytokine secretion and oxidative defense in CIA-induced rats. Sprague-Dawley rats were induced by CIA for 14 days and subjected to daily drug administration at various doses for 20 consecutive days. **(A)** ELISA detection of the serum content of TNF- α , IL-1 β , IL-6, and IL-10. **(B)** Biochemical detection of the content of MDA, SOD, and NO in the serum and synovial tissues. All data are expressed as the mean \pm standard deviation ($n = 3$). * $p < 0.05$. Low, medium, and high doses of COR and PAE were administered, and dose response was analyzed. CIA: collagen-induced arthritis; COR: *Cornus officinalis*; PAE: *Paeonia lactiflora*; PF: paeoniflorin; UA: ursolic acid; DEX: dexamethasone; MDA: malondialdehyde; SOD: superoxide dismutase; NO: nitric oxide.

Joint tissue apoptosis was examined by TUNEL staining after the animals were sacrificed on day 34 (Figures 2C,D). In the control rats, no apoptosis was detected in the joint tissues, but untreated CIA-induced rats showed a substantial amount of joint tissue apoptosis (approximately 70% of cells were apoptotic). Upon treatment using COR or/and PAE, tissue apoptosis was significantly suppressed compared to that in untreated CIA-induced rats, but the difference between treatment groups was not significantly. The individual active compounds paeoniflorin and ursolic acid exhibited similar effects in suppressing the apoptosis of joint tissues in CIA-induced rats, but the effect of the positive drug DEX was the most evident among all drugs tested.

Cornus Officinalis and Paeonia Lactiflora Enhanced Anti-inflammatory Cytokine Secretion and Anti-oxidant Defense in CIA-Induced Rats

We then evaluated the effect of COR and PAE on the expression of inflammatory and oxidative stress-related indicators in CIA-induced rats. First, we examined the secretion of relevant cytokines in the serum of CIA-induced rats (Figure 3A). Compared to Control rats, CIA caused a significant increase in the secretion of pro-inflammatory factors (TNF- α , IL-1 β , and IL-6) and a significant decrease in that of the anti-inflammatory factor IL-10. Both COR and PAE exerted a dose-dependent effect



on cytokine secretion, suppressing inflammation by downregulating TNF- α , IL-1 β , and IL-6 and upregulating IL-10. The combination of COR and PAE also showed a dose-dependent effect, but overall, the combined effect did not exceed that of individual COR or PAE administration. The active compounds paeoniflorin and ursolic acid seemed to exert similar effects as that of the positive control drug DEX in alleviating inflammatory response in CIA-induced rats. In terms of oxidative stress, the levels of factors associated with oxidative defense (MDA, SOD, and NO) were assessed in the serum and synovial tissues of CIA-induced rats (**Figure 3B**). The results showed that CIA induction led to a significant increase in oxidative stress, as shown by the upregulation of MDA and NO and the downregulation of the anti-oxidant SOD. Individual or combined administration of COR and PAE exerted an anti-oxidant effect, as demonstrated by the dose-dependent decrease in the levels of MDA and NO and increase in the

level of SOD upon treatment. The active compounds paeoniflorin and ursolic acid seemed to exert similar effects as that of the positive control drug DEX in attenuating oxidative stress.

Cornus Officinalis and Paeonia Lactiflora Regulated Synovial Apoptosis in CIA-Induced Rats

To evaluate the effect of COR and PAE in synovial apoptosis, we examined the expression of relevant proteins in synovial tissues of control and CIA-induced rats. In terms of apoptosis (**Figure 4**), the expression of pro-apoptotic proteins Bax, cleaved caspase-3, and cytochrome-c was significantly downregulated in synovial tissues of CIA-induced rats compared to that in control rats. Conversely, the expression of the anti-apoptotic Bcl-2 was upregulated, collectively suggesting that synovial apoptosis was

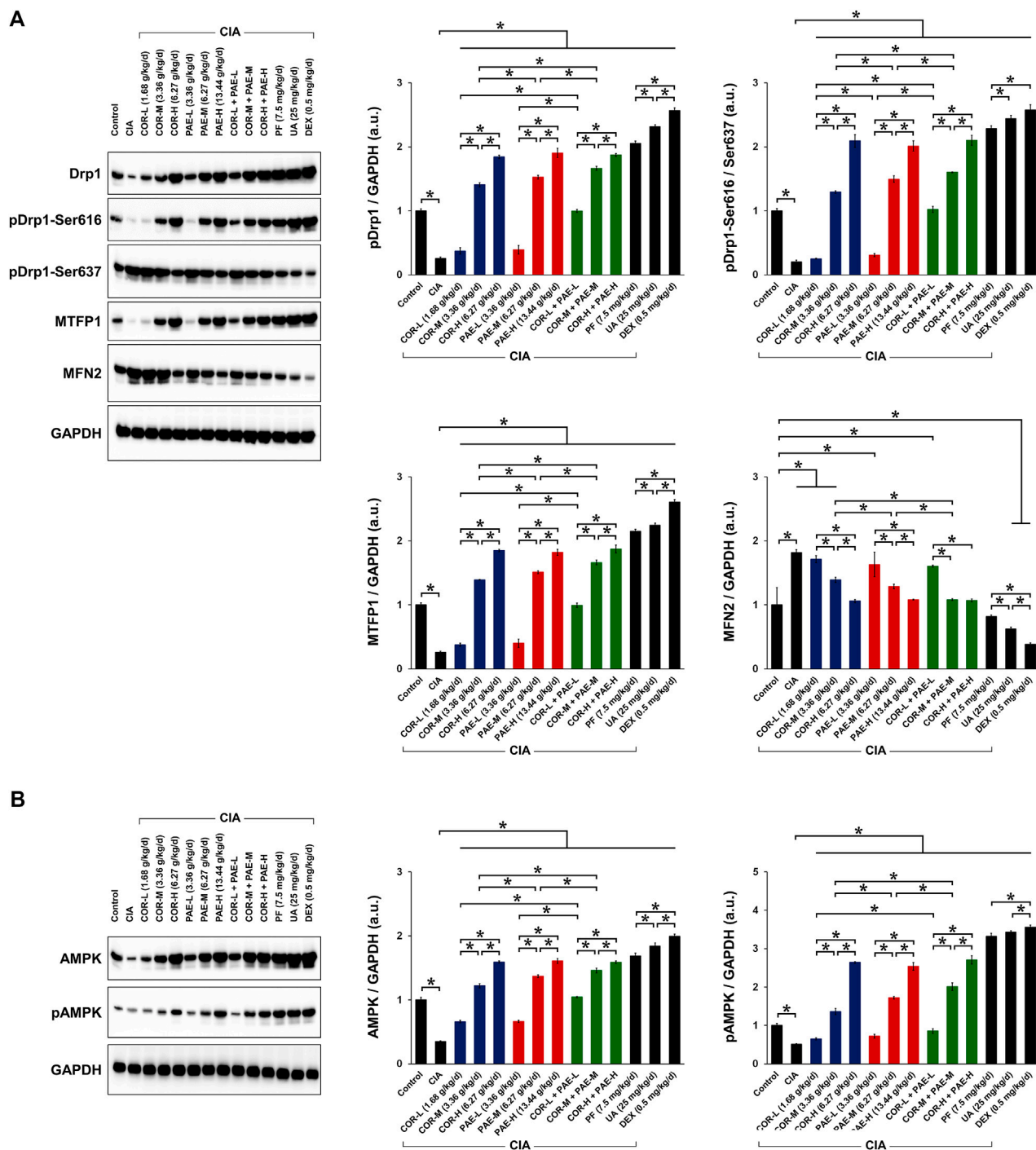


FIGURE 5 | Effect of drug treatment on the expression of proteins associated with mitochondrial function and AMPK signaling in CIA-induced rats. Sprague-Dawley rats were induced by CIA for 14 days and subjected to daily drug administration at various doses for 20 consecutive days. **(A)** Western blot detection and quantification of the expression of mitochondrial function-related proteins (Drp1, Drp1 phosphorylation at Ser616 and Ser637, MTFP1, and MFN2) in synovial tissues. **(B)** Western blot detection and quantification of the expression of AMPK in its non-phosphorylated and phosphorylated form in synovial tissues. All protein expression was normalized to that of GAPDH as a housekeeping control. All data are expressed as the mean \pm standard deviation ($n = 3$). $*p < 0.05$. Low, medium, and high doses of COR and PAE were administered, and dose response was analyzed. CIA: collagen-induced arthritis; COR: *Cornus officinalis*; PAE: *Paeonia lactiflora*; PF: *Paeoniflorin*; UA: ursolic acid; DEX: dexamethasone; Drp1: dynamin-related protein 1; MTFN1: mitochondrial fission process protein 1; MFN2: mitofusin 2; AMPK: AMP-activated protein kinase; GAPDH: glyceraldehyde 3-phosphate dehydrogenase.

suppressed by CIA. Individual administration of COR or PAE in CIA-induced rats appeared to promote synovial apoptosis in a dose-dependent manner, and the combination of the two showed the same trend. Ursolic acid exerted a greater effect than paeoniflorin in affecting the expression of Bax and Bcl-2, but there was no difference between their effect on cleaved caspase-3 and cytochrome-c expression. Taken together, the results suggest that COR and PAE regulated apoptosis in synovial tissues of CIA-induced rats in a dose-dependent manner, and combination treatment exerted similar effects as those of individual treatment.

Cornus Officinalis and Paeonia Lactiflora Promoted Mitochondrial Fission via AMPK Pathway in CIA-Induced Rats

We next evaluated whether COR and PAE affected mitochondrial dynamics in synovial tissues after CIA induction by examining the expression of several mitochondria-related proteins (**Figure 5A**). These proteins include MTFP1, which is expressed as an indication of mitochondrial fission (Morita et al., 2017), and MFN2, which is expressed as an indication of mitochondrial fusion (Hu et al., 2020). We also looked at the phosphorylation of Drp1 at serine 616 and serine 637 as indications of mitochondrial fission activation and deactivation, respectively (Ko et al., 2016; Roe and Qi, 2018). Overall, the expression of MTFP1 and the ratio of pDrp1 (Ser616/Ser637) were significantly decreased in the synovial tissues of rats with CIA compared to those in control rats, whereas the expression of MFN2 was upregulated, signifying that mitochondrial fission was inhibited and fusion was promoted by CIA. This change was counteracted by drug treatment in CIA-induced rats. Specifically, individual administration of COR or PAE in CIA-induced rats promoted mitochondrial fission and suppressed fusion, as demonstrated by the dose-dependent increase in MTFP1 expression and pDrp1 (Ser616/Ser637) ratio and the decrease in MFN2 expression. Furthermore, the combination of the two showed the same trend, but the combined effect did not seem to be much stronger than the individual effects of the drugs. The active compounds ursolic acid and paeoniflorin exerted stronger effects in promoting mitochondrial fission than did individual or combined administration of COR and PAE, and the effect of ursolic acid was overall stronger than that of paeoniflorin at the administered doses.

The activation of AMPK is essential in facilitating mitochondrial fission and maintaining mitochondrial function. We examined the phosphorylation of AMPK in the synovial tissue of CIA-induced rats and investigated the effect of COR and PAE therein (**Figure 5B**). Both total and phosphorylated AMPK expression were downregulated in synovial tissues after the rats were induced by CIA. However, total AMPK expression and AMPK phosphorylation were restored by COR and PAE, whether administered individually or in combination, in a dose-dependent manner. The respective active compounds ursolic acid and paeoniflorin exerted even stronger effects in promoting AMPK phosphorylation. The results indicate that mitochondrial fission, which may contribute to mitochondrial dysfunction and lead to synovial tissue apoptosis, was promoted

by drug administration. These findings are consistent with the previous results on apoptosis and mitochondrial function.

To complement the results of western blot, we performed transmission electron microscopy to observe mitochondrial ultrastructure in synovial tissues (**Figure 6**). Mitochondria were oval and showed normal morphology in the synovial tissues of control animals, with clear and well-defined cristae. In rats subjected to CIA, the synovial mitochondria were smaller, their shape and structure were poorly defined, and cristae were barely recognizable. Mitochondrial structure remained poorly distinguishable upon COR-M treatment, but PAE-M seemed to promote mitochondrial fission (marked with "Fi" pointing to the junction where fission occurred) to a certain degree. When the CIA-induced rats were treated with a combination of COR-M and PAE-M, signs of mitochondrial fission became much clearer. Paeoniflorin and the positive control drug DEX seemed to have exerted the optimal effects in inducing mitochondrial fission, as the shape and ultrastructure of the mitochondria most clearly show a state of separation/division.

DISCUSSION

Traditional Chinese medicine has a history of treating rheumatoid conditions for thousands of years. The "multi-target" characteristics of traditional Chinese medicine have unique advantages in the prevention and control of complex diseases such as RA (Xia et al., 2020). The use of specific herbal or plant-based compounds in traditional Chinese medicine can alleviate symptoms and pathological damage and exert synergistic healing effects when combined with western medicine. Additionally, adverse reactions, drug resistance, and recurrence rate are lowered. Through modern medical theories and research methods (such as network pharmacology), *Cornus officinalis* and *Paeonia lactiflora* Pall have been identified as therapeutic candidates to treat RA. The findings of our study revealed that *Cornus officinalis* and *Paeonia lactiflora*, as well as their main active compounds ursolic acid and paeoniflorin, respectively, reduced synovial hyperplasia and inflammatory infiltration in joint tissues while promoting synovial apoptosis in a rat model of CIA. Each treatment also exerted anti-inflammatory and anti-oxidant defense by regulating the secretion of relevant cytokines and protein indicators. Furthermore, we demonstrated that the effects of the abovementioned compounds were related to synovial apoptosis, and that AMPK-mediated mitochondrial dynamics was involved in this process. In particular, *Cornus officinalis*, *Paeonia lactiflora*, ursolic acid, and paeoniflorin promoted synovial apoptosis. We propose that this occurs as a result of mitochondrial fission via enhanced activation of AMPK signaling in CIA-induced rats.

Overall, the effects of the individual compounds ursolic acid and paeoniflorin appeared to be stronger than those of *Cornus officinalis* and *Paeonia lactiflora*, respectively. As mentioned earlier, traditional Chinese medicine exerts multi-target properties, meaning that each type of herb or prescription is made up of a variety of biologically active compounds. Their role

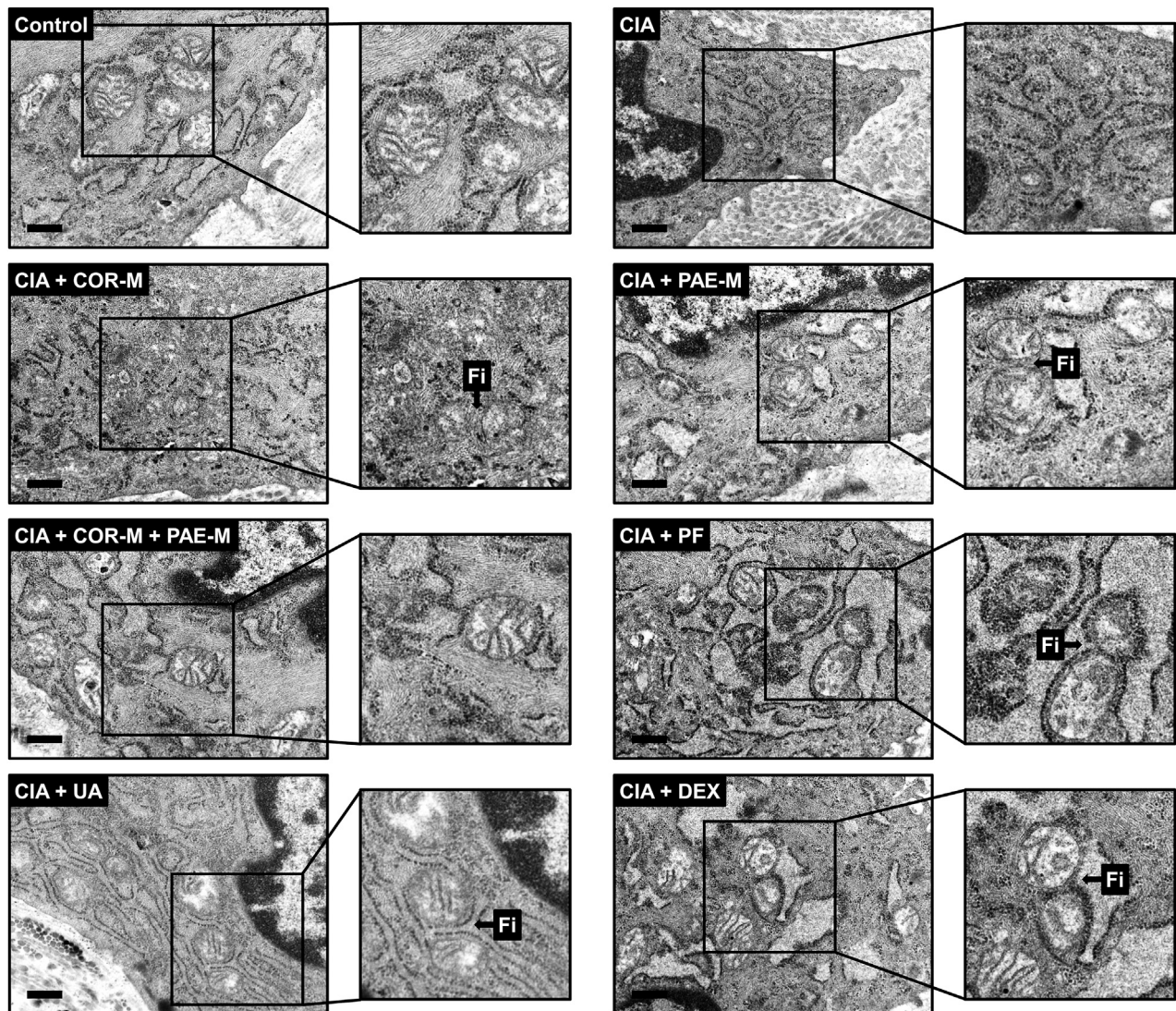


FIGURE 6 | Transmission electron microscopy of mitochondrial morphology in synovial tissues. Sprague-Dawley rats were induced by CIA for 14 days and subjected to daily drug administration at various doses for 20 consecutive days. Selected areas in the microscopic images were magnified to show details of mitochondrial structure (scale bar, 500 nm). Arrows marked by “Fi” indicate areas where mitochondrial fission has occurred. Low, medium, and high doses of COR and PAE were administered, but the medium doses (COR-M and PAE-M) were selected as representatives for analysis. CIA: collagen-induced arthritis; COR: *Cornus officinalis*; PAE: *Paeonia lactiflora*; PF: paeoniflorin; UA: ursolic acid; DEX: dexamethasone.

and potency may differ and each active compound may target different symptoms and biological anomalies. For example, some compounds may be more effective in regulating energy metabolism, while others may exert more potent effects against oxidative stress. In our case, we focused on studying ursolic acid and paeoniflorin, which are active compounds of *Cornus officinalis* and *Paeonia lactiflora*, respectively, that have previously shown strong anti-inflammatory and immunomodulatory activity (Lee et al., 2017; Zhang and Wei, 2020). When administered alone, the anti-inflammatory and immunomodulatory effects of ursolic acid and paeoniflorin are accentuated compared to when they are administered as part of an intricate complex of active compounds. In other words, their

anti-inflammatory and immunomodulatory effects are isolated and concentrated, but as a component of *Cornus officinalis* and *Paeonia lactiflora*, respectively, their therapeutic role may be masked by other co-existing compounds. We suggest that this is the reason why individual administration of ursolic acid or paeoniflorin seemed to be more effective in alleviating RA than *Cornus officinalis* and *Paeonia lactiflora* themselves in this study. It is worth noting that we do not dismiss the utility and value of other active compounds but only focused on inflammation and immunomodulation here. The specific effects of other active compounds of *Cornus officinalis* (such as malic acid and loganin) and *Paeonia lactiflora* (such as albiflorin) will form the basis of future studies.

There is a delicate interplay between oxidative stress, inflammation, and mitochondrial function that governs the regulation of cellular apoptosis, which consequently affects a host of other downstream cellular processes. In the course of RA, fibroblast-like synoviocytes secrete a large number of pro-inflammatory factors such as TNF- α , IL-1 β , IL-6, IL-8, IL-17A, and IL-23, which form a cytokine network to promote and maintain inflammation of the synovial membrane (McInnes and Liew, 2005). Neutrophils and activated macrophages secrete ROS when they are stimulated by excessive production of pro-inflammatory cytokines, making them a mediator of joint damage (Seven et al., 2008; Wendt et al., 2015). The accumulation of ROS may be one of the main causes of RA. Under oxidative stress conditions, overgeneration of ROS leads to lipid peroxidation and DNA fragmentation. This may cause structural and functional modifications of cellular proteins and extracellular components such as collagen and proteoglycans through processes including oxidation and nitration (Nash and Ahmed, 2015). In turn, the accumulation of oxidized cellular components and degradation products may increase synovial inflammation (Phull et al., 2018). In our study, *Cornus officinalis* and *Paeonia lactiflora*, as well as their main active compounds, inhibited inflammatory exacerbation and ROS generation in CIA-induced rats. This is evidenced by the decreased secretion of the pro-inflammatory factors TNF- α , IL-1 β , and IL-6 and the increase in the anti-inflammatory factor IL-10, as well as the decreased secretion of pro-oxidative MDA and NO and the increase in the anti-oxidative SOD. These results exhibited the protective effects of the drugs against arthritic progression.

Mitochondria are the main source of cellular ROS and impaired balance in mitochondrial dynamics may result in cellular dysfunction, thereby leading to pathogenic conditions. It has been shown that hypoxia-induced mitochondrial dysfunction and oxidative damage cause disruptions to cellular metabolism, in turn promoting synovial invasiveness by exacerbating inflammatory response (Fearon et al., 2016). Mutations in mitochondrial DNA have also been identified as a pathological sign of RA (Da Sylva et al., 2005). In the maintenance of mitochondrial homeostasis, the AMPK signaling pathway plays an indispensable role by facilitating mitochondrial fission and recycling (Rabinovitch et al., 2017). Previously, ursolic acid has been shown to exhibit anti-tumor effects against human bladder cancer by activating AMPK signaling (Zheng et al., 2012), and paeoniflorin demonstrated protective effects against ischemia/reperfusion via AMPK activation (Wen et al., 2019). Herein, we showed that *Cornus officinalis* and *Paeonia lactiflora*, as well as their main active compounds, regulated apoptosis by upregulating Bax, cleaved caspase-3, and cytochrome-c and downregulating Bcl-2 via the activation of AMPK in CIA-induced rats. These findings have critical implications in elucidating the molecular basis of RA as they not only establish the importance of apoptosis control in RA development, but also point to AMPK as a potential therapeutic target that could be applied in treatment schemes.

Our study is subject to several limitations that need to be addressed in future research. Of primary interest are the specific

gene and protein targets of *Cornus officinalis*, *Paeonia lactiflora*, ursolic acid, and paeoniflorin pertaining to RA, which were not explored in this study. The identification of such targets requires extensive investigation using tools such as bioinformatics and network pharmacology, which will be carried out as a follow-up. As the multi-target feature of traditional Chinese medicine is one of its unique characteristics, the effect of other active compounds of *Cornus officinalis* and *Paeonia lactiflora* on RA may also provide clues to their mechanisms of action. Bound by restrictions in material acquisition and laboratory conditions, we were unable to study compounds beyond ursolic acid and paeoniflorin here, but other active compounds will form the basis of future research. Additionally, the particular involvement of the AMPK signaling pathway in RA pathogenesis and the effect of ursolic acid and paeoniflorin needs to be confirmed using inhibitors of AMPK. Finally, this study lacks investigation on the effect of ROS and mitochondrial dysfunction on energy metabolism in RA. Future research will focus on this aspect and elucidate whether *Cornus officinalis* and *Paeonia lactiflora* (as well as their active compounds) also regulate energy metabolism to ameliorate RA.

CONCLUSION

We showed here that *Cornus officinalis*, *Paeonia lactiflora*, ursolic acid, and paeoniflorin exhibited clear therapeutic effects against RA in an *in vivo* model of CIA. In particular, the abovementioned drugs promoted synovial apoptosis, favored mitochondrial fission, and enhanced the activation of AMPK signaling in CIA-induced rats. Overall, the effects of ursolic acid and paeoniflorin appeared to be stronger than those of *Cornus officinalis* and *Paeonia lactiflora*, respectively. This research highlights the potential of traditional Chinese medicine in the discovery of new targets and development of treatment strategies for RA, contributing to the advanced clinical management of RA.

DATA AVAILABILITY STATEMENT

The raw data supporting the conclusions of this article will be made available by the authors, without undue reservation.

ETHICS STATEMENT

The animal study was reviewed and approved by Model Animal Research Institute at Wuhan Myhalic Biotechnology Co., Ltd.

AUTHOR CONTRIBUTIONS

GC and JZ conceptualized and designed the study. LH, SH, and MS performed the cell experiments and the network

pharmacology analysis. XW assisted in the experimental operations. LH and MS prepared the draft of the manuscript. GC and JZ revised the manuscript. All authors approved the final version of the manuscript.

REFERENCES

- Chang, J.-S., Chiang, L.-C., Hsu, F.-F., and Lin, C.-C. (2004). Chemoprevention against hepatocellular carcinoma of *Cornus officinalis* in vitro. *Am. J. Chin. Med.* 32 (5), 717–725. doi:10.1142/S0192415X04002296
- Czerwinska, M. E., and Melzig, M. F. (2018). *Cornus mas* and *Cornus officinalis*-analogies and differences of two medicinal plants traditionally used. *Front. Pharmacol.* 9, 894. doi:10.3389/fphar.2018.00894
- Fonseca, L. J. S. d., Nunes-Souza, V., Goulart, M. O. F., and Rabelo, L. A. (2019). Oxidative stress in rheumatoid arthritis: what the future might hold regarding novel biomarkers and add-on therapies. *Oxidative Med. Cell Longevity* 2019, 1. doi:10.1155/2019/7536805
- Da Sylva, T. R., Connor, A., Mburu, Y., Keystone, E., and Wu, G. E. (2005). Somatic mutations in the mitochondria of rheumatoid arthritis synoviocytes. *Arthritis Res. Ther.* 7 (4), R844–R851. doi:10.1186/ar1752
- Deane, K. D., Demoruelle, M. K., Kelmenson, L. B., Kuhn, K. A., Norris, J. M., and Holers, V. M. (2017). Genetic and environmental risk factors for rheumatoid arthritis. *Best Pract. Res. Clin. Rheumatol.* 31 (1), 3–18. doi:10.1016/j.berh.2017.08.003
- Dong, Y., Feng, Z.-L., Chen, H.-B., Wang, F.-S., and Lu, J.-H. (2018). Corni Fructus: a review of chemical constituents and pharmacological activities. *Chin. Med.* 13, 34. doi:10.1186/s13020-018-0191-z
- Endo, T., and Taguchi, H. (1973). Study on the Constituents of *Cornus officinalis* SIEB. et ZUCC. *Yakugaku Zasshi* 93 (1), 30–32. doi:10.1248/yakushi1947.93.1_30
- Fearon, U., Canavan, M., Biniecka, M., and Veale, D. J. (2016). Hypoxia, mitochondrial dysfunction and synovial invasiveness in rheumatoid arthritis. *Nat. Rev. Rheumatol.* 12 (7), 385–397. doi:10.1038/nrrheum.2016.69
- Filippin, L. I., Vercelino, R., Marroni, N. P., and Xavier, R. M. (2008). Redox signalling and the inflammatory response in rheumatoid arthritis. *Clin. Exp. Immunol.* 152 (3), 415–422. doi:10.1111/j.1365-2249.2008.03634.x
- Gong, X., Xu, S.-q., Tong, H., Wang, X.-r., Zong, H.-x., Pan, M.-j., et al. (2019). Correlation between systemic osteoporosis and local bone erosion with rheumatoid arthritis patients in Chinese population. *Rheumatology (Oxford)*. doi:10.1093/rheumatology/kez042
- Guo, Q., Wang, Y., Xu, D., Nossent, J., Pavlos, N. J., and Xu, J. (2018). Rheumatoid arthritis: pathological mechanisms and modern pharmacologic therapies. *Bone Res.* 6, 15. doi:10.1038/s41413-018-0016-9
- Hu, Y., Chen, H., Zhang, L., Lin, X., Li, X., Zhuang, H., et al. (2020). The AMPK-MFN2 axis regulates MAM dynamics and autophagy induced by energy stresses. *Autophagy* 19, 1–15. doi:10.1080/15548627.2020.1749490
- Intriago, M., Maldonado, G., Cárdenas, J., and Ríos, C. (2019). Clinical characteristics in patients with rheumatoid arthritis: differences between genders. *Scientific World J.* 2019, 1. doi:10.1155/2019/8103812
- Ippolito, L., Giannoni, E., Chiarugi, P., and Parri, M. (2020). Mitochondrial redox hubs as promising targets for anticancer therapy. *Front. Oncol.* 10, 256. doi:10.3389/fonc.2020.00256
- Jia, X.-Y., Chang, Y., Sun, X.-J., Wu, H.-X., Wang, C., Xu, H.-M., et al. (2014). Total glucosides of paeony inhibit the proliferation of fibroblast-like synoviocytes through the regulation of G proteins in rats with collagen-induced arthritis. *Int. Immunopharmacology* 18 (1), 1–6. doi:10.1016/j.intimp.2013.09.007
- Kakuwa, T., Izumi, S., Sakamoto, K., Suzuki, T., Iikura, M., and Sugiyama, H. (2019). A successful treatment of rheumatoid arthritis-related interstitial pneumonia with nintedanib. *Respir. Med. Case Rep.* 26, 50–52. doi:10.1016/j.rmcr.2018.10.026
- Kaplan, M. J. (2010). Cardiovascular complications of rheumatoid arthritis: assessment, prevention, and treatment. *Rheum. Dis. Clin. North America* 36 (2), 405–426. doi:10.1016/j.rdc.2010.02.002
- Klareskog, L., Padyukov, L., Rönnelid, J., and Alfredsson, L. (2006). Genes, environment and immunity in the development of rheumatoid arthritis. *Curr. Opin. Immunol.* 18 (6), 650–655. doi:10.1016/j.coi.2006.06.004

FUNDING

This work was financially supported by the National Natural Science Foundation of China (81773900 and 81774255).

- Ko, A.-R., Hyun, H.-W., Min, S.-J., and Kim, J.-E. (2016). The differential DRP1 phosphorylation and mitochondrial dynamics in the regional specific astroglial Death induced by status epilepticus. *Front. Cel. Neurosci.* 10, 124. doi:10.3389/fncel.2016.00124
- Köhler, B. M., Günther, J., Kaudewitz, D., and Lorenz, H. M. (2019). Current therapeutic options in the treatment of rheumatoid arthritis. *JCM.* 8 (7), 938. doi:10.3390/jcm8070938
- Lee, S.-O., Kim, S. Y., Han, S.-M., Kim, H.-M., Ham, S.-S., and Kang, I.-J. (2006). Corni fructus scavenges hydroxy radicals and decreases oxidative stress in endothelial cells. *J. Med. Food* 9 (4), 594–598. doi:10.1089/jmf.2006.9.594
- Lee, J. Y., Choi, J. K., Jeong, N.-H., Yoo, J., Ha, Y. S., Lee, B., et al. (2017). Anti-inflammatory effects of ursolic acid-3-acetate on human synovial fibroblasts and a murine model of rheumatoid arthritis. *Int. Immunopharmacology* 49, 118–125. doi:10.1016/j.intimp.2017.05.028
- McInnes, I. B., and Liew, F. Y. (2005). Cytokine networks-towards new therapies for rheumatoid arthritis. *Nat. Rev. Rheumatol.* 1 (1), 31–39. doi:10.1038/ncprheum0020
- Morita, M., Prudent, J., Basu, K., Goyon, V., Katsumura, S., Hulea, L., et al. (2017). mTOR controls mitochondrial dynamics and cell survival via MTFP1. *Mol. Cell* 67 (6), 922–935. doi:10.1016/j.molcel.2017.08.013
- Nair, A. B., and Jacob, S. (2016). A simple practice guide for dose conversion between animals and human. *J. Basic Clin. Pharm.* 7 (2), 27–31. doi:10.4103/0976-0105.177703
- Nash, K. M., and Ahmed, S. (2015). Nanomedicine in the ROS-mediated pathophysiology: applications and clinical advances. *Nanomedicine* 11 (8), 2033–2040. doi:10.1016/j.nano.2015.07.003
- Obiri, D. D., Osafo, N., Ayande, P. G., and Antwi, A. O. (2014). *Xylopia aethiopica* (Annonaceae) fruit extract suppresses Freund's adjuvant-induced arthritis in Sprague-Dawley rats. *J. Ethnopharmacology* 152 (3), 522–531. doi:10.1016/j.jep.2014.01.035
- Phull, A.-R., Nasir, B., Haq, I. U., and Kim, S. J. (2018). Oxidative stress, consequences and ROS mediated cellular signaling in rheumatoid arthritis. *Chemico-Biological Interact.* 281, 121–136. doi:10.1016/j.cbi.2017.12.024
- Rabinovitch, R. C., Samborska, B., Faubert, B., Ma, E. H., Gravel, S.-P., Andrzejewski, S., et al. (2017). AMPK maintains cellular metabolic homeostasis through regulation of mitochondrial reactive oxygen species. *Cel Rep.* 21 (1), 1–9. doi:10.1016/j.celrep.2017.09.026
- Roe, A. J., and Qi, X. (2018). Drp1 phosphorylation by MAPK1 causes mitochondrial dysfunction in cell culture model of Huntington's disease. *Biochem. Biophysical Res. Commun.* 496 (2), 706–711. doi:10.1016/j.bbrc.2018.01.114
- Seven, A., Güzel, S., Aslan, M., and Hamuryudan, V. (2008). Lipid, protein, DNA oxidation and antioxidant status in rheumatoid arthritis. *Clin. Biochem.* 41 (7–8), 538–543. doi:10.1016/j.clinbiochem.2008.01.029
- Tseng, C.-C., Chen, Y.-J., Chang, W.-A., Tsai, W.-C., Ou, T.-T., Wu, C.-C., et al. (2020). Dual role of chondrocytes in rheumatoid arthritis: the chicken and the egg. *IJMS.* 21 (3), 1071. doi:10.3390/ijms21031071
- Valcárcel-Ares, M. N., Riveiro-Naveira, R. R., Vaamonde-García, C., Loureiro, J., Hermida-Carballo, L., Blanco, F. J., et al. (2014). Mitochondrial dysfunction promotes and aggravates the inflammatory response in normal human synoviocytes. *Rheumatology (Oxford)* 53 (7), 1332–1343. doi:10.1093/rheumatology/keu016
- Wang, C., and Youle, R. J. (2009). The role of mitochondria in apoptosis. *Annu. Rev. Genet.* 43, 95–118. doi:10.1146/annurev-genet-102108-134850
- Wang, T., Li, J., Ge, J., Cheng, W., Jin, Y., Lv, X., et al. (2007). Effects and partial mechanism of total flavonoids from *Cinnamomum Cassiae* on adjuvant arthritis in rats. *Chin. Pharmacol. Bull.* 23 (12), 1618–1623.
- Wen, J., Xu, B., Sun, Y., Lian, M., Li, Y., Lin, Y., et al. (2019). Paeoniflorin protects against intestinal ischemia/reperfusion by activating LKB1/AMPK and promoting autophagy. *Pharmacol. Res.* 146, 104308. doi:10.1016/j.phrs.2019.104308

- Wendt, M. M. N., de Sá-Nakanishi, A. B., de Castro Ghizoni, C. V., Bersani Amado, C. A., Peralta, R. M., Bracht, A., et al. (2015). Oxidative state and oxidative metabolism in the brain of rats with adjuvant-induced arthritis. *Exp. Mol. Pathol.* 98 (3), 549–557. doi:10.1016/j.yexmp.2015.04.002
- Xia, X., May, B. H., Zhang, A. L., Guo, X., Lu, C., Xue, C. C., et al. (2020). Chinese herbal medicines for rheumatoid arthritis: text-mining the classical literature for potentially effective natural products. *Evidence-Based Complement. Altern. Med.* 2020, 7531967. doi:10.1155/2020/7531967
- Xu, H., Cai, L., Zhang, L., Wang, G., Xie, R., Jiang, Y., et al. (2018). Paeoniflorin ameliorates collagen-induced arthritis via suppressing nuclear factor- κ B signalling pathway in osteoclast differentiation. *Immunology* 154, 593–603. doi:10.1111/imm.12907
- Yamahara, J., Mibu, H., Sawada, T., Fujimura, H., Takino, S., Yoshikawa, M., et al. (1981). Biologically active principles of crude drugs. Antidiabetic principles of Corni fructus in experimental diabetes induced by streptozotocin. *Yakugaku Zasshi* 101 (1), 86–90. doi:10.1248/yakushi1947.101.1_86
- Zhang, L., and Wei, W. (2020). Anti-inflammatory and immunoregulatory effects of paeoniflorin and total glucosides of paeony. *Pharmacol. Ther.* 207, 107452. doi:10.1016/j.pharmthera.2019.107452
- Zhang, J., Song, X., Cao, W., Lu, J., Wang, X., Wang, G., et al. (2016). Autophagy and mitochondrial dysfunction in adjuvant-arthritis rats treatment with resveratrol. *Sci. Rep.* 6, 32928. doi:10.1038/srep32928
- Zheng, Q.-y., Jin, F.-s., Yao, C., Zhang, T., Zhang, G.-h., and Ai, X. (2012). Ursolic acid-induced AMP-activated protein kinase (AMPK) activation contributes to growth inhibition and apoptosis in human bladder cancer T24 cells. *Biochem. Biophysical Res. Commun.* 419 (4), 741–747. doi:10.1016/j.bbrc.2012.02.093

Conflict of Interest: The authors declare that the research was conducted in the absence of any commercial or financial relationships that could be construed as a potential conflict of interest.

Copyright © 2021 Huang, Hu, Shao, Wu, Zhang and Cao. This is an open-access article distributed under the terms of the Creative Commons Attribution License (CC BY). The use, distribution or reproduction in other forums is permitted, provided the original author(s) and the copyright owner(s) are credited and that the original publication in this journal is cited, in accordance with accepted academic practice. No use, distribution or reproduction is permitted which does not comply with these terms.



Development of an Advanced Multicellular Intestinal Model for Assessing Immunomodulatory Properties of Anti-Inflammatory Compounds

OPEN ACCESS

Edited by:

Yihai Wang,
Guangdong Pharmaceutical
University, China

Reviewed by:

Nicole Clemence Roy,
University of Otago, New Zealand
Zifei Qin,
First Affiliated Hospital of Zhengzhou
University, China
Jingwen Xu,
Guangdong Pharmaceutical
University, China

*Correspondence:

Diego Marescotti
diego.marescotti@pmi.com

[†]These authors have contributed
equally to this work and share first
authorship

Specialty section:

This article was submitted to
Inflammation Pharmacology,
a section of the journal
Frontiers in Pharmacology

Received: 09 December 2020

Accepted: 06 April 2021

Published: 16 April 2021

Citation:

Marescotti D, Lo Sasso G, Guerrera D,
Renggli K, Ruiz Castro PA, Piault R,
Jaquet V, Moine F, Luettich K,
Frentzel S, Peitsch MC and Hoeng J
(2021) Development of an Advanced
Multicellular Intestinal Model for
Assessing Immunomodulatory
Properties of Anti-
Inflammatory Compounds.
Front. Pharmacol. 12:639716.
doi: 10.3389/fphar.2021.639716

Diego Marescotti^{†*}, Giuseppe Lo Sasso[†], Diego Guerrera[†], Kasper Renggli,
Pedro A. Ruiz Castro, Romain Piault, Vincent Jaquet, Fabian Moine, Karsta Luettich,
Stefan Frentzel, Manuel C. Peitsch and Julia Hoeng

PMI R&D, Philip Morris Products S.A., Neuchâtel, Switzerland

Intestinal inflammation is the collective term for immune system-mediated diseases of unknown, multifactorial etiology, with often complex interactions between genetic and environmental factors. To mechanistically investigate the effect of treatment with compounds possessing immunomodulating properties in the context of intestinal inflammation, we developed an immunocompetent *in vitro* triculture intestinal model consisting of a differentiated intestinal epithelial layer (Caco-2/HT29-MTX) and immunocompetent cells (differentiated THP-1). The triculture mimicked a healthy intestine with stable barrier integrity. Lipopolysaccharide treatment triggered a controlled and reversible inflammatory state, resulting in significant impairment of barrier integrity and release of pro-inflammatory cytokines and chemokines, which are known hallmarks of intestinal inflammation. Treatment with known anti-inflammatory reference compounds (TPCA-1 and budenoside) prevented the induction of an inflammatory state; the decreasing triculture responses to this treatment measured by cytokine release, transepithelial electric resistance (TEER), and epithelial layer permeability proved the suitability of the intestinal model for anti-inflammatory drug screening. Finally, selected tobacco alkaloids (nicotine and anatabine (*R/S* and *S* forms)) were tested in the *in vitro* triculture for their potential anti-inflammatory properties. Indeed, naturally occurring alkaloids, such as tobacco-derived alkaloids, have shown substantial anti-inflammatory effects in several *in vitro* and *in vivo* models of inflammation, gaining increasing interest. Similar to the anti-inflammatory reference compounds, one of the tobacco alkaloids under investigation partially prevented the decrease in the TEER and increase in permeability and reduced the release of pro-inflammatory cytokines and chemokines. Taken together, these data confirm that our *in vitro* model is suitable for screening potential anti-inflammatory compounds in the context of intestinal inflammation.

Keywords: immune competent cells, inflamed intestine, nicotine, inflammatory bowel disease, intestinal inflammation, *in vitro* co-culture, tobacco alkaloids, anatabine

INTRODUCTION

The gastrointestinal tract is composed of an epithelial layer, which is exposed to an overwhelming load of foreign antigens arising from commensal microorganisms, dietary products, and occasional pathogens (Tilg and Moschen, 2015). In the physiological state, the gastrointestinal mucosa forms a unique immunological environment in which tolerance to commensal microbes and/or food antigens and specific immunity to pathogens coexist in a fine-tuned immune equilibrium (Schenk and Mueller, 2008; Honda and Littman, 2012; Tilg and Moschen, 2015). When this tightly regulated immune homeostasis becomes altered, pathological inflammation and disruption of the epithelial barrier might occur (Peterson et al., 2015). The resulting intestinal inflammation is becoming increasingly relevant as one of the more commonly occurring diseases in developed countries (Ng et al., 2017). The indications range from irritable bowel syndrome to chronic inflammatory conditions of the gut related to a combination of genetic, environmental, and immunological factors that impact on normal host–microbe interactions. (Abraham and Medzhitov, 2011; Kaistha and Levine, 2014; Atreya and Neurath, 2015; Ramos and Papadakis, 2019). The etiology of intestinal inflammation remains poorly understood; thus, development of new approaches for predicting disease evolution and personalized response to treatment are of primary clinical relevance (Molodecky et al., 2012; Ponder and Long, 2013). Although no unique cause has been determined for inflamed intestine, environmental factors, including medication, stress, diet, and smoking, are known to impact disease onset and progression (Abraham et al., 2017).

Naturally occurring alkaloids derived from plants or medicinal herbs gained much interest as a potential treatment against inflamed intestine due to their significant antioxidant and anti-inflammatory effect (Niu et al., 2015; Wu et al., 2018; Peng et al., 2019). These natural derived bioactive compounds can be sourced from living organisms, such as bacteria, fungi, plants, and animals (Moreira et al., 2018). Plant-derived alkaloids have been shown to possess anti-inflammatory properties as demonstrated in animal models of disease, including inflammatory bowel disease (IBD), a group of disorders characterized by chronic inflammation of the gastrointestinal tract (Niu et al., 2013; Chen et al., 2017; Ruiz Castro et al., 2020). The positive effects of alkaloid have been linked to a modulation of intestinal oxidative stress (Karatay et al., 2017; Rodrigues de Carvalho et al., 2018), a strengthening of the epithelial barrier function (Zhang et al., 2017), and a boost of gut microbiota (Zhang et al., 2018).

Among the most studied plant-derived alkaloids are pyridine alkaloids derived from the tobacco plant (*Nicotiana tabacum*) (Saitoh et al., 1985). Nicotine—the major alkaloid in tobacco—as well as all minor tobacco alkaloids have been shown to be pharmacologically active (Clark et al., 1965). Nicotine is addictive and not risk free. Minors, pregnant or breast-feeding women, and people with heart disease, severe high blood pressure or diabetes should not use tobacco or nicotine containing products (McNeill et al., 2018). However, several *in vitro* and

in vivo studies that mimicked intestinal inflammation have supported the notion of nicotine-dependent anti-inflammatory effects (Cloëz-Tayarani and Changeux, 2007; McGilligan et al., 2007; Verschuere et al., 2012; Hayashi et al., 2014), which might be mediated by the activation of nicotinic acetylcholine receptors (nAChR) and the consequent activation of cholinergic anti-inflammatory pathways (Wang et al., 2003; Ulloa, 2005). However, the contrasting results obtained by both *in vivo* and clinical studies on the role of nicotine in the context of intestinal inflammation (AlSharari et al., 2013; Gomes et al., 2018), as well as the high frequency of nicotine-related adverse events observed in those clinical studies (Lunney and Leong, 2012), triggered the investigation of other minor tobacco-alkaloids (Olsson et al., 1993; Bai et al., 2007; Paris et al., 2013a; Paris et al., 2013b).

To support the investigation of compounds with potential anti-inflammatory properties in the gastrointestinal system, we developed an immunocompetent *in vitro* intestinal model that recapitulates the intestinal barrier and contains a functional mucus layer and immunocompetent cells. Thus, we developed a tri-culture model using the classical Transwell® configuration, in which epithelial cells, such as Caco-2 and HT29-MTX, are seeded in the apical compartment, while the immune cells, THP-1, are added to the basolateral side.

The epithelial cell line Caco-2 has been the most widely used intestinal cell line model for interrogating various endpoints, including intestinal absorption, cell membrane permeability, passive and active diffusion of drug molecules, and inflammatory response (Hidalgo et al., 1989; Hillgren et al., 1995; Cheng et al., 2008). Upon reaching full confluence, Caco-2 cells spontaneously differentiate over the following 3 to 4 weeks of culture and form a polarized cell monolayer, which is characterized by apical and basolateral membranes, tight junctions, and a brush border with microvilli on the apical side typical of human enterocytes (Chantret et al., 1988; Hidalgo et al., 1989). To better replicate the *in vivo* physiology of the intestine, we decided to coculture Caco-2 cells with a mucus-producing cell line, the stable clone HT29-MTX (Lesuffleur et al., 1990; Chen et al., 2010). Finally, to further complete the model and increase its relevance for anti-inflammatory compound assessment, we included the monocytic cell line THP-1 because of its potential for differentiation into macrophage- or dendritic cell-like cells. Finally, we established the triculture by using the classical Transwell® configuration, in which epithelial cells are seeded in the apical compartment, while immune cells are added to the basolateral side.

Although similar models have already been established (Leonard et al., 2010; Kaulmann et al., 2016; Susewind et al., 2016; Kampfer et al., 2017), we intended to design and obtain an *in vitro* model characterized by i) less laborious cell culture handling, ii) immune-to-epithelial cell pro-inflammatory crosstalk, and iii) functional readouts. As a proof of concept, after establishing and assessing the model with known anti-inflammatory drugs, we evaluated the putative anti-inflammatory effects of two well-known tobacco alkaloids, namely nicotine and anatabine. Therefore, using our model, we were able to investigate the crosstalk between intestinal

epithelial cells and immune cells in the context of intestinal inflammation and its response to natural derived compounds.

MATERIALS AND METHODS

Cell Lines

The human colon adenocarcinoma cell line Caco-2 (86010202, Sigma, St. Louis, MO, United States) was cultured in Eagle's minimum essential medium (EMEM; 30-2003, ATCC, Manassas, VI, United States) supplemented with 10% fetal bovine serum (FBS; 16140-071, Gibco, Gaithersburg, MD, United States), 1% non-essential amino acids (NEAA; 11140-050, Life Tech, Carlsbad, CA, United States), and 1% penicillin/streptomycin (P4333, Sigma). The human colon cell line HT29-MTX-E16 (86010202, Sigma) was cultured in Dulbecco's modified Eagle's medium (DMEM; D6546, Sigma) supplemented with 10% FBS (16140-071, Gibco), 1% NEAA (11140-050, Life Tech), 1% Glutamax (35050-061, Gibco), and 1% penicillin/streptomycin (P4333, Sigma). The human acute monocytic leukemia cell line THP-1 (Tib-202, ATCC) was cultured in Roswell Park Memorial Institute (RPMI) 1640 (R0883, Sigma) supplemented with 10% FBS (16140-071, Gibco), 1% Glutamax (35050-061, Gibco), and 1% penicillin/streptomycin (P4333, Sigma). The cells were tested for *mycoplasma* contamination and found negative.

Triculture Assembly

Human Caco-2 and HT29-MTX cells (2×10^4 in total) were seeded at a 9:1 ratio in 6.5-mm Transwell® with 0.4-μm pore polyester membrane inserts (Costar #3470) and allowed to grow and differentiate for 14 or 21 (depending on the aim of the experiment) days after full confluence in DMEM (Earle's balanced salt solution) (M2279, Sigma) containing 2 mM glutamine (G7513, Sigma), 1% NEAA, 10% heat-inactivated FBS, and 1% penicillin/streptomycin. The culture medium (200 μL in the apical and 700 μL in the basolateral compartments) was replaced every 2 days. A day before the Transwell® containing epithelial cells was moved into the well containing THP-1 cells, the basolateral medium was replaced with 400 μL of RPMI. THP-1 cells (2.4×10^5) were seeded in 600 μL of RPMI in 24-well plates and differentiated with 10, 20, or 40 ng/ml PMA (phorbol-12-myristate-13-acetate; P1585, Sigma) for ~65 h. The PMA was removed after differentiation, and the cells were rested for 24 h. Then, the Caco-2/HT29-MTX-containing Transwell® insert was added into the well, with a basolateral medium volume of 400 μL. After assembly the triculture was rested for 24 h in preparation for pro-inflammatory induction and compound assessment.

Histological Analysis

Histological sections were obtained from cultures harvested on day 12 of culture after the cells reached full confluence. The cultures were processed in accordance with previously published protocols (Iskandar et al., 2018; Zanetti et al., 2018). Briefly, the cultures were washed three times with PBS (phosphate-buffered saline; Merck, Darmstadt, Germany) and fixed for 2 h in 4% (w/v) paraformaldehyde solution in PBS (Thermo Fisher Scientific).

After fixation, the cultures were washed three times in PBS and bisected; the resulting two pieces were placed in cassettes and processed with the Leica ASP300 S Tissue Processor (Leica Biosystems Nussloch GmbH, Nussloch, Germany). The processed cultures were embedded vertically and in parallel by using the MEDITE TES Valida Tissue Embedding System (MEDITE GmbH, Burgdorf, Germany), and 5-μm-thick sections were cut by using a Leica RM2255 microtome (Leica Biosystems Nussloch GmbH). The cut sections were mounted on Superfrost™ Plus slides (Thermo Fisher Scientific) and transferred to the Leica ST5020 automated stainer (Leica Biosystems Nussloch GmbH) for staining with hematoxylin, eosin, and Alcian blue. The stained slides were covered with coverslips automatically by using the Leica CV5030 automated coverslipper (Leica Biosystems Nussloch GmbH). Digital images of the stained slides were generated by using the NanoZoomer 2.0 slide scanner (Hamamatsu Photonics, Hamamatsu, Japan) at $\times 40$ magnification.

Immunofluorescence Staining

To detect goblet cells and tight junctions, we used antibodies targeting Muc5Ac and ZO-1, respectively. The cultures were first fixed with 4% (w/v) paraformaldehyde (Sigma, Saint Louis, United States) for 15 min and then blocked for 1 h in a blocking solution (0.5% Triton X-100, 5% normal goat serum, and 2% bovine serum albumin; all reagents from Thermo Fisher Scientific, Waltham, MA, United States) in $1\times$ Dulbecco's phosphate-buffered saline (D-PBS; without calcium, magnesium, or Phenol red; STEMCELL Technologies). The cultures were stained with a Muc5AC antibody conjugated to Alexa 550 (1:250, ab218714, Abcam) or a ZO-1 antibody (1:250, 339194, ThermoFisher), diluted in D-PBS with 2% normal goat serum (Thermo Fisher Scientific, Waltham, MA, United States) and 1% bovine serum albumin (Thermo Fisher Scientific). Nuclei were counterstained by using ProLong™ Diamond Antifade Mountant with DAPI (4',6-diamidino-2-phenylindole; Thermo Fisher Scientific). Images were acquired with the CellInsight™ CX7 HCS platform (Thermo Fisher).

Chemicals

All compounds, including reference compounds, test compounds, and pro-inflammatory inducers, used in the study are reported in **Supplementary Table S5**.

TEER

Cellular transepithelial electric resistance (TEER) was measured by using chopstick electrodes (STX-2) connected to an EVOM_Epithelial Voltohmmeter (World Precision Instruments, Berlin, Germany) after addition of 200 ml medium to the apical side of the tissues.

WST-8 Cell Viability Assay

WST-8 bioreduction in single cell lines was measured by using Cell Counting Kit-8 (CCK-8, Sigma #96992). WST-8 is bioreduced by cellular dehydrogenases to an orange formazan product that is soluble in tissue culture medium; the amount of formazan produced is directly proportional to the number of

living cells. WST-8 was added to the cells by diluting it 1:10 in the volume of medium present in the wells (i.e., 10–100 μ L medium present in the 96-well plates for single cell lines, 20–200 μ L medium present in the apical compartment of Transwell® inserts containing epithelial cocultures, or 40–400 μ L medium present in the basolateral compartment containing the THP-1 cell part of the triculture). After 1 h of incubation at 37°C, 100 μ L the medium was transferred to a 96-well plate and measured for absorbance at 450 nm by using a FluoStar Omega reader (BMG Labtech GmbH, Ortenberg, Germany). A blank consisting of WST-8 incubated with medium only was also added to the plate and subtracted from the measured absorbance values recorded from the samples.

Permeability

Permeability was assessed by using FITC (fluorescein isothiocyanate)–dextran 4 kDa (FD4, Sigma-Aldrich) by adding 200 μ L of growth medium (MEM) containing 1 mg/ml FD4 to the apical compartment. After a 1-h incubation at 37°C, 100 μ L of basolateral medium was transferred to a 96-well plate (Sterilin black microtiter plates, 611F96BK, Thermo Fisher). Fluorescence intensity was measured at excitation and emission wavelengths of 400 and 535 nm, respectively, by using a FluoStar Omega reader. Fluorescence values from known serial dilutions of FD4 (0–5 μ g/ml) were used to generate a standard curve. FD4 translocation from the apical to basolateral compartments was quantified by interpolation of fluorescence intensity values on the 4-parameter fit standard curve obtained. A blank consisting of cell culture medium was also added to the plate, and the corresponding values were subtracted from the measured concentrations of all samples. FD4 passage (in μ g) was calculated by multiplying the values obtained with the volume present in the basolateral compartment (700 μ L). Additionally, apparent permeability coefficient was calculated by using the following equation:

$$P_{app} = \left(\frac{dQ}{dt} \right) \times \left(\frac{1}{A \times C_0} \right)$$

defined as:

P_{app} = apparent permeability coefficient (cm/s)

dQ/dt [μ g/s] = rate of appearance of FD4 on the basolateral side

A = surface area of the monolayers

C_0 [μ g/ml] = initial FD4 concentration in the apical compartment.

Fold change was calculated over the untreated control used as reference. Subsequently, data were normalized by setting the fold-change values of samples treated with only the inflammation inducer as 100% (reference). A *t*-test was performed for comparing cell cultures treated with the reference/test items as well as the inflammation inducer with those treated with only the inflammation inducer.

Cytokine Measurement

Secreted cytokines were measured in medium collected from cell cultures treated with inflammation inducers or reference/test

items along with inflammation inducers at various time points. Specific ELISA kits (interleukin (IL)-6, IL-8, tumor necrosis factor (TNF) α , and IL-1 β) from R&D systems were used in accordance with the manufacturers' instructions.

Statistical Analysis

This study consisted of an exploratory phase and a confirmation phase, with the latter illustrated in **Figures 4** and **5**. Several independent experiments were performed only for the confirmation phase. For the exploratory phase, the technical replicates, generally different wells in a culture plate, were considered independently. Statistical differences between conditions were determined by two-tailed *t*-tests. Statistical equivalences between conditions were determined by two-one-sided *t*-tests (TOST) with a magnitude of region of similarity of $\pm 20\%$. Statistical trends were determined by a fitting linear model. The *p* value for the linear model, *t*-test, and TOST were reported with asterisks: **p* \leq 0.05; ***p* \leq 0.01; ****p* \leq 0.001; not significant (ns), *p* > 0.05. The *t*-test, linear model, and equivalence test were performed in R 3.5.1 with the *t.test* and *lm* functions from the stats package and the *tost* function from the equivalence package, respectively.

Datasets, detailed protocols, and additional data visualizations are available on the INTERVALS platform.

RESULTS

Establishment of Caco-2/HT29-MTX Coculture and Evaluation of Pro-Inflammatory Response

Caco-2 and HT29-MTX, seeded at a 9:1 ratio (Hilgendorf et al., 2000; Chen et al., 2010), were cocultured over a period of 32 days and monitored for barrier integrity by evaluating the increase in TEER. TEER values reached a maximum of $\sim 900 \Omega \cdot \text{cm}^2$ 12 days after the cells reached full confluence (approximately 3 days after seeding), after which they remained stable in the range of 700–900 $\Omega \cdot \text{cm}^2$ up to day 26 (**Supplementary Figure S1A**). Muc5AC and ZO-1 staining confirmed the presence of functional mucus-secreting HT29-MTX cells and establishment of tight junctions, respectively (**Supplementary Figure S1B**). Additionally, longitudinal slices were stained with hematoxylin, eosin, and Alcian blue for histological examination (**Supplementary Figure S1C**).

We first evaluated the effects of different pro-inflammatory inducers and the route of administration over 24 h after 21 days of maturation of the coculture. In particular, single concentrations of TNF α , IL-1 β , and lipopolysaccharide (LPS) were added either apically or basolaterally on day 22, and TEER, membrane permeability, and basolateral IL-8 release were measured as pro-inflammatory readouts. Interestingly, none of the apical treatments affected membrane integrity, as no changes were observed in TEER (**Supplementary Figure S2A**) or membrane permeability (**Supplementary Figure S2B**) relative to the untreated control. IL-8 release, however, was increased when TNF α or IL-1 β was applied apically (**Supplementary**

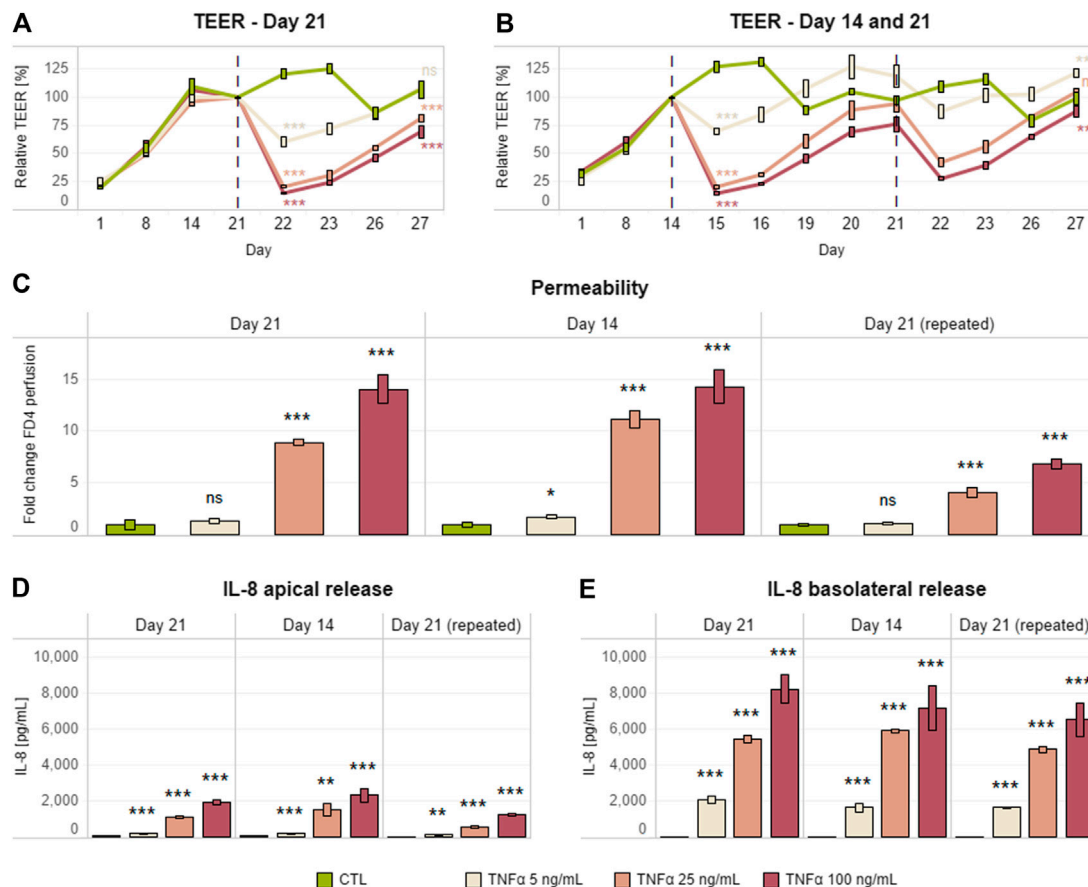


FIGURE 1 | Single and repeated Caco-2/HT29-MTX pro-inflammatory induction after days 14 and 21. TEER (**A,B**), permeability (**C**), and IL-8 release (**D,E**) in a differentiated Caco-2/HT29-MTX coculture basolaterally treated with different concentrations of TNF α (0–100 ng/ml) on day 21 (single) or days 14 and 21 (repeated). Each inflammatory stimulus (red dashed line) was left for up to 24 h; this was followed by a recovery period of up to 120 h without an inflammatory inducer. TEER values are represented in percentage; zero-hour treatment was used as reference (100%). Permeability is expressed as fold change over the untreated control (CTL). Data are presented as the average of three technical replicates with the corresponding standard deviations ($n = 1$; $m > 3$). On the day at the end of the simulation and the last day recorded, statistical differences between the control without TNF α and each of the three concentrations of TNF α were determined by a two-tailed t -test, * $p \leq 0.05$; ** $p \leq 0.01$; *** $p \leq 0.001$; ns, $p > 0.05$. Equivalence comparisons and linear regression analysis are provided in **Supplementary Tables S1 and S2**. Abbreviations: TEER, transepithelial electrical resistance; TNF, tumor necrosis factor; CTL, control.

Figure S2C). On the other hand, a marked decrease in TEER (**Supplementary Figure S2D**) together with an increase in membrane permeability (**Supplementary Figure S2E**) and IL-8 release (**Supplementary Figure S2F**) were observed when the coculture was treated basolaterally with TNF α . In contrast, basolateral IL-1 β treatment showed only a weak effect on TEER and IL-8 release and no effect on membrane permeability (**Supplementary Figures S2D,F,E**, respectively). Of note, as previously documented, LPS treatment had no effect on any of the three readouts in the cells (Abreu et al., 2001).

Although the generally accepted Caco-2 differentiation period is 21 days (Sambuy et al., 2005; Leonard et al., 2010; Pereira et al., 2015; Susewind et al., 2016), we evaluated the possibility of shortening the coculture incubation period from 21 to 14 days (Antunes et al., 2013) and still maintain an equivalent pro-inflammatory response. Differentiated Caco-2/HT29-MTX cocultures on day 14 or 21 were basolaterally treated with

different concentrations of TNF α (5, 25, or 100 ng/ml) for 24 h. TNF α cause a dose-dependent decrease in TEER (**Figures 1A,B**) and increase in permeability (**Figure 1C**) and IL-8 release (**Figures 1D,E**), independent of the age of the coculture/duration of coculture maturation (**Figures 1A,B**). Upon removal of the pro-inflammatory stimulus, we also observed a time-dependent increase in TEER over the following 5 days.

We also tested a protocol involving two consecutive cycles of inflammatory induction and recovery on days 14 and 21. Thus, the Caco-2/HT29-MTX coculture treated on day 14 was further treated on day 21 with the same TNF α concentrations for an additional 24 h (**Figure 1B**). The dose-response outcomes of inflammatory induction on days 14 and 21 were similar in terms of TEER and permeability. However, the coculture appeared to be more resistant to the second stimulus, as the magnitude of effects on TEER and permeability was lower (**Figures 1B-E**).

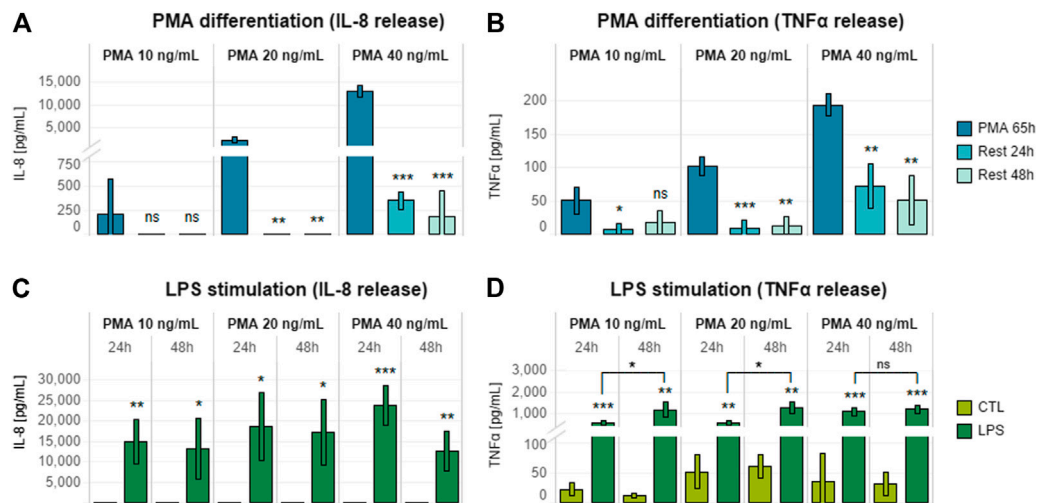


FIGURE 2 | Effects of different PMA concentrations on THP-1 post-differentiation cytokine release. **(A)** IL-8 and **(B)** TNFα release by THP-1 cells differentiated for 65 h with increasing concentrations of PMA (10, 20, and 40 ng/ml) and rested for 24 or 48 h after PMA removal. **(C)** IL-8 and **(D)** TNFα release by THP-1 cells differentiated with increasing concentrations of PMA (10, 20, and 40 ng/ml) for 65 h, rested for 24 or 48 h after PMA removal, and treated with 10 ng/ml LPS for 24 h. Data are presented as the average of three technical replicates with corresponding standard deviation. Statistical differences were calculated between the 65-h induced sample and the rested samples **(A,B)** or between LPS-treated and untreated cultures **(C,D)** by means of two-tailed *t*-tests. **p* ≤ 0.05; ***p* ≤ 0.01; ****p* ≤ 0.001; ns, *p* > 0.05 **(A,B)**. Equivalence comparisons and linear regression analysis are provided in **Supplementary Tables S3 and S4**. R24h = cells rested for 24 h; R48h = cells rested for 48 h. Abbreviations: PMA, phorbol 12-myristate.

Finally, a medium compatibility test was performed with a view toward assembly of the final triculture with THP-1 cells. The coculture medium (DMEM) in the basolateral compartment was fully replaced with THP-1 cell culture medium (RPMI) on day 12, and the effects on coculture monolayer integrity were evaluated by TEER measurement over the following 72 h. The medium switch did not cause any significant difference in TEER (**Supplementary Figure S3**).

Taken together, these results suggest that shortening the Caco-2/HT29-MTX coculture differentiation period from 21 to 14 days enables repeated pro-inflammatory treatment without affecting epithelium integrity or inflammatory response. Finally, in contrast to previous suggestions (Kampfer et al., 2017), the epithelial coculture can be fully switched to RPMI medium without any effect on coculture physiology in terms of tissue barrier integrity.

THP-1 Differentiation Protocol

Previous studies have described several different THP-1 differentiation protocols, with great variation in PMA concentration, treatment duration, and inclusion or omission of resting period (Daigneault et al., 2010; Maess et al., 2014; Lund et al., 2016). To optimize laboratory timing and workload, we optimized a THP-1 differentiation protocol for over-the-weekend induction (~65 h), thereby creating a wider time window for triculture assembly and compound assessment. Cells were seeded in a 24-well plate by adapting previous internally established 96-well plate format conditions (20,000 cells/well in 100 μl). In particular, 12×10^4 cells were seeded in 600 μl of cell culture medium. Before stimulation of differentiated THP-1 cells with a pro-inflammatory inducer for an additional 24 h, a combination of different concentrations of PMA

(10, 20, and 40 ng/ml) and post-differentiation resting times (24 and 48 h) were evaluated to assess the release of IL-8 and TNFα. LPS (10 ng/ml) was chosen as the pro-inflammatory inducer because LPS treatment had no effect on Caco-2/HT29-MTX cocultures (**Supplementary Figures S2D–F**), and, therefore, any effect on the epithelial coculture would be due to activation of the immune cells.

Increasing PMA concentrations caused a dose-dependent increase in both IL-8 and TNFα release by THP-1 cells (**Figures 2A,B**). PMA removal and 24 h of resting were required to obtain a significant decrease in the levels of both mediators; an additional 24-h rest did not result in any further decrease in IL-8 or TNFα levels. LPS treatment after 24 or 48 h of resting induced increased levels of IL-8 and TNFα release relative to untreated rested controls (**Figures 2C,D**). Interestingly, TNFα release was higher when a 48-h resting time was applied after stimulation with PMA (**Figure 2D**).

Taking into account the results of the LPS dose-response analysis, it was interesting to see that 48 h of resting was beneficial for achieving a greater pro-inflammatory response (**Figure 2D**). This aspect fitted well the concept of allowing 24 h of stabilization upon triculture assembly. In addition, we decided to exclude the differentiation with 40 ng/ml, as we observed no further increase in cytokines release relative to 10 or 20 ng/ml.

In order to choose the most appropriate condition for THP-1 maturation, differentiation with both 10 and 20 ng/ml PMA was further assessed in the context of the assembled triculture response.

Coculture Assembly and Pro-Inflammatory Induction

THP-1 cells (12×10^4) differentiated with 10 or 20 ng/ml PMA and rested for 24 h were assembled in a triculture with the Caco-

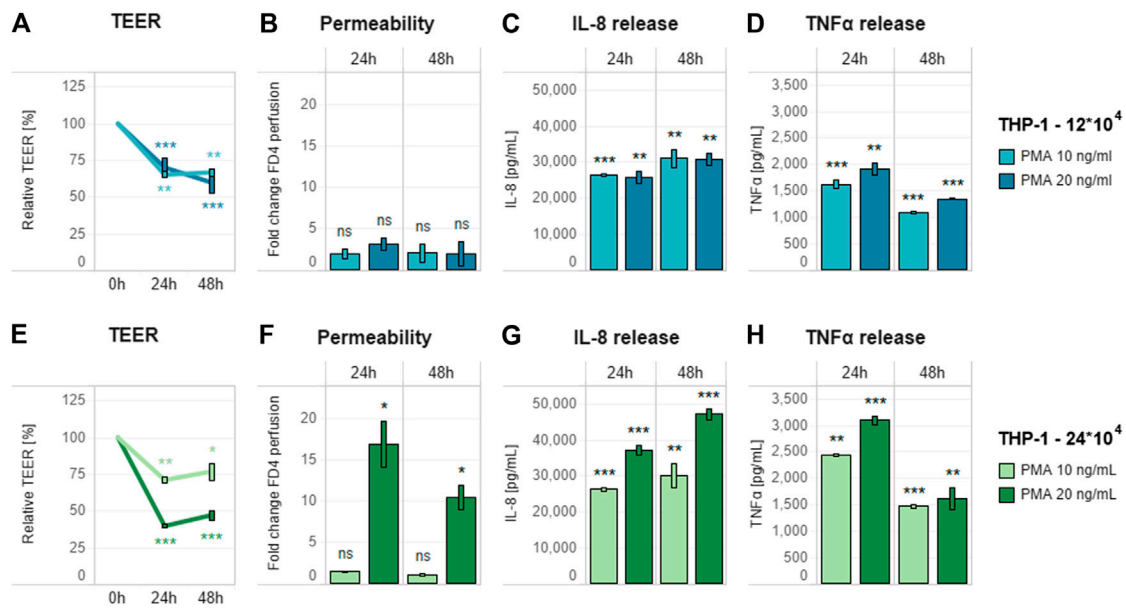


FIGURE 3 | Effect of pro-inflammatory stimulation on optimized triculture. Pro-inflammatory effect of 10 ng/ml LPS added basolaterally to a triculture containing (A–D) 12×10^4 and (E–H) 24×10^4 THP-1 cells in 400 μ l of cell culture medium in the basolateral compartment. (A,E) TEER (B,F) membrane permeability, and (C,D,G,H) cytokine release (IL-8 and TNF α , respectively) of the triculture. For each THP-1 seeding condition, different PMA concentrations (10 and 20 ng/ml) were tested for optimizing the triculture response. TEER values are represented in percentage; zero-hour treatment was used as the reference (100%). Permeability is expressed as fold change over the untreated control without LPS. Data are presented as the average of three technical replicates with the corresponding standard deviations. Statistical differences between the LPS- and PMA-treated cultures and the control culture without the compounds (with 12×10^4 THP-1 cells) were determined by a two-tailed *t*-test. **p* \leq 0.05; ***p* \leq 0.01; ****p* \leq 0.001; ns, *p* > 0.05. Abbreviations: PMA, phorbol 12-myristate; TNF, tumor necrosis factor; IL, interleukin; CTL, control.

2/HT29-MTX coculture on day 13, and the stability of the triculture was evaluated by TEER and permeability measurement. Neither endpoint decreased over the following 72 h (Supplementary Figures S4A,B). Following addition of a single concentration of LPS (10 ng/ml) to the basolateral side 24 h after triculture assembly, only small changes in TEER were observed in the subsequent 24 or 48 h (Supplementary Figure S5A), with no sign of increased permeability (Supplementary Figure S5B). These results confirmed that both concentrations of PMA were suitable for obtaining a stable triculture under pro-inflammatory induction.

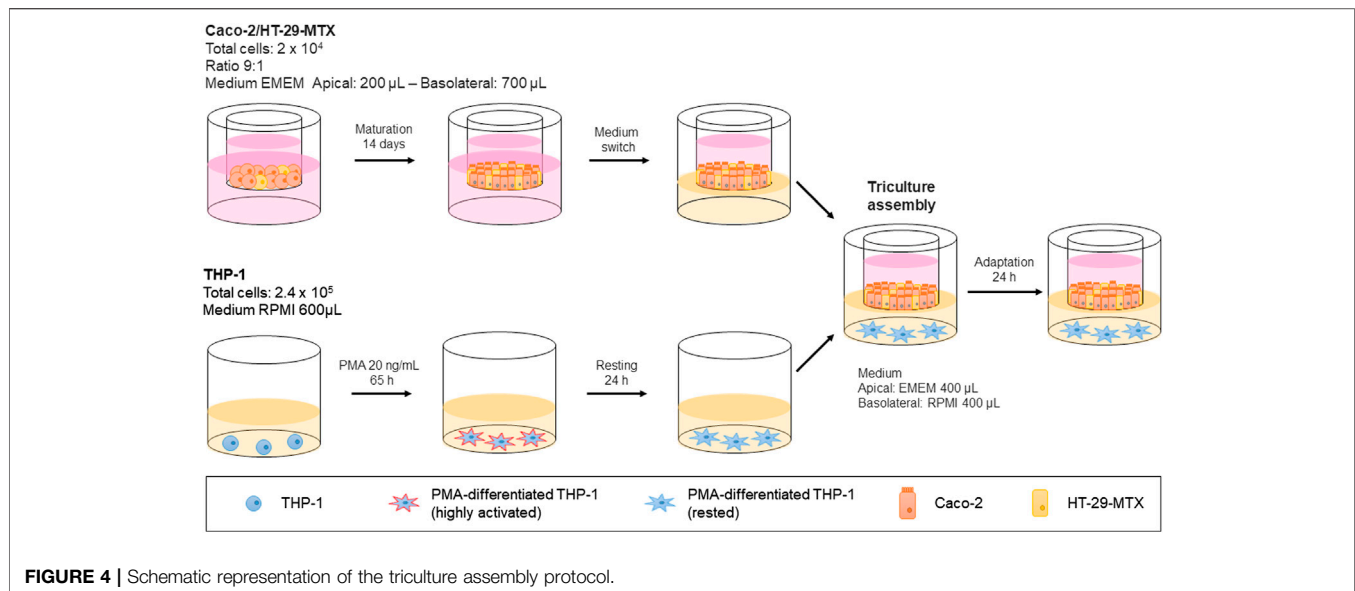
However, they also suggested that the pro-inflammatory induction was not sufficient to affect the epithelial monolayer, thus reducing the applicability of these conditions for anti-inflammatory compound screening. This weak effect could be related to the levels of the released cytokines (Supplementary Figure S5B), especially TNF α , which is known to be the main factor responsible for the pro-inflammatory effects on the epithelial layer. To overcome these limitations and obtain a higher concentration of secreted TNF α , we first decided to decrease the cell culture medium volume in the basolateral compartment from 600 to 400 μ l. Then, while assessing both concentrations of PMA (10 and 20 ng/ml), we also evaluated a higher number of THP-1 cells (24×10^4). All selected conditions were assessed in the presence of the same previously tested pro-inflammatory stimulus (10 ng/ml LPS). Decreasing cell culture medium volume alone was not sufficient to induce an increase in

epithelial layer permeability, because it only caused a decrease in TEER, as in the previous evaluation (Figures 3A,B). Differentiation of 2.4×10^5 THP-1 cells in combination with 20 ng/ml PMA treatment appeared to be the most effective condition, as it caused the greatest decrease in TEER (Figure 3E) and increase in membrane permeability (Figure 3F). This combination also showed the highest level of cytokine release (Figures 3G,H).

With the conditions for triculture assembly (Figure 4) and proinflammatory induction defined, we continued by evaluating the suitability of the assay protocol for assessing anti-inflammatory properties by using known reference compounds. To this end, we chose budesonide and TPCA-1, because the former represents an effective drug that leads to remission in a subset of UC patients, while the latter is a known nuclear factor (NF)- κ B pathway inhibitor.

Reference Compound Assessment

The triculture was pretreated on the basolateral side for 6 h with different concentrations of selected reference compounds—TPCA-1 (0–10 μ M) and budesonide (0–10 nM)—before addition of the pro-inflammatory stimulus (10 ng/ml LPS). After an additional 18 h (24-h time point) of incubation, TEER and monolayer permeability were assessed to evaluate epithelial monolayer integrity. In addition, IL-8 and TNF α release into the basolateral compartment was quantified, and cell viability was evaluated by WST-8 bioreduction separately



in Caco-2-HT29-MTX cocultures and THP-1 cells (**Supplementary Figure S6**).

Both TPCA-1 and budesonide, when compared against the LPS-treated-only control, induced dose–response changes in the investigated inflammation-related endpoints—that is, TEER and permeability—in the context of the epithelial monolayer. Pretreatment with these anti-inflammatory compounds prevented the LPS-induced effects on both TEER and membrane permeability (**Figures 5A,B**). The effects in the immune cell compartment appeared to be stronger upon pre-exposure to budesonide. In fact, the levels of both investigated cytokines were decreased in a dose-dependent manner (**Figure 5D**). On the other hand, treatment with TPCA-1 resulted in a decrease in TNF α levels only (**Figure 5C**). Finally, the absence of cytotoxicity in both cell compartments (apical: **Figures 5A,B**; basolateral: **Figures 5C,D**) proved the suitability of the established anti-inflammatory protocol for measuring the efficacy of anti-inflammatory compounds in a specific way.

Alkaloid Assessment

Using the approach developed and verified with the reference compounds (**Supplementary Figure S4**), we assessed the anti-inflammatory properties of known tobacco alkaloids such as nicotine and anatabine. Of note, anatabine was tested as a citrate salts in both racemic (*R/S*) and *S* forms. Although the anti-inflammatory effects of nicotine have been previously described (Wang et al., 2003; de Jonge et al., 2005; Cloëz-Tayarani and Changeux, 2007), we observed no such effect within the concentration range tested in this study (**Figures 6A,D**). Unlike nicotine, racemic anatabine showed concentration-dependent effects on both epithelial membrane integrity and TEER (**Figure 6B**). The observed effect is most likely due to an anti-inflammatory effect exerted on THP-1 cells, as evident from the decrease in cytokine release (**Figure 6E**). The *S* form exhibited comparable anti-inflammatory effects to those

of the racemate. Nonetheless, *S* form-mediated effects appeared to be unspecific because the *S* form also induced greater cytotoxicity in the immune cells (**Figures 6C,F**). It is, in fact, reasonable to believe that the observed phenotype was caused by the decreased viability and functionality of the THP-1 cells. Comparison of the results of the racemic (*R/S*) and *S* forms of anatabine suggests that the *R* form is most likely less toxic and more specific with regard to anti-inflammatory effects.

DISCUSSION

In the present study, we established a biologically relevant intestinal *in vitro* system for assessing the potential anti-inflammatory effects of immunomodulating natural compounds. We leveraged previously established and published *in vitro* models (Ponce de León-Rodríguez et al., 2018) in which different intestinal epithelial cells were cultured in the presence or absence of immunocompetent cells. Although most features of the adaptive immune response are beyond the scope of current *in vitro* models, the features of innate immune response can be mimicked.

Although not fully representative of the true physiology of cells in their original tissues, immortalized cell lines still represent an adequate solution for profiling therapeutically active compounds. In fact, compared to primary cells, cell lines are characterized by an extended lifespan while still retaining some of their key functional features. The use of cell lines also offers the advantage of decreased experimental variability in screening approaches. For these reasons we selected the most commonly used epithelial cells, namely Caco-2 cells, complemented with mucus-secreting HT29-MTX cells (Huet et al., 1987; Lesuffleur et al., 1990) to better resemble the *in vivo* tissue counterpart. Caco-2 cells can respond to various cytokines or chemokines secreted by immune cells by modulating their membrane permeability, thus further amplifying or attenuating the

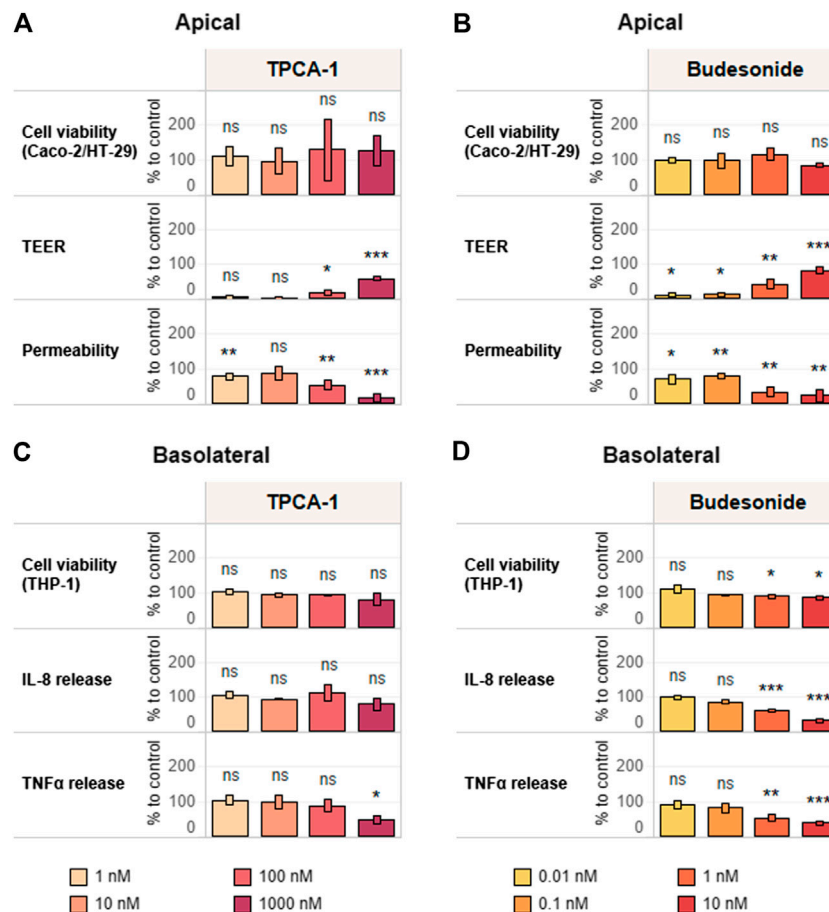


FIGURE 5 | Reference item assessment and verification of the anti-inflammatory protocol. Tricucultures were treated basolaterally with increasing concentrations of **(A,C)** TPCA-1 and **(B,D)** budesonide for 6 h and subsequently stimulated with 10 ng/ml LPS for 18 h. TEER, epithelial layer permeability, cell viability of differentiated Caco-2/HT29-MTX cells **(A,B)** and cytokine release and cell viability of differentiated THP-1 cells **(C,D)** were measured. TEER values are normalized to control (CTL; 100%) and LPS treatment (0%). Permeability is normalized by using LPS treatment as reference (100%). Basolateral IL-8 and TNFα release are expressed as percentage of control (cells treated with LPS only; CTL; 100%). Cell viability values of Caco-2-HT29-MTX cocultures and THP-1 cells are expressed as percentage of control (cells treated with LPS only, CTL; 100%). $n = 3$ independent experiments. Statistical differences between reference compound-treated vs. LPS-treated-only cultures were determined by a two-tailed t -test. $p \leq 0.05$; $**p \leq 0.01$; $***p \leq 0.001$; ns, $p > 0.05$. Abbreviations: LPS, lipopolysaccharide; TEER, transepithelial electrical resistance; TNF, tumor necrosis factor; IL, interleukin.

inflammatory process (Jung et al., 1995; Panja et al., 1998; Bruewer et al., 2005; Weglarz et al., 2007; Hollebeeck et al., 2012; Rodriguez-Ramiro et al., 2013). Altogether, these features make Caco-2 cells one of the most accepted *in vitro* models of human enterocytes currently available.

Furthermore, the presence of mucus—secreted by HT29-MTX—in the cell system is essential for estimating intestinal permeability and adsorption (Mahler et al., 2009). In fact, it acts as a barrier against certain compounds, particularly those that are lipophilic (Behrens et al., 2001), preventing easy access of highly diffusible small molecules (Artursson et al., 2001). In the intestinal mucosa, the close localization of epithelial cells with immune cells with the ability to differentiate into macrophages or dendritic cells has prompted the hypothesis that their interactions are paramount for tissue homeostasis and, in some instances, might promote inflammation (Vitale et al., 2016). Consequently, we selected the monocyte-like cell line THP-1 for the immune

component because of its capacity to be differentiated into macrophage- or dendritic cell-like cells.

Of note, the above-described characteristics do not allow us to exactly define which part of the intestine, small or large, this *in vitro* intestinal system may represent. In fact, although the differentiated Caco-2 cells form a polarized epithelial cell monolayer that resembles the enterocytes lining the small intestine, they have been shown to express both enterocyte and colonocyte genes (Grasset et al., 1984; Engle et al., 1998). Moreover, the presence of HT29-MTX cells further complicates the search for a definition, which may ultimately be considered forced. In fact, on the one hand, the HT29-MTX cells decrease the overall tightness of the monolayer, again pushing the model toward a small intestinal system (Hilgendorf et al., 2000); on the other hand, acting as goblet cells and being present at a fairly abundant level (9:1 ratio) (Hilgendorf et al., 2000; Chen et al., 2010), the HT29-MTX cells may better represent a condition closer to that in the large intestine. Thus, a more accurate and deeper

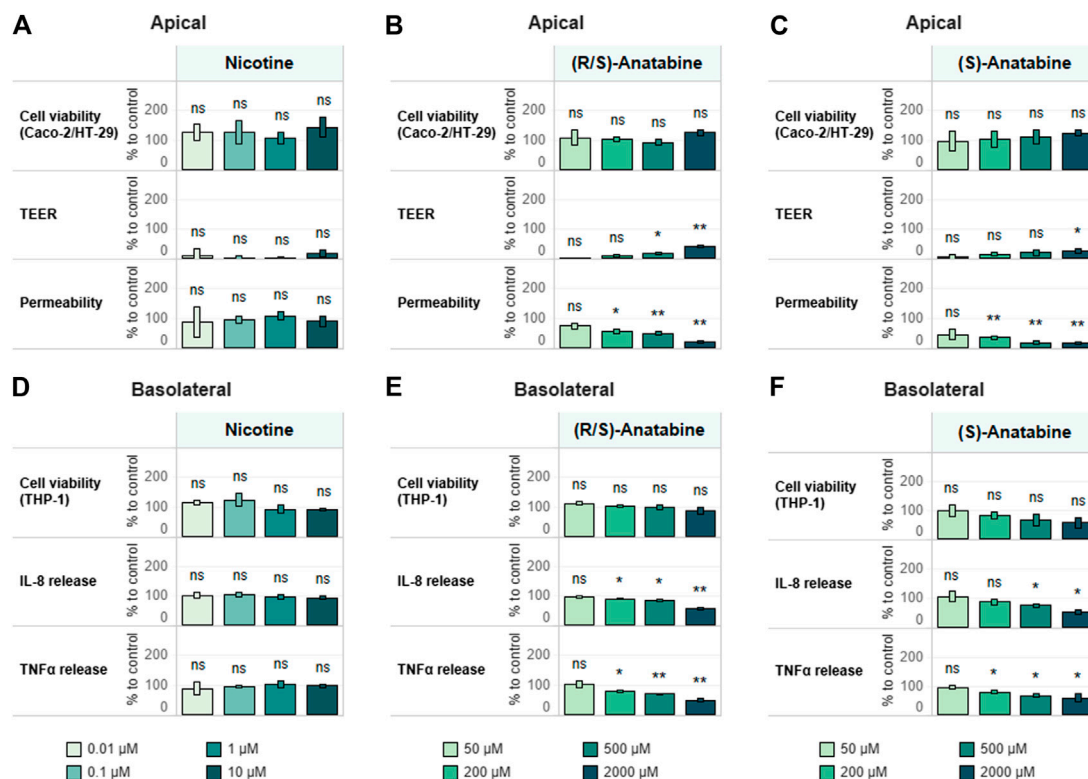


FIGURE 6 | Test item assessment. Tricultures were treated basolaterally with increasing concentrations of (A,D) nicotine (B,E) (R/S)-anatabine, or (C,F) (S)-anatabine for 6 h and subsequently stimulated with 10 ng/ml LPS for 18 h. TEER, epithelial layer permeability, cell viability of differentiated Caco-2/HT29-MTX cells (A–C) and cytokine release and cell viability of differentiated THP-1 cells (D–F) were measured. TEER values are normalized to control (CTL; 100%) and LPS treatment (0%). Permeability is normalized by using LPS treatment as the reference (100%). Basolateral IL-8 and TNFα release are expressed as percentage of control (cells treated with LPS only; CTL; 100%). Cell viability values of Caco-2–HT29-MTX cocultures and THP-1 cells are expressed as percentage of control (cells treated with LPS only; CTL; 100%). $n = 3$ independent experiments. Statistical differences between the reference compound-treated vs. LPS-treated-only cultures were determined by a two-tailed t -test. * $p \leq 0.05$; ** $p \leq 0.01$; *** $p \leq 0.001$; ns, $p > 0.05$. Abbreviations: LPS, lipopolysaccharide; TEER, transepithelial electrical resistance; TNF, tumor necrosis factor; IL, interleukin; CTL, control.

characterization of the model at both molecular and physiological levels is necessary to clearly define it.

The triculture was generated with a dual-compartment geometry by using a Transwell® system, where the epithelial compartment is cultured on the apical side, and the immunocompetent cells are seeded on the basolateral side. The triculture assembly and stimulus protocol developed in this study allowed us to produce an *in vitro* model characterized by several advantages: i) less laborious cell culture handling, which did not require adaptation of cell culture medium, use of extracellular matrix, or pro-inflammatory cell priming; ii) direct immune-to-epithelial cell pro-inflammatory activation, as the selected pro-inflammatory stimulus selectively activated the immune cells, which further extended the effect to the epithelial component; iii) a set of functional readouts that well recapitulate the *in vivo* phenotype; and iv) feasibility for multiple cycles of pro-inflammatory stimulus for assessing repeated treatment.

We also proved the suitability of the model for use as a screening tool for anti-inflammatory compounds by assessing two known anti-inflammatory drugs, both of which successfully prevented LPS-induced pro-inflammatory effects in a dose-dependent manner. The model also allowed further characterization of known tobacco

alkaloids, such as nicotine and anatabine, which have previously been shown to have anti-inflammatory abilities in animal models of intestinal diseases (Paris et al., 2013b; Zabrodskii et al., 2015; Maruta et al., 2018). Several studies have reported nicotine-dependent anti-inflammatory effects in animal models of IBD (Maruta et al., 2018). In Caco-2 cells, nicotine has been shown to up-regulate the expression of the tight junction proteins occludin and claudin-1, and improve barrier function, followed by anatabine and the primary metabolite of nicotine cotinine, although to a lower extent (McGilligan et al., 2007). Conversely, nicotine showed no such effects in our *in vitro* intestinal model, highlighting the importance of using *in vitro* models that replicate key features of the intestinal mucosa for compound testing. On the other hand, the administration route of nicotine *in vivo* models (i.e., oral administration, subcutaneous injection) plays a crucial role in the potential anti-inflammatory effects of nicotine in intestinal inflammation (AlSharari et al., 2013) therefore we might have not been able to capture the full potential of nicotine with our model as nicotine dissemination through the blood stream, intestinal absorption, or gastrointestinal metabolism might play a crucial role in nicotine bioavailability and anti-inflammatory effects in the gut.

Of note, other minor tobacco alkaloids, nAChR agonists as well, were also suggested as having potential anti-inflammatory effects (Olsson et al., 1993; Bai et al., 2007; Alijevic et al., 2020; Ruiz Castro et al., 2020). Among these, the alkaloids anatabine and cotinine have displayed protective effects in animal models of inflammatory conditions, including Alzheimer's disease (Paris et al., 2011), Parkinson's disease (Barreto et al., 2014), sepsis (Zabrodskii et al., 2015), and IBD (Bai et al., 2007; Ruiz Castro et al., 2020). Our results on anatabine are thus substantiated by the findings of previous studies that have demonstrated the anti-inflammatory effects of anatabine in *in vivo* disease models, indicating that this pyridine alkaloid might be a potential candidate for development of anti-inflammatory therapies (Paris et al., 2011; Paris et al., 2013b).

In summary, our results show that our *in vitro* triculture intestinal model exhibits mucosal immune responses and stable barrier function analogous to those *in vivo* and is suitable for screening compounds with anti-inflammatory properties. By capturing the key features of intestinal inflammation, this *in vitro* tool provides a means to investigate immunomodulating therapeutic intervention of the inflamed intestine.

DATA AVAILABILITY STATEMENT

The original data presented in the study are included in the article/**Supplementary Material**. Further inquiries can be directed to the corresponding author.

REFERENCES

- Abraham, B. P., Ahmed, T., and Ali, T. (2017). Inflammatory Bowel Disease: Pathophysiology and Current Therapeutic Approaches. *Handb. Exp. Pharmacol.* 239, 115–146. doi:10.1007/164_2016_122
- Abraham, C., and Medzhitov, R. (2011). Interactions between the Host Innate Immune System and Microbes in Inflammatory Bowel Disease. *Gastroenterology* 140 (6), 1729–1737. doi:10.1053/j.gastro.2011.02.012
- Abreu, M. T., Vora, P., Faure, E., Thomas, L. S., Arnold, E. T., and Arditi, M. (2001). Decreased Expression of Toll-like Receptor-4 and MD-2 Correlates with Intestinal Epithelial Cell Protection against Dysregulated Proinflammatory Gene Expression in Response to Bacterial Lipopolysaccharide. *J. Immunol.* 167 (3), 1609–1616. doi:10.4049/jimmunol.167.3.1609
- Alijevic, O., McHugh, D., Rufener, L., Mazurov, A., Hoeng, J., and Peitsch, M. (2020). An Electrophysiological Characterization of Naturally Occurring Tobacco Alkaloids and Their Action on Human $\alpha 4\beta 2$ and $\alpha 7$ Nicotinic Acetylcholine Receptors. *Phytochemistry* 170, 112187. doi:10.1016/j.phytochem.2019.112187
- AlSharari, S. D., Akbarali, H. I., Abdullah, R. A., Shahab, O., Auttachoat, W., Ferreira, G. A., et al. (2013). Novel Insights on the Effect of Nicotine in a Murine Colitis Model. *J. Pharmacol. Exp. Ther.* 344 (1), 207–217. doi:10.1124/jpet.112.198796
- Antunes, F., Andrade, F., Araújo, F., Ferreira, D., and Sarmento, B. (2013). Establishment of a Triple Co-culture In Vitro Cell Models to Study Intestinal Absorption of Peptide Drugs. *Eur. J. Pharmaceutics Biopharmaceutics* 83 (3), 427–435. doi:10.1016/j.ejpb.2012.10.003
- Artursson, P., Palm, K., and Luthman, K. (2001). Caco-2 Monolayers in Experimental and Theoretical Predictions of Drug Transport. *Adv. Drug Deliv. Rev.* 46 (1–3), 27–43. doi:10.1016/s0169-409x(00)00128-9

AUTHOR CONTRIBUTIONS

DM, GS, and DG contributed to the conception and design of the research, performed data interpretation, and drafted the manuscript. DG performed all the experiments. KR and PC contributed to the interpretation of data and to the manuscript draft. RP and VJ computed and analyzed the data. FM designed the figures. KL, SF, MP, and JH edited and revised the manuscript. All authors approved the final version of the manuscript.

FUNDING

Philip Morris International is the sole source of funding and sponsor of this research.

ACKNOWLEDGMENTS

We thank Sindhoora Bhargavi Gopala Reddy for language editing support.

SUPPLEMENTARY MATERIAL

The Supplementary Material for this article can be found online at: <https://www.frontiersin.org/articles/10.3389/fphar.2021.639716/full#supplementary-material>.

- Atreya, R., and Neurath, M. F. (2015). Molecular Pathways Controlling Barrier Function in IBD. *Nat. Rev. Gastroenterol. Hepatol.* 12 (2), 67–68. doi:10.1038/nrgastro.2014.201
- Bai, A., Guo, Y., and Lu, N. (2007). The Effect of the Cholinergic Anti-inflammatory Pathway on Experimental Colitis. *Scand. J. Immunol.* 66 (5), 538–545. doi:10.1111/j.1365-3083.2007.02011.x
- Barreto, G. E., Iarkov, A., and Moran, V. E. (2014). Beneficial Effects of Nicotine, Cotinine and its Metabolites as Potential Agents for Parkinson's Disease. *Front. Aging Neurosci.* 6, 340. doi:10.3389/fnagi.2014.00340
- Behrens, I., Stenberg, P., Artursson, P., and Kissel, T. (2001). Transport of Lipophilic Drug Molecules in a New Mucus-Secreting Cell Culture Model Based on HT29-MTX Cells. *Pharm. Res.* 18 (8), 1138–1145. doi:10.1023/a:1010974909998
- Bruewer, M., Utech, M., Ivanov, A. I., Hopkins, A. M., Parkos, C. A., and Nusrat, A. (2005). Interferon- γ Induces Internalization of Epithelial Tight Junction Proteins via a Macropinocytosis-like Process. *FASEB J.* 19 (8), 923–933. doi:10.1096/fj.04-3260com
- Chantret, I., Barbat, A., Dussaulx, E., Brattain, M. G., and Zweibaum, A. (1988). Epithelial Polarity, Villin Expression, and Enterocytic Differentiation of Cultured Human Colon Carcinoma Cells: a Survey of Twenty Cell Lines. *Cancer Res.* 48 (7), 1936–1942.
- Chen, X.-M., Elisia, I., and Kitts, D. D. (2010). Defining Conditions for the Co-culture of Caco-2 and HT29-MTX Cells Using Taguchi Design. *J. Pharmacol. Toxicol. Methods* 61 (3), 334–342. doi:10.1016/j.vascn.2010.02.004
- Chen, Y.-Y., Li, R.-Y., Shi, M.-J., Zhao, Y.-X., Yan, Y., Xu, X.-X., et al. (2017). Demethyleneberberine Alleviates Inflammatory Bowel Disease in Mice through Regulating NF- κ B Signaling and T-Helper Cell Homeostasis. *Inflamm. Res.* 66 (2), 187–196. doi:10.1007/s00011-016-1005-3
- Cheng, K.-C., Li, C., and Uss, A. S. (2008). Prediction of Oral Drug Absorption in Humans - from Cultured Cell Lines and Experimental

- Animals. *Expert Opin. Drug Metab. Toxicol.* 4 (5), 581–590. doi:10.1517/17425255.4.5.581
- Clark, M. S., Rand, M. J., and Vanos, S. (1965). Comparison of Pharmacological Activity of Nicotine and Related Alkaloids Occurring in Cigarette Smoke. *Arch. Int. Pharmacodyn Ther.* 156 (2), 363–379.
- Cloëz-Tayarani, I., and Changeux, J. P. (2007). Nicotine and Serotonin in Immune Regulation and Inflammatory Processes: a Perspective. *J. Leukoc. Biol.* 81 (3), 599–606. doi:10.1189/jlb.0906544
- Daigneault, M., Preston, J. A., Marriott, H. M., Whyte, M. K. B., and Dockrell, D. H. (2010). The Identification of Markers of Macrophage Differentiation in PMA-Stimulated THP-1 Cells and Monocyte-Derived Macrophages. *PLoS One* 5 (1), e8668. doi:10.1371/journal.pone.0008668
- de Jonge, W. J., van der Zanden, E. P., The, F. O., Bijlsma, M. F., van Westerloo, D. J., Bennis, R. J., et al. (2005). Stimulation of the Vagus Nerve Attenuates Macrophage Activation by Activating the Jak2-STAT3 Signaling Pathway. *Nat. Immunol.* 6 (8), 844. doi:10.1038/nri1229
- Engle, M. J., Goetz, G. S., and Alpers, D. H. (1998). Caco-2 Cells Express a Combination of Colonocyte and Enterocyte Phenotypes. *J. Cel. Physiol.* 174 (3), 362–369. doi:10.1002/(SICI)1097-4652(199803)174:3<362::AID-JCP10>3.0.CO;2-B
- Gomes, J. P., Watad, A., and Shoenfeld, Y. (2018). Nicotine and Autoimmunity: The lotus' Flower in Tobacco. *Pharmacol. Res.* 128, 101–109. doi:10.1016/j.phrs.2017.10.005
- Grasset, E., Pinto, M., Dussaulx, E., Zweibaum, A., and Desjeux, J. F. (1984). Epithelial Properties of Human Colonic Carcinoma Cell Line Caco-2: Electrical Parameters. *Am. J. Physiology-Cell Physiol.* 247 (3), C260–C267. doi:10.1152/ajpcell.1984.247.3.C260
- Hayashi, S., Hamada, T., Zaidi, S. F., Oshiro, M., Lee, J., Yamamoto, T., et al. (2014). Nicotine Suppresses Acute Colitis and Colonic Tumorigenesis Associated with Chronic Colitis in Mice. *Am. J. Physiology-Gastrointestinal Liver Physiol.* 307 (10), G968–G978. doi:10.1152/ajpgi.00346.2013
- Hidalgo, I. J., Raub, T. J., and Borchardt, R. T. (1989). Characterization of the Human Colon Carcinoma Cell Line (Caco-2) as a Model System for Intestinal Epithelial Permeability. *Gastroenterology* 96 (3), 736–749. doi:10.1016/s0016-5085(89)80072-1
- Hilgendorf, C., Spahn-Langguth, H., Regårdh, C. G., Lipka, E., Amidon, G. L., and Langguth, P. (2000). Caco-2 versus Caco-2/HT29-MTX Co-cultured Cell Lines: Permeabilities via Diffusion, inside- and Outside-Directed Carrier-Mediated Transport. *J. Pharm. Sci.* 89 (1), 63–75. doi:10.1002/(SICI)1520-6017(200001)89:1<63::AID-JPS7>3.0.CO;2-6
- Hillgren, K. M., Kato, A., and Borchardt, R. T. (1995). *In vitro* systems for Studying Intestinal Drug Absorption. *Med. Res. Rev.* 15 (2), 83–109. doi:10.1002/med.2610150202
- Hollebeek, S., Winand, J., Hérent, M.-F., During, A., Leclercq, J., Larondelle, Y., et al. (2012). Anti-inflammatory Effects of Pomegranate (*Punica Granatum* L.) Husk Ellagitannins in Caco-2 Cells, an In Vitro Model of Human Intestine. *Food Funct.* 3 (8), 875–885. doi:10.1039/c2fo10258g
- Honda, K., and Littman, D. R. (2012). The Microbiome in Infectious Disease and Inflammation. *Annu. Rev. Immunol.* 30, 759–795. doi:10.1146/annurev-immunol-020711-074937
- Huet, C., Sahuquillo-Merino, C., Coudrier, E., and Louvard, D. (1987). Absorptive and Mucus-Secreting Subclones Isolated from a Multipotent Intestinal Cell Line (HT-29) Provide New Models for Cell Polarity and Terminal Differentiation. *J. Cel Biol* 105 (1), 345–357. doi:10.1083/jcb.105.1.345
- Iskandar, A. R., Martin, F., Leroy, P., Schlage, W. K., Mathis, C., Titz, B., et al. (2018). Comparative Biological Impacts of an Aerosol from Carbon-Heated Tobacco and Smoke from Cigarettes on Human Respiratory Epithelial Cultures: A Systems Toxicology Assessment. *Food Chem. Toxicol.* 115, 109–126. doi:10.1016/j.fct.2018.02.063
- Jung, H. C., Eckmann, L., Yang, S. K., Panja, A., Fierer, J., Morzycka-Wroblewska, E., et al. (1995). A Distinct Array of Proinflammatory Cytokines Is Expressed in Human Colon Epithelial Cells in Response to Bacterial Invasion. *J. Clin. Invest.* 95 (1), 55–65. doi:10.1172/jci117676
- Kaistha, A., and Levine, J. (2014). Inflammatory Bowel Disease: the Classic Gastrointestinal Autoimmune Disease. *Curr. Probl. Pediatr. Adolesc. Health Care* 44 (11), 328–334. doi:10.1016/j.cppeds.2014.10.003
- Kämpfer, A. A. M., Urbán, P., Gioria, S., Kanase, N., Stone, V., and Kinsner-Ovaskainen, A. (2017). Development of an In Vitro Co-culture Model to Mimic the Human Intestine in Healthy and Diseased State. *Toxicol. Vitro* 45 (Pt 1), 31–43. doi:10.1016/j.tiv.2017.08.011
- Karatay, E., Gül Utku, Ö., Erdal, H., Arhan, M., Önal, İ. K., İbiş, M., et al. (2017). Pentoxifylline Attenuates Mucosal Damage in an Experimental Model of Rat Colitis by Modulating Tissue Biomarkers of Inflammation, Oxidative Stress, and Fibrosis. *Turk J. Med. Sci.* 47 (1), 348–356. doi:10.3906/sag-1508-98
- Kaulmann, A., Legay, S., Schneider, Y.-J., Hoffmann, L., and Bohn, T. (2016). Inflammation Related Responses of Intestinal Cells to Plum and Cabbage Digesta with Differential Carotenoid and Polyphenol Profiles Following Simulated Gastrointestinal Digestion. *Mol. Nutr. Food Res.* 60 (5), 992–1005. doi:10.1002/mnfr.201500947
- Leonard, F., Collnot, E.-M., and Lehr, C.-M. (2010). A Three-Dimensional Coculture of Enterocytes, Monocytes and Dendritic Cells to Model Inflamed Intestinal Mucosa In Vitro. *Mol. Pharmaceutics* 7 (6), 2103–2119. doi:10.1021/mp1000795
- Lesuffleur, T., Barbat, A., Dussaulx, E., and Zweibaum, A. (1990). Growth Adaptation to Methotrexate of HT-29 Human Colon Carcinoma Cells Is Associated with Their Ability to Differentiate into Columnar Absorptive and Mucus-Secreting Cells. *Cancer Res.* 50 (19), 6334–6343.
- Lund, M. E., To, J., O'Brien, B. A., and Donnelly, S. (2016). The Choice of Phorbol 12-myristate 13-acetate Differentiation Protocol Influences the Response of THP-1 Macrophages to a Pro-inflammatory Stimulus. *J. Immunological Methods* 430, 64–70. doi:10.1016/j.jim.2016.01.012
- Lunney, P. C., and Leong, R. W. L. (2012). Review Article: Ulcerative Colitis, Smoking and Nicotine Therapy. *Aliment. Pharmacol. Ther.* 36 (11–12), 997–1008. doi:10.1111/apt.12086
- Maess, M. B., Wittig, B., Cignarella, A., and Lorkowski, S. (2014). Reduced PMA Enhances the Responsiveness of Transfected THP-1 Macrophages to Polarizing Stimuli. *J. Immunol. Methods* 402 (1–2), 76–81. doi:10.1016/j.jim.2013.11.006
- Mahler, G. J., Shuler, M. L., and Glahn, R. P. (2009). Characterization of Caco-2 and HT29-MTX Cocultures in an In Vitro Digestion/cell Culture Model Used to Predict Iron Bioavailability☆. *J. Nutr. Biochem.* 20 (7), 494–502. doi:10.1016/j.jnutbio.2008.05.006
- Maruta, K., Watanabe, C., Hozumi, H., Kurihara, C., Furuhashi, H., Takajo, T., et al. (2018). Nicotine Treatment Ameliorates DSS-Induced Colitis by Suppressing MAdCAM-1 Expression and Leukocyte Recruitment. *J. Leukoc. Biol.* 104 (5), 1013–1022. doi:10.1002/JLB.3A0717-304R
- McGilligan, V. E., Wallace, J. M. W., Heavey, P. M., Ridley, D. L., and Rowland, I. R. (2007). The Effect of Nicotine In Vitro on the Integrity of Tight Junctions in Caco-2 Cell Monolayers. *Food Chem. Toxicol.* 45 (9), 1593–1598. doi:10.1016/j.fct.2007.02.021
- McNeill, A., Brose, L. S., Calder, R., Bauld, L., and Robson, D. (2018). *Evidence Review of E-Cigarettes and Heated Tobacco Products 2018*. A Report Commissioned by Public Health England. London: Public Health England.
- Molodecky, N. A., Soon, I. S., Rabi, D. M., Ghali, W. A., Ferris, M., Chernoff, G., et al. (2012). Increasing Incidence and Prevalence of the Inflammatory Bowel Diseases with Time, Based on Systematic Review. *Gastroenterology* 142 (1), 46–54 e42; quiz e30. doi:10.1053/j.gastro.2011.10.001
- Moreira, R., Pereira, D., Valentão, P., and Andrade, P. (2018). Pyrrolizidine Alkaloids: Chemistry, Pharmacology, Toxicology and Food Safety. *Ijms* 19 (6), 1668. doi:10.3390/ijms19061668
- Ng, S. C., Shi, H. Y., Hamidi, N., Underwood, F. E., Tang, W., Benchimol, E. I., et al. (2017). Worldwide Incidence and Prevalence of Inflammatory Bowel Disease in the 21st Century: a Systematic Review of Population-Based Studies. *The Lancet* 390 (10114), 2769–2778. doi:10.1016/S0140-6736(17)32448-0
- Niu, X., Fan, T., Li, W., Huang, H., Zhang, Y., and Xing, W. (2013). Protective Effect of Sanguinarine against Acetic Acid-Induced Ulcerative Colitis in Mice. *Toxicol. Appl. Pharmacol.* 267 (3), 256–265. doi:10.1016/j.taap.2013.01.009
- Niu, X., Zhang, H., Li, W., Mu, Q., Yao, H., and Wang, Y. (2015). Anti-inflammatory Effects of Cavidine In Vitro and In Vivo, a Selective COX-2 Inhibitor in LPS-Induced Peritoneal Macrophages of Mouse. *Inflammation* 38 (2), 923–933. doi:10.1007/s10753-014-0054-4
- Olsson, E., Holth, A., Kumlin, E., Bohlin, L., and Wahlberg, I. (1993). Structure-Related Inhibiting Activity of Some Tobacco Cembranoids on the Prostaglandin Synthesis in Vitro. *Planta Med.* 59 (4), 293–295. doi:10.1055/s-2006-959684

- Panja, A., Goldberg, S., Eckmann, L., Krishen, P., and Mayer, L. (1998). The Regulation and Functional Consequence of Proinflammatory Cytokine Binding on Human Intestinal Epithelial Cells. *J. Immunol.* 161 (7), 3675–3684.
- Paris, D., Beaulieu-Abdelahad, D., Abdullah, L., Bachmeier, C., Ait-Ghezala, G., Reed, J., et al. (2013a). Anti-inflammatory Activity of Anatabine via Inhibition of STAT3 Phosphorylation. *Eur. J. Pharmacol.* 698 (1–3), 145–153. doi:10.1016/j.ejphar.2012.11.017
- Paris, D., Beaulieu-Abdelahad, D., Bachmeier, C., Reed, J., Ait-Ghezala, G., Bishop, A., et al. (2011). Anatabine Lowers Alzheimer's A β Production In Vitro and In Vivo. *Eur. J. Pharmacol.* 670 (2–3), 384–391. doi:10.1016/j.ejphar.2011.09.019
- Paris, D., Beaulieu-Abdelahad, D., Mullan, M., Ait-Ghezala, G., Mathura, V., Bachmeier, C., et al. (2013b). Amelioration of Experimental Autoimmune Encephalomyelitis by Anatabine. *PLoS One* 8 (1), e55392. doi:10.1371/journal.pone.0055392
- Peng, J., Zheng, T.-T., Li, X., Liang, Y., Wang, L.-J., Huang, Y.-C., et al. (2019). Plant-Derived Alkaloids: The Promising Disease-Modifying Agents for Inflammatory Bowel Disease. *Front. Pharmacol.* 10, 351. doi:10.3389/fphar.2019.00351
- Pereira, C., Araújo, F., Barrias, C. C., Granja, P. L., and Sarmento, B. (2015). Dissecting Stromal-Epithelial Interactions in a 3D In Vitro Cellularized Intestinal Model for Permeability Studies. *Biomaterials* 56, 36–45. doi:10.1016/j.biomaterials.2015.03.054
- Peterson, C. T., Sharma, V., Elmén, L., and Peterson, S. N. (2015). Immune Homeostasis, Dysbiosis and Therapeutic Modulation of the Gut Microbiota. *Clin. Exp. Immunol.* 179 (3), 363–377. doi:10.1111/cei.12474
- Ponce de León-Rodríguez, M. d. C., Guyot, J.-P., and Laurent-Babot, C. (2018). Intestinal In Vitro Cell Culture Models and Their Potential to Study the Effect of Food Components on Intestinal Inflammation. *Crit. Rev. Food Sci. Nutr.* 59 (22), 3648–3666. doi:10.1080/10408398.2018.1506734
- Ponder, A., and Long, M. D. (2013). A Clinical Review of Recent Findings in the Epidemiology of Inflammatory Bowel Disease. *Clin. Epidemiol.* 5, 237–247. doi:10.2147/clep.s33961
- Ramos, G. P., and Papadakis, K. A. (2019). Mechanisms of Disease: Inflammatory Bowel Diseases. *Mayo Clinic Proc.* 94 (1), 155–165. doi:10.1016/j.mayocp.2018.09.013
- Rodrigues de Carvalho, L., de Brito, T. V., Simião da C. Júnior, J., José Dias Júnior, G., de Aguiar Magalhães, D., Guimarães Sousa, S., et al. (2018). Epiisopiloturine, an Imidazole Alkaloid, Reverses Inflammation and Lipid Peroxidation Parameters in the Crohn Disease Model Induced by Trinitrobenzenesulfonic Acid in Wistar Rats. *Biomed. Pharmacother.* 102, 278–285. doi:10.1016/j.biopha.2018.03.090
- Rodríguez-Ramiro, I., Ramos, S., López-Oliva, E., Agis-Torres, A., Bravo, L., Goya, L., et al. (2013). Cocoa Polyphenols Prevent Inflammation in the Colon of Azoxymethane-Treated Rats and in TNF- α -Stimulated Caco-2 Cells. *Br. J. Nutr.* 110 (2), 206–215. doi:10.1017/s0007114512004862
- Ruiz Castro, P. A., Kogel, U., Lo Sasso, G., Phillips, B. W., Sewer, A., Titz, B., et al. (2020). Anatabine Ameliorates Intestinal Inflammation and Reduces the Production of Pro-inflammatory Factors in a Dextran Sulfate Sodium Mouse Model of Colitis. *J. Inflamm.* 17 (1), 29. doi:10.1186/s12950-020-00260-6
- Saitoh, F., Noma, M., and Kawashima, N. (1985). The Alkaloid Contents of Sixty Nicotiana Species. *Phytochemistry* 24 (3), 477–480. doi:10.1016/S0031-9422(00)80751-7
- Sambuy, Y., De Angelis, I., Ranaldi, G., Scarino, M. L., Stamatii, A., and Zucco, F. (2005). The Caco-2 Cell Line as a Model of the Intestinal Barrier: Influence of Cell and Culture-Related Factors on Caco-2 Cell Functional Characteristics. *Cell Biol Toxicol* 21 (1), 1–26. doi:10.1007/s10565-005-0085-6
- Schenk, M., and Mueller, C. (2008). The Mucosal Immune System at the Gastrointestinal Barrier. *Best Pract. Res. Clin. Gastroenterol.* 22 (3), 391–409. doi:10.1016/j.bpg.2007.11.002
- Susewind, J., de Souza Carvalho-Wodarz, C., Repnik, U., Collnot, E.-M., Schneider-Daum, N., Griffiths, G. W., et al. (2016). A 3D Co-culture of Three Human Cell Lines to Model the Inflamed Intestinal Mucosa for Safety Testing of Nanomaterials. *Nanotoxicology* 10 (1), 1–10. doi:10.3109/17435390.2015.1008065
- Tilg, H., and Moschen, A. R. (2015). Food, Immunity, and the Microbiome. *Gastroenterology* 148 (6), 1107–1119. doi:10.1053/j.gastro.2014.12.036
- Ulloa, L. (2005). The Vagus Nerve and the Nicotinic Anti-inflammatory Pathway. *Nat. Rev. Drug Discov.* 4 (8), 673–684. doi:10.1038/nrd1797
- Verschuere, S., De Smet, R., Allais, L., and Cuvelier, C. A. (2012). The Effect of Smoking on Intestinal Inflammation: What Can Be Learned from Animal Models? *J. Crohn's Colitis* 6 (1), 1–12. doi:10.1016/j.crohns.2011.09.006
- Vitale, S., Picascia, S., and Gianfrani, C. (2016). The Cross-Talk between Enterocytes and Intraepithelial Lymphocytes. *Mol. Cell Pediatr* 3 (1), 20. doi:10.1186/s40348-016-0048-4
- Wang, H., Yu, M., Ochani, M., Amella, C. A., Tanovic, M., Susarla, S., et al. (2003). Nicotinic Acetylcholine Receptor $\alpha 7$ Subunit Is an Essential Regulator of Inflammation. *Nature* 421 (6921), 384. doi:10.1038/nature01339
- Weglarz, L., Wawarczyk, J., Orchel, A., Jaworska-Kik, M., and Dzierzewicz, Z. (2007). Phytic Acid Modulates In Vitro IL-8 and IL-6 Release from Colonic Epithelial Cells Stimulated with LPS and IL-1 β . *Dig. Dis. Sci.* 52 (1), 93–102. doi:10.1007/s10620-006-9320-0
- Wu, X., Guo, Y., Min, X., Pei, L., and Chen, X. (2018). Neferine, a Bisbenzylisoquinoline Alkaloid, Ameliorates Dextran Sulfate Sodium-Induced Ulcerative Colitis. *Am. J. Chin. Med.* 46 (6), 1263–1279. doi:10.1142/s0192415x18500660
- Zabrodski, P. F., Gromov, M. S., and Maslyakov, V. V. (2015). Effect of $\alpha 7$ -n-Acetylcholine Receptor Activation and Antibodies to TNF- α on Mortality of Mice and Concentration of Proinflammatory Cytokines during Early Stage of Sepsis. *Bull. Exp. Biol. Med.* 159 (6), 740–742. doi:10.1007/s10517-015-3063-x
- Zanetti, F., Sewer, A., Scotti, E., Titz, B., Schlage, W. K., Leroy, P., et al. (2018). Assessment of the Impact of Aerosol from a Potential Modified Risk Tobacco Product Compared with Cigarette Smoke on Human Organotypic Oral Epithelial Cultures under Different Exposure Regimens. *Food Chem. Toxicol.* 115, 148–169. doi:10.1016/j.fct.2018.02.062
- Zhang, L.-C., Wang, Y., Tong, L.-C., Sun, S., Liu, W.-Y., Zhang, S., et al. (2017). Berberine Alleviates Dextran Sodium Sulfate-Induced Colitis by Improving Intestinal Barrier Function and Reducing Inflammation and Oxidative Stress. *Exp. Ther. Med.* 13 (6), 3374–3382. doi:10.3892/etm.2017.4402
- Zhang, X.-J., Yuan, Z.-W., Qu, C., Yu, X.-T., Huang, T., Chen, P. V., et al. (2018). Palmatine Ameliorated Murine Colitis by Suppressing Tryptophan Metabolism and Regulating Gut Microbiota. *Pharmacol. Res.* 137, 34–46. doi:10.1016/j.phrs.2018.09.010

Conflict of Interest: All authors are employees of Philip Morris International R&D or had worked for Philip Morris International R&D under contractual agreements.

Copyright © 2021 Marescotti, Lo Sasso, Guerrera, Renggli, Ruiz Castro, Piault, Jaquet, Moine, Luetlich, Frentzel, Peitsch and Hoeng. This is an open-access article distributed under the terms of the Creative Commons Attribution License (CC BY). The use, distribution or reproduction in other forums is permitted, provided the original author(s) and the copyright owner(s) are credited and that the original publication in this journal is cited, in accordance with accepted academic practice. No use, distribution or reproduction is permitted which does not comply with these terms.



Xiao-Yin-Fang Therapy Alleviates Psoriasis-like Skin Inflammation Through Suppressing $\gamma\delta$ T17 Cell Polarization

OPEN ACCESS

Edited by:

Xiao Bin Zeng,
Jinan University, China

Reviewed by:

Jingxia Zhao,
Capital Medical University, China
Yuchao Chen,
Guangdong Provincial Hospital of
Chinese Medicine, China
Jingwen Deng,
Guangdong Provincial Hospital of
Chinese Medicine, China
Erle Dang,
Fourth Military Medical University,
China

*Correspondence:

Jun Gu
gujun79@163.com
Yuling Shi
shiyuling1973@tongji.edu.cn
Yangfeng Ding
dingyangfeng@hotmail.com

[†]These authors have contributed
equally to this work

Specialty section:

This article was submitted to
Ethnopharmacology,
a section of the journal
Frontiers in Pharmacology

Received: 15 November 2020

Accepted: 30 March 2021

Published: 16 April 2021

Citation:

Zhang X, Li X, Chen Y, Li B, Guo C,
Xu P, Yu Z, Ding Y, Shi Y and Gu J
(2021) Xiao-Yin-Fang Therapy
Alleviates Psoriasis-like Skin
Inflammation Through Suppressing
 $\gamma\delta$ T17 Cell Polarization.
Front. Pharmacol. 12:629513.
doi: 10.3389/fphar.2021.629513

Xilin Zhang^{1,2,3†}, Xiaorui Li^{4†}, Youdong Chen^{2,5†}, Bingjie Li^{1,2}, Chunyuan Guo^{1,2}, Peng Xu^{2,5}, Zengyang Yu^{1,2}, Yangfeng Ding^{1,2*}, Yuling Shi^{1,2*} and Jun Gu^{1,2,3,5*}

¹Department of Dermatology, Shanghai Skin Disease Hospital, School of Medicine, Tongji University, Shanghai, China, ²Institute of Psoriasis, School of Medicine, Tongji University, Shanghai, China, ³Department of Dermatology, Changhai Hospital, Second Military Medical University, Shanghai, China, ⁴Department of Dermatology, Longhua Hospital, Shanghai University of Traditional Chinese Medicine, Shanghai, China, ⁵Department of Dermatology, Shanghai Tenth People's Hospital, School of Medicine, Tongji University, Shanghai, China

Psoriasis is an immune-mediated chronic inflammatory skin disease primarily mediated by the activation of interleukin (IL)-17-producing T cells. Traditional Chinese Medicine (TCM) represents one of the most effective complementary and alternative medicine (CAM) agents for psoriasis, which provides treasured sources for the development of anti-psoriasis medications. Xiao-Yin-Fang (XYF) is an empirically developed TCM formula that has been used to treat psoriasis patients in Shanghai Changhai Hospital for over three decades. Imiquimod (IMQ)-induced psoriasis-like dermatitis mouse model was utilized to investigate the therapeutic effects of XYF by the assessment of disease severity and skin thickness. Flow cytometric assay was performed to explore the influence of XYF on skin-related immunocytes, primarily T cells. And, RNA sequencing analysis was employed to determine the alternation in gene expression upon XYF therapy. We discovered that XYF alleviated psoriasis-like skin inflammation mainly through suppressing dermal and draining lymph-node IL-17-producing $\gamma\delta$ T ($\gamma\delta$ T17) cell polarization. Moreover, XYF therapy ameliorated the relapse of psoriasis-like dermatitis and prohibited dermal $\gamma\delta$ T cell reactivation. Transcriptional analysis suggested that XYF might regulate various inflammatory signaling pathways and metabolic processes. In conclusion, our results clarified the therapeutic efficacy and inner mechanism of XYF therapy in psoriasis, which might promote its clinical application in psoriasis patients and facilitate the development of novel anti-psoriasis drugs based on the bioactive components of XYF.

Keywords: psoriasis, traditional Chinese medicine, Xiao-Yin-Fang therapy, $\gamma\delta$ T cells, interleukin-17, relapse

Abbreviations: CAM, complementary and alternative medicine; DC, dendritic cells; ddH₂O, double-distilled H₂O; DEG, differentially expressed genes; FC, fold change; GSEA, gene set enrichment analysis; GTW, multi-glycoside of Tripterygium wilfordii Hook. f.; H&E, hematoxylin-eosin; IL, interleukin; $\gamma\delta$ T17, IL-17-producing $\gamma\delta$ T cells; IMQ, imiquimod; IS, intensity score; KEGG, kyoto encyclopedia of genes and genomes; LN, lymph nodes; PASI, psoriasis area and severity index; PMA, phorbol-12-myristate-13-acetate; PS, proportion score; SEM, standard error of mean; SPF, specific pathogen-free; Tc17, T cytotoxic 17 cells; Th17, T helper 17 cells; TCM, traditional chinese medicine; UPLC-Q/TOF-MS, Ultra-high performance liquid chromatography with quadrupole time-of-flight mass spectrometry, VAS, vaseline; XYF, Xiao-Yin-Fang.

INTRODUCTION

Psoriasis is a common, recurrent inflammatory skin disease, which can be triggered in genetically susceptible individuals by diverse etiological factors, including infection, stress, trauma, medication, tobacco, and alcohol consumption (Schleicher, 2016). Men and women are evenly affected at all ages with an estimated prevalence of psoriasis in adults and children ranging between 0.51 to 11.43% and 0–1.37%, respectively, (Michalek et al., 2017). Psoriasis and its associated comorbidities massively influence the physical and mental health of psoriasis patients, which bring about heavy socioeconomic burdens (Pilon et al., 2019).

Psoriasis is clinically characterized by erythematous plaques covered with lamellar silver scales, which pathological features involve abnormal keratinocyte proliferation and immune cell infiltration. The interplay between T lymphocytes, dendritic cells (DC) and keratinocytes, forming a self-perpetuating loop to amplify cutaneous inflammation, has been well described in psoriasis formation (Diani et al., 2015). During the process, the activation of interleukin (IL)-17-producing T cells, mainly including T helper 17 (Th17) cells and IL-17-producing $\gamma\delta$ T ($\gamma\delta$ T17) cells, play an essential role in the pathogenesis of psoriasis (Cai et al., 2013; Casciano et al., 2018).

The management of psoriasis comprises a variety of local and systemic therapies, involving phototherapy, retinoids, corticosteroids, vitamin D3 analogues, immunosuppressants, and recently emerged biologics targeting inflammatory factors, especially IL-17 (Kim and Krueger, 2017). Nevertheless, anti-psoriasis treatments are inevitably accompanied by adverse effects, such as irritation, skin atrophy, impaired hematopoiesis, visceral dysfunction and compromised immune function (Rapalli et al., 2018). A recent survey discovered that around half of the patients treated with oral therapy or biologics discontinued medication due to lack or loss of efficacy, tolerability reasons and safety issues, which signified that treatment dissatisfaction hindered the optimal care of psoriasis patients (Lebwohl et al., 2014). Hence, there is an urgent need to develop novel strategies and medicines for psoriasis management.

Complementary and alternative medicine (CAM) represents a group of various medical systems, practices, and products beyond conventional Western medication. Up to 62% of patients with psoriasis replaced or supplemented conventional therapies with CAM owing to their fewer side effects (Magin et al., 2006; Damevska et al., 2014; Murphy et al., 2019). The commonly utilized CAM for psoriasis includes Traditional Chinese Medicine (TCM), botanical therapy, vitamin supplement, dietary change, and behavioral intervention. Despite limited published evidence, TCM appeared to be the most effective CAM agent (Farahnik et al., 2017). TCM generally exploits topical or oral formulations, which are the mixtures of herbal, animal and/or mineral substances, and physical therapeutics, primarily including acupuncture and massage. Psoriasis was firstly recorded in the Treatise on the Causes and Manifestations of Diseases of Chinese Sui dynasty (581–618 CE) and has been efficaciously handled with TCM in China for over a thousand years. Therefore, TCM provides treasured sources for the development of anti-psoriasis medications.

Xiao-Yin-Fang (XYF), which is composed of *Isatis tinctoria* L., *Scutellaria baicalensis* Georgi, *Salvia miltiorrhiza* Bunge, *Sophora*

TABLE 1 | Constituents of Xiao-Yin-Fang (XYF).

Herb	Taxonomic nomenclature	Used parts	Weight (g)
Banlangen	<i>Isatis tinctoria</i> L.	Root	30
Huangqin	<i>Scutellaria baicalensis</i> Georgi	Root	15
Danshen	<i>Salvia miltiorrhiza</i> Bunge	Root	30
Kushen	<i>Sophora flavescens</i> Aiton	Root	10
Dahuang	<i>Rheum officinale</i> Baill.	Root	3

flavescens Aiton, and *Rheum officinale* Baill., represents an empirically developed formula that originates from Doctor Ming Chen and Doctor Jun Gu. XYF has been prescribed to treat psoriasis patients for over three decades in Shanghai Changhai Hospital, which therapeutic efficacy has been proven by clinical research (Zhang et al., 2008; Wang et al., 2012b). Our previous research has shown that XYF decoction combined with calcipotriol ointment repressed peripheral T cell secretion of IL-17 in patients with psoriasis (Wang et al., 2012a). However, the pharmacological effect and underlying mechanism of XYF in the treatment of psoriasis remained unclear.

In this study, we utilized imiquimod (IMQ)-induced psoriasis-like dermatitis mouse model to explore the therapeutic effect of XYF and its impact on the immune functions of conventional Th and $\gamma\delta$ T cells. We discovered that XYF alleviated psoriasis-like skin inflammation mainly through suppressing dermal and draining lymph-node (LN) $\gamma\delta$ T17 cell polarization. Moreover, XYF therapy ameliorated the relapse of psoriasis-like dermatitis and prohibited dermal $\gamma\delta$ T cell reactivation.

MATERIALS AND METHODS

Mice

C57BL/6J mice were purchased from LINGCHANG Biotech (Shanghai, China), which were bred and maintained in specific pathogen-free (SPF) units with controlled temperature ($22 \pm 2^\circ\text{C}$), relative humidity ($50 \pm 5\%$), artificial light (12 h light/dark cycle) and free access to food/water in the animal facilities of Tongji University, Shanghai, China. Age-matched male mice (6–8 weeks of age; 18–22 g) were randomly used for all experiments in a non-blind manner. Handling of mice and experimental procedures were approved by the Animal Care and Use Committee of Shanghai Tongji University.

Preparation of Xiao-Yin-Fang

Xiao-Yin-Fang (XYF) is an empirically developed Chinese medicine formula summarized and optimized by Chinese famous dermatologists Doctor Ming Chen and Doctor Jun Gu, which has been used to treat psoriasis in Shanghai Changhai Hospital. Its formula primarily includes five Chinese herbs: *Isatis tinctoria* L., *Scutellaria baicalensis* Georgi, *Salvia miltiorrhiza* Bunge, *Sophora flavescens* Aiton, and *Rheum officinale* Baill. with a weight ratio of 30:15:30:10:3 (Table 1). The standardized powder of each herb, which was extracted under optimum condition and corresponded to a standard dosage of raw herb, was purchased from LongHua Hospital, University of

Traditional Chinese Medicine, Shanghai, China. Voucher specimen of herb powder was deposited in Shanghai Skin Disease Hospital with reference No. XYF01-05, respectively. XYF powder was dissolved in double-distilled H₂O, filtered through a 0.45 μ m filter and stored at -20°C for subsequent application. All the procedures were in accordance with the rules and regulations of the 2015 Edition of China Pharmacopoeia.

Qualitative and Quantitative Analysis of Xiao-Yin-Fang by UPLC-Q/TOF-MS

Chemical profiling of XYF was performed on an Agilent 1290 UPLC System (Agilent Technologies Co., Santa Clara, CA, United States) coupled with AB SCIEX Triple TOF 4600[®] quadrupole time-of-flight mass spectrometry (AB SCIEX, Foster City, CA, United States). Chromatographic separation was conducted on an Acquity UPLC[®] HSS T3 Column (2.1 \times 100 mm i.d., 1.8 μ m; Waters, Milford, MA, United States) at 30°C , using a mixed mobile phase consisting of 0.1 formic acid in water (mobile phase A) and 0.1 formic acid in acetonitrile (mobile phase B). The gradient elution program was used as follows: 0–5 min, 0–0% B; 5–7 min, 0–3% B; 7–15 min, 3–5% B; 15–17 min, 5–16% B; 17–19 min, 16–17% B; 19–30 min, 17% B; 30–34 min, 17–20% B; 34–42 min, 20% B; 42–44 min, 20–22% B; 44–49 min, 22% B; 49–54 min, 22–60% B; 54–58 min, 60–95% B; 58–60 min, 95% B; 60–60.1 min, 95–0% B; 60.1–63 min, 0% B. The flow rate was 0.3 ml/min, and the sample injection volume was 1 μ l. Data acquisition was performed on AB SCIEX Triple TOF 4600[®] system equipped with an electrospray ionization (ESI) source in the negative and positive ion modes. The mass spectrometry was operated in full-scan TOF-MS (m/z 50–1700) and information-dependent acquisition (IDA) MS/MS modes. The parameters of mass spectrometry were as follows: ion source gas 1 and 2 were 50 psi; curtain gas was 35 psi; ion source temperature was 500°C ; ion spray voltage floating was 5000 V (positive)/4500 V (negative). In the tandem mass spectrometry (MS/MS) experiments, mass range was 50–1250, collision energy was 40 ± 20 eV, ion release delay was 30 ms and ion release width was 15 ms. All data acquisition and processing were validated using Analyst TF 1.7.1 software (AB SCIEX).

For content determination, seven standards of representative components from five constitutive herbs of XYF, including (R, S)-goitrin (#8508), baicalin (#5719), salvianolic acid B (#4065), tanshinone II a (#7503), matrine (#844), oxymatrine (#8678), and emodin (#8171), were purchased from Standard Technology Co., Shanghai, China (<http://www.nature-standard.com/>). Quantitative analysis of these components in XYF by UPLC-DAD was performed on a Waters H-Class UPLC system (Waters, Milford, MA, United States) as previously reported (Xiang et al., 2018). UV detector was monitored at 225 nm (matrine/oxymatrine), 245 nm ((R, S)-goitrin), 254 nm (emodin), 270 nm (tanshinone II a), 280 nm (baicalin) and 286 nm (salvianolic acid B).

Imiquimod-Induced Psoriasis-like Skin Inflammation

Mice received a daily topical dose of 50 mg of imiquimod (IMQ) cream (5%; #H20030128, Sichuan Med-Shine Pharmaceutical) or

control Vaseline (VAS; #180102, Shandong Mint) on shaved back (an approximate size of $2 \times 3 \text{ cm}^2$) or bilateral ears for five consecutive days. For the induction of disease relapse, 25 mg of IMQ was applied on mouse left ear once daily from day 0 to day 4, and 25 mg of IMQ was reapplied on mouse right ear once daily from day 12 to day 16. Mouse skin inflammation was evaluated by cumulative psoriasis area and severity index (PASI) score, calculated by the adding up of erythema score (0–4), infiltration score (0–4), and desquamation score (0–4). The severity of each symptom was assessed comparing with reference pictures. Skin thickness was recorded as the average value of three measurements by vernier calipers at the center of mouse dorsal or ear lesion before topical treatment.

Experiment Design and Drug Administration

Mice were randomly allocated into the following groups: control group, model group, low-dose XYF group, medium-dose XYF group, high-dose XYF group, and multi-glycoside of *Tripterygium wilfordii* Hook. f (GTW) group. GTW tablets (#Z42021212, Hubei Huangshi Yunfei Pharmaceutical Company) were ground down and dissolved in ddH₂O, which were filtered and stored at -20°C . Based on drug-dose conversion between human and mouse, 200 μ l of XYF decoction (low-dose: 5.8 mg/g; medium-dose: 11.6 mg/g; high-dose: 23.3 mg/g), GTW (7.89 μ g/g) or ddH₂O was administered once daily by gavage for 10 successive days, and VAS or IMQ was topically applied from day 6 to day 10.

Immunohistochemical Analysis

Paraffin-embedded skin specimens were prepared by routine methods, and the sections were stained by hematoxylin-eosin (H&E) with additional immunostaining for Ki-67. The sections were deparaffinized with xylene and rehydrated through the incubation with graded alcohol into water. For H&E staining, the sections were then stained with hematoxylin, washed with PBS, differentiated with hydrochloric acid ethanol, and stained with eosin. Pathological change was examined under the Olympus CX33/BX53 optical microscope (Olympus, Southborough, MA, United States). Epidermal hyperplasia (acanthosis) was measured as the average length between the basement membrane and the stratum corneum. Papillomatosis index is the ratio of the length of the dermal-epidermal junction to the surface length of the epidermis. For Ki-67 staining, heat-induced epitope retrieval was performed in EDTA buffer (#RC016, RecordBio) at pH 8.3% hydrogen peroxide was utilized to block endogenous peroxidase activity. The sections were then incubated with anti-Ki-67 antibody (#ab16667, Abcam) overnight at 4°C , followed by incubation with REAL EnVision and visualized by DAB⁺ (#K5007, DAKO). Ki-67 staining was evaluated semi-quantitatively according to the expression level of cytoplasmic brown staining in five random epidermal fields under 400x magnification performed independently by two researchers. The intensity of staining (IS, intensity score) was assessed as: absent (0), weak (1), moderate (2), and strong (3). The percentage of stained cells (PS, proportion score) was scored: 0–5% (0), 6–25% (1), 26–50% (2), 51–75% (3), and 75–100% (4). H-score was computed as the

average value of the multiplication of IS and PS and interpreted by the following way: 0 as negative staining, 1 to 4 as weak positive staining, 5 to 8 as medium positive staining and 9 to 12 as strong positive staining.

Enzyme-Linked Immunosorbent Assay

IL-17 levels in the serum samples collected from experimental mice were measured using mouse IL-17A ELISA kit (RayBio, Norcross, GA, United States) according to the manufacturers' instructions.

Dermal Single-Cell Suspension Preparation

Mouse ears were harvested and incubated in dispase II (5 mg/ml; #D4693, Sigma) for 1 h at 37°C. Dermal sheet was peeled from epidermal sheet, cut into little pieces, and digested at 37°C in DMEM (#SH30022.01, Hyclone) containing collagenase IV (1 mg/ml; #SH30256.01B, Hyclone) and DNase (0.015 mg/ml; #B002004, Diamond) for one and a half hour. Dermal single-cell suspension was harvested by passing through a 40 μ m cell strainer (#CSS-010-040, Biofil).

In Vitro PMA and Ionomycin Activation Assay

T cell culture medium was RPMI 1640 (#11875119, Gibco) supplemented with heat-inactivated fetal bovine serum (10%; #SH30084.03, Hyclone), penicillin G (100U/ml; #B540733, Sangon), streptomycin sulfate (100 μ g/ml; #B540733, Sangon) and amphotericin B (2.5 μ g/ml; #B540733, Sangon). Mouse skin-draining axillary, brachial and inguinal lymph nodes (LN) were harvested. LN single-cell suspensions were prepared through grinding by glass slides and filtering through a 40 μ m cell strainer. LN and dermal cells were cultured in T cell culture medium in the presence of phorbol-12-myristate-13-acetate (PMA; 50 ng/ml; #P1585, Sigma), ionomycin (1mM; #abs42019871, Absin) and brefeldin A (1:1000; #347688, BD) for 4 h.

Flow Cytometric Analysis

Single-cell suspensions were preincubated with anti-CD16/CD32 antibodies (Ab; clone 2.4G2; #553141, BD Biosciences) for 15 min at 4°C. To discriminate viable cells from dead cells, cells were stained with fixable viability stain (#564406, BD Biosciences) for 10 min at room temperature. For the analysis of surface markers, cells were stained with anti-CD3 Ab (clone 145-2C1; #553061, BD Biosciences), anti-CD4 Ab (clone GK1.5; #562891, BD Biosciences), anti-CD25 Ab (clone 3C7; #101904, Biolegend), anti-CD45 Ab (clone 30-F11; #103134, Biolegend), anti-CD11b Ab (clone M1/70; #553310/#564455, BD Biosciences), anti-TCR β Ab (clone H57-597; #560657, BD Biosciences), anti- $\gamma\delta$ TCR Ab (clone GL3; #118115, Biolegend), anti-MHC-II Ab (clone M5/114.15.2; #563414, BD Biosciences), anti-F4/80 Ab (clone T45-2342; #565410, BD Biosciences), anti-CD11c Ab (clone HL3; #566505, BD Biosciences), anti-Ly6C Ab (clone AL-21; #553104, BD Biosciences), and anti-Ly6G Ab (clone 1A8; #560599, BD Biosciences) for 30 min at 4°C protected from light. For cytoplasmic staining, cells were fixed and permeabilized with

BD Cytofix/Cytoperm (#51-2090KZ, BD Biosciences) and were stained with anti-mouse IFN- γ Ab (clone XMG1.2; #505810, Biolegend), anti-mouse IL-4 Ab (clone 11B11; #560699, BD Biosciences), anti-mouse IL-17 Ab (clone TC11-18H10; #559502, BD Biosciences) and incubated for 30 min at 4°C. For intranuclear staining, cells were fixed and permeabilized with Foxp3/Transcription Factor Fixation/Permeabilization Concentrate and Diluent (#00-5521-00, eBioscience), and were then stained with anti-mouse Foxp3 Ab (clone MF-14; #126408, Biolegend), anti-Ki-67 Ab (clone B56; #556027, BD Biosciences) and anti-ROR- γ t Ab (clone Q31-378; #564723, BD Biosciences). For Annexin-V staining, cells were resuspended in 1x annexin-binding buffer (#556454, BD Biosciences) and stained with Annexin-V (#640908, Biolegend) for 15 min at room temperature. Finally, cells were assayed with BD LSRFortessa Cytometer, and analyzed with FlowJo software (Treestar). Gate strategy of LN CD4⁺ T cells, LN $\gamma\delta$ T cells, dermal neutrophils, dermal inflammatory monocytes, dermal CD4⁺ T cells, and dermal $\gamma\delta$ T cells were demonstrated in **Supplementary Figure S3**.

RNA Sequencing Analysis

Total RNA samples were prepared from intact epidermal or dermal ear sheets of mouse ear skin from two mice. Double-strand cDNA was generated from equal amounts of total RNA by following TruSeq8 RNA Library Prep Kit v2 (#RS-122-2001/2002, Illumina). The cDNA libraries were sequenced using Illumina Hi-seq2500. STAR software was utilized for sequence alignment between the preprocessing sequence and reference genome sequence of mice downloaded from the Ensembl database (Mus_musculus.GRCm38.90, ftp://ftp.ensembl.org/pub/release-90/gtf/mus_musculus/Mus_musculus.GRCm38.90.chr.gtf.gz). Transcript assembly of mRNA sequencing data was performed by StringTie software. DESeq 2 was applied to conduct the analysis of differentially expressed genes (DEG). The cutoffs of DEG were determined as the adjusted *P* value ≤ 0.05 and the $|\log_2FC| \geq 1$. Functional annotations of the DEGs were conducted using Kyoto Encyclopedia of Genes and Genomes (KEGG) pathways analysis and Gene Set Enrichment Analysis (GSEA).

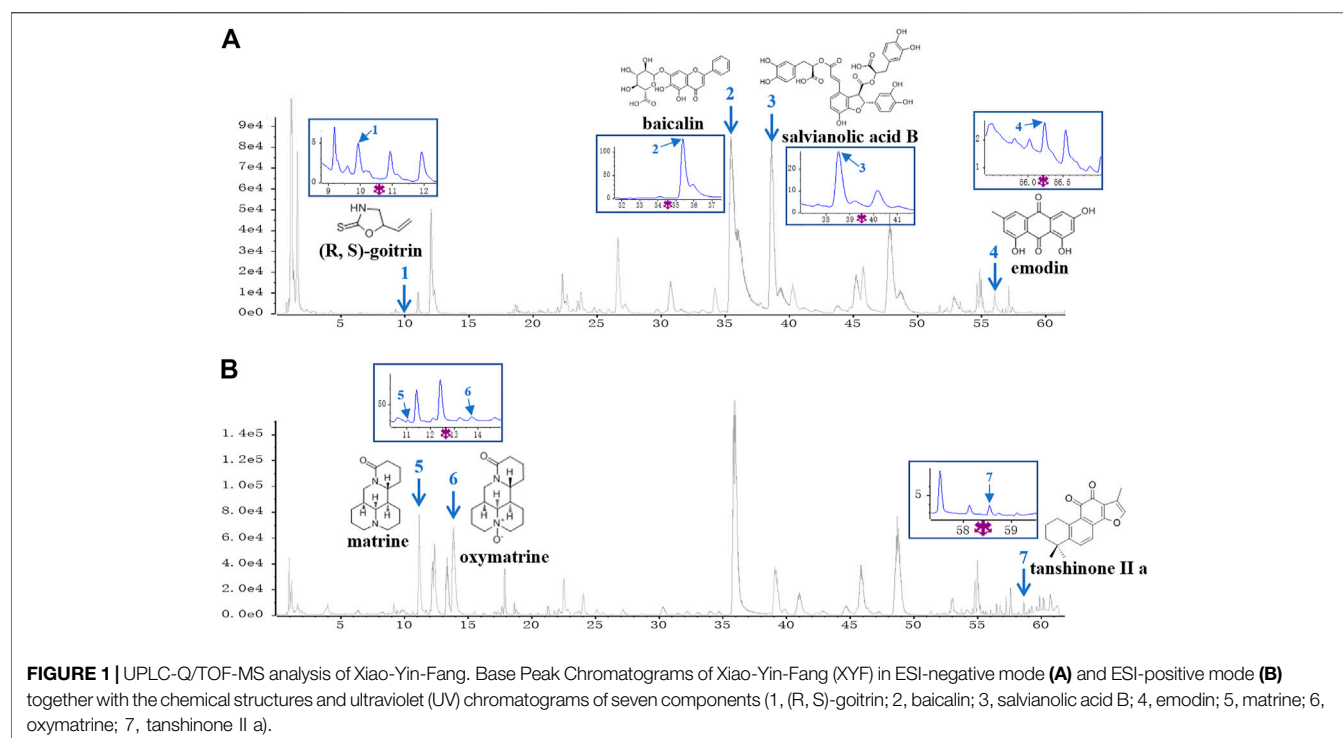
Statistical Analysis

GraphPad Prism 6.0 software was utilized for statistical analysis. Student's t-test or one-way ANOVA were utilized to analyze the differences between the groups following Gaussian distributions with homogeneity of variance. Data that did not follow Gaussian distributions were analyzed using the Kruskal-Wallis test. Differences were statistically significant when *P* < 0.05.

RESULTS

UPLC-Q/TOF-MS Analysis of Xiao-Yin-Fang

A UPLC-Q/TOF-MS method in both negative and positive ion modes was employed to rapidly characterize the major constituents in XYF. A total of 57 compounds were unambiguously or tentatively characterized by comparing their retention times and MS data with reference standards or with



data reported in the literature (**Supplementary Figure S1**). These compounds were all derived from five medicinal materials that composed XYF, and did not contain any conventional immunosuppressants. Seven representative chemical compounds were chosen as chemical markers and quantified to evaluate the quality of relevant medicinal materials, including (R, S)-goitrin (1, Rt 9.928 min), baicalin (2, Rt 35.44 min), salvianolic acid B (3, Rt 38.63 min), tanshinone II a (7, Rt 58.63 min), matrine (5, Rt 11.03 min), oxymatrine (6, Rt 13.75 min), and emodin (4, Rt 56.12 min) (**Figure 1**). Quantitative determination of these seven compounds by UPLC-DAD was performed on a Waters H-Class UPLC system at different wavelengths. As a result, the contents of these seven compounds in XYF were 0.132 mg/g, 12.626 mg/g, 6.154 mg/g, 0.014 mg/g, 2.514 mg/g, 1.757 mg/g, and 0.007 mg/g, respectively.

Xiao-Yin-Fang Alleviates Imiquimod-Induced Psoriasis-like Skin Inflammation

To explore the potential mechanism of XYF in psoriasis, we utilized IMQ-induced psoriasis-like dermatitis mouse model. Mice were divided into six groups and treated as depicted in **Figure 2A**. Multi-glycoside of *Tripterygium wilfordii* Hook. f (GTW), also termed as Tripterygium glycosides, is a widely acknowledged efficacious psoriasis-treating TCM agent and has been proven to ameliorate murine psoriasis-like dermatitis, which was therefore chosen as positive drug in our study (Han et al., 2012; Wu et al., 2015a; Zhao et al., 2016; Lv et al., 2018;

Nguyen et al., 2020a; Ru et al., 2020). As modeling with IMQ generated skin lesions resembling human plaque psoriasis, mice pretreated with XYF displayed lighter erythema, smoother skin, and thinner scales than mice treated with IMQ alone (**Figure 2B**). Moreover, XYF exerted therapeutic effects in a dose-dependent manner that high-dose XYF was as potent as GTW in alleviating psoriasis-like dermatitis (**Figure 2B**). These findings were verified by the evaluation of PASI score (**Figure 2C**) and back skin thickness (**Figure 2D**). Besides, the application of XYF did not cause any behavioral abnormality or extra weight loss in mice (**Figure 2E**). Subcutaneous vessel dilation was also less prominent in the mice from high-dose XYF group than model group (**Supplementary Figure S2**). In accordance, the histological examination showed that both high-dose XYF and GTW significantly reduced epidermal acanthosis and elevated papillomatosis index in an equal manner (**Figures 2F–H**). As the expression of Ki-67 in keratinocytes was upregulated in model mice, high-dose XYF group considerably decreased Ki-67⁺ H-score to a similar degree as GTW (**Figures 2I,J**). Overall, XYF therapy substantially alleviated IMQ-induced psoriasis-like skin inflammation when administered at the high dosage, which demonstrated a comparable efficacy as GTW. Therefore, high-dose XYF was employed in the following study.

Xiao-Yin-Fang Prevents Lymphnode $\gamma\delta$ T Cell Secretion of IL-17

Since T lymphocytes play a vital role in the pathogenesis of psoriasis, we next sought to investigate the impact of XYF on T cell subsets within skin-draining lymph nodes (LN). Compared with control mice, we detected a decreased ratio of LN CD4⁺

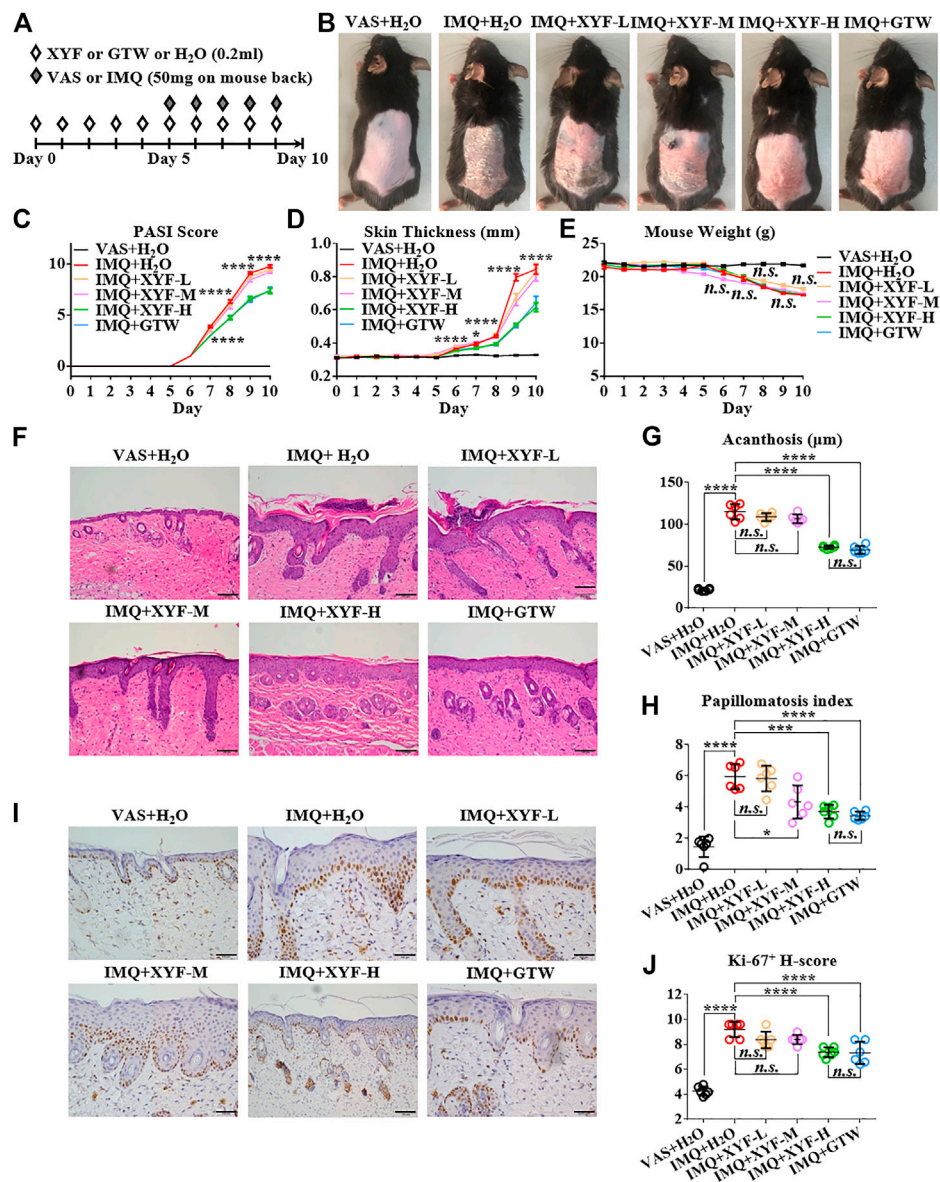


FIGURE 2 | High-dose Xiao-Yin-Fang alleviated imiquimod-induced psoriasis-like skin inflammation on mouse back. **(A)** Schematic of the experimental procedures. Mice were given different-dose Xiao-Yin-Fang (XYF), multi-glycoside of *Tripterygium wilfordii* Hook. f. (GTW) solution or distilled water (H₂O) by gavage twice daily from day 0 to day 9, and received imiquimod (IMQ) or Vaseline (VAS) application on shaved back skin once a day from day 5 to day 9. **(B)** Representative pictures of mouse skin lesions (XYF-L, low-dose XYF; XYF-M, medium-dose XYF; XYF-H, high-dose XYF). **(C–E)** Evaluation of PASI score **(C)**, skin thickness **(D)** and body weight **(E)** of mice. The statistic differences between IMQ + XYF-H group and IMQ + H₂O group were annotated ($n = 54$, three independent experiments). **(F)** H&E staining and calculated epidermal acanthosis **(G)** and papillomatosis index **(H)** (x200; bar = 100 μ m; $n = 36$, three independent experiments). **(I)** Ki-67 staining and assessment of its H-score of epidermal fields **(J)** (x200; bar = 100 μ m; $n = 36$, three independent experiments). The data were presented as mean \pm s.e.m.

T cells with greater IL-17 production in model mice (**Supplementary Figure S4A–D**). The proportion of regulatory T (Treg; CD25⁺Foxp3⁺) cells in CD4⁺ T cells was also increased (**Supplementary Figure S4E**). However, neither XYF nor GTW disturb the balance in Th and Treg cells (**Supplementary Figure S4**). While serum IL-17 levels were upregulated in model mice, the application of XYF reduced the serum contents of IL-17 (**Supplementary Figure S5**). Previous research demonstrated that $\gamma\delta$ T cells are the main source of IL-17 in psoriasis-like

dermatitis (Cai et al., 2011). Accordingly, the percentage and number of LN $\gamma\delta$ T cells were substantially elevated in model mice (**Figure 3A**), and their secretion of IL-17 was raised approximately threefold (**Figure 3B**). Although XYF failed to suppress the expansion of LN $\gamma\delta$ T cells (**Figure 3A**), it drastically hindered their polarization into $\gamma\delta$ T17 cells to a comparable extent as GTW (**Figure 3B**). Hence, XYF therapy might exert its anti-inflammatory role in psoriasis-like dermatitis mainly through its inhibition of $\gamma\delta$ T17 polarization.

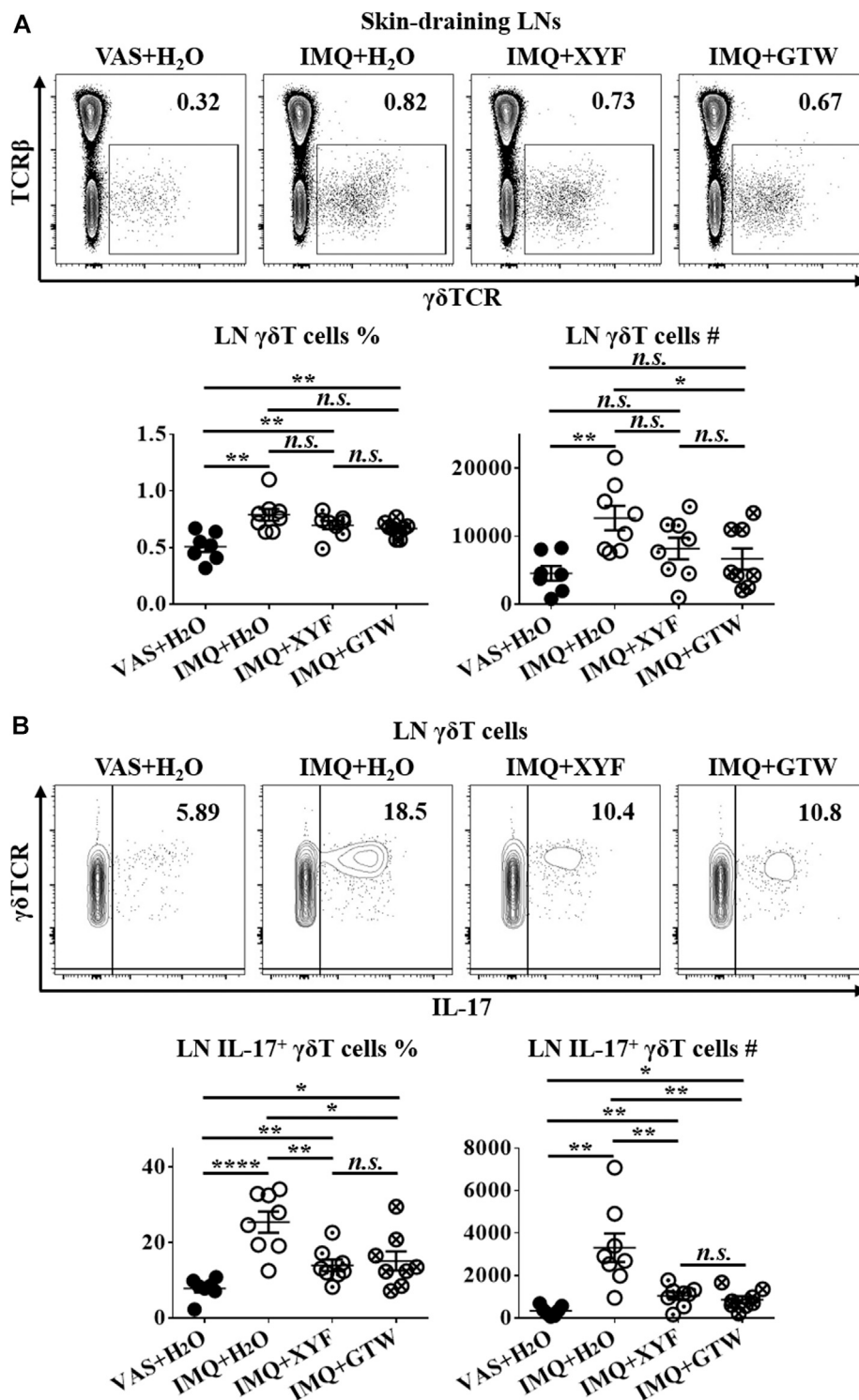


FIGURE 3 | Xiao-Yin-Fang therapy prevented lymphnode $\gamma\delta$ T cell secretion of IL-17. Mice were treated as in **Figure 2**. Skin-draining axillary, brachial and inguinal lymph nodes (LN) were harvested on day 10. Freshly isolated LN cells were *in vitro* cultured in the presence of PMA, ionomycin and Brefeldin A for 4 h. LN cells were then stained with anti-CD45, TCR β , $\gamma\delta$ TCR, CD11b, and IL-17 antibodies, which were analyzed by flow cytometry. Representative scatter plots, the ratios, and numbers of LN $\gamma\delta$ T cells (**A**) and IL-17⁺ $\gamma\delta$ T cells (**B**). $n = 31$, three independent experiments. The data were presented as mean \pm s.e.m.

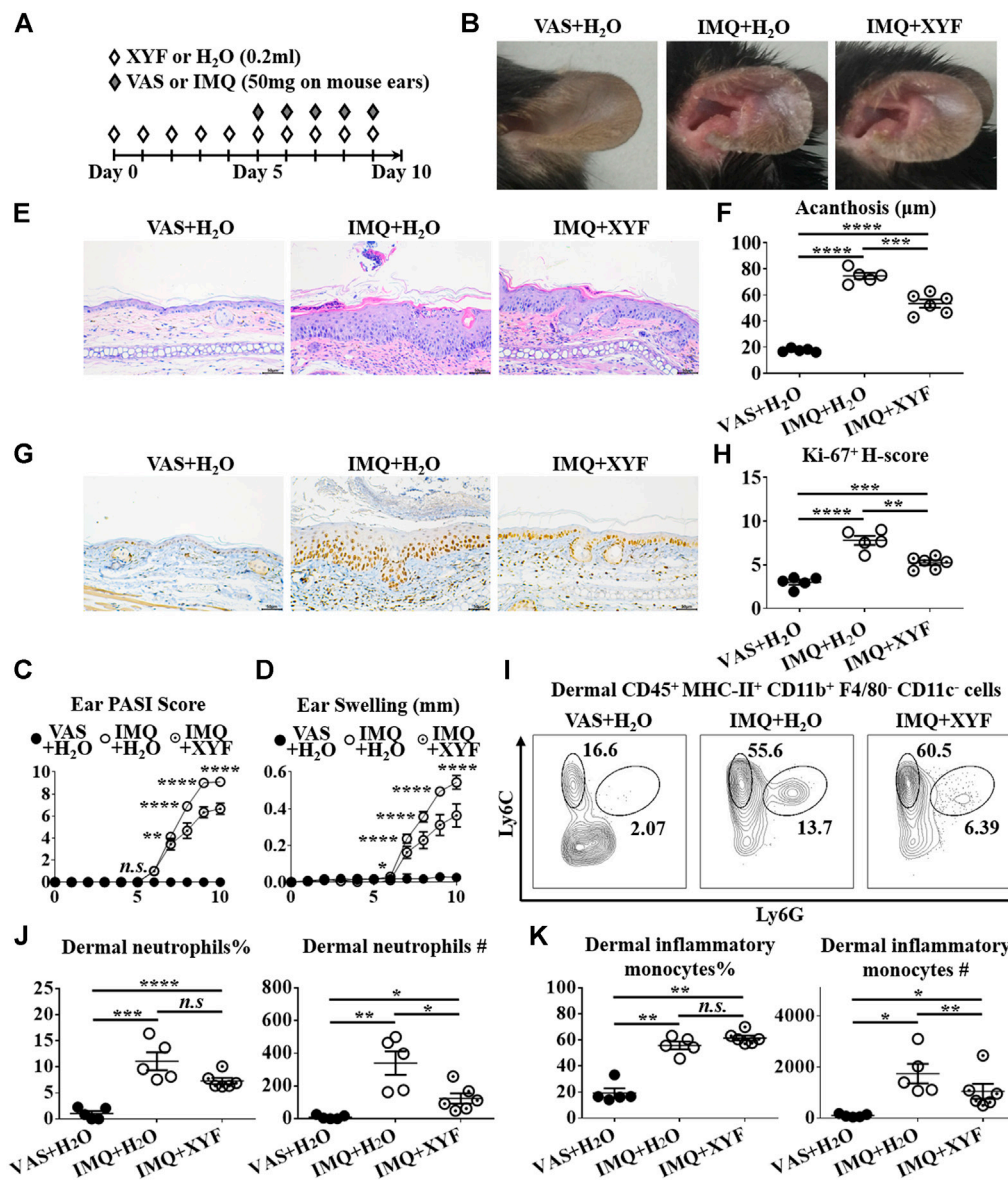


FIGURE 4 | Xiao-Yin-Fang lessened imiquimod-induced psoriasis-like dermatitis on mouse ears. **(A)** Schematic of the experimental procedures. Mice were given XYF or H₂O by gavage twice daily from day 0 to day 9, and received IMQ or VAS application on mouse ears once a day from day 5 to day 9 **(B)** Representative pictures of mouse ear lesions. **(C, D)** Evaluation of PASI score **(C)** and skin swelling **(D)** of mouse ears ($n = 27$, three independent experiments) **(E)** H&E staining and calculated epidermal acanthosis **(F)** ($\times 200$; bar = 50 μm ; $n = 18$, three independent experiments). **(G)** Ki-67 staining and assessment of its H-score of epidermal fields **(H)** ($\times 200$; bar = 50 μm ; $n = 18$, three independent experiments). **(I–K)** Freshly isolated dermal cells were obtained and stained with anti-CD45, MHC-II, CD11b, F4/80, CD11c, Ly6C, and Ly6G antibodies, which were analyzed by flow cytometry. **(I)** Representative scatter plots of dermal neutrophils and inflammatory monocytes. The ratios and cell numbers of dermal neutrophils **(J)** and inflammatory monocytes **(K)** ($n = 16$, three independent experiments). The data were presented as mean \pm s.e.m.

Xiao-Yin-Fang Suppresses Dermal $\gamma\delta$ T17 Cell Polarization

Given that skin-resident $\gamma\delta$ T cells elicited direct action in local inflammation, we established the model of psoriasis-like dermatitis on mouse ears to assess the role of dermal $\gamma\delta$ T cells in the curative effects of XYF (Figure 4A). As depicted in Figures 4B–H, XYF significantly reduced the disease severity of psoriasis-like dermatitis on mouse ears. While neutrophils (Ly6C⁺Ly6G⁺) and inflammatory monocytes (Ly6C⁺Ly6G[−]) gathered in the

dermis following IMQ application, XYF considerably lowered their cell numbers rather than their percentages (Figures 4I–K), corroborating the anti-psoriasis effect of XYF. In line with the findings of LNs, XYF did not affect the homeostasis and function of dermal conventional T cells (Supplementary Figure S6).

Previous studies have uncovered that dermal $\gamma\delta$ T cells were predominantly $\gamma\delta^{\text{int}}$ T cells with a minor population being $\gamma\delta^{\text{high}}$ T cells (Cai et al., 2011). And, dermal $\gamma\delta^{\text{int}}$ T cells were the main source of IL-17 in psoriasis-like dermatitis, whereas $\gamma\delta^{\text{high}}$ T cells

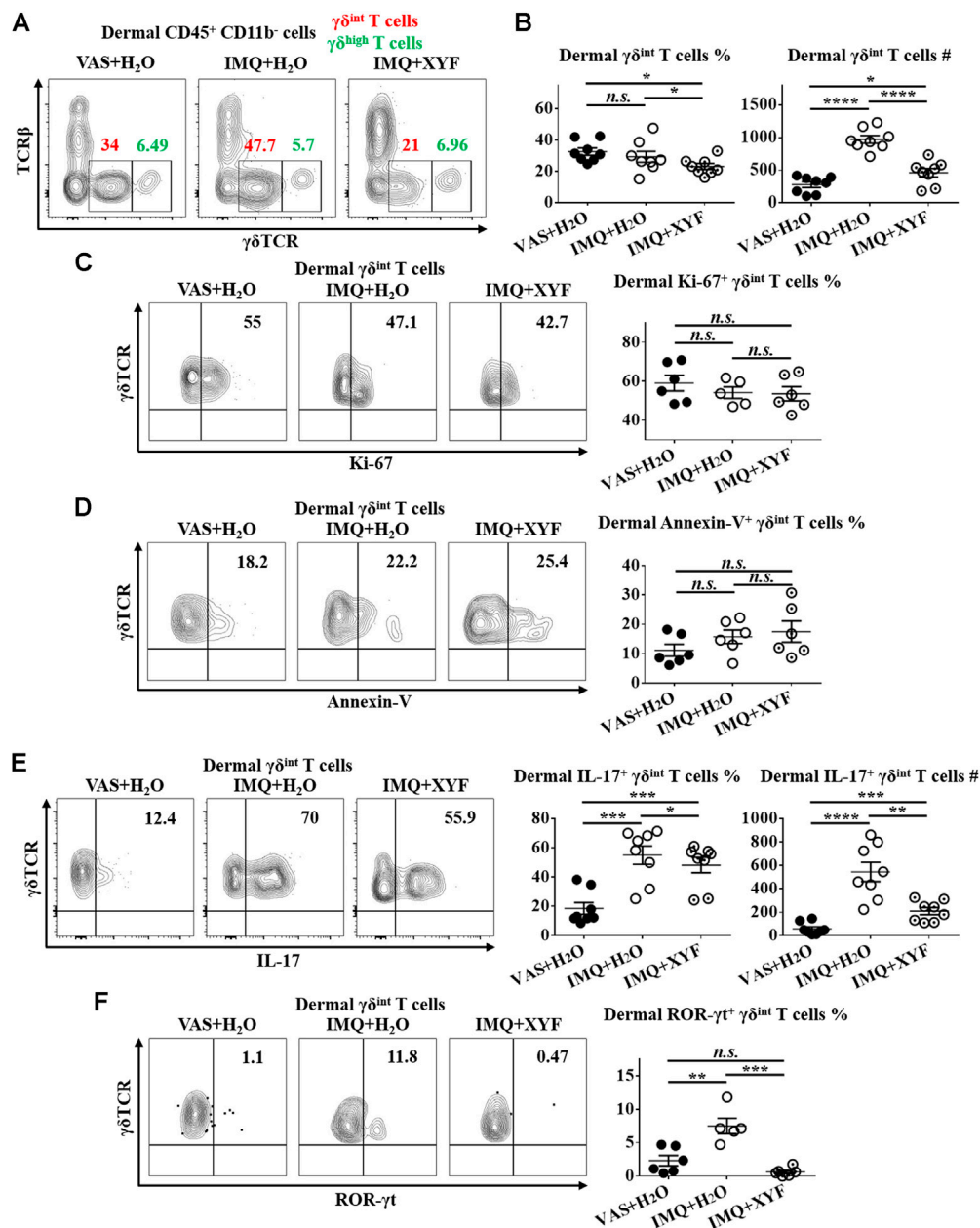


FIGURE 5 | XIAO-YIN-FANG suppressed dermal $\gamma\delta$ T17 cell polarization. Mice were treated as in **Figure 4**, and the dermal cells of mouse ears were harvested. **(A–C)** Freshly isolated dermal cells were *in vitro* cultured in the presence of PMA, ionomycin and Brefeldin A for 4 h. Cultured dermal cells were stained with anti-CD45, TCRβ, γδTCR, and CD11b antibodies ($n = 24$, four independent experiments) **(A)** Representative scatter plots of dermal $\gamma\delta^{\text{int}}$ T cells and $\gamma\delta^{\text{high}}$ T cells. **(B)** The ratios and numbers of dermal $\gamma\delta^{\text{int}}$ T cells. **(C)** Uncultured dermal cells were stained with anti-CD45, TCRβ, γδTCR, CD11b and Ki-67 antibodies. Representative scatter plots and the ratios of dermal Ki-67⁺ $\gamma\delta^{\text{int}}$ T cells ($n = 17$, three independent experiments). **(D)** Uncultured dermal cells were stained with anti-CD45, TCRβ, γδTCR, CD11b and Annexin-V antibodies. Representative scatter plots and the ratios of dermal Annexin-V⁺ $\gamma\delta^{\text{int}}$ T cells ($n = 18$, three independent experiments). **(E)** Cultured dermal cells were stained with anti-CD45, TCRβ, γδTCR, CD11b, and IL-17 antibodies. Representative scatter plots, the ratios and numbers of dermal IL-17⁺ $\gamma\delta^{\text{int}}$ T cells ($n = 24$, three independent experiments). **(F)** Uncultured dermal cells were stained with anti-CD45, TCRβ, γδTCR, CD11b, and ROR-γt antibodies. Representative scatter plots and the ratios of dermal ROR-γt⁺ $\gamma\delta^{\text{int}}$ T cells ($n = 17$, three independent experiments). The data were presented as mean \pm s.e.m.

barely produced IL-17 (Cai et al., 2011; Riolo-Blanco et al., 2014). Hence, we focused on dermal $\gamma\delta^{\text{int}}$ T cells in the following research. While dermal $\gamma\delta^{\text{int}}$ T cells were expanded in model mice, XYF diminished the quantity of $\gamma\delta^{\text{int}}$ T cells (**Figures**

5A,B). The expressions of Ki-67 and Annexin-V in $\gamma\delta^{\text{int}}$ T cells were comparable between model and XYF group (**Figures 5C,D**), suggesting that XYF did not influence $\gamma\delta^{\text{int}}$ T cell survival. Thus, the decrease in $\gamma\delta^{\text{int}}$ T cells triggered by

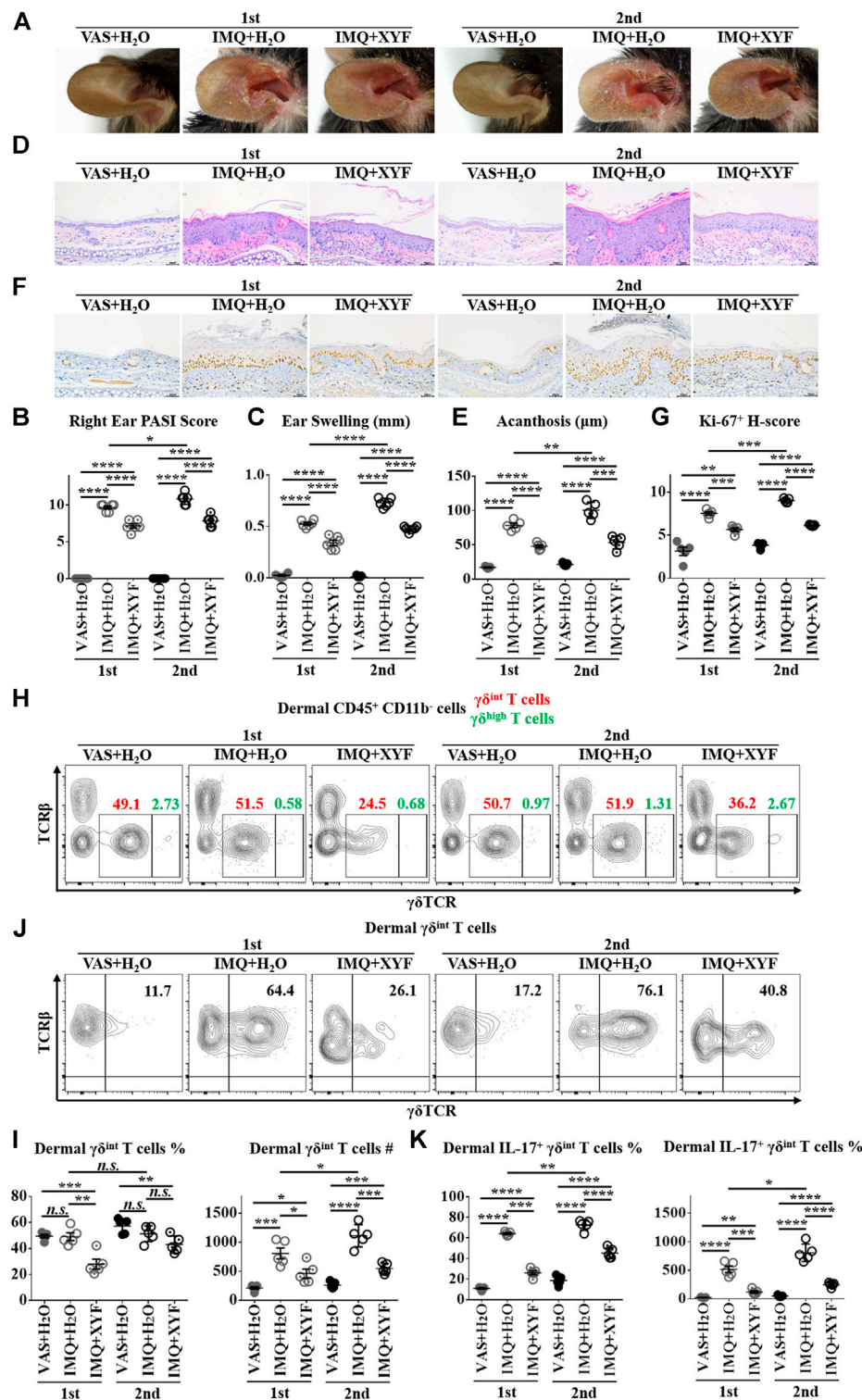


FIGURE 6 | Xiao-Yin-Fang alleviated the relapse of psoriasis-like dermatitis and prohibited dermal $\gamma\delta^{\text{int}}$ T cell reactivation. Mice were treated as in **Supplementary Figure S7**. **(A)** Representative pictures of mouse right ear lesions (1st: the initial occurrence of psoriasis-like dermatitis; 2nd: the recurrence of psoriasis-like dermatitis). **(B, C)** Evaluation of PASI score **(B)** and skin swelling **(C)** of mouse right ears ($n = 36$, two independent experiments). **(D)** H&E staining and calculated epidermal acanthosis **(E)** (x200; bar = 50 μm; $n = 30$, two independent experiments). **(F)** Ki-67 staining and assessment of its H-score of epidermal fields **(G)** (x200; bar = 50 μm; $n = 30$, two independent experiments). **(H–K)** Freshly isolated dermal cells were *in vitro* cultured in the presence of PMA, ionomycin and Brefeldin A for 4 h. Cultured dermal cells were stained with anti-CD45, TCRβ, $\gamma\delta$ TCR, CD11b, and IL-17 antibodies ($n = 30$, two independent experiments). **(H)** Representative scatter plots of dermal $\gamma\delta^{\text{int}}$ T cells and $\gamma\delta^{\text{high}}$ T cells. **(I)** The ratios and numbers of dermal $\gamma\delta^{\text{int}}$ T cells. **(J)** Representative scatter plots of dermal IL-17⁺ $\gamma\delta^{\text{int}}$ T cells. **(K)** The ratios and numbers of dermal IL-17⁺ $\gamma\delta^{\text{int}}$ T cells. The data were presented as mean ± s.e.m.

XYF might result from its impact on cell trafficking. Remarkably, while IL-17 secretion by $\gamma\delta^{\text{int}}$ T cells tripled in model mice versus control mice, XYF significantly repressed $\gamma\delta^{\text{int}}$ T cell production of IL-17 (**Figure 5E**). In accordance, the expression of ROR- γ t, which was a house-keeping transcription factor of $\gamma\delta$ T17 cells, was enhanced in $\gamma\delta^{\text{int}}$ T cells from model mice, whereas XYF considerably downregulated its expression (**Figure 5F**). In total, XYF might ameliorate psoriasis-like skin inflammation mainly through hampering dermal $\gamma\delta^{\text{int}}$ T cell trafficking and suppressing their polarization into $\gamma\delta$ T17 cells.

Xiao-Yin-Fang Alleviates The Relapse of Psoriasis-Like Dermatitis and Prohibits Dermal $\gamma\delta^{\text{int}}$ T Cell Reactivation.

As psoriasis has a notable propensity for recurrence, we exploited a relapsing model of psoriasis-like dermatitis to examine the therapeutic effects of XYF in psoriasis recurrence by applying IMQ cream on left ear and reapplying them on right ear one week later (**Supplementary Figure S7**) (Ramirez-Valle et al., 2015). As expected, the restimulation with IMQ exacerbated the severity of psoriasis-like dermatitis, which was successfully lessened by the treatment with XYF (**Figure 6A**). Evaluations of PASI score, ear swelling, epidermal acanthosis and Ki-67 H-score confirmed the therapeutic effects of XYF (**Figures 6B–G**). Consistently, the secondary application of IMQ further augmented $\gamma\delta^{\text{int}}$ T cells and increased their IL-17 production, whereas XYF decreased $\gamma\delta^{\text{int}}$ T cells and suppressed their secretion of IL-17 (**Figures 6H–J**). In sum, XYF might be beneficial to prevent the relapse of psoriasis through impeding $\gamma\delta^{\text{int}}$ T cell reactivation and their polarization into $\gamma\delta$ T17 cells.

Transcriptional Analysis of Therapeutic Effects of Xiao-Yin-Fang

To further explore the potential mechanisms of XYF therapy, RNA sequencing analysis was performed (**Supplementary Table S1**). Heatmap analysis of differentially expressed genes (DEG) revealed distinct transcriptomes between different groups (**Figures 7A,B**). And, XYF partially reversed the pathological transcriptional alternations in psoriasis-like dermatitis (**Figures 7A,B**). Detailed comparison identified the overlapping genes of DEGs between control/model group and DEGs between model/XYF group (**Figure 7C, Supplementary Table S2, S3**). Kyoto Encyclopedia of Genes and Genomes (KEGG) pathway analysis uncovered that epidermis from model group was enriched in cytokine-cytokine receptor interaction, PI3K-Akt signaling pathway, IL-17 signaling pathway, and cGMP-PKG signaling pathway whereas the dermis from model group was enriched in cytokine-cytokine receptor interaction, chemokine signaling pathway, IL-17 signaling pathway, TNF signaling pathway, Wnt signaling pathway, and PI3K-Akt signaling pathway when compared with control group (**Figures 7D,F**). XYF therapy modulated PI3K-Akt signaling pathway, Calcium signaling, Hippo signaling pathway and cGMP-PKG signaling pathway in the epidermis, whereas it affected several metabolic pathways, Calcium signaling, cAMP signaling pathway and

cGMP-PKG signaling pathway in the dermis (**Figures 7E,G**). Further Gene Set Enrichment Analysis (GSEA) uncovered XYF downregulated focal adhesion and ECM receptor interaction in the epidermis, whereas disturbed arachidonic acid metabolism in the dermis (**Supplementary Figure S8**). Altogether, these results suggested that XYF might regulate multiple inflammatory signaling pathways and metabolic processes, which impact on $\gamma\delta$ T17 cell biology awaits future study.

DISCUSSION

As one major population of skin-located innate immunocytes, dermal $\gamma\delta$ T cells might fundamentally contribute to the immunopathogenesis of psoriasis. Enrichment of $\gamma\delta$ T17 cells was observed in the dermis of psoriatic skin lesions (Cai et al., 2011). A subclass of V γ 9V δ 2⁺ T cells, which expressed IL-17 and tumor necrosis factor α (TNF- α), was distributed in normal skin from healthy individuals, non-lesional and lesional skin of psoriatic patients in increasing order (Laggner et al., 2011). In addition, the ratio of V γ 9V δ 2⁺ $\gamma\delta$ T cells were negatively correlated with the disease severity, indicating that V γ 9V δ 2⁺ $\gamma\delta$ T cell population might be recruited from the blood circulation to the cutaneous tissue when disease flares (Laggner et al., 2011). In line with the findings in psoriasis patients, $\gamma\delta$ T17 cells also played a dominant role in psoriasis-like dermatitis mouse model. The IL-17-secreting dermal cells were substantially decreased in TCR $\delta^{-/-}$ mice accompanied with lessened psoriasiform symptoms, whereas TCR $\alpha^{-/-}$ mice normally develop dermatitis (Cai et al., 2011). Previous studies have uncovered that IL-17 was mostly limited to dermal $\gamma\delta^{\text{int}}$ T cells (Cai et al., 2011; Riol-Blanco et al., 2014). The IL-17-producing $\gamma\delta^{\text{int}}$ T cells in the mouse dermis was primarily composed of V γ 4⁺ and V γ 6⁺ subsets (Cai et al., 2014; O'Brien and Born, 2015; Akitsu and Iwakura, 2018). Amongst, V γ 4⁺ T cells produced more IL-17 than V γ 6⁺ T cells, indicating that V γ 4⁺ T cells might play a more essential role in psoriasis-like dermatitis than V γ 6⁺ T cells (Cai et al., 2014). Moreover, pathogenic V γ 4⁺ T cells expanded and persisted within the dermis for a long time after initial exposure to IMQ, and these experienced $\gamma\delta$ T cells demonstrated heightened effector functions and aggravated secondary inflammation (Hartwig et al., 2015). Furthermore, V γ 4⁺ T cells traveled to noninflamed skin and peripheral LNs where they exacerbated psoriasiform dermatitis at distant sites (Ramirez-Valle et al., 2015). The quasi-innate memory capacity of $\gamma\delta$ T cells might provide a novel mechanistic insight into psoriasis relapse. In summary, although multiple cellular sources of IL-17 have been identified in psoriasis, $\gamma\delta$ T cells might represent a potent contributor in the pathogenesis of psoriasis (Keijsers et al., 2014; Durham et al., 2015; Blauvelt and Chiricozzi, 2018). Therefore, the investigation of $\gamma\delta$ T17-targeted medication is of great importance in the management of psoriasis.

Xiao-Yin-Fang (XYF) is comprised of five Chinese herb medicines, involving *Isatis tinctoria* L. (Banlangen), *Scutellaria baicalensis* Georgi (Huangqin), *Salvia miltiorrhiza* Bunge (Danshen), *Sophora flavescens* Aiton. (Kushen), and *Rheum officinale* Baill. (Dahuang). As bacterial infection has been reported to trigger and aggravate psoriasis, Banlangen

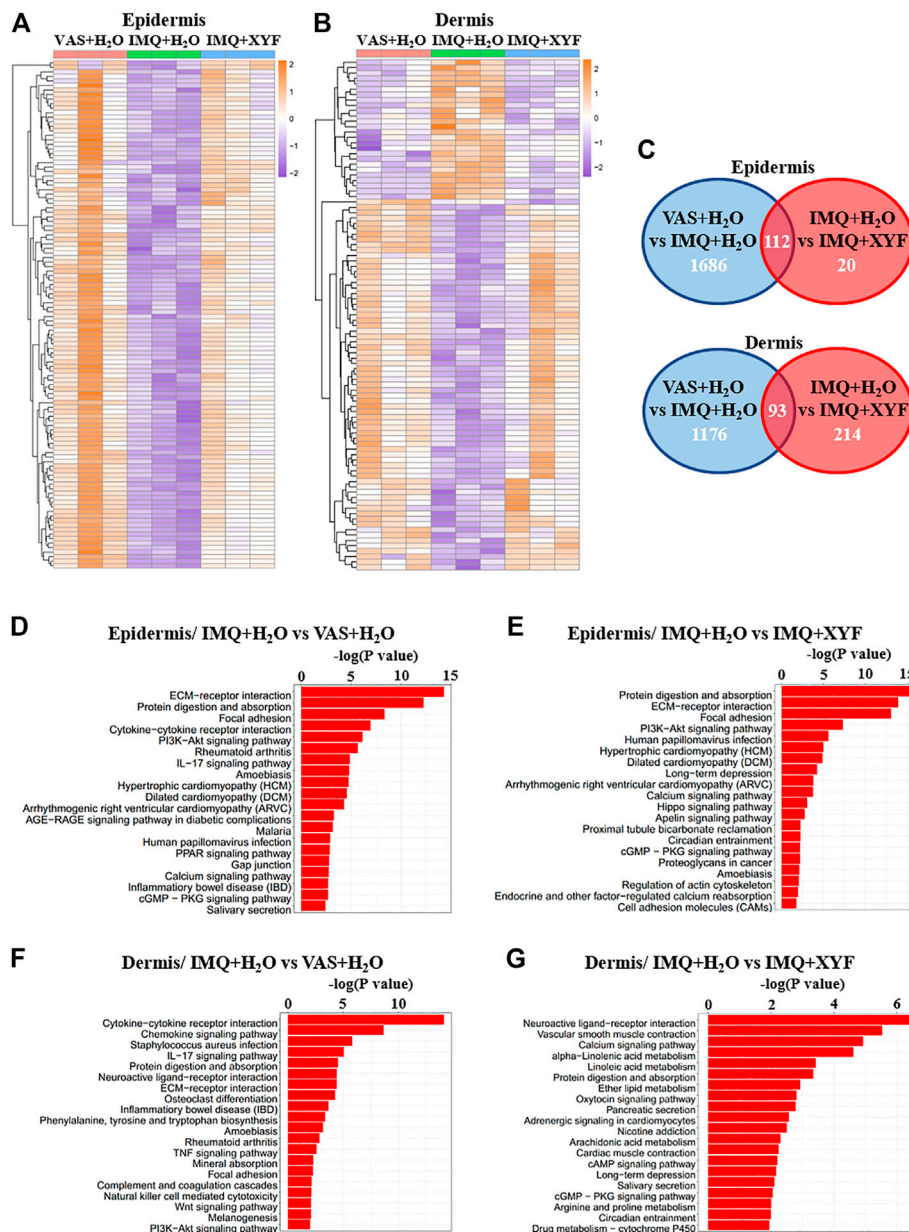


FIGURE 7 | Transcriptional analysis of Xiao-Yin-Fang therapeutic effects. Epidermal and dermal sheets of mouse ears were freshly obtained from VAS + H₂O, IMQ + H₂O and IMQ + XYF group ($n = 3$ for each group), which underwent RNA sequencing analysis. **(A, B)** Heatmap clustering analysis of epidermal and dermal differentially expressed genes (DEG). **(C)** Venn diagrams showed the numbers of overlapping epidermal DEGs (upper panel) and dermal DEGs (lower panel) between VAS + H₂O vs. IMQ + H₂O and IMQ + H₂O vs. IMQ + XYF. **(D-G)** KEGG pathway analysis of DEGs.

contained multiple organic acids with potent antimicrobial activities, which included syringic acid, 2-amino-benzoic acid, salicylic acid and benzoic acid (Kong et al., 2008a; Kong et al., 2008b). Besides, N, N'-dicyclohexyl-N-arachidonic acylurea, a highly unsaturated fatty acid from Balangen, could inhibit TCR-mediated PI3K-Akt signaling pathway, resulting in arrested cell cycle transition from G1 to S phase and lymphocyte hypoproliferation (An et al., 2020). Erucic acid, an active component of Banlangen, markedly reduced CD8⁺ cytotoxic T lymphocyte recruitment (Liang et al., 2020). It is possible that the

chemical constituents of Banlangen might affect the immune function of $\gamma\delta$ T cells.

Former research on Huangqin centered on its major bioactive flavonoid baicalin, which is also the highest-level chemical compound in XYF. Previous studies suggest that baicalin has the advantage of multi-target actions in treating psoriasis (Kim et al., 2013; Liu et al., 2015; Wu et al., 2015b; Bae et al., 2016; Huang et al., 2016; Hung et al., 2018). Stimulation with baicalein *in vitro* hindered HaCaT cell growth and augmented their expressions of keratin 1 and 10 via the inhibition of ERK

phosphorylation (Huang et al., 2016). Consistently, the topical application of baicalin cream dose-dependently promoted the orthokeratosis of granular layers (Wu et al., 2015b). Moreover, baicalin suppressed the expressions of MHC class I/II and costimulatory molecules as well as inhibited IL-12 production from lipopolysaccharide-activated DCs, which repressed Th1/Th2/Th17 but promoted Treg cell differentiation (Kim et al., 2013; Liu et al., 2015; Bae et al., 2016). It has been reported that baicalin cream lessened IMQ-induced psoriasis-like dermatitis, which was accompanied with less infiltration of $\gamma\delta$ T cells into the skin lesions (Hung et al., 2018). Whether baicalin directly regulate the immune activity of $\gamma\delta$ T17 cells remained unexplored.

Danshen exhibited anti-inflammatory and anti-proliferative functions in psoriasis studies (Zhang et al., 2014; May et al., 2015). In silico screening revealed that Danshen contained compounds modulating apoptosis regulator Bcl-2, Bcl-2-Associated X, Caspase-3 along with TNF- α and Prostaglandin G/H synthase 2 (May et al., 2015). Salvianolic acid B reduced psoriatic changes by inhibiting psoriatic inflammatory and keratin markers by abolishing PI3K/Akt signaling pathway (Wang et al., 2020). Tanshinone IIA hindered keratinocyte growth via cell cycle arrest and apoptosis (Li et al., 2012). Cryptotanshinone (CTS), an active component of Danshen with antibacterial and antineoplastic effects, considerably relieved IMQ-induced epidermal hyperplasia through inhibiting STAT3-induced keratinocyte growth (Tang et al., 2018). Danshensu, the most abundant water-soluble component of Danshen, prevented abnormal keratinocyte proliferation in psoriasis by modulating YAP expression (Jia et al., 2020). The impact of Danshen on the immunofunctions of T lymphocytes require further investigation.

Matrine and oxymatrine, two main active phytochemicals of Kushen, have therapeutic potentials for psoriasis. Matrine lessened IMQ-induced psoriasiform cutaneous lesions by decreasing keratinocyte proliferation and MyD88 expression on the surface of DCs derived from bone marrow (Li et al., 2018). Matrine synergized with acitretin to induce cell cycle arrest and autophagy in keratinocytes by regulating PI3K/Akt/mTOR pathway (Jiang et al., 2019). Oxymatrine ameliorated skin inflammation in the patients with psoriasis and psoriasis-like mouse model via inhibiting keratinocyte proliferation probably through MAPK signaling pathway (Chen et al., 2017; Zhou et al., 2017; Shi et al., 2019; Xiang et al., 2020). Whether Kushen or its active components influence T cell biology remains unclear.

Emodin, which is a natural anthraquinone derivative of Dahuang, possesses broad-spectrum pharmacological properties, including antineoplastic, hepatoprotective, anti-inflammatory, antioxidant, and antimicrobial functions. The topical application of a natural compound mixture (PSM) of herbs, containing emodin, genipin, chlorogenic acid, cimigenoside, and ginsenoside Rb1, alleviated IMQ-induced psoriasis-like dermatitis and reduced the proliferation rate of IL-22-stimulated keratinocytes (Nguyen et al., 2020b). The therapeutic effects of Dahuang and its chemical compounds in psoriasis requires further study.

The RNA sequencing analysis revealed that XYF might regulate multiple inflammatory signaling pathways and metabolic processes. Amongst, PI3K-Akt, Calcium, and cAMP

signaling pathways have been reported to influence $\gamma\delta$ T cell biology (Takano et al., 1998; Chen et al., 2005; Chen et al., 2020). Selective inhibition of PI3K δ by Seletalisib hampered the production of IL-17 from peripheral blood $\gamma\delta$ T cells (Chen et al., 2020). Vitamin D, which profoundly regulates calcium metabolism, hindered the proinflammatory activity of $\gamma\delta$ T cells in a dose-dependent fashion (Chen et al., 2005). Prostaglandin E2 inhibited $\gamma\delta$ T cell cytotoxicity triggered by TCR receptors V γ 9V δ 2, NKG2D, and CD16 through a cAMP-mediated PKA type I-dependent signaling (Takano et al., 1998). Whether XYF suppress $\gamma\delta$ T17 cell polarization through these signaling pathways awaits future exploration.

In conclusion, XYF alleviated psoriasis-like skin inflammation mainly through suppressing dermal and draining lymph-node $\gamma\delta$ T17 cell polarization. Moreover, XYF therapy ameliorated the relapse of psoriasis-like dermatitis and prohibited dermal $\gamma\delta$ T cell reactivation. Transcriptional analysis suggested that XYF might regulate various inflammatory signaling and metabolic processes. Our results clarified the therapeutic efficacy and inner mechanisms of XYF therapy in psoriasis, which might promote its clinical application in psoriasis patients and facilitate the development of novel anti-psoriasis drugs based on the bioactive components of XYF.

DATA AVAILABILITY STATEMENT

The datasets presented in this study can be found in online repositories. The names of the repository/repositories and accession numbers can be found below: <https://www.ncbi.nlm.nih.gov/geo/>, GSE161084 <https://www.ncbi.nlm.nih.gov/geo/>, GSE161350.

ETHICS STATEMENT

The animal study was reviewed and approved by the Animal Experimental Ethics Committee of Shanghai Tongji University.

AUTHOR CONTRIBUTIONS

Experimental design by JG, YS, YD, XZ, and XL. Experiments were conducted by XZ, XL, YC, BL, CG, ZY, and PX. Data analysis by XZ, XL, YC and BL. The manuscript written by XZ, XL and YC, and edited by all authors.

FUNDING

This work was sponsored by grants from National Natural Science Foundation of China (No. 81673052, 81602751, 81872522, 82073429), Innovation Program of Shanghai Municipal Education Commission (No.2019-01-07-00-07-E00046), the Program of Science and Technology Commission of Shanghai Municipality (No. 18140901800), Excellent Subject Leader Program of Shanghai Municipal

Commission of Health and Family Planning (No. 2018BR30), Clinical Research Program of Shanghai Hospital Development Center (No. SHDC2020CR1014B, SHDC12018X06) and Program of Shanghai Academic Research Leader (No. 20XD1403300).

REFERENCES

- Akitsu, A., and Iwakura, Y. (2018). Interleukin-17-producing $\gamma\delta$ T ($\gamma\delta$ 17) cells in inflammatory diseases. *Immunology* 155, 418–426. doi:10.1111/imm.12993
- An, K., Qin, Q., Yu, S., Xue, M., Wang, Z., Lin, Q., et al. (2020). Combination of N, N'-dicyclohexyl-N- α -arachidonic acylurea and tacrolimus prolongs cardiac allograft survival in mice. *Immunol. Cell Biol.* 98, 382–396. doi:10.1111/imcb.12327
- Bae, M.-J., Shin, H. S., See, H.-J., Jung, S. Y., Kwon, D.-A., and Shon, D.-H. (2016). Baicalein induces CD4+Foxp3+ T cells and enhances intestinal barrier function in a mouse model of food allergy. *Sci. Rep.* 6, 32225. doi:10.1038/srep32225
- Blauvelt, A., and Chiricozzi, A. (2018). The immunologic role of IL-17 in psoriasis and psoriatic arthritis pathogenesis. *Clinic Rev. Allerg Immunol.* 55, 379–390. doi:10.1007/s12016-018-8702-3
- Cai, Y., Shen, X., Ding, C., Qi, C., Li, K., Li, X., et al. (2011). Pivotal role of dermal IL-17-producing $\gamma\delta$ T cells in skin inflammation. *Immunity* 35, 596–610. doi:10.1016/j.immuni.2011.08.001
- Cai, Y., Fleming, C., and Yan, J. (2013). Dermal $\gamma\delta$ T cells - a new player in the pathogenesis of psoriasis. *Int. Immunopharmacology* 16, 388–391. doi:10.1016/j.intimp.2013.02.018
- Cai, Y., Xue, F., Fleming, C., Yang, J., Ding, C., Ma, Y., et al. (2014). Differential developmental requirement and peripheral regulation for dermal V γ 4 and V γ 6T17 cells in health and inflammation. *Nat. Commun.* 5, 3986. doi:10.1038/ncomms4986
- Casciano, F., Pigatto, P. D., Secchiero, P., Gambari, R., and Reali, E. (2018). T cell hierarchy in the pathogenesis of psoriasis and associated cardiovascular comorbidities. *Front. Immunol.* 9, 1390. doi:10.3389/fimmu.2018.01390
- Chen, L., Cencioni, M. T., Angelini, D. F., Borsellino, G., Battistini, L., and Brosnan, C. F. (2005). Transcriptional profiling of $\gamma\delta$ T cells identifies a role for vitamin D in the immunoregulation of the V γ 9V δ 2 response to phosphate-containing ligands. *J. Immunol.* 174, 6144–6152. doi:10.4049/jimmunol.174.10.6144
- Chen, Q., Zhou, H., Yang, Y., Chi, M., Xie, N., Zhang, H., et al. (2017). Investigating the potential of Oxymatrine as a psoriasis therapy. *Chemico-Biological Interactions* 271, 59–66. doi:10.1016/j.cbi.2017.04.020
- Chen, S., Paveley, R., Kraal, L., Sritharan, L., Stevens, E., Dedi, N., et al. (2020). Selective targeting of PI3K δ suppresses human IL-17-producing T cells and innate-like lymphocytes and may be therapeutic for IL-17-mediated diseases. *J. Autoimmun.* 111, 102435. doi:10.1016/j.jaut.2020.102435
- Damevska, K., Neloska, L., Nikolovska, S., Gocev, G., and Duma, S. (2014). Complementary and alternative medicine use among patients with psoriasis. *Dermatol. Ther.* 27, 281–283. doi:10.1111/dth.12139
- Diani, M., Altomare, G., and Reali, E. (2015). T cell responses in psoriasis and psoriatic arthritis. *Autoimmun. Rev.* 14, 286–292. doi:10.1016/j.autrev.2014.11.012
- Durham, L. E., Kirkham, B. W., and Taams, L. S. (2015). Contribution of the IL-17 pathway to psoriasis and psoriatic arthritis. *Curr. Rheumatol. Rep.* 17, 55. doi:10.1007/s11926-015-0529-9
- Farahnik, B., Sharma, D., Alban, J., and Sivamani, R. (2017). Oral (systemic) botanical agents for the treatment of psoriasis: a review. *J. Altern. Complement. Med.* 23, 418–425. doi:10.1089/acm.2016.0324
- Han, R., Rostami-Yazdi, M., Gerdes, S., and Mrowietz, U. (2012). Triptolide in the treatment of psoriasis and other immune-mediated inflammatory diseases. *Br. J. Clin. Pharmacol.* 74, 424–436. doi:10.1111/j.1365-2125.2012.04221.x
- Hartwig, T., Pantelyushin, S., Croxford, A. L., Kulig, P., and Becher, B. (2015). Dermal IL-17-producing $\gamma\delta$ T cells establish long-lived memory in the skin. *Eur. J. Immunol.* 45, 3022–3033. doi:10.1002/eji.201545883
- Huang, K.-F., Ma, K.-H., Liu, P.-S., Chen, B.-W., and Chueh, S.-H. (2016). Baicalein increases keratin 1 and 10 expression in HaCaT keratinocytes via TRPV4 receptor activation. *Exp. Dermatol.* 25, 623–629. doi:10.1111/exd.13024
- Hung, C.-H., Wang, C.-N., Cheng, H.-H., Liao, J.-W., Chen, Y.-T., Chao, Y.-W., et al. (2018). Baicalin ameliorates imiquimod-induced psoriasis-like inflammation in mice. *Planta. Med.* 84, 1110–1117. doi:10.1055/a-0622-8242
- Jia, J., Mo, X., Liu, J., Yan, F., Wang, N., Lin, Y., et al. (2020). Mechanism of danshensu-induced inhibition of abnormal epidermal proliferation in psoriasis. *Eur. J. Pharmacol.* 868, 172881. doi:10.1016/j.ejphar.2019.172881
- Jiang, W.-W., Wang, Y.-M., Wang, X.-Y., Zhang, Q., Zhu, S.-M., and Zhang, C.-L. (2019). Role and mechanism of matrine alone and combined with acitretin for HaCaT cells and psoriasis-like murine models. *Chin. Med. J. (Engl.)* 132, 2079–2088. doi:10.1097/CM9.0000000000000412
- Keijsers, R. R. M. C., Joosten, I., Van Erp, P. E. J., Koenen, H. J. P. M., and Van De Kerkhof, P. C. M. (2014). Cellular sources of IL-17 in psoriasis: a paradigm shift? *Exp. Dermatol.* 23, 799–803. doi:10.1111/exd.12487
- Kim, J., and Krueger, J. G. (2017). Highly effective new treatments for psoriasis target the IL-23/type 17 T cell autoimmune Axis. *Annu. Rev. Med.* 68, 255–269. doi:10.1146/annurev-med-042915-103905
- Kim, M. E., Kim, H. K., Park, H.-Y., Kim, D. H., Chung, H. Y., and Lee, J. S. (2013). Baicalin from *Scutellaria baicalensis* impairs Th1 polarization through inhibition of dendritic cell maturation. *J. Pharmacol. Sci.* 121, 148–156. doi:10.1254/jphs.12200fp
- Kong, W., Zhao, Y., Shan, L., Xiao, X., and Guo, W. (2008a). Microcalorimetric studies of the action on four organic acids in *Radix isatidis* on the growth of microorganisms. *Chin. J. Biotechnol.* 24, 646–650. doi:10.1016/s1872-2075(08)60033-3
- Kong, W.-J., Zhao, Y.-L., Shan, L.-M., Xiao, X.-H., and Guo, W.-Y. (2008b). Investigation on the spectrum-effect relationships of EtOAc extract from *Radix Isatidis* based on HPLC fingerprints and microcalorimetry. *J. Chromatogr. B.* 871, 109–114. doi:10.1016/j.jchromb.2008.06.053
- Laggner, U., Di Meglio, P., Perera, G. K., Hundhausen, C., Lacy, K. E., Ali, N., et al. (2011). Identification of a novel proinflammatory human skin-homing V γ 9V δ 2 T cell subset with a potential role in psoriasis. *J. Immunol.* 187, 2783–2793. doi:10.4049/jimmunol.1100804
- Lebwohl, M. G., Bachelez, H., Barker, J., Girolomoni, G., Kavanaugh, A., Langley, R. G., et al. (2014). Patient perspectives in the management of psoriasis: results from the population-based multinational assessment of psoriasis and psoriatic arthritis survey. *J. Am. Acad. Dermatol.* 70, 871–881. e830. doi:10.1016/j.jaad.2013.12.018
- Li, F.-L., Xu, R., Zeng, Q.-C., Li, X., Chen, J., Wang, Y.-F., et al. (2012). Tanshinone IIA inhibits growth of keratinocytes through cell cycle arrest and apoptosis: underlying treatment mechanism of psoriasis. *Evidence-Based Complement. Altern. Med.* 2012, 1. doi:10.1155/2012/927658
- Li, N., Zhao, J., Di, T., Meng, Y., Wang, M., Li, X., et al. (2018). Matrine alleviates imiquimod-induced psoriasiform dermatitis in BALB/c mice via dendritic cell regulation. *Int. J. Clin. Exp. Pathol.* 11, 5232–5240.
- Liang, X., Huang, Y., Pan, X., Hao, Y., Chen, X., Jiang, H., et al. (2020). Erucic acid from *Isatis indigotica* Fort. suppresses influenza A virus replication and inflammation *in vitro* and *in vivo* through modulation of NF- κ B and p38 MAPK pathway. *J. Pharm. Anal.* 10, 130–146. doi:10.1016/j.jpha.2019.09.005
- Liu, T., Dai, W., Li, C., Liu, F., Chen, Y., Weng, D., et al. (2015). Baicalin alleviates silica-induced lung inflammation and fibrosis by inhibiting the Th17 response in C57bl/6 mice. *J. Nat. Prod.* 78, 3049–3057. doi:10.1021/acs.jnatprod.5b00868
- Lv, M., Deng, J., Tang, N., Zeng, Y., and Lu, C. (2018). Efficacy and safety of Tripterygium wilfordii Hook F on psoriasis vulgaris: a systematic review and meta-analysis of randomized controlled trials. *Evidence-Based Complement. Altern. Med.* 2018, 1. doi:10.1155/2018/2623085
- Magin, P. J., Adams, J., Heading, G. S., Pond, D. C., and Smith, W. (2006). Complementary and alternative medicine therapies in acne, psoriasis, and atopic eczema: results of a qualitative study of patients' experiences and perceptions. *J. Altern. Complement. Med.* 12, 451–457. doi:10.1089/acm.2006.12.451

SUPPLEMENTARY MATERIAL

The Supplementary Material for this article can be found online at: <https://www.frontiersin.org/articles/10.3389/fphar.2021.629513/full#supplementary-material>.

- May, B. H., Deng, S., Zhang, A. L., Lu, C., and Xue, C. C. L. (2015). In silico database screening of potential targets and pathways of compounds contained in plants used for psoriasis vulgaris. *Arch. Dermatol. Res.* 307, 645–657. doi:10.1007/s00403-015-1577-8
- Michalek, I. M., Loring, B., and John, S. M. (2017). A systematic review of worldwide epidemiology of psoriasis. *J. Eur. Acad. Dermatol. Venereol.* 31, 205–212. doi:10.1111/jdv.13854
- Murphy, E. C., Nussbaum, D., Prussick, R., and Friedman, A. J. (2019). Use of complementary and alternative medicine by patients with psoriasis. *J. Am. Acad. Dermatol.* 81, 280–283. doi:10.1016/j.jaad.2019.03.059
- Nguyen, T., Lestienne, F., Cousy, A., Meneaud, V., and Castex-Rizzi, N. (2020a). Effective inhibition of Th17/Th22 pathway in 2D and 3D human models of psoriasis by Celastrol enriched plant cell culture extract. *J. Eur. Acad. Dermatol. Venereol.* 34 (Suppl. 6), 3–9. doi:10.1111/jdv.16475
- Nguyen, U. T., Nguyen, L. T. H., Kim, B.-A., Choi, M.-J., Yang, I.-J., and Shin, H.-M. (2020b). Natural compound mixture, containing emodin, genipin, chlorogenic acid, cimigenoside, and ginsenoside Rb1, ameliorates psoriasis-like skin lesions by suppressing inflammation and proliferation in keratinocytes. *Evidence-Based Complement. Altern. Med.* 2020, 1. doi:10.1155/2020/9416962
- O'Brien, R. L., and Born, W. K. (2015). Dermal $\gamma\delta$ T cells--What have we learned? *Cell Immunol.* 296, 62–69. doi:10.1016/j.cellimm.2015.01.011
- Pilon, D., Teeple, A., Zhdanava, M., Ladouceur, M., Ching Cheung, H., Muser, E., et al. (2019). The economic burden of psoriasis with high comorbidity among privately insured patients in the United States. *J. Med. Econ.* 22, 196–203. doi:10.1080/13696998.2018.1557201
- Ramírez-Valle, F., Gray, E. E., and Cyster, J. G. (2015). Inflammation induces dermal V γ 4+ $\gamma\delta$ T17 memory-like cells that travel to distant skin and accelerate secondary IL-17-driven responses. *Proc. Natl. Acad. Sci. USA.* 112, 8046–8051. doi:10.1073/pnas.1508990112
- Rapalli, V. K., Singhvi, G., Dubey, S. K., Gupta, G., Chellappan, D. K., and Dua, K. (2018). Emerging landscape in psoriasis management: from topical application to targeting biomolecules. *Biomed. Pharmacother.* 106, 707–713. doi:10.1016/j.biopha.2018.06.136
- Riol-Blanco, L., Ordovas-Montanes, J., Perro, M., Naval, E., Thiriot, A., Alvarez, D., et al. (2014). Nociceptive sensory neurons drive interleukin-23-mediated psoriasiform skin inflammation. *Nature* 510, 157–161. doi:10.1038/nature13199
- Ru, Y., Li, H., Zhang, R., Luo, Y., Song, J., Kuai, L., et al. (2020). Role of keratinocytes and immune cells in the anti-inflammatory effects of *Tripterygium wilfordii* Hook. f. in a murine model of psoriasis. *Phytomedicine* 77, 153299. doi:10.1016/j.phymed.2020.153299
- Schleicher, S. M. (2016). Psoriasis. *Clin. Podiatric Med. Surg.* 33, 355–366. doi:10.1016/j.cpm.2016.02.004
- Shi, H. J., Zhou, H., Ma, A. L., Wang, L., Gao, Q., Zhang, N., et al. (2019). Oxymatrine therapy inhibited epidermal cell proliferation and apoptosis in severe plaque psoriasis. *Br. J. Dermatol.* 181, 1028–1037. doi:10.1111/bjd.17852
- Takano, M., Nishimura, H., Kimura, Y., Washizu, J., Mokuno, Y., Nimura, Y., et al. (1998). Prostaglandin E2 protects against liver injury after *Escherichia coli* infection but hampers the resolution of the infection in mice. *J. Immunol.* 161, 3019–3025.
- Tang, L., He, S., Wang, X., Liu, H., Zhu, Y., Feng, B., et al. (2018). Cryptotanshinone reduces psoriatic epidermal hyperplasia via inhibiting the activation of STAT3. *Exp. Dermatol.* 27, 268–275. doi:10.1111/exd.13511
- Wang, W., Gao, Z., Guo, Z., Guo, Q., Yang, Q., and Gu, J. (2012a). Efficacy of Xiaoyin decoction combined with calcipotriol ointment in patients with vulgaris psoriasis of blood heat type and their effects on related cytokines. *Chin. J. Dermatol.* 45, 647–649.
- Wang, W., Wang, F., Gao, Z., Bu, X., and Gu, J. (2012b). Clinical effects of xiaoyin tang in treating psoriasis of blood-heat type and its impact on T-bet/GATA3. *Chin. J. Dermatovenereology Integrated Traditional West. Med.* 11 (2), 74–77.
- Wang, S., Zhu, L., Xu, Y., Qin, Z., and Xu, A. (2020). Salvianolic acid B ameliorates psoriatic changes in imiquimod-induced psoriasis on BALB/c mice by inhibiting inflammatory and keratin markers via altering phosphatidylinositol-3-kinase/protein kinase B signaling pathway. *Korean J. Physiol. Pharmacol.* 24, 213–221. doi:10.4196/kjpp.2020.24.3.213
- Wu, C., Jin, H.-Z., Shu, D., Li, F., He, C.-X., Qiao, J., et al. (2015a). Efficacy and safety of *Tripterygium wilfordii* Hook F versus acitretin in moderate to severe psoriasis vulgaris. *Chin. Med. J. (Engl.)* 128, 443–449. doi:10.4103/0366-6999.151069
- Wu, J., Li, H., and Li, M. (2015b). Effects of baicalin cream in two mouse models: 2,4-dinitrofluorobenzene-induced contact hypersensitivity and mouse tail test for psoriasis. *Int. J. Clin. Exp. Med.* 8, 2128–2137.
- Xiang, W., Suo, T.-C., Yu, H., Li, A.-P., Zhang, S.-Q., Wang, C.-H., et al. (2018). A new strategy for choosing “Q-markers” via network pharmacology, application to the quality control of a Chinese medical preparation. *J. Food Drug Anal.* 26, 858–868. doi:10.1016/j.jfda.2017.10.003
- Xiang, X., Tu, C., Li, Q., Wang, W., Huang, X., Zhao, Z., et al. (2020). Oxymatrine ameliorates imiquimod-induced psoriasis pruritus and inflammation through inhibiting heat shock protein 90 and heat shock protein 60 expression in keratinocytes. *Toxicol. Appl. Pharmacol.* 405, 115209. doi:10.1016/j.taap.2020.115209
- Zhang, H., Xu, X. G., and Gu, J. (2008). [Effect of xiaoyin recipe in treatment of psoriasis patients of blood-heat syndrome type and its impact on peripheral Th1/Th2 equilibrium]. *Zhongguo Zhong Xi Yi Jie He Za Zhi* 28, 683–685.
- Zhang, C. S., Yu, J. J., Parker, S., Zhang, A. L., May, B., Lu, C., et al. (2014). Oral Chinese herbal medicine combined with pharmacotherapy for psoriasis vulgaris: a systematic review. *Int. J. Dermatol.* 53, 1305–1318. doi:10.1111/ijd.12607
- Zhao, J., Di, T., Wang, Y., Liu, X., Liang, D., Zhang, G., et al. (2016). Multi-glycoside of *Tripterygium wilfordii* Hook. f. ameliorates imiquimod-induced skin lesions through a STAT3-dependent mechanism involving the inhibition of Th17-mediated inflammatory responses. *Int. J. Mol. Med.* 38, 747–757. doi:10.3892/ijmm.2016.2670
- Zhou, H., Shi, H.-J., Yang, J., Chen, W.-G., Xia, L., Song, H.-B., et al. (2017). Efficacy of oxymatrine for treatment and relapse suppression of severe plaque psoriasis: results from a single-blinded randomized controlled clinical trial. *Br. J. Dermatol.* 176, 1446–1455. doi:10.1111/bjd.15316

Conflict of Interest: The authors declare that the research was conducted in the absence of any commercial or financial relationships that could be construed as a potential conflict of interest.

Copyright © 2021 Zhang, Li, Chen, Li, Guo, Xu, Yu, Ding, Shi and Gu. This is an open-access article distributed under the terms of the Creative Commons Attribution License (CC BY). The use, distribution or reproduction in other forums is permitted, provided the original author(s) and the copyright owner(s) are credited and that the original publication in this journal is cited, in accordance with accepted academic practice. No use, distribution or reproduction is permitted which does not comply with these terms.



Pharmacological Benefits of Triphala: A Perspective for Allergic Rhinitis

Salinee Jantrapirom^{1,2}, Pannaphak Hirunsatitpron^{1,3}, Saranyapin Potikanond¹, Wutigri Nimlamool¹ and Nutthiya Hanprasertpong^{1*}

¹Department of Pharmacology, Faculty of Medicine, Chiang Mai University, Chiang Mai, Thailand, ²Drosophila Center for Human Diseases and Drug Discovery (DHD), Faculty of Medicine, Chiang Mai University, Chiang Mai, Thailand, ³Graduate School, Chiang Mai University, Chiang Mai, Thailand

OPEN ACCESS

Edited by:

Michael Heinrich,
UCL School of Pharmacy,
United Kingdom

Reviewed by:

Jen-Tsung Chen,
National University of
Kaohsiung, Taiwan
Tan Loh Teng Hern,
Monash University Malaysia, Malaysia

*Correspondence:

Nutthiya Hanprasertpong
nutthiya.h@cmu.ac.th

Specialty section:

This article was submitted to
Ethnopharmacology,
a section of the journal
Frontiers in Pharmacology

Received: 11 November 2020

Accepted: 16 March 2021

Published: 30 April 2021

Citation:

Jantrapirom S, Hirunsatitpron P,
Potikanond S, Nimlamool W and
Hanprasertpong N (2021)
Pharmacological Benefits of Triphala: A
Perspective for Allergic Rhinitis.
Front. Pharmacol. 12:628198.
doi: 10.3389/fphar.2021.628198

Allergic rhinitis (AR) is considered a major nasal condition impacting a large number of people around the world, and it is now becoming a global health problem. Because the underlying mechanisms of AR are complex, the development of single-drug treatment might not be enough to treat a wide spectrum of the disease. Although the standard guidelines classify and provide suitable diagnosis and treatment, the vast majority of people with AR are still without any means of controlling it. Moreover, the benefits of AR drugs are sometimes accompanied by undesirable side effects. Thus, it is becoming a significant challenge to find effective therapies with limited undesirable side effects for a majority of patients suffering from uncontrolled AR. Aller-7/NR-A2, a polyherbal formulation, has revealed promising results in patients by reducing nasal symptoms and eosinophil counts without serious adverse effects. Interestingly, three out of seven of the herbals in the Aller-7/NR-A2 formulation are also found in an Ayurvedic polyherbal formulation known as “Triphala,” which is a potential candidate for the treatment of AR. However, there are no current studies that have examined the effects of Triphala on the disease. This review aims to describe the complexity of AR pathophysiology, currently available treatments, and the effects of Triphala on AR in order to help develop it as a promising alternative treatment in the future.

Keywords: allergic rhinitis, triphala, antioxidant effect, anti-inflammation, immunomodulation

INTRODUCTION

Although allergic rhinitis (AR), commonly known as hay fever, is not considered a serious condition or one with the potential for mortality, it might become a clinical burden if it were to become uncontrollable in a majority of patients. Epidemiological studies have revealed that patients with AR have a high probability of subsequently developing asthma, and a large proportion of asthmatic patients also have AR as a concomitant condition (Simons, 1999; Thomas, 2006; Vujanovic and Domuz, 2018). Moreover, prolonged AR symptoms, particularly nasal congestion, can lead to the development of obstructive sleep apnea (Young et al., 1997). Currently, three acceptable strategies for managing AR are employed: 1) avoiding sensitized allergenic exposure, 2) starting pharmacotherapy, and 3) starting immunotherapy (Klimek et al., 2019). However, to achieve final outcomes, it is often suggested to patients that they use long-term multiple therapies, which sometimes come with problems of compliance, leading to failures in treatment (Small et al., 2018). Therefore, combinations of two drugs in one device, such as antihistamine/steroid or anticholinergic/steroid, are becoming

TABLE 1 | The medications for allergic rhinitis.

Treatment	Mechanism of action	Adverse effects
Antihistamines (oral)	Block H ₁ receptor on effector cells to reduce histamine-mediated symptoms such as rhinorrhea, sneezing, nasal itching, and eye symptoms	1st generation: Sedation, dry mouth, decrease cognitive function, orthostatic hypotension etc. 2nd generation: Bitter taste (azelastine), rare cardiac arrhythmia in some drugs etc.
Antihistamines (intranasal, intraocular)	Block H ₁ receptor on effector cells located in nasal and ocular area to reduce histaminic effects as mentioned above	Nasal irritation and epistaxis, septal perforation, bitter taste (azelastine) etc.
Intranasal corticosteroids	Bind to glucocorticoid receptor leading to nasal inflammatory cells flux reduction	Nasal irritation, nasal dryness, epistaxis etc.
Oral/IM corticosteroids	Bind to glucocorticoid receptor leading to systematic inflammatory cells flux reduction	Adrenocortical insufficiency, infection, peptic ulcer, glaucoma etc. Depot injections may cause local tissue atrophy
Oral decongestants (sympathomimetic decongestants)	Stimulate systematic α adrenergic receptor to constrict dilated blood vessels	Hypertension, palpitations, restlessness, agitation, tremor, insomnia, headache, dry mucous membrane, urinary retention
Intranasal decongestants (sympathomimetic decongestants)	Stimulate nasal α adrenergic receptor to constrict dilated blood vessels located in nasal mucosa	Nasal irritation, nasal dryness, hypertension in some cases etc.
Intranasal anticholinergics	Block muscarinic receptor leading to reduction of nasal mucosa gland activation	Long term used may cause rebound congestion Nasal irritation, nasal dryness, epistaxis etc.
Leukotriene receptor antagonists (oral)	Block cysteinyl leukotriene receptor on effector cells to reduce vascular permeability and inflammatory cell recruitment	Urticaria, diarrhea, abdominal pain, agitation, suicidal thinking, hallucination etc.
Immunotherapies (subcutaneous, SCIT) (sublingual, SLIT)	Induce specific allergen tolerance and help restoration of immune system	Scit: Local irritation, swelling at the site of injection, anaphylaxis etc. Slit: Lip, mouth, and tongue irritation etc.

novel strategic treatments that have been found to be more effective than using a monotherapy (Seresirikachorn et al., 2018).

Several studies have highlighted the beneficial effects of phytochemicals in attenuating allergic responses and the overall symptoms of AR. Curcumin, ginger, ginseng, resveratrol, and quercetin compounds have all shown effective results in relieving nasal symptoms and suppressing AR-related mediators in animal models by controlling the main anti-inflammatory mitogen-activated protein kinase/nuclear factor κ B (MAPK/NF- κ B) pathway (Jung et al., 2011, 2013; Zhang et al., 2015; Kashiwabara et al., 2016; Kawamoto et al., 2016; Lv et al., 2018). A major component of ginger, 6-gingerol, possesses the ability to suppress T helper 2 (Th2) cytokines by attenuating the activation of MAPK/NF- κ B signaling in ovalbumin (OVA)-sensitized spleen cells (Kawamoto et al., 2016). In addition, resveratrol nasal spray has recently been developed to overcome the problem of drug absorption, and specifically to retain bioactive activities in the affected area, such as the nasal mucosa. An intranasal resveratrol formulation has been shown to be successful in alleviating allergic symptoms and reducing eosinophils and mast cell infiltration in the nasal mucosa of both animals and AR patients (Lv et al., 2018). Moreover, children with AR have significantly reduced nasal symptoms following administration of a combined resveratrol and carboxymethyl β -glucan nasal spray (Miraglia Del Giudice et al., 2014).

Triphala possesses several activities that could be beneficial for respiratory and immune systems. However, there is no study directly evidencing the potential benefits of Triphala on AR, even though its constituent phytochemicals have been suggested to serve many aspects of AR therapeutic strategies. Therefore, it is important to review and clarify the possible mechanism of action of Triphala and its active constituents on AR. This review focuses

mainly on the antioxidative, anti-inflammatory, immunomodulatory, and other effects of Triphala on the AR-affected respiratory system. The quality of the articles relevant to the scope of AR has been evaluated according to the guideline reported by Heinrich et al. (2020) and the Good Research for Comparative Effectiveness (GRACE) tool (Dreyer et al., 2016) (**Supplementary Table S1**).

ALLERGIC RHINITIS

AR is a condition of nasal hypersensitivity caused by an immunologically mediated inflammation by non-infectious stimulants or environmental allergens, such as pollen, dust, fungi, cockroaches, etc. AR is becoming a global health problem affecting approximately 10–40% of the global population (Björkstén et al., 2008; World Allergy Organization, 2013; Bernstein et al., 2016). Although it is not a condition that is associated with high morbidity and mortality, it generates a heavy burden and has a negative impact on the patients' quality of life (QoL) by reducing performance at work and disturbing sleep. In some cases, the condition can persist throughout the patient's life. The common symptoms of AR include nasal congestion, rhinorrhea, nasal itchiness and/or itchy eyes, sneezing, and postnasal drip (Klimek et al., 2019). Uncontrolled moderate or severe AR may also impact the control of asthma (Thomas, 2006).

Currently, AR is classified according to the duration (intermittent or persistent) and severity (mild, moderate/severe) of symptoms. Intermittent AR is diagnosed if the frequency of symptoms is fewer than four times per week or a month per year. A frequency greater than this is classified as persistent. Moreover, the impact of the disease on a patient's QoL

TABLE 2 | Plant's constituents in Triphala exhibiting potential benefits in alleviating AR symptoms.

Compound	Mechanism of action	Potential benefits in AR
Quercetin	<p>Suppresses pro-inflammatory cytokines and inflammatory inducers such as COX-2, VIP, substance P, CGRP, NGF, and HIR gene upregulation in animal models of antigen-induced AR (Mlcek et al., 2016)</p> <p>Reduces periostin production from IL-4-induced HNEpC through inhibition of signal transducer and activator of STAT6 activation and reduces RANTES and eotaxin production in periostin-stimulated HNEpC through suppression of activation of NF-κB p65 (Irie et al., 2016)</p> <p>Reduces NO production from nasal epithelial cells after IL-4 stimulation (Ebihara et al., 2018)</p> <p>Reduces neuropeptide production in nasal lavage fluids induced by TDI nasal challenge in rat model (Kashiwabara et al., 2016)</p> <p>Reduces eosinophil count in nasal mucosa in rat model of AR (Sagit et al., 2017)</p> <p>Inhibits expression of inflammatory cytokines in stimulated human mast cell line (Min et al., 2007)</p> <p>Inhibits the release of histamine, LTs, PGD2, and GM-CSF from human cultured mast cell (Kimata et al., 2000)</p> <p>Inhibits the production of IL-5 and IL-13 and increases IFN-γ production from CD4⁺ T cells induced by IL-4 stimulation (modulate Th1/Th2 balance) (Tanaka et al., 2020)</p> <p>Increases thioredoxin levels in H₂O₂-induced nasal epithelial cells and in nasal lavage fluid of OVA-sensitized mice and decreases nasal symptoms (Edo et al., 2018)</p> <p>Reduces histamine- and PMA-induced up-regulation of H1R gene expression in HeLa cells (Hattori et al., 2013)</p> <p>Reduces secretion of allergic mediators in RBL-2H3 cells, decreases CD23 mRNA expression and p38 MAPK activation in IL-4 stimulated Caco-2 cells, and suppresses IgE-OVA-induced ERK activation and chemokine release (Lee et al., 2010)</p>	<p>Reduction of the release of histamine, inflammatory cytokines, and chemokines</p> <p>Reduction of nasal symptoms</p>
Kaempferol	<p>Moderates several kinds of cytokines and inflammatory markers in both the eosinophil cell line and the OVA-induced AR mouse model (Oh et al., 2013)</p> <p>Inhibits IgE-mediated anaphylaxis <i>in vivo</i> and in human mast cells, reduces serum concentrations of histamine, TNF-α, IL-8, and monocyte chemo-attractant protein-1 (Cao et al., 2020)</p> <p>Reduces serum histamine and COX-2 protein expression in lung tissues in OVA-sensitized mice (Kang et al., 2018)</p> <p>Reduces inflammatory cells in blood sample of BSA-challenged asthmatic mice and inhibits airway wall thickening through disturbing Syk-PLCγ signaling and PKCμ-ERK-cPLA2-COX2 signaling in antigen-exposed mast cells (Shin et al., 2015)</p> <p>Reduces LPS-induced epithelial eotaxin-1 expression, decreases TNF-α-induced eosinophil recruitment, reduces epithelial inflammation, and reduces allergic and inflammatory airway in OVA-challenged mice through disturbing NF-κB signaling (Gong et al., 2012)</p> <p>Inhibits IL-4 activation of STAT6 through type I receptors expressing JAK3 (Cortes et al., 2007)</p> <p>Reduces fibrotic airway remodeling via bronchial epithelial-to-mesenchymal transition by modulating PAR1 activation (Gong et al., 2014)</p> <p>Reduces secretion histamine in IgE-stimulated RBL-2H3 cells and suppressed mast-cell-dependent PCA in IgE-sensitized mice (Kim et al., 2014)</p> <p>Suppresses LPS-induced Th1, Th2, and neutrophil-related chemokines in THP-1 cells (Huang et al., 2010)</p> <p>Reduces secretion of allergic mediators in RBL-2H3 cells, decreases CD23 mRNA expression and p38 MAPK activation in IL-4 stimulated Caco-2 cells, and suppresses IgE-OVA-induced ERK activation and chemokine release (Lee et al., 2010)</p>	<p>Reduction of the release of histamine, inflammatory cytokines, and chemokines</p> <p>Reduction of allergic reaction</p>
Ellagic acid	<p>Accelerates the resolution of allergic airways inflammation in mouse model of ovalbumin-induced asthma and reduces total leukocytes and eosinophils numbers in the BALF, the mucus production, and lung inflammation in part by reducing IL-5 concentration, EPO activity, and P-selectin expression (De Freitas Alves et al., 2013)</p> <p>Reduces the vascular permeability changes, reduces IL-6, increases levels of IL-10, reduces neutrophil recruitment to the BALF, and reduces COX-2-induced exacerbation of inflammation (Cornélio Favarin et al., 2013)</p> <p>Inhibits anti-DNP IgE-mediated passive cutaneous anaphylaxis, reduces histamine release and the expression and secretion of pro-inflammatory cytokines, such as TNF-α and IL-6, and reduces activation of NF-κB (Choi and Yan, 2009)</p> <p>Antioxidant (free radical scavenging activity) (Rios et al., 2018)</p>	<p>Clearance of allergic airways inflammation and asthma</p>

(Continued on following page)

TABLE 2 | (Continued) Plant's constituents in Triphala exhibiting potential benefits in alleviating AR symptoms.

Compound	Mechanism of action	Potential benefits in AR
Gallic acid	Alleviates nasal inflammation in a mouse model of OVA-induced AR (Fan et al., 2019) Inhibits of pro-inflammatory cytokines and histamine release (Kim et al., 2006) Suppresses AR-related mediators both <i>in vitro</i> and <i>in vivo</i> (Ebihara et al., 2018; Edo et al., 2018) Suppresses pro-inflammatory cytokines and inflammatory inducers (Mlcek et al., 2016) Reduces markers of respiratory inflammation (Irie et al., 2016; Edo et al., 2018) Inhibits IL-33-mediated ILC2 activation and subsequent Th2 cytokine release via downregulation of the MyD88/NF- κ B signaling pathway in ovalbumin-induced asthma in mice (Wang et al., 2018) Antioxidant (Roidoung et al., 2016)	Alleviation of nasal symptoms caused by inflammatory cytokines and autacoids Reduction of oxidative stress in AR and may suppress exacerbation of AR-related symptoms
Vitamin C	Reduces MDA, an important oxidative stress marker (Seo et al., 2013; Tongtako et al., 2018) Combined with exercise helps increase PNIF, reduce rhinitis symptoms, nasal blood flow, and MDA levels, decreases nasal secretion IL-4, and increase nasal secretion IL-2 levels (Tongtako et al., 2018) Less decline in pulmonary function when compared to placebo in crossover RCT (Forte et al., 2018) Reduces eosinophil infiltration and increases ratio of IFN- γ /IL-5 cytokines in bronchoalveolar lavage fluid in OVA-challenged mouse model (Chang et al., 2009)	Reduction of oxidative stress in AR and may suppress exacerbation of AR-related symptoms Reduce rhinitis symptoms and other nasal symptoms
Chebulinic acid	A strong antioxidant (Lee et al., 2007) Inhibits influenza viral neuraminidase (Li et al., 2020) DNA gyrase inhibitors (Khan et al., 2018)	Reduction of oxidative stress in AR and may suppress exacerbation of AR-related symptoms Alleviation of symptoms resulted from viral and bacterial infection in AR patients
Chebulagic acid	Inhibits enterovirus 71 replication, inhibits influenza viral neuraminidase (Yang et al., 2013) Reduces onset and progression of collagen-induced arthritis in mice (reduces serum levels of total and anti-collagen IgG, IL-10, and IL-6 but increases TGF- β) (Lee et al., 2005) Inhibits the LPS-induced expression of TNF- α and IL-1 β in endothelial cells (Liu et al., 2015) Inhibits COX-2 and 5-LOX enzymes (Reddy et al., 2009; Athira et al., 2013)	Alleviation of symptoms resulted from viral infection in AR patients Reduction of inflammatory signaling in the airway
Embicanin	Possesses strong free radical-scavenging activity (>gallic acid > ellagic acid > ascorbic acid) (Pozharitskaya et al., 2007)	Reduction of oxidative stress in AR and may suppress exacerbation of AR-related symptoms

BALF, bronchoalveolar lavage fluid; cPLA2, cytosolic phospholipase A2; DNA, deoxyribonucleic acid; DNP, dinitrophenyl; EPO, eosinophil peroxidase; ERK, extra signal-regulated protein kinase; GM-CSF, granulocyte-macrophage colony-stimulating factor; H1R, histamine H1 receptor; THP-1, human monocyte cell line; H₂O₂, hydrogen peroxide; LTs, leukotrienes; LPS, lipopolysaccharide; LOX, lipoxygenases; PAC, passive cutaneous anaphylaxis; PNIF, peak nasal inspiratory flow; PMA, phorbol-12-myristate-13-acetate; PLC γ , phospholipase C γ ; PAR-1, protease-activated receptor-1; PKC μ , protein kinase C μ ; RCT, randomized clinical trial; RANTES, regulated on activation; normal T-cell expressed and secreted; TGF- β , transforming growth factor- β ; TBI, toluene 2,4-diisocyanate.

is also used to evaluate the severity of the symptoms. Symptoms are considered to be mild if normal daily activities, such as sleep, study, and work, can be undertaken without troublesome or interfering symptoms. On the other hand, if a patient presents at least one symptomatic difficulty, then the symptoms are defined as moderate/severe (Figure 1) (Klimek et al., 2019). Therefore, consideration of both duration and severity is an important guide to choosing the most suitable treatment for each patient.

The key elements for AR management are as follows: 1) avoidance of suspected allergens in sensitized individuals, 2) providing appropriate therapeutic agents to reduce nasal symptoms and improve patients' QoL, and/or 3) considering allergen-specific immunotherapy (AIT) (Varshney and Varshney, 2015). The list of medications used for AR, their mechanism of action, and their known adverse effects are listed in Table 1 (Bousquet et al., 2008; Klimek et al., 2019;

Hossenbaccus et al., 2020). Although these treatments alleviate many AR-causing symptoms effectively, their use may also cause additional adverse effects.

The pathophysiology of AR is quite complex (Figure 2), beginning with sensitization and early and late-phase responses (Min, 2010; Sin and Togias, 2011). Allergens can enter the submucosal area guided by antigen-presenting cells (APCs), which are mainly dendritic cells and macrophages, or pass through disturbed epithelial cells (Bharadwaj et al., 2007; Lambrecht and Hammad, 2010). Some allergens may have an additional protease-related activity to help them cleave the tight junctions between epithelial cells (Reithofer and Jahn-Schmid, 2017). After recognizing the antigen, the activated APCs then undergo maturation, migrate to regional lymph nodes, and present allergen peptides to naïve T cells (Th0). The presentation of peptides requires the involvement of major histocompatibility

TABLE 3 | Triphala and its constituents with anti-oxidative properties.

Herbs	Extracts	Models		Results	References
		<i>In vitro</i>	<i>In vivo</i>		
Triphala <i>P. emblica</i> L. (T1) <i>T. chebula</i> retz. (T2) <i>T. bellirica</i> (gaertn.) roxb. (T3)	50% ethanol	Bleomycin and paraquat- induced ROS in HeLa cells		↓ROS levels in bleomycin induction (Triphala > T3 > T2 > T1), in paraquat induction (T1 > Triphala > T2 > T3) (dose = diluted at 3×10^{-5})	(Takauji et al., 2016)
Triphala	n/a (powder mixed with diet)		Mice DMH-induced ER stress in mouse liver. (5% w/w mixed with diet for 14 days; negative control: normal diet)	↓Hepatic oxidative stress (↓MDA and LDH) ↑Anti-oxidative enzymes (↑GSH and GST)	(Sharma and Sharma, 2011)
Triphala	Mixed with normal saline		Rat LPO, SOD, CAT, and GPx levels in noise-induced stress rats (extract = 1 g/kg, p.o. for 48 days; negative control: Saline)	↓MDA and corticosterone while ↑SOD, GPx, and vitamin C level in plasma and spleen (MAC = 1 g/kg) ↑CAT in spleen (MAC = 1 g/kg)	(Srikumar et al., 2006)
<i>P. emblica</i> L. (T1)	70% methanol		Mice SOD, CAT, GST, GSH in liver (extract = 10, 50, and 100 mg/kg, p.o. for 7 days) negative control: normal saline	↑SOD, CAT, GST, and GSH content in liver (MAC = 10 mg/kg)	(Hazra et al., 2010)
<i>T. chebula</i> retz. (T2) <i>T. bellirica</i> (gaertn.) Roxb.(T3) <i>P. emblica</i> L.	Water	H ₂ O ₂ - induced U937 human myeloleukemic model Positive control: Gallic acid, trolox		↓ROS production in H ₂ O ₂ -induced human myeloleukemic U937 cells (IC50 = 295.0 µg/ml)	(Charoenteeraboon et al., 2010)
<i>T. chebula</i> retz	Distilled water		Young and aged rats (extract = 200 mg/kg, p.o. for 4 weeks; negative control: sterile water)	↑Enzymatic (MnSOD, CAT, GR, GST, GSH, G6PDH) and non-enzymatic antioxidants (GPx, vitamin E, and vitamin C levels) in liver and kidney of aged rats ↓Oxidative stress markers (MDA, PCO, LF, XO) in liver and kidney of aged rats ↑Enzymatic (GST, G6PD) and non-enzymatic antioxidants (GST) as well as ↓Oxidative stress marker (MDA, PCO, XO) in liver of young rats	(Mahesh et al., 2009)

DMH, 1,2-dimethylhydrazinedihydrochloride; ABTS^{•+}, 2,2'-azino-bis(3-ethylbenzthiazoline-6-sulphonic acid); IC50, 50% inhibitory concentration; ER, endoplasmic reticulum; EDTA, ethylenediaminetetraacetic acid; FRAP, ferric reducing ability of plasma; G6PD, glucose-6-phosphate dehydrogenase; GR, glutathione reductase; HDF, human dermal fibroblast; H₂O₂^{•-}, hydrogen peroxide; [•]OH, hydroxyl radical; HOCl, hypochlorous acid; LPO, lipid peroxidation; LF, lipofuscin; Mn-SOD, manganese superoxide dismutase; MAC, minimal active concentration; NO, nitric oxide; ONOO⁻, peroxynitrite; PCO, protein carbonyl; RBC, red blood cell; Roxb., *Triphala*; GSH, reduced glutathione; TEAC, Trolox equivalent antioxidant concentration; ¹O₂, singlet oxygen; O₂^{•-}, superoxide anion radical; XO, xanthine oxidase.

complex (MHC) class II molecules expressed on the APC surface, together with T cell receptors located on naïve T lymphocyte (Th0) surfaces (Bharadwaj et al., 2007). Depending on the cytokine-stimulated pattern, the Th0 cells can be differentiated into T helper type 1 (Th1) and T helper type 2 (Th2) cells (Zhu et al., 2010). Recognition of the antigenic peptides, together with activation by interleukin-4 (IL-4) derived from various resident cells, drives the Th0 cells to preferentially acquire the differentiated form of Th2 cells (Zhu et al., 2010). Furthermore, the release of IL-4, IL-5, and IL-13 by Th2 cells induces B-cell immunoglobulin class-switch recombination (Poulsen and Hummelshøj, 2007). The gene segments responsible for encoding the immunoglobulin heavy

chain are rearranged in order to produce allergen-specific IgE antibodies (Gadermaier et al., 2014).

The early phase occurs in sensitized individuals within minutes of exposure to allergens. Soluble IgE antibodies, which are produced by B cells in the sensitization phase, locally diffuse and systematically enter the body fluids via lymphatic vessels (Burton and Oettgen, 2011). IgE can strongly bind to the tetrameric (αβγ2) high-affinity surface receptors for IgE (FcεRI) on tissue mast cells and basophils (Turner and Kinet, 1999). Any cells with surface-bound IgE antibodies are called sensitized cells, and they are prompted to respond to specific antigens through the membrane-bound IgE

TABLE 4 | Triphala and its constituents with anti-inflammatory properties.

Herbs	Extracts	Models		Results	References
		<i>In vitro</i>	<i>In vivo</i>		
Triphala	Water		Mice CFA-induced arthritis (extract = 1 g/kg, p.o. for 8 days) Positive control: indomethacin (3 mg/kg, p.o. for 8 days)	↓paw edema ↓lysosomal enzymes (acid phosphatase, E-glucuronidase, N-acetyl glucosaminidase, and E-galactosidase) in plasma, liver, and spleen ↓protein-bound carbohydrates (hexose, hexosamine, hexuronic acid, fucose, and sialic acid) in liver and spleen ↓marker enzymes (AST, ALT, and ALP) in plasma, liver, and spleen	(Rasool and Sabina, 2007)
Triphala	Methanol		Rats Carrageenan-induced edema (extract = 100 and 200 mg/kg, p.o. single dose) Cotton pellet induced granuloma (extract = 100 and 200 mg/kg, p.o. for 7 days; negative control: 1% tween 80; positive control: indomethacin = 10 mg/kg, p.o. for 7 days)	↓paw edema (MAC = 100 mg/kg) ↓wet and dried weight of cotton pellet (MAC = 200 mg/kg)	(Prabu et al., 2008)
Triphala	Water		Rats EPP and AA-induced ear edema (extract = 4 mg/ear, topical application; negative control: Mixture of dimethylsulfoxide and acetone, 1:1; positive control: phenylbutazone = 1 mg/ear, phenidone = 2 mg/ear) Carrageenan-induced paw edema (extract = 300–200 mg/kg, p.o.; negative control: distilled water; positive control: aspirin = 300 mg/kg) Cotton pellet-induced granuloma formation (extract = 1,200 mg/kg, p.o. for 7 days; negative control: distilled water; positive control: aspirin = 300 mg/kg, prednisolone = 5 mg/kg)	↓EPP-induced ear edema ↔ AA-induced ear edema ↓carrageenan-induced paw edema (MAC = 300 mg/kg) ↔ granuloma formation	(Sireeratawong et al., 2013)
Triphala	Water		Rats CFA-induced arthritis (extract = 100 mg/kg, i.p. for 7 days; negative control: saline; positive control: indomethacin = 3 mg/kg, i.p.)	↓lipid peroxidation, glycoproteins (hexose, hexosamine, and sialic acid), and lysosomal enzymes (acid phosphatase, β-galactosidase, N-acetyl β-glucosaminidase, and cathepsin-D) in paw tissues ↑SOD, CAT, GPx, GST, and GSH in paw tissues ↓TNF-α, IL-1β, VEGF, MCP-1, and PGE2 levels in serum and paw tissues	(Kalaiselvan and Rasool, 2015)

(Continued on following page)

TABLE 4 | (Continued) Triphala and its constituents with anti-inflammatory properties.

Herbs	Extracts	Models		Results	References
		<i>In vitro</i>	<i>In vivo</i>		
Triphala	Distilled water	LPS stimulated RAW 246.7 macrophage (extract = 100–300 µg/ml)		↓TNF-α, IL-1β, IL-6, MCP-1, VEGF, NO, PGE2 levels (MAC = 200 µg/ml) ↓lysosomal enzymes [β-galactosidase, N-acetyl β-glucosaminidase, cathepsin-D (MAC = 100 µg/ml), and acid phosphatase (MAC = 300 µg/ml)] ↓TNF-α, IL-1β, IL-6, MCP-1, NF-kBp65, COX-2 and ↑HO mRNA expression (MAC = 200 µg/ml) ↓NF-kBp65 and pNF-kBp65 protein expression (MAC = 200 µg/ml) ↓overexpressed TNF-α, IL-17, iNOS, COX-2 (MAC = 200 µg/ml) ↓free radical formation (MAC = 100 µg/ml) ↓p-NF κB p65, IL-17, COX-2 and RANKL protein expression in paw tissues	(Kalaiselvan and Rasool, 2016)
Triphala (AIE)	Ethanol	TNF-α induced inflammation in retinal choroid microvascular endothelial cells (RF/6 A) (AIE = 1–50 µg/ml, CA, CI and GA = 1–100 µg/ml)	Rats CFA-induced arthritis extract = 100 mg/kg, i.p. for 7 days; negative control: Saline; positive control: indomethacin = 3 mg/kg, i.p. for 7 days)	↓MMP-9 expression (MAC of AIE, CA and CI = 10 µg/ml, GA = 50 µg/ml) ↓tube formation, chemotaxis, endothelial cell proliferation (MAC of AIE, CA and CI = 10 µg/ml, GA = 100 µg/ml) ↓IL-6, IL-8, and MCP-1 expression (MAC of AIE = 100 µg/ml, CA and CI = 10 µg/ml, GA = 50 µg/ml) ↓phosphorylation of p38, ERK and NF-κB (MAC of AIE, CA and CI = 10 µg/ml, GA = 100 µg/ml)	(Shanmuganathan and Angayarkanni, 2018)
Chebulagic acid (CA)				Binding energy of CA = 6.4 kcal/mol, CI = 7.7 kcal/mol, GA = 6.3 kcal/mol	
Chebulinic acid (CI)				↓angiogenesis (MAC of AIE, CA and CI = 25 µg/ml, GA = 100 µg/ml)	
Gallic acid (GA)					
		<i>In silico</i> docking study: binding to TNF-α-receptor-1	<i>Ex vivo</i> : TNF-α induced angiogenesis in chick chorioallantoic membrane (AIE = 25 µg, CA = 25 µM, CI = 25 µM, GA = 100 µM)		
<i>P. emblica</i> L.	80% methanol		Rats Acetic acid induced colitis (extract = 100 and 200 mg/kg, p.o. for 7 days; positive control: sulfasalazine = 500 mg/kg, p.o. for 3 days)	↓serum LDH (MAC = 100 mg/kg) ↓macroscopic inflammation scores and wet weight of colonic segments (MAC = 200 mg/kg)	(Deshmukh et al., 2010)
<i>P. emblica</i> L.	Hydroalcohol		Rats KA-induced seizures (extract = 300, 500, and 700 mg/kg, i.p. for 7 days; negative control: Normal saline, i.p.)	↓lipid peroxidation in brain (MAC = 300 mg/kg) ↑brain GSH levels (MAC = 500 mg/kg) ↓TNF-α in brain (MAC = 300 mg/kg)	(Golechha et al., 2011)

(Continued on following page)

TABLE 4 | (Continued) Triphala and its constituents with anti-inflammatory properties.

Herbs	Extracts	Models		Results	References
		<i>In vitro</i>	<i>In vivo</i>		
<i>P. emblica</i> L.	70% ethanol free (FPEO) and bounded (BREO) phenolic compounds		<p>Rats</p> <p>Carrageenan-induced paw edema (FPEO and BREO = 20 and 40 mg/kg, p.o.; positive control: diclofenac sodium = 12.5 mg/kg, p.o.; negative control: 1% of carboxy methyl cellulose = 1 ml, p.o.)</p> <p>Cotton pellet-induced granuloma formation (extract = 20 and 40 mg/kg, p.o. for 16 days; negative control: 1% of carboxy methyl cellulose = 1 ml, p.o.; positive control: diclofenac = 12.5 mg/kg, p.o.)</p>	<p>Both FPEO and BREO</p> <p>↓paw edema (MAC = 40 mg/kg)</p> <p>↓granulomatous tissue mass (MAC = 40 mg/kg)</p> <p>↓lipid peroxidation, myeloperoxidase activity, plasma extravasation levels and ↑GSH level (MAC = 40 mg/kg)</p>	(Muthuraman et al., 2011)
<i>P. emblica</i> L.	Commercial fruit extract (patented enzymatic process)	LPS-induced inflammation in HUVEC (extract = 0–100 µg/ml)	<p>Rats</p> <p>LPS-induced endotoxemia (50 mg/kg, p.o.; negative control: PBS = 50 mg/kg, p.o.)</p>	<p>↓adhesion of THP-1 cells (MAC = 1 µg/ml)</p> <p>↓E-selectin mRNA expression (MAC = 30 µg/ml)</p> <p>↓serum TNF-α and IL-6 levels (MAC = 50 mg/kg)</p>	(Pradyumna Rao et al., 2013)
<i>P. emblica</i> L.	Hydro-alcohol		<p>Rats</p> <p>Carrageenan (positive control: indomethacin 10 mg/kg, p.o.), histamine (positive control: CPM 3 mg/kg, p.o.), serotonin (positive control: CPH 3 mg/kg, p.o.), and PGE2 (positive control: PBZ 100 mg/kg, p.o.)-induced hind paw edema (extract = 300, 500, and 700 mg/kg, i.p.; negative control: saline = 1 ml/kg, i.p.)</p> <p>Cotton pellet-induced granuloma formation (extract = 300, 500, and 700 mg/kg, i.p. for 7 days; negative control: Saline = 1 ml/kg, i.p.; positive control: indomethacin = 10 mg/kg, p.o.)</p>	<p>↓paw edema (MAC = 300 mg/kg)</p> <p>↑GSH, catalase, and SOD level in paw tissues (MAC = 500 mg/kg)</p> <p>↓MDA level in paw tissues (MAC = 300 mg/kg)</p> <p>↓granulomatous tissue mass (MAC = 300 mg/kg)</p>	(Golechha et al., 2014)
<i>P. emblica</i> L.	Methanol		<p>Rats</p> <p>Carrageenan-induced paw edema (extract = 200 and 400 mg/kg; positive control: diclofenac = 10 mg/kg)</p>	<p>↓paw edema (MAC = 200 mg/kg)</p> <p>↓IL-1β, TNF-α levels (MAC = 200 mg/kg)</p>	(Middha et al., 2015)
<i>P. emblica</i> L.	Ethyl acetate fraction		<p>Mice</p> <p>Arsenic-induced inflammation (extract = 500 mg/kg, p.o. for 30 days; negative control: 2% gum acacia)</p>	<p>↓serum TNF-α, IL-1β, IL-6 (MAC = 500 mg/kg)</p> <p>Restore T cells and B cells</p> <p>Reverse thymus and spleen weight</p>	(Singh et al., 2015)

(Continued on following page)

TABLE 4 | (Continued) Triphala and its constituents with anti-inflammatory properties.

Herbs	Extracts	Models		Results	References
		<i>In vitro</i>	<i>In vivo</i>		
<i>T. chebula</i> retz	50% methanol		Rats Formaldehyde-induced arthritis (extract = 20, 40, and 80 mg/kg, p.o. for 10 days)	↓ joint swelling (MAC = 40 mg/kg) ↓ serum TNF- α (MAC = 40 mg/kg) ↓ synovial expression of IL-1 β , IL-6, and TNFR1 (maximum at 80 mg/kg)	(Nair et al., 2010)
<i>T. chebula</i> retz	50% methanol		CFA-induced arthritis (extract = 20, 40, and 80 mg/kg, p.o. for 21 days; positive control: indomethacin = 3 mg/kg) Rats Carrageenan-induced paw edema (extract = 20, 40, and 80 mg/kg, p.o.) Cotton pellet-induced granuloma formation (extract = 20, 40, and 80 mg/kg, p.o. for 6 days)	↓ joint swelling (MAC = 20 mg/kg) ↓ paw edema (MAC = 80 mg/kg) ↓ dry granuloma weight (MAC = 40 mg/kg) ↓ TNF- α , IL-6 and IL- β levels (MAC = 80 mg/kg)	(Nair et al., 2012)
<i>T. chebula</i> retz	95% ethanol		CFA-stimulated peritoneal macrophages (extract = 80 mg/kg, p.o. for 6 days; negative control; 1% gum acacia; positive control: indomethacin = 3 mg/kg) Mice Croton oil-induced ear dermatitis (extract = 100 mg/ml, topical application)	↓ TNF-R1 expression on peritoneal macrophage (MAC = 80 mg/kg) ↓ ear thickness (MAC = 100 mg/kg) ↓ ear plug weight (MAC = 100 mg/kg)	(Sukakul et al., 2013)
<i>T. chebula</i> retz	70% ethanol	Human RBC stablization method (extract = 50, 100, 250, 500 μ g/ml)	Rats Carrageenan-induced high paw edema (extract = 50, 100, 250, and 500 mg/kg p.o.; negative control: normal saline; positive control: indomethacin 5 mg/kg, p.o.)	↓ MDA formation (MAC = 50 mg/kg) ↓ paw edema (MAC = 50 mg/kg) ↑ human RBC membrane stability (MAC = 50 μ g/ml)	(Bag et al., 2013)
<i>T. chebula</i> retz	80% ethanol		Rats Carrageenan-induced paw edema (extract = 300 mg/kg; negative control: normal saline; positive control: diclofenac 100 mg/kg)	↓ paw edema (MAC = 300 mg/kg)	(Ibne Jami et al., 2014)
<i>T. chebula</i> retz	100% methanol	LPS-stimulated mouse macrophage cells (RAW 264.7) (compounds = 10, 50 μ M; positive control: parthenolide 10 μ M, indomethacin 10 μ M)		↓ NO production chebulinic acid (MAC = 50 μ M) 2,3,6-tri-O-galloyl-B-D-glucose (MAC = 50 μ M) arjunuc acid (MAC = 50 μ M) arjulonic acid (MAC = 50 μ M) ↓ expression of iNOS (MAC = 10 μ M) and COX-2 (MAC = 50 μ M)	(Yang et al., 2014)

(Continued on following page)

TABLE 4 | (Continued) Triphala and its constituents with anti-inflammatory properties.

Herbs	Extracts	Models		Results	References
		<i>In vitro</i>	<i>In vivo</i>		
<i>T. chebula</i> retz	Water		<p>Rats</p> <p>EPP- and AA-induced ear edema (extract = 1, 2, 4 mg/20 μL/ear; positive control: phenylbutazone, phenidone 1 and 2 mg/ear)</p> <p>Carrageenan-induced paw edema (extract = 150, 300, and 600 mg/kg; negative control: normal saline; positive control: Aspirin 300 mg/kg)</p> <p>Cotton pellet-induced granuloma formation (extract = 600 mg/kg, p.o. for 7 days; positive control: Aspirin 300 mg/kg, prednisolone 5 mg/kg)</p>	<p>↓EPP-induced ear edema (MAC = 1 mg/ear)</p> <p>↔ AA-induced ear edema</p> <p>↓paw edema (MAC = 1 mg/kg)</p> <p>↔ granulomatous tissue mass</p>	(Sireeratawong et al., 2014)
<i>T. chebula</i> retz	Methanol		<p>Rats</p> <p>Carrageenan-induced paw edema (extract = 100 and 200 mg/kg, p.o.)</p> <p>Cotton pellet-induced granuloma formation in rats (extract = 100 and 200 mg/kg, p.o. for 7 days; negative control: 1% Tween80 2 ml/kg, p.o; positive control: indomethacin" 10 mg/kg, p.o.)</p>	<p>↓paw edema (MAC = 100 mg/kg)</p> <p>↓granulomatous tissue (MAC = 200 mg/kg)</p>	(Kirubanandan et al., 2015)
<i>T. chebula</i> retz	<i>Terminalia chebularin</i> (polyphenolic compound from fruit)	M5 (a cocktail of IL-1 α , IL-17A, IL-22, oncostatin M, and TNF α)-induced HaCaT cells proliferation (extract = 10 μ g/ml)		<p>↓TBARS content, ROS production</p> <p>↑GSH level (MAC = 10 μg/ml)</p> <p>↓TNFα, IL-17A, IL-23b, MMP-9, cyclinD, cyclinE mRNA expression (MAC = 10 μg/ml)</p> <p>↓overexpressed p65 NF-κB expression in tissues and cells (MAC = 10 μg/ml)</p>	(An et al., 2016)
			<p>Mice</p> <p>IMQ-induced psoriatic skin lesion (extract = 50 mg/kg, intragastric; negative control: vehicle vaseline cream)</p>	<p>↓skin lesion through heme oxygenase-I (MAC = 50 mg/kg)</p> <p>↓TNFα, IL-17 A and IL-23 b levels in serum and skin (MAC = 50 mg/kg)</p> <p>↑HO-1 expression (MAC = 50 mg/kg)</p>	
<i>T. chebula</i> retz	Water		<p>Osteoarthritic dogs (extract = 500 mg p.o. bid for 150 days; negative control: placebo capsule)</p>	<p>↓pain upon limb manipulation significance at 90 days</p> <p>↓ESR significance at 120 days</p>	(Murdock, 2015)
<i>T. chebula</i> retz	70% ethanol	LPS-induced primary microglia cells isolated from mice (extract = 5,10,20,40,80 μ g/ml)		<p>↓TNF-α, IL-1β, IL-6, COX-2, PGE-2, NO concentration (MAC = 20 μg/ml)</p> <p>↓TNF-α, IL-1β, IL-6, COX-2, iNOS mRNA expression (MAC = 20 μg/ml)</p> <p>↑Arg-1 mRNA expression (dose dependence) (MAC = 20 μg/ml)</p> <p>↑urea production (MAC = 40 μg/ml)</p>	(Rahimi et al., 2018)

(Continued on following page)

TABLE 4 | (Continued) Triphala and its constituents with anti-inflammatory properties.

Herbs	Extracts	Models		Results	References
		<i>In vitro</i>	<i>In vivo</i>		
<i>T. bellirica</i> (gaertn.) roxb	70% aqueous acetone	Radical scavenging activity		↓ROS generation in LPS stimulated RAW 264.7 macrophage cells (MAC = 100 µg/ml) ↓total COX activity, MPO, total 5- LOX activity (MAC = 25 µg/ml) ↓ <i>TNF-α</i> , <i>IL-6</i> and <i>COX-2</i> mRNA expression (MAC = 25 µg/ml)	(Jayesh et al., 2018)
<i>T. bellirica</i> (gaertn.) roxb	Water	LPS- or palmitic acid-induced macrophage RAW 264.7 cell (extract = 100, 200, 400 µg/ml; negative control: Distilled water; positive control: GA = 46 µg/kg, EA = 1.6 µg/kg)	LPS-shock model mice (extract = 400 mg/kg, p.o.; negative control: Distilled water)	↓ROS production (MAC = 100 µg/ml) ↓ <i>TNF-α</i> , <i>IL-1β</i> , <i>IL-6</i> , <i>MCP-1</i> , <i>CCL-2</i> , <i>MSR</i> , <i>NOS2</i> mRNA expression (MAC = 400 µg/ml) ↓SR-A protein expression ↓ROS production (MAC = 100 µg/ml) ↓NF-κB nuclear translocation, ↓phosphorylation of NF-κB p65, p38, JNK, and ERK (MAC = 400 µg/ml) Activate Akt/AMPK/Nrf2 pathway (MAC = 100 µg/ml) ↑mRNA expression of antioxidant enzymes (catalase, NQO1, and GCLM) ↓ <i>TNF-α</i> and <i>IL-6</i> mRNA expression Prevent oxidative stress and inflammation in endotoxemic mice ↓paw edema (MAC = 100 mg/kg)	(Tanaka et al., 2018)
<i>T. bellirica</i> (gaertn.) roxb	Ethanol		Rats Carrageenan-induced paw edema (extract = 100, 200, and 400 mg/kg; negative control: distilled water, positive control: Indomethacin 3 mg/kg)		(Chauhan et al., 2018)

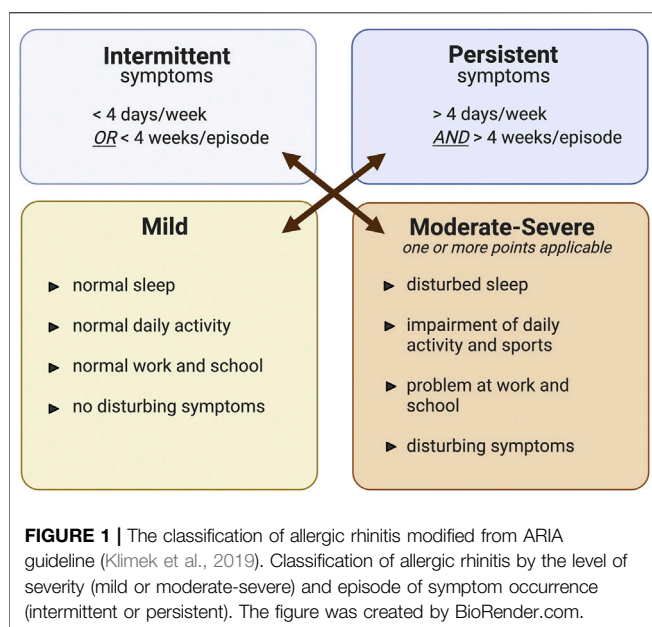
ALP, alanine aminotransferase; ALT, alkaline phosphatase; AA, arachidonic acid; AST, aspartate aminotransferase; CCL-2, C-C motif chemokine ligand 2 gene; CPM, chlorpheniramine; SR-A, class A scavenger receptor A; CFA, complete Freund's adjuvant; CPH, cyproheptadine; ESR, erythrocyte sedimentation rate; GCLM, glutamate-cysteine ligase modifier subunit; HUVEC, human umbilical vein endothelial cells; IMQ, imiquimod; KA, kainic acid; MSR, macrophage scavenger receptor gene; MPO, myeloperoxidase; NQO1, NADPH quinone oxidoreductase 1; PBZ, phenylbutazone; RANKL, receptor activator of nuclear kappa-B ligand; TBARS, thiobarbituric acid reactive substances; vWF, von Willebrand factor.

antibodies. The crosslinking of adjacent IgE antibodies by allergens induces aggregation of FcεRI and then triggers a rapid degranulation and secretion of various mediators, including histamine and tryptase (Turner and Kinet, 1999). Mast cells also release newly synthesized lipid mediators, including leukotrienes (LTC₄, LTD₄, and LTE₄) and prostaglandins (PGD₂) to help sustain inflammation by neutrophil and eosinophil infiltration (Fanning and Boyce, 2013).

There are many signs and symptoms associated with the early phase of AR, such as nasal pruritus, sneezing, and coughing caused by the histamine-stimulated sensory nerve endings of the trigeminal nerves (Taylor-Clark et al., 2005; Rosa and Fantozzi, 2013). The activation of sympathetics and parasympathetics by histamines can also stimulate the mucous glands to produce a watery discharge that is presented as rhinorrhea (Al Suleimani and Walker, 2007). Histamines, together with leukotrienes and

prostaglandins, act on blood vessels, causing vasodilation and nasal congestion (White, 1990).

The late phase response is characterized by recruitment of T cells, eosinophils, basophils, and neutrophils following a release of their various mediators, which leads to a continuation of the symptoms and inflammatory induction. This phase usually begins around 4–5 h following exposure to allergens and can last for 24 h. Some cytokines, such as IL-4, IL-13, and tumor necrosis factor-α (TNF-α) released from mast cells, have the ability to upregulate two adhesion molecules, which are vascular cell adhesion molecule-1 (VCAM-1) and intracellular cell adhesion molecule-1 (ICAM-1) (Lee et al., 1994). These adhesion molecules subsequently induce migration of basophils, eosinophils, neutrophils, and T cells to the nasal mucosa. Moreover, an activated form of group 2 innate lymphoid cells (ILC2), which are induced by mast cell-related



cytokines (leukotrienes, prostaglandins, and platelet-activating factor (PAF)) play a role in continuing the inflammation by releasing large amounts of Th2 cytokines (Li and Hendriks, 2013). Neutrophils that are recruited into the nasal mucosa can harm the epithelium by inducing reactive oxygen species (ROS) and enzyme (protease, matrix metalloproteinase 9 (MMP-9), and myeloperoxidase) production (Lacy, 2006; Ventura et al., 2014). Persistent inflammation in the late phase is associated with tissue remodeling, which might also lead to alteration of organ function and nasal hyperresponsiveness (Galli et al., 2008).

TRIPHALA

Triphala, one of the polyherbal formulations used in Ayurvedic medicine, comprises the dried fruits of three plants, namely, *Terminalia chebula* Retz (Family Combretaceae R. Br), *Terminalia bellirica* (Gaertn.) Roxb (Family Combretaceae R. Br), and *Phyllanthus emblica* L (Family Phyllanthaceae Martinov). The composition of Triphala is derived from a rational combination of *T. chebula* Retz., *T. bellirica* (Gaertn.) Roxb., and *P. emblica* L., which are combined to balance the three pillars of life or elemental substances, known in Sanskrit as the three doshas, namely, Vata (elements of space and air), Kapha (elements of earth and water), and Pitta (elements of fire and water) (Peterson et al., 2017). Normally, the herbs are mixed in equal proportions (1:1:1), but sometimes the ratios can be modified to be one part *T. chebula* Retz., two parts *T. bellirica* (Gaertn.) Roxb., and three parts *P. emblica* L (1:2:3) (Gajendra et al., 2016) or one part each of *T. chebula* Retz. and *T. bellirica* (Gaertn.) Roxb. and two parts *P. emblica* L (1:1:2) (Ginsburg et al., 2009). According to a traditional Thai medicine textbook, Triphala is used to provide relief for different disease conditions related to the imbalance of water element (Kapha); specifically,

the difficulty of breathing caused by excessive water-soluble element and mucus retention in the lungs. Although there is no specific definition of AR in Traditional Thai medicine, Triphala is used to reduce runny nose, cough, the viscosity of phlegm, sore and dry throat, and thirst. These symptoms are somehow related to AR symptoms.

Several phytochemicals have been detected in the fruits of these three plants. These include phenolic compounds (gallic acid, ellagic acid, chebulinic acid, chebulagic acid, and emblicanin A and B), flavonoids (quercetin and kaempferol), alkaloids (phyllanthidine and phyllantin), ascorbic acid, carbohydrates, proteins, etc. (Parveen et al., 2018). The amount of each phytochemical varies depending on the methods used to extract it, the solvents used, and the region in which the parent plant was grown (Parveen et al., 2018). One study by Liu et al. found that samples collected from different regions in China contained a range of phenolic contents in *P. emblica* L. methanolic extracts (Liu et al., 2008). Moreover, methanolic extraction appeared to yield more phytochemicals than aqueous extraction (Parveen et al., 2018). Therefore, characterization of the compound to be extracted should be a mandatory procedure before undertaking extraction experiments.

The phytochemicals contained in Triphala may be beneficial for the treatment of AR. Gallic acid and quercetin are prominent phenolic compounds and are well-known antioxidants in AR-related studies. Gallic acid was shown to alleviate nasal inflammation by shifting the immune response toward Th1 in a mouse model of OVA-induced AR (Fan et al., 2019). The increment of Th2 cytokines, including IL-4, IL-5, IL-13, and IL-17 was attenuated, whereas Th1-related cytokines, including interferon- γ (IFN- γ) and IL-12, were upregulated in nasal larval fluid (NALF) upon treatment with gallic acid (Fan et al., 2019). Moreover, histopathological improvements such as nasal mucosa thickening, goblet cell hyperplasia, and eosinophil infiltration, have been observed in a gallic acid-treated group of patients (Fan et al., 2019). One study also found that the AR-positive effects of gallic acid were caused by inhibition of pro-inflammatory cytokines and histamine release via the modulation of cyclic adenosine monophosphate (cAMP), intracellular calcium regulation, NF- κ B), and a p38 mitogen-activated protein kinase (p38 MAPK)-dependent mechanism (Kim et al., 2006).

Quercetin, a flavonoid aglycone, functions extensively as a major active compound in anti-allergic supplements. Both transcriptional and translational levels of AR-related mediators can be suppressed by quercetin both *in vitro* and *in vivo*. In IL-4-induced human nasal epithelial cells (HNEpCs), nitric oxide (NO) production, inducible nitric oxide synthase (iNOS) mRNA expression, and signal transducer and activator of transcription 6 (STAT6) activation are all attenuated (Ebihara et al., 2018; Edo et al., 2018). Quercetin has the ability to suppress pro-inflammatory cytokines and inflammatory inducers such as cyclooxygenase-2 (COX-2), vasoactive intestinal peptide (VIP), substance P, calcitonin gene-related peptide (CGRP), nerve growth factor (NGF), and HIR gene upregulation in animal models of antigen-induced AR (Mlcek et al., 2016). In

TABLE 5 | Triphala and its constituents with immunomodulating properties.

Herbs	Models	Extracts		Results	References
		<i>in vitro</i>	<i>in vivo/clinical</i>		
Triphala	Fruit powder mixed with saline		Rats Noise-induced stress (extract = 1 g/kg/day for 48 days, p.o.; negative control: Saline)	↑Neutrophil function (adherence, phagocytic index, avidity index, NBT reduction) ↓Corticosterone level	(Srikumar et al., 2005)
Triphala	Fruit powder mixed with saline		Rats Noise-induced stress (extract = 1 g/kg/day for 48 days, p.o.; negative control: Normal saline)	↑Pan T cells, CD4 ⁺ /CD8 ⁺ T cells ↑IL-2, IFN-gamma ↓IL-4	(Srikumar et al., 2007)
Triphala	Aqueous fruit powder suspension in 2%gum acacia	PHA induced T-lymphocyte (human blood isolation) proliferation (extract 50, 100 ug/ml for 4 days)	Mice CFA-induced arthritis (extract = 500 and 1,000 mg/kg, p.o. for 5 days) Intraperitoneal SRBC-induced humoral antibody titer (extract = 500 and 1,000 mg/kg, p.o. for 7 days) DTH: SRBC-induced foot paw swelling (extract = 500 and 1,000 mg/kg, p.o. for 4 days)	↓T-lymphocyte proliferation (MAC = 50 ug/ml) ↓Complement activity (MAC = 500 mg/ml) ↓Antibody titer response (MAC = 500 mg/ml) ↓DTH response (MAC = 500 mg/ml)	(Sabina et al., 2009)
Triphala	95% ethanol		healthy volunteer (extract = 1,050 mg/day, p.o. for 2 weeks)	↑Cytotoxic T-cell (CD3 ⁺ CD8 ⁺ CD45 ⁺) and natural killer cells (CD16 ⁺ CD56 ⁺ CD45 ⁺) ↓Cytotoxicity of chromium (MAC = 100 µg/ml) ↓Lymphocyte suppression ↑Restore IL-2, IFN-gamma production ↓Apoptosis and DNA fragmentation	(Phetkate et al., 2012)
<i>P. emblica</i> L.	90% ethanol	Lymphocyte isolation from chromium (10 µg/ml)-induced immunosuppressed rats (extract = 100 µg/ml)		↓CD8 ⁺ T cell, ↑CD4 ⁺ (Th) ↑T (CD3 ⁺) and B(CD19 ⁺) sub cells population	(Sai Ram et al., 2002)
<i>P. emblica</i> L.	95% ethanol		Mice Arsenic induced immunotoxicity (extract = 500 mg/kg, p.o. for 30 days; negative control: 2% gum acacia solution in distilled water)		(Singh et al., 2015)
<i>T. chebula</i> retz	Ethanol		Rats SRBC-induced immune response (extract = 100 mg/kg, p.o. for 11 days; negative control: 1% gum acacia solution in distilled water, cyclophosphamide 100 mg/kg; positive control: SRBC-sensitized rats)	↑Phagocytic activity ↑Neutrophil, lymphocyte, and monocyte ↑Phagocytic activity ↑Serum immunoglobulin	(Aher et al., 2010)
<i>T. chebula</i> retz	70% ethanol		Rats SRBC-induced immune response (extract = 100 mg/kg, p.o. for 14 days; negative control: 1% gum acacia solution in distilled water, cyclophosphamide 100 mg/kg, positive control: SRBC- sensitized rats)	↑Liver mitochondrial enzyme (CAT, SOD, GSH) ↓Liver LPO ↑Lymphocyte proliferation ↑IL-2, IL-10 and TNF-α mRNA expression in spleen cells	(Aher and Wahi, 2011)
<i>T. chebula</i> retz	Water		Mice DNFB-induced atopic symptoms (extract = 100 ug/ml, topical application for 8 days)	↓Ear swelling (thickness) ↓Eosinophil level ↓Atopic biomarkers (MMP-9, IL-31, and T-bet)	(Nam et al., 2011)

(Continued on following page)

TABLE 5 | (Continued) Triphala and its constituents with immunomodulating properties.

Herbs	Models	Extracts		Results	References
		<i>in vitro</i>	<i>in vivo/clinical</i>		
<i>T. chebula</i> <i>retz</i>	Water		Mice Goat RBC or ovalbumin-induced immune system (extract = 100, 200, 300, and 400 mg/kg, p.o. for 10 days)	↑Antibody titer of gRBC (MAC = 200 mg/kg) ↑IFN-gamma (MAC = 300 mg/kg) ↓IL-4 (MAC = 300 mg/kg) ↑Lymphocyte proliferation and macrophage response ↑Bone marrow cellularity and WBC count (MAC = 300 mg/kg)	(Rubab and Ali, 2016)
<i>T. chebula</i> <i>retz</i>	Methanol extract followed by water fraction	Compound 48/80-induced histamine release from RPMC (extract = 0.005–1.0 g/kg)	Compound 48/80-induced anaphylactic shock in mice (extract = 0.001–1.0 g/kg, i.p.; negative control: Saline)	↓Histamine release (MAC = 0.01 g/kg) ↓Mortality rate (MAC = 0.01 g/kg) ↓Serum histamine level (MAC = 0.1 g/kg)	(Shin et al., 2001)
			Anti-DNP IgE-induced passive cutaneous anaphylaxis reaction in rats (extract = 0.001–1.0 g/kg, p.o.)	↓Passive cutaneous anaphylaxis reaction (MAC = 1.0 g/kg) ↑IgE-mediated TNF- α production (MAC = 1 mg/ml)	

NBT, nitro blue tetrazolium; PHA, phytohemagglutinin; RPMC, rat peritoneal mast cells.

addition, periostin, a novel marker of respiratory inflammation, and thioredoxin, an antioxidant enzyme, were found to be moderated by quercetin, resulting in an improvement in AR clinical condition (Irie et al., 2016; Edo et al., 2018). The effects of quercetin were also revealed in the clinical setting in which the combination of herbs [quercetin, *Perilla frutescens* (L.) Britton, and vitamin D3] known as “Lertal[®]” was effective in relieving the overall symptoms of AR and reducing the use of anti-allergic drugs without additional adverse effects (Thornhill and Kelly, 2000).

Other active compounds in Triphala are ascorbic acid (vitamin C) and kaempferol. In particular, the plasma level of ascorbic acid has been found to be reduced in allergic-related diseases in which patients with allergy-related respiratory and cutaneous symptoms can derive benefits after receiving an exogenous vitamin C treatment (Vollbracht et al., 2018). One study found that vitamin C in combination with exercise potentially reduced inflammatory cytokines in nasal secretion, reduced malondialdehyde (MDA), an important oxidative stress marker, and exhibited improvement in physiological function in rhinitis patients (Seo et al., 2013; Tongtako et al., 2018). Kaempferol moderates several kinds of cytokines and inflammatory markers in both the eosinophil cell line and the mouse model of OVA induction, leading to a reduction in AR-related inflammation (Oh et al., 2013).

Considering the beneficial aspect of Triphala for manipulating the pathophysiology of AR, specific convincing compounds (shown in Table 2.) are likely to be major responsible molecules since many previous studies have revealed their

pharmacological activities specifically for physiological processes related to airway inflammation and AR development.

Triphala: Antioxidative Effects

All living cells of organisms are a major source of ROS. Moreover, other exogenous sources of oxidative stress can also induce an exacerbation of AR symptoms. For example, 1) urban pollutants aggravate nasal inflammation and AR-related symptoms, 2) pollen grains that contain endogenous reduced nicotinamide adenine dinucleotide phosphate (NADPH) oxidase damage airway epithelial cells and trigger granulocyte recruitment (Boldogh et al., 2005). However, our bodies have sophisticated antioxidant defense mechanisms, for example, enzymatic mechanisms, including glutathione-S-transferase (GST), superoxide dismutase (SOD), catalase (CAT), glutathione peroxidase (GPx), as well as non-enzymatic mechanisms involving glutathione, ascorbate, urate, α -tocopherol, bilirubin, lipoic acid, transferrin, and albumin, in order to prevent overwhelming by and accumulation of oxidative stress (Frei et al., 1988; Adwas et al., 2019). The imbalance between ROS production and endogenous antioxidant defense leads to an exhaustion of oxidative stress markers such as NO, MDA, and nitrite/nitrate (Birben et al., 2012; Ayala et al., 2014; Nadif et al., 2014).

Oxidative stress is now considered to be one of the markers of the pathogenesis of AR, asthma, and chronic obstructive pulmonary disease (COPD). Epidemiological and clinical studies of AR have found that aeroallergen and pollutant co-exposure can induce immunological effects, leading to recruitment of inflammatory cells, cytokines, chemokines, and

TABLE 6 | Triphala and its constituents in the respiratory system (Antitussive effect + Bronchodilator).

Herbs	Extracts	Models		Results	References
		<i>In vitro</i>	<i>In vivo/Ex-vivo</i>		
<i>P. emblica</i> L.	Absolute ethanol	Cats Mechanical stimulation-induced coughing (extract = 50,200 mg/kg, p.o.; positive control: Codeine 10 mg/kg, i.p., dropropizine 100 mg/kg, i.p.)		↓number of cough efforts, cough frequency, and intensity during expiration and inspiration (MAC = 50 mg/kg)	(Nosál'Ovác et al., 2003)
<i>T. chebula</i> Retz	Polysaccharide extract (water-extracted carbohydrate polymer)	Guineapig Aerosol citric acid (0.3 M) induced cough (extract = 50 mg/kg p.o.; negative control: Water; positive control: Codeine phosphate 10 mg/kg)		↓number of cough efforts	(Nosalova et al., 2013)
<i>T. bellirica</i> (Gaertn.) Roxb	70% methanol	Rats Carbachol (1 µM/kg)-induced bronchoconstriction (extract = 30,100, and 300 mg/kg, i.v.; positive control: salbutamol = 0.001, 0.03, and 0.1 mg/kg, i.v.) Carbachol; CCh 1 µM/kg and K ⁺ 80 mM/kg induced-isolated guineapig's trachea (extract = 0.1–10 mg/ml; negative control: Saline; positive control: Dicyclomine, nifedipine, atropine)		↓bronchoconstriction (18, 39, and 98% inhibition at dose of 30, 100, and 300 mg/kg, respectively) ↓tracheal contraction (IC ₅₀ of CCh = 3.3 mg/ml and IC ₅₀ of K ⁺ = 8.5 mg/ml)	(Gilani et al., 2008)

finally AR-related symptoms (Naclerio et al., 2020). Ozone exposure was also found to exacerbate antigen-induced rhinitis, nasal symptoms such as rhinorrhea, sneezing, nasal hyperresponsiveness, and eosinophil infiltration in guinea pigs (Iijima et al., 2001). An increase in plasma total oxidant status (TOS) and a decrease in the plasma antioxidative enzyme paraoxonase (PON-1) have both been detected in children with persistent AR, and these two factors were correlated with their nasal symptoms. TOS and PON-1 may serve as disease markers in children with AR (Ozkaya et al., 2013). Therefore, any treatments that can attenuate this increase in oxidants and prevent the decrease in endogenous antioxidants may help improve AR-related symptoms and can be considered a new strategy for treating AR.

In recent decades, several studies have examined and described the antioxidative properties of Triphala, as shown in **Table 3**. Even with different extraction methods, Triphala retains its ability to scavenge free radicals in both *in vitro* and *in vivo* models. For this aspect, several studies reported the activity of Triphala by using chemical assays in which the results do not directly represent the antioxidative properties of Triphala in the actual physiological condition and cannot guarantee its intracellular antioxidant activities (Naik et al., 2006; Liu et al., 2008; Mehrotra et al., 2011; Babu et al., 2013; Gajendra et al., 2016; Varma et al., 2016). However, screening by using such *in vitro* chemical assays provide beneficial information related to potential antioxidant activities of Triphala, which may be further verified in the cell models or animal models. An enrichment of polyphenolic compounds such as phenolic acids, flavonoids, and tannins is considered to be one of the most important oxidant defensive mechanisms of Triphala (Rice-Evans et al., 1997; Francenia Santos-Sánchez et al., 2019). Thus, quantification of total phenolic content using gallic acid as a standard is necessary (Chandra et al., 2014). Parveen et al. discovered that the

methanolic extract of Triphala and its constituents showed a more intense chromogenic reaction than aqueous extracts, and this result supports its greater free radical scavenging ability (Parveen et al., 2018). Interestingly, Triphala possesses radical scavenging effects by reducing the concentrations of oxidative stress molecules and products, and it also works to increase the number of antioxidant enzymes present (**Figure 2**) (Gupta et al., 2010). Giving Triphala in dimethylhydrazine (DMH)-induced endoplasmic reticulum (ER)-stressed mice for 35 days can prevent an increase in hepatic oxidative products, including MDA and lactate dehydrogenase (LDH), and it also helps to maintain the levels of antioxidative enzymes (GST and GSH) (Sharma and Sharma, 2011). These effects have also been found in a noise-stress induction model, with additional benefits for the restoration of plasma vitamin C and corticosterone levels (Srikumar et al., 2006). Because Triphala contains three different herbs, some researchers have tried to compare the overall ability of Triphala in terms of the potency of different herb extracts. Hazra et al. found that each herb contained individual polyphenolic profiles. The methanolic extract of *P. emblica* L. expresses higher phenolic and ascorbic contents than those of *T. chebula* Retz. and *T. bellirica* (Gaertn.) Roxb., and its scavenging ability for 2,2-diphenyl-1-picrylhydrazyl (DPPH) and peroxyxynitrite radicals seems to be superior. On the other hand, although *T. bellirica* (Gaertn.) Roxb. contains fewer polyphenolic compounds than the other two herbs, it still has a greater effect in reducing the number of superoxide, nitric oxide, and hydroxyl radicals (Hazra et al., 2010). However, different sample sources, herbal proportions, and extraction methods can cause variations in the medicinal profiles (Liu et al., 2008; Parveen et al., 2018). Therefore, it is important to carry out herb qualification and characterization before examining the effects of these herbs or permitting their consumption by humans.

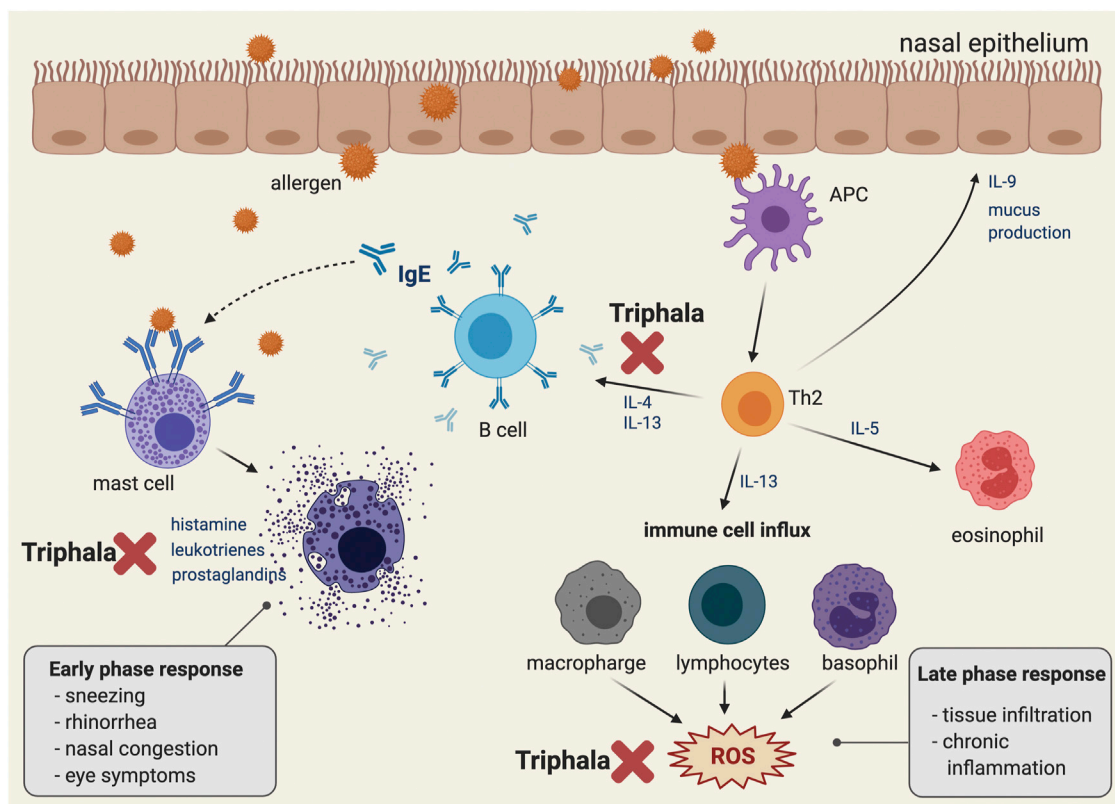


FIGURE 2 | Pathophysiology of allergic rhinitis and the conceptual representative of a possible mechanism of action of Triphala in suppressing IgE dependent allergic reaction. A schematic illustration representing the pathophysiology of the IgE-associated allergic reaction. Immediately following exposure to the allergen, the latter is bound to the IgE on the surface of the mast cell and eventually activates mast cell degranulation, which releases inflammatory mediators. In addition, late phase and chronic allergic inflammation occur as a result of eosinophil, macrophage, lymphocyte, and basophil activation. Eventually, following these cell activations, the intracellular ROS are generated. Triphala may play an inhibitory role at the early phase response by suppressing the release of autacoids (including histamine, leukotrienes, and prostaglandins) and by down-regulating the production and secretion of IL-4 and IL-13, which are key AR mediators for enhancing inflammation and IgE production in B cells. Moreover, Triphala may help modulate the late phase response by scavenging the oxidative stress molecules and products. The figure was created by BioRender.com.

Triphala: Anti-Inflammation

Inflammation plays an important role during AR progression (Gelfand, 2004). Several kinds of inflammatory cytokines have been found to be increased in AR patients in both the early and late phases of allergen-induced inflammation. IgE-mediated mast cell degranulation in the early phase is an initial factor in inducing Th2 and T helper cell 17 (Th17) differentiation (Iwakura et al., 2008; Mukai et al., 2018). Cytokines, such as IL-4, IL-13, and IL-17, released by these T cells possess an ability to aggravate nasal mucosa inflammation and disturb the intact mucosal barrier (Wise et al., 2014; Ramezanpour et al., 2016). Many studies in both *in vitro* and *in vivo* models have revealed the marked benefits of inflammatory modulation of AR conditions by using various anti-inflammatory approaches (Holgate et al., 2005; Canonica and Baiardini, 2006). An *in vitro* IL-4 and IL-13 antagonizing treatment and an *in vivo* anti-IL-4 treatment in mice were found to prevent epithelial barrier disruption (Steelant et al., 2018). Suppression of IL-4, TNF- α , IgE, and eosinophil levels in serum significantly alleviated symptoms and improved QoL in AR patients (Lv et al., 2018). Additionally, the strategy of

upregulating anti-inflammatory signaling pathways, nuclear factor erythroid 2-related factor 2/heme oxygenase-1 (Nrf2/HO-1), and suppression of toll-like receptor-myeloid differentiation primary response 88-nuclear factor kappa B (TLR-MyD88-NF- κ B) are all promising strategies for relieving nasal inflammation and improving airway epithelial barrier integrity (Bui et al., 2020).

Regardless of the prominent effects of a single herb, the polyherbal Triphala formulation possesses anti-inflammatory activity by acting through several mechanisms (Figure 2; Table 4). Using different extraction methodologies, the herbs retain their ability to reduce both acute and chronic inflammation. For example, at a dose of 100–200 mg/kg, Triphala was shown to be effective in reducing inflammation in carrageenan- and ethyl phenylpropionate (EPP)-induced paw edema, which are both used as acute inflammatory models (Prabu et al., 2008). Similarly, chronic inflammation in a granuloma formation induced by a cotton pellet was also reduced by a Triphala pretreatment (Prabu et al., 2008). Sireeratawong et al. reported that even though the animal received a high dose of

Triphala water extracted at 1,200 mg/kg, the granuloma formation was not reduced by the cotton pellet induction model (Sireeratawong et al., 2013). On the other hand, another study using a similar induction model found that the methanolic extract was beneficial, especially at lower doses (100–200 mg/kg) (Prabu et al., 2008). These results suggest that the methanolic extract might possess higher potency than the water extract, hence further comparisons of the active compounds identified in each extract are needed in order to address this point.

Most of the anti-inflammatory properties of Triphala have been reported in arthritis models. Pretreatment with the herbs significantly alleviated the inflammatory markers and enzymes associated with arthritis (Rasool and Sabina, 2007). Moreover, over-activation and overexpression of the NF- κ B pathway and the production of cytokines, chemokines, and growth factors, such as TNF- α , IL-17, TNF- α , IL-1 β , IL-6, monocyte chemoattractant protein-1 (MCP-1), vascular endothelial growth factor (VEGF), prostaglandin E2 (PGE2), COX-2, NO, and iNOS, were attenuated when patients were pretreated with Triphala compared with the untreated groups (Kalaiselvan and Rasool, 2016). Compound identification was partially accomplished by Shanmuganathan et al. by focusing on the TNF- α modulatory effect in which chebulinic acid, gallic acid, and the whole Triphala extract showed inhibitory characteristics on inflammation markers. These effects were mediated through the MAPK and NF- κ B signaling pathways. Moreover, the authors confirmed the binding capability of these active compounds to TNF- α -receptor-1 by using an in silico (i.e., computer simulated) approach (Shanmuganathan and Angayarkanni, 2018).

Although the effect of Triphala on AR has not yet been investigated, this polyherbal recipe counteracts various kinds of inflammation, suggesting the possibility of using these herbs to treat many inflammation-related diseases, including AR. High penetrating capacity and high toxic threshold are considered to be the advantages of Triphala for developing a preferential therapeutic formulation in the future. Its highly penetrative ability is evident in different parts of various body systems, such as the effects of *P. emblica* L. in attenuating brain inflammation in epileptic models and the reduction in psoriasis-related skin inflammation by *T. chebula* Retz (Golechha et al., 2011; An et al., 2016).

Activation and translocation of NF- κ B are fundamental steps for increasing inflammation-related gene expression and maintaining airway inflammation (Hart et al., 1998; Schuliga, 2015). Although no study has reported a direct effect of Triphala on airway inflammation, there is some evidence that suggests that this polyherbal recipe might be a good candidate for use in AR treatment. Triphala and its active constituents (*T. bellirica* (Gaertn.) Roxb. and *T. chebula* Retz.) exhibited an ability to decrease NF- κ B activation and nuclear translocation by suppressing the phosphorylation of p38, c-Jun N-terminal kinase (JNK), and ERK and activating the Akt/AMP-activated protein kinase/nuclear factor erythroid 2-related factor (Akt/AMPK/Nrf) signaling pathway (Tanaka et al., 2018). Therefore, further studies need to be undertaken in order to explore the effects of Triphala in AR models.

Triphala: Immunomodulation

A balance between immunostimulation and immunosuppression is important for helping our bodies maintain physiological function. In both autoimmune and inflammatory diseases, immunological imbalance occurs mainly in helper and regulatory T cells (Dejaco et al., 2006; Noack and Miossec, 2014). Especially in AR, which is known as a type I hypersensitivity condition, several immune cells are prone to activation and to be aberrant in both the sensitization and response phases (Kiboneka and Kibuule, 2019). A shift predominantly to Th2 cell responses or a lowering of the Th1/Th2 ratio has been found in several allergic diseases (Romagnani, 2004). Normally, Th1 responses result in IL-2, IFN- γ , IgG2a, IgG2b, and IgG3 production, whereas Th2 responses lead to IL-3, IL-4, IL-5, IL-13, and IgG1 production (Gelfand, 2004; Galli et al., 2008). Most of the Th2 cytokines act as enhancers of the inflammatory process. For example, IL-3 and IL-5 affect mast cells and eosinophil proliferation and differentiation (Denburg et al., 1994; Kouro and Takatsu, 2009). IL-13 participates in the recruitment of inflammatory cells to inflammation sites by enhancing VCAM-1 expression (De Vries, 1998). An increment in IL-4, which is considered to be a major mediator in AR, can activate IgE production in B cells (Poulsen and Hummelshoj, 2007).

In herbal medicine, quercetin is a well-known candidate compound for AR-related cytokine modulation. This compound is one of the essential elements in the Triphala formulation. Quercetin has been reported to inhibit cytokines such as IL-5, RANTES, and eotaxin released by eosinophils and mast cells (Sakai-Kashiwabara and Asano, 2013). Moreover, Th1 and Th2 markers including IFN- γ and IL-4, which are aberrantly expressed in an asthmatic model, were found to be modulated by quercetin (Park et al., 2009).

Researchers have found that Triphala and its active constituents have dual activities in relation to both immunostimulant and immunosuppressive effects that might be beneficial in AR treatment (Figure 2; Table 5). Pretreatment with Triphala (1 g/kg/day) improved neutrophil function and reduced *Pan* T and CD4⁺/CD8⁺ along with an increase in corticosteroid levels in a noise-induced stress model (Srikumar et al., 2007). Interestingly, these herbs also reduced IL-4 (Th2 cytokine) and increased IL-2 and IFN- γ (Th1 cytokines), suggesting an influence on Th1 shifting (Srikumar et al., 2005, 2007). In nonspecific mitogen-induced T lymphocyte proliferation, the application of Triphala reduced T cell proliferation, together with a reduced complement, antibody titer, and a delayed-type hypersensitivity (DTH) response following CFA and sheep red blood cell (SRBC) induction (Sabina et al., 2009). Similar results have also been observed in a single constituent, especially with *T. chebula* Retz. Atopic lesions induced by 2,4-dinitrofluorobenzene (DNFB) were relieved following topical application of *T. chebula* Retz. extract. As well as lesion improvement, the extract attenuated atopic markers (MMP-9 and IL-31) and eosinophil infiltration in affected and adjacent areas, respectively (Nam et al., 2011). Another interesting finding was that this extract was able to shift forward the Th1 response by attenuating IL-4 and increasing

IFN-gamma in an OVA-induced allergic model (Rubab and Ali, 2016). The results strongly suggest the benefits of using *T. chebula* Retz. extract for treating AR because the shifting of immunity from Th2 to Th1 is also used to define a successful response following treatment with allergen-specific immunotherapy (AIT) (Lam et al., 2020), and alteration of Th2 cytokines by reducing the Th2 response may offer a kind of protective effect in treating allergic diseases (Bosnjak et al., 2011). Moreover, upregulation of IFN-gamma in T cells is correlated with a reduction in nasal symptoms following exposure to allergens (Durham et al., 1999).

In theory, it is accepted that a balance of the numbers and ratios of Th cells and Tc cells is considered to be a homeostasis marker of the intrinsic immune system. Significant increments in Th cells, Tc cells, and natural killer cells following exposure to Triphala and its active constituents could confirm an additional improvement in the general cellular-mediated immunity of these agents in order to deal with harsh environments and exogenous microorganisms.

Although intranasal corticosteroids are now considered to be the most effective treatment for AR, their mechanism of action acts mainly preferentially through immunosuppression rather than immunomodulation (Bousquet et al., 2008; Hossenbaccus et al., 2020). It will be of interest to find any alternative treatments having dual immunostimulatory and immunosuppressive effects. Luckily, Triphala and its active constituents possess these properties. Thus, this polyherbal formulation might be an important potential candidate in the area of AR therapeutic development.

Triphala: Respiratory System

Following exposure to allergens or the start of the pollen season, some AR patients may have symptoms of cough (dry cough or a cough containing phlegm that is loose in character) together with nasal symptoms (Galway and Shields, 2019). Chronic cough and bronchoconstriction may be caused by bronchial hyper-responsiveness (BHR), which has been reported in AR patients even without asthma (Eggleston, 1988; Polosa et al., 2000). The relationship between AR and BHR may be explained by the following: 1) evidence of the neuronal connection between the upper and lower airways in which the exposure of nasal mucosal to certain stimuli, such as allergens and histamine, has been found to be associated with bronchospasm, and 2) direct contact with local topical nasal inflammatory or systemic inflammatory circulating cytokines from the upper airways might cause inflammation of the lower airways (Braunstahl, 2005; Taylor-Clark et al., 2005; Undem and Taylor-Clark, 2014). IL-13, in particular, which has been reported to not only mediate airway inflammation but is also considered to be a compounding factor driving BHR, may play a role in both upper and lower airway communication (Townley et al., 2009).

The effects of Triphala and its constituents on the lower respiratory system have been reported mainly in animal models. *P. emblica* L. and *T. chebula* Retz. extracts have the ability to alleviate coughs induced by mechanical stimulation and citric acid, respectively (Table 6) (Nosál'Ovák et al., 2003; Nosalova et al., 2013). *T. bellirica* (Gaertn.) Roxb. itself can dose dependently reduce BHR induced by carbachol (Gilani et al., 2008). One study showed that Triphala alleviated bronchial hyper-reactivity via immunomodulation and anti-oxidative pathways in OVA-induced asthma in murines

(Horani et al., 2012). Interestingly, some of the airway hypersensitivity endpoints using a whole-body plethysmograph, such as improvement of the pulmonary Penh value, have revealed that Triphala is superior to classical treatments such as the corticosteroid budesonide (Horani et al., 2012). However, although the immunomodulatory effects of these two treatments seem to play an important role in relieving bronchial hyper-reactivity, there are some differences in the immune response. Budesonide acts mainly through an anti-humoral mechanism by inhibiting antibody production. On the other hand, Triphala has no effect on antibody production, but its effects are selective toward lymphocyte distribution in both intra- and extrapulmonary organs (Horani et al., 2012).

PERSPECTIVES AND CONCLUSION

AR inflammation is a complex disease that involves several different types of cells and mediators. Specific treatments that aim to manipulate only a single mediator or one type of cell are less likely to be effective. On this basis, it is necessary to employ agents with a broader spectrum of action that can alleviate the complex symptoms of this disease. The realm of complementary and alternative medicine has gained greater attention since much evidence from different study models for specific pharmacological properties (as well as the results from clinical trials) has been accumulated, and that increases the reliability and confidence of using this lineage of medicine. Recently, several plants and their constituents are approved to be safe, effective, and less expensive for managing the development and progression of various diseases, and many of them are already on the WHO's list of essential medicines. Therefore, Triphala which contains three different plants may be one of the effective remedies to alleviate AR-related symptoms. Experimental data from previous *in vitro* and *in vivo* studies of Triphala or individual plants in this remedy have demonstrated potential natural compounds that may be the main acting molecules able to promote the attenuation of AR symptoms. The current review (as shown in Table 2) helps reveal phytochemicals in Triphala that exhibit the promising pharmacological activities that may provide potential benefits in alleviating AR symptoms. Specifically, Triphala contains flavonoids like quercetin. The benefits of quercetin on AR may be through its ability to decrease histamine release from mast cells, and that may help reduce the process of allergic inflammation at the early phase. Moreover, its effects on suppressing the production of cytokines and eosinophil chemoattractants may help reduce the late phase inflammation and eventually the AR symptoms. However, in the clinical view, it may be challenging to utilize quercetin as a monotherapy since the pathophysiology of AR is complex. It would be more convincing to incorporate this compound in the standard regimen if there is more scientific data identifying its pharmacological targets that explain the specific effects of quercetin on alleviating AR. Besides quercetin, kaempferol is another flavonoid that shows interesting inhibitory effects on inflammation in the airways. This compound can suppress mast cell stimulation, production, and release of inflammatory cytokines and chemokines. Triphala also contains ellagic acid which has been

shown to reduce histamine release and inflammation in the lung via suppressing the activity of NF- κ B, and these effects help speed up the resolution of allergic airway inflammation. Another functional compound found in Triphala is gallic acid which has been reported to suppress nasal histamine release and inflammation. This compound is one of the active components that may help reduce nasal symptoms caused by autacoids and inflammatory cytokines. Similarly, chebulagic acid has been shown to possess anti-inflammatory properties by reducing cytokine production and inflammatory enzymes including COX-2 and LOX. Moreover, Triphala contains various natural compounds that may help suppress allergic responses through their antioxidant potential. Those compounds include vitamin C, chebulinic acid, and emblicanin. These compounds function mainly in scavenging free radicals and reducing oxidative stress; therefore, they may be the responsible compounds to help suppress exacerbation of AR-related symptoms. In short, Triphala is explored to be an important source of bioactive compounds able to be used for AR treatments. The orchestration of these compounds may create synergistic effects to decrease the exacerbation of inflammatory response and oxidative stress that lead to AR development.

The anti-inflammatory, immunomodulatory, antioxidant, and antibacterial activities of Triphala are similar to those of other herbal formulas clinically proven to treat AR effectively, such as Shi-Bi-Lin (a Chinese herbal formula), butterbur, and *Nigella sativa* (black caraway or black cumin). However, there have not been any *in vivo* studies that utilize a direct model for AR to test the effects of Triphala. The ovalbumin-induced guinea pig model of AR could well be a proper assay to definitively evaluate if Triphala can reduce AR-associated inflammation. However, there is a limitation to these types of study models because it is not a direct AR model to give us enough reliable information specific to AR. It would provide strong evidence if in the future there are direct experimental designs specifically developed for animal AR models to verify the effectiveness of Triphala.

During allergic inflammation, the nasal epithelial barriers of AR patients appear to become impaired. Consequently, this condition leads to the development of sinusitis and otitis media, with effusion caused by bacteria, viruses, and fungi. Although Triphala shows promise in being an effective bacteriostatic/bactericidal agent, most studies have focused only on oral streptococci. Thus, further studies are needed to address whether Triphala is effective in killing other types of bacteria, as well as viruses and fungi that are related to allergic rhinosinusitis. Additionally, clinical studies should be conducted to verify the efficacy of this herbal formula. As a step toward the clinical investigation of Triphala for its efficacy and safety, our research team has created the study design/clinical trial, and the study protocol has already been registered in Thai Clinical Trials Registry (TCTR20191008005). Moreover, study models for pharmacokinetics are crucial to fulfill all aspects of the pharmacology of Triphala and to obtain valuable information about the active compound profiles. If the accumulated data clearly show that Triphala can be used effectively to inhibit inflammation, modulate immunity, alleviate unwanted symptoms in patients with AR, and prevent AR-related

infections, this will provide a novel alternative treatment for patients. For example, Triphala could be used as a monotherapy in patients with mild AR. For patients with moderate-to-severe AR (for which intranasal corticosteroids are usually prescribed) but who do not want to use steroidal drugs, Triphala may be used in combination with an antihistamine. For patients using steroids who have inadequate control of AR, Triphala may be added to the treatment plan to reduce the use of high-dose steroids. Similarly, for patients who require immunotherapy, a Triphala supplement may offer a faster and better response to immunotherapy.

In conclusion, Triphala exhibits beneficial effects if used as an alternative treatment for AR. However, extensive investigations in both animals and humans are first needed to be certain about its definitive mechanisms of action and the efficacy/safety of treatments. Although most studies reported the pharmacological effects of Triphala in a reasonable range of concentrations, some studies evaluated the effects of Triphala at relatively high doses. This may create concerns about its low efficacy and toxicity. With this, specifying the efficacy and adverse effects of Triphala is a vital base to ensure its safe use. Triphala should be carefully examined further to gain adequate data about toxic target organs, safe dose range, safety window of effective dose, and minimum toxic dose. Considering the actual applications, appropriate dosage and course of treatment are required to be precisely adjusted to ensure that Triphala is safe and effective. The accumulated evidence obtained from such studies will be beneficial to properly prescribe Triphala to individual AR patients with different clinical symptoms and varying degrees of severity in order to achieve the highest efficacy with the fewest side effects.

AUTHOR CONTRIBUTIONS

Conceptualization, NH and SP; writing—original draft preparation, SJ, NH, SP, PH and WN; writing—review and editing, SJ, NH, SP, and WN. All authors have read and agreed to the published version of the manuscript.

FUNDING

This work was supported by the Faculty of Medicine, Chiang Mai University (Grant Number 061–2563).

ACKNOWLEDGMENTS

PH was supported in part by Grants from the Teaching Assistant and Research Assistant. (TA/RA) scholarships, Graduate School, Chiang Mai University, Chiang Mai, Thailand.

SUPPLEMENTARY MATERIAL

The Supplementary Material for this article can be found online at: <https://www.frontiersin.org/articles/10.3389/fphar.2021.628198/full#supplementary-material>.

REFERENCES

- Adwas, A. A., Sedik, A., Elsayed, I., Azab, A. E., and Quwaydir, F. A. (2019). Oxidative stress and antioxidant mechanisms in human body. *J. Appl. Biotechnol. Bioeng.* 11, 23. doi:10.15406/jabb.2019.06.00173
- Aher, V. D., Kumar, A., and Wahi (2010). Immunomodulatory effect of alcoholic extract of *Terminalia chebula* ripe fruits. *J. Pharm. Sci. Res.* 6, 121. doi:10.21276/ap.2017.6.2.15
- Aher, V., and Wahi, A. (2011). Immunomodulatory activity of alcohol extract of *Terminalia chebula* retz combretaceae. *Trop. J. Pharm. Res.* 10 (5), 37. doi:10.4314/tjpr.v10i5.5
- Alsuleimani, Y. M., and Walker, M. J. A. (2007). Allergic rhinitis and its pharmacology. *Pharmacol. Ther.* 114 (3), 233–260. doi:10.1016/j.pharmthera.2007.01.012
- An, J., Li, T., Dong, Y., Li, Z., and Huo, J. (2016). *Terminalia chebulanin* attenuates psoriatic skin lesion via regulation of heme oxygenase-1. *Cell. Physiol. Biochem* 39 (2), 531–43. doi:10.1159/000445645
- Athira, A. P., Helen, A., Saja, K., Reddanna, P., and Sudhakaran, P. R. (2013). Inhibition of Angiogenesis in vitro by chebulagic acid: a COX-LOX dual inhibitor. *Int. J. Vasc. Med.* 13, 1–8. doi:10.1155/2013/843897
- Ayala, A., Muñoz, M. F., and Argüelles, S. (2014). Lipid peroxidation: production, metabolism, and signaling mechanisms of malondialdehyde and 4-hydroxy-2-nonenal. *Oxidative Med. Cell Longevity* 2014, 360438. doi:10.1155/2014/360438
- Babu, D., Gurumurthy, P., Borra, S. K., and Cherian, K. M. (2013). Falling through the safety net: Americans without health insurance. *Choice Reviews Online* 7, 2898–2905. doi:10.5897/JMPR2013
- Bag, A., Kumar Bhattacharyya, S., Kumar Pal, N., and Ranjan Chattopadhyay, R. (2013). Anti-inflammatory, anti-lipid peroxidative, antioxidant and membrane stabilizing activities of hydroalcoholic extract of *Terminalia chebulafruits*. *Pharm. Biol.* 51 (12), 1515–1520. doi:10.3109/13880209.2013.799709
- Bernstein, D. I., Schwartz, G., and Bernstein, J. A. (2016). Allergic rhinitis: mechanisms and treatment. *Immunol. Allergy Clin. North America* 36 (2), 261–78. doi:10.1016/j.jiac.2015.12.004
- Bharadwaj, A. S., Bewtra, A. K., and Agrawal, D. K. (2007). Dendritic cells in allergic airway inflammation This article is one of a selection of papers published in the Special Issue on Recent Advances in Asthma Research. *Can. J. Physiol. Pharmacol.* 85 (7), 686–699. doi:10.1139/Y07-062
- Birben, E., Sahiner, U. M., Sackesen, C., Erzurum, S., and Kalayci, O. (2012). Oxidative stress and antioxidant defense. *World Allergy Organ. J.* 5, 9. doi:10.1097/WOX.0b013e3182439613
- Björkstén, B., Clayton, T., Ellwood, P., Stewart, A., Strachan, D., Phase III Study Group, et al. (2008). Worldwide time trends for symptoms of rhinitis and conjunctivitis: phase III of the international study of asthma and allergies in childhood. *Pediatr. Allergy Immunol.* 19 (2), 110–124. doi:10.1111/j.1399-3038.2007.00601.x
- Boldogh, I., Bacs, A., Choudhury, B. K., Dharajiya, N., Alam, R., Hazra, T. K., et al. (2005). ROS generated by pollen NADPH oxidase provide a signal that augments antigen-induced allergic airway inflammation. *J. Clin. Invest.* 115 (8), 2169–2179. doi:10.1172/JCI24422
- Bosnjak, B., Stelzmueller, B., Erb, K. J., and Epstein, M. M. (2011). Treatment of allergic asthma: modulation of Th2 cells and their responses. *Respir. Res.* 12(1), 114. doi:10.1186/1465-9921-12-114
- Bousquet, J., Khaltaev, N., Cruz, A. A., Denburg, J., Fokkens, W. J., Togias, A., et al. (2008). Allergic rhinitis and its impact on asthma (ARIA) 2008 update (in collaboration with the world health organization, GA(2)len and AllerGen). *Allergy* 63 Suppl 86, 8–160. doi:10.1111/j.1398-9995.2007.01620.x
- Braunstahl, G.-J. (2005). The unified immune system: respiratory tract-nasobronchial interaction mechanisms in allergic airway disease. *J. Allergy Clin. Immunol.* 115 (1), 142–148. doi:10.1016/j.jaci.2004.10.041
- Bui, T. T., Fan, Y., Piao, C. H., Nguyen, T. V., Shin, D.-u., Jung, S. Y., et al. (2020). Piper Nigrum extract improves OVA-induced nasal epithelial barrier dysfunction via activating Nrf2/HO-1 signaling. *Cell Immunol.* 351, 104035. doi:10.1016/j.cellimm.2019.104035
- Burton, O. T., and Oettgen, H. C. (2011). Beyond immediate hypersensitivity: evolving roles for IgE antibodies in immune homeostasis and allergic diseases. *Immunol. Rev.* 242 (1), 128–183. doi:10.1111/j.1600-065X.2011.01024.x
- Canonica, G., and Baiardini, I. (2006). Minimal persistent inflammation in allergic rhinitis: Its clinical implications. *Allergy Clin. Immunol. Int. - J. World Allergy Organ.* 18, 169. doi:10.1027/0838-1925.18.4.169
- Cao, J., Li, C., Ma, P., Ding, Y., Gao, J., Jia, Q., et al. (2020). Effect of kaempferol on IgE-mediated anaphylaxis in C57BL/6 mice and LAD2 cells. *Phytomedicine* 79, 153346. doi:10.1016/j.phymed.2020.153346
- Chandra, S., Khan, S., Avula, B., Lata, H., Yang, M. H., Elsohly, M. A., et al. (2014). Assessment of total phenolic and flavonoid content, antioxidant properties, and yield of aeroponically and conventionally grown leafy vegetables and fruit crops: a comparative study. *Evidence-Based Complement. Altern. Med.* 2014, 253875. doi:10.1155/2014/253875
- Chang, H.-H., Chen, C.-S., and Lin, J.-Y. (2009). High dose vitamin C supplementation increases the Th1/Th2 cytokine secretion ratio, but decreases eosinophilic infiltration in bronchoalveolar lavage fluid of ovalbumin-sensitized and challenged mice. *J. Agric. Food Chem.* 57 (21), 10471–10476. doi:10.1021/jf902403p
- Charoenteeraboon, J., Ngamkitdechakul, C., Soonthornchareonnon, N., Jaijoo, K., and Sireeratawong, S. (2010). Antioxidant activities of the standardized water extract from fruit of *phyllanthus emblica* linn. *Songklanakarin J. Sci. Technol.* 77, 547. doi:10.1055/s-0031-1282780
- Chauhan, P., Singh, S., Gupta, Y., and Kumar, U. (2018). Evaluation of toxicity studies and anti-inflammatory activity of *Terminalia Bellerica* in carrageenan-induced paw edema in experimental rats. *J. Nat. Sci. Biol. Med.* 9 (2), 169–174. doi:10.4103/jnsbm.JNSBM_159_17
- Choi, Y. H., and Yan, G. H. (2009). Ellagic acid attenuates immunoglobulin e-mediated allergic response in mast cells. *Biol. Pharm. Bull.* 32 (6), 1118–1121. doi:10.1248/bpb.32.1118
- Cornélio Favarin, D., Martins Teixeira, M., Lemos De Andrade, E., De Freitas Alves, C., Lazo Chica, J. E., Artério Sorgi, C., et al. (2013). Anti-inflammatory effects of ellagic acid on acute lung injury induced by acid in mice. *Mediators Inflamm.* 2013, 1. doi:10.1155/2013/164202
- Cortes, J. R., Perez-G, M., Rivas, M. D., and Zamorano, J. (2007). Kaempferol inhibits IL-4-induced STAT6 activation by specifically targeting JAK3. *J. Immunol.* 179 (6), 3881–3887. doi:10.4049/jimmunol.179.6.3881
- De Freitas Alves, C., Angeli, G. N., Favarin, D. C., Lemos De Andrade, E., Lazo Chica, J. E., Faccioli, L. H., et al. (2013). The effects of proresolution of ellagic acid in an experimental model of allergic airway inflammation. *Mediators Inflamm.* 2013, 1. doi:10.1155/2013/863198
- De Vries, J. E. (1998). The role of IL-13 and its receptor in allergy and inflammatory responses. *J. Allergy Clin. Immunol.* 102 (9), 165–169. doi:10.1016/S0091-6749(98)70080-6
- Dejaco, C., Duftner, C., Grubeck-Loebenstien, B., and Schirmer, M. (2006). Imbalance of regulatory T cells in human autoimmune diseases. *Immunology* 117 (3), 289–300. doi:10.1111/j.1365-2567.2005.02317.x
- Denburg, J. A., Woolley, M., Leber, B., Linden, M., and O'Byrne, P. (1994). Basophil and eosinophil differentiation in allergic reactions. *J. Allergy Clin. Immunol.* 94 (6 pt 2), 1135–1141. doi:10.1016/0091-6749(94)90321-2
- Deshmukh, C. D., Veeresh, B., and Pawar, A. T. (2010). Protective effect OF *emblica officinalis* fruit extract ON acetic acid induced colitis IN rats. *J. Herb. Med. Toxicol.* 7, 127. doi:10.18535/jmscr/v7i7.122
- Dreyer, N. A., Bryant, A., and Velentgas, P. (2016). The GRACE checklist: a validated assessment tool for high quality observational studies of comparative effectiveness. *Jmcp* 22 (10), 1107–1113. doi:10.18553/jmcp.2016.22.10.1107
- Durham, S. R., Walker, S. M., Varga, E.-M., Jacobson, M. R., O'Brien, F., Noble, W., et al. (1999). Long-term clinical efficacy of grass-pollen immunotherapy. *N. Engl. J. Med.* 341 (7), 468–475. doi:10.1056/NEJM199908123410702
- Ebihara, N., Takahashi, K., Takemura, H., Akanuma, Y., Asano, K., and Sunagawa, M. (2018). Suppressive effect of quercetin on nitric oxide production from nasal epithelial cells in vitro. *Evid-Based Complement. Altern. Med.* 2018, 1. doi:10.1155/2018/6097625
- Edo, Y., Otaki, A., and Asano, K. (2018). Quercetin enhances the thioredoxin production of nasal epithelial cells in vitro and in vivo. *Medicines* 5 (4), 124. doi:10.3390/medicines5040124
- Eggleston, P. A. (1988). Upper airway inflammatory diseases and bronchial hyperresponsiveness. *J. Allergy Clin. Immunol.* 81 (5 pt 2), 1036–1041. doi:10.1016/0091-6749(88)90176-5
- Fan, Y., Piao, C. H., Hyeon, E., Jung, S. Y., Eom, J.-E., Shin, H. S., et al. (2019). Gallic acid alleviates nasal inflammation via activation of Th1 and inhibition of Th2

- and Th17 in a mouse model of allergic rhinitis. *Int. Immunopharmacol.* 70, 512–519. doi:10.1016/j.intimp.2019.02.025
- Fanning, L. B., and Boyce, J. A. (2013). Lipid mediators and allergic diseases. *Ann. Allergy Asthma Immunol.* 111 (3), 155–162. doi:10.1016/j.anaai.2013.06.031
- Forte, G. C., da Silva, D. T. R., Hennemann, M. L., Sarmiento, R. A., Almeida, J. C., and de Tarso Roth Dalcin, P. (2018). Diet effects in the asthma treatment: a systematic review. *Crit. Rev. Food Sci. Nutr.* 58 (11), 1878–1887. doi:10.1080/10408398.2017.1289893
- Francenia Santos-Sánchez, N., Salas-Coronado, R., Villanueva-Cañongo, C., and Hernández-Carlos, B. (2019). Antioxidant compounds and their antioxidant mechanism. *Antioxidation* 7, 347. doi:10.5772/intechopen.85270
- Frei, B., Stocker, R., and Ames, B. N. (1988). Antioxidant defenses and lipid peroxidation in human blood plasma. *Proc. Natl. Acad. Sci.* 85 (24), 9748–9752. doi:10.1073/pnas.85.24.9748
- Gadermaier, E., Levin, M., Flicker, S., and Ohlin, M. (2014). The human IgE repertoire. *Int. Arch. Allergy Immunol.* 163 (2), 77–91. doi:10.1159/000355947
- Gajendra, S., Pushkar, C., Syed, A. Y., Rajveer, S. R., and Bhanwar, L. J. (2016). Research article antibacterial and antioxidant activity of triphala extracts. *Int. J. Curr. Res.* 8, 38335–38348. doi:10.7176/cm/11-6-01
- Galli, S. J., Tsai, M., and Piliponsky, A. M. (2008). The development of allergic inflammation. *Nature* 454 (7203), 445–454. doi:10.1038/nature07204
- Galway, N. C., and Shields, M. D. (2019). The child with an incessant dry cough. *Paediatric Respir. Rev.* 30, 58–64. doi:10.1016/j.prrv.2018.08.002
- Gelfand, E. (2004). Inflammatory mediators in allergic rhinitis. *J. Allergy Clin. Immunol.* 114 (5 Suppl), S135–S138. doi:10.1016/j.jaci.2004.08.043
- Gilani, A. H., Khan, A.-u., Ali, T., and Ajmal, S. (2008). Mechanisms underlying the antispasmodic and bronchodilatory properties of *Terminalia bellerica* fruit. *J. Ethnopharmacol.* 116 (3), 528–538. doi:10.1016/j.jep.2008.01.006
- Ginsburg, I., Koren, E., Horani, A., Mahamid, M., Doron, S., Muhanna, N., et al. (2009). Amelioration of hepatic fibrosis via Padma Hepaten is associated with altered natural killer T lymphocytes. *Clin. Exp. Immunol.* 157 (1), 155–164. doi:10.1111/j.1365-2249.2009.03936.x
- Golechha, M., Bhatia, J., Ojha, S., and Arya, D. S. (2011). Hydroalcoholic extract of *Emblica officinalis* protects against kainic acid-induced status epilepticus in rats: evidence for an antioxidant, anti-inflammatory, and neuroprotective intervention. *Pharm. Biol.* 49 (11), 1128–1136. doi:10.3109/13880209.2011.571264
- Golechha, M., Sarangal, V., Ojha, S., Bhatia, J., and Arya, D. S. (2014). Anti-inflammatory effect of *Emblica officinalis* in rodent models of acute and chronic inflammation: involvement of possible mechanisms. *Int. J. Inflamm.* 2014, 1. doi:10.1155/2014/178408
- Gong, J.-H., Cho, L.-H., Shin, D., Han, S.-Y., Park, S.-H., and Kang, Y.-H. (2014). Inhibition of airway epithelial-to-mesenchymal transition and fibrosis by kaempferol in endotoxin-induced epithelial cells and ovalbumin-sensitized mice. *Lab. Invest.* 94 (3), 297–308. doi:10.1038/labinvest.2013.137
- Gong, J.-H., Shin, D., Han, S.-Y., Kim, J.-L., and Kang, Y.-H. (2012). Kaempferol suppresses eosinophil infiltration and airway inflammation in airway epithelial cells and in mice with allergic asthma. *J. Nutr.* 142 (1), 47–56. doi:10.3945/jn.111.150748
- Gupta, S., Kalaiselvan, V., Srivastava, S., Agrawal, S., and Saxena, R. (2010). Evaluation of anticataract potential of Triphala in selenite-induced cataract: in vitro and in vivo studies. *J. Ayurveda Integr. Med.* 1 (4), 280–286. doi:10.4103/0975-9476.74425
- Hart, L. A., Krishnan, V. L., Adcock, I. M., Barnes, P. J., and Chung, K. F. (1998). Activation and localization of transcription factor, nuclear factor- κ B, in asthma. *Am. J. Respir. Crit. Care Med.* 158, 1585. doi:10.1164/ajrccm.158.5.9706116
- Hattori, M., Mizuguchi, H., Baba, Y., Ono, S., Nakano, T., Zhang, Q., et al. (2013). Quercetin inhibits transcriptional up-regulation of histamine H1 receptor via suppressing protein kinase C- δ /extracellular signal-regulated kinase/poly(ADP-ribose) polymerase-1 signaling pathway in HeLa cells. *Int. Immunopharmacology* 15 (2), 232–239. doi:10.1016/j.intimp.2012.12.030
- Hazra, B., Sarkar, R., Biswas, S., and Mandal, N. (2010). Comparative study of the antioxidant and reactive oxygen species scavenging properties in the extracts of the fruits of *Terminalia chebula*, *Terminalia bellerica* and *Emblica officinalis*. *BMC Complement. Altern. Med.* 10, 20. doi:10.1186/1472-6882-10-20
- Heinrich, M., Appendino, G., Efferth, T., Fürst, R., Izzo, A. A., Kayser, O., et al. (2020). Best practice in research - overcoming common challenges in phytopharmacological research. *J. Ethnopharmacology* 246, 112230. doi:10.1016/j.jep.2019.112230
- Holgate, S., Casale, T., Wenzel, S., Bousquet, J., Deniz, Y., and Reisner, C. (2005). The anti-inflammatory effects of omalizumab confirm the central role of IgE in allergic inflammation. *J. Allergy Clin. Immunol.* 115 (3), 459–465. doi:10.1016/j.jaci.2004.11.053
- Horani, A., Shoseyov, D., Ginsburg, I., Mruwat, R., Doron, S., Amer, J., et al. (2012). Triphala (PADMA) extract alleviates bronchial hyperreactivity in a mouse model through liver and spleen immune modulation and increased anti-oxidative effects. *Ther. Adv. Respir.* 6 (4), 199–210. doi:10.1177/1753465812452194
- Hossenbaccus, L., Linton, S., Garvey, S., and Ellis, A. K. (2020). Towards definitive management of allergic rhinitis: best use of new and established therapies. *Allergy Asthma Clin. Immunol.* 16, 39. doi:10.1186/s13223-020-00436-y
- Huang, C.-H., Jan, R.-L., Kuo, C.-H., Chu, Y.-T. W. L., Wang, W.-L., Lee, M.-S., et al. (2010). Natural flavone kaempferol suppresses chemokines expression in human monocyte THP-1 cells through MAPK pathways. *J. Food Sci.* 75 (8), H254–H259. doi:10.1111/j.1750-3841.2010.01812.x
- Ibne Jami, M. S., Sultana, Z., Ali, M. E., Begum, M. M., and Haque, M. M. (2014). Evaluation of analgesic and anti-inflammatory activities on ethanolic extract of *Terminalia chebula* fruits in experimental animal models. *Am. J. Plant Sci* 05 (01), 63–69. doi:10.4236/ajps.2014.51010
- Iijima, M. K., Kobayashi, T., Kamada, H., and Shimojo, N. (2001). Exposure to ozone aggravates nasal allergy-like symptoms in Guinea pigs. *Toxicol. Lett.* 123 (1), 77–85. doi:10.1016/S0378-4274(01)00392-7
- Irie, S., Kashiwabara, M., Yamada, A., and Asano, K. (2016). Suppressive activity of quercetin on periotin functions in vitro. *In Vivo* 30 (1), 17–25. doi:10.4172/2155-6121.1000253
- Iwakura, Y., Nakae, S., Saijo, S., and Ishigame, H. (2008). The roles of IL-17A in inflammatory immune responses and host defense against pathogens. *Immunol. Rev.* 226, 57–59. doi:10.1111/j.1600-065X.2008.00699.x
- Jayesh, K., Karishma, R., Vysakh, A., Gopika, P., and Latha, M. S. (2018). *Terminalia bellirica* (Gaertn.) Roxb fruit exerts anti-inflammatory effect via regulating arachidonic acid pathway and pro-inflammatory cytokines in lipopolysaccharide-induced RAW 264.7 macrophages. *Inflammopharmacol* 28, 265. doi:10.1007/s10787-018-0513-x
- Jung, J.-W., Kang, H.-R., Ji, G.-E., Park, M.-S., Song, W.-J., Kim, M.-H., et al. (2011). Therapeutic effects of fermented red ginseng in allergic rhinitis: a randomized, double-blind, placebo-controlled study. *Allergy Asthma Immunol. Res.* 3 (2), 103–110. doi:10.4168/aa.2011.3.2.103
- Jung, J. H., Kang, I. G., Kim, D. Y., Hwang, Y. J., and Kim, S. T. (2013). The effect of Korean red ginseng on allergic inflammation in a murine model of allergic rhinitis. *J. Ginseng Res.* 37 (2), 167–175. doi:10.5142/jgr.2013.37.167
- Kalaiselvan, S., and Rasool, M. K. (2015). The anti-inflammatory effect of triphala in arthritic-induced rats. *Pharm. Biol.* 53, 51. doi:10.3109/13880209.2014.910237
- Kalaiselvan, S., and Rasool, M. K. (2016). Triphala herbal extract suppresses inflammatory responses in LPS-stimulated RAW 264.7 macrophages and adjuvant-induced arthritic rats via inhibition of NF- κ B pathway. *J. Immunotoxicol.* 13 (4), 509–525. doi:10.3109/1547691X.2015.1136010
- Kang, D. R., Belal, S. A., Choe, H. S., Shin, D. K., and Shim, K. S. (2018). Effect of kaempferol on cyclooxygenase 2 (Cox2) and cytosolic phospholipase A2 (cPLA2) protein expression in BALB/c mice. *Iran J Allergy Asthma Immunol* 17 (5), 428–435. doi:10.18502/ijaa.v17i5.301
- Kashiwabara, M., Asano, K., Mizuyoshi, T., and Kobayashi, H. (2016). Suppression of neuropeptide production by quercetin in allergic rhinitis model rats. *BMC Complement. Altern. Med.* 16, 132. doi:10.1186/s12906-016-1123-z
- Kawamoto, Y., Ueno, Y., Nakahashi, E., Obayashi, M., Sugihara, K., Qiao, S., et al. (2016). Prevention of allergic rhinitis by ginger and the molecular basis of immunosuppression by 6-gingerol through T cell inactivation. *J. Nutr. Biochem.* 27, 112–122. doi:10.1016/j.jnutbio.2015.08.025
- Khan, T., Sankhe, K., Suvarna, V., Sherje, A., Patel, K., and Dravyakar, B. (2018). DNA gyrase inhibitors: progress and synthesis of potent compounds as antibacterial agents. *Biomed. Pharmacother.* 103, 923–938. doi:10.1016/j.biopha.2018.04.021
- Kiboneka, A., and Kibuule, D. (2019). The immunology of asthma and allergic rhinitis. *Rhinosinusitis* 12, 77. doi:10.5772/intechopen.86964
- Kim, M., Lim, S. J., Kang, S. W., Um, B.-H., and Nho, C. W. (2014). Aceriphyllum rossii Extract and its active compounds, quercetin and kaempferol inhibit IgE-

- mediated mast cell activation and passive cutaneous anaphylaxis. *J. Agric. Food Chem.* 62 (17), 3750–3758. doi:10.1021/jf405486c
- Kim, S.-H., Jun, C.-D., Suk, K., Choi, B.-J., Lim, H., Park, S., et al. (2006). Gallic acid inhibits histamine release and pro-inflammatory cytokine production in mast cells. *Toxicol. Sci.* 91 (1), 123–131. doi:10.1093/toxsci/kfj063
- Kimata, M., Shichijo, M., Miura, T., Serizawa, I., Inagaki, N., and Nagai, H. (2000). Effects of luteolin, quercetin and baicalein on immunoglobulin E-mediated mediator release from human cultured mast cells. *Clin. Exp. Allergy* 30 (4), 501–508. doi:10.1046/j.1365-2222.2000.00768.x
- Kirubanandan, S., Ravi, B., and Renganathan, S. (2015). Anti-inflammatory and analgesic activities of methanol extract of *Terminalia chebula* fruits. *Int. J. Pharm. Chem. Sci.* 4, 400–404. doi:10.4236/pp.2015.612056
- Klimek, L., Bachert, C., Pfaar, O., Becker, S., Bieber, T., Brehler, R., et al. (2019). ARIA guideline 2019: treatment of allergic rhinitis in the German health system. *Allergo J. Int.* 28, 255. doi:10.1007/s40629-019-00110-9
- Kouro, T., and Takatsu, K. (2009). IL-5- and eosinophil-mediated inflammation: from discovery to therapy. *Int. Immunol.* 21, 1303–1309. doi:10.1093/intimm/dxp102
- Lacy, P. (2006). Mechanisms of degranulation in neutrophils. *Allergy Asthma Clin. Immunol.* 2 (3), 98–108. doi:10.1186/1710-1492-2-3-98
- Lam, H. Y., Tergaonkar, V., and Ahn, K. S. (2020). Mechanisms of allergen-specific immunotherapy for allergic rhinitis and food allergies. *Biosci. Rep.* 40 (4). BSR20200256. doi:10.1042/BSR20200256
- Lambrecht, B. N., and Hammad, H. (2010). The role of dendritic and epithelial cells as master regulators of allergic airway inflammation. *Lancet* 376 (9743), 835–843. doi:10.1016/S0140-6736(10)61226-3
- Lee, B. J., Naclerio, R. M., Bochner, B. S., Taylor, R. M., Lim, M. C., and Baroody, F. M. (1994). Nasal challenge with allergen upregulates the local expression of vascular endothelial adhesion molecules. *J. Allergy Clin. Immunol.* 94 (6 pt 1), 1006–1016. doi:10.1016/0091-6749(94)90119-8
- Lee, E.-J., Ji, G.-E., and Sung, M.-K. (2010). Quercetin and kaempferol suppress immunoglobulin E-mediated allergic inflammation in RBL-2H3 and Caco-2 cells. *Inflamm. Res.* 59 (10), 847–854. doi:10.1007/s00011-010-0196-2
- Lee, H.-S., Jung, S.-H., Yun, B.-S., and Lee, K.-W. (2007). Isolation of chebulic acid from *Terminalia chebula* Retz. and its antioxidant effect in isolated rat hepatocytes. *Arch. Toxicol.* 81, 211. doi:10.1007/s00204-006-0139-4
- Lee, S.-I., Hyun, P.-M., Kim, S.-H., Kim, S.-K., Kim, B.-S., et al. (2005). Suppression of the onset and progression of collagen-induced arthritis by chebulagic acid screened from a natural product library. *Arthritis Rheum.* 52, 345. doi:10.1002/art.20715
- Li, B. W. S., and Hendriks, R. W. (2013). Group 2 innate lymphoid cells in lung inflammation. *Immunology* 140 (3), 281–287. doi:10.1111/imm.12153
- Li, P., Du, R., Wang, Y., Hou, X., Wang, L., Zhao, X., et al. (2020). Identification of chebulinic acid and chebulagic acid as novel influenza viral neuraminidase inhibitors. *Front. Microbiol.* 11, 182. doi:10.3389/fmicb.2020.00182
- Liu, X., Zhao, M., Wang, J., Yang, B., and Jiang, Y. (2008). Antioxidant activity of methanolic extract of emblica fruit (*Phyllanthus emblica* L.) from six regions in China. *J. Food Compos. Anal.* 21, 219. doi:10.1016/j.jfca.2007.10.001
- Liu, Y., Bao, L., Xuan, L., Song, B., Lin, L., and Han, H. (2015). Chebulagic acid inhibits the LPS-induced expression of TNF- α and IL-1 β in endothelial cells by suppressing MAPK activation. *Exp. Ther. Med.* 10 (1), 263–268. doi:10.3892/etm.2015.2447
- Lv, C., Zhang, Y., and Shen, L. (2018). Preliminary clinical effect evaluation of resveratrol in adults with allergic rhinitis. *Int. Arch. Allergy Immunol.* 175, 231. doi:10.1159/000486959
- Mahesh, R., Bhuvana, S., and Hazeena Begum, V. M. (2009). Effect of *Terminalia chebula* aqueous extract on oxidative stress and antioxidant status in the liver and kidney of young and aged rats. *Cell Biochem. Funct.* 27 (6), 358–363. doi:10.1002/cbf.1581
- Mehrotra, S., Jamwal, R., Shyam, R., Meena, D. K., Mishra, K., Patra, R., et al. (2011). Anti-helicobacter *pylori* and antioxidant properties of *Embllica officinalis* pulp extract: a potential source for therapeutic use against gastric ulcer. *J. Med. Plants Res.* 14, 203–209. doi:10.1046/j.1365-2036.2000.00679.x
- Middha, S. K., Goyal, A. K., Lokesh, P., Yardi, V., Mojamdar, L., Keni, D. S., et al. (2015). Toxicological evaluation of emblica officinalis fruit extract and its anti-inflammatory and free radical scavenging properties. *Pharmacogn. Mag.* 11, S427. doi:10.4103/0973-1296.168982
- Min, Y.-D., Choi, C.-H., Bark, H., Son, H.-Y., Park, H.-H., Lee, S., et al. (2007). Quercetin inhibits expression of inflammatory cytokines through attenuation of NF- κ B and p38 MAPK in HMC-1 human mast cell line. *Inflamm. Res.* 56 (5), 210. doi:10.1007/s00011-007-6172-9
- Min, Y.-G. (2010). The pathophysiology, diagnosis and treatment of allergic rhinitis. *Allergy Asthma Immunol. Res.* 2, 65. doi:10.4168/aa.2010.2.2.65
- Miraglia Del Giudice, M., Maiello, N., Decimo, F., Capasso, M., Campana, G., Leonardi, S., et al. (2014). Resveratrol plus carboxymethyl- β -glucan may affect respiratory infections in children with allergic rhinitis. *Pediatr. Allergy Immunol.* 25 (7), 724–728. doi:10.1111/pai.12279
- Mrcek, J., Jurikova, T., Skrovankova, S., and Sochor, J. (2016). Quercetin and its anti-allergic immune response. *Molecules* 21 (5), 623. doi:10.3390/molecules21050623
- Mukai, K., Tsai, M., Saito, H., and Galli, S. J. (2018). Mast cells as sources of cytokines, chemokines, and growth factors. *Immunol. Rev.* 282 (1), 121–150. doi:10.1111/immr.12634
- Murdock, N. (2015). Evaluation of *Terminalia chebula* extract for anti-arthritis efficacy and safety in osteoarthritic dogs. *J. Veterinar Sci. Technol.* 7, 28. doi:10.4172/2157-7579.1000290
- Muthuraman, A., Sood, S., and Singla, S. K. (2011). The antiinflammatory potential of phenolic compounds from *Embllica officinalis* L. in rat. *Inflammopharmacol* 19 (6), 327–334. doi:10.1007/s10787-010-0041-9
- Naclerio, R., Ansotegui, I. J., Bousquet, J., Canonica, G. W., D'Amato, G., Rosario, N., et al. (2020). International expert consensus on the management of allergic rhinitis (AR) aggravated by air pollutants. *World Allergy Organ. J.* 13 (3), 100106. doi:10.1016/j.waojou.2020.100106
- Nadif, R., Rava, M., Decoster, B., Huyvaert, H., Le Moual, N., Bousquet, J., et al. (2014). Exhaled nitric oxide, nitrite/nitrate levels, allergy, rhinitis and asthma in the EGEA study. *Eur. Respir. J.* 44 (2), 351–360. doi:10.1183/09031936.00202413
- Naik, G. H., Priyadarsini, K. I., and Mohan, H. (2006). Free radical scavenging reactions and phytochemical analysis of triphala, an ayurvedic formulation. *Curr. Sci.* 90 (8), 49.
- Nair, V., Kumar, R., Singh, S., and Gupta, Y. K. (2012). Anti-granuloma activity of *Terminalia chebula* Retz. in wistar Rats. *Eur. J. Inflamm.* 10 (2), 185–192. doi:10.1177/1721727X1201000203
- Nair, V., Singh, S., and Gupta, Y. K. (2010). Anti-arthritis and disease modifying activity of *Terminalia chebula* Retz. in experimental model experimental models. *J. Pharm. Pharmacol.* 62 (12), 1801–1811. doi:10.1111/j.2042-7158.2010.01193.x
- Nam, D. Y., Lee, J. M., Heo, J. C., and Lee, S. H. (2011). Mitigation of 2,4-dinitrofluorobenzene-induced atopic dermatitis-related symptoms by *Terminalia chebula* Retz. *Int. J. Mol. Med.* 28, 1013–1018. doi:10.3892/ijmm.2011.792
- Noack, M., and Miossec, P. (2014). Th17 and regulatory T cell balance in autoimmune and inflammatory diseases. *Autoimmun. Rev.* 13 (6), 668–677. doi:10.1016/j.autrev.2013.12.004
- Nosalova, G., Jurecek, L., Chatterjee, U. R., Majee, S. K., Nosal, S., and Ray, B. (2013). Antitussive activity of the water-extracted carbohydrate polymer from *Terminalia chebula* citric acid-induced cough. *Evidence-Based Complement. Altern. Med.* 2013, 1. doi:10.1155/2013/650134
- Nosál'Ovák, G., Mokry, J., and Hassan, K. M. T. (2003). Antitussive activity of the fruit extract of *Embllica officinalis* Gaertn. (Euphorbiaceae). *Phytomedicine* 10 (6-7), 583–589. doi:10.1078/094471103322331872
- Oh, H.-A., Han, N.-R., Kim, M.-J., Kim, H.-M., and Jeong, H.-J. (2013). Evaluation of the effect of kaempferol in a murine allergic rhinitis model. *Eur. J. Pharmacol.* 718 (1-3), 48–56. doi:10.1016/j.ejphar.2013.08.045
- Ozkaya, E., Akduman, H., Erenberk, U., Demir, A., and Dundaroz, M. R. (2013). Plasma paraoxonase activity and oxidative stress and their relationship to disease severity in children with allergic rhinitis. *Am. J. Rhinol Allergy* 27, 13. doi:10.2500/ajra.2013.27.3837
- Park, H.-j., Lee, C.-M., Jung, I. D., Lee, J. S., Jeong, Y.-i., Chang, J. H., et al. (2009). Quercetin regulates Th1/Th2 balance in a murine model of asthma. *Int. Immunopharmacology* 9 (3), 261–267. doi:10.1016/j.intimp.2008.10.021
- Parveen, R., Shamsi, T. N., Singh, G., Athar, T., and Fatima, S. (2018). Phytochemical analysis and *In-vitro* Biochemical Characterization of aqueous and methanolic extract of Triphala, a conventional herbal remedy. *Biotechnol. Rep.* 17, 126–136. doi:10.1016/j.btre.2018.02.003

- Peterson, C. T., Denniston, K., and Chopra, D. (2017). Therapeutic uses of triphala in ayurvedic medicine. *J. Altern. Complement. Med.* 23, 607–614. doi:10.1089/acm.2017.0083
- Phetkate, P., Kummalue, T., U-Pratya, Y., and Kietinun, S. (2012). Significant increase in cytotoxic T lymphocytes and natural killer cells by triphala: a clinical phase I study. *Evidence-Based Complement. Altern. Med.* 2012, 239856. doi:10.1155/2012/239856
- Polosa, R., Ciamarra, L., Mangano, G., Prosperini, G., Pistorio, M. P., Vancheri, C., et al. (2000). Bronchial hyperresponsiveness and airway inflammation markers in nonasthmatics with allergic rhinitis. *Eur. Respir. J.* 15 (1), 30–35. doi:10.1034/j.1399-3003.2000.15a07.x
- Poulsen, L. K., and Hummelshøj, L. (2007). Triggers of IgE class switching and allergy development. *Ann. Med.* 39 (6), 440–456. doi:10.1080/07853890701449354
- Pozharitskaya, O. N., Ivanova, S. A., Shikov, A. N., and Makarov, V. G. (2007). Separation and evaluation of free radical-scavenging activity of phenol components of *Embolica officinalis* extract by using an HPTLC-DPPH method. *J. Sep. Sci.* 30 (9), 1250–1254. doi:10.1002/jssc.200600532
- Prabu, D., Kirubanandan, S., Ponnudurai, K., Nappinnai, M., Jinu, A. J. S., and Renganathan, S. (2008). Anti-inflammatory and analgesic activities of methanol extract of Triphala - a poly herbal formulation. *Oriental Pharm. Exp. Medicine Pharm. Exp. Med* 8, 423. doi:10.3742/opem.2008.8.4.423
- Pradyumna Rao, T., Okamoto, T., Akita, N., Hayashi, T., Kato-Yasuda, N., and Suzuki, K. (2013). Amla (*Embolica officinalis* Gaertn.) extract inhibits lipopolysaccharide-induced procoagulant and pro-inflammatory factors in cultured vascular endothelial cells. *Br. J. Nutr.* 110 (12), 2201–2206. doi:10.1017/S0007114513001669
- Rahimi, V. B., Askari, V. R., Shirazinia, R., Soheili-Far, S., Askari, N., Rahmanian-Devin, P., et al. (2018). Protective effects of hydro-ethanolic extract of *Terminalia chebula* on primary microglia cells and their polarization (M1/M2 balance). *Mult. Scler. Relat. Disord.* 25, 5–3. doi:10.1016/j.msard.2018.07.015
- Ramezanzpour, M., Moraitis, S., Smith, J. L. P., Wormald, P. J., and Vreugde, S. (2016). Th17 cytokines disrupt the airway mucosal barrier in chronic rhinosinusitis. *Mediators Inflamm.* 2016, 9798206. doi:10.1155/2016/9798206
- Rasool, M., and Sabina, E. P. (2007). Antiinflammatory effect of the Indian ayurvedic herbal formulation Triphala on adjuvant-induced arthritis in mice. *Phytother. Res.* 21 (9), 889–894. doi:10.1002/ptr.2183
- Reddy, D. B., Reddy, T. C. M., Jyotsna, G., Sharan, S., Priya, N., Lakshmpathi, V., et al. (2009). Chebulagic acid, a COX-LOX dual inhibitor isolated from the fruits of *Terminalia chebula* Retz., induces apoptosis in COLO-205 cell line. *J. Ethnopharmacology* 124 (3), 506–512. doi:10.1016/j.jep.2009.05.022
- Reithofer, M., and Jahn-Schmid, B. (2017). Allergens with protease activity from house dust mites. *Int. J. Mol. Sci.* 18 (7), 1368. doi:10.3390/ijms18071368
- Rice-Evans, C. A., Miller, N. J., and Paganga, G. (1997). Antioxidant properties of phenolic compounds. *Trends Plant Sci.* 2 (4), 152–159. doi:10.1016/S1360-1385(97)01018-2
- Ríos, J.-L., Giner, R., Marín, M., and Recio, M. (2018). A pharmacological update of ellagic acid. *Planta Med.* 84 (15), 1068–1093. doi:10.1055/a-0633-9492
- Roidoung, S., Dolan, K. D., and Siddiq, M. (2016). Gallic acid as a protective antioxidant against anthocyanin degradation and color loss in vitamin-C fortified cranberry juice. *Food Chem.* 210, 422–427. doi:10.1016/j.foodchem.2016.04.133
- Romagnani, S. (2004). Immunologic influences on allergy and the TH1/TH2 balance. *J. Allergy Clin. Immunol.* 113 (3), 395–400. doi:10.1016/j.jaci.2003.11.025
- Rosa, A. C., and Fantozzi, R. (2013). The role of histamine in neurogenic inflammation. *Br. J. Pharmacol.* 170 (1), 38–45. doi:10.1111/bph.12266
- Rubab, I., and Ali, S. (2016). Dried fruit extract of *Terminalia chebulam* modulates the immune response in mice. *Food Agric. Immunol.* 27, 1. doi:10.1080/09540105.2015.1055554
- Sabina, E. P., Rasool, M. K., and Mathew, L. (2009). *Vivo and in vitro immunomodulatory effects of Indian ayurvedic herbal formulation triphala on experimental induced inflammation*. London: Pharmacologyonline.
- Sagit, M., Polat, H., Gorgen, S. G., Berk, E., Guler, S., and Yasar, M. (2017). Effectiveness of quercetin in an experimental rat model of allergic rhinitis. *Eur. Arch. Otorhinolaryngol.* 274 (8), 3087–3095. doi:10.1007/s00405-017-4602-z
- Sai Ram, M., Neetu, D., Yogesh, B., Anju, B., Dipti, P., Pauline, T., et al. (2002). Cyto-protective and immunomodulating properties of Amla (*Embolica officinalis*) on lymphocytes: an *in-vitro* study. *J. Ethnopharmacol.* 81 (1), 5–10. doi:10.1016/S0378-8741(01)00421-4
- Sakai-Kashiwabara, M., and Asano, K. (2013). Inhibitory action of quercetin on eosinophil Activation *in vitro*. *Evidence-Based Complement. Altern. Med.* 2013, 1. doi:10.1155/2013/127105
- Schuliga, M. (2015). NF-kappaB signaling in chronic inflammatory airway disease. *Biomolecules* 5 (3), 1266–1283. doi:10.3390/biom5031266
- Seo, J.-H., Kwon, S.-O., Lee, S.-Y., Kim, H. Y., Kwon, J.-W., Kim, B.-J., et al. (2013). Association of antioxidants with allergic rhinitis in children from Seoul. *Allergy Asthma Immunol. Res.* 5 (2), 81–87. doi:10.4168/air.2013.5.2.81
- Seresirikachorn, K., Chitsuthipakorn, W., Kanjanawase, D., Khattiyawattayakun, L., and Snidvongs, K. (2018). Effects of H1 antihistamine addition to intranasal corticosteroid for allergic rhinitis: a systematic review and meta-analysis. *Int. Forum Allergy Rhinol.* 8 (10), 1083–1092. doi:10.1002/alr.22166
- Shanmuganathan, S., and Angayarkanni, N. (2018). Chebulagic acid Chebulinic acid and Gallic acid, the active principles of Triphala, inhibit TNF α induced pro-angiogenic and pro-inflammatory activities in retinal capillary endothelial cells by inhibiting p38, ERK and NFkB phosphorylation. *Vasc. Pharmacol.* 108, 23–35. doi:10.1016/j.vph.2018.04.005
- Sharma, A., and Sharma, K. K. (2011). Chemoprotective role of triphala against 1,2-dimethylhydrazine dihydrochloride induced carcinogenic damage to mouse liver. *Ind. J. Clin. Biochem.* 26 (3), 290–295. doi:10.1007/s12291-011-0138-y
- Shin, D., Park, S.-H., Choi, Y.-J., Kim, Y.-H., Antika, L., Habibah, N., et al. (2015). Dietary compound kaempferol inhibits airway thickening induced by allergic reaction in a bovine serum albumin-induced model of asthma. *Ijms* 16 (12), 29980–29995. doi:10.3390/ijms161226218
- Shin, T. Y., Jeong, H. J., Kim, D. K., Kim, S. H., Lee, J. K., Kim, D. K., et al. (2001). Inhibitory action of water soluble fraction of *Terminalia chebula* on systemic and local anaphylaxis. *J. Ethnopharmacol.* 74 (2), 133–140. doi:10.1016/S0378-8741(00)00360-3
- Simons, F. E. R. (1999). Allergic rhinobronchitis: the asthma-allergic rhinitis link. *J. Allergy Clin. Immunol.* 104 (3 Pt 1), 534–540. doi:10.1016/S0091-6749(99)70320-9
- Sin, B., and Togias, A. (2011). Pathophysiology of allergic and nonallergic rhinitis. *Proc. Am. Thorac. Soc.* 8 (1), 106–114. doi:10.1513/pats.201008-057RN
- Singh, M. K., Yadav, S. S., Yadav, R. S., Chauhan, A., Katiyar, D., and Khattri, S. (2015). Protective effect of *Embolica-officinalis* in arsenic induced biochemical alteration and inflammation in mice. *Springerplus* 4, 438. doi:10.1186/s40064-015-1227-9
- Sireeratawong, S., Jaijoy, K., Khonsung, P., and Soonthornchareonnon, N. (2014). Analgesic and anti-inflammatory activities of the water extract from *terminalia chebula* rezt. *Afr. J. Trad. Compl. Alt. Med.* 11, 77. doi:10.4314/ajtcam.v11i6.8
- Sireeratawong, S., Jaijoy, K., and Soonthornchareonnon, N. (2013). Evaluation of anti-inflammatory and antinociceptive activity of Triphala recipe. *Afr. J. Trad. Compl. Alt. Med.* 10 (2), 246–250. doi:10.4314/ajtcam.v10i2.8
- Small, P., Keith, P. K., and Kim, H. (2018). Allergic rhinitis. *Allergy Asthma Clin. Immunol.* 14, 139. doi:10.1186/s13223-018-0280-7
- Srikumar, R., Jeya Parthasarathy, N., and Sheela Devi, R. (2005). Immunomodulatory activity of triphala on neutrophil functions. *Biol. Pharm. Bull.* 28 (8), 1398–403. doi:10.1248/bpb.28.1398
- Srikumar, R., Parthasarathy, N. J., Manikandan, S., Muthuvel, A., Rajamani, R., and Sheeladevi, R. (2007). Immunomodulatory effect of Triphala during experimentally induced noise stress in albino rats. *J. Health Sci.* 53, 142. doi:10.1248/jhs.53.142
- Srikumar, R., Parthasarathy, N. J., Manikandan, S., Narayanan, G. S., and Sheeladevi, R. (2006). Effect of Triphala on oxidative stress and on cell-mediated immune response against noise stress in rats. *Mol. Cel. Biochem.* 283 (1–2), 67–74. doi:10.1007/s11010-006-2271-0
- Steelant, B., Seys, S. F., Van Gerven, L., Van Woensel, M., Farré, R., Wawrzyniak, P., et al. (2018). Histamine and T helper cytokine-driven epithelial barrier dysfunction in allergic rhinitis. *J. Allergy Clin. Immunol.* 141 (3), 951–963. doi:10.1016/j.jaci.2017.08.039
- Sukakul, T., Kettawan, A., Chompoopong, S., and Rungruang, T. (2013). Topical application of *Terminalia chebula* extract helps croton oil-induced dermatitis in mice. *Int. Food Res. J.* 20 (5), 2269–2272.

- Takauji, Y., Miki, K., Mita, J., Hossain, M. N., Yamauchi, M., Kioi, M., et al. (2016). Triphala, a formulation of traditional Ayurvedic medicine, shows protective effect against X-radiation in HeLa cells. *J. Biosci.* 41 (4), 569–575. doi:10.1007/s12038-016-9639-4
- Tanaka, M., Kishimoto, Y., Sasaki, M., Sato, A., Kamiya, T., Kondo, K., et al. (2018). *Terminalia* bellirica (gaertn.) Roxb. Extract and gallic acid attenuate LPS-induced inflammation and oxidative stress via MAPK/NF- κ B and Akt/AMPK/Nrf2 pathways. *Oxidative Med. Cell Longevity* 2018, 9364364. doi:10.1155/2018/9364364
- Tanaka, Y., Atsuko, F., Asano, K., and Koyabashi, H. (2020). Modulation of Th1/Th2 cytokine balance by. *Medicines* 7, 1–9. doi:10.3390/medicines7080046
- Taylorclark, T., Kollarik, M., Macglashanjr, D., and Udem, B. (2005). Nasal sensory nerve populations responding to histamine and capsaicin. *J. Allergy Clin. Immunol.* 116 (6), 1282–1288. doi:10.1016/j.jaci.2005.08.043
- Thomas, M. (2006). Allergic rhinitis: evidence for impact on asthma. *BMC Pulm. Med.* 6 Suppl 1 (Suppl 1), S4. doi:10.1186/1471-2466-6-S1-S4
- Thornhill, S. M., and Kelly, A. M. (2000). Natural treatment of perennial allergic rhinitis. *Altern. Med. Rev.* 5 (5), 448–454. doi:10.1007/bf03297230
- Tongtak, W., Klaewsongkram, J., Mickleborough, T. D., and Suksom, D. (2018). Effects of aerobic exercise and vitamin C supplementation on rhinitis symptoms in allergic rhinitis patients. *Asian Pac. J. Allergy Immunol.* 36 (4), 222–231. doi:10.12932/AP-040417-0066
- Townley, R. G., Gendapodi, P. R., Qutna, N., Evans, J., Romero, F. A., and Abel, P. (2009). Effect of interleukin 13 on bronchial hyperresponsiveness and the bronchoprotective effect of beta-adrenergic bronchodilators and corticosteroids. *Ann. Allergy Asthma Immunol.* 102 (3), 190–197. doi:10.1016/S1081-1206(10)60080-4
- Turner, H., and Kinet, J.-P. (1999). Signalling through the high-affinity IgE receptor Fc ϵ RI. *Nature* 402 (S6760), 24–30. doi:10.1038/35037021
- Udem, B. J., and Taylor-Clark, T. (2014). Mechanisms underlying the neuronal-based symptoms of allergy. *J. Allergy Clin. Immunol.* 133 (6), 1521–1534. doi:10.1016/j.jaci.2013.11.027
- Varma, S. R., Sivaprakasam, T. O., Mishra, A., Kumar, L. M. S., Prakash, N. S., Prabhu, S., et al. (2016). Protective effects of triphala on dermal fibroblasts and human keratinocytes. *PLoS One* 11 (1), e0145921. doi:10.1371/journal.pone.0145921
- Varshney, J., and Varshney, H. (2015). Allergic rhinitis: an overview. *Indian J. Otolaryngol. Head Neck Surg.* 67, 143. doi:10.1007/s12070-015-0828-5
- Ventura, I., Vega, A., Chacón, P., Chamorro, C., Aroca, R., Gómez, E., et al. (2014). Neutrophils from allergic asthmatic patients produce and release metalloproteinase-9 upon direct exposure to allergens. *Allergy* 69 (7), 898–905. doi:10.1111/all.12414
- Vollbracht, C., Raithel, M., Krick, B., Kraft, K., and Hagel, A. F. (2018). Intravenous vitamin C in the treatment of allergies: an interim subgroup analysis of a long-term observational study. *J. Int. Med. Res.* 46 (9), 3640–3655. doi:10.1177/0300060518777044
- Vujnovic, S. D., and Domuz, A. (2018). Epidemiological aspects of rhinitis and asthma: comorbidity or united airway disease in asthma diagnosis and management—approach based on phenotype and endotype. *Asthma Diag. Manage. Approach Based Phenotype Endotype* 33, 237. doi:10.5772/intechopen.76773
- Wang, X., Zhao, H., Ma, C., Lv, L., Feng, J., and Han, S. (2018). Gallic acid attenuates allergic airway inflammation via suppressed interleukin-33 and group 2 innate lymphoid cells in ovalbumin-induced asthma in mice. *Int. Forum Allergy Rhinol.* 8 (11), 1284–1290. doi:10.1002/alr.22207
- White, M. V. (1990). The role of histamine in allergic diseases. *J. Allergy Clin. Immunol.* 86 (4 Pt 2), 599–605. doi:10.1016/S0091-6749(05)80223-4
- Wise, S. K., Laury, A. M., Katz, E. H., Den Beste, K. A., Parkos, C. A., and Nusrat, A. (2014). Interleukin-4 and interleukin-13 compromise the sinonasal epithelial barrier and perturb intercellular junction protein expression. *Int. Forum Allergy Rhinology* 4 (5), 361–370. doi:10.1002/alr.21298
- World Allergy Organization (2013). White book on allergy: update 2013, executive summary. *World Allergy Organ.* 12, 49. doi:10.1080/14693062.2006.9685626
- Yang, M. H., Ali, Z., Khan, I. A., and Khan, S. I. (2014). Anti-inflammatory activity of constituents isolated from *Terminalia* chebula. *Nat. Product. Commun.* 9 (7), 965–968. doi:10.1177/1934578x1400900721
- Yang, Y., Xiu, J., Liu, J., Zhang, L., Li, X., Xu, Y., et al. (2013). Chebulagic acid, a hydrolyzable tannin, exhibited antiviral activity *in vitro* and *in vivo* against human enterovirus 71. *Ijms* 14 (5), 9618–9627. doi:10.3390/ijms14059618
- Young, T., Finn, L., and Kim, H. (1997). Nasal obstruction as a risk factor for sleep-disordered breathing. The university of Wisconsin sleep and respiratory research group. *J. Allergy Clin. Immunol.* 99, S757.
- Zhang, N., Li, H., Jia, J., and He, M. (2015). Anti-inflammatory effect of curcumin on mast cell-mediated allergic responses in ovalbumin-induced allergic rhinitis mouse. *Cell Immunol.* 298 (1–2), 88–95. doi:10.1016/j.cellimm.2015.09.010
- Zhu, J., Yamane, H., and Paul, W. E. (2010). Differentiation of effector CD4 T cell populations. *Annu. Rev. Immunol.* 28 (1), 445–489. doi:10.1146/annurev-immunol-030409-101212

Conflict of Interest: The authors declare that the research was conducted in the absence of any commercial or financial relationships that could be construed as a potential conflict of interest.

Copyright © 2021 Jantrapirom, Hirunsatitpran, Potikanond, Nimlamool and Hanprasertpong. This is an open-access article distributed under the terms of the Creative Commons Attribution License (CC BY). The use, distribution or reproduction in other forums is permitted, provided the original author(s) and the copyright owner(s) are credited and that the original publication in this journal is cited, in accordance with accepted academic practice. No use, distribution or reproduction is permitted which does not comply with these terms.



Rhoifolin Ameliorates Osteoarthritis via Regulating Autophagy

Jiyuan Yan¹, Bowei Ni¹, Gaohong Sheng¹, Yingchi Zhang⁴, Yifan Xiao³, Yongzhuang Ma⁵, Hao Li¹, Hua Wu^{1*} and Chang Tu^{2*}

¹Department of Orthopedics, Tongji Hospital, Tongji Medical College, Huazhong University of Science and Technology, Wuhan, China, ²Department of Orthopedics, Renmin Hospital of Wuhan University, Wuhan, China, ³Department of Pathology and Pathophysiology, Medical College, Jiangnan University, Wuhan, China, ⁴Department of Traumatology, Tongji Hospital, Tongji Medical College, Huazhong University of Science and Technology, Wuhan, China, ⁵Department of Orthopedics, Shanxi Bethune Hospital, Taiyuan, China

OPEN ACCESS

Edited by:

Jun Tian,
Jiangsu Normal University, China

Reviewed by:

Aida Habib,
American University of Beirut,
Lebanon
Shrikant Anant,
University of Kansas Medical Center,
United States

*Correspondence:

Hua Wu
wuhua360@aliyun.com
Chang Tu
tuchang@whu.edu.cn

Specialty section:

This article was submitted to
Inflammation Pharmacology,
a section of the journal
Frontiers in Pharmacology

Received: 30 January 2021

Accepted: 07 May 2021

Published: 28 May 2021

Citation:

Yan J, Ni B, Sheng G, Zhang Y, Xiao Y,
Ma Y, Li H, Wu H and Tu C (2021)
Rhoifolin Ameliorates Osteoarthritis via
Regulating Autophagy.
Front. Pharmacol. 12:661072.
doi: 10.3389/fphar.2021.661072

Osteoarthritis (OA) is a common age-related joint disease. Its development has been generally thought to be associated with inflammation and autophagy. Rhoifolin (ROF), a flavanone extracted from *Rhus succedanea*, has exhibited prominent anti-oxidative and anti-inflammatory properties in several diseases. However the exact role of ROF in OA remains unclear. Here, we investigated the therapeutic effects as well as the underlying mechanism of ROF on rat OA. Our results indicated that ROF could significantly alleviate the IL-1 β -induced inflammatory responses, cartilage degradation, and autophagy downregulation in rat chondrocytes. Moreover, administration of autophagy inhibitor 3-methyladenine (3-MA) could reverse the anti-inflammatory and anti-cartilage degradation effects of ROF. Furthermore, P38/JNK and PI3K/AKT/mTOR signal pathways were involved in the protective effects of ROF. *In vivo*, intra-articular injection of ROF could notably ameliorate the cartilage damage in rat OA model. In conclusion, our work elucidated that ROF ameliorated rat OA via regulating autophagy, indicating the potential role of ROF in OA therapy.

Keywords: rhoifolin, osteoarthritis, autophagy, 3-methyladenine, MAPK, PI3K/AKT/mTOR

INTRODUCTION

Osteoarthritis, featured with cartilage loss, joint pain, and physical disability, has attracted worldwide attention in recent years (Kontio et al., 2020). As an age-related joint disease, OA afflicts over 240 million people globally. Furthermore, the prevalence of OA continues to rise since the mid-twentieth century (Nelson 2018; Mandl 2019). Currently, most therapeutic strategies targeted for OA focus on relieving the symptom rather than reversing the disease progression. Therefore, patients at the late stage of OA have to accept joint replacement without better choices (Glyn-Jones et al., 2015).

Chronic inflammatory responses and cartilage metabolic imbalances are vital to the progression of OA (Appleton, 2018). Excessive release of proinflammatory cytokine interleukin-1 β (IL-1 β) was found in the synovial fluid of OA patient (Pelletier et al., 2001). Previous study indicated that IL-1 β could induce the production of matrix metallo-proteinases (MMPs) and aggrecanase-2 (ADAMTS5), which resulted in the loss of cartilage matrix (Tu et al., 2019). Moreover, elevated level of IL-1 β had been shown to exacerbate the inflammatory responses via overproducing the inflammatory mediators including cyclooxygenase-2 (COX-2) and inducible nitric oxide synthase (iNOS) (Tu et al., 2019). Autophagy is a highly conserved catabolic process which is essential for

maintaining cell homeostasis (He and Klionsky 2009). In OA pathological progression, autophagy induction could promote chondrocyte survival and cartilage matrix synthesis (Carames et al., 2010). Besides, intra-articular injection of autophagy inhibitor ameliorated the cartilage degradation in mouse OA model (Takayama et al., 2014). Furthermore, it is reported that IL-1 β could significantly induce the autophagy downregulation in chondrocytes (Wang et al., 2019). Therefore, strategies targeting IL-1 β may lead to new ideas in OA treatment.

Due to mild side effects and definite efficacy, more and more herb medicines have been accepted by OA patients (Li et al., 2017). Rhoifolin, a bioactive product first extracted from *Rhus succedanea*, has proved its anti-oxidative and anti-inflammatory properties in several diseases (Fang et al., 2020; Gandhi et al., 2020; Peng et al., 2020). *In vitro*, ROF attenuated osteoclasts-stimulated osteolysis *via* suppressing MAPK and NF κ B signal pathways, indicating the possible mechanism of its action (Liao et al., 2019). However, the detailed role of ROF in OA remains unclear. In this study, we aim to clarify therapeutic potential of ROF in OA and in the underlying mechanism. We expect to explore a new way in OA treatment.

MATERIALS AND METHODS

Ethics Approval

This study was conducted in strict accordance with the Guidelines of Animal Care and Use Committee for Teaching and Research, Tongji Medical College, Huazhong University of Science and Technology. The experimental procedures were approved by the Institutional Animal Care and Use Committee, Tongji Medical College, Huazhong University of Science and Technology. All efforts were made to reduce animal suffering.

Reagents

Rhoifolin (ROF, #PHL83302) was procured from Sigma Aldrich (St. Louis, MO, United States). ROF was dissolved in DMSO and all experiment groups were treated with equal volume of DMSO. Recombinant rat IL-1 β was purchased from R and D systems (Minneapolis, MN, United States). Fetal bovine serum (FBS) and Dulbecco's Modified Eagle's Medium F12 (DMEM/F12) were acquired from Gibco (NY, United States). Antibodies specific for MMP13 (#ab219620) and iNOS (#ab136918) were provided by Abcam (Cambridge, MA, United States). Antibody against Collagen II (#15943-1-AP) was obtained from Proteintech Group (Wuhan, Hubei, China). Antibodies against COX-2 (#12882), ATG5(#12994), ATG12 (#4180), Beclin-1 (#3495), P62-sequestosome (#39749), LC3 I/II (#12741), P-PI3K(#4228), PI3K(#4249), P-AKT (#4060), AKT(#4691), P-mTOR (#5536), mTOR (#2983), P-JNK (#9255), JNK (#9258), P-P38 (#4511), P38 (#8690), P-ERK (#4370), and ERK (#4695) were supplied by Cell Signaling Technology (Beverly, MA, United States). Antibodies specific for ADAMTS5 (#BA3020) and GAPDH (#BM3876) were procured from Boster (Wuhan, Hubei, China).

Cell Culture

Chondrocytes were harvested from 5 days-old Sprague-Dawley (SD) rats as reported previously (Ma et al., 2019; Tu et al., 2019). Briefly, the cartilage obtained from the knee joints was first sliced into small pieces and digested with 0.25% trypsin-EDTA for 30 min. Then, the cartilage fragments were fully digested with 0.25% collagenase II overnight. Subsequently, the cell suspension was centrifuged with a speed of 1,500 rpm for 5 min to obtain primary chondrocytes. Cells were finally cultured in DMEM/F12 supplemented with 10% FBS and 1% penicillin/streptomycin solution at 37°C with 5% CO₂. Chondrocytes of second or third passages were used in following experiments.

Cell Viability

Cell Counting Kit-8 (CCK-8, #AR1160, Boster) assay was employed to explore the cell viability. Concisely, rat chondrocytes were seeded onto 96-well plates at a density of 1×10^4 cells per well. After adhesion, the cells were treated with different concentrations of ROF (0, 5, 10, and 20 μ M) alone or combined with IL-1 β (10 ng/ml) for 24 h. Next, 100 μ L culture medium supplemented with 10 μ L CCK-8 reagent was added to each well. After 1 h incubation at room temperature, the absorbance at 450 nm of each well was detected by a microplate reader (Bio-Rad, Richmond, CA, United States).

Western Blot

Rat chondrocytes were collected and washed with phosphate buffered saline (PBS). Next, the cells were lysed with RIPA buffer containing 1% protease/phosphatase inhibitor cocktail (Boster). The protein concentration of isolated cell lysis solution was determined by bicinchoninic acid (BCA) kit. Afterward, 25 μ g protein samples were separated on 8–12% SDS-polyacrylamide gels and transferred to PVDF membranes using a Bio-Rad system. The membranes were blocked with 5% BSA for 1 h at room temperature and then incubated with primary antibodies overnight at 4°C. Subsequently, the membranes were washed with TBST and incubated with corresponding secondary antibodies for 1 h at room temperature. Finally, enhanced ECL kit (Thermo Fisher Scientific, United States) was used to visualize the blots. The relative protein expression was calculated by ImageJ software compared to internal control.

Tandem GFP-RFP-LC3 Adenovirus Transfection

For autophagy flux evaluation, rat chondrocytes were transfected with tandem GFP-RFP-LC3 adenovirus transfection vectors (HanBio Technology, China). Autophagosomes (shown in green) and autolysosomes (shown in red) were observed with a nanoscale laser scanning confocal microscope system (Nikon, NY, United States).

Transmission Electron Microscopy

Rat chondrocytes were trypsinized, centrifuged and blocked in 10% BSA. Then cells were fixed using 2.5% glutaraldehyde overnight at 4°C. Subsequently, the cells were washed with PBS and fixed with 1% osmium tetroxide for 1 h. Next, the

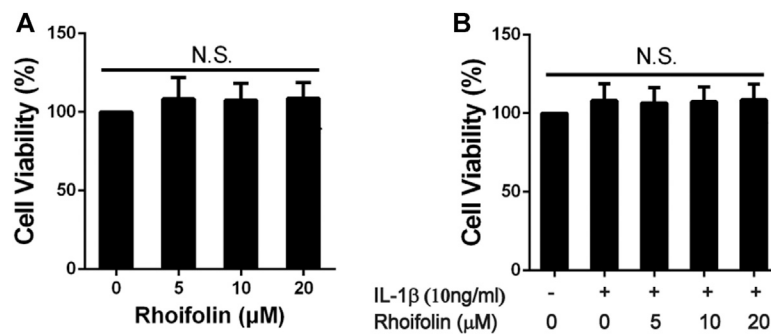


FIGURE 1 | Effects of ROF on Cell Viability. **(A)** Rat chondrocytes were exposed to ROF (5, 10, 20 μM) alone or **(B)** with IL-1β (10 ng/ml) for 24 h and cell viability was assessed by CCK-8 assay. N.S. indicated no significance.

cells were washed with distilled water and stained using 2% uranyl acetate for 1 h. After dehydration, the samples were mixed with resin and propylene oxide (1:1) for 2 h and transferred into pure resin overnight. Finally, the samples were embedded, sectioned, and stained with uranyl acetate and lead citrate. A TECNAI G20 transmission electron microscopy (TEM) was employed to observe the autophagosomes in cells.

Rat Osteoarthritis Model

Eighteen 8-week-old male SD rats (weight 280–320 g) were obtained from the Laboratory Animal Center of Tongji Hospital. The rat OA model was built by anterior cruciate ligament transaction (ACL-T) and medial meniscus destabilization as described before (Appleton et al., 2007). All rats accepted the surgery on the right knee and were randomly divided into three groups. For the ROF group ($n = 6$), rats were performed the operation and intra-articular injection of 20 μM ROF weekly. For the sham group ($n = 6$), rats accepted sham surgery without ACL-T or meniscus destabilization and were treated with equal volume of saline. For the OA group ($n = 6$), rats were performed the operation and intra-articular injection of equal volume of saline. 8 weeks postsurgery, all rats were sacrificed and the samples were fixed with 4% paraformaldehyde for further study.

Histological Evaluation

Fixed samples were decalcified in 10% EDTA solution for 1 month and embedded in paraffin. Then the whole knee joints were cut into 5 μm-thick sections coronally, and stained with H and E and Safranin-O-Fast green. Further immunohistological staining was performed using antibodies against Collagen II, MMP13, and LC3B. Furthermore, the Osteoarthritis Research Society International (OARSI) scoring system was employed to evaluate the histological changes.

Statistical Analysis

Data are exhibited as mean ± standard deviation. All data were analyzed using one-way analysis of variance (ANOVA) followed by Turkey's post hoc test. Comparisons were considered significant for $p < 0.05$. All experiments were repeated at least three times.

RESULTS

Effects of Rhoifolin on Cell Viability

CCK-8 assay was performed to evaluate the cytotoxic effects of ROF on rat chondrocytes. As shown in **Figure 1**, after 24 h reaction, ROF at the concentrations of 5, 10, and 20 μM had no toxic effects on chondrocytes with or without IL-1β treatment (10 ng/ml).

Rhoifolin Alleviates IL-1β-Induced Inflammatory Responses and Cartilage Degradation

To confirm the protective effects of ROF on the IL-1β-induced inflammatory responses and cartilage degradation in rat chondrocytes, Western blotting was performed. As exhibited in **Figures 2A,B**, IL-1β could significantly increase the expression of inflammatory cytokines, including iNOS and COX-2, while administration of different concentrations of ROF could alleviate this process. Moreover, the expression of collagen II, MMP13, and ADAMTS5 was used to evaluate the cartilage degradation. As shown in **Figures 2C,D**, IL-1β could notably induce the upregulation of MMP13 and ADAMTS5 and the downregulation of collagen II. However, ROF could reverse this change.

Rhoifolin Attenuates IL-1β-Induced Autophagy Downregulation in Chondrocytes

A previous study indicated that autophagy played an important role in OA development. We next explored the effects of ROF on autophagy in IL-1β-treated rat chondrocytes. As shown in **Figures 3A,B**, IL-1β treatment significantly decreased the expression of ATG5, ATG12, Beclin-1, and the ratio of LC3 II/LC3 I, while increased the expression of P62-sequestosome in rat chondrocytes. However, administration of 20 μM ROF could markedly reverse this change. The tandem GFP-RFP-LC3 adenovirus transfection was further used to observe the autophagosome formation. As exhibited in **Figures 3C,D**, the number of autophagosomes (green puncta) and autophagolysosomes (red puncta) in chondrocytes decreased significantly after IL-1β treatment. However, when treated with

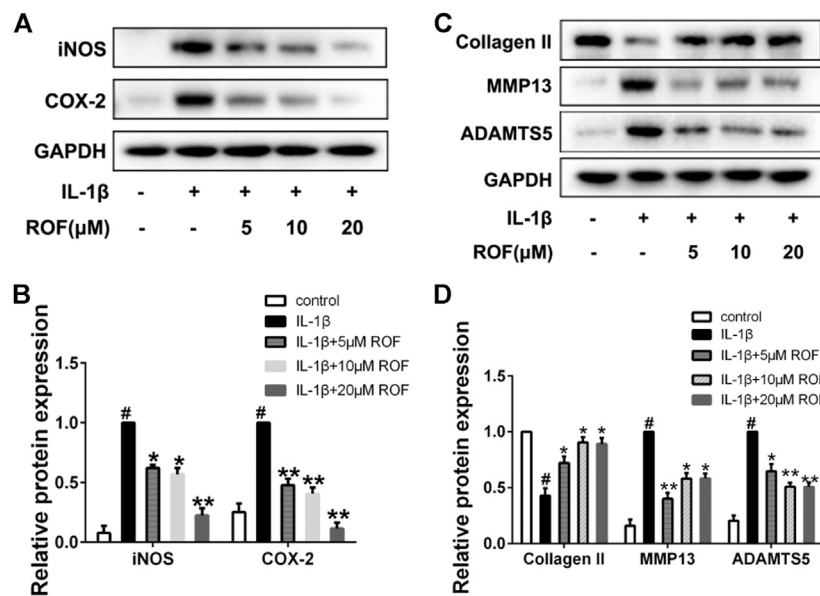


FIGURE 2 | ROF inhibits IL-1 β -induced inflammatory responses and cartilage degradation in chondrocytes. Cells were treated with different concentrations of ROF in the presence or absence of IL-1 β (10 ng/ml) for 24 h. **(A)** Western blots and **(B)** quantitative analysis of iNOS and COX-2. **(C)** Western blots and **(D)** quantitative analysis of collagen II, MMP13, and ADAMTS5. GAPDH was employed as the loading control ($n = 3$). # $p < 0.05$ vs. control group; * $p < 0.05$ and ** $p < 0.01$ vs. IL-1 β group.

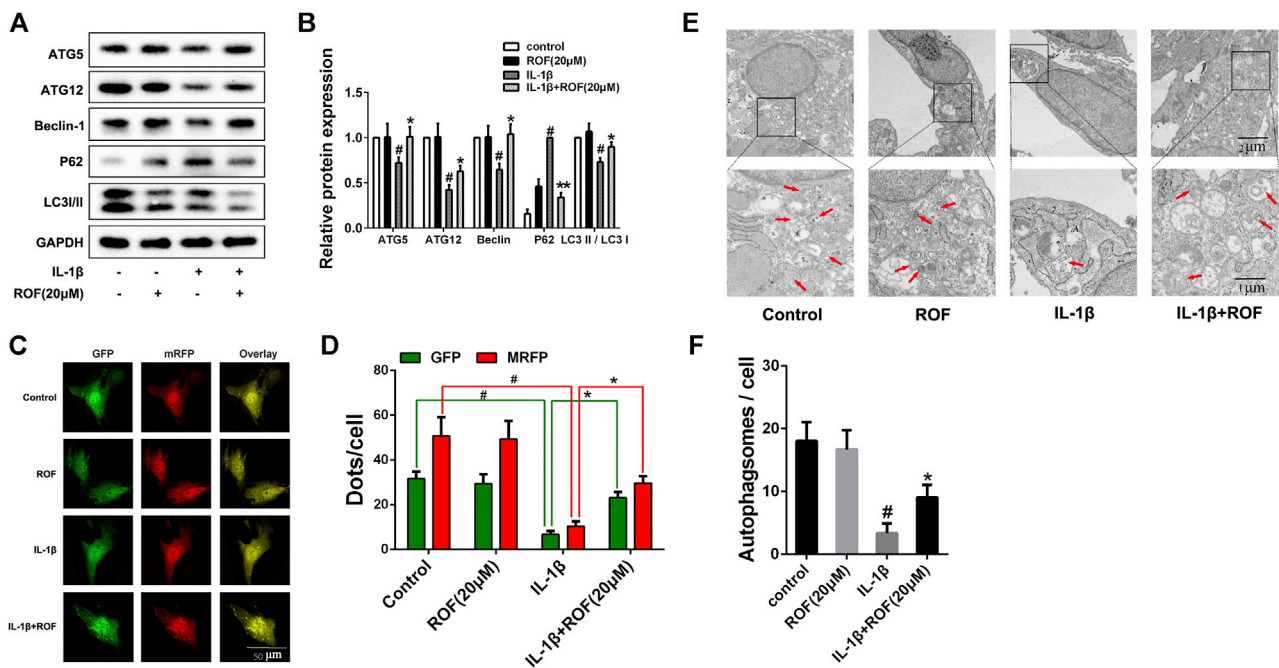


FIGURE 3 | ROF suppresses IL-1 β -induced autophagy downregulation in chondrocytes. **(A)** Western blots and **(B)** quantitative analysis of ATG5, ATG12, Beclin-1, P62-sequestosome and LC3 II/LC3 I in each group. **(C)** Fluorescence microscopy and **(D)** quantitative analysis of cells transfected with tandem GFP-RFP-LC3 adenovirus in each group. **(E)** TEM images and **(F)** quantitative analysis of autophagosomes in each group. Red arrow indicated autophagosome. GAPDH was employed as the internal control ($n = 3$). # $p < 0.05$ vs. control group; * $p < 0.05$ vs. IL-1 β group.

20 μ M ROF, more autophagosomes and autophagolysosomes were observed in chondrocytes. Moreover, transmission electron microscopy (TEM) was used to further observe the

autophagosomes in each group. As shown in **Figures 3E,F**, the ROF treatment could significantly alleviate the IL-1 β -induced autophagosomes decrease in rat chondrocytes.

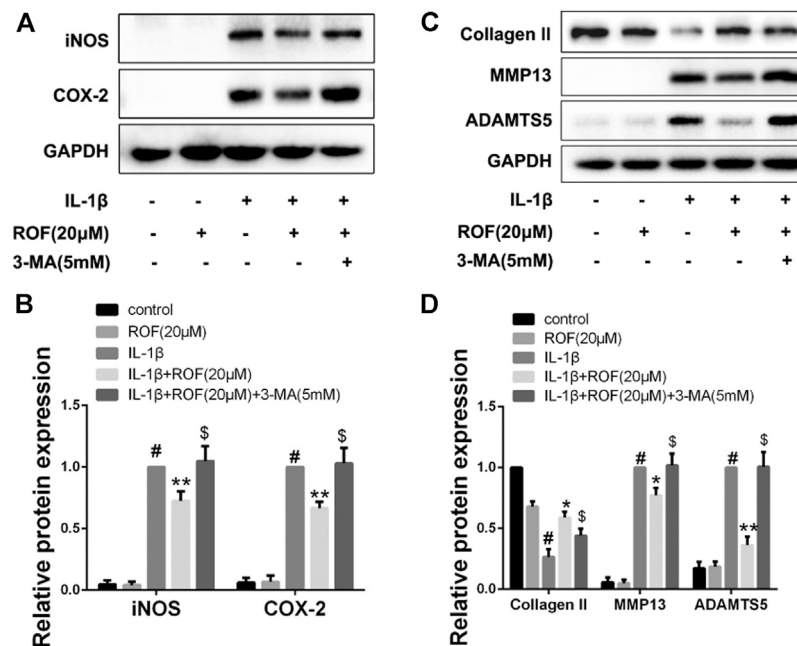


FIGURE 4 | Autophagy inhibitor 3-MA attenuates the anti-inflammatory and anti-cartilage degradation effects of ROF in chondrocytes. **(A)** Western blots and **(B)** quantitative analysis of iNOS and COX-2 in each group. **(C)** Western blots and **(D)** quantitative analysis of collagen II, MMP13, and ADAMTS5 in each group. GAPDH was employed as the internal control ($n = 3$). # $p < 0.05$ vs. control group; * $p < 0.05$ and ** $p < 0.01$ vs. IL-1 β group; \$ $p < 0.05$ vs. IL-1 β + ROF (20 μ M) group.

Methyladenine Reverses the Anti-Inflammatory and Anti-Cartilage Degradation Effects of Rhoifolin in Chondrocytes

To elucidate whether ROF exerts anti-inflammatory and anti-cartilage degradation effects by regulating autophagy, autophagy inhibitor 3-methyladenine (3-MA) was employed. As shown in **Figure 4**, ROF could effectively ameliorate the IL-1 β -induced inflammatory response and cartilage matrix degradation in chondrocytes. However, when 3-MA was added simultaneously, the protective effects of ROF were blocked. The results suggested that ROF may function via promoting autophagy in IL-1 β -treated rat chondrocytes.

Effects of Rhoifolin on Interleukin-1 β -Induced MAPK and PI3K/AKT/mTOR Signal Activation in Chondrocytes

MAPK and PI3K/AKT/mTOR pathways are highly associated with inflammatory reaction and autophagy in OA development. In this study, chondrocytes were first serum-starved overnight and then treated with IL-1 β alone or in combination with 20 μ M ROF for 30 min. As shown in **Figure 5**, ROF could dramatically block the phosphorylations of JNK, P38, PI3K, AKT, and mTOR induced by IL-1 β in chondrocytes.

Effects of Rhoifolin on Rat Osteoarthritis Model

To clarify the effects of ROF on rat OA *in vivo*, we built rat OA models by anterior cruciate ligament transaction and medial

meniscus destabilization. All animals recovered with no infection or complications. ROF was injected into the knee joint weekly postsurgery. H&E and Safranin-O-Fast green staining were employed to access the histomorphology differences among samples from the three groups. As shown in **Figure 6A**, compared with normal structure of cartilage in the sham group, obvious cartilage damage, including surface erosion, disorganized sequence of chondrocytes, and loss of proteoglycan, was observed in the OA group. However, less cartilage lesion was observed in the ROF group. We further compared the OARSI scores in the three groups; results indicated that intra-articular injection of 20 μ M ROF could markedly alleviate the OA progression (**Figure 6B**). In consistent with *in vitro* results, the immunohistochemistry staining showed that ROF could significantly increase collagen II and LC3B and reduce MMP13 expression in rat OA cartilage (**Figures 6C,D**). All data indicated ROF could ameliorate OA progression *in vivo*.

DISCUSSION

Due to unsatisfactory therapeutic strategies available, osteoarthritis undoubtedly brings endless pain to the elderly (Robinson et al., 2016). In recent years, natural plant extract has attracted wide attention in OA therapy for its potential anti-inflammatory properties and mild side effects (Dragos et al., 2017). Rhoifolin (ROF), a flavanone first extracted from *Rhus succedanea*, has showed its anti-inflammatory potential in lipopolysaccharide-induced acute inflammation (Fang et al., 2020), Freund's

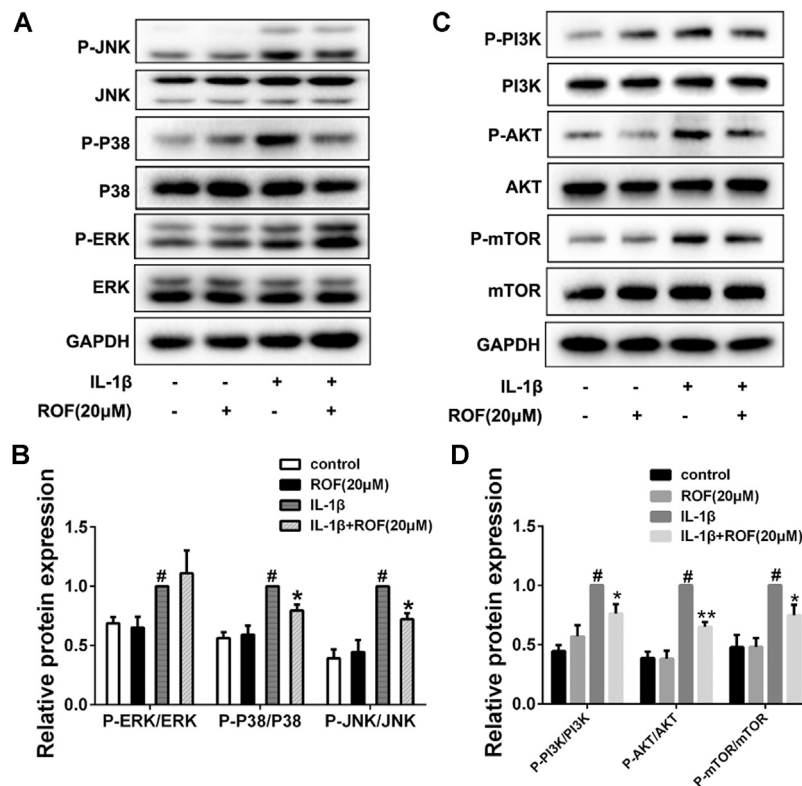


FIGURE 5 | ROF blocks the activation of P38/JNK and PI3K/AKT/mTOR pathways induced by IL-1 β in chondrocytes. Cells were exposed to L-1 β (10 ng/ml) with or without 20 μ M ROF for 30 min as above. **(A)** Western blots and **(B)** quantitative analysis of MAPK pathways in each group. **(C)** Western blots and **(D)** quantitative analysis of PI3K/AKT/mTOR pathways in each group. JNK, P38, ERK, PI3K, AKT, and mTOR were used as loading control ($n = 3$). [#] $p < 0.05$ vs. control group; ^{*} $p < 0.05$ and ^{**} $p < 0.01$ vs. IL-1 β group.

adjuvant-induced rheumatoid arthritis (Peng et al., 2020), and age-related inflammation (Lim et al., 2017). In this study, for the first time, we report the therapeutic effects of ROF in rat OA as well as the underlying mechanisms.

Local inflammatory responses and metabolic dysfunction are essential to the progression of OA. During the OA process, massive proinflammatory cytokines such as IL-1 β and TNF α were secreted in the joint. These proteins can induce excessive production of inflammatory mediators and cartilage matrix-degrading enzymes (Dumond et al., 2004; Murphy and Nagase 2008). Previous study indicated that IL-1 β at the dose of 10 ng/ml shared the maximum effects in rat chondrocytes (Wang, et al., 2018). Therefore, in our study, IL-1 β treatment (10 ng/ml) was employed as a stimulus *in vitro*. We first confirmed ROF could significantly alleviate the IL-1 β -induced upregulation of iNOS and COX-2. Moreover, our data revealed that ROF could reduce the IL-1 β -induced production of MMP13 and ADAMTS5, thus contributing to the elevated level of collagen II in chondrocytes. Taken together, we proved the anti-inflammatory and anti-cartilage degenerative effects of ROF on the IL-1 β -treated rat chondrocytes.

Autophagy is considered as a protective process in normal cartilage (Carames et al., 2010). Enhancement of autophagy can

delay the progression of OA via regulating intracellular metabolic activity (Luo et al., 2019). In our study, reduced levels of autophagy were observed in IL-1 β -treated rat chondrocytes compared to normal ones. However, administration of ROF could partly reverse the IL-1 β -induced autophagy downregulation. To further verify whether ROF exerts anti-inflammatory and anti-cartilage degradation effects via regulating autophagy, we used autophagy inhibitor 3-methyladenine (3-MA). It is interesting to see that ROF lost its protective properties when mixed with 3-MA. These results suggested that ROF ameliorated OA by regulating autophagy.

MAPK and PI3K/AKT/mTOR pathways are crucial to the onset and development of OA (Malemud 2017). Meanwhile, these two pathways are highly related to autophagy process (Yu et al., 2018). Previous study revealed inactivating MAPK signaling resulted in reduced cartilage and subchondral bone damage in OA (Zhou et al., 2019). Besides, inhibition of PI3K/AKT/mTOR promoted the autophagy and attenuated inflammation in OA (Xue et al., 2017). In our results, ROF could dramatically block the IL-1 β -induced phosphorylations of P38/JNK and PI3K/AKT/mTOR pathways, indicating the underlying mechanisms. Since numerous natural compounds had been reported to block the IL-1 β -induced activation of ERK in chondrocytes, it is interesting to see that ERK was not involved in the protective role of ROF in IL-1 β -treated rat chondrocytes.

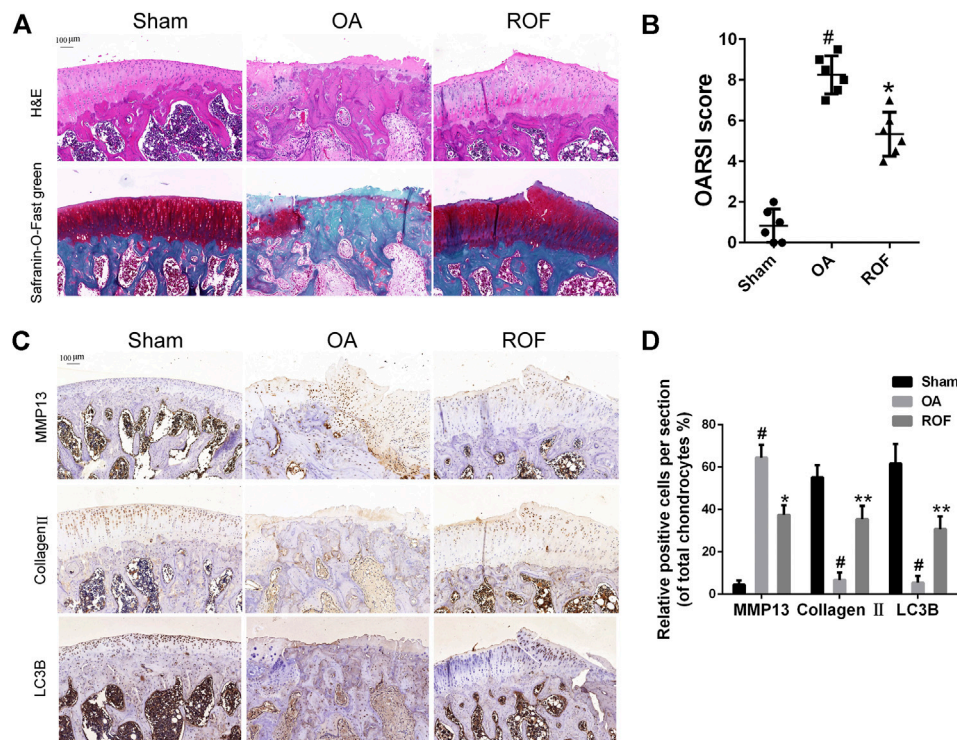


FIGURE 6 | ROF alleviates cartilage damage in the rat OA model. **(A)** H&E and Safranin-O-Fast green staining of cartilage samples from three groups 8 weeks after surgery. **(B)** OARSI scores of three groups. **(C)** Immunohistochemical staining and **(D)** quantitative analysis of MMP13, collagen II, and LC3B in the cartilage samples from three groups. The rate of positively stained chondrocytes in each section was calculated and quantitated from six rats of each group. # $p < 0.05$ vs. sham group; * $p < 0.05$ and ** $p < 0.01$ vs. OA group.

To clarify the therapeutic effects of ROF in OA, the *in vitro* study is far from enough. We next constructed the rat OA model and evaluated the protective properties of ROF *in vivo*. Results from the histological analysis indicated intra-articular injection of ROF could alleviate the cartilage damage. The *in vivo* data further confirmed the protective role of ROF in OA progression. However, the direct target of ROF in OA therapy is still unknown. Furthermore, the most suitable dose of ROF for *in vivo* application remains unclear. Considering the results we have achieved, further work is needed.

CONCLUSION

In summary, we are the first to report the anti-inflammatory, anti-cartilage degradation and autophagy promoting properties of ROF in OA. We further proved ROF functioned by regulating autophagy. Moreover, P38/JNK and PI3K/AKT/mTOR pathways were involved in this process. Our study would contribute to the knowledge of the therapeutic effects of ROF and provide new ideas for future OA treatment.

DATA AVAILABILITY STATEMENT

The raw data supporting the conclusion of this article will be made available by the authors, without undue reservation.

ETHICS STATEMENT

The animal study was reviewed and approved by the Guidelines of Animal Care and Use Committee for Teaching and Research, Tongji Medical College, Huazhong University of Science and Technology. Written informed consent was obtained from the owners for the participation of their animals in this study.

AUTHOR CONTRIBUTIONS

CT worked on conception and design. *In vivo* experiments were conducted by JY, YX conducted the *in vitro* experiments. CT wrote the paper.

FUNDING

This work was financially supported by the National Natural Science Foundation for Young Scientists of China (Grant No. 82001281) to Yifan Xiao and the National Natural Science Foundation of China (Grant No.51537004) to Hua Wu.

REFERENCES

- Appleton, C. T. G., McErlain, D. D., Pitelka, V., Schwartz, N., Bernier, S. M., Henry, J. L., et al. (2007). Forced Mobilization Accelerates Pathogenesis: Characterization of a Preclinical Surgical Model of Osteoarthritis. *Arthritis Res. Ther.* 9 (1), R13. doi:10.1186/ar2120
- Appleton, C. T. (2018). Osteoarthritis Year in Review 2017: Biology. *Osteoarthritis and Cartilage* 26 (3), 296–303. doi:10.1016/j.joca.2017.10.008
- Caramés, B., Taniguchi, N., Otsuki, S., Blanco, F. J., and Lotz, M. (2010). Autophagy Is a Protective Mechanism in normal Cartilage, and its Aging-Related Loss Is Linked with Cell Death and Osteoarthritis. *Arthritis Rheum.* 62 (3), 791–801. doi:10.1002/art.27305
- Dragos, D., Gilca, M., Gaman, L., Vlad, A., Iosif, L., Stoian, I., et al. (2017). Phytomedicine in Joint Disorders. *Nutrients* 9 (1). doi:10.3390/nu9010070
- Dumond, H., Presle, N., Pottier, P., Pacquelet, S., Terlain, B., Netter, P., et al. (2004). Site Specific Changes in Gene Expression and Cartilage Metabolism during Early Experimental Osteoarthritis. *Osteoarthritis and Cartilage* 12 (4), 284–295. doi:10.1016/j.joca.2003.11.008
- Fang, J., Cao, Z., Song, X., Zhang, X., Mai, B., Wen, T., et al. (2020). Rhoifolin Alleviates Inflammation of Acute Inflammation Animal Models and LPS-Induced RAW264.7 Cells via IKK β /NF-K β Signaling Pathway. *Inflammation* 43 (6), 2191–2201. doi:10.1007/s10753-020-01286-x
- Gandhi, G. R., Vasconcelos, A. B. S., Wu, D. T., Li, H. B., Antony, P. J., Li, H., et al. (2020). Citrus Flavonoids as Promising Phytochemicals Targeting Diabetes and Related Complications: A Systematic Review of *In Vitro* and *In Vivo* Studies. *Nutrients* 12 (10). doi:10.3390/nu12102907
- Glyn-Jones, S., Palmer, A. J. R., Agricola, R., Price, A. J., Vincent, T. L., Weinans, H., et al. (2015). Osteoarthritis. *The Lancet* 386 (9991), 376–387. doi:10.1016/s0140-6736(14)60802-3
- He, C., and Klionsky, D. J. (2009). Regulation Mechanisms and Signaling Pathways of Autophagy. *Annu. Rev. Genet.* 43, 67–93. doi:10.1146/annurev-genet-102808-114910
- Kontio, T., Viikari-Juntura, E., and Solovieva, S. (2020). Effect of Osteoarthritis on Work Participation and Loss of Working Life-Years. *J. Rheumatol.* 47 (4), 597–604. doi:10.3899/jrheum.181284
- Li, L., Liu, H., Shi, W., Liu, H., Yang, J., Xu, D., et al. (2017). Insights into the Action Mechanisms of Traditional Chinese Medicine in Osteoarthritis. *Evid. Based Complement. Alternat Med.* 2017, 5190986. doi:10.1155/2017/5190986
- Liao, S., Song, F., Feng, W., Ding, X., Yao, J., Song, H., et al. (2019). Rhoifolin Ameliorates Titanium Particle-stimulated Osteolysis and Attenuates Osteoclastogenesis via RANKL-induced NF- κ B and MAPK Pathways. *J. Cell Physiol.* 234 (10), 17600–17611. doi:10.1002/jcp.28384
- Lim, H., Park, B. K., Shin, S. Y., Kwon, Y. S., and Kim, H. P. (2017). Methyl Caffate and Some Plant Constituents Inhibit Age-Related Inflammation: Effects on Senescence-Associated Secretory Phenotype (SASP) Formation. *Arch. Pharm. Res.* 40 (4), 524–535. doi:10.1007/s12272-017-0909-y
- Luo, P., Gao, F., Niu, D., Sun, X., Song, Q., Guo, C., et al. (2019). The Role of Autophagy in Chondrocyte Metabolism and Osteoarthritis: A Comprehensive Research Review. *Biomed. Res. Int.* 2019, 5171602. doi:10.1155/2019/5171602
- Ma, Y., Tu, C., Liu, W., Xiao, Y., and Wu, H. (2019). Isorhapontigenin Suppresses Interleukin-1 β -Induced Inflammation and Cartilage Matrix Damage in Rat Chondrocytes. *Inflammation* 42 (6), 2278–2285. doi:10.1007/s10753-019-01092-0
- Malemud, C. J. (2017). Negative Regulators of JAK/STAT Signaling in Rheumatoid Arthritis and Osteoarthritis. *Int. J. Mol. Sci.* 18 (3). doi:10.3390/ijms18030484
- Mandl, L. A. (2019). Osteoarthritis Year in Review 2018: Clinical. *Osteoarthritis and Cartilage* 27 (3), 359–364. doi:10.1016/j.joca.2018.11.001
- Murphy, G., and Nagase, H. (2008). Reappraising Metalloproteinases in Rheumatoid Arthritis and Osteoarthritis: Destruction or Repair?. *Nat. Rev. Rheumatol.* 4 (3), 128–135. doi:10.1038/ncprheum0727
- Nelson, A. E. (2018). Osteoarthritis Year in Review 2017: Clinical. *Osteoarthritis and Cartilage* 26 (3), 319–325. doi:10.1016/j.joca.2017.11.014
- Pelletier, J.-P., Martel-Pelletier, J., and Abramson, S. B. (2001). Osteoarthritis, an Inflammatory Disease: Potential Implication for the Selection of New Therapeutic Targets. *Arthritis Rheum.* 44 (6), 1237–1247. doi:10.1002/1529-0131(200106)44:6<1237::aid-art214>3.0.co;2-f
- Peng, S., Hu, C., Liu, X., Lei, L., He, G., Xiong, C., et al. (2020). Rhoifolin Regulates Oxidative Stress and Proinflammatory Cytokine Levels in Freund's Adjuvant-Induced Rheumatoid Arthritis via Inhibition of NF-K β . *Braz. J. Med. Biol. Res.* 53 (6), e9489. doi:10.1590/1414-431x20209489
- Robinson, W. H., Lepus, C. M., Wang, Q., Raghu, H., Mao, R., Lindstrom, T. M., et al. (2016). Low-grade Inflammation as a Key Mediator of the Pathogenesis of Osteoarthritis. *Nat. Rev. Rheumatol.* 12 (10), 580–592. doi:10.1038/nrrheum.2016.136
- Takayama, K., Kawakami, Y., Kobayashi, M., Greco, N., Cummins, J. H., Matsushita, T., et al. (2014). Local Intra-articular Injection of Rapamycin Delays Articular Cartilage Degeneration in a Murine Model of Osteoarthritis. *Arthritis Res. Ther.* 16 (6), 482. doi:10.1186/s13075-014-0482-4
- Tu, C., Huang, X., Xiao, Y., Song, M., Ma, Y., Yan, J., et al. (2019). Schisandrin A Inhibits the IL-1 β -Induced Inflammation and Cartilage Degradation via Suppression of MAPK and NF-kappaB Signal Pathways in Rat Chondrocytes. *Front. Pharmacol.* 10, 41. doi:10.3389/fphar.2019.00041
- Tu, C., Ma, Y., Song, M., Yan, J., Xiao, Y., and Wu, H. (2019). Liquiritigenin Inhibits IL-1 β -induced Inflammation and Cartilage Matrix Degradation in Rat Chondrocytes. *Eur. J. Pharmacol.* 858, 172445. doi:10.1016/j.ejphar.2019.172445
- Wang, F., Liu, J., Chen, X., Zheng, X., Qu, N., Zhang, B., et al. (2019). IL-1 β Receptor Antagonist (IL-1Ra) Combined with Autophagy Inducer (TAT-Beclin1) Is an Effective Alternative for Attenuating Extracellular Matrix Degradation in Rat and Human Osteoarthritis Chondrocytes. *Arthritis Res. Ther.* 21 (1), 171. doi:10.1186/s13075-019-1952-5
- Wang, P., Mao, Z., Pan, Q., Lu, R., Huang, X., Shang, X., et al. (2018). Histone Deacetylase-4 and Histone Deacetylase-8 Regulate Interleukin-1 β -Induced Cartilage Catabolic Degradation through MAPK/JNK and ERK Pathways. *Int. J. Mol. Med.* 41 (4), 2117–2127. doi:10.3892/ijmm.2018.3410
- Xue, J.-F., Shi, Z.-M., Zou, J., and Li, X.-L. (2017). Inhibition of PI3K/AKT/mTOR Signaling Pathway Promotes Autophagy of Articular Chondrocytes and Attenuates Inflammatory Response in Rats with Osteoarthritis. *Biomed. Pharmacother.* 89, 1252–1261. doi:10.1016/j.biopha.2017.01.130
- Yu, L., Chen, Y., and Tooze, S. A. (2018). Autophagy Pathway: Cellular and Molecular Mechanisms. *Autophagy* 14 (2), 207–215. doi:10.1080/15548627.2017.1378838
- Zhou, F., Mei, J., Han, X., Li, H., Yang, S., Wang, M., et al. (2019). Kinsenoside Attenuates Osteoarthritis by Repolarizing Macrophages through Inactivating NF-K β /MAPK Signaling and Protecting Chondrocytes. *Acta Pharmaceutica Sinica B* 9 (5), 973–985. doi:10.1016/j.apsb.2019.01.015

Conflict of Interest: The authors declare that the research was conducted in the absence of any commercial or financial relationships that could be construed as a potential conflict of interest.

Copyright © 2021 Yan, Ni, Sheng, Zhang, Xiao, Ma, Li, Wu and Tu. This is an open-access article distributed under the terms of the Creative Commons Attribution License (CC BY). The use, distribution or reproduction in other forums is permitted, provided the original author(s) and the copyright owner(s) are credited and that the original publication in this journal is cited, in accordance with accepted academic practice. No use, distribution or reproduction is permitted which does not comply with these terms.



The Effect of Chinese Medicine Compound in the Treatment of Rheumatoid Arthritis on the Level of Rheumatoid Factor and Anti-Cyclic Citrullinated Peptide Antibodies: A Systematic Review and Meta-Analysis

Xuan Tang^{1†}, Zehao Liu^{1†}, Zhihua Yang^{1†}, Shengmei Xu¹, Maojie Wang^{1,2,3}, Xiumin Chen^{1,4,5}, Zehuai Wen^{1,3} and Runyue Huang^{1,3,4,5*}

¹The Second Affiliated Hospital of Guangzhou University of Chinese Medicine (Guangdong Provincial Hospital of Chinese Medicine), Guangzhou, China, ²Center for Molecular Medicine, University Medical Center Utrecht, Utrecht, Netherlands, ³Guangdong Provincial Key Laboratory of Clinical Research on Traditional Chinese Medicine Syndrome, Guangzhou, China, ⁴Guangdong-Hong Kong-Macau Joint Lab on Chinese Medicine and Immune Disease Research, Guangzhou University of Chinese Medicine, Guangzhou, China, ⁵State Key Laboratory of Dampness Syndrome of Chinese Medicine, The Second Affiliated Hospital of Guangzhou University of Chinese Medicine, Guangzhou, China

OPEN ACCESS

Edited by:

Yihai Wang,
Guangdong Pharmaceutical
University, China

Reviewed by:

Jianing Zhu,
Zhejiang University, China
Chao Xie,
University of Rochester, United States

*Correspondence:

Runyue Huang
ryhuang@gzucm.edu.cn

[†]These authors have contributed
equally to this work

Specialty section:

This article was submitted to
Ethnopharmacology,
a section of the journal
Frontiers in Pharmacology

Received: 26 March 2021

Accepted: 17 June 2021

Published: 30 June 2021

Citation:

Tang X, Liu Z, Yang Z, Xu S, Wang M,
Chen X, Wen Z and Huang R (2021)
The Effect of Chinese Medicine
Compound in the Treatment of
Rheumatoid Arthritis on the Level of
Rheumatoid Factor and Anti-Cyclic
Citrullinated Peptide Antibodies: A
Systematic Review and Meta-Analysis.
Front. Pharmacol. 12:686360.
doi: 10.3389/fphar.2021.686360

Objectives: To evaluate the current evidence whether Chinese medicine compound (CMC) can reduce the serum levels of rheumatoid factor (RF) and anti-cyclic citrullinated peptide antibodies (anti-CCP).

Methods: We comprehensively searched PubMed, Embase, the Cochrane Library, China National Knowledge Infrastructure (CNKI), the Database for Chinese Technical Periodicals (VIP), and Wanfang data. We then performed a systematic review and meta-analysis of all randomized controlled trials (RCTs) assessing the CMC therapy methods. This study is registered with PROSPERO, number CRD42020216284.

Results: In total, 65 studies were eligible for inclusion, including 6099 patients. The result of the meta-analysis showed that compared with common Western medicine therapy, CMC monotherapy or combined with Western medicine was able to reduce serum RF (SMD = -0.85, 95%CI -1.04 to -0.67) and anti-CCP (SMD = -0.56, 95%CI -0.79 to -0.32) levels to some extent. In the efficacy meta-analysis, a greater number of CMC-treated patients achieved the efficacy criteria after a period of treatment, where the relative risk (RR) was 1.20 [1.08, 1.33] for achieving ACR20, 1.57 [1.38, 1.78] for ACR50, and 2.21 [1.72, 2.84] for ACR70. At the same time, there was a statistically significant difference in the effective rate of the patient's TCM symptoms (RR = 1.22, 95%CI 1.19–1.26).

Conclusions: Through this meta-analysis and systematic review, we found that CMC for the treatment of RA is effective in reducing RF and anti-CCP levels and might have better clinical efficacy than Western medicine monotherapy. Some active components are responsible for this efficacy and worth further exploring.

Keywords: Chinese medicine compound, rheumatoid arthritis, rheumatoid factor, anti-cyclic citrullinated peptide antibodies, meta-analysis

HIGHLIGHTS

1. Through this meta-analysis and systematic review, we found that CMC to treat RA is effective in reducing RF and anti-CCP levels and might have better clinical efficacy than Western medicine monotherapy.
2. Through frequency analysis of the CMC constituent herbs involved in the 65 literatures included in the meta-analysis, we summarized the active ingredients and pharmacological effects of five high-frequency representative Chinese herbs and found that CMC can reduce RF and anti-CCP levels possibly by regulating the immune response and inhibiting B lymphocyte proliferation.
3. CMC may be a potential and efficacious therapeutic adjunct to delay the progression and improve outcomes of RA.

INTRODUCTION

As an incurable autoimmune disease, rheumatoid arthritis (RA) can cause cartilage and bone damages as well as disability, and finally lead to poor quality of life. The average prevalence of RA is estimated at 0.5–1.0% globally (Ngian, 1999). In China, the people suffer from RA with an estimated prevalence of 0.42% (Zeng et al., 2013). Although remission is now an achievable goal for the majority of patients owing to advances in early diagnosis, new drugs and improved treatment strategies, the rate of reaching the standard of domestic RA treatment in China is still low at present. Currently, mainstream therapeutic strategy, i.e. Western medical treatment, including disease-modifying anti-rheumatic drugs (DMARDs), biologic agents, glucocorticoids (GC), which are considered to be effective means to rapidly alleviate and control the progression of RA, but the toxic side effects caused by Western medicine long-term use (Rainsford, 1999; Wang et al., 2018), the non-response of some patients to drugs (He et al., 2019), and the expensive price of biologic agents are the main problems faced by Western medical treatment. Therefore, there is still a considerable unmet need in RA treatment, which has led to an increasing number of patients with RA to seek complementary and integrative medicines.

Traditional Chinese Medicine (TCM), the most common complementary and alternative therapeutic approach for Western medicine, also has a long history in the treatment of RA, whether taken internally or externally, monotherapy or in combination, it has obvious therapeutic effects with few side effects. Chinese medicine compound (CMC) is the main form and means of clinical use of TCM, which concentrates the advantages and characteristics of TCM in the treatment of diseases. Under the guidance of the theoretical system that the concept of holism and treatment based on syndrome differentiation, CMC is formulated as a mixture of different kinds of Chinese herbal medicines, including decoction, granule and Chinese patent medicine, etc. In China, it is quite common that DMARDs are combined with various CMC in the treatment of RA. Modern scholars of TCM have carried out many clinical studies on CMC for the treatment of RA, but the literature reported in these clinical studies is of varying quality and results.

One study (Yao, 2010) showed that the efficacy of the CMC experimental group was better than that of the control group after two months of treatment, and the difference was statistically significant ($p < 0.05$). On the contrary, the results of Chen's randomized controlled trial (Chen et al., 2010) found that the total effective rate in the CMC group was lower than that in the Western medicine group. Especially the efficacy in alleviating pain symptoms was inferior to that of the Western medicine group, and the difference was statistically significant ($p < 0.05$). It is precisely because of the differences in conclusions between studies that we need to conduct a systematic review to objectively evaluate the role and underlying mechanisms of CMC in the treatment of RA.

RF and anti-CCP are serological indicators for the diagnosis of RA. Anti-CCP has higher specificity and sensitivity for RA than RF, which combined detection with RF can compensate for the lack of specificity and sensitivity of RF, and has good diagnostic value for RA (van Venrooij et al., 2008). There are several studies showing that anti-CCP is a sensitive serological indicator of the degree of bone erosion and predict the prognosis of RA patients, thus assisting in the optimal therapeutic management of RA patients (Forslind et al., 2004; Ronnelid et al., 2005; Schoels et al., 2011). So far, no systematic review has been found to describe the efficacy of CMC in reducing RF and CCP levels in RA patients.

The following is a systematic review and meta-analysis of randomized controlled trials (RCTs) of CMC in the treatment of RA, to provide some references for improving RA therapeutic strategy.

METHODS

Literature Search and Strategy

According to the Preferred Reporting Items for Systematic Reviews and Meta-analyses (PRISMA), we searched the PubMed, embase, Cochrane Library, China National Knowledge Infrastructure (CNKI), the database for Chinese Technical Periodicals (VIP) and Wanfang data from the inception dates to September 31, 2020. The keywords used were as follows: Chinese keywords were Chinese pinyin such as “Zhongyi, Zhongyao and Zhongyiyao” (which means “Traditional Chinese Medicine”) and “Leifengshiguanjieyan, Leifengshixingguanjieyan” (which means “rheumatoid arthritis”). while English searches combined subject terms (MeSH) and free words, with a retrieval strategy of “Arthritis, Rheumatoid” or “rheumatoid arthritis” AND “Medicine, Chinese Traditional” or “Chinese medicine” or “herbal medicine” or “Traditional Chinese Medicine”.

Study Selection Criteria

Study Type

We merely included the RCTs that involved CMC to treat RA, regardless of blinding, publication status or language.

Participant Type

Adults (usually over 18 years of age) with a diagnosis of RA either using the 1987 American College of Rheumatology (ACR)

classification criteria (Arnett et al., 1988) for RA, or using the 2010 ACR/European League Against Rheumatism (EULAR) classification criteria (Aletaha et al., 2010) for RA, and regardless of gender, age, the severity of disease, duration of disease, etc.

Intervention Measures

All experimental groups were administered orally with any types of CMC, including CMC monotherapy or combined with Western medicine. The control groups received only oral Western medicine treatment.

Major Research Indicators

Primary Outcomes

The primary outcomes include mean serum RF and anti-CCP levels after CMC treatment.

Secondary Outcomes

The secondary outcomes pertained to the clinical efficacy.

- 1) The efficacy of response of RA to treatment with CMC by the ACR outcome measure ACR20, 50 and 70. The ACR20, 50 and 70 response is defined as at least a 20, 50 and 70% reduction from baseline in the number of both tender and swollen joints and at least a 20, 50 and 70% improvement in three or more of the five remaining ACR core set measures (patient's assessment of pain, level of disability, C-reactive protein level, global assessment of disease by the patient, and global assessment of disease by the physician) (Felson et al., 1995).
- 2) Standard of curative effect of TCM symptoms. Refer to the "Guiding Principles for Clinical Research of New Chinese Medicines": 1) Effective: decrease of integral symptoms scored $\geq 30\%$, some relief of TCM symptoms; 2) Ineffective: integral symptoms score lower $< 30\%$, no relief or even aggravation of TCM symptoms (Zheng, 2002).

Exclusion Criteria

Exclusion criteria included republished literature; the literature whose research topic is complications of RA; animal experiments, reviews, conference papers, incomplete case reports or important data reports with no reply from the corresponding author(s).

Data Selection

Three authors participated in the data extraction of all the studies included in the review. Two authors (Xuan Tang and Zehao Liu) independently extracted the relevant data from the eligible studies. A third author (Zhihua Yang) resolved any divergence still present after discussion. Data extracted from the selected studies included authors' name, publication year, trial design, characteristics of participants, intervention methods, components of CMC, duration of treatment and endpoint evaluation indicators.

Quality Assessment

Assessment of risk of bias was undertaken for each included study using the Cochrane Collaboration's risk of bias assessment tool (Green and Higgins, 2008). Seven sources of bias were assessed: random sequence generation, allocation concealment, blinding of

participants and personnel, blinding of outcome assessment, incomplete outcome data, selective outcome reporting, and other sources of bias. The evaluation criteria of each item were judged as "low risk of bias", "unclear risk of bias" and "high risk of bias".

Statistical Analysis

Extracted data were combined for meta-analysis using R4.0.3 and Stata12.0 software. The dichotomous data was evaluated using the relative risk (RR) and 95% confidence interval (CI), and the continuous data were combined using the standardized mean difference (SMD) and 95% CI. The *I*-squared [*I*(Zeng et al., 2013)] statistic was used to assess the heterogeneity across the included studies, as suggested by literature (Higgins et al., 2003). The analysis was carried out using a fixed-effects model according to if *I*-squared $\leq 50\%$. Instead, a random-effects model was adopted when significant heterogeneity (*I*-squared $> 50\%$) was found. In addition, Egger's test was used to estimate and represent the risk of potential publication bias if the number of included trials reached 10 (Begg and Mazumdar, 1994).

At the same time, we performed descriptive statistics on the frequency of each component of CMC involved in the 65 literature that was finally included in the meta-analysis, in order to explore the high-frequency Chinese medicine for RA treatment and their active ingredients and pharmacological effects, and to find out the potential mechanism that reduces serum RF and anti-CCP levels.

Subgroup Analysis and Investigation of Heterogeneity

Where sufficient studies were available and the data were heterogeneous, we carried out separate meta-analyses for studies according to some factors including intervention duration and intervention measures of the experimental group.

Sensitivity Analysis

We performed a sensitivity analysis to explore heterogeneity and the differences in effect size. After excluding different studies in turn and re-performing the meta-analysis of the remaining studies, we assessed whether the results obtained were significantly different from those before the exclusion so as to assess whether the results of the meta-analysis were robust.

RESULTS

Literature Search Results

According to the retrieval strategy, 1,063 literature was initially detected, including 471 of CNKI. After removal of duplicates via literature management software across databases, 793 studies were screened. Through reading titles and abstracts, 610 literature was excluded because they did not meet the inclusion criteria. And 118 literature was excluded after examination of the full text. Finally, 65 studies that met the inclusion criteria were included in our meta-analysis. **Figure 1** shows the process and consequences of literature screening. The

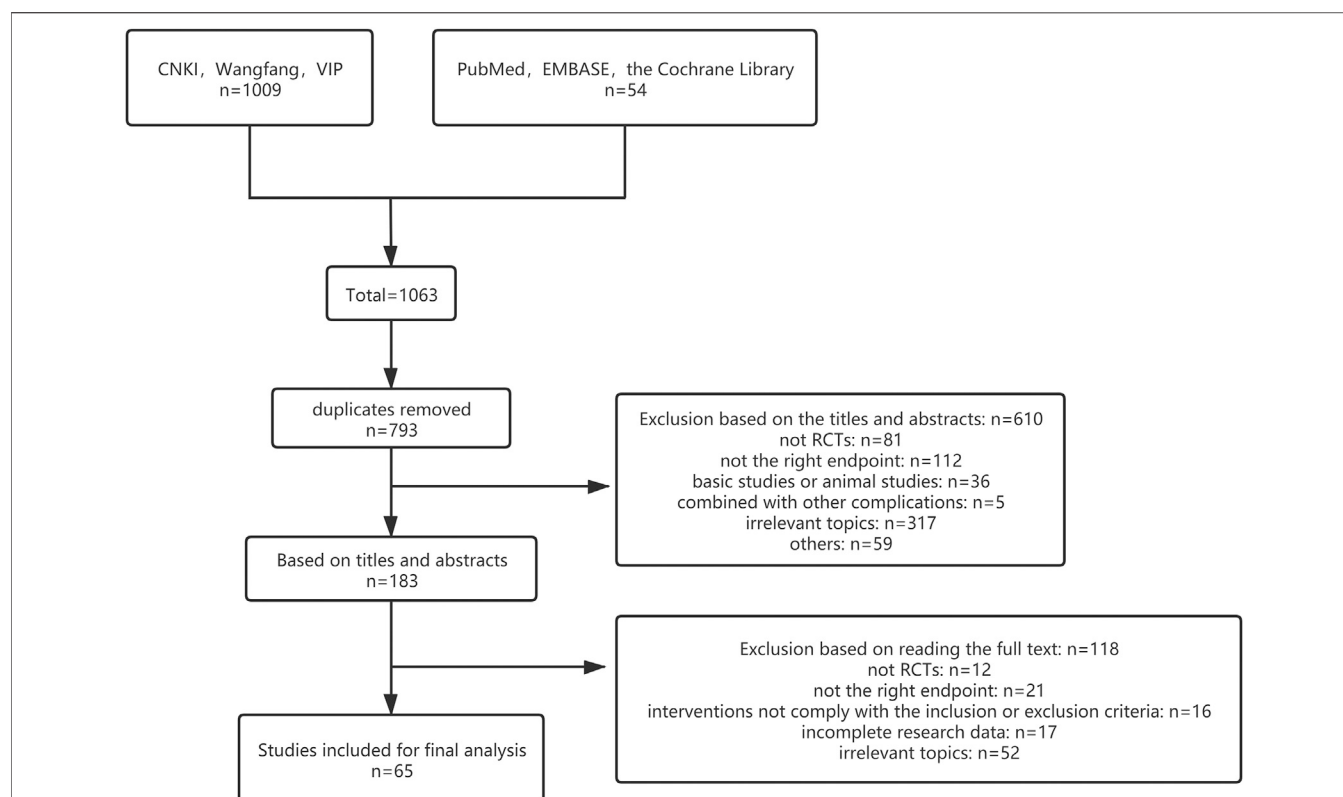


FIGURE 1 | Flow diagram of study selection.

process followed for the selection of eligible studies is described in a flow diagram (Figure 1).

Characteristics of Studies

A total of 65 studies were included in the meta-analysis were conducted in China. These studies, published between 2006 to 2020, included 6,131 patients, 3139 RA patients that received CMC, and 2992 RA patients that received Western medicine monotherapy. In the end, 6,099 patients completed the study. A total of 63 studies (Huang et al., 2006; Li, 2006; Wang et al., 2006; Liu et al., 2007; Luo, 2008; Shen et al., 2008; Li, 2009; Liu et al., 2009; Ma et al., 2009; Xiang et al., 2009; Chen et al., 2010; Yao, 2010; Zhou et al., 2010; Han and Song, 2011; Shen et al., 2011; Yang et al., 2011; Li et al., 2012a; Li, 2013; Liu et al., 2013; Wei et al., 2013; Wei and Liu, 2013; Yang, 2013; Cao and Liu, 2014; He and Xiao, 2014; Niu, 2014; Wang and Tao, 2014; Yu and Chen, 2014; Zhang and Chen, 2014; Li et al., 2015a; Shu et al., 2015; Su et al., 2015; Zhao, 2015; Zheng and Shi, 2015; Chen et al., 2016; Han et al., 2016; Jia et al., 2016; Jiang and Wu, 2016; Liu et al., 2016; Qian et al., 2016; You et al., 2016; Gao and Bu, 2017; Guo et al., 2017; Li et al., 2017; Pang et al., 2017; Wang, 2017; Wang and Tu, 2017; Bian and Wang, 2018; Ge, 2018; Guo et al., 2018; Hu, 2018; Ma et al., 2018; Shi and Yang, 2018; Xu et al., 2018; Zeng and Chen, 2018; Fang et al., 2019; Li et al., 2019; Pang et al., 2019; Song et al., 2019; Yuan et al., 2019; Zhang, 2019; Zhao, 2019; Cao et al., 2020; Jiang and Ma, 2020) and 8 studies (Liu et al., 2009; Chen et al., 2010; Han et al., 2016; Gao and Bu, 2017; Pang

et al., 2017; Bian and Wang, 2018; Pang et al., 2019; Li, 2020) explored RF and anti-CCP levels respectively after treatment. In addition, 14 studies (Chen et al., 2010; Shen et al., 2011; Yang, 2013; Cao and Liu, 2014; He and Xiao, 2014; Wang and Tao, 2014; Zhang and Chen, 2014; Li et al., 2015b; Shu et al., 2015; Zhao, 2015; Jiang and Wu, 2016; Qian et al., 2016; Wang and Tu, 2017; Pang et al., 2019; Cao et al., 2020) researched the efficacy of response of ACR20, 50 and 70. Moreover, 33 studies (Huang et al., 2006; Li, 2006; Luo, 2008; Shen et al., 2008; Liu et al., 2009; Xiang et al., 2009; Yao, 2010; Zhou et al., 2010; Liu et al., 2013; Wei et al., 2013; Wei and Liu, 2013; Yang, 2013; He and Xiao, 2014; Li et al., 2015a; Shu et al., 2015; Zheng and Shi, 2015; Chen et al., 2016; Han et al., 2016; Jiang and Wu, 2016; Liu et al., 2016; You et al., 2016; Guo et al., 2017; Li et al., 2017; Wang and Tu, 2017; Bian and Wang, 2018; Ge, 2018; Guo et al., 2018; Ma et al., 2018; Shi and Yang, 2018; Xu et al., 2018; Li et al., 2019; Song et al., 2019; Yuan et al., 2019) reported the effective rate of TCM symptoms.

The experimental group received oral CMC or CMC combined with Western medicine as intervention measures, while the control group received conventional Western medicine for the treatment of RA as the positive control. Among all the medications included in the study, CMC included decoction, patent medicines (including capsules, tablets, and pills), and powder. Western medicine mainly included DMARDs such as methotrexate (MTX), leflunomide (LEF), sulfasalazine (SSZ), hydroxychloroquine sulfate (HCQ), as

TABLE 1 | Characteristics of the included studies.

Author	Year	Sample size		Disease stage		Age (Y)		Intervention methods		Intervention duration	Outcomes
		EG	CG	EG	CG	EG	CG	EG	CG		
Li, X.	2015	36	36	—	—	37.5 ± 11.9	38.6 ± 12.7	MTX + NSAIDs + CMC	MTX + NSAIDs	12W	①③
Li, Y.	2015	29	30	—	—	49.03 ± 13.8	47.98 ± 12.92	CMC	LEF	12W	①③
Cao, Y. H.	2014	31	31	5.6 ± 3.3Y	5.8 ± 3.1Y	42.2 ± 8.6	41.3 ± 9.0	LEF + NSAIDs + CMC	LEF + NSAIDs	12W	①③
Li, J. H.	2019	40	39	6.64 ± 2.65Y	6.18 ± 2.53Y	59.43 ± 9.69	58.36 ± 9.15	MTX + NSAIDs + CMC	MTX + NSAIDs	12W	①④
Bian, Z. Q.	2018	84	79	6.58 ± 2.24Y	5.89 ± 2.01Y	48.58 ± 14.36	50.66 ± 13.57	NASIDs + CMC	NASIDs	12W	①②③
Yuan, L.	2019	15	15	6–12 M	4–12M	30–50	25–50	MTX + NSAIDs + CMC	MTX + NSAIDs	12W	①④
Yu, M.	2014	32	32	5.8 ± 3.6Y	6.1 ± 3.9Y	38.2 ± 6.8	38.5 ± 7.2	MTX + SSZ + NSAIDs + CMC	MTX + SSZ + NSAIDs	12W	①
Shen, Y. P.	2008	30	10	4.65 ± 2.47Y	4.01 ± 2.55Y	35.32 ± 14.43	34.98 ± 14.67	GC + NSAIDs + CMC	GC + NSAIDs	12W	①④
Niu, J. H.	2014	31	30	0.5–40Y	0.5–42Y	14–68	13–65	MTX + CMC	MTX	14W	①
Zhang, H. J.	2014	30	30	3.6 ± 1.7Y	3.9 ± 2.1Y	36.8 ± 10.3	37.8 ± 10.7	NASIDs + CMC	NASIDs	12W	①③
Xiang, C. C.	2009	40	40	4.5 ± 1.5Y	4.9 ± 1.3Y	50.24 ± 7.25	51.12 ± 6.85	MTX + SSZ + NSAIDs + CMC	MTX + SSZ + NSAIDs	12W	①④
Luo, Y. H.	2008	32	28	1–16Y	1–15Y	60–75	62–74	CMC	MTX + SSZ + NSAIDs	12W	①④
Shi, L.	2018	40	38	7.33 ± 4.67Y	7.45 ± 4.30Y	51.47 ± 8.36	53.24 ± 8.65	NASIDs + CMC	NASIDs	8W	①④
Ge, S.	2018	46	46	4.6 ± 0.7Y	4.5 ± 0.8Y	44.8 ± 4.8	44.5 ± 5.3	MTX + NSAIDs + CMC	MTX + NSAIDs	12W	①④
Liu, Y.	2016	35	30	5.97 ± 2.88Y	6.03 ± 2.70Y	46.89 ± 9.15	45.40 ± 8.63	MTX + LEF + CMC	MTX + LEF	4W	①④
Song, W. H.	2019	66	66	6.68 ± 0.84Y	6.73 ± 0.88M	53.27 ± 6.56	52.89 ± 6.41	MTX + CMC	MTX	12W	①④
Guo, H. M.	2017	340	300	5.3 ± 4.5Y	4.9 ± 4.7M	37.4 ± 8.5	36.5 ± 7.8	CMC + NSAIDs	MTX + NSAIDs	12W	①④
Hu, H.	2018	43	43	23.64 ± 3.05M	24.82 ± 4.08M	43.26 ± 4.82	44.05 ± 4.71	MTX + CMC	MTX	8W	①④
Li, J.P.	2013	40	40	41.52 ± 5.62M	42.82 ± 2.69M	72.38 ± 6.16	72.32 ± 6.38	LEF + CMC	LEF	12W	①
Wang, S. M.	2006	40	20	2.8 ± 1.4Y	2.6 ± 1.3Y	41.4 ± 11.6	40.2 ± 12.9	MTX + SSZ + NSAIDs + CMC	MTX + SSZ + NSAIDs	36W	①
Jiang, D. et al.	2016	44	44	5.5 ± 1.6Y	5.3 ± 1.4Y	47.3 ± 11.2	48.2 ± 10.1	LEF + CMC	LEF	24W	①③④
Fang, X.G. et al.	2019	57	57	3.03 ± 0.36Y	3.02 ± 0.38Y	46.68 ± 7.59	45.59 ± 7.82	LEF + NSAIDs + CMC	LEF + NSAIDs	12W	①
Mang, Z. L. et al.	2018	25	25	11.60 ± 1.16Y	10.80 ± 1.08Y	49.68 ± 2.47	46.88 ± 2.11	MTX + NSAIDs + CMC	MTX + NSAIDs	6W	①④
Zhao, F. C.	2015	55	55	24.15 ± 12.03M	22.35 ± 14.32M	46.32 ± 12.31	48.34 ± 10.65	MTX + GC + CMC	MTX + GC	9W	①③
He, D. C. et al.	2014	30	30	169.38 ± 25.8D	155.47 ± 24.94D	49.69 ± 11.84	50.16 ± 12.14	MTX + LEF + CMC	MTX + LEF	12W	①③④
Ma, W. K. et al.	2009	34	34	4.71 ± 4.64Y	4.42 ± 4.92Y	48.35 ± 13.24	47.74 ± 14.92	MTX + SSZ + NSAIDs + CMC	MTX + SSZ + NSAIDs	24W	①
Jia, F. Y. et al.	2016	62	58	87 ± 50.97M	81.52 ± 56.27M	49.18 ± 11.40	49.10 ± 13.06	LEF + NSAIDs + CMC	LEF + NSAIDs	8W	①④
Li, D.	2020	55	55	4.76 ± 1.56Y	4.21 ± 1.63Y	54.06 ± 8.89	53.56 ± 10.06	MTX + SSZ + NSAIDs + CMC	MTX + SSZ + NSAIDs	12W	②
Jiang, P. et al.	2020	96	90	8.67 ± 3.23Y	8.48 ± 3.40Y	45.41 ± 4.87	45.65 ± 4.90	MTX + SSZ + NSAIDs + CMC	MTX + SSZ + NSAIDs	4W	①
Han, L. et al.	2016	40	36	7.36 ± 6.23Y	7.46 ± 6.35Y	67.53 ± 7.24	68.14 ± 7.72	LEF + GC + CMC	LEF + GC	12W	①②③
Huang, G. D. et al.	2006	47	47	7.8 ± 3.2Y	7.9 ± 3.5Y	38 ± 7	38 ± 7	MTX + D-PEN + CMC	MTX + D-PEN	24W	①④
Zhang, K. L.	2019	82	78	4.3 ± 1.0Y	4.2 ± 1.1Y	54.9 ± 4.9	55.9 ± 5.4	MTX + LEF + CMC	MTX + LEF	4W	①
Li, A. M.	2009	67	67	68 ± 47M	69 ± 43M	50.12 ± 11.67	50.01 ± 12.35	CMC	MTX + NSAIDs	16W	①
Li, J. et al.	2017	47	45	3.2 ± 1.3Y	3.4 ± 1.2Y	51.6 ± 5.8	50.3 ± 6.1	MTX + NSAIDs + CMC	MTX + NSAIDs	12W	①④
Qian, X. et al.	2016	41	41	4.9 ± 1.1Y	4.3 ± 0.8Y	45.7 ± 12.6	46.4 ± 14.2	NASIDs + CMC	NASIDs	12W	①③
Cao, M. Z. et al.	2020	42	38	2.55 ± 0.69Y	2.65 ± 0.72Y	38.67 ± 9.52	39.11 ± 9.37	MTX + CMC	MTX	6W	①③
Yang, Y. J.	2013	60	60	2.1 ± 0.8Y	1.9 ± 0.9Y	32.2 ± 10.6	33.6 ± 10.2	CMC	LEF + NSAIDs + Thymosins	24W	①③
Zhou, C. Y. et al.	2010	50	50	52.74 ± 65.82M	50.37 ± 53.81M	48.03 ± 9.47	49.42 ± 10.16	CMC	MTX	12W	①④
Liu, X. D. et al.	2009	30	30	5.35 ± 2.61Y	4.65 ± 2.42Y	46.55 ± 9.21	47.86 ± 8.30	MTX + SSZ + NSAIDs + CMC	MTX + SSZ + NSAIDs	12W	①②③
Liu, B. et al.	2007	50	50	16M	15M	50	52	MTX + CMC	MTX	16W	①
Wei, Y. et al.	2013	80	80	3.1 ± 1.5Y	4.65 ± 2.42Y	35.1 ± 11.5	36.5 ± 10.1	LEF + SSZ + NSAIDs + CMC	LEF + SSZ + NSAIDs	12W	①④
Zheng, X. B. et al.	2015	30	30	52.3 ± 10.8M	53.6 ± 11.5M	49.6 ± 18.9	49.1 ± 19.4	MTX + CMC	MTX	12W	①④
Shu, C. et al.	2015	22	20	4.57 ± 3.41Y	4.08 ± 2.95Y	45.35 ± 10.42	46.59 ± 10.84	CMC	MTX + LEF	12W	①③④
Wei, W. et al.	2013	45	45	3.5 ± 2.2Y	3.4 ± 2.3Y	68.4 ± 2.5	69.2 ± 2.8	MTX + HCQ + NSAIDs + TNFi + CMC	MTX + HCQ + NSAIDs + TNFi	12W	①④
Han, S. L. et al.	2011	35	35	4.1 ± 1.35Y	3.88 ± 2.12Y	47.22 ± 8.13	46.86 ± 7.20	MTX + SSZ + NSAIDs + CMC	MTX + SSZ + NSAIDs	12W	①
Xu, G. S. et al.	2018	38	38	48.00M	46.50M	50.32 ± 10.99	48.56 ± 14.15	MTX + LEF + NSAIDs + CMC	MTX + LEF + NSAIDs	12W	①④
Pang, A. M. et al.	2017	39	39	7.61 ± 2.13M	6.85 ± 2.91M	41.63 ± 10.72	42.16 ± 9.82	MTX + NSAIDs + CMC	MTX + NSAIDs	12W	①②
Pang, J. et al.	2019	31	31	44.80 ± 27.40M	46.27 ± 28.92M	47.50 ± 13.04	46.13 ± 12.73	MTX + NSAIDs + CMC	MTX + NSAIDs	24W	①②③
Zhao, L.	2019	30	30	118.6 ± 49.6M	117.4 ± 46.5M	52.6 ± 6.8	53.4 ± 6.6	MTX + CMC	MTX	8W	①
Zeng, J. Y. et al.	2018	40	40	-	-	58.62 ± 5.09	58.74 ± 5.16	MTX + HCQ + NSAIDs + CMC	MTX + HCQ + NSAIDs	8W	①
Wang, H. T.	2017	40	40	3 ± 0.35Y	3 ± 0.21Y	42 ± 1.36	40 ± 1.32	CMC	LEF + NSAIDs	4W	①
Su, S. Z. et al.	2015	34	36	6 ± 2.3Y	5 ± 3.1Y	53 ± 1.2	55 ± 0.9	MTX + LEF + NSAIDs + CMC	MTX + LEF + NSAIDs	NR	①
Wang, Y. et al.	2017	52	52	4.7 ± 2.2Y	4.4 ± 2.1Y	45.1 ± 17.2	43.7 ± 14.8	MTX + LEF + CMC	MTX + LEF	12W	①③④
Gao, D. et al.	2017	60	60	7.73 ± 1.48Y	7.43 ± 1.37Y	55.02 ± 7.99	54.26 ± 6.78	MTX + CMC	MTX	12W	①②
Guo, H. L. et al.	2018	40	40	3.95 ± 3.00Y	3.67 ± 2.61Y	39.65 ± 12.99	40.83 ± 10.7	MTX + CMC	MTX	12W	①④
You, B. R. et al.	2016	43	43	2.1 ± 0.8Y	2.3 ± 0.6Y	42.3 ± 5.8	41.7 ± 5.2	MTX + CMC	MTX	24W	①④
Liu, E. C. et al.	2013	50	50	56.37 ± 65.30M	52.26 ± 52.61M	46.23 ± 9.68	49.62 ± 8.62	CMC	MTX	12W	①④
Li, S.W.	2006	31	30	5.17 ± 3.37Y	6.22 ± 4.65Y	49.5	51.7	MTX + SSZ + CMC	MTX + SSZ	8W	①④
Chen, F. et al.	2016	35	35	26.40 ± 6.12M	25.2 ± 4.48M	37.52 ± 6.61	37.34 ± 6.48	MTX + LEF + NSAIDs + CMC	MTX + LEF + NSAIDs	8W	①④
Li, Z. L. et al.	2012	30	31	1.15 ± 0.61Y	1.00 ± 0.60Y	50.40 ± 9.19	57.28 ± 11.39	CMC	Alfacalcidol capsule + caltrate D tablet	12W	①
Yang, B. et al.	2011	20	20	5.3Y	5.1Y	43	41	MTX + NSAIDs + CMC	MTX + NSAIDs	12W	①
Yao, J. H.	2010	58	38	4.08 ± 1.32Y	3.98 ± 1.42Y	36.52 ± 4.85	35.80 ± 4.92	CMC	LEF + NSAIDs + placebo	8W	①④
Shen, H. B. et al.	2011	40	40	32.5 ± 28.0M	38.0 ± 24.3M	49.0 ± 12.6	52.6 ± 10.1	CMC	MTX + NSAIDs	12W	①③
Chen, Z. W. et al.	2010	45	45	47.32 ± 48.32M	52.21 ± 41.31M	45.76 ± 10.21	46.23 ± 12.21	CMC	MTX	24W	①②③
Wang, Z. et al.	2014	47	41	3.8 ± 6.2Y	4.0 ± 6.4Y	42.82 ± 12.45	44.78 ± 12.38	MTX + LEF + CMC	MTX + LEF	12W	①③

EG, experimental group; CG, control group; CMC, Chinese medicine compound; SSZ, Sulfasalazine; MTX, Methotrexate; LEF, leflunomide; GC, glucocorticoid; HCQ, Hydroxychloroquine; NSAIDs, Nona-steroidal anti-inflammatory drugs; D-PEN, D-penicillamine; TNFi, TNF- α inhibitor; NR, Not Reported; W, weeks. ①RF; ②Anti-CCP; ③ACR20/ACR50/ACR70; ④ Standard of curative effect of TCM syndromes.

TABLE 2 | A summary table describing the composition of the CMCs.

Study	Source	Species, concentration	Quality control reported? (Y/N)	Chemical analysis reported? (Y/N)
Li. (2006)	The First Affiliated Hospital of Henan College of Traditional Chinese Medicine	Gentiana macrophylla Pall.[Gentianaceae;Radix Gentianae Macrophyllae], 9 g; Angelica dahurica (Hoffm.) Benth. & Hook.f. ex Franch. & Sav. [Apiaceae;Radix Angelicae Pubescentis], 9 g; Saposhnikovia divaricata (Turcz. ex Ledeb.) Schischk. [Apiaceae;Radix Saposhnikoviae], 6 g; Asarum sieboldii [Aristolochiaceae; Herba cum Radix Asari], 3 g; Conioselinum anthriscoides 'Chuanxiong'[Apiaceae; Rhizoma Ligustici], 9 g; Angelica sinensis (Oliv.) Diels[Apiaceae;Radix Angelicae Sinensis], 12 g; Rehmannia glutinosa (Gaertn.) DC. [Orobanchaceae;Radix Rehmanniae Preparata], 15 g; Paeonia lactiflora Pall.[Paeoniaceae;Radix Paeoniae Alba], 12 g; Neolitsea cassia (L.) Kosterm.[Lauraceae; Ramulus Cinnamomi], 6 g; Poria[Polyporaceae; Sclerotium Poriae Cocos], 12 g; Eucommia ulmoides Oliv. [Eucommiaceae; Cortex Eucommiae], 15 g; Achyranthes bidentata Blume [Amaranthaceae;Radix Achyranthis Bidentatae], 30 g; Codonopsis pilosula[Campanulaceae; Radix Codonopsis], 12 g; Glycyrrhiza glabra[Fabaceae; Radix Glycyrrhizae], 10 g; Astragalus mongholicus Bunge[Fabaceae;Radix Astragali seu Hedysari], 20 g; Dipsacus asper[Caprifoliaceae; Radix Dipsaci], 15 g; Citrus × aurantium L.[Rutaceae;Pericarpium Citri Reticulatae], 9 g; Zingiber officinale[Zingiberaceae; Rhizoma Zingiberis], 9 g	N	N
Huang et al. (2006)	Xiangya Hospital of Central South University & Hengyang Hospital affiliated with Hunan College of Traditional Chinese Medicine	Centipede[Scolopendridae; Scolopendra], 1 g; Pheretima asiatica Michaelsen[Megascolecidae; Lumbricus], 10 g; Agkistrodon[Deinagkistrodon;Bungarus], 1 g; Aconitum carmichaeli Debeaux [Ranunculaceae;Radix Aconiti], 3g(decocted earlier); Linderia aggregata (Sims) Kosterm. [Lauraceae; Radix Linderiae], 3g(decocted earlier); Calamus draco Willd. [Calamus draco Willd.; Sanguis Draconis], 3 g; Arisaema heterophyllum Blume [Araceae; Rhizoma Arisaematis], 5g(decocted earlier); Eupolyphaga [Corydidae;Eupolyphaga Seu Steleophaga], 5 g; Smilax nipponica [Magnoliaceae; Dashenjin], 10 g; Clematis chinensis Osbeck[Ranunculaceae;Radix Clematidis], 10 g; Frankincense[Burseraceae; Olibanum], 10 g; Commiphora myrrha[Burseraceae; Resina Commiphorae], 10 g; Dipsacus asper [Caprifoliaceae; Radix Dipsaci], 10 g; Angelica dahurica (Hoffm.) Benth. & Hook.f. ex Franch. & Sav.[Apiaceae;Radix Angelicae Dahuricae], 10 g; Garden Balsam Stem [Euphorbiaceae; Speranskia tuberculata (Bunge) Baill], 10 g; Angelica sinensis (Oliv.) Diels[Apiaceae;Radix Angelicae Sinensis], 20 g; Conioselinum anthriscoides 'Chuanxiong'[Apiaceae;Rhizoma Ligustici], 20 g; Glycyrrhiza glabra [Fabaceae; Radix Glycyrrhizae], 20 g	Y-Prepared according to Chinese Pharmacopeia 2005	N
Wang et al. (2006)	Shiyan City Hospital of Traditional Chinese Medicine	Rehmannia glutinosa (Gaertn.) DC. [Orobanchaceae;Radix Rehmanniae Preparata], 12 g; Paeonia lactiflora Pall. [Paeoniaceae;Radix Paeoniae Rubra], 10 g; Paeonia lactiflora Pall.[Paeoniaceae;Radix Paeoniae Alba], 10 g; Angelica sinensis (Oliv.) Diels[Apiaceae;Radix Angelicae Sinensis], 15 g; Conioselinum anthriscoides 'Chuanxiong'[Apiaceae;Rhizoma Ligustici], 10 g; Sinomenium acutum [Menispermaceae; Caulis Sinomenii], 15-30 g; Tripterygium wilfordii[Celastraceae; Radix Tripterygii Wilfordii], 10 g; Trachelospermum jasminoides (Lindl.) Lem. [Apocynaceae; Caulis Trachelospermi], 15-30 g; Spatholobus suberectus Dunn[Fabaceae;Caulis Spatholobi], 30 g; Reynoutria multiflora (Thunb.) Moldenke [Polygonaceae; Caulis Polygoni Multiflori], 30 g	N	N
Liu et al. (2007)	The First Affiliated Hospital of Tianjin College of Traditional Chinese Medicine	Angelica sinensis (Oliv.) Diels[Apiaceae;Radix Angelicae Sinensis], 10 g; Conioselinum anthriscoides 'Chuanxiong'[Apiaceae;Rhizoma Ligustici], 8 g; Paeonia lactiflora Pall.[Paeoniaceae;Radix Paeoniae Alba], 10 g; Rehmannia glutinosa (Gaertn.) DC. [Orobanchaceae;Radix Rehmanniae Preparata], 15 g	N	N
Luo et al. (2008)	Hospital attached to Beiliu Health School of Guangxi Autonomous Region	Astragalus mongholicus Bunge[Fabaceae;Radix Astragali seu Hedysari], 30 g; Codonopsis pilosula [Campanulaceae; Radix Codonopsis], 15 g; Atractylodes macrocephala Koidz.[Asteraceae;Rhizoma Atractylodis Macrocephalae], 15 g; Paeonia × suffruticosa [Paeoniaceae;Cortex Moutan Radicis], 15 g; Gentiana macrophylla Pall.[Gentianaceae;Radix Gentianae Macrophyllae], 15 g; Zaocys dhumnades(Cantor)[Natricinae;Zaocys dhumnades], 15 g; Dioscorea oppositifolia[Dioscoreaceae; Rhizoma Dioscoreae], 18 g; Coix lacryma-jobi L.[Poaceae;Semen Coicis], 18 g; Curcuma longa [Zingiberaceae; Rhizoma Curcuma Longae], 12 g; Bombyx mori Linnaeus[Bombyx Linnaeus;Bombyx Batryticatus], 9 g; Carthamus tinctorius[Asteraceae; Flos Carthami], 6 g; Buthus martensii Karsch [Scorpiones;Scorpio], 3 g; Asarum sieboldii[Aristolochiaceae; Herba cum Radix Asari], 3 g	N	N

(Continued on following page)

TABLE 2 | (Continued) A summary table describing the composition of the CMCs.

Study	Source	Species, concentration	Quality control reported? (Y/N)	Chemical analysis reported? (Y/N)
Shen et al. (2008)	Hongmiaopo Hospital, Xi'an, Shaanxi Province	Rehmannia glutinosa[Orobanchaceae; Radix Rehmanniae]; Ophiopogon japonicus (Thunb.) Ker Gawl. [Asparagaceae; Radix Ophiopogonis]; Rehmannia glutinosa (Gaertn.) DC. [Orobanchaceae;Radix Rehmanniae Preparata]; Eucommia ulmoides Oliv. [Eucommiaceae; Cortex Eucommiae]; Achyranthes bidentata Blume [Amaranthaceae;Radix Achyranthes Bidentatae]; Taxillus chinensis (DC.) Danser [Loranthaceae; Herba Taxilli]; Astragalus mongholicus Bunge[Fabaceae;Radix Astragali seu Hedysari]; Pseudostellaria heterophylla (Miq.) Pax [Caryophyllaceae; Radix Pseudostellariae heterophylla]; Angelica sinensis (Oliv.) Diels[Apiaceae;Radix Angelicae Sinensis]; Salvia miltiorrhiza Bunge[Lamiaceae; Radix Salviae Miltiorrhizae]; Polygonatum sibiricum Redouté [Asparagaceae; Rhizoma Polygonati]; Gentiana macrophylla Pall.[Gentianaceae;Radix Gentianae Macrophyllae]; Angelica dahurica (Hoffm.) Benth. & Hook.f. ex Franch. & Sav. [Apiaceae;Radix Angelicae Pubescentis]; Spatholobus suberectus Dunn[Fabaceae;Caulis Spatholobi]; Silkworm shit [Bombycidae; Bombyx mori L.]; Glycyrrhiza glabra[Fabaceae; Radix Glycyrrhizae]	N	N
Xiang et al. (2009)	The First Affiliated Hospital of Guangxi College of Traditional Chinese Medicine	Gentiana macrophylla Pall.[Gentianaceae;Radix Gentianae Macrophyllae], 15 g; Eucommia ulmoides Oliv. [Eucommiaceae; Cortex Eucommiae], 15 g; Dipsacus asper[Caprifoliaceae; Radix Dipsaci], 15 g; Rehmannia glutinosa (Gaertn.) DC. [Orobanchaceae;Radix Rehmanniae Preparata], 15 g; Angelica dahurica (Hoffm.) Benth. & Hook.f. ex Franch. & Sav. [Apiaceae;Radix Angelicae Pubescentis], 15 g; Taxillus chinensis (DC.) Danser[Loranthaceae; Herba Taxilli], 15 g; Reynoutria multiflora (Thunb.) Moldenke[Polygonaceae;Radix Polygoni Multiflori], 15 g; Linderaggregata (Sims) Kosterm. [Lauraceae; Radix Linderaggregatae], 15 g; Pheretima asiatica Michaelson[Megascolecidae;Lumbricus], 10 g; Bombyx mori Linnaeus[Bombyx Linnaeus;Bombyx Batryticatus], 10 g; Neolitsea cassia[Lauraceae; Cortex Cinnamomi], 10 g; Astragalus mongholicus Bunge[Fabaceae;Radix Astragali seu Hedysari], 30 g	N	N
Ma et al. (2009)	The Second Affiliated Hospital of Guiyang College of Traditional Chinese Medicine	Panax notoginseng (Burkill) F.H.Chen[Araliaceae;Radix Notoginseng]; Linderaggregata (Sims) Kosterm. [Lauraceae; Radix Linderaggregatae]; Sinomenium acutum[Menispermaceae; Caulis Sinomenii]; Cibotium barometz (L.) J.Sm.[Cyatheaceae;Rhizoma Cibotii]; Homalomena occulta (Lour.) Schott [Araceae; Rhizoma Homalomenae]; Curcuma longa[Zingiberaceae; Rhizoma Curcuma Longae]; Paeonia lactiflora Pall.[Paeoniaceae;Radix Paeoniae Alba]; etc.	Y-Prepared according to Chinese Pharmacopeia 2005	N
Li et al. (2009)	Qingdao Fifth People's Hospital	Tripterygium wilfordii[Celastraceae; Radix Tripterygii Wilfordii], 15 g; Sinomenium acutum [Menispermaceae; Caulis Sinomenii], 20 g; Lonicera japonica Thunb. [Caprifoliaceae;Caulis Lonicerae], 20 g; Spatholobus suberectus Dunn[Fabaceae;Caulis Spatholobi], 30 g; Morus alba[Moraceae; Ramulus Mori], 30 g; Paeonia lactiflora Pall.[Paeoniaceae;Radix Paeoniae Alba], 30 g; Anemarrhena asphodeloides[Liliaceae; Rhizoma Anemarrhenae], 8 g; Saposhnikovia divaricata (Turcz. ex Ledeb.) Schischk. [Apiaceae;Radix Saposhnikoviae], 12 g; Epimedium sagittatum (Siebold & Zucc.) Maxim. [Berberidaceae;Herba Epimedi], 15 g; Conioselinum anthriscoides 'Chuanxiong'[Apiaceae;Rhizoma Ligustici], 15 g; Pheretima asiatica Michaelson[Megascolecidae;Lumbricus], 12 g; Buthus martensii Karsch[Scorpiones;Scorpio], 10 g; Taxillus chinensis (DC.) Danser[Loranthaceae; Herba Taxilli], 15 g; Angelica sinensis (Oliv.) Diels[Apiaceae;Radix Angelicae Sinensis], 10 g; Rehmannia glutinosa (Gaertn.) DC. [Orobanchaceae;Radix Rehmanniae Preparata], 15 g	N	N
Liu et al. (2009)	Zhejiang Integrated Chinese and Western Medicine Hospital	Saposhnikovia divaricata (Turcz. ex Ledeb.) Schischk. [Apiaceae;Radix Saposhnikoviae]; Angelica dahurica (Hoffm.) Benth. & Hook.f. ex Franch. & Sav.[Apiaceae;Radix Angelicae Dahuricae]; Clematis chinensis Osbeck[Ranunculaceae;Radix Clematidis]; Buthus martensii Karsch[Scorpiones;Scorpio]; Centipede[Scolopendridae; Scolopendra]; Sinapis alba L. [Brassicaceae;Semen sinapis.]; Lonicera japonica Thunb. [Caprifoliaceae;Caulis Lonicerae]; Salvia miltiorrhiza Bunge[Lamiaceae; Radix Salviae Miltiorrhizae]; Coix lacryma-jobi L.[Poaceae;Semen Coicis]; Bombyx mori Linnaeus[Bombyx Linnaeus; Bombyx Batryticatus]; Corydalis yanhusuo[Papaveraceae;Rhizoma Corydalis]; Atractylodes macrocephala Koidz.[Asteraceae;Rhizoma Atractylodis Macrocephalae]	Y-Prepared according to Chinese Pharmacopeia 2005	N
Chen et al. (2010)	Shanghai Hospital of Traditional Chinese Medicine	Hansenia weberbaueriana (Fedde ex H.Wolff) Pimenov & Kljuykov [Apiaceae;Rhizoma et Radix Notopterygii], 30 g; Rehmannia glutinosa[Orobanchaceae; Radix Rehmanniae], 30 g; Astragalus mongholicus Bunge[Fabaceae;Radix Astragali seu Hedysari], 30 g; Aconitum carmichaeli Debeaux [Ranunculaceae;Radix Aconiti], 9 g; Sauromatum giganteum (Engl.) Cusimano [Araceae;Rhizoma Typhonii], 9 g; Caragana sinica (Buc'hoz) Rehde, 30 g; Rumex japonicus Houtt. [Polygonaceae; Radix Rumicis Japonici], 30 g; Sinapis alba L. [Brassicaceae;Semen sinapis.], 12 g; Curcuma longa [Zingiberaceae; Rhizoma Curcuma Longae], 12 g	Y-Prepared according to Chinese Pharmacopeia 2005	N

TABLE 2 | (Continued) A summary table describing the composition of the CMCs.

Study	Source	Species, concentration	Quality control reported? (Y/N)	Chemical analysis reported? (Y/N)
Yao et al. (2010)	Heze Hospital of Traditional Chinese Medicine	Tripterygium wilfordii[Celastraceae; Radix Tripterygii Wilfordii], (decocted earlier)20 g; Sarcandra glabra (Thunb.) Nakai[Chloranthaceae;Herba Sarcandrae], 15 g; Lonicera japonica [Caprifoliaceae;Flos Lonicerae], 24 g; Equus asinus L. [Equidae; Colla Corii Asini], 24 g; Scleromitron diffusum (Willd.) R.J.Wang[Rubiaceae;Herba Hedyotis], 30 g; Phellodendron amurense Rupr. [Rutaceae;Cortex Phellodendri], 12 g; Atractylodes lancea (Thunb.) DC.[Asteraceae;Rhizoma Atractylodis], 9 g; Coix lacryma-jobi L.[Poaceae;Semen Coicis], 30 g; TuPoria[Polyporaceae; Sclerotium Poriae Cocos], 20 g; Bolbostemma paniculatum (Maxim.) Franquet [Cucurbitaceae;Rhizoma Bolbostematis], 12 g; Paeonia lactiflora Pall. [Paeoniaceae;Radix Paeoniae Rubra], 20 g; Hansenia weberbaueriana (Fedde ex H.Wolff) Pimenov & Kijuykov [Apiaceae;Rhizoma et Radix Notopterygii], 9 g; Angelica dahurica (Hoffm.) Benth. & Hook.f. ex Franch. & Sav. [Apiaceae;Radix Angelicae Pubescentis], 9 g	N	N
Zhou et al. (2010)	Xiyuan Hospital, Chinese Academy of Traditional Chinese Medicine	Lonicera japonica [Caprifoliaceae;Flos Lonicerae], 30 g; Angelica sinensis (Oliv.) Diels[Apiaceae;Radix Angelicae Sinensis], 20 g; Scrophularia ningpoensis[Scrophulariaceae; Radix Scrophulariae], 20 g; Glycyrrhiza glabra[Fabaceae; Radix Glycyrrhizae], 10 g; Scleromitron diffusum (Willd.) R.J.Wang [Rubiaceae;Herba Hedyotis], 30 g; Cremastra appendiculata (D.Don) Makino[Orchidaceae; Pseudobulbus Cremastrae seu Pleiones], 9 g; Sigesbeckia orientalis[Asteraceae; Herba Siegesbeckiae], 30 g; Reynoutria japonica Houtt. [Polygonaceae; Rhizoma Polygoni Cuspidati], 15 g; TuPoria [Polyporaceae; Sclerotium Poriae Cocos], 20 g; Paeonia lactiflora Pall.[Paeoniaceae;Radix Paeoniae Alba], 30 g; Clematis chinensis Osbeck[Ranunculaceae;Radix Clematidis], 20 g; Dioscorea colletii var. hypoglauca (Palib.) S.J.Pei & C.T.Ting[Dioscoreaceae;Rhizome Dioscoreae Hypoglaucae], 20 g	N	N
Shen et al. (2011)	the Third Hospital of Beijing University, Beijing Military General Hospital and Wangjing Hospital of China Academy of Chinese Medical Sciences	Erodium stephanianum Willd. [Geraniaceae; Herba Geranii], 15 g; Manis pentadactyla Linnaeus [Manidae; Radix Actinidiae chinensis], 15 g; Sigesbeckia orientalis[Asteraceae; Herba Siegesbeckiae], 15 g; TuPoria[Polyporaceae; Sclerotium Poriae Cocos], 15 g; Reynoutria japonica Houtt. [Polygonaceae; Rhizoma Polygoni Cuspidati], 15 g; Sanguisorba officinalis L. [Rosaceae; Radix Sanguisorbae], 15 g; Xuchangqin g 10 g; Ephedra sinica Stapf [Ephedraceae;Herba Ephedrae], 5 g	N	N
Han and Song (2011)	Hangzhou Xixi Street Community Health Service Center	Clematis chinensis Osbeck[Ranunculaceae;Radix Clematidis], 30 g; Buthus martensii Karsch [Scorpiones;Scorpio], 3 pieces; Centipede[Scolopendridae; Scolopendra], 1 piece; Sinapis alba L. [Brassicaceae;Semen sinapis.], 12 g; Salvia miltiorrhiza Bunge[Lamiaceae; Radix Salviae Miltiorrhizae], 20 g; Coix lacryma-jobi L.[Poaceae;Semen Coicis], 30 g	N	N
Yang et al. (2011)	Institute of Integrated Chinese and Western Medicine, Xiangya Hospital, Central South University	Atractylodes lancea (Thunb.) DC.[Asteraceae;Rhizoma Atractylodis], 12 g; Phellodendron amurense Rupr. [Rutaceae;Cortex Phellodendri], 12 g; Achyranthes bidentata Blume [Amaranthaceae;Radix Achyranthis Bidentatae], 12 g; Coix lacryma-jobi L.[Poaceae;Semen Coicis], 12 g	Y-Prepared according to Chinese Pharmacopeia 2005	N
Li et al. (2012)	Shanghai Guanghua Hospital of Integrative Medicine	Kidney-Yin deficiency syndrome: Rehmannia glutinosa (Gaertn.) DC. [Orobanchaceae;Radix Rehmanniae Preparata], 15 g; Shanyu 12 g; Eucommia ulmoides Oliv. [Eucommiaceae; Cortex Eucommiae], 12 g; Dipsacus asper[Caprifoliaceae; Radix Dipsaci], 10 g; Psoralea fructus[Fabaceae; Fructus Psoralliae], 15 g; Angelica sinensis (Oliv.) Diels[Apiaceae;Radix Angelicae Sinensis], 10 g; Achyranthes bidentata Blume [Amaranthaceae;Radix Achyranthis Bidentatae], 15 g; Pheretima asiatica Michaelsen[Megascolecidae;Lumbricus], 10g. kidney-Yang deficiency syndrome: Aconitum carmichaeli [Ranunculaceae; Radix Aconiti Lateralis Preparata], 10 g; Curculigo orchoides Gaertn.[Hydroxylaceae; Rhizoma Curculigins], 30 g; Gynochthodes officinalis (F.C.How) Razafim. [Rubiaceae; Radix Morindae Officinalis], 15 g; Epimedium sagittatum (Siebold & Zucc.) Maxim. [Berberidaceae;Herba Epimedii], 12 g; Angelica sinensis (Oliv.) Diels[Apiaceae;Radix Angelicae Sinensis], 10 g; Buthus martensii Karsch [Scorpiones;Scorpio], 2 g	N	N
Liu et al. (2013)	Anhui Mengcheng County Hospital of Traditional Chinese Medicine	Strychnos nux-vomica L. [Loganiaceae; Semen Strychni]; Frankincense[Burseraceae; Olibanum] ; Commiphora myrrha[Burseraceae; Resina Commiphorae] ; Glycyrrhiza glabra[Fabaceae; Radix Glycyrrhizae]; etc.	N	N

(Continued on following page)

TABLE 2 | (Continued) A summary table describing the composition of the CMCs.

Study	Source	Species, concentration	Quality control reported? (Y/N)	Chemical analysis reported? (Y/N)
Wei et al. (2013)	Hangzhou Economic and Technological Development Zone Maternal and Child Health Hospital	Lonicera japonica [Caprifoliaceae;Flos Loniceræ], 30 g; Scrophularia ningpoensis [Scrophulariaceae; Radix Scrophulariæ], 20 g; Angelica sinensis (Oliv.) Diels[Apiaceae;Radix Angelicæ Sinensis], 20 g; Glycyrrhiza glabra[Fabaceae; Radix Glycyrrhizæ], 10 g; Chrysanthemum × morifolium (Ramat.) Hemsl.[Asteraceae;Flos Chrysanthemi], 20 g; Phellodendron amurense Rupr. [Rutaceae;Cortex Phellodendri], 12 g; Atractylodes lancea (Thunb.) DC.[Asteraceae;Rhizoma Atractylodis],12 g; TuPoria[Polyporaceae; Sclerotium Poriae Cocos], 20 g; Achyranthes bidentata Blume [Amaranthaceae;Radix Achyranthis Bidentatæ], 12 g; Sinomenium acutum[Menispermaceae; Caulis Sinomenii], 20 g; Zaocys dhumnades(Cantor) [Natricinae;Zaocys dhumnades], 6 g; Pheretima asiatica Michaelsen[Megascolecidae; Lumbricus], 10 g	N	N
Li (2013)	The Second Affiliated Hospital of Tianjin University of Traditional Chinese Medicine	Caragana sinica (Buc'hoz) Rehde, 30 g; Scrophularia ningpoensis[Scrophulariaceae; Radix Scrophulariæ], 25 g; Coix lacryma-jobi L.[Poaceae;Semen Coicis], 25 g; Hansenia weberbaueriana (Fedde ex H.Wolff) Pimenov & Kljuykov [Apiaceae;Rhizoma et Radix Notopterygii], 15 g; Angelica dahurica (Hoffm.) Benth. & Hook.f. ex Franch. & Sav. [Apiaceae;Radix Angelicæ Pubescentis], 15 g; Sinomenium acutum[Menispermaceae; Caulis Sinomenii], 15 g; Paeonia lactiflora Pall. [Paeoniaceae;Radix Paeoniae Rubra], 15 g; Sigesbeckia orientalis[Asteraceae; Herba Siegesbeckiæ],15 g; Atractylodes lancea (Thunb.) DC.[Asteraceae;Rhizoma Atractylodis],15 g; Salvia miltiorrhiza Bunge[Lamiaceae; Radix Salviae Miltiorrhizæ], 10 g; Clematis chinensis Osbeck[Ranunculaceae;Radix Clematidis], 10 g; Bombyx mori Linnaeus[Bombyx Linnaeus;Bombyx Batryticatus], 10 g; Eupolyphaga[Corydidae;Eupolyphaga Seu Steleophaga], 5 g	N	N
Wei et al. (2013)	People's Hospital of Yuyao City, Zhejiang Province	Centipede[Scolopendridae; Scolopendra], 2 pieces; Agkistrodon[Deinagkistrodon;Bungarus], 1 piece; Buthus martensii Karsch[Scorpiones;Scorpio], 10 g; Hansenia weberbaueriana (Fedde ex H.Wolff) Pimenov & Kljuykov [Apiaceae;Rhizoma et Radix Notopterygii], 15 g; Angelica dahurica (Hoffm.) Benth. & Hook.f. ex Franch. & Sav. [Apiaceae;Radix Angelicæ Pubescentis], 15 g; Corydalis yanhusuoi[Papaveraceae;Rhizoma Corydalis], 15 g; Gentiana macrophylla Pall.[Gentianaceae;Radix Gentianæ Macrophyllæ], 15 g; Stephania tetrandra[Menispermaceae; Radix Stephaniae Tetrandrae], 15 g; Poria[Polyporaceae; Sclerotium Poriae Cocos], 20 g; Liquidambar formosana Hance [Altingiaceae; Fructus Liquidambaris], 20 g; Astragalus mongholicus Bunge[Fabaceae;Radix Astragali seu Hedysari], 30 g; Codonopsis pilosula [Campanulaceae; Radix Codonopsis], 30 g; Atractylodes macrocephala Koidz.[Asteraceae; Rhizoma Atractylodis Macrocephalæ], 15 g; Glycyrrhiza glabra[Fabaceae; Radix Glycyrrhizæ], 10 g	N	N
Yang et al. (2013)	The Third Hospital of Baoding City, Hebei Province	Strychnos nux-vomica L. [Loganiaceae; Semen Strychni], 0.2 g; Dioscorea nipponica Makino [Dioscoreaceae;Rhizoma Dioscoreæ Nipponicæ], 8 g; Rhododendron molle (Blume) G.Don [Ericaceae; Rhododendri mollis flos], 0.2 g; Epimedium sagittatum (Siebold & Zucc.) Maxim. [Berberidaceae;Herba Epimedii], 3 g; Paeonia lactiflora Pall.[Paeoniaceae;Radix Paeoniae Alba], 3 g; Wushe 3 g; Dibiechong 3 g; Sarcandra glabra (Thunb.) Nakai[Chloranthaceae;Herba Sarcandrae], 4 g	N	N
Wang Tao (2014)	Zhejiang Integrated Chinese and Western Medicine Hospital	Yangtao Actinidia Root [Actinidiaceae; Actinidia chinensis Planch.], 30 g; Pheretima asiatica Michaelsen[Megascolecidae;Lumbricus], 10 g; Bombyx mori Linnaeus[Bombyx Linnaeus;Bombyx Batryticatus], 10 g; Poria[Polyporaceae; Sclerotium Poriae Cocos], 15 g; Glycyrrhiza glabra [Fabaceae; Radix Glycyrrhizæ], 5 g; Spatholobus suberectus Dunn[Fabaceae;Caulis Spatholobii], 30 g; Angelica sinensis (Oliv.) Diels[Apiaceae;Radix Angelicæ Sinensis], 15 g; Rehmannia glutinosa (Gaertn.) DC. [Orobanchaceae;Radix Rehmanniæ Preparata], 15 g; Coix lacryma-jobi L.[Poaceae; Semen Coicis], 30 g; Astragalus mongholicus Bunge[Fabaceae;Radix Astragali seu Hedysari], 30 g; Paeonia lactiflora Pall. [Paeoniaceae;Radix Paeoniae Rubra], 15 g	Y-Prepared according to <i>Chinese Pharmacopeia 2010</i>	N

(Continued on following page)

TABLE 2 | (Continued) A summary table describing the composition of the CMCs.

Study	Source	Species, concentration	Quality control reported? (Y/N)	Chemical analysis reported? (Y/N)
He Xiao (2014)	Wuhan General Hospital of Guangzhou Military Region	Deerhorn glue[Cervidae;Colla Corni Cervi], 10 g; Aconitum carmichaeli[Ranunculaceae; Radix Aconiti Lateralis Preparata], 10 g; Neolitsea cassia (L.) Kosterm.[Lauraceae;Ramulus Cinnamomi], 10 g; Angelica dahurica (Hoffm.) Benth. & Hook.f. ex Franch. & Sav. [Apiaceae;Radix Angelicae Pubescentis], 10 g; Asarum sieboldii[Aristolochiaceae; Herba cum Radix Asari], 5 g; Angelica sinensis (Oliv.) Diels[Apiaceae;Radix Angelicae Sinensis], 15 g; Clematis chinensis Osbeck[Ranunculaceae; Radix Clematidis], 15 g; Sinomenium acutum[Menispermaceae; Caulis Sinomenii], 20 g; Paeonia lactiflora Pall. [Paeoniaceae;Radix Paeoniae Rubra], 10 g; Paeonia lactiflora Pall.[Paeoniaceae;Radix Paeoniae Alba], 10 g; Pheretima asiatica Michaelsen[Megascolecidae;Lumbricus], 10 g; Coix lacryma-jobi L.[Poaceae;Semen Coicis], 30 g; Rehmannia glutinosa[Orobanchaceae; Radix Rehmanniae], 10 g; Glycyrrhiza glabra[Fabaceae; Radix Glycyrrhizae], 15 g; Centipede [Scolopendridae; Scolopendra], 2 pieces ; Vincetoxicum mukdenense Kitag.[Apocynaceae;Radix Cynanchi Paniculati], 15 g	Y-Prepared according to <i>Chinese Pharmacopeia 2010</i>	N
Zhang et al. (2014)	263 Clinical Department, General Hospital of Beijing Military Region	Angelica dahurica (Hoffm.) Benth. & Hook.f. ex Franch. & Sav. [Apiaceae;Radix Angelicae Pubescentis], 15 g; Clematis chinensis Osbeck[Ranunculaceae;Radix Clematidis], 15 g; Buthus martensii Karsch [Scorpiones;Scorpio], 6 g; Pheretima asiatica Michaelsen[Megascolecidae; Lumbricus], 12 g; Atractylodes lancea (Thunb.) DC.[Asteraceae; Rhizoma Atractylodis], 12 g;Neolitsea cassia (L.) Kosterm.[Lauraceae; Ramulus Cinnamomi], 10 g; Phellodendron amurense Rupr. [Rutaceae; Cortex Phellodendri], 10 g; Zhechong10 g; Wuqiaoshe 10 g; Carthamus tinctorius[Asteraceae; Flos Carthami], 10 g; Achyranthes bidentata Blume [Amaranthaceae; Radix Achyranthis Bidentatae], 15 g; Curcuma longa[Zingiberaceae; Rhizoma Curcuma Longae], 15 g	N	N
Niu (2014)	Xi'an Hospital of Traditional Chinese Medicine	Paeonia lactiflora Pall.[Paeoniaceae;Radix Paeoniae Alba], 20 g; Chaenomeles lagenaria (Loisel.) Koidz. [Rosaceae; Fructus Chaenomelis], 15 g; Pyrola calliantha Andres [Ericaceae; Herba Pyrolae], 15 g; Lycopodium japonicum[Lycopodiaceae; Herba Lycopodii], 15 g; Atractylodes macrocephala Koidz.[Asteraceae;Rhizoma Atractylodis Macrocephalae], 15 g; Neolitsea cassia (L.) Kosterm.[Lauraceae;Ramulus Cinnamomi], 12 g; Gentiana macrophylla Pall.[Gentianaceae;Radix Gentianae Macrophyllae], 12 g; Piper kadsura[Piperaceae; Caulis Piperis Kadsurae], 12 g; Aconitum carmichaeli Debeaux [Ranunculaceae;Radix Aconiti], 10 g; Saposhnikovia divaricata (Turcz. ex Ledeb.) Schischk. [Apiaceae;Radix Saposhnikoviae], 10 g; Angelica sinensis (Oliv.) Diels[Apiaceae;Radix Angelicae Sinensis], 10 g; Achyranthes bidentata Blume [Amaranthaceae;Radix Achyranthis Bidentatae], 10 g; Frankincense[Burseraceae; Olibanum], 10 g; Cremastra appendiculata (D.Don) Makino [Orchidaceae;Pseudobulbus Cremastrae seu Pleiones], 10 g; Glycyrrhiza glabra[Fabaceae; Radix Glycyrrhizae], 6 g; Ephedra sinica Stapf [Ephedraceae;Herba Ephedrae], 4 g	N	N
Cao et al. (2014)	Anhui Provincial Hospital of Traditional Chinese Medicine	Compound QiYi Capsule: Coix lacryma-jobi L.[Poaceae;Semen Coicis] ; Astragalus mongholicus Bunge [Fabaceae;Radix Astragali seu Hedysari] ; Centipede[Scolopendridae; Scolopendra] ; Tripterygium wilfordii[Celastraceae; Radix Tripterygii Wilfordii]; Astragalus mongholicus Bunge[Fabaceae;Radix Astragali seu Hedysari],n Qingre Chubi Capsules: Astragalus mongholicus Bunge[Fabaceae;Radix Astragali seu Hedysari],n ; Gardenia jasminoides J.Ellis[Rubiaceae;Fructus Gardeniae] ; Prunus persica (L.) Batsch[Rosaceae;Semen Persicae] ; Clematis chinensis Osbeck[Ranunculaceae;Radix Clematidis]; etc.	Y-Prepared according to <i>Chinese Pharmacopeia 2010</i>	N
Yu and Chen (2014)	Guangxi Yongfu County People's Hospital	Coix lacryma-jobi L.[Poaceae;Semen Coicis], 20 g; Atractylodes lancea (Thunb.) DC.[Asteraceae; Rhizoma Atractylodis], 12 g; Glycyrrhiza glabra[Fabaceae; Radix Glycyrrhizae], 6 g; Hansenia weberbaueriana (Fedde ex H.Wolff) Pimenov & Kjiuykov [Apiaceae;Rhizoma et Radix Notopterygii], 10 g; Angelica dahurica (Hoffm.) Benth. & Hook.f. ex Franch. & Sav. [Apiaceae;Radix Angelicae Pubescentis], 10 g; Saposhnikovia divaricata (Turcz. ex Ledeb.) Schischk. [Apiaceae;Radix Saposhnikoviae], 10 g; Ephedra sinica Stapf [Ephedraceae;Herba Ephedrae], 6 g; Neolitsea cassia (L.) Kosterm.[Lauraceae; Ramulus Cinnamomi], 10 g; Aconitum carmichaeli Debeaux [Ranunculaceae;Radix Aconiti], 10 g; Angelica sinensis (Oliv.) Diels[Apiaceae;Radix Angelicae Sinensis], 8 g; Conioselinum anthriscoides 'Chuanxiong'[Apiaceae;Rhizoma Ligustici], 8 g	N	N

(Continued on following page)

TABLE 2 | (Continued) A summary table describing the composition of the CMCs.

Study	Source	Species, concentration	Quality control reported? (Y/N)	Chemical analysis reported? (Y/N)
Su et al. (2015)	Dongguan City Hospital of Traditional Chinese Medicine	Angelica dahurica (Hoffm.) Benth. & Hook.f. ex Franch. & Sav. [Apiaceae; Radix Angelicae Pubescentis], 20 g; Taxillus chinensis (DC.) Danser [Loranthaceae; Herba Taxilli], 30 g; Eucommia ulmoides Oliv. [Eucommiaceae; Cortex Eucommiae], 15 g; Asarum sieboldii [Aristolochiaceae; Herba cum Radix Asari], 3 g; Angelica sinensis (Oliv.) Diels [Apiaceae; Radix Angelicae Sinensis], 10 g; Paeonia lactiflora Pall. [Paeoniaceae; Radix Paeoniae Alba], 20 g; Glycyrrhiza glabra [Fabaceae; Radix Glycyrrhizae], 6 g; Rehmannia glutinosa (Gaertn.) DC. [Orobanchaceae; Radix Rehmanniae Preparata], 15 g; Conioselinum anthriscoides 'Chuanxiong' [Apiaceae; Rhizoma Ligustici], 15 g; Neolitsea cassia (L.) Kosterm. [Lauraceae; Ramulus Cinnamomi], 15 g; Codonopsis pilosula [Campanulaceae; Radix Codonopsis], 15 g; Gleditsia sinensis Lam. [Fabaceae; Spina Gleditsiae], 12 g; Quanchong 5 g; Centipede [Scolopendridae; Scolopendra], 2 pieces; Spatholobus suberectus Dunn [Fabaceae; Caulis Spatholobi], 30 g	N	N
Shu et al. (2015)	Tongling Hospital of Traditional Chinese Medicine	Sophora flavescens Aiton [Fabaceae; Radix Sophorae Flavescentis], 9 g; Sinomenium acutum [Menispermaceae; Caulis Sinomenii], 9 g; Phellodendron amurense Rupr. [Rutaceae; Cortex Phellodendri], 9 g; Dioscorea colletii var. hypoglauca (Palib.) S.J. Pei & C.T. Ting [Dioscoreaceae; Rhizome Dioscoreae Hypoglaucae], 10 g; Astragalus mongholicus Bunge [Fabaceae; Radix Astragali seu Hedysari], 30 g; Angelica sinensis (Oliv.) Diels [Apiaceae; Radix Angelicae Sinensis], 15 g; Sargentodoxa cuneata (Oliv.) Rehder [Lardizabalaceae; Caulis Sargentodoxae], 15 g; Spatholobus suberectus Dunn [Fabaceae; Caulis Spatholobi], 15 g; Tripterygium wilfordii [Celastraceae; Radix Tripterygii Wilfordii], (decocted earlier) 10 g; Equus asinus L. [Equidae; Colla Corii Asini], 25 g; Citrus x aurantium L. [Rutaceae; Pericarpium Citri Reticulatae], 9 g; Taxillus chinensis (DC.) Danser [Loranthaceae; Herba Taxilli], 15 g; Centipede [Scolopendridae; Scolopendra], 1 piece; Zaocys dhumnades (Cantor) [Natricinae; Zaocys dhumnades], 10 g	N	N
Li et al. (2015)	Yiji Mountain Hospital of Wannan Medical College	Astragalus mongholicus Bunge [Fabaceae; Radix Astragali seu Hedysari], 30 g; Equus asinus L. [Equidae; Colla Corii Asini], 20 g; Angelica sinensis (Oliv.) Diels [Apiaceae; Radix Angelicae Sinensis], 15 g; Sargentodoxa cuneata (Oliv.) Rehder [Lardizabalaceae; Caulis Sargentodoxae], 15 g; Spatholobus suberectus Dunn [Fabaceae; Caulis Spatholobi], 15 g; Cuscuta chinensis Lam. [Convolvulaceae; Semen Cuscutae], 12 g; Dioscorea colletii var. hypoglauca (Palib.) S.J. Pei & C.T. Ting [Dioscoreaceae; Rhizome Dioscoreae Hypoglaucae], 12 g; Epimedium sagittatum (Siebold & Zucc.) Maxim. [Berberidaceae; Herba Epimedi], 12 g; Sinomenium acutum [Menispermaceae; Caulis Sinomenii], 9 g; Pinellia ternata (Thunb.) Makino [Araceae; Rhizoma Pinelliae], 9 g; Sophora flavescens Aiton [Fabaceae; Radix Sophorae Flavescentis], 9 g; Phellodendron amurense Rupr. [Rutaceae; Cortex Phellodendri], 9 g	N	N
Zhao (2015)	Shandong Provincial Hospital of Traditional Chinese Medicine	Saposhnikovia divaricata (Turcz. ex Ledeb.) Schischk. [Apiaceae; Radix Saposhnikoviae], 30 g; Gypsum [Mineral; Gypsum Fibrosum], 30 g; Gardenia jasminoides J. Ellis [Rubiaceae; Fructus Gardeniae], 30 g; Astragalus mongholicus Bunge [Fabaceae; Radix Astragali seu Hedysari], 30 g; Citrus x aurantium L. [Rutaceae; Pericarpium Citri Reticulatae], 30 g; Atractylodes macrocephala Koidz. [Asteraceae; Rhizoma Atractylodis Macrocephalae], 25 g; Pogostemon cablin (Blanco) Benth. [Lamiaceae; Pogostemon Cablin (Blanco) Benth.], 15 g; Actaea cimicifuga L. [Ranunculaceae; Rhizoma Cimicifugae], 15 g; Bupleurum falcatum L. [Apiaceae; Radix Bupleuri], 15 g; Codonopsis pilosula [Campanulaceae; Radix Codonopsis], 25 g; Angelica sinensis (Oliv.) Diels [Apiaceae; Radix Angelicae Sinensis], 20 g; Glycyrrhiza glabra [Fabaceae; Radix Glycyrrhizae], 10 g	N	N
Li et al. (2015)	Fuyang People's Hospital, Anhui Province	Atractylodes lancea (Thunb.) DC. [Asteraceae; Rhizoma Atractylodis], 10 g; Phellodendron amurense Rupr. [Rutaceae; Cortex Phellodendri], 10 g; Stephania tetrandra [Menispermaceae; Radix Stephaniae Tetrandrae], 10 g; Conioselinum anthriscoides 'Chuanxiong' [Apiaceae; Rhizoma Ligustici], 10 g; Hansenia weberbaueriana (Fedde ex H. Wolff) Pimenov & Kljuykov [Apiaceae; Rhizoma et Radix Notopterygii], 10 g; Angelica dahurica (Hoffm.) Benth. & Hook.f. ex Franch. & Sav. [Apiaceae; Radix Angelicae Dahuricae], 6 g; Clematis chinensis Osbeck [Ranunculaceae; Radix Clematidis], 10 g; Neolitsea cassia (L.) Kosterm. [Lauraceae; Ramulus Cinnamomi], 5 g; Sinapis alba L. [Brassicaceae; Semen sinapis.], 10 g; Prunus persica (L.) Batsch [Rosaceae; Semen Persicae], 10 g; Carthamus tinctorius [Asteraceae; Flos Carthami], 10 g; Zaocys dhumnades (Cantor) [Natricinae; Zaocys dhumnades], 10 g; Sigesbeckia orientalis [Asteraceae; Herba Siegesbeckiae], 30 g; Medicated leaven [Massa Medicata Fermentata], 10 g	N	N

(Continued on following page)

TABLE 2 | (Continued) A summary table describing the composition of the CMCs.

Study	Source	Species, concentration	Quality control reported? (Y/N)	Chemical analysis reported? (Y/N)
Zheng and Shi (2015)	Jiangxi Guangfeng County People's Hospital	Aconitum carmichaeli Debeaux [Ranunculaceae;Radix Aconiti]; Aconitum kusnezoffii Rchb.[Ranunculaceae;Radix Aconiti Kusnezoffii]; Cyperus rotundus L. [Cyperaceae; Rhizoma Cyperi]; Conioselinum anthriscoides 'Chuanxiong'[Apiaceae;Rhizoma Ligustici]; Ephedra sinica Stapf [Ephedraceae;Herba Ephedrae];,Angelica sinensis (Oliv.) Diels[Apiaceae;Radix Angelicae Sinensis]; Arisaema heterophyllum Blume [Araceae; Rhizoma Arisaematis];Angelica dahurica (Hoffm.) Benth. & Hook.f. ex Franch. & Sav.[Apiaceae;Radix Angelicae Dahuricae];Commiphora myrrha[Burseraceae; Resina Commiphorae];Frankincense[Burseraceae; Olibanum];Pheretima asiatica Michaelsen [Megascolecidae; Lumbricus]	N	N
Qian et al. (2016)	The First Affiliated Hospital of Nanjing University of Chinese Medicine	Angelica dahurica (Hoffm.) Benth. & Hook.f. ex Franch. & Sav. [Apiaceae;Radix Angelicae Pubescentis], 10 g; Eucommia ulmoides Oliv. [Eucommiaceae; Cortex Eucommiae], 15 g; Achyranthes bidentata Blume [Amaranthaceae;Radix Achyranthis Bidentatae], 10 g; Asarum sieboldii[Aristolochiaceae; Herba cum Radix Asari], 6 g; Panax ginseng C.A.Mey.[Araliaceae;Radix Ginseng], 10 g; Taxillus chinensis (DC.) Danser[Loranthaceae; Herba Taxilli], 20 g; Saposhnikovia divaricata (Turcz. ex Ledeb.) Schischk. [Apiaceae;Radix Saposhnikoviae], 10 g; Neolitsea cassia[Lauraceae; Cortex Cinnamomi], 10 g; Angelica sinensis (Oliv.) Diels[Apiaceae;Radix Angelicae Sinensis], 10 g; Gentiana macrophylla Pall.[Gentianaceae; Radix Gentianae Macrophyllae], 10 g; Conioselinum anthriscoides 'Chuanxiong'[Apiaceae;Rhizoma Ligustici], 10 g; Glycyrrhiza glabra[Fabaceae; Radix Glycyrrhizae], 6 g; Paeonia lactiflora Pall.[Paeoniaceae; Radix Paeoniae Alba], 10 g	N	N
Jia et al. (2016)	Linfen Fourth People's Hospital	Astragalus mongholicus Bunge[Fabaceae;Radix Astragali seu Hedysari], 30 g; Angelica sinensis (Oliv.) Diels[Apiaceae;Radix Angelicae Sinensis], 20 g; Conioselinum anthriscoides 'Chuanxiong'[Apiaceae; Rhizoma Ligustici], 15 g; Shudi 15 g; Saposhnikovia divaricata (Turcz. ex Ledeb.) Schischk. [Apiaceae; Radix Saposhnikoviae], 15 g; Hanseria weberbaueriana (Fedde ex H.Wolff) Pimenov & Kljuykov [Apiaceae;Rhizoma et Radix Notopterygii], 10 g; Angelica dahurica (Hoffm.) Benth. & Hook.f. ex Franch. & Sav. [Apiaceae;Radix Angelicae Pubescentis], 10 g; Neolitsea cassia (L.) Kosterm.[Lauraceae;Ramulus Cinnamomi], 15 g; Cucumis melo L. [Cucurbitaceae; Retinervus Luffae Fructus], 15 g; Gentiana macrophylla Pall.[Gentianaceae;Radix Gentianae Macrophyllae], 15 g; Piper kadsura[Piperaceae; Caulis Piperis Kadsurae], 12 g; Trachelospermum jasminoides (Lindl.) Lem. [Apocynaceae; Caulis Trachelospermi], 20 g; Uncaria rhynchophylla (Miq.) Miq. [Rubiaceae; Ramulus Uncariae Cum Uncis], 20 g; Spatholobus suberectus Dunn[Fabaceae;Caulis Spatholobi], 30 g; Paeonia lactiflora Pall.[Paeoniaceae;Radix Paeoniae Alba], 30 g; Paeonia lactiflora Pall. [Paeoniaceae;Radix Paeoniae Rubra], 15 g;Epimedium sagittatum (Siebold & Zucc.) Maxim. [Berberidaceae;Herba Epimedio], 15 g; Taxillus chinensis (DC.) Danser[Loranthaceae; Herba Taxilli], 12 g; Pheretima asiatica Michaelsen [Megascolecidae;Lumbricus], 12 g; Buthus martensii Karsch[Scorpiones;Scorpio], 10 g; Curcuma longa [Zingiberaceae; Rhizoma Curcuma Longae], 10 g; Coix lacryma-jobi L.[Poaceae;Semen Coicis],10 g; Glycyrrhiza glabra[Fabaceae; Radix Glycyrrhizae], 10 g	N	N
You et al. (2016)	The Fifth Affiliated Hospital of Xinjiang Medical University	Rehmannia glutinosa (Gaertn.) DC. [Orobanchaceae;Radix Rehmanniae Preparata], 15 g; Astragalus mongholicus Bunge[Fabaceae;Radix Astragali seu Hedysari],n 15 g; Shanyu 12 g; Paeonia x suffruticosa [Paeoniaceae;Cortex Moutan Radicis], 12 g; Poria[Polyporaceae; Sclerotium Poriae Cocos], 12 g; Coptis chinensis Franch.[Ranunculaceae;Rhizoma Coptidis], 12 g; Dioscorea oppositifolia[Dioscoreaceae; Rhizoma Dioscoreae], 10 g; Chrysanthemum x morifolium (Ram.) Hemsl.[Asteraceae;Flos Chrysanthemi], 10 g; Alisma plantago-aquatica subsp. orientale (Sam.) Sam.[Alismataceae;Rhizoma Alismatis], 10 g; Angelica sinensis (Oliv.) Diels[Apiaceae;Radix Angelicae Sinensis], 10 g	N	N
Han et al. (2016)	Xinjiang Uyghur Autonomous Region Hospital of Traditional Chinese Medicine	Zaocys dhumnades(Cantor)[Natricinae;Zaocys dhumnades], 12 g; Taxillus chinensis (DC.) Danser [Loranthaceae; Herba Taxilli], 20 g; Buthus martensii Karsch[Scorpiones;Scorpio], 6 g; Lonicera japonica Thunb. [Caprifoliaceae;Caulis Lonicerae], 30 g; Coix lacryma-jobi L.[Poaceae;Semen Coicis], 30 g; Atractylodes lancea (Thunb.) DC.[Asteraceae;Rhizoma Atractylodis],12 g; Astragalus mongholicus Bunge[Fabaceae;Radix Astragali seu Hedysari], 30 g; Saposhnikovia divaricata (Turcz. ex Ledeb.) Schischk. [Apiaceae;Radix Saposhnikoviae], 12 g; Conioselinum anthriscoides 'Chuanxiong'[Apiaceae; Rhizoma Ligustici], 12 g; Epimedium sagittatum (Siebold & Zucc.) Maxim. [Berberidaceae;Herba Epimedio], 10 g; Rehmannia glutinosa (Gaertn.) DC. [Orobanchaceae;Radix Rehmanniae Preparata], 10 g; Psoralea fructus[Fabaceae; Fructus Psoraliae], 10 g	N	N

TABLE 2 | (Continued) A summary table describing the composition of the CMCs.

Study	Source	Species, concentration	Quality control reported? (Y/N)	Chemical analysis reported? (Y/N)
Liu et al. (2016)	Henan Provincial Chinese Medicine Hospital, Zhengzhou Henan, China	Forsythia suspensa (Thunb.) Vahl [Oleaceae; Fructus Forsythiae], 10 g; Phellodendron amurense Rupr. [Rutaceae; Cortex Phellodendri], 10 g; Paeonia lactiflora Pall. [Paeoniaceae; Radix Paeoniae Alba], 10 g; Stephanian tetrandra [Menispermaceae; Radix Stephaniae Tetrandrae], 15 g; Coix lacryma-jobi L. [Poaceae; Semen Coicis], 15 g; Grona styracifolia (Osbeck) H. Ohashi & K. Ohashi [Fabaceae; Herba Lysimachiae], 10 g; Lonicera japonica [Caprifoliaceae; Flos Lonicerae], 10 g; Clematis chinensis Osbeck [Ranunculaceae; Radix Clematidis], 15 g; Viola philippica Cav. [Violaceae; Herba Viola], 10 g; Agkistrodon [Deinagkistrodon; Bungarus], 10 g; Patrinia scabiosifolia Link [Caprifoliaceae; Herba Patriniae], 10 g; Saposhnikovia divaricata (Turcz. ex Ledeb.) Schischk. [Apiaceae; Radix Saposhnikoviae], 10 g; Lonicera japonica Thunb. [Caprifoliaceae; Caulis Lonicerae], 10 g; Morus alba [Moraceae; Ramulus Mori], 10 g; Pheretima asiatica Michaelsen [Megascolecidae; Lumbricus], 6 g; Glycyrrhiza glabra [Fabaceae; Radix Glycyrrhizae], 6 g	N	N
Chen et al. (2016)	Jingfukang Pharmaceutical Co., Ltd.	Ant; Panax ginseng C.A. Mey. [Araliaceae; Radix Ginseng]; Aconitum carmichaeli Debeaux [Ranunculaceae; Radix Aconiti]; Neolitsea cassia (L.) Kosterm. [Lauraceae; Ramulus Cinnamomi]; Atractylodes lancea (Thunb.) DC. [Asteraceae; Rhizoma Atractylodis]; Phellodendron amurense Rupr. [Rutaceae; Cortex Phellodendri]; Coix lacryma-jobi L. [Poaceae; Semen Coicis]; Alisma plantago-aquatica subsp. orientale (Sam.) Sam. [Alismataceae; Rhizoma Alismatis]; Centipede [Scolopendridae; Scolopendra]; Zaoocys dhumnades (Cantor) [Natriciniae; Zaoocys dhumnades]; Lycopodium japonicum [Lycopodiaceae; Herba Lycopodii]; Strychnos nux-vomica L. [Loganiaceae; Semen Strychni]; Spatholobus suberectus Dunn [Fabaceae; Caulis Spatholobi]; Garden Balsam Stem [Euphorbiaceae; Speranskia tuberculata (Bunge) Baill]; Salvia miltiorrhiza Bunge [Lamiaceae; Radix Salviae Miltiorrhizae]	Y-Prepared according to Chinese Pharmacopeia 2015	N
Jiang and Wu (2016)	Nantong Hospital of Traditional Chinese Medicine, Jiangsu Province, China	Aconitum carmichaeli Debeaux [Ranunculaceae; Radix Aconiti], 8 g; Neolitsea cassia (L.) Kosterm. [Lauraceae; Ramulus Cinnamomi], 8 g; Angelica sinensis (Oliv.) Diels [Apiaceae; Radix Angelicae Sinensis], 10 g; Shengdi 15 g; Paeonia lactiflora Pall. [Paeoniaceae; Radix Paeoniae Alba], 20 g; Anemarrhena asphodeloides [Liliaceae; Rhizoma Anemarrhenae], 20 g; Lonicera japonica Thunb. [Caprifoliaceae; Caulis Lonicerae], 20 g; Pheretima asiatica Michaelsen [Megascolecidae; Lumbricus], 12 g; Bombyx mori Linnaeus [Bombyx Linnaeus; Bombyx Batryticatus], 12 g; Zaoocys dhumnades (Cantor) [Natriciniae; Zaoocys dhumnades], 10 g; Glycyrrhiza glabra [Fabaceae; Radix Glycyrrhizae], 6 g	N	N
Wang and Tu (2017)	Dazhou Central Hospital, Sichuan Province, China	Astragalus mongholicus Bunge [Fabaceae; Radix Astragali seu Hedysari], 60 g; Neolitsea cassia (L.) Kosterm. [Lauraceae; Ramulus Cinnamomi], 20 g; Paeonia lactiflora Pall. [Paeoniaceae; Radix Paeoniae Alba], 20 g; Zingiber officinale [Zingiberaceae; Rhizoma Zingiberis], 10 g; Ziziphus jujuba Mill. [Rhamnaceae; Fructus Jujubae], 10 g; Glycyrrhiza glabra [Fabaceae; Radix Glycyrrhizae], 5 g; Tripterygium wilfordii [Celastraceae; Radix Tripterygii Wilfordii], 15 g; Spatholobus suberectus Dunn [Fabaceae; Caulis Spatholobi], 30 g; Piper kadsura [Piperaceae; Caulis Piperis Kadsurae], 30 g; Trachelospermum jasminoides (Lindl.) Lem. [Apocynaceae; Caulis Trachelospermi], 30 g; Yinhuateng 30 g	N	N
Pang et al. (2017)	Affiliated Hospital of Shandong University of Chinese Medicine, Jinan, China	Angelica sinensis (Oliv.) Diels [Apiaceae; Radix Angelicae Sinensis], 20 g; Paeonia lactiflora Pall. [Paeoniaceae; Radix Paeoniae Alba], 30 g; Atractylodes macrocephala Koidz. [Asteraceae; Rhizoma Atractylodis Macrocephalae], 15 g; Atractylodes lancea (Thunb.) DC. [Asteraceae; Rhizoma Atractylodis], 10 g; Sinomenium acutum [Menispermaceae; Caulis Sinomenii], 20 g; Sarcandra glabra (Thunb.) Nakai [Chloranthaceae; Herba Sarcandrae], 30 g; Conioselinum anthriscoides 'Chuanxiong' [Apiaceae; Rhizoma Ligustici], 20 g; Saposhnikovia divaricata (Turcz. ex Ledeb.) Schischk. [Apiaceae; Radix Saposhnikoviae], 9 g; Glycyrrhiza glabra [Fabaceae; Radix Glycyrrhizae], 30 g	N	N
Li et al. (2017)	First Affiliated Hospital of Tianjin University of Traditional Chinese Medicine, Tianjin, China	Angelica dahurica (Hoffm.) Benth. & Hook. f. ex Franch. & Sav. [Apiaceae; Radix Angelicae Pubescentis], 15 g; Hansenia weberbaueriana (Fedde ex H. Wolff) Pimenov & Kljuykov [Apiaceae; Rhizoma et Radix Notopterygii], 15 g; Conioselinum anthriscoides 'Chuanxiong' [Apiaceae; Rhizoma Ligustici], 15 g; Frankincense [Burseraceae; Olibanum], 10 g; Gentiana macrophylla Pall. [Gentianaceae; Radix Gentianae Macrophyllae], 10 g; Aucklandia costus Falc. [Asteraceae; Radix Aucklandiae], 10 g; Morus alba [Moraceae; Ramulus Mori], 10 g; Piper kadsura [Piperaceae; Caulis Piperis Kadsurae], 10 g; Angelica sinensis (Oliv.) Diels [Apiaceae; Radix Angelicae Sinensis], 20 g; Neolitsea cassia (L.) Kosterm. [Lauraceae; Ramulus Cinnamomi], 12 g; Glycyrrhiza glabra [Fabaceae; Radix Glycyrrhizae], 6 g	N	N

(Continued on following page)

TABLE 2 | (Continued) A summary table describing the composition of the CMCs.

Study	Source	Species, concentration	Quality control reported? (Y/N)	Chemical analysis reported? (Y/N)
Gao and Bu, (2017)	The Second Traditional Chinese Medicine Hospital of Jiangsu, Nanjing Jiangsu, China	Rehmannia glutinosa (Gaertn.) DC. [Orobanchaceae; Radix Rehmanniae Preparata], 30 g; Astragalus mongholicus Bunge [Fabaceae; Radix Astragali seu Hedysari], 15 g; Shanyu 20 g; Paeonia x suffruticosa [Paeoniaceae; Cortex Moutan Radicis], 10 g; Poria [Polyporaceae; Sclerotium Poriae Cocos], 15 g; Coptis chinensis Franch. [Ranunculaceae; Rhizoma Coptidis], 10 g; Dioscorea oppositifolia [Dioscoreaceae; Rhizoma Dioscoreae], 20 g; Chrysanthemum x morifolium (Ramat.) Hemsl. [Asteraceae; Flos Chrysanthemi], 10 g; Alisma plantago-aquatica subsp. orientale (Sam.) Sam. [Alismataceae; Rhizoma Alismatis], 10 g; Paeonia lactiflora Pall. [Paeoniaceae; Radix Paeoniae Rubra], 15 g; Angelica sinensis (Oliv.) Diels [Apiaceae; Radix Angelicae Sinensis], 10 g	N	N
Gao and Bu (2017)	Rheumatism Hospital of Shanxi Jinkang, Taiyuan, Chian	Ant ; Atractylodes macrocephala Koidz. [Asteraceae; Rhizoma Atractylodis Macrocephalae] ; Aconitum carmichaeli [Ranunculaceae; Radix Aconiti Lateralis Preparata] ; Neolitsea cassia (L.) Kosterm. [Lauraceae; Ramulus Cinnamomi]; etc.	N	N
Wang and Tu (2017)	Tongji Hospital Affiliated to Tongji Medical School of Huazhong University of Science and Technology, Wuhan Hubei, China	Aconitum carmichaeli Debeaux [Ranunculaceae; Radix Aconiti], 20 g; Ephedra sinica Stapf [Ephedraceae; Herba Ephedrae], 6 g; Astragalus mongholicus Bunge [Fabaceae; Radix Astragali seu Hedysari], 30 g; Paeonia lactiflora Pall. [Paeoniaceae; Radix Paeoniae Alba], 20 g; Glycyrrhiza glabra [Fabaceae; Radix Glycyrrhizae], 10 g; Neolitsea cassia (L.) Kosterm. [Lauraceae; Ramulus Cinnamomi], 10 g; Clematis chinensis Osbeck [Ranunculaceae; Radix Clematidis], 10 g; Asarum sieboldii [Aristolochiaceae; Herba cum Radix Asari], 3 g; Eupolyphaga [Corydidae; Eupolyphaga Seu Steleophaga], 10 g; Morus alba [Moraceae; Ramulus Mori], 20 g; Lycopodium japonicum [Lycopodiaceae; Herba Lycopodii], 20 g; Angelica dahurica (Hoffm.) Benth. & Hook.f. ex Franch. & Sav. [Apiaceae; Radix Angelicae Pubescentis], 20 g; Taxillus chinensis (DC.) Danser [Loranthaceae; Herba Taxilli], 20 g; Reynoutria multiflora (Thunb.) Moldenke [Polygonaceae; Radix Polygoni Multiflori], 20 g; Dipsacus asper [Caprifoliaceae; Radix Dipsaci], 15 g	N	N
Ma et al. (2018)	Lanzhou Traditional Chinese Medicine Orthopedics Hospital, Gansu Province, China	Paeonia lactiflora Pall. [Paeoniaceae; Radix Paeoniae Rubra], 15 g; Angelica sinensis (Oliv.) Diels [Apiaceae; Radix Angelicae Sinensis], 15 g; Pheretima asiatica Michaelsen [Megascolecidae; Lumbricus], 10 g; Astragalus mongholicus Bunge [Fabaceae; Radix Astragali seu Hedysari], 25 g; Conioselinum anthriscoides 'Chuanxiong' [Apiaceae; Rhizoma Ligustici], 10 g; Arisaema erubescens [Araceae; Arisaemae cum Bile], 10 g; Sinapis alba L. [Brassicaceae; Semen sinapis.], 10 g; Buthus martensii Karsch [Scorpiones; Scorpio], 5 g; Angelica dahurica (Hoffm.) Benth. & Hook.f. ex Franch. & Sav. [Apiaceae; Radix Angelicae Pubescentis], 15 g; Hansenia weberbaueriana (Fedde ex H. Wolff) Pimenov & Kljuykov [Apiaceae; Rhizoma et Radix Notopterygii], 15 g; Neolitsea cassia (L.) Kosterm. [Lauraceae; Ramulus Cinnamomi], 10 g; Paeonia lactiflora Pall. [Paeoniaceae; Radix Paeoniae Alba], 15 g; Glycyrrhiza glabra [Fabaceae; Radix Glycyrrhizae], 5 g	N	N
Guo et al. (2018)	Affiliated Hospital of Gansu University of Traditional Chinese Medicine, Gansu Province, China	Cervus nippon Temminck [Cervidae; Cornu Cervi Degelatinatum] ; Equus asinus L. [Equidae; Colla Corii Asini] ; Buthus martensii Karsch [Scorpiones; Scorpio] ; Panax notoginseng (Burkill) F.H.Chen [Araliaceae; Radix Notoginseng] ; Neolitsea cassia [Lauraceae; Cortex Cinnamomi] ; Coptis chinensis Franch. [Ranunculaceae; Rhizoma Coptidis] ; Ligustrum lucidum W.T.Aiton [Oleaceae; Fructus Ligustri Lucidi] ; Chinemys reevesii (Gray) [Testudinidae; Plastrum Testudinis] ; Trionyx sinensis Wiegmann [Trionychidae; Carapax Trionycis] ; Drynaria roosii [Polypodiaceae; Rhizoma Drynariae] ; Spatholobus suberectus Dunn [Fabaceae; Caulis Spatholobi] ; Glycyrrhiza glabra [Fabaceae; Radix Glycyrrhizae]	N	N
Xu et al. (2018)	Kangmei Pharmaceutical Co., Ltd.	Lonicera japonica Thunb. [Caprifoliaceae; Caulis Lonicerae], 30 g; Angelica sinensis (Oliv.) Diels [Apiaceae; Radix Angelicae Sinensis], 30 g; Scrophularia ningpoensis [Scrophulariaceae; Radix Scrophulariae], 20 g; Glycyrrhiza glabra [Fabaceae; Radix Glycyrrhizae], 10 g; Dioscorea nipponica Makino [Dioscoreaceae; Rhizoma Dioscoreae Nipponicae], 30 g; Arctium lappa L. [Arctium lappa L.; Fructus Arctii], 15 g; Bombyx mori Linnaeus [Bombyx Linnaeus; Bombyx Batryticatus], 10 g; etc.	N	N

(Continued on following page)

TABLE 2 | (Continued) A summary table describing the composition of the CMCs.

Study	Source	Species, concentration	Quality control reported? (Y/N)	Chemical analysis reported? (Y/N)
Bian and Wang (2018)	Guangdong Shengkang Pharmaceutical Co., Ltd.	Astragalus mongholicus Bunge[Fabaceae;Radix Astragali seu Hedysari], 30 g; Neolitsea cassia (L.) Kosterm.[Lauraceae;Ramulus Cinnamomi], 15 g; Paeonia lactiflora Pall. [Paeoniaceae;Radix Paeoniae Rubra], 15 g; Paeonia lactiflora Pall.[Paeoniaceae;Radix Paeoniae Alba], 15 g; Angelica sinensis (Oliv.) Diels[Apiaceae;Radix Angelicae Sinensis], 20 g; Arisaema erubescens[Araceae; Arisaemae cum Bile], 15 g; Zingiber officinale[Zingiberaceae; Rhizoma Zingiberis],10 g; Bombyx mori Linnaeus[Bombyx Linnaeus;Bombyx Batryticatus], 15 g; Cremastra appendiculata (D.Don) Makino[Orchidaceae; Pseudobulbus Cremastrae seu Pleiones], 15 g; Sinapis alba L. [Brassicaceae;Semen sinapis.], 9 g; Corydalis yanhusuol[Papaveraceae;Rhizoma Corydalis], 15 g; Pheretima asiatica Michaelsen [Megasclecoideae;Lumbricus], 15 g; Lonicera japonica Thunb. [Caprifoliaceae;Caulis Lonicerae], 30 g; Glycyrrhiza glabra[Fabaceae; Radix Glycyrrhizae], 6 g	N	N
Shi et al. (2018)	Tongling City Hospital of Traditional Chinese Medicine, Shanxi Province, China	Damp-heat obstruction type: Gentiana macrophylla Pall.[Gentianaceae;Radix Gentianae Macrophyllae], 15 g; Angelica dahurica (Hoffm.) Benth. & Hook.f. ex Franch. & Sav. [Apiaceae;Radix Angelicae Pubescentis], 15 g; Stephania tetrandra[Menispermaceae; Radix Stephaniae Tetrandrae], 9 g; Poria [Polyporaceae; Sclerotium Poriae Cocos], 15 g; Coix lacryma-jobi L.[Poaceae;Semen Coicis], 30 g; Lycium barbarum L. [Lycium barbarum L.; Lycii Cortex], 15 g; Lonicera japonica Thunb. [Caprifoliaceae; Caulis Lonicerae], 30 g; Dipsacus asper[Caprifoliaceae; Radix Dipsaci], 15 g; Drynaria roosii [Polypodiaceae; Rhizoma Drynariae], 15 g; Anemarrhena asphodeloides[Liliaceae; Rhizoma Anemarrhenae], 15 g; Phellodendron amurense Rupr. [Rutaceae;Cortex Phellodendri], 15 g; Frankincense[Burseraceae; Olibanum], 9 g; Glycyrrhiza glabra[Fabaceae; Radix Glycyrrhizae], 6 g. Kidney qi deficiency and cold type: Epimedium sagittatum (Siebold & Zucc.) Maxim. [Berberidaceae; Herba Epimedium], 15 g; Curculigo orchoides Gaertn.[Hypoxidaceae;Rhizoma Curculiginis], 12 g; Angelica dahurica (Hoffm.) Benth. & Hook.f. ex Franch. & Sav. [Apiaceae;Radix Angelicae Pubescentis], 15 g; Hansenia weberbaueriana (Fedde ex H.Wolff) Pimenov & Kljuykov [Apiaceae;Rhizoma et Radix Notopterygii], 9 g; Neolitsea cassia (L.) Kosterm.[Lauraceae;Ramulus Cinnamomi], 15 g; Dipsacus asper [Caprifoliaceae; Radix Dipsaci], 15 g; Drynaria roosii[Polypodiaceae; Rhizoma Drynariae], 15 g; Clematis chinensis Osbeck[Ranunculaceae;Radix Clematidis], 15 g; Psoralea fructus[Fabaceae; Fructus Psoraliae], 15 g; Achyranthes bidentata Blume [Amaranthaceae;Radix Achyranthis Bidentatae], 15 g; Lycopodium japonicum[Lycopodiaceae; Herba Lycopodii], 30 g; Saposhnikovia divaricata (Turcz. ex Ledeb.) Schischk. [Apiaceae;Radix Saposhnikoviae], 10 g; Aconitum carmichaeli[Ranunculaceae; Radix Aconiti Lateralis Preparata], 9 g; Glycyrrhiza glabra[Fabaceae; Radix Glycyrrhizae], 6g. Blood stasis type: Eucommia ulmoides Oliv. [Eucommiaceae; Cortex Eucommiae], 15 g; Dipsacus asper[Caprifoliaceae; Radix Dipsaci], 15 g; Deerhorn glue[Cervidae;Colla Corni Cervi], 10 g; Cyperus rotundus L. [Cyperaceae; Rhizoma Cyperi], 15 g; Psoralea fructus[Fabaceae; Fructus Psoraliae], 15 g; Drynaria roosii[Polypodiaceae; Rhizoma Drynariae], 15 g; Salvia miltiorrhiza Bunge[Lamiaceae; Radix Salviae Miltiorrhizae], 20 g; Reynoutria multiflora (Thunb.) Moldenke[Polygonaceae;Radix Polygoni Multiflori], 15 g; Frankincense[Burseraceae; Olibanum], 9 g; Commiphora myrrha[Burseraceae; Resina Commiphorae], 9 g; Angelica dahurica (Hoffm.) Benth. & Hook.f. ex Franch. & Sav. [Apiaceae;Radix Angelicae Pubescentis], 15 g; Spatholobus suberectus Dunn [Fabaceae;Caulis Spatholobi], 30 g; Achyranthes bidentata Blume [Amaranthaceae;Radix Achyranthis Bidentatae], 15 g; Angelica sinensis (Oliv.) Diels[Apiaceae;Radix Angelicae Sinensis], 15 g; Paeonia lactiflora Pall. [Paeoniaceae;Radix Paeoniae Rubra], 12 g	N	N
Ge et al. (2018)	Jiaozuo Traditional Chinese Medicine Hospital, Henan Province, China	Piper kadsura[Piperaceae; Caulis Piperis Kadsurae], 12 g; Sinomenium acutum[Menispermaceae; Caulis Sinomenii], 12 g; Spatholobus suberectus Dunn[Fabaceae;Caulis Spatholobi], 12 g; Yinhuateng 12 g; Saposhnikovia divaricata (Turcz. ex Ledeb.) Schischk. [Apiaceae;Radix Saposhnikoviae], 10 g; Dioscorea nipponica Makino[Dioscoreaceae;Rhizoma Dioscoreae Nipponicae], 10 g; Sinapis alba L. [Brassicaceae;Semen sinapis.], 10 g; Buthus martensii Karsch [Scorpiones;Scorpio], 6 g; Angelica sinensis (Oliv.) Diels[Apiaceae;Radix Angelicae Sinensis], 15 g; Arisaema erubescens[Araceae; Arisaemae cum Bile], 10 g; Conioselinum anthriscoides 'Chuanxiong'[Apiaceae;Rhizoma Ligustici], 8 g; Paeonia lactiflora Pall.[Paeoniaceae;Radix Paeoniae Alba], 10 g; Prunus persica (L.) Batsch[Rosaceae;Semen Persicae], 9 g; Carthamus tinctorius[Asteraceae; Flos Carthami], 6 g	N	N

TABLE 2 | (Continued) A summary table describing the composition of the CMCs.

Study	Source	Species, concentration	Quality control reported? (Y/N)	Chemical analysis reported? (Y/N)
Zeng and Chen (2018)	Liaoning Good Nurse Pharmaceutical Co., Ltd.	Rehmannia glutinosa (Gaertn.) DC. [Orobanchaceae; Radix Rehmanniae Preparata] ; Epimedium sagittatum (Siebold & Zucc.) Maxim. [Berberidaceae; Herba Epimedi] ; Clematis chinensis Osbeck [Ranunculaceae; Radix Clematidis] ; Cibotium barometz (L.) J.Sm. [Cyatheaaceae; Rhizoma Cibotii] ; Anemarrhena asphodeloides [Liliaceae; Rhizoma Anemarrhenae] ; Lycopodium japonicum [Lycopodiaceae; Herba Lycopodii] ; Drynaria roosii [Polypodiaceae; Rhizoma Drynariae]; etc.	Y-Prepared according to <i>Chinese Pharmacopeia 2015</i>	N
Hu (2018)	Neijiang Hospita of Traditional Chinese Medicine, Sichuan Neijiang, China	Wind-cold-dampness syndrome: Clematis chinensis Osbeck [Ranunculaceae; Radix Clematidis], 15 g; Hansenia weberbaueriana (Fedde ex H.Wolff) Pimenov & Kijuykov [Apiaceae; Rhizoma et Radix Notopterygii], 9 g; Neolitsea cassia (L.) Kosterm. [Lauraceae; Ramulus Cinnamomi], 9 g; Commiphora myrrha [Burseraceae; Resina Commiphorae], 9 g; Conioselinum anthriscoides 'Chuanxiong' [Apiaceae; Rhizoma Ligustici], 9 g; Gentiana macrophylla Pall. [Gentianaceae; Radix Gentianae Macrophyllae], 9 g; Angelica dahurica (Hoffm.) Benth. & Hook.f. ex Franch. & Sav. [Apiaceae; Radix Angelicae Pubescentis], 9 g; Frankincense [Burseraceae; Olibanum], 9 g; Angelica sinensis (Oliv.) Diels [Apiaceae; Radix Angelicae Sinensis], 9g. Wind-heat-dampness syndrome: Morus alba [Moraceae; Ramulus Mori], 20 g; Lonicera japonica Thunb. [Caprifoliaceae; Caulis Lonicerae], 20 g; Paeonia lactiflora Pall. [Paeoniaceae; Radix Paeoniae Alba], 15 g; Stephania tetrandra [Menispermaceae; Radix Stephaniae Tetrandrae], 12 g; Erythrina indica Lam. [Leguminosae; Cortex Erythrinae], 12 g; Anemarrhena asphodeloides [Liliaceae; Rhizoma Anemarrhenae], 10 g; Saposhnikovia divaricata (Turcz. ex Ledeb.) Schischk. [Apiaceae; Radix Saposhnikoviae], 9 g; Neolitsea cassia (L.) Kosterm. [Lauraceae; Ramulus Cinnamomi], 6g. of Phlegm and blood stasis syndrome: Codonopsis pilosula [Campanulaceae; Radix Codonopsis], 15 g; Taxillus chinensis (DC.) Danser [Loranthaceae; Herba Taxilli], 12 g; Gentiana macrophylla Pall. [Gentianaceae; Radix Gentianae Macrophyllae], 12 g; Rehmannia glutinosa (Gaertn.) DC. [Orobanchaceae; Radix Rehmanniae Preparata], 12 g; Poria [Polyporaceae; Sclerotium Poriae Cocos], 12 g; Paeonia lactiflora Pall. [Paeoniaceae; Radix Paeoniae Alba], 12 g; Eucommia ulmoides Oliv. [Eucommiaceae; Cortex Eucommiae], 10 g; Angelica sinensis (Oliv.) Diels [Apiaceae; Radix Angelicae Sinensis], 10 g; Achyranthes bidentata Blume [Amaranthaceae; Radix Achyranthis Bidentatae], 10 g; Conioselinum anthriscoides 'Chuanxiong' [Apiaceae; Rhizoma Ligustici], 10 g; Angelica dahurica (Hoffm.) Benth. & Hook.f. ex Franch. & Sav. [Apiaceae; Radix Angelicae Pubescentis], 9 g; Saposhnikovia divaricata (Turcz. ex Ledeb.) Schischk. [Apiaceae; Radix Saposhnikoviae], 9 g; Neolitsea cassia [Lauraceae; Cortex Cinnamomi], 3 g; Asarum sieboldii [Aristolochiaceae; Herba cum Radix Asari], 3g. Kidney-Yang deficiency syndrome: Woolly datvhmanspipe herb [Aristolochiaceae; Herba Aristolochiae Mollissimae], 15 g; Atractylodes macrocephala Koidz. [Asteraceae; Rhizoma Atractylodis Macrocephalae], 15 g; Epimedium sagittatum (Siebold & Zucc.) Maxim. [Berberidaceae; Herba Epimedi], 15 g; Clematis chinensis Osbeck [Ranunculaceae; Radix Clematidis], 15 g; Gynochthodes officinalis (F.C.Hov) Razafim. [Rubiaceae; Radix Morindae Officinalis], 12 g; Achyranthes bidentata Blume [Amaranthaceae; Radix Achyranthis Bidentatae], 12 g; Dioscorea oppositifolia [Dioscoreaceae; Rhizoma Dioscoreae], 12 g; Poria [Polyporaceae; Sclerotium Poriae Cocos], 12 g; Cibotium barometz (L.) J.Sm. [Cyatheaaceae; Rhizoma Cibotii], 12 g; Aconitum carmichaeli [Ranunculaceae; Radix Aconiti Lateralis Preparata], 9 g; Shanyu 9 g; Neolitsea cassia (L.) Kosterm. [Lauraceae; Ramulus Cinnamomi], 9 g	N	N
Yuan et al. (2019)	The First Affiliated Hospital of Guangxi University of Chinese Medicine, Nanning Guangxi, China	Gypsum [Mineral; Gypsum Fibrosum], 30 g; Anemarrhena asphodeloides [Liliaceae; Rhizoma Anemarrhenae], 20 g; Non-glutinous rice [Gramineae; Oryza sativa L.], 20 g; Neolitsea cassia (L.) Kosterm. [Lauraceae; Ramulus Cinnamomi], 6 g; Glycyrrhiza glabra [Fabaceae; Radix Glycyrrhizae], 6 g; Angelica sinensis (Oliv.) Diels [Apiaceae; Radix Angelicae Sinensis], 10 g; Rehmannia glutinosa [Orobanchaceae; Radix Rehmanniae], 50 g; Prunus armeniaca L. [Rosaceae; Semen Armeniacae Amarum], 12 g; Coix lacryma-jobi L. [Poaceae; Semen Coicis], 12 g; Clematis chinensis Osbeck [Ranunculaceae; Radix Clematidis], 12 g; Arnebia euchroma (Royle ex Benth.) I.M. Johnst. [Boraginaceae; Radix Lithospermi], 30 g; Paeonia lactiflora Pall. [Paeoniaceae; Radix Paeoniae Rubra], 30 g;	N	N

(Continued on following page)

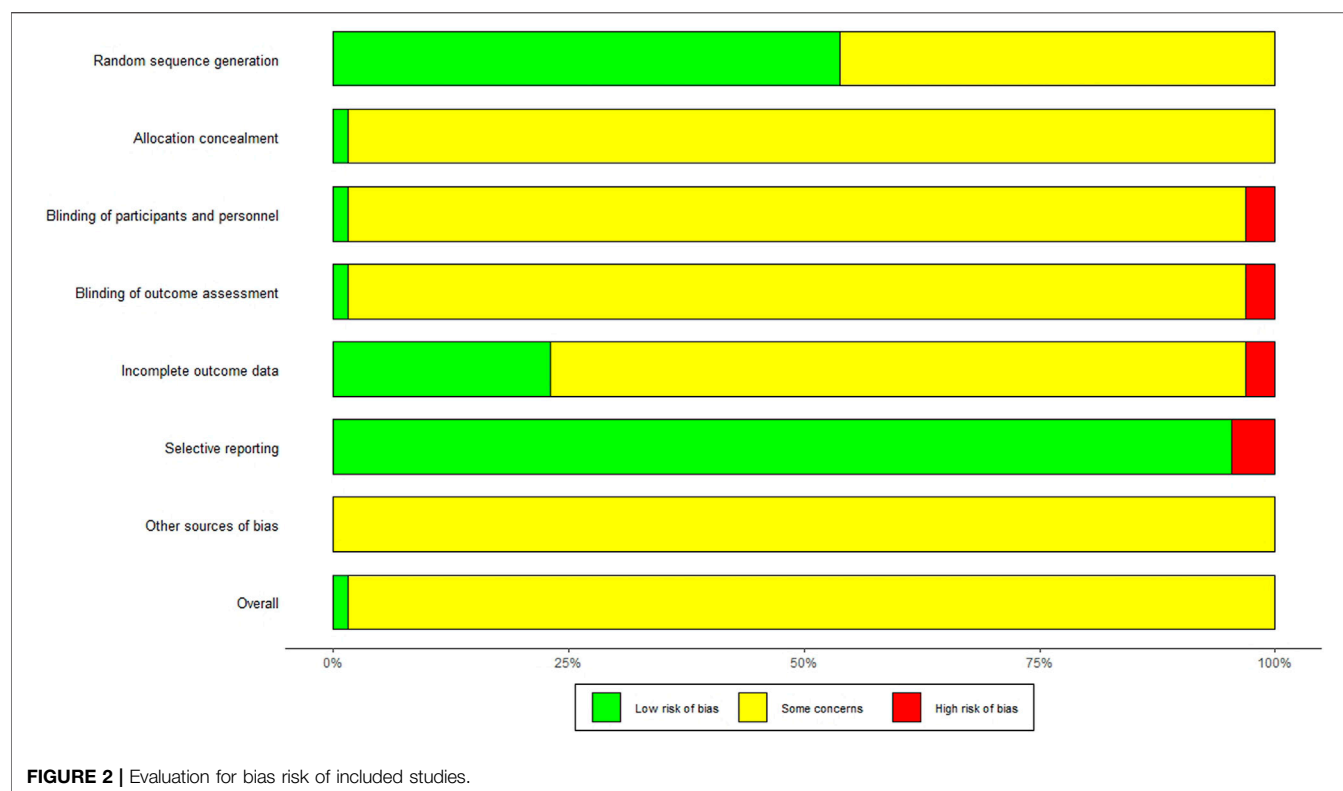
TABLE 2 | (Continued) A summary table describing the composition of the CMCs.

Study	Source	Species, concentration	Quality control reported? (Y/N)	Chemical analysis reported? (Y/N)
Pang et al. (2019)	Zhongshan Hospital of Traditional Chinese Medicine Affiliated to Guangzhou University of Chinese Medicine, Guangdong Zhongshan, China	Neolitsea cassia (L.) Kosterm.[Lauraceae;Ramulus Cinnamomi] ; Tripterygium hypoglaucum (H.Lév.) Hutch. [Celastraceae; Tripterygium hypoglaucum(Devl.)Hutch.] ; Paeonia lactiflora Pall.[Paeoniaceae; Radix Paeoniae Alba] ; Spatholobus suberectus Dunn[Fabaceae;Caulis Spatholobi] ; Zaocys dhumnades(Cantor)[Natricinae;Zaocys dhumnades] ; Coix lacryma-jobi L.[Poaceae;Semen Coicis] ; Zingiber officinale[Zingiberaceae; Rhizoma Zingiberis]; etc.	N	N
Zhao (2019)	Shenzhen Second People's Hospital, Guangdong Shenzhen, China	Paeonia lactiflora Pall.[Paeoniaceae;Radix Paeoniae Alba], 12 g; Anemarrhena asphodeloides[Liliaceae; Rhizoma Anemarrhenae], 12 g; Neolitsea cassia (L.) Kosterm.[Lauraceae;Ramulus Cinnamomi], 9 g; Paeonia lactiflora Pall. [Paeoniaceae;Radix Paeoniae Rubra], 9 g; Ephedra sinica Stapf [Ephedraceae; Herba Ephedrae], 9 g; Atractylodes macrocephala Koidz.[Asteraceae;Rhizoma Atractylodis Macrocephalae], 9 g; Saposhnikovia divaricata (Turcz. ex Ledeb.) Schischk. [Apiaceae;Radix Saposhnikoviae], 9 g; Glycyrrhiza glabra[Fabaceae; Radix Glycyrrhizae], 6 g; Aconitum camichaeli [Ranunculaceae; Radix Aconiti Lateralis Preparata], 6 g; Zingiber officinale[Zingiberaceae; Rhizoma Zingiberis], 3 pieces	N	N
Li et al. (2019)	Kangmei Pharmaceutical Co., Ltd.	Neolitsea cassia (L.) Kosterm.[Lauraceae;Ramulus Cinnamomi], 15 g; Anemarrhena asphodeloides [Liliaceae; Rhizoma Anemarrhenae], 10-15 g; Paeonia lactiflora Pall.[Paeoniaceae;Radix Paeoniae Alba], 10-30 g; Ephedra sinica Stapf [Ephedraceae;Herba Ephedrae], 10 g; Zingiber officinale[Zingiberaceae; Rhizoma Zingiberis],10 g; Saposhnikovia divaricata (Turcz. ex Ledeb.) Schischk. [Apiaceae;Radix Saposhnikoviae], 10 g; Atractylodes macrocephala Koidz.[Asteraceae;Rhizoma Atractylodis Macrocephalae], 10 g; Aconitum camichaeli[Ranunculaceae; Radix Aconiti Lateralis Preparata], 10-30 g; Glycyrrhiza glabra[Fabaceae; Radix Glycyrrhizae], 10 g	N	N
Song et al. (2019)	Qinghai Hospital of Traditional Chinese Medicine, Qinghai Xining, China	Rehmannia glutinosa (Gaertn.) DC. [Orobanchaceae;Radix Rehmanniae Preparata], 30 g; Angelica dahurica (Hoffm.) Benth. & Hook.f. ex Franch. & Sav. [Apiaceae;Radix Angelicae Pubescentis], 15 g; Paeonia lactiflora Pall.[Paeoniaceae;Radix Paeoniae Alba], 15 g; Angelica sinensis (Oliv.) Diels[Apiaceae; Radix Angelicae Sinensis], 12 g; Neolitsea cassia[Lauraceae; Cortex Cinnamomi], 10 g; Deerhorn glue [Cervidae;Colla Corni Cervi], 10 g; Sinapis alba L. [Brassicaceae;Semen sinapis.], 10 g; Ephedra sinica Stapf [Ephedraceae;Herba Ephedrae], 10 g; Glycyrrhiza glabra[Fabaceae; Radix Glycyrrhizae], 9 g; Poria [Polyporaceae; Sclerotium Poriae Cocos], 9 g	N	N
Zhang et al. (2019)	Luoyang Zhenggu Hospital (Henan Orthopaedic Hospital), Zhengzhou, China	Coix lacryma-jobi L.[Poaceae;Semen Coicis], 30 g; Angelica sinensis (Oliv.) Diels[Apiaceae;Radix Angelicae Sinensis], 12 g; Saposhnikovia divaricata (Turcz. ex Ledeb.) Schischk. [Apiaceae;Radix Saposhnikoviae], 10 g; Conioselinum anthriscoides 'Chuanxiong'[Apiaceae;Rhizoma Ligustici], 10 g; Ephedra sinica Stapf [Ephedraceae;Herba Ephedrae], 10 g; Atractylodes lancea (Thunb.) DC.[Asteraceae;Rhizoma Atractylodis],10 g; Glycyrrhiza glabra[Fabaceae; Radix Glycyrrhizae], 10 g; Hansenia weberbaueriana (Fedde ex H.Wolff) Pimenov & Kljuykov [Apiaceae;Rhizoma et Radix Notopterygii], 5 g; Angelica dahurica (Hoffm.) Benth. & Hook.f. ex Franch. & Sav. [Apiaceae;Radix Angelicae Pubescentis], 5 g; Neolitsea cassia (L.) Kosterm.[Lauraceae;Ramulus Cinnamomi], 5 g	N	N
Fang et al. (2019)	Taihe Hospital of Shiyan City, Affiliated Hospital of Hubei Medical College, Shiyan Hubei, China	Astragalus mongholicus Bunge[Fabaceae;Radix Astragali seu Hedysari], 15 g; Conioselinum anthriscoides 'Chuanxiong'[Apiaceae;Rhizoma Ligustici], 15 g; Aconitum camichaeli[Ranunculaceae; Radix Aconiti Lateralis Preparata], 15 g; Zaocys dhumnades(Cantor)[Natricinae;Zaocys dhumnades], 15 g; Paeonia lactiflora Pall.[Paeoniaceae;Radix Paeoniae Alba], 10 g; Zingiber officinale Roscoe [Zingiberaceae; Rhizoma Zingiberis], 10 g; Neolitsea cassia (L.) Kosterm.[Lauraceae;Ramulus Cinnamomi], 10 g; Aconitum camichaeli Debeaux [Ranunculaceae;Radix Aconiti], 10 g; Atractylodes macrocephala Koidz.[Asteraceae;Rhizoma Atractylodis Macrocephalae], 10 g; Angelica sinensis (Oliv.) Diels[Apiaceae;Radix Angelicae Sinensis], 10 g; Glycyrrhiza glabra[Fabaceae; Radix Glycyrrhizae], 6 g; Ephedra sinica Stapf [Ephedraceae;Herba Ephedrae], 9 g; Asarum sieboldii[Aristolochiaceae; Herba cum Radix Asari], 5 g; Centipede[Scolopendridae; Scolopendra], 1 piece; Buthus martensii Karsch [Scorpiones;Scorpio], 1 piece; Spatholobus suberectus Dunn[Fabaceae;Caulis Spatholobi], 30 g	N	N

(Continued on following page)

TABLE 2 | (Continued) A summary table describing the composition of the CMCs.

Study	Source	Species, concentration	Quality control reported? (Y/N)	Chemical analysis reported? (Y/N)
Cao et al. (2020)	Affiliated Hospital of Liaoning University of Traditional Chinese Medicine, Shenyang, China	Angelica dahurica (Hoffm.) Benth. & Hook.f. ex Franch. & Sav. [Apiaceae;Radix Angelicae Pubescentis], 9 g; Taxillus chinensis (DC.) Danser[Loranthaceae; Herba Taxilli], 9 g; Eucommia ulmoides Oliv. [Eucommiaceae; Cortex Eucommiae], 9 g; Achyranthes bidentata Blume [Amaranthaceae;Radix Achyranthis Bidentatae], 9 g; Gentiana macrophylla Pall.[Gentianaceae;Radix Gentianae Macrophyllae], 9 g; Neolitsea cassia[Lauraceae; Cortex Cinnamomi], 9 g; Saposhnikovia divaricata (Turcz. ex Ledeb.) Schischk. [Apiaceae;Radix Saposhnikoviae], 9 g; Conioselinum anthriscoides 'Chuanxiong'[Apiaceae; Rhizoma Ligustici], 9 g; Angelica sinensis (Oliv.) Diels[Apiaceae;Radix Angelicae Sinensis], 9 g; Paeonia lactiflora Pall.[Paeoniaceae;Radix Paeoniae Alba], 9 g; Asarum sieboldii[Aristolochiaceae; Herba cum Radix Asari], 5 g; Rehmannia glutinosa[Orobanchaceae; Radix Rehmanniae], 9 g; Hansenia weberbaueriana (Fedde ex H.Wolff) Pimenov & Kljuykov [Apiaceae;Rhizoma et Radix Notopterygii], 9 g; Neolitsea cassia (L.) Kosterm.[Lauraceae;Ramulus Cinnamomi], 9 g	N	N
Li (2020)	Zhengzhou Hospital of Traditional Chinese Medicine, Zhengzhou, China	Cremastra appendiculata (D.Don) Makino[Orchidaceae;Pseudobulbus Cremastrae seu Pleiones], 10 g; Sinapis alba L. [Brassicaceae;Semen sinapis.], 10 g; Bombyx mori Linnaeus[Bombyx Linnaeus;Bombyx Batryticatus], 10 g; Pheretima asiatica Michaelsen[Megascolecidae;Lumbricus], 10 g; Arisaema erubescens [Araceae; Arisaemae cum Bile], 15 g	N	N
Jiang and Ma (2020)	Jingzhou Hospital of Traditional Chinese Medicine, Jingzhou Hubei, China	Dioscorea nipponica Makino[Dioscoreaceae;Rhizoma Dioscoreae Nipponicae], 20 g; Sinomenium acutum[Menispermaceae; Caulis Sinomenii], 30 g; Sinapis alba L. [Brassicaceae;Semen sinapis.], 10 g; Paeonia lactiflora Pall. [Paeoniaceae;Radix Paeoniae Rubra], 10 g; Bolbostemma paniculatum (Maxim.) Franquet [Cucurbitaceae;Rhizoma Bolbostematis], 8 g; Curcuma kwangsiensis S.G.Lee & C.F.Liang [Zingiberaceae; Rhizoma Curcumae], 6 g	N	N



nonsteroidal anti-inflammatory drugs (NSAIDs) and GC, etc. There were no statistically significant differences between the basic information about the patients. A summary with baseline characteristics of included patients is shown in **Table 1**. The details (including dosages, herbs, quality control and mentions) of interventions in above studies were disposed in **Supplementary Material 1** and **Table 2**. All herbs used in are assessable and well documented in **Supplementary Material 5** (including their Pinyin Names, Accepted Names, Latin Names, Full Formats and Medicinal Sources).

Quality of the Included Studies

The quality of the trials was assessed and graded according to the criteria described in The Cochrane Handbook 4.2.6. Overall, for most of the included studies, the risk of bias was unclear. In addition, although the random design was mentioned in all studies, only 53.85% (35/65) of the studies described specific methods of random sequence generation. The 35 studies all used the simple random grouping method, regarding random sequence generation of which 32 studies used the random number table method and the other 3 studies selected by draw lots. Except for the study of Zhou (Zhou et al., 2010), the use of allocation concealment was not mentioned in the rest literature. Only one trial (Jiang and Wu, 2016) mentioned the double-blind of patients and personnel, and two studies (Huang et al., 2006; Xu et al., 2018) explicitly mentions the absence of the use of blinding, while the rest literature did not mention the use of blindness. There were 14 studies (Huang et al., 2006; Ma et al., 2009; Li et al., 2012a; He and Xiao, 2014; Li et al., 2015a; Li et al., 2015b; Shu et al., 2015; Chen et al., 2016; Li et al., 2017; Bian and Wang, 2018;

Xu et al., 2018; Fang et al., 2019; Li et al., 2019; Pang et al., 2019) described the dropouts, and two trials (Li, 2006; Zhang and Chen, 2014) were not reported the number of people and the reasons for the failure at follow-up. Pre-designed outcomes were reported in most studies, detecting a low risk of reporting bias. The review authors' judgments about each methodological quality item were presented as percentages across all the included studies in **Figure 2**.

Effects of Interventions

Primary Outcomes

Serum RF Level After Treatment

Sixty-three studies including 5,939 patients (3,043 in the experimental group and 2,896 in the control group) provided the serum RF concentration data. The SMD of the RF levels in treatment group (CMC involved) between baseline and follow-up was 2.64 and 95%CI was [2.25, 3.02], while the SMD in control group (no CMC involved) between baseline and follow-up was 2.08 and 95%CI was [1.75, 2.40] (**Supplementary Material 2**). After treatment, the results showed that CMC had a significant difference in reducing serum RF level compared with the control group. (SMD = -0.86, 95%CI = [-1.05, -0.67]) (**Figure 3**).

Serum Anti-CCP Level After Treatment

Eight studies have observed changes in serum anti-CCP level before and after treatment and provided relevant data. The SMD of the anti-CCP levels in treatment group (CMC involved) between baseline and follow-up was 2.15 and 95%CI was [1.28, 3.01], while the SMD in control group (no CMC involved) between

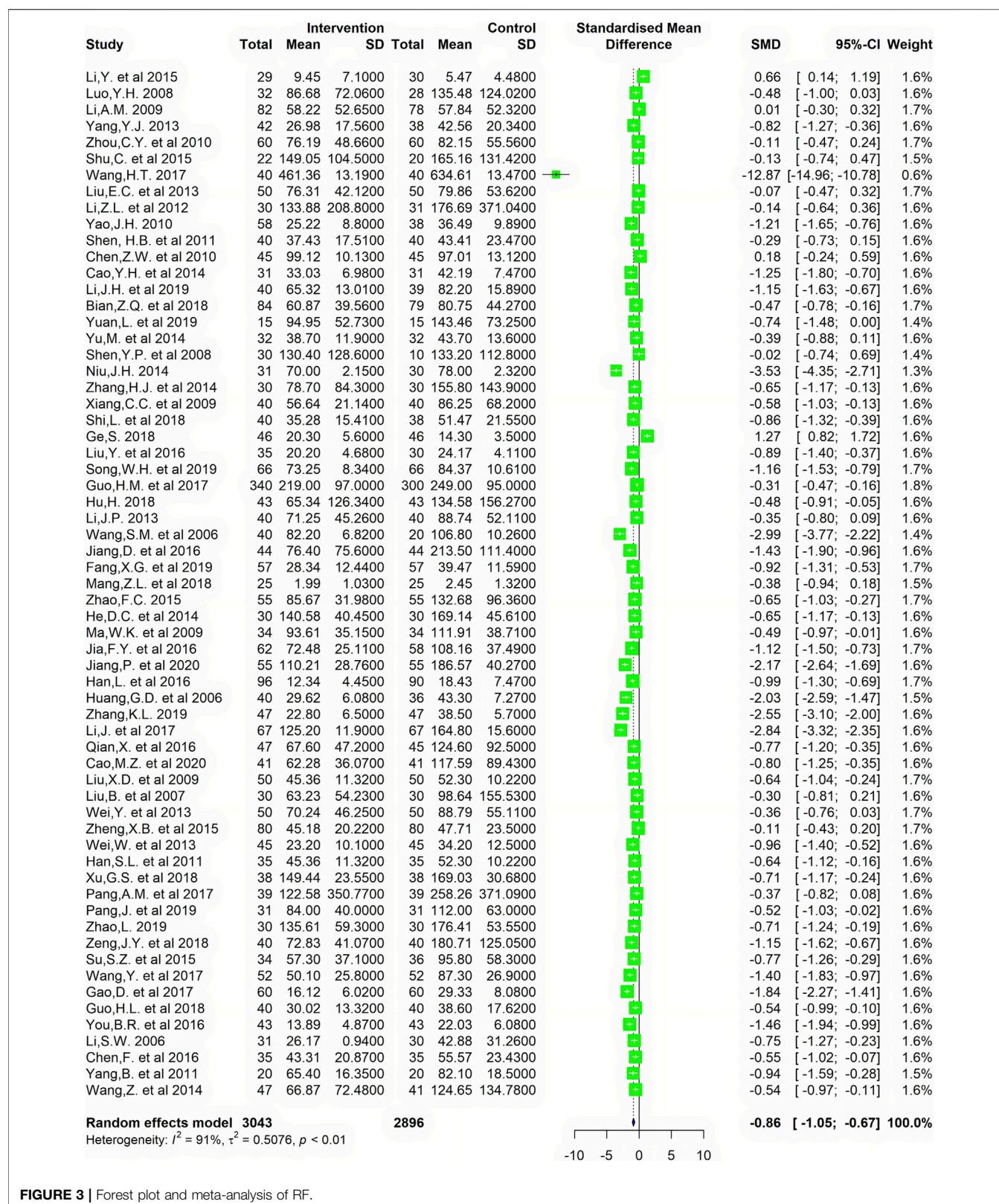


FIGURE 3 | Forest plot and meta-analysis of RF.

baseline and follow-up was 1.62 and 95%CI was [0.91,2.33] (Supplementary Material 3). Since a significant heterogeneity was detected [I^2 (Zeng et al., 2013) = 68%, $p < 0.01$], the

randomized effect model was adopted for analysis and the results indicated that CMC could significantly reduce the level of anti-CCP after treatment (SMD = -0.56, 95%CI = [-0.79, -0.32]) (Figure 4).

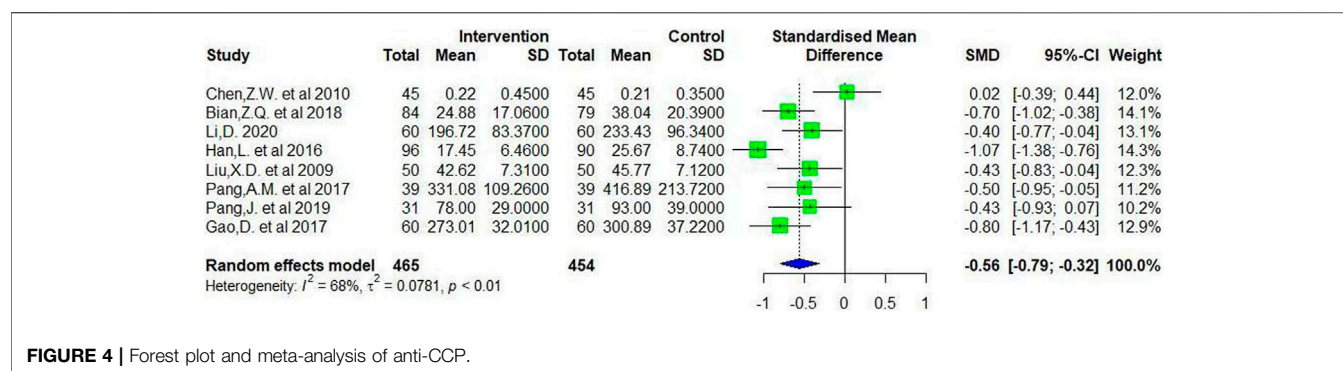


FIGURE 4 | Forest plot and meta-analysis of anti-CCP.

Secondary Outcomes

ACR Response

A total of 14 studies reported ACR20 response rates over the treatment time, and 11 of them also reported the proportion of patients who achieved ACR50 and ACR70 response after treatment. The I -squared was 76% and the p -value was <0.01 , so a random-effects model was adopted for the meta-analysis of ACR20 response. The results of the pooled analysis suggest that the proportion of RA patients who achieved an

ACR20 response after CMC treatment was superior to that of the control group. (SMD = 1.20, 95%CI = [1.08, 1.33]) (Figure 5).

The low risk of heterogeneity was detected among all studies in terms of the ACR50 and ACR70 response of CMC therapy in RA patients. The analysis was performed using a fixed-effects model and the results demonstrated that the RR of achieving ACR50 was 1.50 [1.38, 1.78] and correspondingly the RR of achieving ACR70 was 2.12 [1.65, 2.72] (Figure 5).

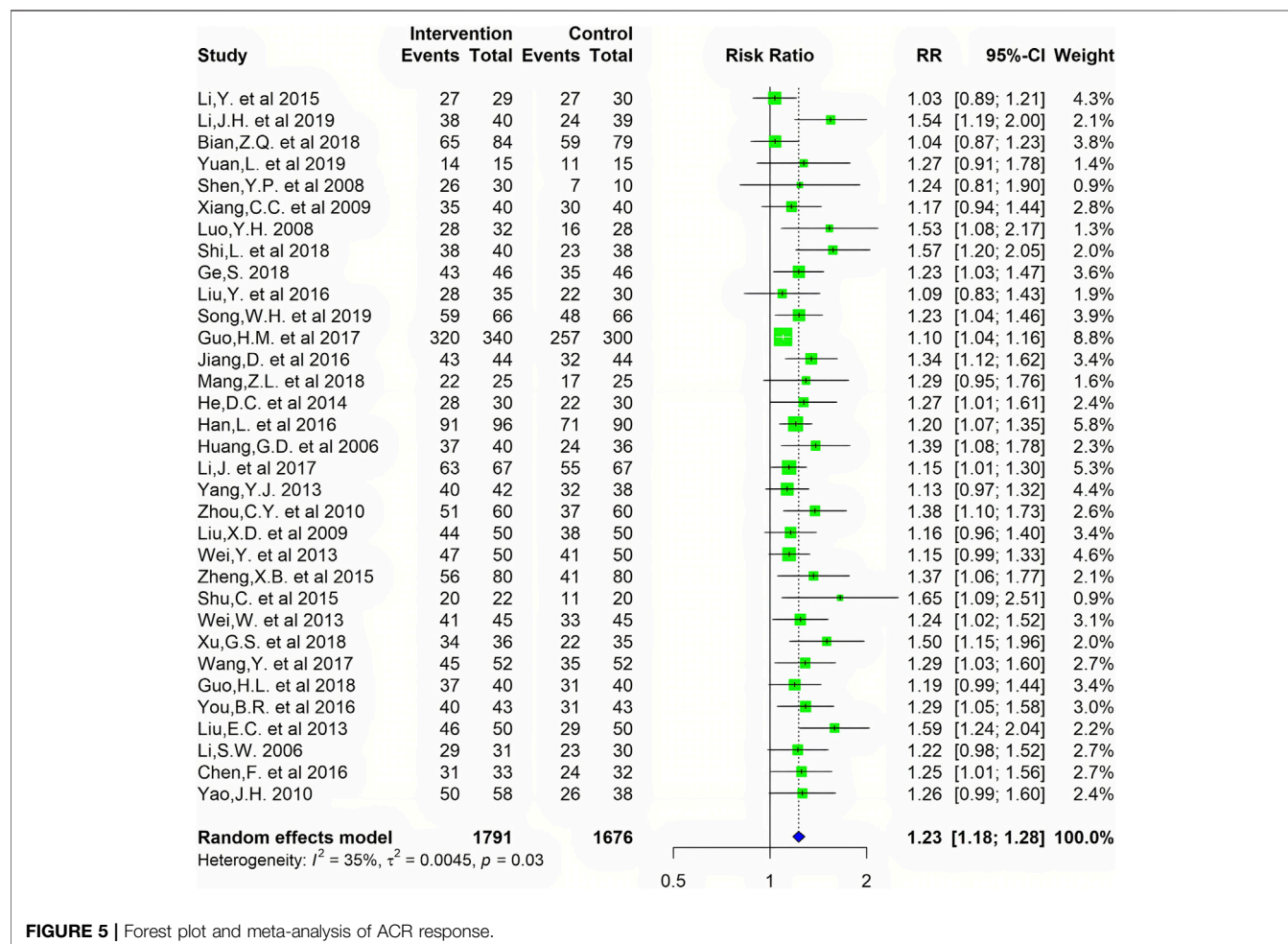


FIGURE 5 | Forest plot and meta-analysis of ACR response.

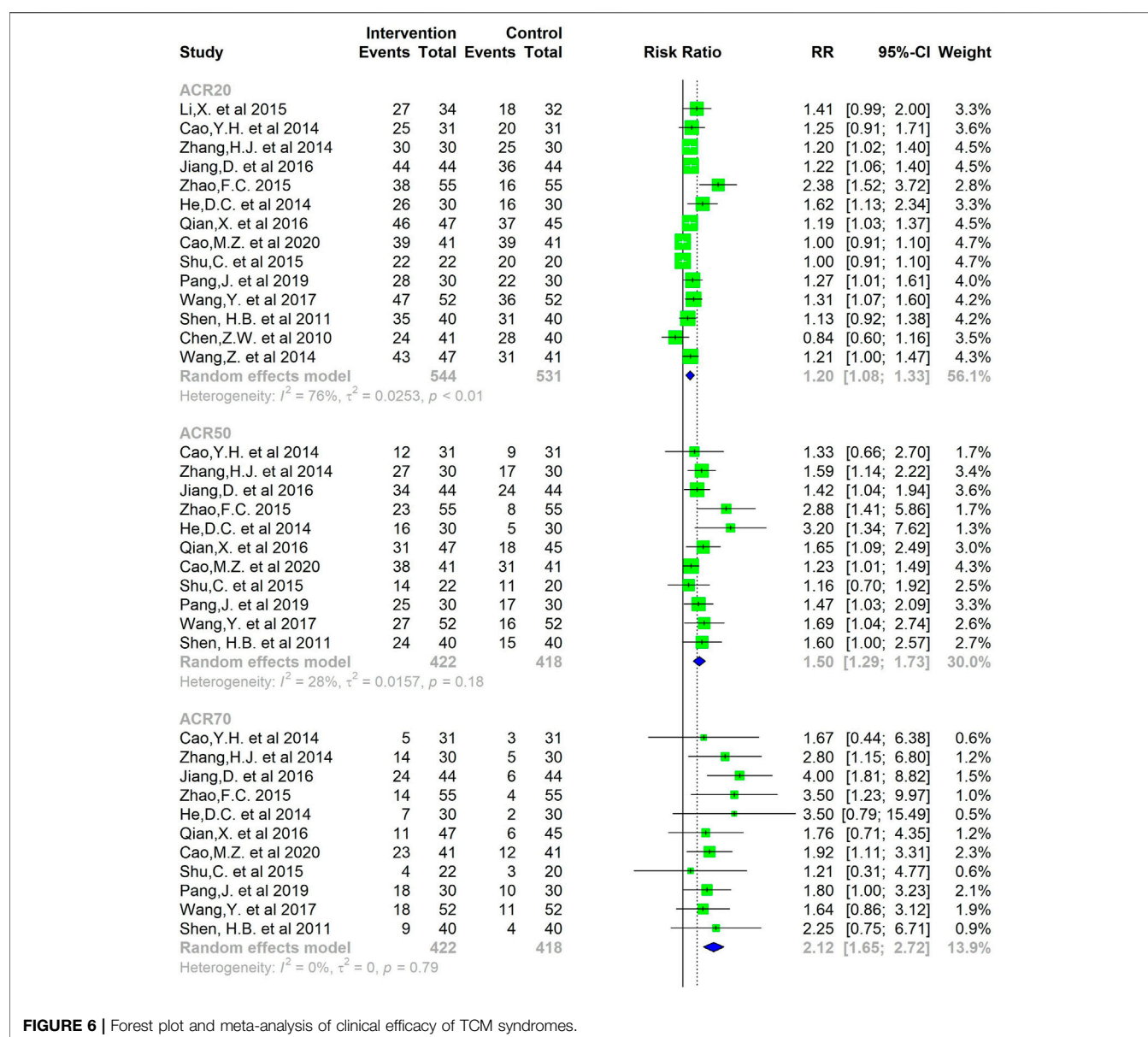


FIGURE 6 | Forest plot and meta-analysis of clinical efficacy of TCM syndromes.

Clinical Efficacy of TCM Syndromes

Data on the clinical efficacy of TCM symptoms were available for 33 studies containing a total of 3,467 cases. The meta-analysis yielded a pooled RR of 1.23 ($I^2 = 35\%$, 95% CI 1.18–1.28). As shown in **Figure 6**, CMC has a good effect on patients with RA.

Sensitivity and Subgroup Analysis

Through sensitivity analysis, after excluding different studies in turn, it was found that there was no change in the significance of any of the outcomes. However, in the sensitivity analysis of the primary outcomes, anti-CCP, it was found that I -squared dropped to 43.4% when a study (Han et al., 2016) was excluded. Considering the difference in the average age of the included patients, unlike other studies, this study included elderly patients with RA, aged ≥ 60 years old. When analyzing the response rate of TCM syndromes, it was found that after a

study (Guo et al., 2017) were excluded, I -squared could be reduced to 11.9%. By reviewing the original article, it was found that the sample size of this study was large compared with other studies (total sample size >600), suggesting that the source of heterogeneity may be caused by the difference in sample size between studies.

After the heterogeneity test, we conducted a subgroup analysis to explore the source of heterogeneity when the heterogeneity between included studies was found to be significant and not negligible. To assess whether the length of the intervention duration and the difference in intervention measures affect that CMC lower levels of RF and anti-CCP, we conducted a subgroup analysis of the primary outcomes RF and anti-CCP. The subgroup analysis was based on the different number of weeks in terms of intervention duration (4 weeks; 6 weeks; 8 weeks; 9 weeks; 12 weeks; 14 weeks; 16 weeks; 24 weeks;

TABLE 3 | The results of meta-analysis of RF and anti-CCP subgroup analysis.

Variable	No. of Trials	No. of EG	No. of CG	SMD (95% CI)	I ² (%)
RF					
Intervention Duration					
4W	4	253	238	-2.93 (-4.56, -1.31)	98
6W	2	67	63	-0.63 (-1.05, -0.21)	27
8W	8	339	312	-0.86 (-1.07, -0.66)	34
9W	1	55	55	-0.65 (-1.03, -0.27)	NA
12W	36	1,600	1,522	-0.73 (-0.95, -0.52)	88
14W	1	31	30	-3.53 (-4.35, -2.71)	NA
16W	2	117	117	-1.60 (-4.02, 0.83)	98
24W	7	304	304	-0.90 (-1.57, -0.23)	93
36W	1	40	20	-2.99 (-3.77, -2.22)	NA
NR	1	34	36	-0.77 (-1.26, -0.29)	NA
Intervention Measure					
CMC	12	530	498	-0.72 (-1.27, -0.17)	94
CMC + WM	51	2,513	2,398	-0.91 (-1.10, -0.73)	91
Anti-CCP					
Intervention Duration					
12W	6	389	378	-0.67 (-0.89, -0.45)	54
24W	2	76	76	-0.18 (-0.62, 0.26)	47
Intervention Measure					
CMC	1	45	45	0.02 (-0.39, 0.44)	NA
CMC + WM	7	420	409	-0.65 (-0.85, -0.45)	49

EG, experimental group; CG, control group; W, weeks; CMC, Chinese medicine compound; WM, Western medicine; SMD, standardized mean difference; NR, not reported; NA, not applicable.

36 weeks; not reported), and different intervention measures (CMC monotherapy or CMC combined with Western medicine) specified the subgroups. **Table 3** summarizes the results of RF and anti-CCP subgroup analysis.

We found that the heterogeneity could not be eliminated after grouping according to the results of subgroup analysis, indicating that differences in intervention duration and intervention measures might not be the underlying source of heterogeneity. Combined with the results of subgroup analysis and sensitivity analysis, we discussed the heterogeneity between studies, considering that the heterogeneity between included studies was mainly related to the following aspects:

- 1) There were differences in the CMC components as well as the dosage regimens of intervention measures among studies;
- 2) The average age and disease course of the included participants were different, resulting in varying severity of the disease;
- 3) Due to the slow-acting of the herbal medicine, it usually takes several months after treatment to show significant therapeutic effects. However, the duration of intervention varies greatly from study to study, which may lead to the heterogeneity of the results.

Publication Bias

Analysis for publication bias was performed using Egger's test for endpoints of RF. Egger's asymmetry coefficient, known to be low powered, did detect potential bias in the meta-analysis of RF ($p < 0.01$). These publication bias may be due to the included studies were all published in Chinese. Moreover, all literature included had positive results, and the articles with negative results were often not able to be published, which caused publication bias to some extent. As described above, the publication bias could not be excluded.

Frequency Distribution Analysis

A total of 71 CMCs were recorded, and 156 single Chinese medicines were obtained, which were sorted by frequency of occurrence from high to low, we listed the Chinese medicine with a frequency of more than 10 times. There were a total of 26 traditional Chinese herbs (**Table 4**). The top five were *Angelica sinensis* (Oliv.) Diels [Apiaceae; *Radix Angelicae Sinensis*] (Danggui), *Glycyrrhiza glabra* L. [Fabaceae; *Radix Glycyrrhizae*] (Gancao), *Neolitsea cassia* (L.) Kosterm. [Lauraceae; *Ramulus Cinnamomi*] (Guizhi), *Paeonia lactiflora* Pall. [Paeoniaceae; *Radix Paeoniae Alba*] (Baishao), and *Angelica dahurica* (Hoffm.) Benth. & Hook.f. ex Franch. & Sav. [Apiaceae; *Radix Angelicae Pubescentis*] (Duhuo).

DISCUSSION

Main Findings

RF and anti-CCP belong to the serum biomarkers involved in the 2010 ACR/EULAR RA classification criteria, and they precede the onset of clinical symptoms and predict a more severe disease course, indicating a pathogenic role in RA (Kay and Upchurch, 2012).

There is a study confirmed that the combined presence of anti-CCP and IgM-RF mediates increased production of proinflammatory cytokine *in vitro* and this combination is associated with increased systemic inflammation and disease activity in RA (Moura et al., 2012). Accumulating evidences suggest that the presence of high titers of RF in combination with anti-CCP associated with increased disease activity, more aggressive arthritis, worse prognosis and reduced rates of remission in patients with RA (Jónsson et al., 1995; Moez et al., 2013; Sokolove et al., 2014; Valesini et al., 2015). Moreover, anti-

TABLE 4 | The frequency of Chinese medicine (more than 10 times of traditional Chinese medicine).

No.	Pinyin name	Full format	Frequency
1	Danggui	<i>Angelica sinensis</i> (Oliv.) Diels [Apiaceae; Radix Angelicae Sinensis]	38
2	Gancao	<i>Glycyrrhiza glabra</i> L.[Fabaceae; Radix Glycyrrhizae]	32
3	Guizhi	<i>Neolitsea cassia</i> (L.) Kosterm.[Lauraceae; Ramulus Cinnamomi]	27
4	Baishao	<i>Paeonia lactiflora</i> Pall.[Paeoniaceae; Radix Paeoniae Alba]	27
5	Duhuo	<i>Angelica dahurica</i> (Hoffm.) Benth. & Hook.f. ex Franch. & Sav. [Apiaceae; Radix Angelicae Pubescentis]	22
6	Chuanxiong	<i>Conioselinum anthriscoides</i> 'Chuanxiong'[Apiaceae; Rhizoma Ligustici]	21
7	Yiyiren	<i>Coix lacryma-jobi</i> L.[Poaceae; Semen Coicis]	18
8	Huangqi	<i>Astragalus mongholicus</i> Bunge[Fabaceae; Radix Astragali seu Hedysari]	17
9	Fangfeng	<i>Saposhnikovia divaricata</i> (Turcz. ex Ledeb.) Schischk. [Apiaceae; Radix Saposhnikoviae]	17
10	Weilingxian	<i>Clematis chinensis</i> Osbeck[Ranunculaceae; Radix Clematidis]	16
11	Shudihuang	<i>Rehmannia glutinosa</i> (Gaertn.) DC. [Orobanchaceae; Radix Rehmanniae Preparata]	16
12	Dilong	<i>Pheretima asiatica</i> Michaelsen[Megascopidae; Lumbricus]	15
13	Jixueteng	<i>Spatholobus suberectus</i> Dunn[Fabaceae; Caulis Spatholobi]	15
14	Qinjiao	<i>Gentiana macrophylla</i> Pall.[Gentianaceae; Radix Gentianae Macrophyllae]	13
15	Niuxi	<i>Achyranthes bidentata</i> Blume [Amaranthaceae; Radix Achyranthis Bidentatae]	13
16	Qianghuo	<i>Hanseria weberbaueriana</i> (Fedde ex H.Wolff) Pimenov & Kljuykov [Apiaceae; Rhizoma et Radix Notopterygii]	12
17	Chishao	<i>Paeonia lactiflora</i> Pall. [Paeoniaceae; Radix Paeoniae Rubra]	12
18	Cangzhu	<i>Atractylodes lancea</i> (Thunb.) DC.[Asteraceae; Rhizoma Atractylodis]	11
19	Rendongteng	<i>Lonicera japonica</i> Thunb. [Caprifoliaceae;Caulis Lonicerae]	11
20	Baizhu	<i>Atractylodes macrocephala</i> Koidz.[Asteraceae; Rhizoma Atractylodis Macrocephalae]	11
21	Sangjisheng	<i>Taxillus chinensis</i> (DC.) Danser[Loranthaceae; Herba Taxilli]	11
22	Wushaosheng	<i>Zaocys dhumnades</i> (Cantor) [Natricinae; Zaocys dhumnades]	11
23	Quanxie	<i>Buthus martensii</i> Karsch[Scorpiones; Scorpio]	11
24	Baijiezi	<i>Sinapis alba</i> L. [Brassicaceae; Semen sinapis.]	10
25	Mahuang	<i>Ephedra sinica</i> Stapf [Ephedraceae; Herba Ephedrae]	10
26	Huangbo	<i>Phellodendron amurense</i> Rupr. [Rutaceae; Cortex Phellodendri]	10

CCP not only has a great diagnostic value for RA in terms of sensitivity and specificity but also seem to be better predictors of poor prognostic features such as progressive joint destruction (Harre et al., 2012). In addition, anti-CCP status predicts response to therapy as well (Burska et al., 2014).

The observations suggest that RF and anti-CCP are capable of promoting a more accurate prognosis and by targeting these two markers will contribute to a better disease management. There is no doubt that underscores the utility of these autoantibodies in RA.

In China, CMC has a long history of treating RA, and several clinical trials have been conducted in recent years on the treatment of RA with CMC. However, to our knowledge, this is the first systematic review and meta-analysis of published RCTs to assess the effect of CMC in reducing the levels of serum RF and anti-CCP in patients with RA. We revealed that 65 RCTs observed the comparison between CMC or CMC combined with Western medicine and Western medicine monotherapy in the treatment of RA in terms of changing the serological markers RF and anti-CCP level. The pooled analysis showed that after treatment, serum RF and anti-CCP levels were decreased more significantly in the experimental group compared to the Western medicine control groups than at baseline. It indicated that CMC in the treatment of RA had a potential role in reducing serum RF and anti-CCP levels. In addition, we found that the CMC group had better ACR response and more effective clinical efficacy of TCM syndromes. The RR of ACR70 was higher than that of ACR20 and ACR50, and the proportion of patients achieving an ACR20 response was not significant than that of ACR50 and ACR70 response. This might be partially explained as

high heterogeneity as well as difference in effect estimates observed in ACR20. The study of Chen (Chen et al., 2010) might be the source of the heterogeneity, which was related to the contradiction between the results reported in his study with other studies. In the results of this study, the ACR20 response rate was lower in the experimental group than in the control group, and the difference was not statistically significant. In addition, in the meta-analysis of ACR50, we found that the two studies of Zhao (Zhao, 2015) and He (He and Xiao, 2014) showed a high confidence interval value, indicating lower external validity.

Furthermore, this study summarized the frequency of CMC constituent involved in 65 research literatures and found that the top five from high to low were *Angelica sinensis* (Oliv.) Diels [Apiaceae;Radix Angelicae Sinensis] (Danggui), *Glycyrrhiza glabra* L.[Fabaceae;Radix Glycyrrhizae] (Gancao), *Neolitsea cassia* (L.) Kosterm.[Lauraceae;Ramulus Cinnamomi] (Guizhi), *Paeonia lactiflora* Pall.[Paeoniaceae;Radix Paeoniae Alba] (Baishao), and *Angelica dahurica* (Hoffm.) Benth. & Hook.f. ex Franch. & Sav. [Apiaceae;Radix Angelicae Pubescentis] (Duhuo). The active ingredients and pharmacological effects of the above five high-frequency representative Chinese herb were summarized in Table 5, and as illustrated in this table, most of the main active ingredients of the five Chinese herbs have immunomodulatory effects. The polysaccharides isolated from *Angelica sinensis* (Oliv.) Diels [Apiaceae;Radix Angelicae Sinensis] (Danggui) can regulate the immune response by regulating expression of Th1 and Th2 related cytokines (Chen et al., 2013). Cinnamaldehyde is isolated from the essential oil produced from the *Neolitsea cassia* (L.) Kosterm.[Lauraceae;Ramulus Cinnamomi] (Guizhi), and it has been reported to reduce the release of pro-inflammatory

TABLE 5 | Main active ingredients, pharmacological effects and mechanisms of the top five Chinese medicine in frequency distribution.

Pinyin name	Full Format	Main active ingredients	Pharmacological effects and mechanisms
Danggui	Angelica sinensis (Oliv.) Diels [Apiaceae; Radix Angelicae Sinensis]	Polysaccharides	Immunomodulatory activity: regulating the expression of Th1- and Th2-related cytokines (Chen et al., 2013)
Gancao	Glycyrrhiza glabra L.[Fabaceae; Radix Glycyrrhizae]	Glycyrrhizin acid, Glycyrrhetic acid, Licorice flavonoids, Licorice polysaccharides	Anti-inflammatory: Inhibiting the transcriptions of iNOS, COX-2, TNF- α and IL-6 by blocking the activation of NF- κ B signaling pathways (Kim et al., 2008; Chang et al., 2010)
Guizhi	Neolitsea cassia (L.) Kosterm.[Lauraceae; Ramulus Cinnamomi]	Cinnamaldehyde	Immuno-modulating: Inhibiting the production of proinflammatory cytokines (IL-1 β , TNF- α , etc.) production within LPS, LTA and polyIC stimulated macrophages and monocytes (Chao et al., 2008)
Baishao	Paeonia lactiflora Pall.[Paeoniaceae; Radix Paeoniae Alba]	Total glucosides of paeony	Anti-inflammatory and immune-regulatory: Inhibiting the activation of macrophages NF- κ B and the release of inflammatory cytokines such as TNF- α , IL-1 β , IL-17, and inhibit the proliferation of B lymphocytes (Zhang et al., 2019; Zhang and Wei, 2020)
Duhuo	Angelica dahurica (Hoffm.) Benth. & Hook.f. ex Franch. & Sav. [Apiaceae; Radix Angelicae Pubescentis]	Angelicae Pubescentis Radix's volatile oil	Anti-inflammatory and analgesic: Inhibiting COX-1 and COX-2 to varying degrees (Fan et al., 2009; Qiu et al., 2011)

Th, T helper; iNOS, inducible nitric oxide synthase; COX-, cyclooxygenase-; TNF- α , tumor necrosis factor- α ; IL-, interleukin-; NF- κ B, nuclear factor-kappa B; LPS, lipopolysaccharide; LTA, lipoteichoic acid; polyIC, polyinosinic-polycytidylic acid.

cytokines by inhibiting the activation of macrophages and monocytes through suppression of the mitogen-activated protein kinases (MAPKs) signaling pathway (Chao et al., 2008). Total glycoside of paeony (TGP) is extracted from the dried root of *Paeonia lactiflora* Pall.[Paeoniaceae;Radix Paeoniae Alba] (Baishao). Paeoniflorin (Pae) is the major active component of TGP. Pae can balance the subsets of immune cells through inhibiting abnormal activated cell subsets and restoring regulatory cell subsets by integrating multiple signaling pathways, such as JAK2/STAT3 pathway, MAPKs/NF- κ B pathway, PI3K/Akt/mTOR pathway, etc. (Zhang et al., 2019; Zhang and Wei, 2020). It is well known that the pathogenesis of RA is related to B lymphocytes, and RF and anti-CCP are considered to be the results of B lymphocyte activation and differentiation into plasma cells (Cambridge et al., 2003; Dörner et al., 2004). One study confirmed through animal experiments that Pae inhibits the activation and proliferation of B cells by selectively blocking the LPS/TLR4 signaling pathway (Zhang et al., 2015). In addition, another study found that Pae can regulate PI3K/Akt/mTOR pathways mediated by BAFF (B-cell activating factor)/BAFF-R, thereby inhibiting antibody production by B lymphocytes in CIA rats. This may be one of the mechanisms of action of Pae to downregulate antibodies production and treat RA (Li et al., 2012b). Therefore, we figured that the mechanism by which TCM or CMC can reduce serum RF and anti-CCP levels might be related to the regulation of the immune response and inhibition of B lymphocytes proliferation.

Limitations for Research

There are some limitations in our systematic review. Firstly, since there has been no standardized CMC abroad, the above researches were all completed in China. Moreover, the foundation and clinical effects of CMC in other countries may be inconsistent with these data. With the successful development and proven definitive efficacy and safety of biologicals worldwide, biologicals are now more commonly used in the treatment of RA

in many places. However, their use is not common in China as Europe, which is due to the more expensive treatment price and economic cost of biologicals compared to traditional treatment options, and this is also one of the reasons why early, adequate, and full course use of biologicals is difficult for RA patients in many developing countries (Joyce et al., 2014). It follows that among the studies included in the systematic review and meta-analysis, we found that only one (Wei and Liu, 2013) of the interventions used biologicals. Therefore, the conclusions of this systematic review have some limitations. Secondly, the overall quality of the literature included was poor, and the design of the methodological part need to be improved. Most of the included studies had inadequate or missing descriptions of randomization, allocation concealment and blinding method, resulting in an inability to fully assess the internal validity of the trials. Additionally, the sample size of most studies was too small to perform robust analysis, which fundamentally affected the strength of synthesis evidence, and therefore resulting in the limitations and conservatism of this systematic review. Thirdly, due to the different dosage forms used in each study intervention (including decoction, capsule, tablet, pill, etc.), the composition and dosage of CMC administered were also different. These had led to a diversity of intervention measures with no uniform standard, which may lead to heterogeneity. If all CMC intervention measures are combined into the same category of treatment for analysis, the inferred results of meta-analysis would be limited to some extent. Finally, outcome measures and measuring instruments for RF and anti-CCP varied from studies.

CONCLUSION

In summary, CMC may be an effective treatment to treat RA. In terms of reducing the levels of RF and anti-CCP, CMC (or CMC combined with Western medicine) is more effective than only Western medicine.

Through a systematic review of the potency of CMC to change serum biomarkers levels and the clinical efficacy for the treatment of RA, we found that CMC may be a potential and efficacious therapeutic adjunct to delay the progression and improve outcomes of RA. In the future, RCTs with larger samples and higher quality should be carried out to provide more accurate and complete data to support and verify the potential of TCM compound in the treatment of RA.

DATA AVAILABILITY STATEMENT

The original contributions presented in the study are included in the article/**Supplementary Material**, further inquiries can be directed to the corresponding author.

AUTHOR CONTRIBUTIONS

RH and ZW conceived the study, participated in its design and coordination. XT, ZL, and ZY developed the search strategies. XT, ZL, and ZY conducted data collection, analysis and interpretation. XT drafted the paper. RH, ZW, MW, SX, and XC revised it. All authors have approved the final manuscript.

FUNDING

This study was supported by National Natural Science Foundation of China (No. 81804041), the special project of

State Key Laboratory of Dampness Syndrome of Chinese Medicine (SZ2020ZZ17), Guangdong Provincial Key laboratory of Chinese Medicine for Prevention and Treatment of Refractory Chronic Diseases (2018) (No. 2018B030322012), the 2020 Guangdong Provincial Science and Technology Innovation Strategy Special Fund (Guangdong-HongKong-Macau Joint Lab) (No: 2020B1212030006), Natural Science Foundation of Guangdong Province (No. 2021A1515011477, 2021A1515011593), grant from Guangzhou Basic Research Program (No. 202102010256), the China-Sweden Joint Research Base Project on TCM of Guangdong Provincial Hospital of Chinese Medicine (YN2020RD01), as well as grants from Guangdong Provincial Hospital of Chinese Medicine (No. MB2019ZZ07, YN10101906, YN2018ML08, YN2018ZD06).

ACKNOWLEDGMENTS

The authors thank Professor Bijlsma, EULAR Past-President, for his valuable advice to improve the quality of this study.

SUPPLEMENTARY MATERIAL

The Supplementary Material for this article can be found online at: <https://www.frontiersin.org/articles/10.3389/fphar.2021.686360/full#supplementary-material>

REFERENCES

- Aletaha, D., Neogi, T., Silman, A. J., Funovits, J., Felson, D. T., Bingham, C. O., et al. (2010). 2010 Rheumatoid Arthritis Classification Criteria: An American College of Rheumatology/European League against Rheumatism Collaborative Initiative. *Arthritis Rheum.* 62 (9), 2569–2581. doi:10.1002/art.27584
- Arnett, F. C., Edworthy, S. M., Bloch, D. A., McShane, D. J., Fries, J. F., Cooper, N. S., et al. (1988). The American Rheumatism Association 1987 Revised Criteria for the Classification of Rheumatoid Arthritis. *Arthritis Rheum.* 31 (3), 315–324. doi:10.1002/art.1780310302
- Begg, C. B., and Mazumdar, M. (1994). Operating Characteristics of a Rank Correlation Test for Publication Bias. *Biometrics* 50 (4), 1088–1101. doi:10.2307/2533446
- Bian, Z. Q., and Wang, Y. D. (2018). Warm Yang Dehumidification, Phlegm Tongluo Prescription Combined with Conventional Therapy to Treat 90 Cases of Cold and Dampness Bizu Rheumatoid Arthritis. *Glob. Chin. Med.* 11 (03), 447–450.
- Burska, A. N., Hunt, L., Boissinot, M., Strollo, R., Ryan, B. J., Vital, E., et al. (2014). Autoantibodies to Posttranslational Modifications in Rheumatoid Arthritis. *Mediators Inflamm.* 2014, 492873. doi:10.1155/2014/492873
- Cambridge, G., Leandro, M. J., Edwards, J. C. W., Ehrenstein, M. R., Salden, M., Bodman-Smith, M., et al. (2003). Serologic Changes Following B Lymphocyte Depletion Therapy for Rheumatoid Arthritis. *Arthritis Rheum.* 48 (8), 2146–2154. doi:10.1002/art.11181
- Cao, M. Z., Wang, Z. L., and Jiang, X. S. (2020). Clinical Efficacy of Modified Duhuo Jisheng Decoction Combined with Methotrexate in Treatment of Patients with Rheumatoid Arthritis of Active Stage. *China J. Pharm. Econ.* 15 (04), 55–58+62.
- Cao, Y. H., and Liu, J. (2014). Clinical Observation of Heat Clearing and Wetting Combined with Western Medicine in the Treatment of Dampness-Heat Type Rheumatoid Arthritis. *J. Anhui Univ. Chin. Med.* 33 (06), 19–22.
- Chang, Y.-L., Chen, C.-L., Kuo, C.-L., Chen, B.-c., and You, J.-s. (2010). Glycyrrhetic Acid Inhibits ICAM-1 Expression via Blocking JNK and NF- κ B Pathways in TNF- α -Activated Endothelial Cells. *Acta Pharmacol. Sin.* 31 (5), 546–553. doi:10.1038/aps.2010.34
- Chao, L. K., Hua, K.-F., Hsu, H.-Y., Cheng, S.-S., Lin, I.-F., Chen, C.-J., et al. (2008). Cinnamaldehyde Inhibits Pro-inflammatory Cytokines Secretion from Monocytes/macrophages through Suppression of Intracellular Signaling. *Food Chem. Toxicol.* 46 (1), 220–231. doi:10.1016/j.fct.2007.07.016
- Chen, F., Min, C. H., Zhou, Y., and Zhang, H. Y. (2016). Clinical Observation of 35 Cases of Rheumatoid Arthritis of Kidney Qi Deficiency and Cold Type Treated by Antshen Juanbi Capsule Combined with Western Medicine. *J. Traditional Chin. Med.* 57 (12), 1045–1048.
- Chen, X.-P., Li, W., Xiao, X.-F., Zhang, L.-L., and Liu, C.-X. (2013). Phytochemical and Pharmacological Studies on Radix Angelica Sinensis. *Chin. J. Nat. Medicines* 11 (6), 577–587. doi:10.1016/s1875-5364(13)60067-9
- Chen, Z., Sun, J., Li, Y. M., and Chen, Y. Q. (2010). Efficacy of Shenshi Qianghuo Dihuang Decoction in Rheumatoid Arthritis: a Randomized Controlled Trial. *J. Chin. Integr. Med.* 8 (1), 35–39. doi:10.3736/jcim20100107
- Dörner, T., Egerer, K., Feist, E., and Burmester, G. R. (2004). Rheumatoid Factor Revisited. *Curr. Opin. Rheumatol.* 16 (3), 246–253. doi:10.1097/00002281-200405000-00013
- Fan, L., Li, L., and He, H. F. (2009). Study on the Anti-inflammatory and Analgesic Pharmacological Effects of Volatile Oil. *Anhui Med. Pharm. J.* 13 (02), 133–134.
- Fang, X. G., Wang, M., Chen, H. Y., Bai, Z. X., Chen, Z. F., and Lan, P. M. (2019). Self-designed Tongluo Powder Combined with Leflumide in the Treatment of

- Wind-Cold and Rheumatism Type Rheumatoid Arthritis and its Effect on Serum WNT-3 and BMP-2 Levels. *Mod. J. Integrated Traditional Chin. West. Med.* 28 (13), 1408–1411+1453.
- Felson, D. T., Anderson, J. J., Boers, M., Bombardier, C., Furst, D., Goldsmith, C., et al. (1995). American College of Rheumatology Preliminary Definition of Improvement in Rheumatoid Arthritis. *Arthritis Rheum.* 38 (6), 727–735. doi:10.1002/art.1780380602
- Forslind, K., Ahlmen, M., Eberhardt, K., Hafstrom, I., and Svensson, B. (2004). Prediction of Radiological Outcome in Early Rheumatoid Arthritis in Clinical Practice: Role of Antibodies to Citrullinated Peptides (Anti-CCP). *Ann. Rheum. Dis.* 63 (9), 1090–1095. doi:10.1136/ard.2003.014233
- Gao, D., and Bu, S. S. (2017). Clinical Research on Liuwei Dihuang Tang and Siwu Tang Treatment of Rheumatoid Arthritis. *ACTA Chin. Med.* 32 (06), 1079–1081.
- Ge, S. (2018). Observation on the Curative Effect of Combined Chinese and Western Medicine on Rheumatoid Arthritis. *J. Pract. Traditional Chin. Med.* 34 (11), 1371–1372.
- Green, S., and Higgins, J. P. T. (2008). *Cochrane Handbook for Systematic Reviews of Interventions*. Chichester, England: Wiley-Blackwell.
- Guo, H. L., Wang, G., and Tian, J. X. (2018). Yukang Pills Combined with Methotrexate Tablets in the Treatment of 40 Cases of Rheumatoid Arthritis. *TCM Res.* 31 (11), 23–26.
- Guo, H. M., Guo, L. W., and Xing, J. Y. (2017). Clinical Observation on 340 Cases of Rheumatoid Arthritis Treated by Ant Tongbi Capsule. *World Chin. Med.* 12 (08), 1859–1862.
- Han, L., Ba, Y., Gu, J. N. T. H., Shi, R., Ba, H. E. G. L., and Wei, R. (2016). Effect of Removing Wind, Dehumidifying and Tonifying Kidney in the Treatment of Senile Rheumatoid Arthritis and the Influence of Antibody Levels against Cyclic Citrulline Polypeptide, Rheumatoid Factor, Erythrocyte Sedimentation Rate, C-Reactive Protein and Keratin. *Chin. J. Gerontol.* 36 (18), 4558–4560.
- Han, S. L., and Song, Y. W. (2011). A Randomized Controlled Study of Eliminating Phlegm, Eliminating Stasis and Eliminating Rheum in the Treatment of Rheumatoid Arthritis. *Chin. Arch. Traditional Chin. Med.* 29 (12), 2808–2810.
- Harre, U., Georgess, D., Bang, H., Bozec, A., Axmann, R., Ossipova, E., et al. (2012). Induction of Osteoclastogenesis and Bone Loss by Human Autoantibodies against Citrullinated Vimentin. *J. Clin. Invest.* 122 (5), 1791–1802. doi:10.1172/jci60975
- He, D. C., and Xiao, J. J. (2014). Clinical Efficacy and Safety of Bizhengning in the Treatment of Rheumatoid Arthritis. *Mod. J. Integrated Traditional Chin. West. Med.* 23 (28), 3090–3092+3095.
- He, D., Liu, Z., Wang, M., Shu, Y., Zhao, S., Song, Z., et al. (2019). Synergistic Enhancement and Hepatoprotective Effect of Combination of Total Phenolic Extracts of Citrus Aurantium L. And Methotrexate for Treatment of Rheumatoid Arthritis. *Phytotherapy Res.* 33 (4), 1122–1133. doi:10.1002/ptr.6306
- Higgins, J. P. T., Thompson, S. G., Deeks, J. J., and Altman, D. G. (2003). Measuring Inconsistency in Meta-Analyses. *BMJ* 327 (7414), 557–560. doi:10.1136/bmj.327.7414.557
- Hu, H. (2018). Short-term and Long-Term Effects of Applying Traditional Chinese Medicine Syndrome Differentiation Combined with Methotrexate in the Treatment of Rheumatoid Arthritis. *J. Sichuan Traditional Chin. Med.* 36 (02), 76–79.
- Huang, G. D., Li, J. B., Huang, D. F., Huang, Y. H., Xiao, M. Z., Tang, L. J., et al. (2006). Observation on Effect of Centipede Longsnake Decoction Combined with Western Medicine in Treating Rheumatoid Arthritis. *Chin. J. Clin. Rehabil.* 43, 186–187.
- Jia, F. Y., Wang, J., and Yang, Q. B. (2016). A Clinical Study on Treatment of Rheumatoid Arthritis by Eliminating Rheum Nourishing the Liver and Yishen Decoction. *Asia-Pacific Traditional Med.* 12 (05), 143–144.
- Jiang, D., and Wu, J. (2016). Analysis and Evaluation of the Curative Effect of Self-Prepared Chinese Medicine Combined with Anti-rheumatism Medicine on Active Rheumatoid Arthritis. *J. Mod. Med. Health* 32 (22), 3507–3510.
- Jiang, P., and Ma, L. J. (2020). Clinical Study on the Treatment of Rheumatoid Arthritis by Removing Phlegm and Removing Blood Stasis. *China Cont. Med. Edu.* 12 (17), 158–160.
- Jónsson, T., Arinbjarnarson, S., Thorsteinsson, J., Steinsson, K., Geirsson, Á. J., Jónsson, H., et al. (1995). Raised IgA Rheumatoid Factor (RF) but Not IgM RF or IgG RF Is Associated with Extra-articular Manifestations in Rheumatoid Arthritis. *Scand. J. Rheumatol.* 24 (6), 372–375. doi:10.3109/03009749509095183
- Joyce, A. T., Gandra, S. R., Fox, K. M., Smith, T. W., and Pill, M. W. (2014). National and Regional Dose Escalation and Cost of Tumor Necrosis Factor Blocker Therapy in Biologic-Naïve Rheumatoid Arthritis Patients in US Health Plans. *J. Med. Econ.* 17 (1), 1–10. doi:10.3111/13696998.2013.856314
- Kay, J., and Upchurch, K. S. (2012). ACR/EULAR 2010 Rheumatoid Arthritis Classification Criteria. *Rheumatology* 51 (Suppl. 6), vi5–vi9. doi:10.1093/rheumatology/kes279
- Kim, J.-Y., Park, S. J., Yun, K.-J., Cho, Y.-W., Park, H.-J., and Lee, K.-T. (2008). Isoliquiritigenin Isolated from the Roots of Glycyrrhiza Uralensis Inhibits LPS-Induced iNOS and COX-2 Expression via the Attenuation of NF-Kb in RAW 264.7 Macrophages. *Eur. J. Pharmacol.* 584 (1), 175–184. doi:10.1016/j.ejphar.2008.01.032
- Li, A. M. (2009). Siteng Yin and Siwu Tang Were Used to Treat 160 Cases of Rheumatoid Arthritis. *Chin. ethnic folk Med.* 18 (10), 51–52.
- Li, D. (2020). Effect of Huatan Huoxue Formula on Swollen Joint Count index and Joint Pain Index in Patients with Phlegm and Blood Stasis Type of Rheumatoid Arthritis. *J. Med. Forum* 41 (04), 91–94.
- Li, J., Rong, B., Jia, J., and Pan, M. Z. (2017). Effect of Modified Juanbitang on Inflammatory Factors and Serum MMP-3OPG and ANKL in Synovial Fluid of Patients with Wind-Cold-Wetness Type Rheumatoid Arthritis. *Chin. J. Exp. Traditional Med. Formulae* 23 (22), 165–170.
- Li, J. H., Lin, Y. B., Yu, G. S., Zhang, S. X., Liu, Y. Y., and Xu, H. B. (2019). Clinical Observation on Treating 41 Cases of Rheumatoid Arthritis of Mixed Heat and Cold Type with Guizhi Shaoyao Zhimu Tang Combined with Methotrexate. *Rheum. Arthritis* 8 (02), 31–34+42.
- Li, J. P. (2013). Clinical Analysis of 40 Cases of Rheumatoid Arthritis Treated by Combination of Chinese and Western Medicine. *J. Sichuan Traditional Chin. Med.* 31 (01), 86–88.
- Li, P.-P., Liu, D.-D., Liu, Y.-J., Song, S.-S., Wang, Q.-T., Chang, Y., et al. (2012). BAFF/BAFF-R Involved in Antibodies Production of Rats with Collagen-Induced Arthritis via PI3K-Akt-mTOR Signaling and the Regulation of Paeoniflorin. *J. Ethnopharmacology* 141 (1), 290–300. doi:10.1016/j.jep.2012.02.034
- Li, S. W. (2006). Clinical Observation on Treatment of Rheumatoid Arthritis by Sanbi Decoction. *Chin. Arch. Traditional Chin. Med.* (09), 1738–1739.
- Li, X., Liu, J. F., and Zhao, G. Q. (2015). Clinical Observation on the Treatment of Rheumatoid Arthritis by Adding or Subtracting Judanxi Gout Prescription Combined with Methotrexate. *Anhui Med. J.* 36 (08), 995–998.
- Li, Y., Fan, W. M., Gu, S. F., and Liu, W. H. (2015). Clinical Observation of Kidney-Tonifying Collateral-Activating Blood-Activating Formula in Treating Rheumatoid Arthritis with Mutual junction of Phlegm and Blood Stasis. *J. Anhui Univ. Chin. Med.* 34 (04), 17–20.
- Li, Z. L., Wang, R. S., Shen, J., Xu, L. M., Yue, T., Zhu, Q., et al. (2012). Effect of Tonifying Kidney and Removing Blood Stasis on Bone Metabolism in Patients with Early Rheumatoid Arthritis. *J. Traditional Chin. Med.* 53 (03), 215–218.
- Liu, B., Liu, W., and Wang, Y. (2007). Siwu Decoction Combined with Methotrexate Attenuated and Effective Treatment for Rheumatoid Arthritis. *Chin. J. Integr. Med.* 27 (1).
- Liu, E. C., Liu, Y., Wang, S. H., and Wang, S. F. (2013). Clinical Observation on the Treatment of Rheumatoid Arthritis with Lumbago Capsule. *Clin. J. Traditional Chin. Med.* 25 (02), 109–111.
- Liu, X. D., Zhang, J. L., Ye, L. H., Liu, F. Y., and Chen, Y. (2009). Effect of Wenhua Juanbi Prescription on TNF and IL-1 in Peripheral Blood of Patients with Rheumatoid Arthritis. *Chin. J. Integr. Med.* 29 (09), 787–790.
- Liu, Y., Zhang, H. J., Guo, Y. X., and Meng, Q. L. (2016). Clinical Observation of 35 Cases of Rheumatoid Arthritis of Damp Heat Type Treated with Si Miao San He Xuan Bi Tang and Western Medicine. *World J. Integrated Traditional West. Med.* 11 (6), 800–803.
- Luo, Y. H. (2008). 32 Cases of Senile Rheumatoid Arthritis Were Treated with Spleen-Invigorating and Blood-Activating Formula. *Shaanxi J. Tradit Chin. Med.* (08), 997–999.
- Ma, W. K., Zhong, Q., Liu, Z. Q., and Yao, X. M. (2009). Clinical Study on the Treatment of Rheumatoid Arthritis by Sanwu Capsule Combined with Methotrexate and Salazosulphapyridine. *J. New Chin. Med.* 41 (11), 42–44.

- Ma, Z. L., Wang, C. Y., and Liu, B. B. (2018). Clinical Observation of Buyang Huanwu Decoction in Treating Phlegm and Blood Stasis Type Rheumatoid Arthritis. *Mod. J. Integrated Traditional Chin. West. Med.* 27 (12), 1313–1315.
- Moez, S., John, P., and Bhatti, A. (2013). Anti-citrullinated Protein Antibodies: Role in Pathogenesis of RA and Potential as a Diagnostic Tool. *Rheumatol. Int.* 33 (7), 1669–1673. doi:10.1007/s00296-012-2635-6
- Moura, R. A., Graca, L., and Fonseca, J. E. (2012). To B or Not to B the Conductor of Rheumatoid Arthritis Orchestra. *Clinic Rev. Allerg Immunol.* 43 (3), 281–291. doi:10.1007/s12016-012-8318-y
- Ngian, G. S. (1999). Rheumatoid Arthritis. *Nat. Rev. Dis. Primers* 4:18002. doi:10.1038/nrdp.2018.2
- Niu, J. H. (2014). Observation on the Curative Effect of Guizhi Peony Zhimu Decoction Combined with Juanyu Decoction and Juanyu Decoction in Treating Rheumatoid Arthritis. *Shaanxi J. Tradit Chin. Med.* 35 (08), 984–986.
- Pang, A. M., Jiang, P., Li, J. X., and Chi, X. W. (2017). Effects of Hebi Formula on Bone Erosion in Early Rheumatoid Arthritis of Liver and Spleen Disorder Type. *Chin. J. Traditional Chin. Med.* 32 (12), 5682–5685.
- Pang, J., Xu, J., Li, L., and Li, Y. L. (2019). Clinical Study of Guikun Fengshi Mixture Combined with Methotrexate in the Treatment of Rheumatoid Arthritis. *Pharmacol. Clin. Chin. Mater. Med.* 35 (05), 155–158.
- Qian, X., Chen, X., Wei, G., Guo, Y. K., and Sun, Z. L. (2016). Clinical Effect of Duhuo Jisheng Tang Combined with Meloxicam in Treatment of Rheumatoid Arthritis. *Chin. J. Exp. Traditional Med. Formulae* 22 (7), 173–176.
- Qiu, J. B., Xu, Q., and Jiang, X. H. (2011). Effects of Ethanol Extract of Angelicae Pubescentis Radix on Cyclooxygenase. *China Med. Herald* 8 (16), 42–43.
- Rainsford, K. D. (1999). Profile and Mechanisms of Gastrointestinal and Other Side Effects of Nonsteroidal Anti-inflammatory Drugs (NSAIDs). *Am. J. Med.* 107 (6A), 27–35. doi:10.1016/s0002-9343(99)00365-4
- Ronneld, J., Wick, M. C., Lampa, J., Lindblad, S., Nordmark, B., Klareskog, L., et al. (2005). Longitudinal Analysis of Citrullinated Protein/peptide Antibodies (Anti-CP) during 5 Year Follow up in Early Rheumatoid Arthritis: Anti-CP Status Predicts Worse Disease Activity and Greater Radiological Progression. *Ann. Rheum. Dis.* 64 (12), 1744–1749. doi:10.1136/ard.2004.033571
- Schoels, M., Bombardier, C., and Aletaha, D. (2011). Diagnostic and Prognostic Value of Antibodies and Soluble Biomarkers in Undifferentiated Peripheral Inflammatory Arthritis: a Systematic Review. *J. Rheumatol. Suppl.* 87, 20–25. doi:10.3899/jrheum.101070
- Shen, H.-b., Bai, Y.-j., Huo, Z.-j., Li, W.-n., and Tang, X.-p. (2011). Assessment of Clinical Effect of Therapy Combining Disease with Syndrome on Rheumatoid Arthritis. *J. Traditional Chin. Med.* 31 (1), 39–43. doi:10.1016/s0254-6272(11)60009-5
- Shen, Y. P., Chuan, X. W., and Liu, Y. (2008). Effect of Nourishing Yin and Supplementing Qi on Hormone Withdrawal in Rheumatoid Arthritis. *Shandong J. Traditional Chin. Med.* (02), 95–96.
- Shi, L., and Yang, F. (2018). 40 Cases of Rheumatoid Arthritis Were Treated by Renal Differentiation. *J. Shaanxi Univ. Traditional Chin. Med.* 041 (001), 66–69.
- Shu, C., Hua, D. P., and Li, Y. (2015). Clinical Observation on Yishen Qingluo Huoxue Formula in Treatment of Intermingled Phlegm and Blood Stasis Type of Rheumatoid Arthritis. *Chin. Arch. Traditional Chin. Med.* 33 (01), 34–37.
- Sokolove, J., Johnson, D. S., Lahey, L. J., Wagner, C. A., Cheng, D., Thiele, G. M., et al. (2014). Rheumatoid Factor as a Potentiator of Anti-citrullinated Protein Antibody-Mediated Inflammation in Rheumatoid Arthritis. *Arthritis Rheumatol.* 66 (4), 813–821. doi:10.1002/art.38307
- Song, W. H., Li, Q., Wang, F. Z., Tao, W. X., and Guan, Q. C. R. (2019). Effects of Wenyang Bushen Method on the Levels of Serum 25 Hydroxyvitamin D3 in Patients with Plateau Rheumatoid Arthritis. *World Chin. Med.* 14 (6), 1466–1470.
- Su, S. Z., Ye, X. Y., Peng, J. H., and Chen, B. (2015). Clinical Observation on Treating Rheumatoid Arthritis by Bushen Huoxue Therapy. *Clin. J. Chin. Med.* (13), 18–20.
- Valesini, G., Gerardi, M. C., Iannuccelli, C., Pacucci, V. A., Pendolino, M., and Shoenfeld, Y. (2015). Citrullination and Autoimmunity. *Autoimmun. Rev.* 14 (6), 490–497. doi:10.1016/j.autrev.2015.01.013
- van Venrooij, W. J., van Beers, J. J. B. C., and Pruijn, G. J. M. (2008). Anti-CCP Antibody, a Marker for the Early Detection of Rheumatoid Arthritis. *Ann. N. Y. Acad. Sci.* 1143, 268–285. doi:10.1196/annals.1443.013
- Wang, H. T. (2017). Clinical Research on Treating Rheumatoid Arthritis by the Buyi Qixue, Qushi Tongluo Therapy. *Clin. J. Chin. Med.* 9 (27), 62–63.
- Wang, S. M., Wang, X., and Gong, Q. (2006). Observation of 40 Cases of Rheumatoid Arthritis Treated by Combination of Traditional Chinese and Western Medicine. *J. Sichuan Traditional Chin. Med.* (06), 47–48.
- Wang, W., Zhou, H., and Liu, L. (2018). Side Effects of Methotrexate Therapy for Rheumatoid Arthritis: A Systematic Review. *Eur. J. Med. Chem.* 158, 502–516. doi:10.1016/j.ejmech.2018.09.027
- Wang, Y., and Tu, S. H. (2017). Clinical Study on Modified Wutou Decoction in Treatment of Rheumatoid Arthritis. *ACTA Chin. Med.* 32 (09), 1716–1719.
- Wang, Z., and Tao, X. J. (2014). [Treatment of Rheumatoid Arthritis by Yangxue Tongluo Recipe Combined with Immunosuppressive Agents: a Clinical Observation]. *Zhongguo Zhong Xi Yi Jie He Za Zhi* 34 (3), 276–278.
- Wei, W., and Liu, K. K. (2013). Clinical Observation of Traditional Chinese Medicine Combined with Etanercept in Treatment of Elderly Rheumatoid Arthritis. *Chin. Arch. Traditional Chin. Med.* 31 (04), 939–941.
- Wei, Y., Yang, X. M., and Wang, S. E. (2013). Clinical Observation of 50 Cases of Active Rheumatoid Arthritis Treated by Combination of Chinese and Western Medicine. *Sci. Tech. Chin. Traditional Med.* 20 (1), 54–55.
- Xiang, C. C., Xiong, Q. D., and Wu, J. Y. (2009). 40 Cases of Rheumatoid Arthritis Were Treated with Bushendecotion and Western Medicine. *Shaanxi J. Tradit Chin. Med.* 30 (12), 1614–1616.
- Xu, G. S., Yu, X. F., Kong, M. Z., Chen, J. C., and Qiu, M. S. (2018). Clinical Observation on the Treatment of Rheumatoid Arthritis with Heat and Blood Stasis by Traditional Chinese Medicine Therapy of Clearing Heat and Activating Blood Circulation. *Chin. J. Traditional Chin. Med.* 33 (03), 1167–1170.
- Yang, B., Liang, Q. H., Wu, D., Tang, T., and Peng, W. J. (2011). Clinical Observation of Simiao Pill Combined with Western Medicine in Treating 20 Cases of Active Rheumatoid Arthritis. *J. Traditional Chin. Med.* 52 (18), 1566–1569.
- Yang, Y. J. (2013). Treatment of 42 Cases of Rheumatoid Arthritis with Compound Ma Qian Zisan. *China Pharm.* 22 (2), 84–85.
- Yao, J. H. (2010). Clinical Observation of 58 Cases of Rheumatoid Arthritis Treated by Heat Bi Decoction. *J. Traditional Chin. Med.* 51 (12), 1086–1088.
- You, B. R., Tian, X. W., and Liu, C. J. (2016). Clinical Observation of Liuwei Dihuanghe Siwu Decoction Combined with Methotrexate in the Treatment of Rheumatoid Arthritis. *Guiding J. TCM* 22 (6), 95–97.
- Yu, M., and Chen, Y. Y. (2014). Observation on Effect of Integrated Chinese Medicine and Western Medicine on 32 Patients with Rheumatoid Arthritis. *Intern. Med. China* 9 (01), 12–14.
- Yuan, L., Wu, J. Y., Tang, J., Chen, Y. G., and Zhang, Z. Y. (2019). Clinical Observation of Baihu Plus Guizhi Decoction Combined with Western Medicine in Treating Rheumatoid Arthritis with Rheumatic Heat Arthralgia Syndrome. *J. Liaoning Univ. TCM* 21 (12), 168–171.
- Zeng, J. Y., and Chen, S. K. (2018). The Clinical Effect of Traditional Chinese Medicine Combined with Antirheumatic Drugs on Rheumatoid Arthritis. *Clin. J. Chin. Med.* 10 (27), 82–83.
- Zeng, X. F., Zhu, S. L., Tan, A. C., and Xie, X. P. (2013). Disease Burden and Quality of Life of Rheumatoid Arthritis in China: A Systematic Review. *Chin. J. Evid-based Med.* 13 (03), 300–307.
- Zhang, H. J., and Chen, T. B. (2014). Clinical Observation of Clearing Damp Analgesic Decoction Combined with Meloxicam in Treatment of Rheumatoid Arthritis. *Shaanxi J. Tradit Chin. Med.* 10, 1336–1338.
- Zhang, J., Li, H., Huo, R., Zhai, T., Li, H., Sun, Y., et al. (2015). Paeoniflorin Selectively Inhibits LPS-Provoked B-Cell Function. *J. Pharmacol. Sci.* 128 (1), 8–16. doi:10.1016/j.jphs.2015.02.011
- Zhang, K. L. (2019). Research on the Clinical Effect of Integrated Chinese and Western Medicines in Treatment of 47 Cases of Rheumatoid Arthritis. *Chin. ethnic folk Med.* 28 (11), 83–85.
- Zhang, L., and Wei, W. (2020). Anti-inflammatory and Immunoregulatory Effects of Paeoniflorin and Total Glucosides of Paeony. *Pharmacol. Ther.* 207, 107452. doi:10.1016/j.pharmthera.2019.107452
- Zhang, L., Yu, J., Wang, C., and Wei, W. (2019). The Effects of Total Glucosides of Paeony (TGP) and Paeoniflorin (Pae) on Inflammatory-Immune Responses in

- Rheumatoid Arthritis (RA). *Funct. Plant Biol.* 46 (2), 107–117. doi:10.1071/fp18080
- Zhao, F. C. (2015). Observation on the Curative Effect of Combined Chinese and Western Medicine on Rheumatoid Arthritis. *Mod. J. Integrated Traditional Chin. West. Med.* 24 (19), 2107–2109.
- Zhao, L. (2019). Clinical Efficacy of the Guizhi Shaoyao Zhimu Decoction on Rheumatoid Arthritis of the Fenghan Shibi Type. *Clin. J. Chin. Med.* 11 (34), 51–53.
- Zheng, X. B., and Shi, C. H. (2015). Zhuithmg Tougu Capsules Combined with Methotmxate on the Treatment of Rheumatoid Arthritis for 80 Cases. *Chin. Med. Mod. distance Educ.* 13 (09), 63–65.
- Zheng, X. Y. (2002). *Guiding Principles for Clinical Research of New Chinese Medicines*. Beijing: China Medical Science and Technology Press.
- Zhou, C. Y., Tang, J. Y., Fang, D. Y., Pan, Z., and Ma, F. (2010). A Clinical Study on Simiao Xiaobi Decoction in the Treatment of Rheumatoid Arthritis in Active Stage. *Chin. J. Integr. Med.* 30 (03), 275–279.
- Conflict of Interest:** The authors declare that the research was conducted in the absence of any commercial or financial relationships that could be construed as a potential conflict of interest.

Copyright © 2021 Tang, Liu, Yang, Xu, Wang, Chen, Wen and Huang. This is an open-access article distributed under the terms of the Creative Commons Attribution License (CC BY). The use, distribution or reproduction in other forums is permitted, provided the original author(s) and the copyright owner(s) are credited and that the original publication in this journal is cited, in accordance with accepted academic practice. No use, distribution or reproduction is permitted which does not comply with these terms.



Salvianolate Ameliorates Osteopenia and Improves Bone Quality in Prednisone-Treated Rheumatoid Arthritis Rats by Regulating RANKL/RANK/OPG Signaling

Xiang Gao^{1,2†}, Qingyun Wu^{1,3†}, Xinle Zhang^{1†}, Jia Tian¹, Dahong Liang¹, Yalin Min¹, Jiaqi Lu¹, Xuemei Zhang¹, Liao Cui², Bilian Xu^{1*} and Yanzhi Liu^{1,4*}

OPEN ACCESS

Edited by:

Yihai Wang,
Guangdong Pharmaceutical
University, China

Reviewed by:

Jwu-Lai Yeh,
Kaohsiung Medical University, Taiwan
Cecilia Engdahl,
University of Gothenburg, Sweden
Hong Xing Zheng,
Shaanxi University of Technology,
China

*Correspondence:

Bilian Xu
xubilianq@126.com
Yanzhi Liu
liuyanzhi02@163.com

[†]These authors have contributed
equally to this work

Specialty section:

This article was submitted to
Ethnopharmacology,
a section of the journal
Frontiers in Pharmacology

Received: 15 May 2021

Accepted: 23 August 2021

Published: 06 September 2021

Citation:

Gao X, Wu Q, Zhang X, Tian J, Liang D,
Min Y, Lu J, Zhang X, Cui L, Xu B and
Liu Y (2021) Salvianolate Ameliorates
Osteopenia and Improves Bone
Quality in Prednisone-Treated
Rheumatoid Arthritis Rats by
Regulating RANKL/RANK/
OPG Signaling.
Front. Pharmacol. 12:710169.
doi: 10.3389/fphar.2021.710169

¹Department of Pharmacology, Guangdong Key Laboratory for Research and Development of Natural Drug, Guangdong Medical University, Zhanjiang, China, ²Stem Cell Research and Cellular Therapy Center, The Affiliated Hospital of Guangdong Medical University, Zhanjiang, China, ³Department of Pharmacy, Yangjiang People's Hospital, Yangjiang, China, ⁴Clinic Research Institute of Zhanjiang, Affiliated Central People's Hospital of Zhanjiang of Guangdong Medical University, Zhanjiang, China

Rheumatoid arthritis (RA) is closely associated with periarticular osteopenia and leads to a high risk of generalized osteoporosis. Although glucocorticoid (GC) treatment ameliorates joint degradation and manages inflammation in RA, GC application may induce further bone quality deterioration in RA patients. Current treatments for RA lack relevant strategies for the prevention and treatment of osteopenia in RA. In this study, we aimed to investigate whether salvianolate treatment ameliorated osteopenia in prednisone-treated RA rats. Lewis rats with collagen-induced arthritis (CIA) were administered prednisone (PDN) or PDN plus salvianolate (PDN+Sal) treatment for 90 days. The effects of Sal were investigated in PDN-treated CIA rats. To further evaluate the effects of Sal under inflammatory conditions, we investigated the effects of Sal treatment on the TNF- α -induced inflammatory response in MC3T3-E1 osteoblasts. Bone histomorphometry, bone mineral density (BMD), bone biomechanical properties, micro-computed tomography (micro-CT), immunohistochemistry, RT-PCR and western blot analyses were performed to evaluate the effects of Sal. The results demonstrated that RA induced bone loss and bone quality deterioration, with high bone turnover in CIA rats. PDN+Sal treatment significantly increased BMD and trabecular/cortical bone mass, suppressed inflammation, and improved bone biomechanical properties compared to CIA control and PDN treatment. PDN+Sal treatment significantly suppressed bone resorption and the RANKL and RANKL/OPG ratios compared to PDN. PDN+Sal and PDN treatment significantly inhibited TNF- α by 82 and 83%, respectively, and both suppressed inflammation in CIA rats. However, there was no significant difference between PDN+Sal and PDN treatment alone in regard to bone formation parameters or the management of inflammation and arthropathy. Sal significantly increased Osterix, OPN, and Col1a1 while decreasing RANKL, TRAF6, and TRAIL gene in TNF- α -induced MC3T3-E1 osteoblasts. Sal significantly increased Osterix, OPN and RUNX2 while decreasing NF- κ B, TRAF6 and IL-1 β protein in TNF- α -induced MC3T3-E1 osteoblasts.

The results suggested that salvianolate treatment ameliorated osteopenia and improved bone quality in prednisone-treated RA rats, and the potential mechanism may be related to the regulation of the RANKL/RANK/OPG signaling pathway, TRAIL-TRAF6-NF κ B signal axis, and downregulation of inflammatory cytokines. Salvianolate could be used as a promising supplemental therapeutic strategy to ameliorate osteopenia and improve bone quality in GC-treated RA patients.

Keywords: rheumatoid arthritis, osteoporosis, salvianolate, glucocorticoid, collagen-induced arthritis, rats

INTRODUCTION

Rheumatoid arthritis (RA) is a chronic inflammatory disease that often leads to severe joint damage, disability and even death (Guler-Yuksel et al., 2010). Bone loss and bone erosion around joints are serious issues in RA. RA is closely associated with periarticular osteopenia and leads to a high risk of generalized osteoporosis (Fassio et al., 2016; Okano et al., 2017; Coury et al., 2019). Current treatments for RA, such as nonsteroidal anti-inflammatory drugs (NSAIDs), disease-modifying antirheumatic drugs (DMARDs), biologics and glucocorticoids (GCs), have limited bone protection effects and even accelerate bone loss around joints or induce generalized osteopenia. GCs play an important role in the treatment of severe RA patients. Their potent anti-inflammatory effect significantly ameliorates RA symptoms; however, their potential side effects (e.g., GC-induced osteoporosis, GIOP) significantly limits the application of GCs in RA. Secondary osteoporosis is one of the major problems associated with long-term GC therapy. Bone mineral density (BMD) seemed to increase immediately in response to GC therapy but was ultimately reduced at a later time (Earp et al., 2008). Another report indicated that GCs (dosage ≥ 7.5 mg/day) were related to treatment failure in osteoporotic patients with RA (Wen et al., 2016). Concerns about these effects have prompted the development of new strategies to prevent bone loss and the deterioration of bone quality induced by RA or RA treatment with GCs.

Salvia miltiorrhiza Bunge is a traditional Chinese medicine that is widely used in clinical practice for the prevention and treatment of cardio-cerebral vascular diseases. Previous studies have shown that *Salvia miltiorrhiza* has anticoagulant, vasodilatory, and anti-inflammatory effects and other activities (Ji et al., 2000; Adams et al., 2006; Li et al., 2018; Jiang et al., 2019; Ren et al., 2019). *Salvia miltiorrhiza*-extracted cryptotanshinone significantly ameliorated inflammation and joint destruction in rats with collagen-induced arthritis (Wang et al., 2015). *Salvia miltiorrhiza* injection decreased the protein expression of NF- κ B and TNF- α in RA rats (Liu et al., 2015). In addition, our previous studies demonstrated that bioactive components of *Salvia miltiorrhiza* prevented bone loss in prednisone-treated rats by stimulating osteogenesis, inhibiting bone absorption and suppressing adipogenesis in the bone (Cui et al., 2009; Cui et al., 2012; Yang et al., 2016). Salvianolate contains the total polyphenols extracted from *Salvia miltiorrhiza*. Salvianolate injection has been approved by the China SFDA for coronary heart disease treatment since 2005 (Approval number:

Z20050248). Accordingly, salvianolate injection has been used for coronary heart disease treatment in the clinic for more than 15 years in China. It has been used in clinical practice for the treatment and prevention of cardio-cerebral vascular diseases, and its safety profile is well established in China (Chen et al., 2016; Zhang et al., 2016; Dong et al., 2018; NanZhu et al., 2018; Shen et al., 2020; Chai et al., 2021). Our previous study showed that salvianolate attenuated osteogenic inhibition and suppressed hyperactive bone resorption, which lead to the recovery of bone mass and bone mechanical properties in prednisone-treated lupus mice (Liu et al., 2016). However, whether salvianolate can ameliorate bone loss in RA or GC-treated RA individuals is still unknown. Since GCs are potent anti-inflammatory agents, it would be greatly beneficial if the burden of side effects of GC treatment could be reduced, especially the side effects involving the bone. Based on previous studies, we speculated that salvianolate might ameliorate osteopenia and provide joint protection in GC-treated RA individuals. In this study, we aimed to investigate the combined effect of prednisone and salvianolate on preventing joint damage and systemic bone loss in a CIA rat model.

MATERIALS AND METHODS

Drugs and Reagents

Bovine type II collagen (Collagen II) was purchased from Sichuan University (Chengdu, China). Incomplete Freund's adjuvant (IFA) was purchased from Sigma-Aldrich, China. Prednisone acetate was obtained from Guangdong South China Pharmaceutical Group Co., Ltd. (Guangdong, China). The salvianolate commercial injection product was purchased from Shanghai Green Valley Pharmaceutical Co., Ltd. (Shanghai, China). Salvianolate injection has been approved by the China SFDA for coronary heart disease treatment since 2005 (Approved number: Z20050248). Accordingly, salvianolate injection has been used for coronary heart disease treatment in the clinic for more than 15 years in China. According to the manufacturer's instructions, one unit of salvianolate injection (50 mg) contained 40 mg salvianolic acid B magnesium salt (Magnesium lithospermate B, CAS. No: 122021-74-3 **Supplementary Figure S1**). The certificate of analysis and HPLC analysis were provided by manufacturer (**Supplementary Figures S2, S3**).

Experimental Protocols

Forty-three female 6-week-old Lewis rats weighing 122 ± 12 g were obtained from Beijing Vital River Laboratory Animal Co. Ltd. (Beijing, China) [permit number: SCXK (Beijing) 2012-001]. All rats were housed in the animal facility of Guangdong Medical University for 2 weeks prior to the study. All protocols followed the Principles of the Care and Use of the National Laboratory Animal Monitoring Institute of China and were approved by the Academic Committee on the Ethics of Animal Experiments of Guangdong Medical University, Zhanjiang, People's Republic of China, Permit Number: SYXK (GUANGDONG) 2008-0007. Forty-three 8-week-old female Lewis rats weighing 138 ± 13 g were randomly divided into two groups: a control (CON) group included seven rats, and the remaining 36 rats were used to induce the CIA rat model. The CIA rat model was induced as previously described (Mohammad Shahi et al., 2012). Briefly, rats were injected intradermally on the back at the base of the tail with 0.4 ml of collagen II emulsion (1.5 mg/ml). The same immunization procedure was performed again 1 week later to strengthen arthritis induction. Rats in the CON group were administered 0.4 ml acetic acid (0.05 mol/L) as a control. Four weeks after immunization, twenty-one CIA model rats had been successfully established (arthritis index ≥ 4) for further study. The twenty-one CIA rats were randomly divided into three groups with seven rats per group: 1. the CIA rat group; 2. The prednisone-treated CIA rat group (CIA+PND); and 3. The prednisone and salvianolate combination treatment CIA rat group (CIA+PND+Sal). Rats in the CON and CIA groups were administered saline as a control, while rats in the CIA+PND and CIA+PND+Sal groups were treated with prednisone at 4.5 mg/kg/day (gavage) or/and salvianolate at 20 mg/kg/day (intraperitoneal injection). Drugs were administered every day after the CIA model was established, and the treatment continued for 90 days. On the 14th, 13th, fourth, and third days before the end point, all rats received subcutaneous injections of calcein (7 mg/kg) for *in vivo* bone formation fluorescence labeling. Rats were sacrificed by cardiac puncture under anesthesia.

Bone Mineral Density and Biomechanical Property Analysis

The left femurs were collected and used for BMD analysis with a dual-energy X-ray absorptiometry system (DEX) (QDR-4500A, Hologic Inc. Bedford, MA, United States). After BMD analysis, the femurs were used for bone mechanical property analysis with a three-point bending test using an MTS Mini Bionix testing system (Mini Bionix 858, MTS System Co., Eden Prairie, MN, United States). Samples were tested with a 15-mm span at a speed of 0.01 mm/s. Force (F) and deflection (D) were automatically recorded in the system. The elastic load, maximum load, break load and stiffness coefficient were calculated for each sample.

Micro-computed Tomography Analysis

The left distal femurs were collected for micro-CT analysis using a Viva CT40 analysis system (Scanco Medical, Zurich, Switzerland). The scan region was set to 500 slices with a

9.50-mm thickness in the distal femur, an integration time of 200 ms, energy of 70 kVp and a current of 114 mA. The lower and upper threshold was set at 170–1,000. The regions of interest (cancellous bone between 1- and 4-mm distal to the growth plate-metaphyseal junctions of the distal femur) were chosen for analysis. Bone volume/total volume (BV/TV), trabecular number (Tb.N), trabecular separation (Tb.Sp), trabecular thickness (Tb.Th), connectivity density (Conn.D), and the structure model index (SMI) were calculated with the built-in analysis software provided by the vendor.

Bone Histomorphometric Analysis

The right proximal tibial metaphysis (PTM) and the fourth lumbar vertebra (LV) were processed to generate nondecalcified sections. The samples were cut to expose the bone marrow cavity with an Isomet Low Speed Saw (Buehler, Lake Bluff, Illinois, United States) and fixed in 10% formalin for 24 h, followed by 70% ethanol fixation and gradient alcohol dehydration. They were embedded in methyl methacrylate for nondecalcified sectioning. Frontal sections of the PTM/LV were prepared at thicknesses of 5 and 8 μ m. The 5- μ m sections were stained with Masson-Goldner Trichrome for static histomorphometric analysis. The 8- μ m sections without staining were used for dynamic histomorphometric fluorescence measurements.

The region of interest in the PTM was located between 1- and 4-mm distal to the growth plate-epiphyseal junction. A semiautomatic digitizing image analysis system (Osteometrics, Decatur, GA, United States) was used for bone histomorphometric analysis. Static histomorphometric parameters included the total tissue area, trabecular area, trabecular perimeter, and osteoclast number (Oc.N). Dynamic histomorphometric parameters included the single-labeled perimeter, double-labeled perimeter, and interlabeled width. These parameters were used to calculate the percentage of trabecular bone volume (BV/TV), Tb.N, Tb. Sp, Oc.N number, the percentage of the osteoclast surface perimeter (%Oc.S.Pm), the percentage of the osteoblast surface perimeter (%Ob.S.Pm), the percentage of the labeled perimeter (%L.Pm), mineral apposition rate (MAR) and bone formation rate (BFR) per unit of bone surface (BFR/BS).

For the midtibial diaphyseal cortical bone, cross sections of the tibial shaft (3 sections per site) were cut to a 200 μ m thickness using a low-speed metallurgical saw. Then, sections were ground to a thickness of 20 μ m and cover slipped for histomorphometric analysis. The total cross-sectional area, cortical area, marrow area, single- and double-fluorescently labeled perimeter and interlabeling width for both periosteal and endocortical surfaces were measured, and the percentage of cortical area (%Ct.Ar), the percentage of marrow area (%Ma.Ar), and bone formation rates for periosteal (P-BFR/BS) and endocortical surfaces (E-BFR/BS) were calculated. The abbreviations of the bone histomorphometric parameters used were recommended by the American Society for Bone and Mineral Research Histomorphometric Nomenclature Committee (Dempster et al., 2013). All histomorphometric parameters and

procedures were in accordance with a previously published study (Liang et al., 2019).

Histological Evaluation

Right hind ankle samples were collected and fixed in 10% formalin. Then, the samples were decalcified in 15% ethylenediaminetetraacetic acid (EDTA) solution before paraffin embedding. The tissues were prepared in 4 μ m-thick paraffin sections, followed by staining with hematoxylin and eosin (H&E) and histological score evaluation (Sajti et al., 2004). The histological scores were calculated with a comprehensive histological scoring system as described previously (Wu et al., 2016).

Enzyme-Linked Immunosorbent Assay

Blood was collected from cardiac puncture under anesthesia. The serum was separated and stored at -80°C before analyses. Serum levels of tumor necrosis factor- α (TNF- α , catalog number: E-EL-R2856c), interleukin-6 (IL-6, catalog number: E-EL-R0015c), receptor activator of nuclear factor- κ B ligand (RANKL, catalog number: E-EL-R0841c), and osteoprotegerin (OPG, catalog number: E-EL-R3005) were detected by enzyme-linked immunosorbent assay (ELISA) kits (Elabscience Biotechnology Co., Ltd., Wuhan, China.) according to the manufacturer's instructions.

Immunohistochemical Analysis

Immunostaining for tumor necrosis factor- α (TNF- α), RANKL and osteoprotegerin (OPG) was performed on 4- μ m decalcified right distal femoral sections. Briefly, all sections were deparaffinized in xylene, rehydrated, and washed in PBS. The sections were then heated for 20 min in citrate buffer (pH 6.0) at 95°C and incubated with an anti-tumor necrosis factor- α (TNF- α) monoclonal antibody (1:100, catalog number: ab199013, Abcam, United States), anti-RANKL polyclonal antibody (1:200, catalog number: BA1323, Wuhan Boster, China), and anti-Osteoprotegerin (OPG) polyclonal antibody (1:500, catalog number: ab73400, Abcam, United States) overnight at 4°C . Phosphate-buffered saline (PBS) was used as a negative control. Then, the sections were incubated with secondary antibodies for 30 min at 26°C . 3,3'-Diaminobenzidine (DAB) staining and hematoxylin counterstaining were performed to visualize the expression of biomarkers. Immunohistochemical analysis was performed with Image-Pro Plus 6.0 software to evaluate immunostaining.

Western Blot Analysis

Left hind ankles were snap-frozen in liquid nitrogen and ground into powder. Tissue homogenates were prepared and analyzed by western blotting. Protein expression of RANKL and OPG was detected using an anti-RANKL polyclonal antibody (1:200, catalog number: BA1323, Wuhan Boster, China) and anti-OPG polyclonal antibody (1:3,000, catalog number: ab203061, Abcam, United States), respectively. An anti- β -actin antibody (1:2,000, Catalog number: AP80340, SAB, United States) was used as a control. IgG antibodies (Beyotime, China) were used as

TABLE 1 | The biomarker primers for RT-PCR analysis.

No.	Genes	Primers
1	OPN-Forward	GAGATGGAGTCTTGCTCTGTCAACC
	OPN-Reverse	AGGCGGATCACGAGGTGCTAGG
2	Osterix-Forward	TCGTCTGACTGCCTGCCTAGTG
	Osterix-Reverse	CTGCGTGGATGCCTGCCTTG
3	Col1a1-Forward	TGAACGTGGTGACAAAGGTC
	Col1a1-Reverse	CCATCTTTACCAGGAGAACCAT
4	TRAF6-Forward	AGGAATCACTTGGCACGACACTTG
	TRAF6-Reverse	TGCGACGGACGCAAGCAAG
5	TRAIL-Forward	CCTCAGCTTCAGTCAGCACTTCAG
	TRAIL-Reverse	GTAAGTCACAGCCACAGACACAGC

secondary antibodies. Quantification was performed using Gel-Pro analyzer 4 software.

MC3T3-E1 cells were treated with TNF- α (50 ng/ml) or TNF- α (50 ng/ml) + Sal (1 μ M), and the cells were collected for western blot analysis. The osteogenesis-related biomarkers OPN, Osterix and RUNX2 were analyzed after treatment for 24 h, while NF- κ B, TRAF6 and IL-1 β were analyzed after treatment for 72 h. Cell proteins were extracted and separated by SDS-PAGE. Proteins were then transferred to polyvinylidene fluoride (PVDF) membranes. The membranes were blocked with 5% skim milk in TBST, followed by incubation with primary antibodies overnight at 4°C . OPN (1:1,000, catalog number: ab8448, Abcam, United States), Osterix (1:1,000, catalog number: ab22552, Abcam), RUNX2 (1:1,000, catalog number: 12556, Cell Signaling, United States), NF- κ B (1:1,000, catalog number: sc-8008, Santa Cruz, United States), TRAF6 (1:1,000, catalog number: ab33915, Abcam, United States), IL-1 β (1:1,000, catalog number: 12242, Cell Signaling, United States), α -tubulin (1:1,000, catalog number: sc-32293, Santa Cruz, United States), and phosphor-NF- κ B (1:1,000, Cell Signaling, catalog number: 3033S, United States) primary antibodies were used. After washing with TBST three times, the membranes were incubated with a horseradish peroxidase-conjugated secondary antibody (1:5,000 dilution, Santa Cruz, United States) at room temperature for 1 h. The immunoreactive bands were visualized by using an Immobilon[®] western chemiluminescent HRP substrate (WBKLS0100, Millipore, United States). The protein band images were subjected to semiquantitative analysis using ImageJ software and normalized to α -tubulin. Western blots were repeated a minimum of three times.

Quantitative RT-PCR Assay

MC3T3-E1 cells were treated with TNF- α or TNF- α +Sal for 24 h, and the cells were collected for RT-PCR analysis. Total RNA was isolated from cells with TRIzol Reagent and quantified by a microspectrophotometer. HiScript[®] III All-in-one RT SuperMix Perfect for qPCR (333-01, Vazyme, China) was used to generate reverse-transcribed cDNA. PCR was performed using TB Green[™] Premix Ex Taq[™] II (RR820A, TaKaRa, Japan) with the corresponding primers (Table 1). Osteopontin (OPN), Osterix (Ox), Collagen 1a1 (Col1a1), receptor activator of nuclear factor- κ B ligand (RANKL), TNF-related apoptosis-inducing ligand (TRAIL), and TNF receptor associated factor 6 (TRAF6) were analyzed by RT-PCR. The

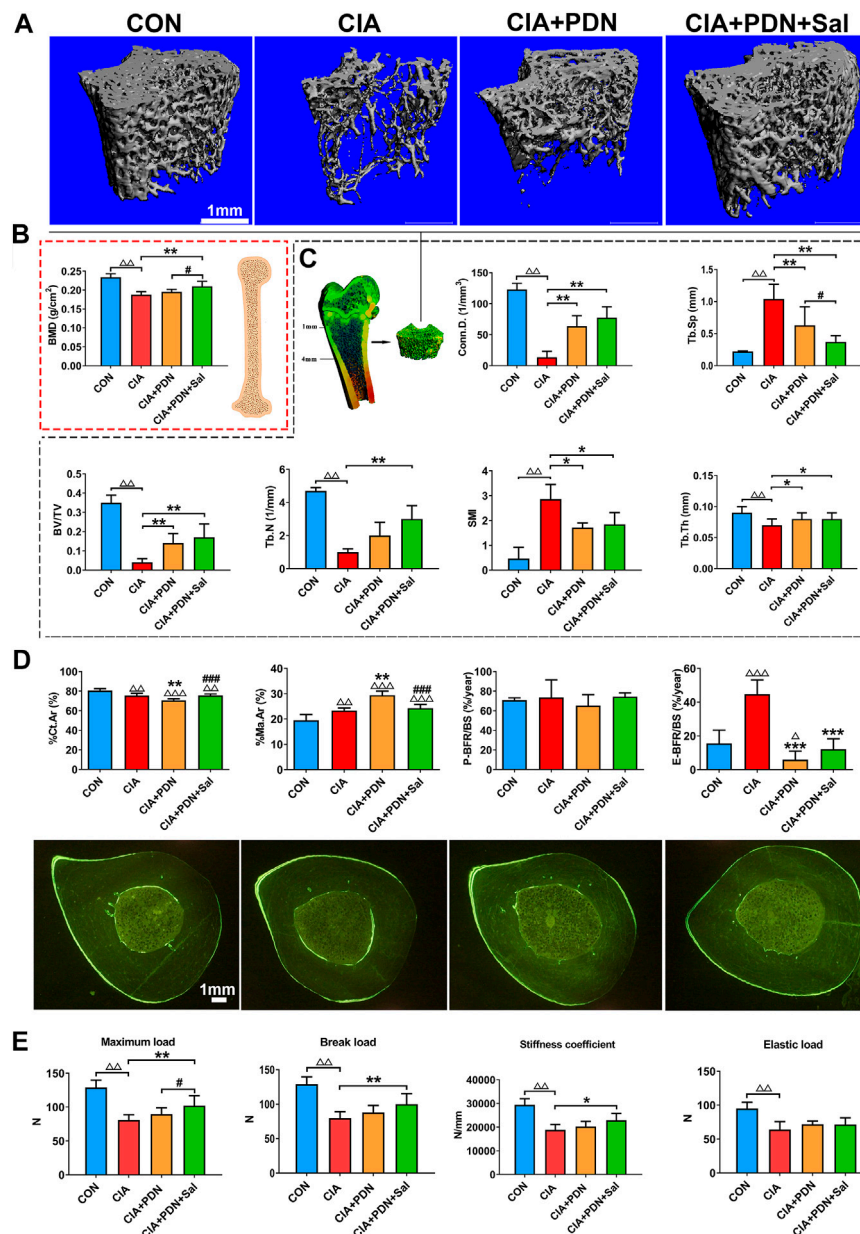


FIGURE 1 | Representative micro-CT images (A); micro-CT analysis of the distal femur metaphysis (B); BMD analyses of the whole femurs (C); bone histomorphometric analysis and representative images of the midshaft of the tibia (D) and bone biomechanical analysis of the femur (E) in different groups of rats. The femurs were collected for BMD analysis with a dual-energy X-ray absorptiometry system (DEX) and further used for biomechanical analysis. The distal femur metaphysis of rats was scanned and analyzed by a micro-CT system. The midshaft of the tibia were prepared for bone histomorphometric analysis. CON: healthy control rat group; CIA: collagen II-induced arthritis rat group; CIA+PDN: prednisone-treated CIA rat group; CIA+PDN+Sal: combination treatment with prednisone and salvianolate CIA rat group. $\Delta\Delta p < 0.01$ vs. CON, $\Delta\Delta\Delta p < 0.001$ vs. CON; $*p < 0.05$, $**p < 0.01$, $***p < 0.001$ vs. CIA; $\#p < 0.05$, $###p < 0.05$ vs. CIA+PDN ($n = 7$).

real-time PCR primers were synthesized by Shanghai Sangon Biotech, Shanghai, China.

The PCR program was as follows: preheating at 95°C for 30 s, 95°C heating for 5 s, and 60°C heating for 34 s, followed by 40 cycles of 95°C heating for 15 s and 60°C heating for 1 min. A Roche Light Cycler Detection System (Roche Diagnostics, Mannheim, Germany) was used to record the fluorescence signal and convert it into numerical values for statistical analysis. Relative

gene expression was calculated by employing the comparative CT method, and the expression of the target gene was normalized to that of the housekeeping gene glyceraldehyde 3-phosphate dehydrogenase (GAPDH). The experiment was repeated 3 times.

Statistical Analysis

Data are presented as the means \pm SD and were analyzed using SPSS software 17.0 (SPSS Inc., Chicago, IL, United States). Data

were analyzed by one-way ANOVA followed by post hoc Fisher's protected least significant difference test with the homogeneity of variance or Dunnett's T3 test with the heterogeneity of variance. $p < 0.05$ was considered significant.

RESULTS

The Micro-CT and BMD Analysis of the Femur

Representative micro-CT analysis images are shown in **Figure 1**. Compared with the control group, BV/TV, Tb.N, Tb.Th and Conn. D were significantly decreased, while Tb. Sp and SMI were significantly increased, in the CIA group (**Figure 1A**). BMD in the CIA group was significantly decreased by 19.6% compared to that in the control group ($p < 0.01$) (**Figure 1B**). Prednisone treatment in CIA rats (CIA+PDN) significantly increased BV/TV, Tb.Th, and Conn. D while decreasing Tb. Sp and SMI compared to those in CIA model rats (**Figure 1C**). Prednisone and salvianolate combination treatment in CIA rats (CIA+PDN+Sal group) significantly increased femur BMD and decreased Tb. Sp compared to those in the CIA and CIA+PDN group. Compared to the CIA model group, prednisone and salvianolate combination treatment significantly increased BV/TV, Tb.N, Tb.Th and Conn. D while significantly decreasing Tb. Sp and SMI (**Figures 1A–C**).

Bone Biomechanical Property Analysis and Bone Histomorphometry Analysis of Cortical Bone

Histomorphometric analyses of the midshaft of the tibia demonstrated that %Ct.Ar in CIA group was significantly decreased, while %Ma.Ar and E-BFR/BS were increased in the CIA model group compared to those in the control. CIA+PDN significantly decreased %Ct.Ar and E-BFR/BS while increasing %Ma.Ar compared to that in the CIA control. CIA+PDN+Sal significantly increased %Ct.Ar, while decreasing %Ma.Ar compared to those in the CIA+PDN group. There was no significant difference in P-BFR/BS among the groups (**Figure 1D**).

The biomechanical properties of the femur (maximum load, break load, elastic load, and stiffness coefficient) in the CIA group were significantly decreased compared with those in the control group. Compared with those in the CIA group, the maximum load, break load, and stiffness coefficient were significantly increased in the CIA+PDN+Sal group. Compared to the CIA+PDN group, the CIA+PDN+Sal group had a significantly increased maximum load (**Figure 1E**).

Bone Histomorphometry Analysis of the PTM

Histomorphometric analysis demonstrated that %Tb.Ar and Tb.N of PTM in CIA rats were significantly decreased, while Tb. Sp, Oc. N, %Oc.S.Pm, MAR, %Ob.S.Pm and BFR/BS were significantly increased in the CIA model group compared to the control group. CIA+PDN significantly increased %Tb.Ar and

Tb.N while decreasing Tb. Sp, Oc. N, %Oc.S.Pm, MAR and BFR/BS compared to those in the CIA control. CIA+PDN+Sal significantly increased %Tb.Ar, %Ob.S.Pm and Tb.N while decreasing Oc. N and %Oc.S.Pm compared to those in the CIA group and CIA+PDN group. Combination treatment with CIA+PDN+Sal did not increase MAR or BFR/BS compared to those in the CIA+PDN group (**Figures 2A,C**). The histomorphometric images of the lumbar vertebra showed the same trend as the PTM (**Figure 2B**).

Histological and Immunohistochemistry Analyses

As shown in **Figure 3**, the histopathologic scores of ankle sections in the CIA group were significantly increased compared to those in the control group. The histopathologic scores were significantly decreased in the CIA+PDN and CIA+PDN+Sal groups compared to the CIA and control groups. Although CIA+PDN+Sal decreased histopathologic scores compared to CIA+PDN, there was no significant difference between the two groups.

Immunohistochemistry analyses demonstrated that the expression of TNF- α and RANKL in CIA rats was significantly increased compared to that in the control group. Compared with that in the CIA group, the expression of TNF- α and RANKL was decreased in the CIA+PDN group and CIA+PDN+Sal group. OPG expression in the CIA group was decreased compared to that in the control group. The CIA+PDN+Sal group had increased OPG expression compared to the CIA group (**Figure 3**).

Western Blot Analyses of *in vivo* Samples

The results of femur western blotting analysis showed that the expression of RANKL and the RANKL/OPG ratio in CIA rats were significantly increased by 308 and 276%, respectively, while the expression of OPG was not significantly changed. The expression of RANKL and the RANKL/OPG ratio were significantly decreased by 72 and 49%, respectively, compared to that in the CIA group. CIA+PDN+Sal also significantly increased OPG by 118% and decreased the RANKL/OPG ratio by 65% compared to those in the CIA+PDN group (**Figure 4A**).

Serum Biomarker Analyses

Compared with the control group, the levels of IL-6, TNF- α , RANKL and the RANKL/OPG ratio were significantly increased in the CIA group. CIA model induction caused a decrease in OPG expression in the serum. CIA+PDN and CIA+PDN+Sal decreased serum IL-6 and TNF- α levels compared to those in the CIA group. CIA+PDN+Sal significantly decreased sRANKL and sRANKL/OPG and increased OPG levels in serum compared to those in the CIA group (**Figure 4B**).

RT-PCR and Western Blot Analyses of *in vitro* Samples

RT-qPCR results demonstrated that TNF- α -induced inflammatory medium significantly decreased Osterix, OPN, and Col1a1 expression and increased RANKL, TRAF6, and

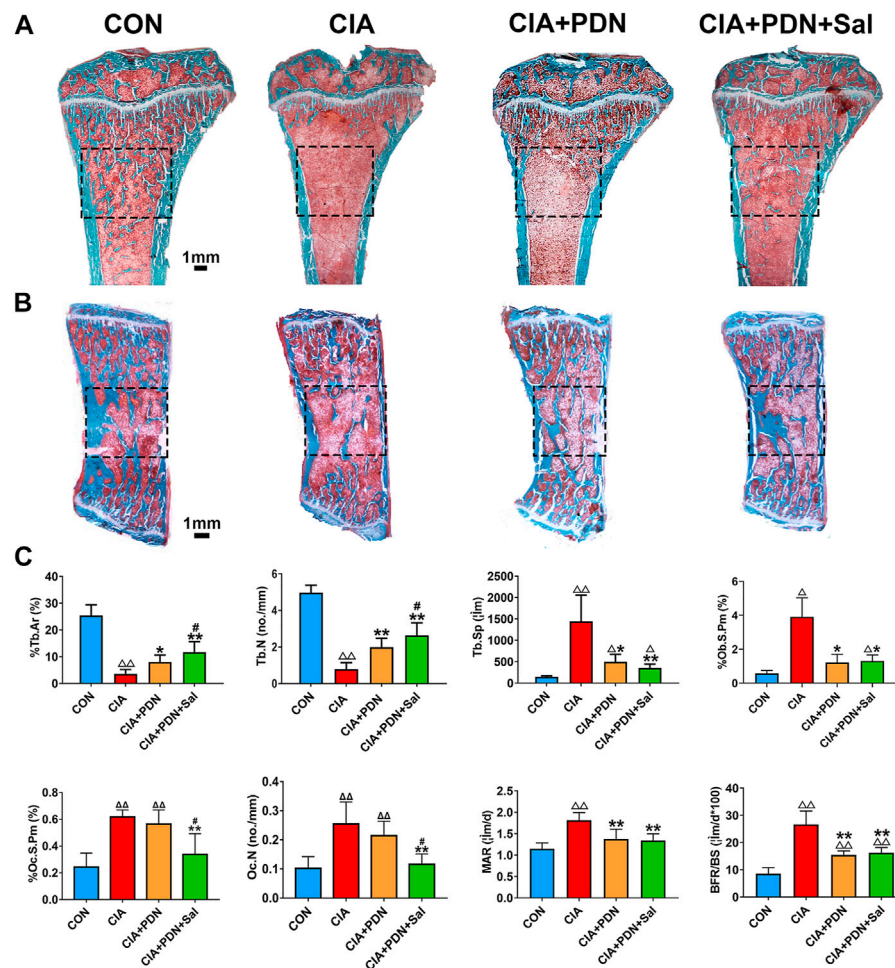


FIGURE 2 | Representative images of the tibial metaphysis (A) and the lumbar vertebra (B) and bone histomorphometric analysis of the proximal tibial metaphysis (C) Nondecalcified tissue sections of the tibial metaphysis and lumbar vertebra were stained with Masson-Goldner trichrome. $\Delta\Delta p < 0.01$ vs. CON, $^{*}p < 0.05$, $^{**}p < 0.01$ vs. CIA, $^{#}p < 0.05$ vs. CIA+PDN ($n = 7$).

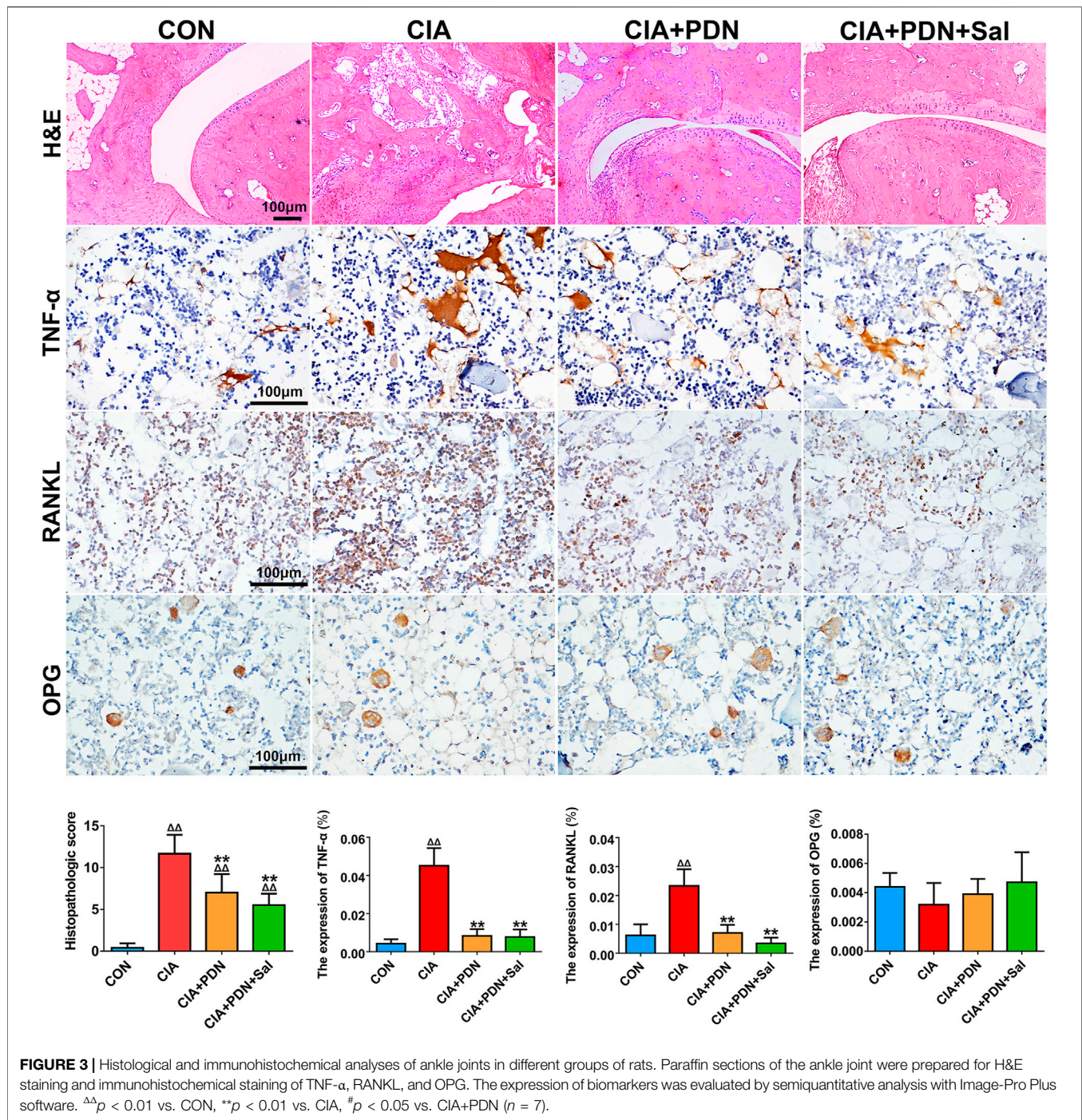
TRAIL gene expression in MC3T3-E1 osteoblasts compared to that in the control. Salvianolate treatment significantly upregulated Osterix, OPN, and Col1a1 gene expression and downregulated RANKL, TRAF6 and TRAIL gene expression in TNF- α -induced MC3T3-E1 osteoblasts compared to that in the TNF- α -induced group (Figure 5A).

The results of western blotting revealed that TNF- α significantly decreased OPN and RUNX2 protein expression and increased NF κ B, TRAF6, and IL-1 β protein expression. Salvianolate treatment significantly increased OPN, Osterix, and RUNX2 protein expression and decreased NF κ B, TRAF6, and IL-1 β protein expression compared to that in the TNF- α -induced group (Figure 5B).

DISCUSSION

A previous report revealed that 24.8% of female RA patients developed osteoporosis after an average follow-up of 7.4 years

after diagnosis (Hwang et al., 2017). There is a large amount of evidence suggesting that accelerated BMD loss occurred in the hands, spine and femoral neck of RA patients compared to that in healthy individuals (Guler-Yuksel et al., 2010; Fassio et al., 2016). Our data showed that CIA induced significant joint destruction and inflammation, and systemic osteoporosis was also found in CIA rats with trabecular and cortical bone degradation, BMD reduction, and bone biomechanical deterioration (Figures 1–3). In our previous study, we found that CIA rats developed systemic osteoporosis along with CIA development (Wu et al., 2016). These results are consistent with previous clinical reports on RA (Kim et al., 2010; Hoes et al., 2015). Previous studies indicated that inflammatory cytokines (such as TNF- α , IL-1 β , and IL-6) significantly promoted osteoclastogenesis (Lam et al., 2000; Moon et al., 2013; Wu et al., 2017; Shiratori et al., 2018). In this study, TNF- α and IL-6 in the serum were significantly increased in CIA rats compared to that in normal control rats. Our data indicated that bone resorption (including parameters of Oc. N, %Oc.S.Pm, and RANKL in the serum and femur) was significantly enhanced



in CIA rats compared to that in healthy controls (Figures 2C, 3, 4). In addition, our data also demonstrated that the bone formation rate and osteoblast number parameter in the PTM was significantly increased in the CIA group compared to the normal control group (Figure 2C). Interestingly, we noticed that periosteal bone formation did not show a significant difference among the groups; however, endocortical bone formation rates significantly increased in the CIA group compared to the other groups (Figure 3B). These results suggest that RA induced high

bone turnover in the trabecular and endocortical regions and that elevated bone formation was insufficient to compensate for the higher bone resorption, ultimately resulting in bone loss.

Glucocorticoid (GC) therapy is a main treatment strategy in RA because of its ability to effectively manage inflammation and reduce disease progression in RA (Bakker et al., 2012; Engvall et al., 2013). In this study, GC therapy effectively controlled progressive inflammation in CIA rats (Figure 4). However, some reports have suggested that long-term, high-dose or even low-

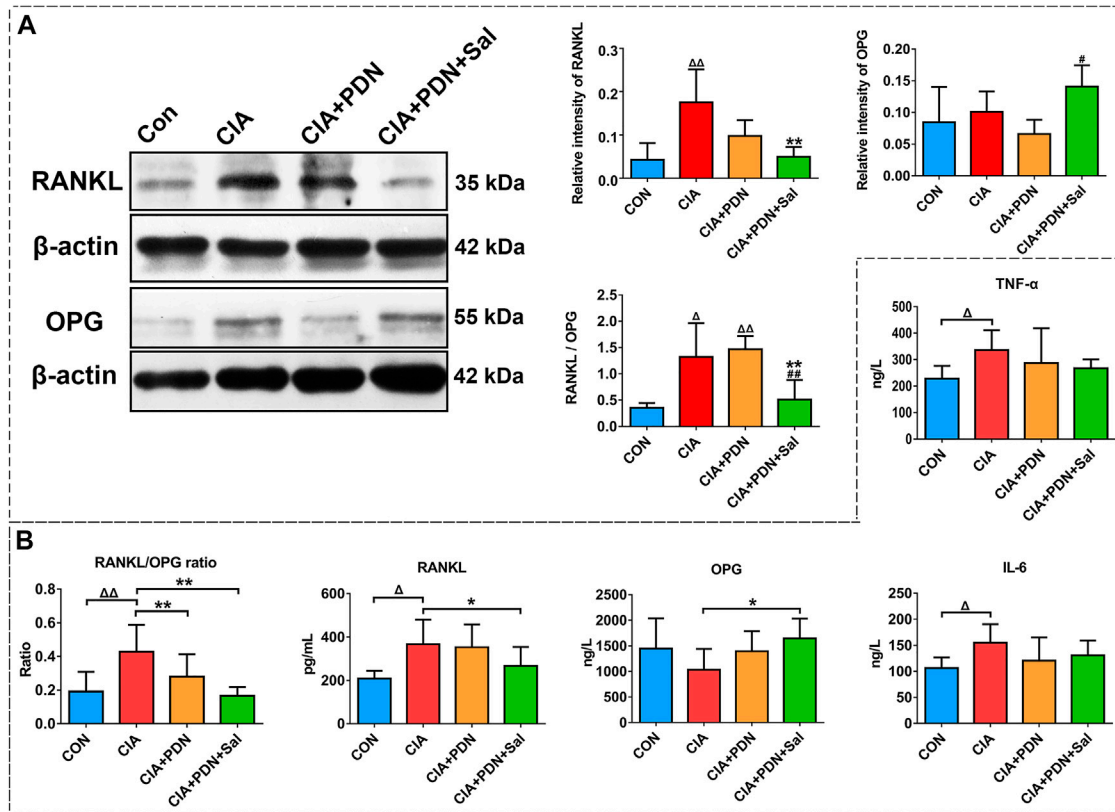


FIGURE 4 | Western blot analysis of RANKL and OPG expression in the hind ankle (A) and serum biomarker analysis (B) in different groups of rats. ^{ΔΔ} $p < 0.01$ vs. CON, ^{**} $p < 0.01$ vs. CIA, [#] $p < 0.05$ vs. CIA+PDN ($n = 7$).

dose GC therapy in RA accelerated bone loss and led to a high risk of fractures (Engvall et al., 2008; Wang et al., 2020). A previous study demonstrated that the BMD of the spine and femoral neck continued to decrease after GC therapy in RA patients and that subsequent GC dose adjustments did not help to ameliorate the decline in BMD (Fassio et al., 2016). A high dose of daily GCs *via* systemic administration was associated with elevated fracture risk in RA patients (Balasubramanian et al., 2016). In this study, compared to the CIA group, the CIA+PDN group had significantly suppressed the elevated osteogenesis and osteoclastogenesis and decreased the high bone turnover induced by RA. Prednisone treatment partially alleviated the bone loss in trabecular and trabecular bone microstructure deterioration induced by RA, which may have been due to its effective control of inflammation and the decreased in the high bone turnover of RA. However, prednisone treatment still significantly induced cortical bone loss and increased cortical bone marrow area in CIA rats (Figure 1D). These results suggest that prednisone monotherapy partially ameliorates joint damage and bone loss in trabecular, but still induces cortical bone loss and does not improve bone quality or reduce fracture risk in CIA rats.

In this study, our data demonstrated that CIA+PDN+Sal significantly increased BMD and biomechanical properties, ameliorated bone loss in both trabecular and cortical bone and improved trabecular microstructure compared to those in the

CIA and CIA+PDN groups, which suggests that salvianolate treatment significantly improved bone quality. Our previous study demonstrated that salvianolate treatment significantly decreased bone loss in prednisone-treated lupus mice (Liu et al., 2016). In this study, salvianolate significantly inhibited osteoclast number and activity (Oc.N and %Oc.S.Pm), and bone resorption decreased accordingly. RANKL and the RANKL/OPG ratio significantly decreased in the serum, femur and ankle of the CIA+PDN+Sal group, while the serum level of OPG increased significantly.

In addition, we found that salvianolate did not adequately improve bone formation in prednisone-treated CIA rats compared to prednisone treatment alone according to bone histomorphometric analysis. These results were different from those of a previous study in which salvianolic acid B (one of the main bioactive components in salvianolate) promoted the osteogenesis of bone marrow stromal cells and human mesenchymal stem cells *in vitro* (Xu et al., 2014) and increased bone formation by promoting osteoblastic differentiation and bone matrix mineralization in zebrafish larvae (Luo et al., 2016). This may be partly because RA induced significantly increased bone formation with high bone turnover compared to that in the normal control, and salvianolate did not adequately increase bone formation. In addition, prednisone treatment may provide some suppression of bone

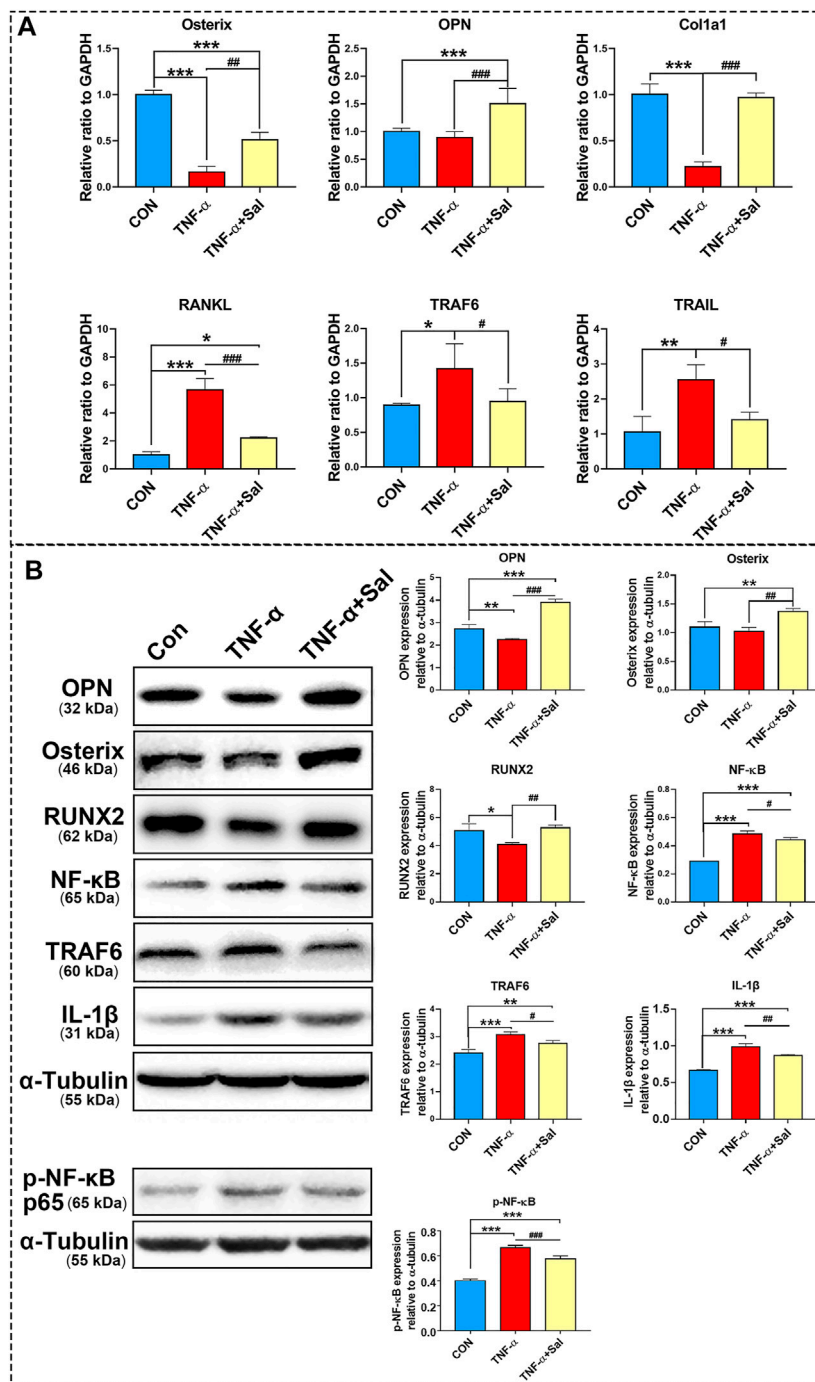


FIGURE 5 | The impacts of salvianolate treatment on TNF- α -induced MC3T3-E1 cells. **(A)** Osterix, OPN, Col1a1, RANKL, TRAF6, and TRAIL gene expression in TNF- α -induced MC3T3-E1 cells after salvianolate treatment based on RT-PCR analyses. **(B)** OPN, RUNX2, NF- κ B, TRAF6, IL-1 β , and p-NF- κ B p65 protein expression in TNF- α -induced MC3T3-E1 cells after salvianolate treatment based on western blot analyses. * p < 0.05, ** p < 0.01, *** p < 0.001 vs. CON, # p < 0.05, ## p < 0.01, ### p < 0.001 vs. TNF- α .

formation (Rauch et al., 2010; Chotiarnwong and McCloskey, 2020) to partially block the effects of salvianolate in prednisone-treated CIA rats. Salvianolate showed some synergistic anti-inflammatory effects with prednisone treatment (serum TNF- α). However, the synergistic effect did not reveal a significant difference

compared to prednisone treatment alone. These results suggest that combination therapy with prednisone and salvianolate ameliorated bone loss mainly by inhibiting bone resorption through the regulation of the RANKL/RANK/OPG signaling pathway. Previous studies demonstrated that the main bioactive components of salvianolate

(salvianic acid A and salvianic acid B) increased the expression of OPG in GC-induced osteoporosis rats (Cui et al., 2009; Cui et al., 2012). In addition, salvianolate ameliorated bone loss in prednisone-treated lupus mice partially through the RANK/RANKL/OPG signaling pathway (Liu et al., 2016). The results of this study were consistent with those of previous reports and indicated that combination therapy with prednisone and salvianolate was superior to prednisone treatment alone for ameliorating systemic bone loss and joint damage in RA rats.

In vivo results suggested that RANKL overexpression and OPG suppression in CIA rats and salvianolate treatment could suppress RANKL, increase OPG, and decrease RANKL/OPG ratio. First, we wondered where the OPG and RANKL came from? OPG is a glycoprotein secreted by bone marrow stromal cells (BMSCs) and osteoblasts. OPG acts as an effective inhibitor of osteoclast differentiation, activation and survival and therefore inhibits bone resorption. RANKL is an important cytokine secreted by osteoblasts and their immature precursors, T lymphocytes, B lymphocytes and megakaryocytes and endothelial cells. RANKL/RANK/OPG is an important osteoclastogenesis signaling pathway that regulates bone resorption (Kong et al., 2000; Thirunavukkarasu et al., 2000; Buckley and Fraser, 2002; Wright et al., 2009; Fumoto et al., 2014; Lee et al., 2018).

To further evaluate the effects of salvianolate under inflammatory conditions, we investigated the effects of salvianolate in MC3T3-E1 osteoblast in this study, as osteoblast secreted both OPG and RANKL to regulate osteoclast activity. The role of osteoblast is important in regulating osteoclast function and activity.

The results demonstrated that salvianolate significantly downregulated *RANKL*, *TRAF6*, and *TRAIL* gene expression a TNF- α -induced inflammatory osteoblast model. In addition, salvianolate significantly upregulated the gene expression of osteogenic markers (Osterix, OPN, and *Col1a1*). The results further revealed that salvianolate significantly suppressed the protein expression of IL-1 β , NF- κ B, and TRAF6 and promoted the protein expression of osteogenic markers (Osterix, OPN, and RUNX2) (Figure 5). TRAF6 is a downstream protein of RANKL. The decrease in TRAF6 further downregulated the NF- κ B signaling pathway. The suppression of the RANKL/TRAF6/NF- κ B signaling axis and inflammatory cytokine inhibition contributed to osteoclastogenesis suppression. In addition, salvianolate also downregulated TRAIL levels compared to those in the TNF- α -induced group. Decreased TRAIL expression was reported to decrease the apoptosis of osteoblasts (Mori et al., 2009), inhibit RANK signaling and suppress osteoclast activation (Yen et al., 2008; Yen et al., 2012).

In vitro study, we confirmed that osteoblast involves in the regulation of the overexpression RANKL and TRAIL-TRAF6-NF κ B signal axis was further activated to stimulate osteoclastogenesis *in vitro*. Salvianolate treatment significant increased osteogenesis (Osterix, OPN, and *Col1a1*) and suppress RANKL/RANK/OPG signaling pathway and TRAIL-TRAF6-NF κ B signal axis *in vitro* (Figure 6). RANKL and inflammatory cytokines play a key role in the pathogenesis of joint damage and systemic bone mass loss

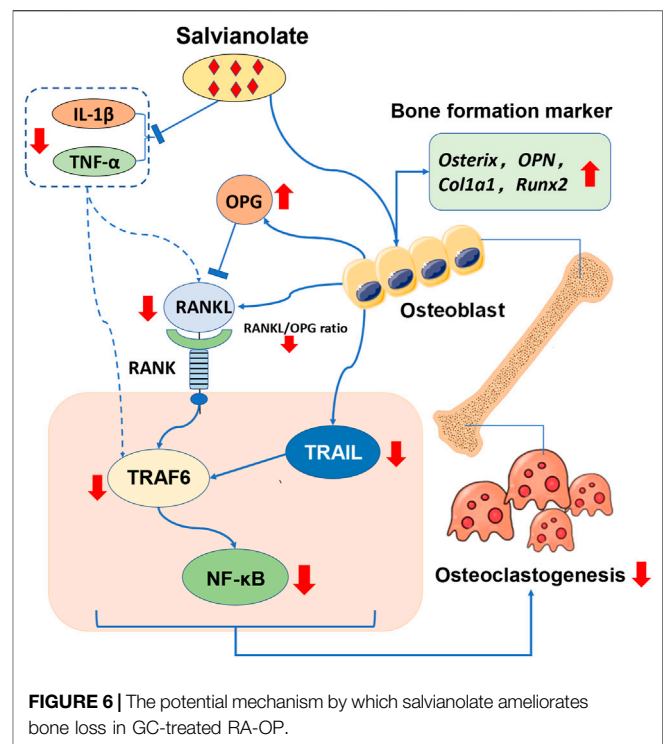


FIGURE 6 | The potential mechanism by which salvianolate ameliorates bone loss in GC-treated RA-OP.

during RA. Previous studies have suggested that the RANKL/RANK/OPG signaling pathway plays a critical role in joint and bone destruction in the pathology of RA. A close relationship among inflammatory cytokines and the NF- κ B and RANKL/RANK/OPG signaling pathways has been reported (Zhang et al., 2001; Popova et al., 2019; Ilchovska and Barrow, 2021). It was reported that RANKL-targeted peptides inhibited osteoclastogenesis and attenuated adjuvant-induced arthritis by inhibiting RANKL activation and downregulating inflammatory cytokines (Naidu et al., 2013). In this study, salvianolate inhibited RANKL/RANK/OPG activation, suppress TRAIL-TRAF6-NF κ B signal axis, downregulated inflammatory cytokines, and promoted osteogenesis under inflammatory conditions *in vitro*. Due to the high bone turnover of CIA rats and the potent anti-inflammatory effects of GC, salvianolate did not have significant osteogenic and anti-inflammatory effects *in vivo*; however, salvianolate significantly inhibited bone resorption and improved bone quality in the CIA+PDN+Sal group compared to that in the CIA+PDN group *in vivo*.

In this study, the effect of Salvianolate on CIA/GC-treated rat model is more based on bone resorption inhibition other than the stimulation of bone formation. The effects of salvianolate on bone resorption inhibition may due to salvianolate suppress osteoblast-mediated RANKL/OPG signal and TRAIL-TRAF6-NF κ B signal axis.

There is a limitation in this study, osteoclast is an important cell in CIA and it is currently unknown whether salvianolate have a direct effect on osteoclast in CIA/GC-treated CIA rats and the underlying mechanism. Further studies are needed to investigate on this point.

In conclusion, combination therapy with prednisone and salvianolate was superior to prednisone monotherapy for ameliorating joint damage and improved bone quality in CIA rats through the regulation of the RANKL/RANK/OPG signaling pathway and TRAIL-TRAF6-NF κ B signal axis, thus reducing fracture risk. Salvianolate demonstrated significant osteoclastogenesis suppression, ameliorates osteopenia and improves bone quality, which could be used as a promising antiosteopenia therapeutic strategy to improve bone quality in RA patients.

DATA AVAILABILITY STATEMENT

The original contributions presented in the study are included in the article/**Supplementary Material**, further inquiries can be directed to the corresponding author/s.

ETHICS STATEMENT

The animal study was reviewed and approved by The Academic Committee on the Ethics of Animal Experiments of the Guangdong Medical University.

REFERENCES

- Adams, J. D., Wang, R., Yang, J., and Lien, E. J. (2006). Preclinical and Clinical Examinations of Salvia Miltiorrhiza and its Tanshinones in Ischemic Conditions. *Chin. Med.* 1, 3. doi:10.1186/1749-8546-1-3
- Bakker, M. F., Jacobs, J. W., Welsing, P. M., Verstappen, S. M., Tekstra, J., Ton, E., et al. (2012). Low-dose Prednisone Inclusion in a Methotrexate-Based, Tight Control Strategy for Early Rheumatoid Arthritis: a Randomized Trial. *Ann. Intern. Med.* 156, 329–339. doi:10.7326/0003-4819-156-5-201203060-00004
- Balasubramanian, A., Wade, S. W., Adler, R. A., Lin, C. J. F., Maricic, M., O'malley, C. D., et al. (2016). Glucocorticoid Exposure and Fracture Risk in Patients with New-Onset Rheumatoid Arthritis. *Osteoporos. Int.* 27, 3239–3249. doi:10.1007/s00198-016-3646-z
- Buckley, K. A., and Fraser, W. D. (2002). Receptor Activator for Nuclear Factor κ B Ligand and Osteoprotegerin: Regulators of Bone Physiology and Immune Responses/potential Therapeutic Agents and Biochemical Markers. *Ann. Clin. Biochem.* 39, 551–556. doi:10.1177/000456320203900602
- Chai, Y. N., Luo, M., Liang, W. J., Qiu, J. L., Li, D., Wang, L. C., et al. (2021). The Safety and Effectiveness of Salvianolate in Preventing Perioperative Venous Thromboembolism in China: A PRISMA-Compliant Meta-Analysis Based on RCTs. *Medicine (Baltimore)* 100, e25639. doi:10.1097/MD.00000000000025639
- Chen, Z. W., Xie, Y. M., Liao, X., and Wang, G. Q. (2016). Systematic Review on Safety of Salvianolate Injection. *Zhongguo Zhong Yao Za Zhi* 41, 3686–3695. doi:10.4268/cjcm20161931
- Chotiarnwong, P., and McCloskey, E. V. (2020). Pathogenesis of Glucocorticoid-Induced Osteoporosis and Options for Treatment. *Nat. Rev. Endocrinol.* 16, 437–447. doi:10.1038/s41574-020-0341-0
- Coury, F., Peyruchaud, O., and Machuca-Gayet, I. (2019). Osteoimmunology of Bone Loss in Inflammatory Rheumatic Diseases. *Front. Immunol.* 10, 679. doi:10.3389/fimmu.2019.00679
- Cui, L., Li, T., Liu, Y., Zhou, L., Li, P., Xu, B., et al. (2012). Salvianolic Acid B Prevents Bone Loss in Prednisone-Treated Rats through Stimulation of Osteogenesis and Bone Marrow Angiogenesis. *PLoS One* 7, e34647. doi:10.1371/journal.pone.0034647
- Cui, L., Liu, Y. Y., Wu, T., Ai, C. M., and Chen, H. Q. (2009). Osteogenic Effects of D+beta-3,4-dihydroxyphenyl Lactic Acid (Salvianic Acid A, SAA) on Osteoblasts and Bone Marrow Stromal Cells of Intact and Prednisone-Treated Rats. *Acta Pharmacol. Sin.* 30, 321–332. doi:10.1038/aps.2009.9
- Dempster, D. W., Compston, J. E., Drezner, M. K., Glorieux, F. H., Kanis, J. A., Malluche, H., et al. (2013). Standardized Nomenclature, Symbols, and Units for Bone Histomorphometry: a 2012 Update of the Report of the ASBMR Histomorphometry Nomenclature Committee. *J. Bone Miner. Res.* 28, 2–17. doi:10.1002/jbmr.1805
- Dong, P., Hu, H., Guan, X., Ung, C. O. L., Shi, L., Han, S., et al. (2018). Cost-consequence Analysis of Salvianolate Injection for the Treatment of Coronary Heart Disease. *Chin. Med.* 13, 28. doi:10.1186/s13020-018-0185-x
- Earp, J. C., Dubois, D. C., Molano, D. S., Pyszczyński, N. A., Keller, C. E., Almon, R. R., et al. (2008). Modeling Corticosteroid Effects in a Rat Model of Rheumatoid Arthritis I: Mechanistic Disease Progression Model for the Time Course of Collagen-Induced Arthritis in Lewis Rats. *J. Pharmacol. Exp. Ther.* 326, 532–545. doi:10.1124/jpet.108.137372
- Engvall, I. L., Svensson, B., Boonen, A., Van Der Heijde, D., Lerner, U. H., Hafström, I., et al. (2013). Low-dose Prednisolone in Early Rheumatoid Arthritis Inhibits Collagen Type I Degradation by Matrix Metalloproteinases as Assessed by Serum ICTP-Aa Possible Mechanism for Specific Inhibition of Radiological Destruction. *Rheumatology (Oxford)* 52, 733–742. doi:10.1093/rheumatology/kes369
- Engvall, I. L., Svensson, B., Tengstrand, B., Brismar, K., Hafström, I., and Better Anti-Rheumatic Pharmac. O. T. S. G. (2008). Impact of Low-Dose Prednisolone on Bone Synthesis and Resorption in Early Rheumatoid Arthritis: Experiences from a Two-Year Randomized Study. *Arthritis Res. Ther.* 10, R128. doi:10.1186/ar2542
- Fassio, A., Idolazzi, L., Jaber, M. A., Dartizio, C., Viapiana, O., Rossini, M., et al. (2016). The Negative Bone Effects of the Disease and of Chronic Corticosteroid Treatment in Premenopausal Women Affected by Rheumatoid Arthritis. *Reumatismo* 68, 65–71. doi:10.4081/reumatismo.2016.878
- Fumoto, T., Takeshita, S., Ito, M., and Ikeda, K. (2014). Physiological Functions of Osteoblast Lineage and T Cell-Derived RANKL in Bone Homeostasis. *J. Bone Miner. Res.* 29, 830–842. doi:10.1002/jbmr.2096
- Güler-Yüksel, M., Klarenbeek, N. B., Goekoop-Ruiterman, Y. P., De Vries-Bouwstra, J. K., Van Der Kooij, S. M., Gerards, A. H., et al. (2010). Accelerated Hand Bone mineral Density Loss Is Associated with Progressive

AUTHOR CONTRIBUTIONS

All authors listed have made a substantial, direct, and intellectual contribution to the work and approved it for publication.

FUNDING

This study was supported by grants from the National Natural Science Foundation of China (No. 81373499 and 81703584), The regional joint fund of natural science foundation of Guangdong province (No. 2020B1515120052), Guangdong Province Natural Science Foundation of China (No. 2017A030310614 and 2018A030307036), Discipline construction project of Guangdong Medical University (No.4SG21002G), The Science and Technology Foundation of Zhanjiang, Guangdong Province, China (No. 201018003). Guangdong Medical University scientific research fund (No. B2017001).

SUPPLEMENTARY MATERIAL

The Supplementary Material for this article can be found online at: <https://www.frontiersin.org/articles/10.3389/fphar.2021.710169/full#supplementary-material>

- Joint Damage in Hands and Feet in Recent-Onset Rheumatoid Arthritis. *Arthritis Res. Ther.* 12, R96. doi:10.1186/ar3025
- Hoes, J. N., Bultink, I. E., and Lems, W. F. (2015). Management of Osteoporosis in Rheumatoid Arthritis Patients. *Expert Opin. Pharmacother.* 16, 559–571. doi:10.1517/14656566.2015.997709
- Hwang, J., Lee, E. K., Ahn, J. K., Cha, H. S., Koh, E. M., and Lee, J. (2017). Bone-density Testing Interval and Transition to Osteoporosis in Patients with Rheumatoid Arthritis. *Osteoporos. Int.* 28, 231–237. doi:10.1007/s00198-016-3703-7
- Ilchovska, D. D., and Barrow, D. M. (2021). An Overview of the NF- κ B Mechanism of Pathophysiology in Rheumatoid Arthritis, Investigation of the NF- κ B Ligand RANKL and Related Nutritional Interventions. *Autoimmun. Rev.* 20, 102741. doi:10.1016/j.autrev.2020.102741
- Ji, X. Y., Tan, B. K., and Zhu, Y. Z. (2000). Salvia Miltiorrhiza and Ischemic Diseases. *Acta Pharmacol. Sin.* 21, 1089–1094.
- Jiang, Z., Gao, W., and Huang, L. (2019). Tanshinones, Critical Pharmacological Components in Salvia Miltiorrhiza. *Front. Pharmacol.* 10, 202. doi:10.3389/fphar.2019.00202
- Kim, S. Y., Schneeweiss, S., Liu, J., Daniel, G. W., Chang, C. L., Garneau, K., et al. (2010). Risk of Osteoporotic Fracture in a Large Population-Based Cohort of Patients with Rheumatoid Arthritis. *Arthritis Res. Ther.* 12, R154. doi:10.1186/ar3107
- Kong, Y. Y., Boyle, W. J., and Penninger, J. M. (2000). Osteoprotegerin Ligand: a Regulator of Immune Responses and Bone Physiology. *Immunol. Today* 21, 495–502. doi:10.1016/s0167-5699(00)01718-7
- Lam, J., Takeshita, S., Barker, J. E., Kanagawa, O., Ross, F. P., and Teitelbaum, S. L. (2000). TNF- α Induces Osteoclastogenesis by Direct Stimulation of Macrophages Exposed to Permissive Levels of RANK Ligand. *J. Clin. Invest.* 106, 1481–1488. doi:10.1172/JCI11176
- Lee, D. W., Kwon, J. Y., Kim, H. K., Lee, H. J., Kim, E. S., Kim, H. J., et al. (2018). Propofol Attenuates Osteoclastogenesis by Lowering RANKL/OPG Ratio in Mouse Osteoblasts. *Int. J. Med. Sci.* 15, 723–729. doi:10.7150/ijms.22713
- Li, Z. M., Xu, S. W., and Liu, P. Q. (2018). Salvia miltiorrhizaBurge (Danshen): a golden Herbal Medicine in Cardiovascular Therapeutics. *Acta Pharmacol. Sin.* 39, 802–824. doi:10.1038/aps.2017.193
- Liang, Y., Liu, Y., Lai, W., Du, M., Li, S., Zhou, L., et al. (2019). 1,25-Dihydroxy Vitamin D3 Treatment Attenuates Osteopenia, and Improves Bone Muscle Quality in Goto-Kakizaki Type 2 Diabetes Model Rats. *Endocrine* 64, 184–195. doi:10.1007/s12020-019-01857-5
- Liu, Q. S., Luo, X. Y., Jiang, H., Xing, Y., Yang, M. H., Yuan, G. H., et al. (2015). Salvia Miltiorrhiza Injection Restores Apoptosis of Fibroblast-like Synoviocytes Cultured with Serum from Patients with Rheumatoid Arthritis. *Mol. Med. Rep.* 11, 1476–1482. doi:10.3892/mmr.2014.2779
- Liu, Y., Cui, Y., Zhang, X., Gao, X., Su, Y., Xu, B., et al. (2016). Effects of Salvianolate on Bone Metabolism in Glucocorticoid-Treated Lupus-Prone B6.MRL-Fas (lpr)/J Mice. *Drug Des. Devel. Ther.* 10, 2535–2546. doi:10.2147/DDDT.S110125
- Luo, S. Y., Chen, J. F., Zhong, Z. G., Lv, X. H., Yang, Y. J., Zhang, J. J., et al. (2016). Salvianolic Acid B Stimulates Osteogenesis in Dexamethasone-Treated Zebrafish Larvae. *Acta Pharmacol. Sin.* 37, 1370–1380. doi:10.1038/aps.2016.62
- Mohammad Shahi, M., Rashidi, M. R., Mahboob, S., Haidari, F., Rashidi, B., and Hanaee, J. (2012). Protective Effect of Soy Protein on Collagen-Induced Arthritis in Rat. *Rheumatol. Int.* 32, 2407–2414. doi:10.1007/s00296-011-1979-7
- Moon, S. J., Ahn, I. E., Jung, H., Yi, H., Kim, J., Kim, Y., et al. (2013). Temporal Differential Effects of Proinflammatory Cytokines on Osteoclastogenesis. *Int. J. Mol. Med.* 31, 769–777. doi:10.3892/ijmm.2013.1269
- Mori, G., Brunetti, G., Colucci, S., Oranger, A., Ciccolella, F., Sardone, F., et al. (2009). Osteoblast Apoptosis in Periodontal Disease: Role of TNF-Related Apoptosis-Inducing Ligand. *Int. J. Immunopathol Pharmacol.* 22, 95–103. doi:10.1177/039463200902200111
- Naidu, V. G., Dinesh Babu, K. R., Thwin, M. M., Satish, R. L., Kumar, P. V., and Gopalakrishnakone, P. (2013). RANKL Targeted Peptides Inhibit Osteoclastogenesis and Attenuate Adjuvant Induced Arthritis by Inhibiting NF- κ B Activation and Down Regulating Inflammatory Cytokines. *Chem. Biol. Interact* 203, 467–479. doi:10.1016/j.cbi.2012.12.016
- Nanzhu, Y., Aichun, J., Xin, L., and Xianghua, Y. (2018). Salvianolate Injection in the Treatment of Acute Cerebral Infarction: A Systematic Review and a Meta-Analysis. *Medicine (Baltimore)* 97, e12374. doi:10.1097/MD.00000000000012374
- Okano, T., Inui, K., Tada, M., Sugioka, Y., Mamoto, K., Wakitani, S., et al. (2017). High Frequency of Vertebral Fracture and Low Bone Quality in Patients with Rheumatoid Arthritis-Results from TOMORROW Study. *Mod. Rheumatol.* 27, 398–404. doi:10.1080/14397595.2016.1213943
- Popova, V., Vazhev, Z., Geneva-Popova, M., and Batalov, A. (2019). Comparison of RANKL Expression, Inflammatory Markers, and Cardiovascular Risk in Patients with Acute Coronary Syndrome with and without Rheumatoid Arthritis. *Rheumatol. Int.* 39, 1723–1732. doi:10.1007/s00296-019-04367-9
- Rauch, A., Seitz, S., Baschant, U., Schilling, A. F., Illing, A., Stride, B., et al. (2010). Glucocorticoids Suppress Bone Formation by Attenuating Osteoblast Differentiation via the Monomeric Glucocorticoid Receptor. *Cell Metab* 11, 517–531. doi:10.1016/j.cmet.2010.05.005
- Ren, J., Fu, L., Nile, S. H., Zhang, J., and Kai, G. (2019). Salvia Miltiorrhiza in Treating Cardiovascular Diseases: A Review on its Pharmacological and Clinical Applications. *Front. Pharmacol.* 10, 753. doi:10.3389/fphar.2019.00753
- Sajti, E., Van Meeteren, N., Kavelaars, A., Van Der Net, J., Gispén, W. H., and Heijnen, C. (2004). Individual Differences in Behavior of Inbred Lewis Rats Are Associated with Severity of Joint Destruction in Adjuvant-Induced Arthritis. *Brain Behav. Immun.* 18, 505–514. doi:10.1016/j.bbi.2003.12.004
- Shen, Y., Wang, S., Liu, Y., Ge, L., Xia, L., Zhang, X., et al. (2020). The Effects of Salvianolate Combined with Western Medicine on Diabetic Nephropathy: A Systematic Review and Meta-Analysis. *Front. Pharmacol.* 11, 851. doi:10.3389/fphar.2020.00851
- Shiratori, T., Kyumoto-Nakamura, Y., Kukita, A., Uehara, N., Zhang, J., Koda, K., et al. (2018). IL-1 β Induces Pathologically Activated Osteoclasts Bearing Extremely High Levels of Resorbing Activity: A Possible Pathological Subpopulation of Osteoclasts, Accompanied by Suppressed Expression of Kindlin-3 and Talin-1. *J. Immunol.* 200, 218–228. doi:10.4049/jimmunol.1602035
- Thirunavukkarasu, K., Halladay, D. L., Miles, R. R., Yang, X., Galvin, R. J., Chandrasekhar, S., et al. (2000). The Osteoblast-specific Transcription Factor Cbfa1 Contributes to the Expression of Osteoprotegerin, a Potent Inhibitor of Osteoclast Differentiation and Function. *J. Biol. Chem.* 275, 25163–25172. doi:10.1074/jbc.M000322200
- Wang, Y., Wang, S., Li, Y., Jiang, J., Zhou, C., Li, C., et al. (2015). Therapeutic Effect of Cryptotanshinone on Collagen-Induced Arthritis in Rats via Inhibiting Nuclear Factor Kappa B Signaling Pathway. *Transl. Res.* 165, 704–716. doi:10.1016/j.trsl.2014.12.004
- Wang, Y., Zhao, R., Gu, Z., Dong, C., Guo, G., and Li, L. (2020). Effects of Glucocorticoids on Osteoporosis in Rheumatoid Arthritis: a Systematic Review and Meta-Analysis. *Osteoporos. Int.* 31, 1401–1409. doi:10.1007/s00198-020-05360-w
- Wen, L., Kang, J. H., Yim, Y. R., Lee, J. W., Lee, K. E., Park, D. J., et al. (2016). Risk Factors for Treatment Failure in Osteoporotic Patients with Rheumatoid Arthritis. *Mod. Rheumatol.* 26, 194–199. doi:10.3109/14397595.2015.1069444
- Wright, H. L., McCarthy, H. S., Middleton, J., and Marshall, M. J. (2009). RANK, RANKL and Osteoprotegerin in Bone Biology and Disease. *Curr. Rev. Musculoskelet. Med.* 2, 56–64. doi:10.1007/s12178-009-9046-7
- Wu, Q., Xiong, X., Zhang, X., Lu, J., Zhang, X., Chen, W., et al. (2016). Secondary Osteoporosis in Collagen-Induced Arthritis Rats. *J. Bone Miner. Metab.* 34, 500–516. doi:10.1007/s00774-015-0700-4
- Wu, Q., Zhou, X., Huang, D., Ji, Y., and Kang, F. (2017). IL-6 Enhances Osteocyte-Mediated Osteoclastogenesis by Promoting JAK2 and RANKL Activity In Vitro. *Cell Physiol Biochem* 41, 1360–1369. doi:10.1159/000465455
- Xu, D., Xu, L., Zhou, C., Lee, W. Y., Wu, T., Cui, L., et al. (2014). Salvianolic Acid B Promotes Osteogenesis of Human Mesenchymal Stem Cells through Activating ERK Signaling Pathway. *Int. J. Biochem. Cell Biol* 51, 1–9. doi:10.1016/j.biocel.2014.03.005
- Yang, Y., Su, Y., Wang, D., Chen, Y., Liu, Y., Luo, S., et al. (2016). Tanshinol Rescues the Impaired Bone Formation Elicited by Glucocorticoid Involved in KLF15 Pathway. *Oxid. Med. Cell Longev* 2016, 1092746. doi:10.1155/2016/1092746
- Yen, M. L., Hsu, P. N., Liao, H. J., Lee, B. H., and Tsai, H. F. (2012). TRAF-6 Dependent Signaling Pathway Is Essential for TNF-Related Apoptosis-Inducing Ligand (TRAIL) Induces Osteoclast Differentiation. *PLoS One* 7, e38048. doi:10.1371/journal.pone.0038048
- Yen, M. L., Tsai, H. F., Wu, Y. Y., Hwa, H. L., Lee, B. H., and Hsu, P. N. (2008). TNF-related Apoptosis-Inducing Ligand (TRAIL) Induces Osteoclast

- Differentiation from Monocyte/macrophage Lineage Precursor Cells. *Mol. Immunol.* 45, 2205–2213. doi:10.1016/j.molimm.2007.12.003
- Zhang, D., Wu, J., Liu, S., Zhang, X., and Zhang, B. (2016). Salvianolate Injection in the Treatment of Unstable Angina Pectoris: A Systematic Review and Meta-Analysis. *Medicine (Baltimore)* 95, e5692. doi:10.1097/MD.0000000000005692
- Zhang, Y. H., Heulsmann, A., Tondravi, M. M., Mukherjee, A., and Abu-Amer, Y. (2001). Tumor Necrosis Factor-Alpha (TNF) Stimulates RANKL-Induced Osteoclastogenesis via Coupling of TNF Type 1 Receptor and RANK Signaling Pathways. *J. Biol. Chem.* 276, 563–568. doi:10.1074/jbc.M008198200

Conflict of Interest: The authors declare that the research was conducted in the absence of any commercial or financial relationships that could be construed as a potential conflict of interest.

Publisher's Note: All claims expressed in this article are solely those of the authors and do not necessarily represent those of their affiliated organizations, or those of the publisher, the editors and the reviewers. Any product that may be evaluated in this article, or claim that may be made by its manufacturer, is not guaranteed or endorsed by the publisher.

Copyright © 2021 Gao, Wu, Zhang, Tian, Liang, Min, Lu, Zhang, Cui, Xu and Liu. This is an open-access article distributed under the terms of the Creative Commons Attribution License (CC BY). The use, distribution or reproduction in other forums is permitted, provided the original author(s) and the copyright owner(s) are credited and that the original publication in this journal is cited, in accordance with accepted academic practice. No use, distribution or reproduction is permitted which does not comply with these terms.



The Essential Oil of *Artemisia argyi* H.Lév. and Vaniot Attenuates NLRP3 Inflammasome Activation in THP-1 Cells

Pengxiao Chen^{1,2,3†}, Qi Bai^{1,2†}, Yanting Wu^{1,2}, Qiongzen Zeng^{1,2}, Xiaowei Song^{1,2}, Yuying Guo¹, Pengjun Zhou⁴, Yao Wang⁵, Xiaofeng Liao¹, Qiaoli Wang¹, Zhe Ren^{1,2*} and Yifei Wang^{1,2*}

¹Guangzhou Jinan Biomedicine Research and Development Center, Institute of Biomedicine, College of Life Science and Technology, Jinan University, Guangzhou, China, ²Key Laboratory of Bioengineering Medicine of Guangdong Province, Guangzhou, China, ³Biology Postdoctoral Research Station, Jinan University, Guangzhou, China, ⁴The First Affiliated Hospital of Jinan University, Guangzhou Overseas Chinese Hospital, Guangzhou, China, ⁵Guangdong Provincial Key Laboratory of Large Animal Models for Biomedicine, School of Biotechnology and Health Sciences, Wuyi University, Jiangmen, China

OPEN ACCESS

Edited by:

Xiao Bin Zeng,
Jinan University, China

Reviewed by:

Irem I. Tatli,
Hacettepe University, Turkey
Letizia Mezzaasoma,
University of Perugia, Italy

*Correspondence:

Zhe Ren
rz62@163.com
Yifei Wang
twang-yf@163.com

[†]These authors have contributed
equally to this work and share first
authorship

Specialty section:

This article was submitted to
Ethnopharmacology,
a section of the journal
Frontiers in Pharmacology

Received: 21 May 2021

Accepted: 03 September 2021

Published: 16 September 2021

Citation:

Chen P, Bai Q, Wu Y, Zeng Q, Song X,
Guo Y, Zhou P, Wang Y, Liao X,
Wang Q, Ren Z and Wang Y (2021) The
Essential Oil of *Artemisia argyi* H.Lév.
and Vaniot Attenuates NLRP3
Inflammasome Activation in THP-
1 Cells.
Front. Pharmacol. 12:712907.
doi: 10.3389/fphar.2021.712907

Artemisia argyi H. Lév. and Vaniot is a traditional medical herb that has been used for a long time in China and other Asian countries. Essential oil is the main active fraction of *Artemisia argyi* H. Lév. and Vaniot, and its anti-inflammatory potential has been observed *in vitro* and *in vivo*. Here, we found that the essential oil of *Artemisia argyi* H. Lév. and Vaniot (EOAA) inhibited monosodium urate (MSU)- and nigericin-induced NLRP3 inflammasome activation. EOAA suppressed caspase-1 and IL-1 β processing and pyroptosis. NF- κ B p65 phosphorylation and translocation were also inhibited. In addition, EOAA suppressed nigericin-induced NLRP3 inflammasome activation without blocking ASC oligomerization, suggesting that it may inhibit NLRP3 inflammasome activation by preventing caspase-1 processing. Our study thus indicates that EOAA inhibits NLRP3 inflammasome activation and has therapeutic potential against NLRP3-driven diseases.

Keywords: *Artemisia argyi* H. Lév. & Vaniot, essential oil, NLRP3 inflammasome, NF- κ B, ASC oligomerization

INTRODUCTION

Pattern recognition receptors (PRRs) are responsible for the detection of microbial components, endogenous danger signals and environmental irritants, leading to the activation of inflammatory cascades in immune cells that contribute to pathogen clearance and tissue repair (Takeuchi and Akira, 2010). NLRP3, a member of the Nod-like receptor family, is a vital pattern recognition receptor mediating the response to broad stimuli, including lipopolysaccharide (LPS), bacteria, virus, pore-forming toxin, adenosine triphosphate (ATP) and monosodium urate (MSU) crystals (Swanson et al., 2019). Once activated, NLRP3 self-oligomerizes and binds with ASC, which subsequently recruits caspase-1 to form a multiprotein complex called the NLRP3 inflammasome, resulting in the self-cleavage and maturation of caspase-1 (Fernandes-Alnemri et al., 2007). Activated caspase-1 further cleaves pro-IL-1 β and pro-IL-18 to produce active and mature forms, which are indispensable for the secretion of IL-1 β and IL-18 (Martinon et al., 2002). Gasdermin D (GSDMD) is also cleaved by caspase-1 and migrates to the plasma membrane, forming nonselective pores and inducing pyroptosis (He et al., 2015; Kayagaki et al., 2015; Shi et al., 2015). Typically, NLRP3 inflammasome activation requires two steps: priming and activation. During the

priming process, NF- κ B-mediated upregulation of NLRP3 and pro-IL-1 β is critical for the activation of the NLRP3 inflammasome (Bauernfeind et al., 2009). To date, the NLRP3 inflammasome is the most extensively studied inflammasome. Dysfunction of the NLRP3 inflammasome is implicated in various inflammatory diseases, such as type 2 diabetes (Masters et al., 2010), neuron degenerate diseases (Halle et al., 2008; Venegas et al., 2017; Ising et al., 2019) and gout (Martinon et al., 2006). Therefore, regulating the activation of the NLRP3 inflammasome is a promising therapeutic strategy for controlling inflammation-related disorders.

In recent years, *in vitro* and *in vivo* studies have revealed that several phytochemicals possess inhibitory effects on the NLRP3 inflammasome. Oridonin, a major active ingredient of *Rabdosia rubescens*, directly targets NLRP3 to mediate its preventive effects in mouse models of peritonitis, gouty arthritis and type 2 diabetes (He et al., 2018). Artemisinin attenuates uric acid-induced inflammation by interfering with the interaction between NEK7 and NLRP3 (Kim et al., 2019). Traditional medicine may be potentially useful resource for exploring therapeutic agents for the treatment of NLRP3 inflammasome-related diseases.

Artemisia argyi H. Lév. and Vaniot is a traditional Chinese medicinal herb that has been widely used to treat inflammation, dysmenorrhea, abdominal pain, uterine haemorrhage and pruritus (Song et al., 2019). Essential oil is the main component of *Artemisia argyi* H. Lév. and Vaniot. Gas chromatography-mass spectrometry (GC-MS) revealed that the essential oil of *Artemisia argyi* H. Lév. and Vaniot (EOAA) contains eucalyptol, β -caryophyllene, terpinolene and other ingredients (Guan et al., 2019). According to previous research, EOAA suppressed the inflammatory responses in a 12-O-tetradecanoylphorbol-13-acetate (TPA)-induced mouse ear edema model and downregulated the gene expression of the inflammatory mediators iNOS and COX-2 by inhibiting JAK/STAT activation (Chen et al., 2017). In addition, *Artemisia princeps* extract has been reported to suppress NLRP3 inflammasome activation (Kwak et al., 2018). However, the effect of EOAA on the activation of the NLRP3 inflammasome remains unknown.

Here, we found that EOAA extracted by steam distillation (SDAO) and EOAA extracted from CO₂ supercritical fluid (SFEAO) inhibited the activation of the NLRP3 inflammasome induced by MSU and nigericin. Thus, our results indicate that EOAA has therapeutic potential for NLRP3 inflammasome-related diseases.

MATERIALS AND METHODS

Materials

RPMI 1640 medium, fetal bovine serum (FBS) and penicillin-streptomycin were purchased from Gibco (Grand Island, NY, United States). Phorbol myristate acetate, cocktails of the protease and phosphatase inhibitor, RIPA lysis buffer, PMSF, LDH Cytotoxicity Assay Kit and SDS-PAGE solution kit were obtained from Beyotime Biotech (Shanghai, China). Uric acid

(U2625-25G) was from Sigma-Aldrich (St. Louis, MO, United States) which was used to prepare monosodium urate according to the previous study. Nigericin (tlrl-nig) were purchased from InvivoGen (San Diego, CA, United States). Disuccinimidyl suberate (DSS, RH65890-1G) was from BioRuler (Danbury, CT, United States). The ELISA kit for IL-1 β (CHE0001) and TNF- α (CHE0019) were purchased from Beijing 4A Biotech (Beijing, China). Antibodies against NLRP3 (D4D8T), Phospho-NF- κ B p65 (Ser536), NF- κ B p65 (D14E12) were from Cell Signaling Technology (Boston, MA, United States). Antibody against GSDMDC1 (64-Y) was obtained from Santa cruz (Santa Cruz, CA, United States). Antibody against ASC/TMS1 was from ProteinTech (Des Plaines, IL, United States). IL-1 β antibody (AF-401-SP) was from R&D systems (Minneapolis, MN, United States). Anti-pro-Caspase-1 + p10 + p12 antibody (ab179515) was from Abcam (Cambridge, MA, United States). Donkey anti-Rabbit IgG (H+L) Secondary Antibody (Alexa Fluor 488) and Chicken anti-Rabbit IgG (H+L) Cross-Adsorbed Secondary Antibody (Alexa Fluor 594) were purchased from Life technology (Grand Island, NY, United States). Other ordinary chemicals were from Guangzhou chemical reagent factory (Guangzhou, China).

Extraction of Essential Oils Hydrodistillation

500 g crushed dry leaves of *Artemisia argyi* H. Lév. and Vaniot from Nanyang City in Henan province of China were filled in round bottom boiling flask with 5 L distilled water for 3 h. Then, the essential oil was extracted by hydrodistillation in a glass Clevenger-type apparatus for 5 h as recommended by Chinese Pharmacopoeia and collected into a container. The acquired oil was subsequently dried over anhydrous sodium sulphate and sealed in the dark under refrigeration until used.

Subcritical Extraction

500 g crushed dry leaves of *Artemisia argyi* H. Lév. and Vaniot were filled in the supercritical extraction device. The subcritical extraction system was provided by Guangzhou Fengze Machinery Equipment Installation Co., Ltd. (Guangzhou, China). The extraction temperature was set as 55°C and the extraction pressure was 20 MPa. The flow rate of CO₂ was constant at 25 L/h for 1 h. Resover I pressure was 7 MPa and resover II pressure was 5 MPa. After extraction, two times amount of ethanol was mixed the extract of *Artemisia argyi* H. Lév. and Vaniot and stirred overnight. Precipitated wax composition was removed through vacuum filtration. The ethanol in filtrate was removed by vacuum distillation at 30°C to obtain the volatile oil of *Artemisia argyi* H. Lév. and Vaniot.

Gas Chromatography-Mass Spectrometry Analysis of EOAA

GC/MS analysis of the essential oil was carried out on a GC-MS system (7890A-5975C, Agilent, Little Falls, DE, United States) equipped with Agilent J&W HP-5 ms capillary column (30 m \times 0.25 mm \times 0.25 μ m) in the electron impact mode (Ionization energy: 70 eV). The ion source temperature of mass spectrometer

was 230°C. The temperature program was started at 50°C, remaining at this temperature for 2 min, and increased to 200°C with a flow rate of 5°C/min, then held for 2 min, followed by increasing to 240°C by 30°C/min, and then held for 1 min. Split injection (1 µl) was conducted with a split ratio of 1:20. Helium was used as the carrier gas with a flow rate of 1.0 ml/min. Volatile compounds were identified by comparing the obtained mass spectra of the analytes with those of authentic standards from the NIST libraries using MassHunter software. The identified components were analyzed quantitatively by area normalization.

Cell Culture and Stimulation

THP-1 cells were obtained from the American Type Culture Collection and STR profiling authentication of THP-1 cells (Supplementary material) was conducted by Cellcook Biotech (Guangzhou, China). THP-1 cells were cultured in RPMI 1640 medium containing 10% FBS at 37°C in a humidified incubator with 5% CO₂ and 95% air. The cells were routinely tested for mycoplasma contamination. Differentiated THP-1 cells were acquired by incubation with 500 nM phorbol myristate acetate (PMA) for 3 h. Before induction of inflammasome activation, the medium was replaced with Opti-MEM. Then, the cells were treated with 500 µg/ml MSU with or without essential oil for 6 h. Differentiated THP-1 cells were treated with nigericin for 1 h to induce inflammasome activation. Essential oil was added to the cell culture 1 h before nigericin induction.

Cell Viability Assay

PMA treated THP-1 cells (1×10^4 cells) were added in each well of 96-well plated and allowed the attachment of cells for 12 h. After washing with PBS, cells were exposed to series of diluted SFEAO and SEAO with 1640 medium for additional 24 h. SFEAO and SEAO were original mix with PEG400 at 10% v/v. The medium in each well was then removed followed by washing with PBS. 10 µl CCK-8 in 100 µl 1640 medium was added to each well and the plates were incubated at 37°C continually. The absorbance of each well was measured at 450 nm every 30 min using microplate reader (ELX800, BioTek, Winooski, VT, United States). Until it had reached above 1.0, the data of absorbance was recorded. The percentage of viability was calculated according to the following equation. Percentage of viability = (OD of sample-OD of blank)/(OD of control-OD of blank) × 100%. Wells only contained cell culture medium was set as blank. Cells treated without SFEAO or SEAO were set as control and cell treated with SFEAO or SEAO were set as sample.

ELISA

Cell culture supernatants were collected after separation from the cell debris through centrifugation. Then, the levels of IL-1β and TNF-α in the supernatants were assessed using ELISA kits according to the manufacturer's guidelines. In brief, a series concentrations of standard and diluted cell supernatants were added to the primary antibody coated plate and incubated at 37°C for 90 min. Wash the plate for four times and flap the plate to dry. Add biotinylated primary antibody to each well and incubated at 37°C for 60 min. Again, wash the plate for four times and flap the

plate to dry. Add enzyme conjugated-second antibody and incubate in dark at 37°C for 30 min. Wash the plate for four times and flap the plate to dry. Add chromogenic substrate and incubate in dark at 37°C for 30 min. Finally, add stop solution into wells and measure OD at 450 nm with microplate reader. Calculate the concentration of IL-1β and TNF-α in cell supernatant according to the standard curve fitted by four parameters logistic fitting method.

Lactate Dehydrogenase Assay

The release of LDH in the culture medium was assayed with an LDH cytotoxicity kit according to the manufacturer's guidelines. Cells were seeded on 96 wells plate. Select one group of wells as "group of maximal LDH release rate." Before treating cells as the method in "Cell culture and stimulation" section, wash cells with PBS and change to serum-free medium. 1 h before the end of treatment, add LDH release reagent in wells of "group of maximal LDH release rate." At the end of treatment, the plate was centrifuged at 400 g for 5 min. Transfer 120 µl supernatant in a new plate. Add INT (2-p-iodophenyl-3-nitrophenyl tetrazolium chloride) and lactic acid solution in each well and incubate the plate in dark at room temperature for 30 min. Measure OD at 490 nm and calculate the release rate of LDH as the following equation:

Release rate of LDH = (OD of treated sample-OD of control)/(OD of "group of maximal LDH release rate"-OD of control) × 100%

Immunoblotting

Cells were lysed in RIPA buffer on ice for 30 min, and then supernatants were collected through centrifugation at 14,000 g/min for 15 min. The protein concentration of the supernatants was measured using the BCA method. After the addition of 5× loading buffer, the cell lysate was heated to 100°C. The denatured cell lysate sample was loaded on an 8% or 10% polyacrylamide gel. After transfer to the PVDF membrane and incubation in nonfat milk, the membrane was incubated overnight in the indicated antibody solution at 4°C. The signal on the membrane was detected with an enhanced chemiluminescence detection kit (4AW012-1000, Beijing 4A Biotech) and acquired via an imaging system (Tanon 4600 SF, Biotanon, Shanghai, China). Antibodies against NLRP3 (D4D8T), Phospho-NF-κB p65 (Ser536), NF-κB p65 (D14E12), GSDMDC1 (64-Y), ASC/TMS1, IL-1β and pro-Caspase-1 + p10 + p12 were used for detecting the corresponding proteins.

ASC Oligomerization Assay

After the treatment, the cells were lysed in AO buffer (1% Triton × 100, 20 mM HEPES-KOH, pH 7.5, 150 mM KCl, and complete protease and phosphatase inhibitor cocktail) by syringing 30 times through a 21-gauge needle. The lysates were centrifuged at 3,200 g for 15 min at 4°C and separated into the soluble fraction (the supernatant) and insoluble fraction (the pellet). Equal amount of soluble fraction was collected, and 5× loading buffer was added. The insoluble part was rinsed in PBS twice and resuspended in 60 µl PBS containing 4 mM disuccinimidyl suberate (DSS). The cross-linking reaction was

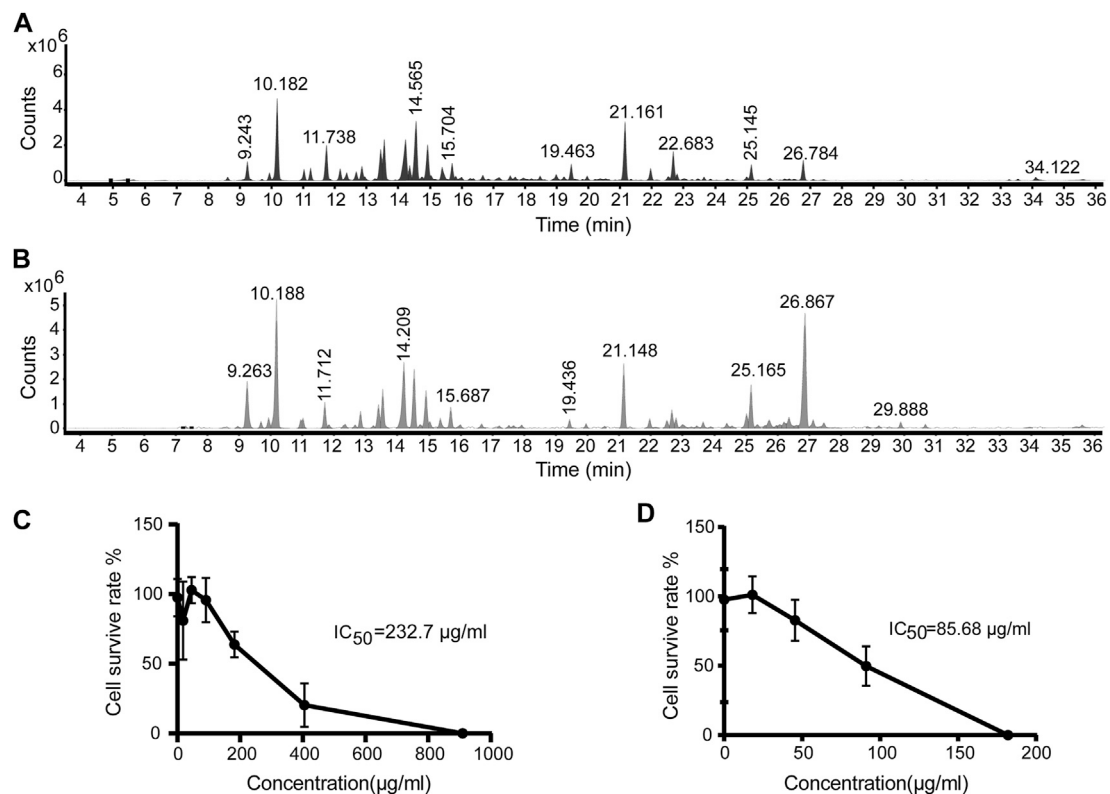


FIGURE 1 | GC-MS analysis of EOAA and the effect of EOAA on cell viability. Typical total ion chromatography (TIC) of SFEAO (**A**) and SDAO (**B**). THP-1 cells were incubated with different concentrations of SFEAO and SDAO. The effect of SFEAO (**C**) and SDAO (**D**) on cell viability were determined by CCK-8 assay. IC_{50} : the half maximal inhibitory concentration. Data were from three independent experiments with biological duplicates in each (**C,D**; mean and SD of $n = 6$).

performed at room temperature for 30 min with rotation (Lugrin and Martinon, 2017). Then, the same volume of nonreducing loading buffer was added. All the samples were boiled for 10 min and loaded on polyacrylamide gels for immunoblotting.

Immunofluorescence

For detection of ASC specks and NF- κ B p65 translocation, cells were seeded on coverslips the day before the following procedures. After the indicated treatment, the cells were fixed with 4% paraformaldehyde, permeabilized with PBS containing 0.1% Triton \times 100, and blocked with 3% BSA in PBST. The cells were stained with ASC antibody and NF- κ B p65 antibody overnight at 4°C. The next day, anti-rabbit antibodies (Alexa Fluor 488 and Alexa Fluor 594) were added for incubation at room temperature for 1 h. The nuclei were counterstained with DAPI. All of the images were acquired with a fluorescence microscope (Zeiss LSM880 Airyscan, Zeiss, Germany).

Statistical Analysis

All data are expressed as the mean \pm SD and are representative of at least three different experiments or biological replications. Statistical analysis was performed in GraphPad using Student's *t*-test for two groups and one-way ANOVA for multiple groups. Differences with *p* values less than 0.05 were considered to be statistically significant.

RESULTS

GC-MS Analysis of EOAA

The *Artemisia argyi* H. Lévl. and Vaniot used in this study was collected from Henan Province of China and EOAA was extracted with supercritical fluid extraction and hydrodistillation. The chemical composition of the essential oil was analyzed by GC-MS and was showed in **Figures 1A,B**. As listed in **Tables 1, 2**, a total of 29 and 26 compounds were identified for the SFEAO and SDAO, accounting for the 85.7 and 81.7% of total oil, respectively. The major components were found to be monoterpenoids, sesquiterpenoids, phenols, ketones, aldehydes in SFEAO and SDAO. Five major compounds in common were eucalyptol, terpinen-4-ol, β -caryophyllene, (+)-borneol, and α -terpineol. The most abundant composition in SFEAO is eucalyptol. Differently, neointermedeol was most abundant in SDAO, accounting for $16.12 \pm 0.95\%$. The cytotoxicity effects of SFEAO and SDAO were determined by CCK-8 assay. As showed in **Figures 1C,D**, the IC_{50} concentrations of SFEAO and SDAO were 232.7 and 85.7 μ g/ml respectively, which indicated that SFEAO was less cytotoxic than SDAO.

EOAA Inhibits the Release of Processed Caspase-1 and IL-1 β Induced by MSU

When the NLRP3 inflammasome is activated, procaspase-1 self-cleaves into activated caspase-1 (p10), which further cleaves

TABLE 1 | Chemical compositions of SFEAO.

Rt (min)	Compound	CAS	Peak area (%)
9.243	2,5,5-trimethyl-3,6-heptadien-2-ol	26127-98-0	2.33 ± 0.14
9.937	p-Cymene	99-87-6	0.91 ± 0.05
10.182	1,8-Cineole	470-82-6	8.96 ± 0.48
11.030	3,3,6-trimethylhepta-1,5-dien-4-one	546-49-6	1.08 ± 0.04
11.235	Sabinene hydrate	546-79-2	1.55 ± 0.12
11.738	3,3,6-trimethylhepta-1,5-dien-4-ol	27644-04-8	3.50 ± 0.38
12.170	trans-Sabinene hydrate	17699-16-0	1.59 ± 0.15
12.376	Thujone	546-80-5	1.02 ± 0.11
12.678	β-Thujone	471-15-8	1.95 ± 0.54
12.856	4-Isopropyl-1-Methyl-2-Cyclohexen-1-ol	619-62-5	4.60 ± 1.40
13.449	cis-Sabinol	3310-2-9	5.24 ± 1.11
13.563	(±)-Camphor	464-49-3	0.29 ± 2.12
13.910	cis-Chrysanthanol	55722-60-6	1.26 ± 0.25
14.233	Borneol	507-70-0	6.31 ± 0.27
14.244	6-Camphenol	3570-04-5	1.93 ± 0.41
14.366	1,5-Heptadien-4-ol, 3,3,6-trimethyl-, 4-acetate, (4S)- (ACI)	3465-88-1	1.62 ± 0.08
14.565	Terpinen-4-ol	562-74-3	8.72 ± 0.36
14.931	α-Terpineol	98-55-5	5.26 ± 0.43
15.164	trans-Piperitol	16721-39-4	1.79 ± 0.23
15.388	(S)-Verbenone	1196-01-6	0.87 ± 0.16
15.704	cis-Carveol	1197-06-4	2.44 ± 0.24
18.987	γ-Terpineol	586-81-2	0.71 ± 0.08
19.463	Eugenol	97-53-0	2.07 ± 0.18
21.161	β-Caryophyllene	87-44-5	8.08 ± 0.45
21.968	Humulene	6753-98-6	1.50 ± 0.10
22.683	(±)-β-Copaene	18252-44-3	4.01 ± 0.36
22.805	(+)-β-Selinene	17066-67-0	0.82 ± 0.09
25.145	Caryophyllene oxide	1139-30-6	2.37 ± 0.28
26.784	Neointermedeol	5945-72-2	2.93 ± 0.32

TABLE 2 | Chemical compositions of SDAO.

Rt (min)	Compound	CAS	Peak area (%)
9.263	2,5,5-trimethyl-3,6-heptadien-2-ol	26127-98-0	4.50 ± 0.13
9.699	4-Carene	29050-33-7	0.36 ± 0.17
9.941	p-Cymene	99-87-6	1.08 ± 0.13
10.068	β-Phellandrene	555-10-2	0.63 ± 0.11
10.188	1,8-Cineole	470-82-6	10.66 ± 1.38
10.947	γ-Terpinene	99-85-4	0.37 ± 0.25
11.003	3,3,6-trimethylhepta-1,5-dien-4-one	546-49-6	0.71 ± 0.06
11.712	3,3,6-trimethylhepta-1,5-dien-4-ol	27644-04-8	2.05 ± 0.12
12.838	trans-4-Isopropyl-1-methyl-2-cyclohexen-1-ol	29803-81-4	1.52 ± 0.07
13.407	cis-Sabinol	3310-2-9	2.06 ± 0.64
13.539	(±)-Camphor	464-49-3	3.39 ± 0.05
14.209	Borneol	507-70-0	7.24 ± 0.10
14.529	Terpinen-4-ol	562-74-3	5.85 ± 0.06
14.905	α-Terpineol	98-55-5	5.17 ± 2.10
15.310	trans-Piperitol	16721-39-4	0.90 ± 0.10
15.687	cis-Carveol	1197-06-4	2.00 ± 0.12
19.436	Eugenol	97-53-0	0.64 ± 0.06
21.148	β-Caryophyllene	87-44-5	5.85 ± 0.16
21.966	Humulene	6753-98-6	0.81 ± 0.04
22.666	β-Copaene	18252-44-3	1.33 ± 0.17
22.792	(+)-β-selinene	17066-67-0	0.80 ± 0.011
25.028	Espatulenol	6750-60-3	1.54 ± 0.19
25.165	Caryophyllene oxide	1139-30-6	4.87 ± 0.66
26.361	Bicyclo [7.2.0]undecan-3-ol, 11,11-dimethyl-4,8-bis(methylene)- (9CI, ACI)	79580-01-1	0.48 ± 0.34
26.867	Neointermedeol	5945-72-2	16.12 ± 0.95
27.123	trans-Longipinocarveol	889109-69-7	0.80 ± 0.11

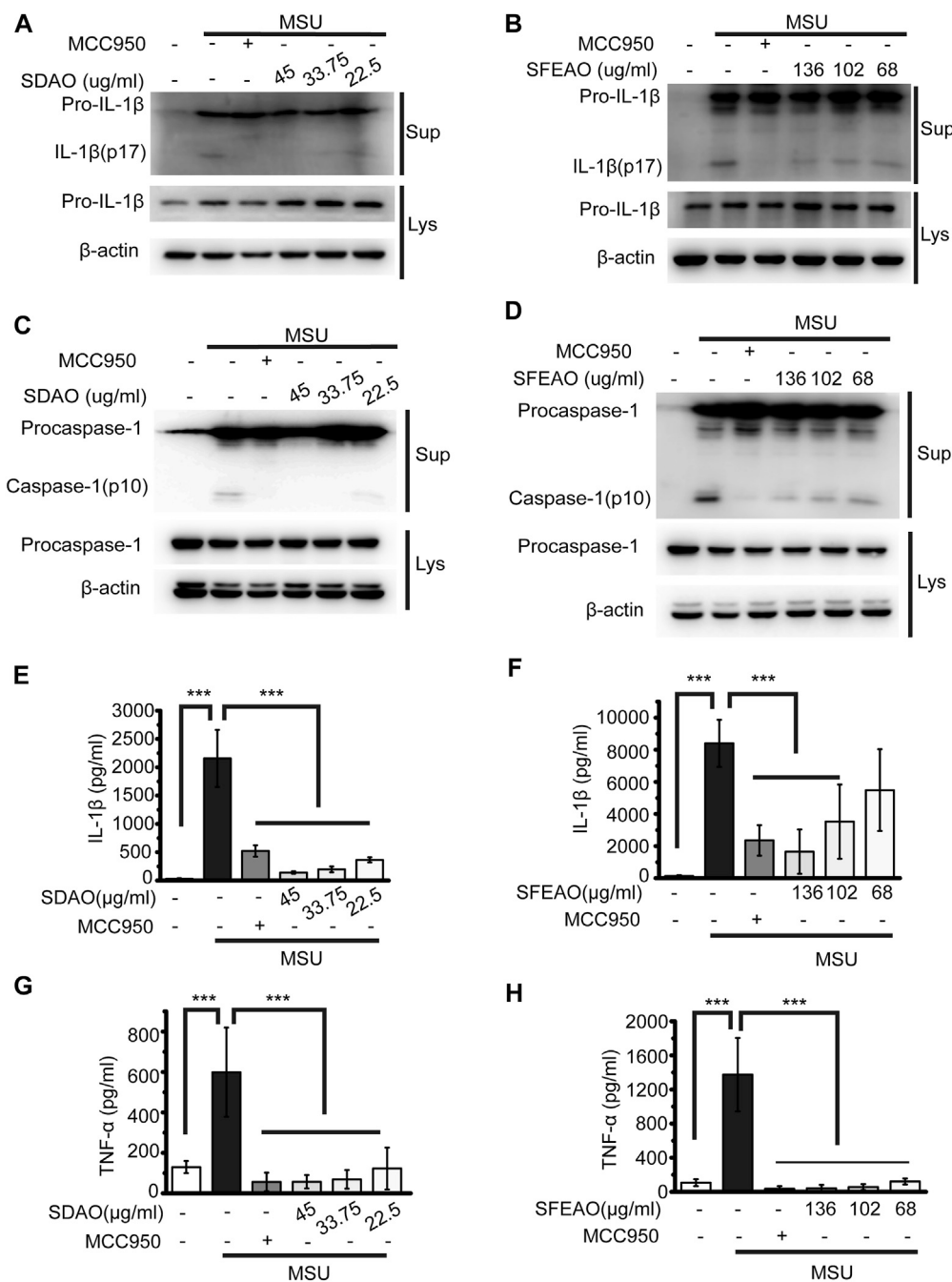


FIGURE 2 | EOAAs inhibit the release of processed caspase-1 and secretion of IL-1 β and TNF- α induced by MSU. PMA-primed THP-1 cells were treated with or without MCC950 (20 μ M) or different concentrations of SDAO or SFEAO and stimulated with MSU (500 μ g/ml) for 6 h. The level of mature IL-1 β (**A,B**) and caspase-1 (**C,D**) cleavage were assessed in the supernatant. The levels of pro-IL-1 β and procaspase-1 were assessed in whole-cell extracts by immunoblotting. β -Actin was used as an internal control. Concentrations of IL-1 β (**E,F**) and TNF- α (**G,H**) in the supernatant were determined by ELISA. Data were from three independent experiments with biological duplicates in each (**E-H**; mean and SD of $n = 6$) or are representative of at least three independent experiments (**A-D**). Statistics were analyzed using one-way ANOVA by Bonferroni post hoc test, * $p < 0.05$, ** $p < 0.01$, *** $p < 0.001$.

pro-IL-1 β to form IL-1 β (p17). The activated fragments of both caspase-1 (p10) and IL-1 β (p17) are secreted and thus can be detected in the cell culture supernatant (Guey and Petrilli, 2016). As shown in **Figures 2A,B**, SDAO and SFEAO at different concentrations inhibited the processing of IL-1 β after MSU

treatment for 6 h. Consistent with these results, the abundance of the activated fragment of caspase-1 was decreased in SDAO- and SFEAO-treated cell culture supernatants (**Figures 2C,D**). In addition, the inhibitory effects of SDAO and SFEAO were dose-dependent. MCC950 was used as a positive control (Coll et al.,

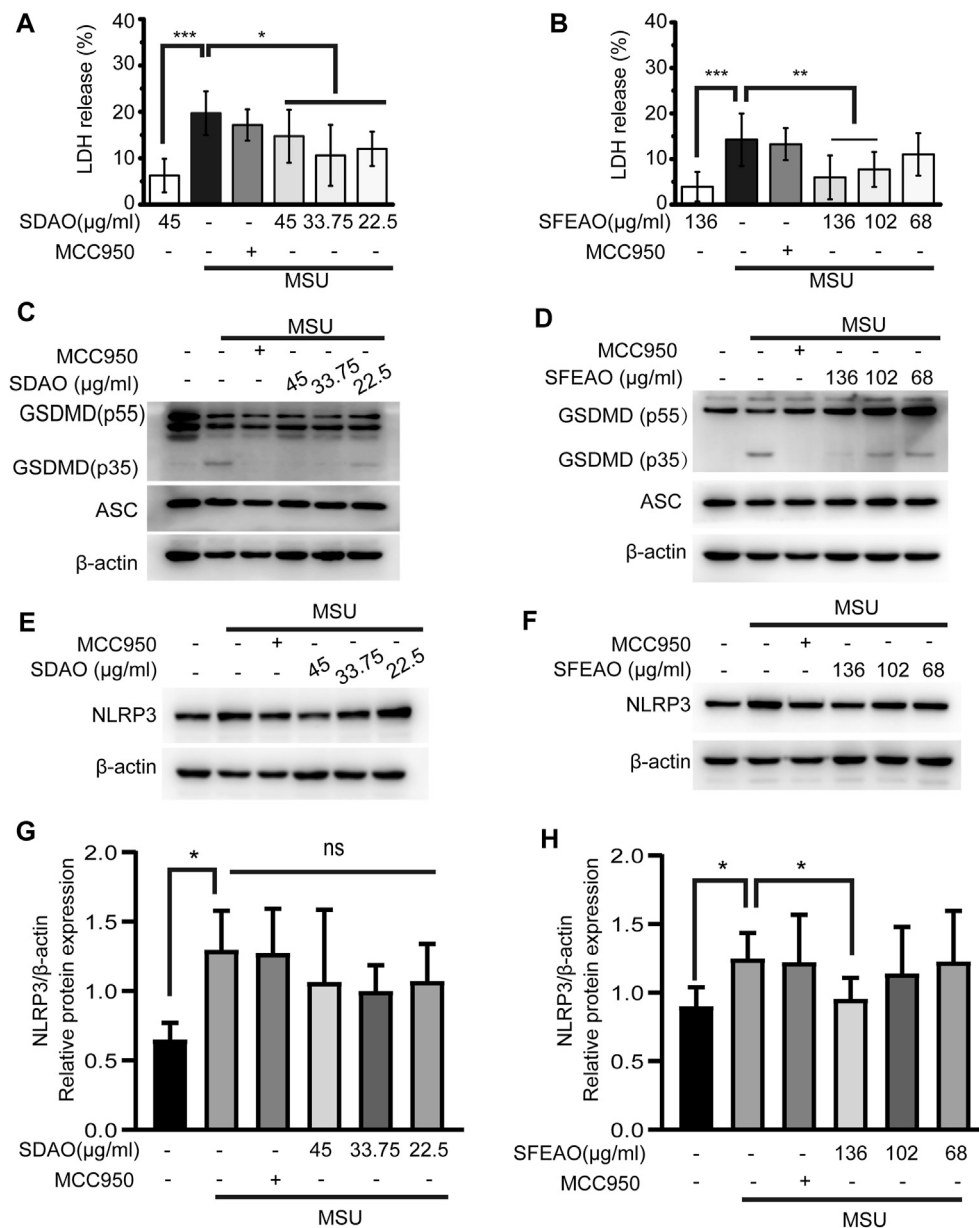


FIGURE 3 | EAOA inhibits the cleavage of GSDMD, the release of LDH and the expression of NLRP3 after MSU treatment. PMA-primed THP-1 cells were treated with or without MCC950 (20 μM) or different concentrations of SDAO or SFEAO upon stimulation with MSU (500 μg/ml) for 6 h. The release of LDH in cell supernatants was measured by LDH assay (**A,B**). The cleavage of GSDMD and the amount of ASC in the whole-cell extract were assessed by immunoblotting (**C,D**). The protein expression levels of NLRP3 (**E,F**) in the cytoplasm were measured utilizing immunoblotting. β-Actin was acted as internal reference. NLRP3 expression was analyzed by densitometric quantification (**G,H**, $n = 3$ for **G**, $n = 5$ for **H**). Data were from three independent experiments with six biological duplicates in each (**A,B**; mean and SD of $n = 18$) or are representative of at least three independent experiments (**C-F**). Arcsine-square root transformation of the percent data was used for statistical analysis. Statistics were analyzed using one-way ANOVA by Bonferroni post hoc test, * $p < 0.05$, ** $p < 0.01$, *** $p < 0.001$.

2015), and the amounts of activated caspase-1 and IL-1 β were lowest with MCC950 among the different treatments. These data indicate that SDAO and SFEAO can inhibit the activation of NLRP3 inflammasome.

The activation of the NLRP3 inflammasome causes cell membrane rupture, which allows the release of cytokines such as IL-1 β and other cellular components. This process is called

pyroptosis. LDH was released into the cell culture supernatant only when the integrity of the cell membrane was disrupted (Evavold et al., 2018). Thus, the concentrations of IL-1 β and LDH in the supernatant can indicate the extent of cell pyroptosis after different treatments. As shown in **Figures 2E,F**, both SDAO and SFEAO decreased the concentration of IL-1 β after MSU treatment. Moreover, the concentration of TNF- α was

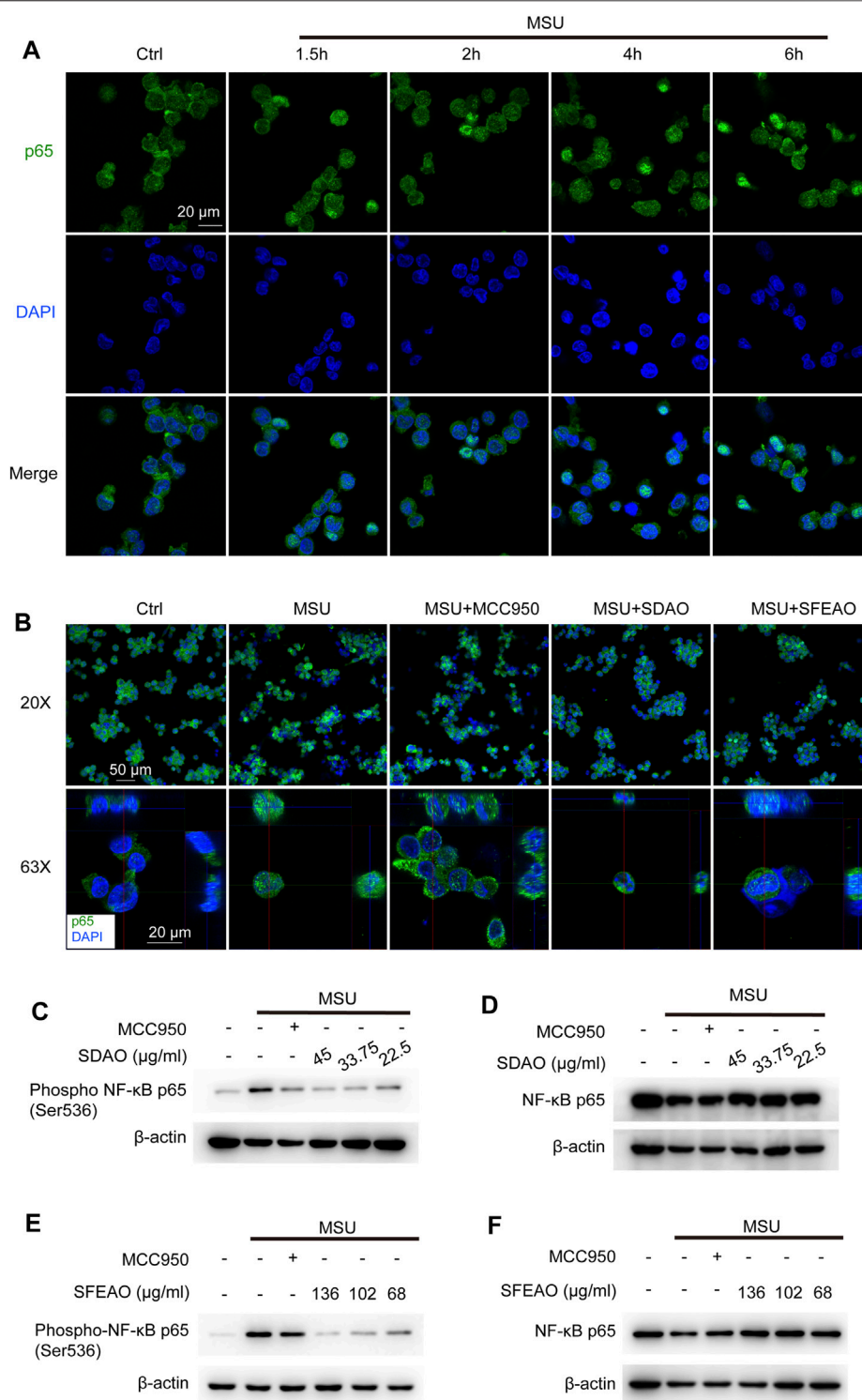


FIGURE 4 | EOAA inhibits the nuclear translocation of p65 and phosphorylation of p65 after MSU stimulation. The subcellular localization of p65 was determined by indirect immunofluorescence using fluorescence microscopy after staining with a p65 antibody (green). Nuclear DNA was revealed by DAPI staining (blue). **(A)** PMA-primed THP-1 cells were stimulated with MSU (500 μg/ml) for different durations. **(B)** PMA-primed THP-1 cells were treated with or without MCC950 (20 μM), SDAO (45 μg/ml) or SFEAO (136 μg/ml) upon stimulation with MSU (500 μg/ml) for 6 h. Two magnifications of immunofluorescence pictures were acquired, and Z-stack pictures at 63X were processed using the Image software package for orthogonal view. The green and red lines in 63X images indicate the positions within the image of the projection given on the upper (XZ surface) and right (YZ surface), respectively. PMA-primed THP-1 cells were treated with or without MCC950 (20 μM) or different concentrations of SDAO or SFEAO upon stimulation with MSU (500 μg/ml) for 6 h. The protein expression levels of p-p65 **(C,E)** and NF-κB p65 **(D,F)** in the cytoplasm were measured utilizing immunoblotting. β-Actin was acted as internal reference.

decreased by SDAO and SFEAO (**Figures 2G,H**). The release rate of LDH was also decreased by SDAO and SFEAO (**Figures 3A,B**). This suggests that SDAO and SFEAO inhibit pyroptosis induced by NLRP3 inflammasome activation.

The mechanism of cell pyroptosis involves the cleavage of GSDMD. Activated caspase-1 cleaves GSDMD into GSDMD-N and other fragments. This cleavage induces the oligomerization of GSDMD-N on the cell membrane, which leads to the formation of a nonselective pore and cell membrane collapse (He et al., 2015; Kayagaki et al., 2015; Shi et al., 2015). We found that SDAO and SFEAO decreased the amount of GSDMD-N (GSDMD p35) (**Figures 3C,D**), which indicates their inhibitory effect on pyroptosis induced by MSU.

EOAA Inhibits the Activation of NF- κ B and has Little Effect on Protein Expression of NLRP3

There are two processes involved in the activation of the NLRP3 inflammasome. The first process is priming, in which the activation of NF- κ B is needed to promote the transcription of NLRP3 and IL-1 β . Without the accumulation of sufficient amounts of NLRP3, the NLRP3 inflammasome cannot be activated (Bauernfeind et al., 2009). We found that NLRP3 expression increased after MSU treatment. SDAO didn't significantly inhibited the expression of NLRP3 in MSU-treated cells (**Figures 3E,G**). However, SFEAO (136 μ g/ml) induced a slight decrease on expression of NLRP3 in MSU-treated cells (**Figures 3F,H**). Additionally, MSU induced a mild increase in gene expression of NLRP3 and IL-1 β (**Supplementary Figure S1**), which was consistent with the result of protein expressions. Notably, both SFEAO (136 μ g/ml) and SDAO (45 μ g/ml) inhibited the gene expression of NLRP3 and IL-1 β upon MSU stimulation (**Supplementary Figure S1**).

NF- κ B is a crucial transcription factor in inflammatory reaction and is composed of p50/p105 (NF- κ B1) and p65 (RelA). In the resting state, NF- κ B localizes to cells and binds to an inhibitory protein, I κ B α (Hayden and Ghosh, 2004). IKK β is the kinase to phosphorylate I κ B α . Phosphorylated I κ B α is ubiquitinated and translocated to the proteasome for degradation, which causes the release of p65 and exposure of nuclear-located guide peptides (Karin and Ben-Neriah, 2000). At the same time, p65 is phosphorylated by IKK β , which is helpful for the maximum activity of NF- κ B (Chen and Greene, 2004). Former study has shown that MSU induced NF- κ B dependent transcriptional activation of IL-8 promotor (Liu et al., 2000). We detected the location of p65 in cells after MSU treatment for different times. The data showed that nuclear p65 began to translocate to the nucleus after MSU treatment for 2 h and was sustained in the nucleus after MSU treatment for 6 h (**Figure 4A**). Then, we detected the effect of SDAO and SFEAO on the translocation of p65. The results shown in **Figure 4B** suggested that SDAO and SFEAO inhibited the translocation of NF- κ B after MSU treatment for 6 h. Further, we detected the phosphorylation of p65 at Ser536. Different concentrations of SDAO and SFEAO decreased the

phosphorylation of p65 at Ser536 (**Figures 4C,E**). However, neither SDAO nor SFEAO changed the expression of total p65 (**Figures 4D,F**). Although SDAO and SFEAO inhibited the activation of NF- κ B and decreased the transcriptional level of NLRP3 slightly, the protein expression of NLRP3 was not altered by SDAO and SFEAO.

EOAA Blocks the Oligomerization of ASC

After the priming process, NLRP3 assembles into an oligomer under the stimulation of some molecules. Then, ASC links to the NLRP3 oligomer through the PYD domain, and ASC molecules aggregate with each other via the PYD domain, forming a large scaffold for the combination of pro-caspase-1 at the CARD domain that can be visualized as a speck (Fernandes-Alnemri et al., 2007). The specks were visible under a microscope when the cells were stained with a fluorescent antibody recognizing ASC (Stutz et al., 2013). As shown in **Figure 5A**, cells treated with MSU exhibited many ASC specks. The percentage of cells with ASC specks was $22.2 \pm 2.4\%$ among the total cells when the cells were treated with MSU. However, MCC950, SDAO and SFEAO significantly decreased the percentage of cells with ASC specks to respectively $4.0 \pm 1.1\%$, $1.8 \pm 0.4\%$ and $1.7 \pm 0.7\%$ (**Figure 5B**). We found that both the dimerization and oligomerization of ASC were blocked by SDAO and SFEAO (**Figures 5C,D**). These results suggest that SDAO and SFEAO block the organization process of the NLRP3 inflammasome, thus inhibiting its activation.

Effect of EOAA on Phosphorylation of MAPKs and I κ B α

Some researchers have reported that the MAPK signaling pathway is involved in the inflammation caused by MSU (Jaramillo et al., 2004; Campillo-Gimenez et al., 2018; Bousoik et al., 2020). In addition, the MAPK signaling pathway is upstream of NF- κ B. Therefore, we detected the phosphorylation of several MAPKs, including p38, JNK1/2, ERK1/2 and p65, to determine whether MAPKs could be phosphorylated before p65. As shown in **Figures 6B,C**, JNK and p65 were phosphorylated 60 min after MSU treatment. p38 was significantly phosphorylated at 90 min (**Figure 6A**). However, the phosphorylation of ERK1/2 appeared in the resting state and decreased gradually (**Figure 6D**). Our data showed that MAPKs were phosphorylated after MSU treatment and that JNK and p65 were phosphorylated at almost the same time point.

Then, we detected whether EOAA inhibited the phosphorylation of p38, JNK, ERK and p65 at 90 min after MSU treatment. **Figures 6E,F** show that SDAO (45 μ g/ml) and SFEAO (136 μ g/ml) inhibited the phosphorylation of p38, JNK and p65. Further, we detected the phosphorylation of IKK α / β and I κ B α , which are indicators of the initiation of NF- κ B activation. Our results showed that MSU treatment increased the phosphorylation of IKK α / β and I κ B α (**Figures 6G,H**). SDAO (45 μ g/ml) and SFEAO (136 μ g/ml) inhibited the phosphorylation of IKK α / β and I κ B α

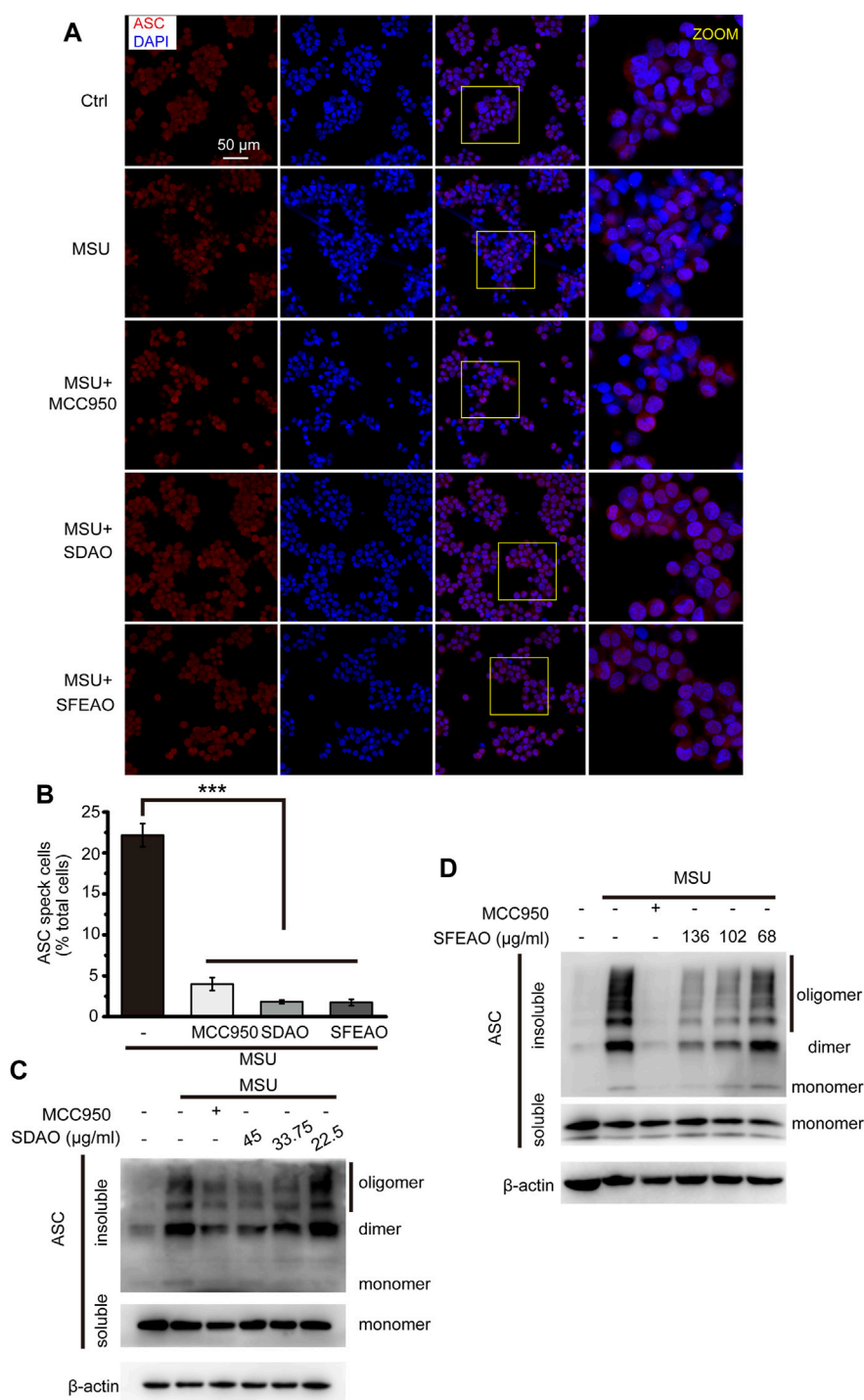


FIGURE 5 | EOAA inhibits the formation of ASC oligomers induced by MSU. PMA-primed THP-1 cells were treated with or without MCC950 (20 μ M) or different concentrations of SDAO or SFEAO upon stimulation with MSU (500 μ g/ml) for 6 h. **(A)** Cells stained with anti-ASC antibody for ASC specks (red) and DAPI for nuclei (blue). The concentrations of SDAO and SFEAO were 45 and 136 μ g/ml, respectively. **(B)** The percentage of cells with ASC specks among all cells is presented. **(C,D)** ASC oligomers were extracted from the Triton X-100 insoluble part of the cell extract by DSS crosslinking and measured by immunoblotting. ASC speck was quantified by the cells with ASC specks relative to the total cells from three individual fields in each experiment. Data were from three independent experiments **(B)**; mean and SEM of $n = 3$) or are representative of at least three independent experiments **(A,C,D)**. Arcsine-square root transformation of the percent data was used for statistical analysis. Statistics were analyzed using one-way ANOVA by Bonferroni post hoc test, * $p < 0.05$, ** $p < 0.01$, *** $p < 0.001$.

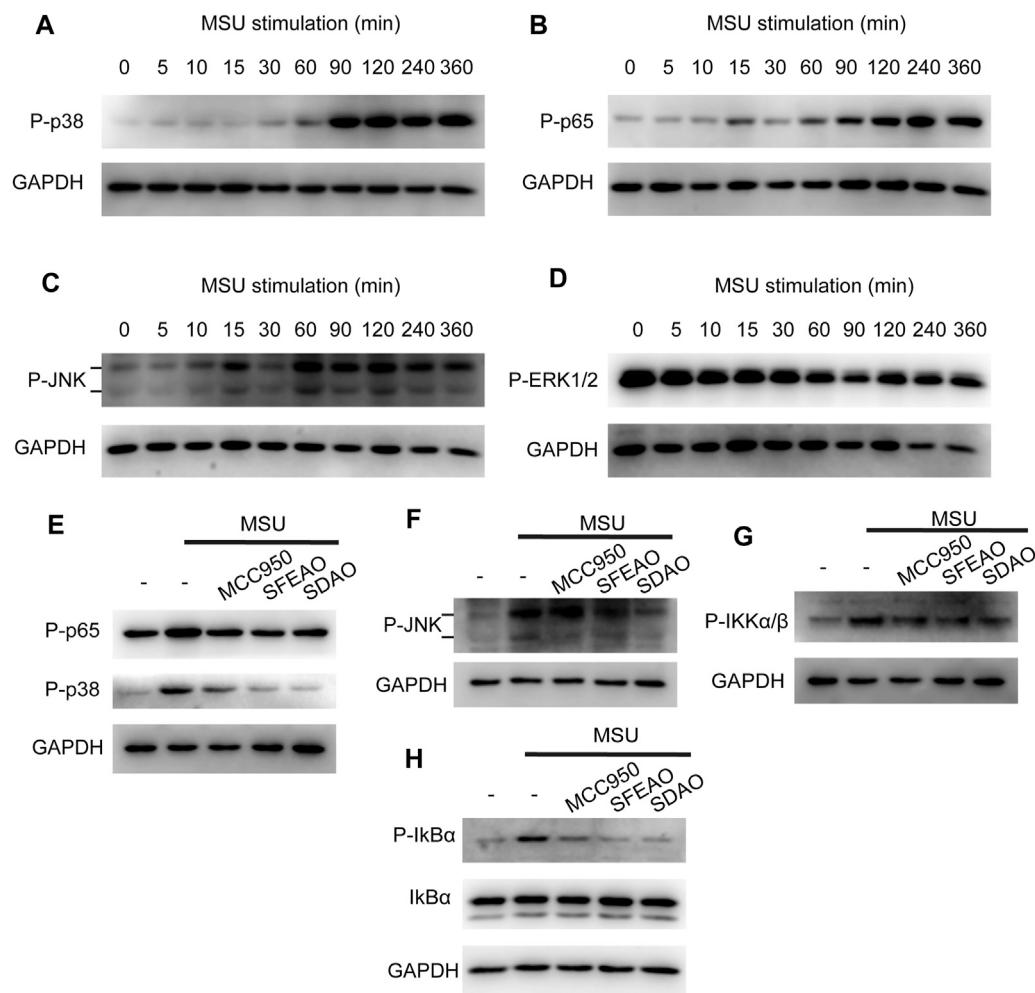


FIGURE 6 | EOAA inhibited the phosphorylation of p65, p38, IKK, IκBα and JNK at 90 min after MSU treatment. PMA-primed THP-1 cells were stimulated with MSU (500 µg/ml) for different durations. The protein expression levels of p-p38 (**A**), p-p65 (**B**), p-JNK (**C**) and p-ERK1/2 (**D**) in the cytoplasm were measured utilizing immunoblotting. PMA-primed THP-1 cells were treated with or without MCC950 (20 µM), SDAO (45 µg/ml) or SFEAO (136 µg/ml) upon stimulation with MSU (500 µg/ml) for 90 min. The phosphorylation of p65, p38 (**E**), JNK (**F**), IKKα/β (**G**), and IκBα (**H**) in whole-cell extracts was measured by immunoblotting. GAPDH was acted as internal reference.

(**Figures 6G,H**). These results indicate that EOAA inhibits the NF-κB and MAPK signaling pathways.

EOAA Inhibits the Release of Processed Caspase-1 and IL-1β Induced by Nigericin

To determine whether EOAA could inhibit the activation of the NLRP3 inflammasome induced by other stimulators, we activated the NLRP3 inflammasome with nigericin. In this model, we found that high concentrations of SDAO and SFEAO were needed to significantly inhibit the activation of the NLRP3 inflammasome. The data showed that both SDAO and SFEAO decreased the level of mature IL-1β (**Figures 7A,B**) and caspase-1 (**Figures 7C,D**) in the cell culture supernatant. MCC950 and different concentrations of EOAA significantly inhibited the secretion of IL-1β

(**Figure 7E**). The secretion of TNF-α was not induced by NLRP3 inflammasome activation after nigericin treatment (**Figure 7F**). Nigericin treatment induced the secretion of TNF-α in an NLRP3 inflammasome activation-independent way. In addition, MCC950 did not inhibit the secretion of TNF-α. We found that only high concentrations of SDAO and SFEAO inhibited the secretion of TNF-α. LDH release was also inhibited by MCC950 and different concentrations of SDAO and SFEAO (**Figure 7G**). Our results indicate that SDAO and SFEAO inhibit the activation of the NLRP3 inflammasome induced by nigericin.

EOAA Inhibits the Cleavage of GSDMD Induced by Nigericin

Along with the inhibitory effect of SDAO and SFEAO on LDH release, we further detected the cleavage of GSDMD in

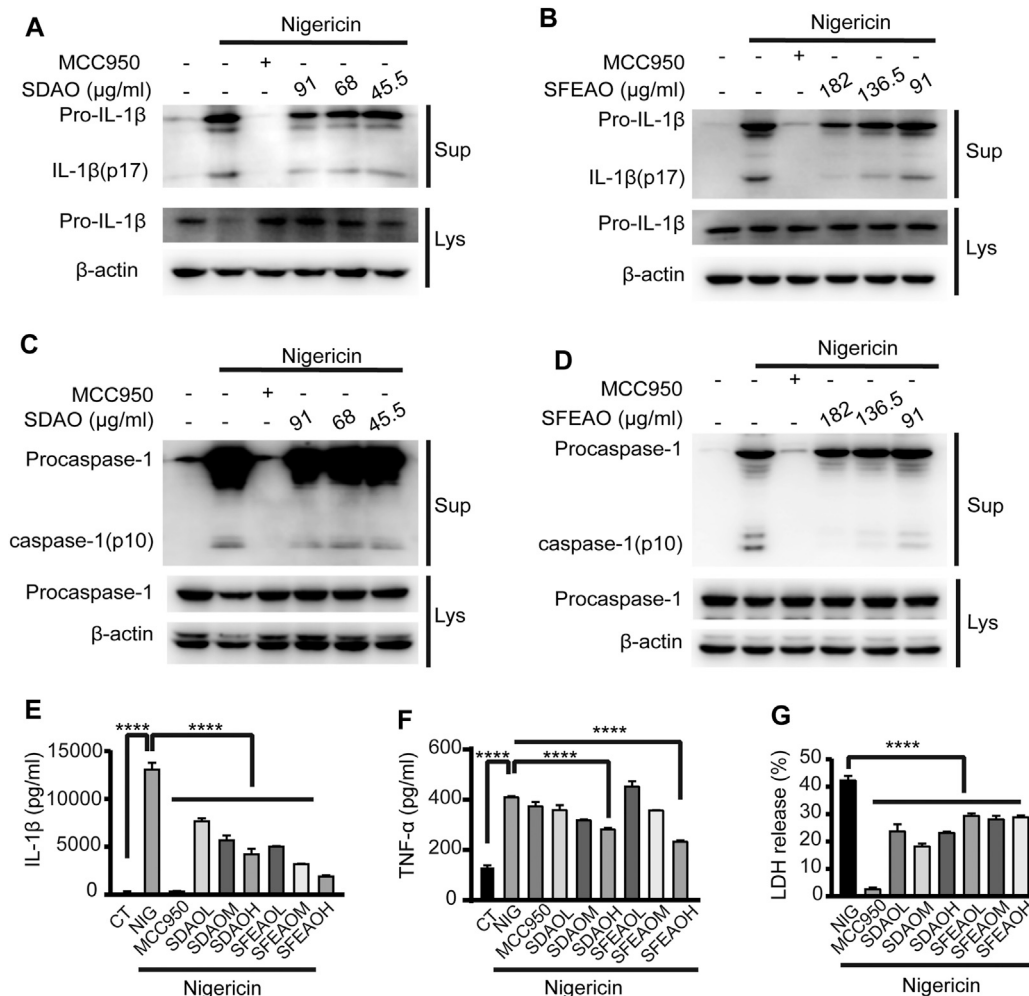


FIGURE 7 | EOAA inhibits the release of processed caspase-1 and IL-1 β induced by nigericin. PMA-primed THP-1 cells were treated with or without MCC950 (20 μ M) or different concentrations of SDAO or SFEAO and stimulated with nigericin (10 μ M) for 1 h. Mature IL-1 β and caspase-1 cleavage were measured in the supernatant. Pro-IL-1 β (A,B) and procaspase-1 (C,D) levels were measured in whole-cell extracts by immunoblotting. β -Actin was used as an internal control. IL-1 β (E) and TNF- α (F) secretion was determined by ELISA. The release of LDH in cell supernatants was assessed by LDH assay (G). CT:Ctrl; NIG:nigericin; SDAOL, SDAOM, SDAOH mean 45.5, 68, 91 μ g/ml SDAO, respectively; SFEAOL, SFEAOM, SFEAOH mean 91, 138.5, 182 μ g/ml SFEAO, respectively. Data were from three independent experiments with biological duplicates in each (E,F; mean and SD of $n = 6$) or from three independent experiments with six biological duplicates in each (G; mean and SD of $n = 18$) or were representative of at least three independent experiments (A–D). Arcsine-square root transformation of the percent data was used for statistical analysis. Statistics were analyzed using one-way ANOVA by Bonferroni post hoc test, * $p < 0.05$, ** $p < 0.01$, *** $p < 0.001$, **** $p < 0.0001$.

nigericin-treated cells. As shown in **Figures 8A,B**, we found that both SDAO and SFEAO decreased the expression of the GSDMD-N fragment. However, the expression of NLRP3 was not influenced under any condition, including nigericin treatment and SDAO and SFEAO treatment (**Figures 8C,D**). These data indicate that SDAO and SFEAO inhibits cell pyroptosis by blocking the cleavage of GSDMD during activation of the NLRP3 inflammasome.

Surprisingly, we found by detecting ASC specks (**Figures 8E,F**) and oligomers (**Figure 8G**) that the SDAO and SFEAO did not influence oligomerization. These results indicate that SDAO and SFEAO do not influence the organization process of the NLRP3 inflammasome. Given that SDAO and SFEAO eventually inhibit the activation of the NLRP3

inflammasome, we hypothesized that EOAA might influence the downstream process of the ASC oligomerization and then inhibit the processing of caspase-1 in nigericin-treated cells.

DISCUSSION

Artemisia argyi H. Lév. and Vaniot is a traditional Chinese medicine that is effective against inflammation. However, the mechanism underlying it is not clear. Here, we demonstrated that EOAA inhibits the activation of the NLRP3 inflammasome induced by MSU and nigericin. Moreover, different mechanisms underlie the inhibitory effects of EOAA on

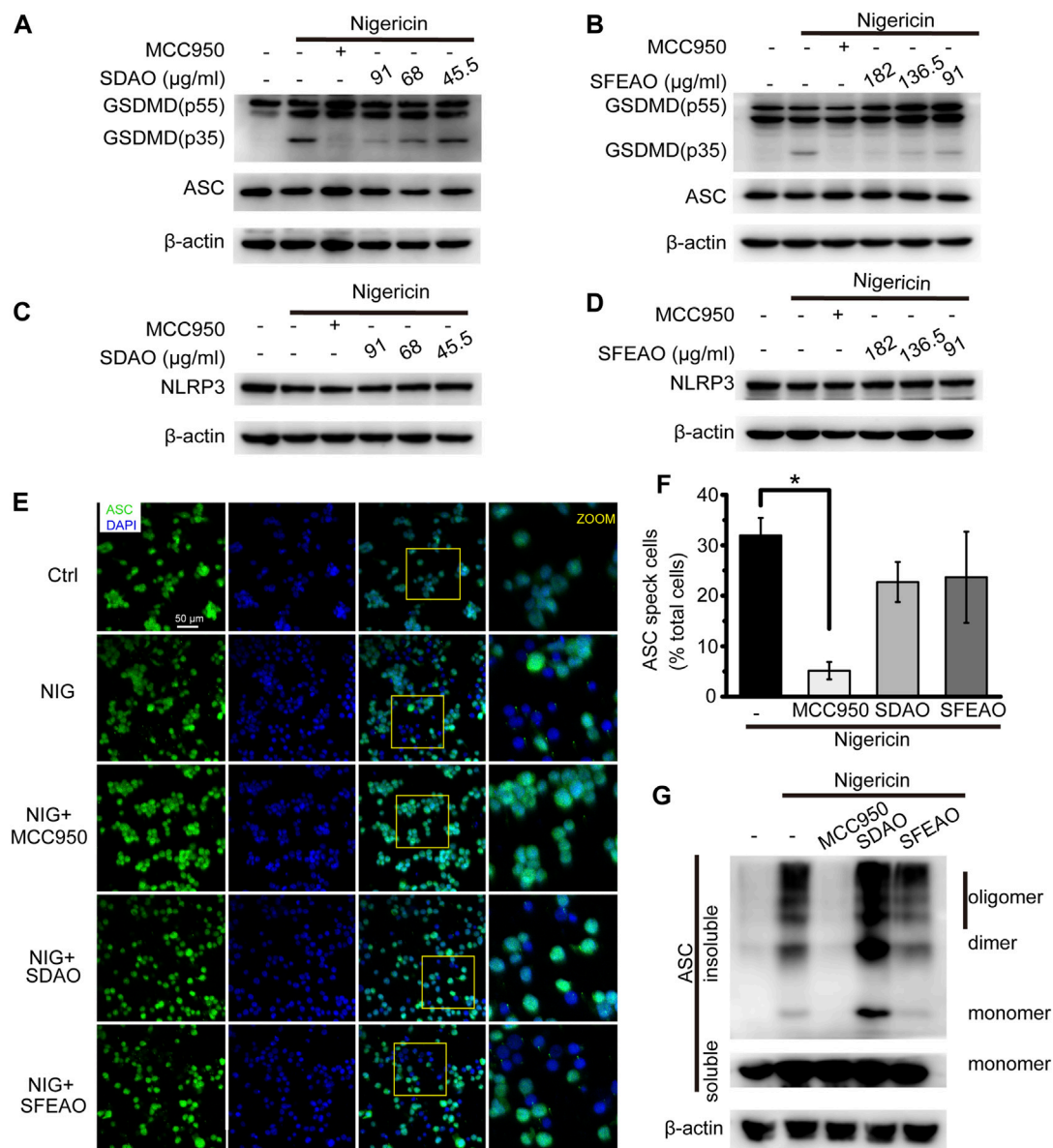


FIGURE 8 | EOAA inhibits GSDMD slicing and has no effect on NLRP3 expression and the formation of ASC oligomers after nigericin treatment. PMA-primed THP-1 cells were treated with or without MCC950 (20 μ M) or different concentrations of SDAO or SFEAO and stimulated with nigericin (10 μ M) for 1 h. The levels of cleaved GSDMD (**A,B**) and NLRP3 in whole-cell extracts were measured by immunoblotting (**C,D**). β -Actin was used as an internal control. PMA-primed THP-1 cells were treated with or without MCC950 (20 μ M), SDAO (91 μ M) or SFEAO (182 μ M) upon stimulation with nigericin (10 μ M) for 1 h. (**E**) Cells stained with anti-ASC antibody to detect ASC specks (green) and with DAPI to detect nuclei (blue). (**F**) The percentage of cells with ASC specks among all cells is presented. (**G**) ASC oligomers were extracted from the Triton X-100 insoluble part of the cell extract by DSS crosslinking and measured by immunoblotting. NIG:nigericin. ASC speck was quantified by the cells with ASC specks relative to the total cells from three individual fields in each experiment. Data were from three independent experiments (**F**; mean and SEM of $n = 3$) or representative of at least three independent experiments (**A–G**). Arcsine-square root transformation of the percent data was used for statistical analysis. Statistics were analyzed using one-way ANOVA by Bonferroni post hoc test, * $p < 0.05$, ** $p < 0.01$, *** $p < 0.001$.

NLRP3 inflammasome activation induced by MSU and nigericin, suggesting that components of EOAA may act on multiple targets to hinder multiple processes during NLRP3 inflammasome activation.

IL-1 β is a critical proinflammatory cytokine belonging to the IL-1 cytokine family. IL-1 β binds with IL-1R to induce the upregulation of MHC-II, adhesion molecules and IFN- γ in

innate immune cells (Dinarello, 2009). IL-1 β exists in the cytosol as a 31-kDa precursor that can be cleaved into 17–18-kDa mature forms by caspase-1 during inflammasome activation (Martinon et al., 2002). According to our results, both MSU and nigericin treatment increased the amount of the mature forms of caspase-1 and IL-1 β in the cell supernatant, which was significantly decreased by EOAA. Thus, our results

demonstrate that EOAA is effective at inhibiting NLRP3 inflammasome activation.

Unlike most cytokines, IL-1 cytokines lack an N-terminal secretion signal sequence and thus are not released through a classical ER–Golgi system (Piccioli and Rubartelli, 2013). Rather, processed IL-1 β is alternatively released via the pyroptotic and the nonpyroptotic effects of GSDMD. Cleaved from GSDMD by active caspase-1, the GSDMD-N domain aggregates at the cell membrane, forming a pore structure with a diameter wide enough for the passage of IL-1 cytokines (He et al., 2015; Evavold et al., 2018). Furthermore, IL-1 β leaks out through the ruptured cell membrane during cell pyroptosis (Kayagaki et al., 2015; Shi et al., 2015). In our research, EOAA inhibited GSDMD cleavage and pyroptosis, as indicated by the release of LDH upon stimulation with MSU and nigericin. These results suggest that EOAA could contribute to suppressing the secretion of IL-1 β by blocking the cleavage of GSDMD and the subsequent induction of pyroptosis.

Artemisia argyi H. Lév. and Vaniot is a well-known medical herb with strong aromatic odours. It contains multiple phytochemicals including essential oil, flavonoids, organic acids, coumarins, and polysaccharides, among which essential oil is the main composition (Ge et al., 2016). Previous studies have demonstrated the anti-inflammatory effect of *Artemisia argyi* H. Lév. and Vaniot extract. *Artemisia argyi* H. Lév. and Vaniot extract from different research groups showed significant inhibitory effect on dermatitis related lesions (Han et al., 2016; Yun et al., 2016). *Artemisia argyi* H. Lév. and Vaniot extract could play a protective role on gastric mucosa in ethanol-induced rat model by decreasing the amount of inflammatory mediators, superoxide dismutase, and malonaldehyde (Li et al., 2018), suggesting that *Artemisia argyi* H. Lév. and Vaniot contains effective anti-inflammatory components.

Essential oil is the main component of *Artemisia argyi* H. Lév. and Vaniot, and it can be extracted via steam distillation and CO₂ supercritical fluid. EOAA is mainly composed of abundant monoterpenoids, sesquiterpenoids, alcohols, ketones, ethers, phenols and a small quantity of aldehydes, organic acids, esters, and aromatic compounds (Song et al., 2019). In our research, a total of 29 compounds and 26 compounds were identified in SFEAO and SDAO separately using GC–MS. Additionally, monoterpenoids, sesquiterpenoids, took up large proportions of SFEAO and SDAO. These results are in line with those of previous studies (Ge et al., 2016; Guan et al., 2019). The reported chemical composition of essential oil of *Artemisia argyi* H. Lév. and Vaniot varied with localities of growth (Pan et al., 1992), extracting and processing methods of *Artemisia argyi* H. Lév. and Vaniot (Guan et al., 2019). *Artemisia argyi* H. Lév. and Vaniot used in our research was grown at Nanyang City in Henan Province, one of the main producing places of *Artemisia argyi* H. Lév. and Vaniot in China. *Artemisia argyi* H. Lév. and Vaniot from Qichun City in Hubei Province, named as Qi Ai, has long been considered as geo-authentic medicinal plant (Ge et al., 2016). Thus, many researches on essential oil of Qi Ai have been conducted. Extraction methods and experimental parameters may cause the deviation on chemical composition analysis in different researches on essential oil of Qi Ai. However, the

dominant chemical compounds in essential oil of Qi Ai were 1,8-cineole, β -caryophyllene, α -thujone, borneol, terpinen-4-ol, cis-sabinol, caryophyllene oxide and so on (Zheng-You et al., 2009). Compared with the research of Xiao Guan et al. on chemical compounds in essential oil of Qi Ai extracted by CO₂ subcritical fluid (Guan et al., 2019), 18 common compounds, accounting for 41.15% of the whole content, were found in SFEAO of our study. 12 compounds making up a portion of 53.24% in SDAO of our study were same as that in essential oil of Qi Ai. The common compounds separately accounted for 58.68 and 51.51% of essential oil of Qi Ai obtained by subcritical extraction and hydrodistillation. These results indicate that the main chemical composition of essential oil in our research is similar to that of Qi Ai. However, 1,8-cineole and camphor, the major compounds in SFEAO and SDAO, were not detected in research of Xiao Guan et al. Thujone, a common compound made up a portion less than 1% in SFEAO and SDAO, accounted for 7.989 and 11.312% in essential oil of Qi Ai obtained by subcritical extraction and hydrodistillation. Thus, the proportion of some common compounds in essential oil of *Artemisia argyi* H. Lév. and Vaniot varied with its producing area. Remarkably, compared with the research of essential oil extracted from Nanyang *Artemisia argyi* (Duan et al., 2017), we also found many major common compounds with different percentages in SFEAO and SDAO.

EOAA has also been reported to inhibit the release of proinflammatory mediators (NO, PGE₂ and ROS) and cytokines (TNF- α , IL-6, IFN- β and MCP-1) in LPS-induced RAW264.7 macrophages, suggesting that EOAA has anti-inflammatory potential. In addition, EOAA inhibited the release of cytokines by inhibiting the phosphorylation of JAK2 and STAT1/3, but not the activation of MAPK and NF- κ B (Chen et al., 2017). Contrary to this report, our research found that EOAA inhibits the phosphorylation of p65 and the translocation of NF- κ B upon treatment with MSU. The reason for these opposite results may attribute to the difference of cell model and essential oil components. The amount of eucalyptol, also known as 1,8-cineole, account for most in both our research and Chen et al. (2017)'s. However, it was quantified to 33.4% in Chen et al. (2017)' study, which was 12.3% in our study. Meanwhile, the five most abundant compounds were eucalyptol, terpinen-4-ol, β -caryophyllene, borneol, and α -terpineol in SFEAO and SDAO, which is different from eucalyptol, cyclohexanol, α -(-)-thujone, camphor, (-)-borneol in Chen et al. (2017)' study.

Previous studies showed that multiple factors interfered with the assembly of NLRP3 inflammasome, including but not limited to the amount of NLRP3 protein (Bauernfeind et al., 2009), post-translational modification and self-oligomerization of NLRP3 (Py et al., 2013), the interaction of ASC and NLRP3 (Lu et al., 2014), phosphorylation of ASC (Hara et al., 2013) and interaction of NLRP3 with other regulatory proteins (Zhou et al., 2010). In addition to being a transcription factor of inflammatory genes, NF- κ B plays a vital role in priming NLRP3 activation. In the resting state, the intracellular amount of NLRP3 and pro-IL-1 β is not sufficient to initiate activation of the NLRP3 inflammasome. Activation of NF- κ B mediated by pattern recognition and

cytokine receptors upregulates the transcription of pro-IL-1 β and NLRP3, which is necessary but not sufficient for NLRP3 activation (Bauernfeind et al., 2009). Our results showed that EOAA inhibits the activation of NF- κ B by blocking the phosphorylation of its upstream kinase IKK, resulting in low gene expression of NLRP3 after MSU treatment. However, only SFEAO mildly inhibited the protein expression of NLRP3. Thus, the main reason for EOAA inhibit the activation of NLRP3 inflammasome is not lowering the protein expression of NLRP3. Meanwhile, MSU only induced a less than 2-fold increase of NLRP3 at mRNA and protein expression. THP-1 cells used in our study were primed with PMA at 0.5 μ M for 3 h to differentiate into macrophages, which may mask the effect of other stimuli (Park et al., 2007).

Besides, phosphorylation of NLRP3 also indeed regulated the assembly of NLRP3 inflammasome. JNK1-mediated NLRP3 S194 phosphorylation induced NLRP3 deubiquitylation, which is essential for its oligomerization and assembly with ASC (Song et al., 2017). Phosphorylation of NLRP3 on Ser295 by PKD at the Golgi is required for release NLRP3 from MAMs, resulting in assembly of the active inflammasome (Zhang et al., 2017). However, it is contradictory about the effect of phosphorylation on NLRP3. NLRP3 phosphorylation at S295 via NPR1/cGMP/PKG-1 axis contributed to disassembly of NLRP3 inflammasome (Mezzasoma et al., 2020). Additionally, the activation of JNK1 drive the phosphorylation of ASC at CARD domain, which is critical for the assembling of ASC speck (Hara et al., 2013).

Previous studies have noted that MSU treatment induces the phosphorylation of JNK, p38, and ERK1/2, which contributes to the activation of NF- κ B and the inflammatory reaction of MSU (Jaramillo et al., 2004; Campillo-Gimenez et al., 2018; Bousoik et al., 2020). The results of this study showed that MSU treatment induced the phosphorylation of p38 and JNK and slightly decreased the phosphorylation of ERK1/2. EOAA inhibited the phosphorylation of both p38 and JNK in MSU-stimulated THP-1 cells. Therefore, it is possible that EOAA inhibit the phosphorylation of NLRP3 or ASC due to phosphorylation of JNK, which need to be proved based on credible experimental evidence.

Nigericin is an inducer of the NLRP3 inflammasome that causes K⁺ influx and initiates its structural organization (Perregaux and Gabel, 1994). In PMA-induced THP-1 cells, nigericin activated the NLRP3 inflammasome. Administration of EOAA to PMA-induced THP-1 cells before nigericin treatment did not influence NLRP3 inflammasome priming but interfered with the subsequent activation procedure. Our results showed that EOAA did not inhibit the oligomerization of ASC but indeed blocked the activation of the NLRP3 inflammasome, as indicated by the blockade of caspase-1

cleavage. IL-1 β and GSDMD cleavage and the release of LDH are the results of caspase-1 activation. Thus, EOAA might block the process of caspase-1 activation.

At present, it is unclear how EOAA blocks the process of caspase-1 activation. There are many ways to block this process, such as interfering with the binding of ASC to caspase-1 or inactivating the enzymatic activity of caspase-1 directly. In addition, we did not study whether EOAA could inhibit the activation of other forms of inflammasomes, such as AIM and NLRC4 inflammasomes and the nonconventional NLRP3 inflammasome. Caspase-1 is the common effector of the above inflammasomes. Our data indicate that EOAA could inhibit the activation of caspase-1 without interfering with the oligomerization of ASC. Thus, EOAA might inhibit the activation of other inflammasomes. However, more experiments need to be done to verify this assumption.

DATA AVAILABILITY STATEMENT

The raw data supporting the conclusions of this article will be made available by the authors, without undue reservation.

AUTHOR CONTRIBUTIONS

PC, QB, ZR, and YiW conceived the project and designed research. PC and QB conducted experiments, performed statistical analysis, and drafted the manuscript. YWu, XS, QZ, PZ, YG, and YaW provided technical assistance with several protocols. XL and QW revised the manuscript and results. ZR and YiW supervised the study. PC and QB contributed equally to this article. All authors read and approved the final manuscript.

FUNDING

This research was supported by Research start-up fund of Guangzhou City, Program of scientific and technological innovation team funded by Huizhou City (20170217013144015), Daya Bay technological project (2017008) and Innovation team project of modern agricultural industry technology system funded by Guangdong Province (2020KJ142).

SUPPLEMENTARY MATERIAL

The Supplementary Material for this article can be found online at: <https://www.frontiersin.org/articles/10.3389/fphar.2021.712907/full#supplementary-material>

REFERENCES

Bauernfeind, F. G., Horvath, G., Stutz, A., Alnemri, E. S., Macdonald, K., Speert, D., et al. (2009). Cutting Edge: NF- κ B Activating Pattern Recognition and Cytokine Receptors License NLRP3 Inflammasome Activation by Regulating

NLRP3 Expression. *J. Immunol.* 183 (2), 787–791. doi:10.4049/jimmunol.0901363

Bousoik, E., Qadri, M., and Elsaid, K. A. (2020). CD44 Receptor Mediates Urate Crystal Phagocytosis by Macrophages and Regulates Inflammation in A Murine Peritoneal Model of Acute Gout. *Sci. Rep.* 10 (1), 5748. doi:10.1038/s41598-020-62727-z

- Campillo-Gimenez, L., Renaudin, F., Jalabert, M., Gras, P., Gosset, M., Rey, C., et al. (2018). Inflammatory Potential of Four Different Phases of Calcium Pyrophosphate Relies on NF- κ B Activation and MAPK Pathways. *Front. Immunol.* 9, 2248. doi:10.3389/fimmu.2018.02248
- Chen, L. F., and Greene, W. C. (2004). Shaping the Nuclear Action of NF- κ B. *Nat. Rev. Mol. Cell Biol.* 5 (5), 392–401. doi:10.1038/nrm1368
- Chen, L. L., Zhang, H. J., Chao, J., and Liu, J. F. (2017). Essential Oil of Artemisia Argyi Suppresses Inflammatory Responses by Inhibiting JAK/STATs Activation. *J. Ethnopharmacol.* 204, 107–117. doi:10.1016/j.jep.2017.04.017
- Coll, R. C., Robertson, A. A., Chae, J. J., Higgins, S. C., Munoz-Planillo, R., Inerra, M. C., et al. (2015). A Small-Molecule Inhibitor of the NLRP3 Inflammasome for the Treatment of Inflammatory Diseases. *Nat. Med.* 21 (3), 248–255. doi:10.1038/nm.3806
- Dinarello, C. A. (2009). Immunological and Inflammatory Functions of the Interleukin-1 Family. *Annu. Rev. Immunol.* 27 (1), 519–550. doi:10.1146/annurev.immunol.021908.132612
- Duan, K., Gao, M., Liu, Y., Zhang, T., Chen, L., Zhao, S., et al. (2017). Phenolic Compounds and Essential Oil Compositions of Artemisia Argyi Leaves from Two Growing Areas. *Food Sci.* 38 (4), 204–210. doi:10.7506/spkx1002-6630-201704033
- Evavold, C. L., Ruan, J., Tan, Y., Xia, S., Wu, H., and Kagan, J. C. (2018). The Pore-Forming Protein Gasdermin D Regulates Interleukin-1 Secretion from Living Macrophages. *Immunity* 48 (1), 35–36. doi:10.1016/j.immuni.2017.11.013
- Fernandes-Alnemri, T., Wu, J., Yu, J. W., Datta, P., Miller, B., Jankowski, W., et al. (2007). The Pyroptosome: a Supramolecular Assembly of ASC Dimers Mediating Inflammatory Cell Death via Caspase-1 Activation. *Cell Death Differ.* 14 (9), 1590–1604. doi:10.1038/sj.cdd.4402194
- Ge, Y. B., Wang, Z. G., Xiong, Y., Huang, X. J., Mei, Z. N., and Hong, Z. G. (2016). Anti-inflammatory and Blood Stasis Activities of Essential Oil Extracted from Artemisia Argyi Leaf in Animals. *J. Nat. Med.* 70 (3), 531–538. doi:10.1007/s11418-016-0972-6
- Guan, X., Ge, D., Li, S., Huang, K., Liu, J., and Li, F. (2019). Chemical Composition and Antimicrobial Activities of Artemisia argyi Lévl. et Vant Essential Oils Extracted by Simultaneous Distillation-Extraction, Subcritical Extraction and Hydrodistillation. *Molecules* 24 (3). doi:10.3390/molecules24030483
- Guey, B., and Petrilli, V. (2016). “Assessing Caspase-1 Activation,” in *NLR Proteins. Methods in Molecular Biology*. Editors D. V. Francesco and P. Pablo (New York, NY: Humana Press), 1417, 197–206. doi:10.1007/978-1-4939-3566-6_13
- Halle, A., Hornung, V., Petzold, G. C., Stewart, C. R., Monks, B. G., Reinheckel, T., et al. (2008). The NALP3 Inflammasome Is Involved in the Innate Immune Response to Amyloid-Beta. *Nat. Immunol.* 9 (8), 857–865. doi:10.1038/ni.1636
- Han, H. M., Kim, S. J., Kim, J. S., Kim, B. H., Lee, H. W., Lee, Y. T., et al. (2016). Ameliorative Effects of Artemisia Argyi Folium Extract on 2,4-dinitrochlorobenzene-induced A-topic D-dermatitis-like Lesions in BALB/c M-ice. *Mol. Med. Rep.* 14 (4), 3206–3214. doi:10.3892/mmr.2016.5657
- Hara, H., Tsuchiya, K., Kawamura, I., Fang, R., Hernandez-Cuellar, E., Shen, Y., et al. (2013). Phosphorylation of the Adaptor ASC Acts as a Molecular Switch that Controls the Formation of Speck-like Aggregates and Inflammasome Activity. *Nat. Immunol.* 14 (12), 1247–1255. doi:10.1038/ni.2749
- Hayden, M. S., and Ghosh, S. (2004). Signaling to NF- κ B. *Genes Dev.* 18 (18), 2195–2224. doi:10.1101/gad.1228704
- He, H., Jiang, H., Chen, Y., Ye, J., Wang, A., Wang, C., et al. (2018). Oridonin Is a Covalent NLRP3 Inhibitor with strong Anti-inflammasome Activity. *Nat. Commun.* 9 (1), 2550. doi:10.1038/s41467-018-04947-6
- He, W. T., Wan, H., Hu, L., Chen, P., Wang, X., Huang, Z., et al. (2015). Gasdermin D Is an Executor of Pyroptosis and Required for Interleukin-1 β Secretion. *Cell Res* 25 (12), 1285–1298. doi:10.1038/cr.2015.139
- Ising, C., Venegas, C., Zhang, S., Scheiblich, H., Schmidt, S. V., Vieira-Saecker, A., et al. (2019). NLRP3 Inflammasome Activation Drives Tau Pathology. *Nature* 575 (7784), 669–673. doi:10.1038/s41586-019-1769-z
- Jaramillo, M., Godbout, M., Naccache, P. H., and Olivier, M. (2004). Signaling Events Involved in Macrophage Chemokine Expression in Response to Monosodium Urate Crystals. *J. Biol. Chem.* 279 (50), 52797–52805. doi:10.1074/jbc.M403823200
- Karin, M., and Ben-Neriah, Y. (2000). Phosphorylation Meets Ubiquitination: the Control of NF- κ B Activity. *Annu. Rev. Immunol.* 18, 621–663. doi:10.1146/annurev.immunol.18.1.621
- Kayagaki, N., Stowe, I. B., Lee, B. L., O'Rourke, K., Anderson, K., Warming, S., et al. (2015). Caspase-11 Cleaves Gasdermin D for Non-canonical Inflammasome Signalling. *Nature* 526 (7575), 666–671. doi:10.1038/nature15541
- Kim, S. K., Choe, J. Y., and Park, K. Y. (2019). Anti-inflammatory Effect of Artemisinin on Uric Acid-Induced NLRP3 Inflammasome Activation through Blocking Interaction between NLRP3 and NEK7. *Biochem. Biophys. Res. Commun.* 517 (2), 338–345. doi:10.1016/j.bbrc.2019.07.087
- Kwak, S. B., Koppula, S., In, X., Kim, Y. K., Kim, M. K., et al. (2018). Artemisia Extract Suppresses NLRP3 and AIM2 Inflammasome Activation by Inhibition of ASC Phosphorylation. *Mediators Inflamm.* 2018, 6054069. doi:10.1155/2018/6054069
- Li, S., Zhou, S., Yang, W., and Meng, D. (2018). Gastro-protective Effect of Edible Plant Artemisia Argyi in Ethanol-Induced Rats via Normalizing Inflammatory Responses and Oxidative Stress. *J. Ethnopharmacol.* 214, 207–217. doi:10.1016/j.jep.2017.12.023
- Liu, R., O'Connell, M., Johnson, K., Pritzker, K., Mackman, N., and Terkeltaub, R. (2000). Extracellular Signal-Regulated Kinase 1/extracellular Signal-Regulated Kinase 2 Mitogen-Activated Protein Kinase Signaling and Activation of Activator Protein 1 and Nuclear Factor κ B Transcription Factors Play central Roles in Interleukin-8 Expression Stimulated by Monosodium Urate Monohydrate and Calcium Pyrophosphate Crystals in Monocytic Cells. *Arthritis Rheum.* 43 (5), 1145–1155. doi:10.1002/1529-0131(200005)43:5<1145
- Lu, A., Magupalli, V. G., Ruan, J., Yin, Q., Atianand, M. K., Vos, M. R., et al. (2014). Unified Polymerization Mechanism for the Assembly of ASC-dependent Inflammasomes. *Cell* 156 (6), 1193–1206. doi:10.1016/j.cell.2014.02.008
- Lugrin, J., and Martinon, F. (2017). Detection of ASC Oligomerization by Western Blotting. *Bio Protoc.* 7 (10), e2292. doi:10.21769/BioProtoc.2292
- Martinon, F., Burns, K., and Tschopp, J. (2002). The Inflammasome: a Molecular Platform Triggering Activation of Inflammatory Caspases and Processing of proIL- β . *Mol. Cell* 10 (2), 417–426. doi:10.1016/S1097-2765(02)00599-3
- Martinon, F., Pétrilli, V., Mayor, A., Tardivel, A., and Tschopp, J. (2006). Gout-associated Uric Acid Crystals Activate the NALP3 Inflammasome. *Nature* 440 (7081), 237–241. doi:10.1038/nature04516
- Masters, S. L., Dunne, A., Subramanian, S. L., Hull, R. L., Tannahill, G. M., Sharp, F. A., et al. (2010). Activation of the NLRP3 Inflammasome by Islet Amyloid Polypeptide Provides a Mechanism for Enhanced IL-1 β in Type 2 Diabetes. *Nat. Immunol.* 11 (10), 897–904. doi:10.1038/ni.1935
- Mezzasoma, L., Talesa, V. N., Romani, R., and Bellezza, I. (2020). ANP and BNP Exert Anti-inflammatory Action via NPR-1/cGMP Axis by Interfering with Canonical, Non-canonical, and Alternative Routes of Inflammasome Activation in Human THP1 Cells. *Int. J. Mol. Sci.* 22 (1). doi:10.3390/ijms22010024
- Pan, J. G., Xu, Z. L., and Ji, L. (1992). Chemical Studies on Essential Oils from 6 Artemisia Species. *Zhongguo Zhong Yao Za Zhi* 17 (12), 741–764.
- Park, E. K., Jung, H. S., Yang, H. I., Yoo, M. C., Kim, C., and Kim, K. S. (2007). Optimized THP-1 Differentiation Is Required for the Detection of Responses to Weak Stimuli. *Inflamm. Res.* 56 (1), 45–50. doi:10.1007/s00011-007-6115-5
- Perregaux, D., and Gabel, C. A. (1994). Interleukin-1 Beta Maturation and Release in Response to ATP and Nigericin. Evidence that Potassium Depletion Mediated by These Agents Is a Necessary and Common Feature of Their Activity. *J. Biol. Chem.* 269 (21), 15195–15203. doi:10.1016/S0021-9258(17)36591-2
- Piccoli, P., and Rubartelli, A. (2013). The Secretion of IL-1 β and Options for Release. *Semin. Immunol.* 25, 425–429. doi:10.1016/j.smim.2013.10.007
- Py, B. F., Kim, M. S., Vakifahmetoglu-Norberg, H., and Yuan, J. (2013). Deubiquitination of NLRP3 by BRCC3 Critically Regulates Inflammasome Activity. *Mol. Cell* 49 (2), 331–338. doi:10.1016/j.molcel.2012.11.009
- Shi, J., Zhao, Y., Wang, K., Shi, X., Wang, Y., Huang, H., et al. (2015). Cleavage of GSDMD by Inflammatory Caspases Determines Pyroptotic Cell Death. *Nature* 526 (7575), 660–665. doi:10.1038/nature15514
- Song, N., Liu, Z. S., Xue, W., Bai, Z. F., Wang, Q. Y., Dai, J., et al. (2017). NLRP3 Phosphorylation Is an Essential Priming Event for Inflammasome Activation. *Mol. Cell* 68 (1), 185e6–e186. doi:10.1016/j.molcel.2017.08.017
- Song, X., Wen, X., He, J., Zhao, H., Li, S., and Wang, M. (2019). Phytochemical Components and Biological Activities of Artemisia Argyi. *J. Funct. Foods* 52, 648–662. doi:10.1016/j.jff.2018.11.029
- Stutz, A., Horvath, G. L., Monks, B. G., and Latz, E. (2013). “ASC Speck Formation as a Readout for Inflammasome Activation,”. *The Inflammasome. Methods in*

- Molecular Biology (Methods and Protocols)*. Editors D. N. Christine and E. Late (Totowa, NJ: Humana Press), 1040, 91–101. doi:10.1007/978-1-62703-523-1_8
- Swanson, K. V., Deng, M., and Ting, J. P.-Y. (2019). The NLRP3 Inflammasome: Molecular Activation and Regulation to Therapeutics. *Nat. Rev. Immunol.* 19, 477–489. doi:10.1038/s41577-019-0165-0
- Takeuchi, O., and Akira, S. (2010). Pattern Recognition Receptors and Inflammation. *Cell* 140 (6), 805–820. doi:10.1016/j.cell.2010.01.022
- Venegas, C., Kumar, S., Franklin, B. S., Dierkes, T., Brinkschulte, R., Tejera, D., et al. (2017). Microglia-derived ASC Specks Cross-Seed Amyloid- β in Alzheimer's Disease. *Nature* 552 (7685), 355–361. doi:10.1038/nature25158
- Yun, C., Jung, Y., Chun, W., Yang, B., Ryu, J., Lim, C., et al. (2016). Anti-Inflammatory Effects of Artemisia Leaf Extract in Mice with Contact Dermatitis *In Vitro* and *In Vivo*. *Mediators Inflamm.* 2016, 8027537. doi:10.1155/2016/8027537
- Zhang, Z., Meszaros, G., He, W. T., Xu, Y., De Fatima Magliarelli, H., Mailly, L., et al. (2017). Protein Kinase D at the Golgi Controls NLRP3 Inflammasome Activation. *J. Exp. Med.* 214 (9), 2671–2693. doi:10.1084/jem.20162040
- Zheng-You, H., Yan-Hong, Z., Dong, W., Rong-Hua, Y., Hui-Hui, Y., and Min-Bo, L. (2009). Chemical Composition of Essential Oil from Fresh and Dried Folium Artemisia Argyi from Hubei Province. *Chin. Traditional Patent Med.* 31 (7), 1079–1082.
- Zhou, R., Tardivel, A., Thorens, B., Choi, I., and Tschopp, J. (2010). Thioredoxin-interacting Protein Links Oxidative Stress to Inflammasome Activation. *Nat. Immunol.* 11 (2), 136–140. doi:10.1038/ni.1831

Conflict of Interest: The authors declare that the research was conducted in the absence of any commercial or financial relationships that could be construed as a potential conflict of interest.

Publisher's Note: All claims expressed in this article are solely those of the authors and do not necessarily represent those of their affiliated organizations, or those of the publisher, the editors and the reviewers. Any product that may be evaluated in this article, or claim that may be made by its manufacturer, is not guaranteed or endorsed by the publisher.

Copyright © 2021 Chen, Bai, Wu, Zeng, Song, Guo, Zhou, Wang, Liao, Wang, Ren and Wang. This is an open-access article distributed under the terms of the Creative Commons Attribution License (CC BY). The use, distribution or reproduction in other forums is permitted, provided the original author(s) and the copyright owner(s) are credited and that the original publication in this journal is cited, in accordance with accepted academic practice. No use, distribution or reproduction is permitted which does not comply with these terms.



The Mechanism Action of German Chamomile (*Matricaria recutita* L.) in the Treatment of Eczema: Based on Dose–Effect Weight Coefficient Network Pharmacology

Wenfei Wang^{1†}, Yichun Wang^{1†}, Junbo Zou^{1,2}, Yanzhuo Jia¹, Yao Wang¹, Jia Li¹, Changli Wang^{1,2}, Jing Sun^{1,2}, Dongyan Guo^{1,2}, Fang Wang³, Zhenfeng Wu³, Ming Yang³, Lei Wu⁴, Xiaofei Zhang^{1,2,3*} and Yajun Shi^{1,2*}

OPEN ACCESS

Edited by:

Jun Tian,
Jiangsu Normal University, China

Reviewed by:

Soon Yew Tang,
University of Pennsylvania,
United States
Shiliang Li,
East China University of Science and
Technology, China

*Correspondence:

Xiaofei Zhang
2051028@sntcm.edu.cn
Yajun Shi
2051004@sntcm.edu.cn

[†]These authors have contributed
equally to this work and share first
authorship

Specialty section:

This article was submitted to
Inflammation Pharmacology,
a section of the journal
Frontiers in Pharmacology

Received: 08 May 2021

Accepted: 13 August 2021

Published: 30 September 2021

Citation:

Wang W, Wang Y, Zou J, Jia Y,
Wang Y, Li J, Wang C, Sun J, Guo D,
Wang F, Wu Z, Yang M, Wu L, Zhang X
and Shi Y (2021) The Mechanism
Action of German Chamomile
(*Matricaria recutita* L.) in the Treatment
of Eczema: Based on Dose–Effect
Weight Coefficient
Network Pharmacology.
Front. Pharmacol. 12:706836.
doi: 10.3389/fphar.2021.706836

¹Department of Pharmaceutics, College of Pharmacy, Shaanxi University of Chinese Medicine, Xianyang, China, ²Department of Pharmaceutics, The Key Laboratory of Basic and New Drug Research of Traditional Chinese Medicine, Shaanxi University of Chinese Medicine, Xianyang, China, ³Department of Pharmaceutics, Key Laboratory of Modern Preparation of Traditional Chinese Medicine, Ministry of Education, Jiangxi University of Chinese Medicine, Nanchang, China, ⁴Henan Feinari Aromatic Biotechnology Co., Ltd, Zhumadian, China

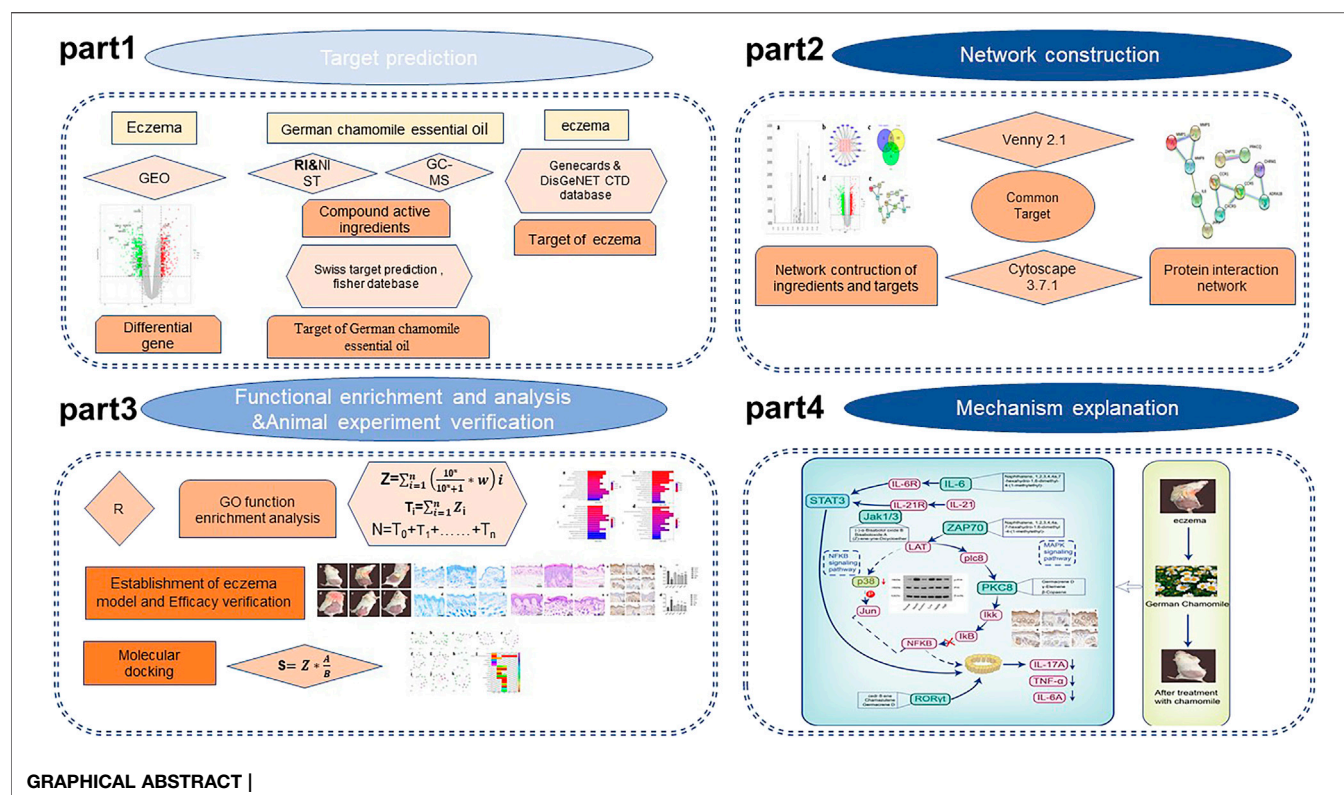
To determine the active ingredients in German chamomile volatile oil and the mechanism of action in the treatment of eczema, this study used two parameters (ingredient content and oil–water partition coefficient) and established a new network pharmacology method based on the dose–effect weight coefficient. Through the new network pharmacology method, we found that German chamomile volatile oil regulated T-cell lymphatic subpopulations to inhibit the Th17 cell differentiation signaling pathway. This resulted in a reduction of interleukin 17 (IL-17), thereby inhibiting the activation of the nuclear factor kappa beta (NF- κ B) and MAPK pathways, decreasing the secretion of the pro-inflammatory factors (tumor necrosis factor alpha (TNF- α) and interleukin 6 (IL-6)), and reducing inflammation. In this study, a new dose–effect relationship synergistic network pharmacology method was established to provide a new method for the screening of effective ingredients and pathways of drugs, and to provide a basis for the follow-up studies of German chamomile volatile oil in the treatment of eczema.

Keywords: German chamomile, eczema, weight coefficient, molecular docking, mechanism verification

INTRODUCTION

Eczema is an inflammatory skin disease usually accompanied by infiltration, hypertrophy, and severe itching. Studies have shown that the occurrence of eczema is related to many factors, including immune, environmental, and genetic factors, as well as infection. Eczema has a long course and recurs easily, seriously affecting the quality of life. At present,

Abbreviations: BP, biological process; DEG, differentially expressed genes; DL, drug-like; ECL, electrochemiluminescence; GC-MS, gas chromatography–mass spectrometer; GEO, gene expression omnibus database; GO, gene ontology; HE, hematoxylin–eosin staining; IL-6, interleukin 6; IL-17, interleukin 17; JAK3, Janus kinase 3; KEGG, Kyoto Encyclopedia of Genes and Genomes; MMP1, matrix metalloproteinases 1; NF- κ B, nuclear factor kappa-beta; OB, oral bioavailability; PPI, protein–protein interaction networks; PRKCCQ, protein kinase C; PVDF, polyvinylidene fluoride; RORC, (human) recombinant protein C; SDS-PAGE, sodium dodecyl sulfate–polyacrylamide gel electrophoresis; SMILES, simplified molecular input line entry specification; TBST, Tris-buffered saline + Tween; TNF- α , tumor necrosis factor alpha; ZAP70, zeta-chain 70.



antihistamines, anti-allergic drugs, and glucocorticoids are commonly used in the clinic. However, these drugs only temporarily relieve symptoms and may result in adverse reactions with long-term use. Thus, it is important to develop natural drugs with minimal side effects for the effective treatment of eczema.

Chamomile (*Matricaria recutita* L.) is one of the oldest aromatic plants, and the flower and essential oils have been shown to exhibit anti-inflammatory and antispasmodic effects. Chamomile is widely used in food, cosmetics, disinfectants, and medicines. Therefore, it is a medicinal plant with great developmental potential. German chamomile belongs to the family Compositae, and its volatile oil is often used in cosmetic care to eliminate inflammation, relieve skin irritation, and reduce redness and swelling of the skin. This oil has been used for healing skin wound and exhibits antibacterial, anti-inflammatory, and antioxidant activities. The cyclic ethers, flavonoids, and total volatile oils in chamomile have also been shown to exhibit an inhibitory effect on fungal growth. Polysaccharides isolated from its inflorescence also exhibit anti-inflammatory activity. Several studies have reported significant effects of German chamomile volatile oil in the treatment of eczema (Anderson et al., 2000; Patzelt-Wenzler and Ponce-Pöschl, 2000; Arsić et al., 2011; El-Salamouni et al., 2020). However, neither the active components nor the pharmacological mechanism of its volatile oil is clear. This study used an eczema mouse model to explore the therapeutic effects of German chamomile volatile oil on eczema and to determine the therapeutic mechanism. The results provide a

reference for further elucidation of the mechanism of action in future studies.

Network pharmacology explains the development of a disease via establishment of a database, network, network analysis, and experimental verification. It also attempts to determine the interaction between drugs and the body and to guide the discovery of new drugs. However, at present, most network pharmacology research treats the content of all components equally, ignoring the effects of both drug content and concentration on efficacy. This may lead to the identification of components with low content as key components. At the same time, components with high content that play a key role in treatment are often ignored. As a result, the existing network pharmacology research has been unable to identify ingredients and the mechanism of action that are responsible for observed effects. Network pharmacology generally uses oral bioavailability (OB) and drug-like (DL) property to screen for active ingredients in drugs. However, this method cannot be applied to predict transdermal drug delivery, resulting in the inability to obtain the targets and mechanisms of transdermal drugs. To address the above issues, a new method, “dose–effect weight coefficient method and network pharmacology” method, has been established, which can be used for transdermal drugs to mine components, targets, and pathways. Component content and oil–water partition coefficient, and molecular docking score are combined to obtain the theoretical transdermal absorption content of each component. Using this method, the contribution score of the corresponding “weight coefficient” is established, compared with the signaling pathways enriched by traditional

network pharmacology, and the key pathways are selected. For the purpose of this study, a mouse eczema model was established using dinitrochlorobenzene (DNCB) to explore the mechanism of action and to verify the efficacy of German chamomile volatile oil in the treatment of eczema.

MATERIALS AND METHODS

Determination of Chemical Composition of Volatile Oil From German Chamomile

German chamomile essential oil (purchased from Henan Feinari Aromatic Biotechnology Co., Ltd.) was identified by gas chromatography–mass spectrometry (GC–MS) analysis (Tai et al., 2020). The chromatographic conditions were HP-5 MS capillary column (30 m × 250 μm × 0.25 μm), carrier gas He, carrier gas as shunt mode, injection of 1.0 μL, and a column flow rate of 1 ml/min. The starting temperature was 40°C, and the temperature was increased to 250°C at a rate of 6°C/min. The mass spectrometry conditions were full scan mode, ionization source EI, an ionization energy of 70 eV, transmission line temperature 280°C, ion source temperature 230°C, quadrupole temperature 150°C, solvent delay time 3 min, and scanning quality range of 20–450 amu (Fu et al., 2018).

Identification of Essential Oil

The data were processed using data analysis software. The NIST standard spectral database was used to search, and the components were screened according to the matching degree, retention index, and related literature. The retention index was defined as the retention time of n-alkanes (C8–C40) under the same gas chromatographic conditions. According to the retention index of n-alkanes, the retention index of German chamomile volatile oil was as follows:

$$RI = 100Z + \frac{100[tR(X) - tR(Z)]}{tR(Z + 1) - tR(Z)} \quad (1-1)$$

where tR is the retention time, X is the compound to be analyzed, and Z and Z + 1 are the number of carbon atoms of the two n-alkanes before and after the analyte, namely, tR (Z) < tR (x) < tR (Z + 1) (Yuandong et al., 2017).

Pharmacological Analysis of the Ingredient-Target Network

Determination of Volatile Oil of German Chamomile Targets

The Swiss Target Prediction database (Le-qi et al., 2020) and meta TarFisher databases were used to predict the volatile oil targets of German chamomile, and the targets of the active components of German chamomile volatile oil were obtained.

Acquisition of Eczema Disease Targets

Taking “eczema” as the keyword and setting the species as humans, we searched the GeneCards database (Liu et al., 2020), DisGeNET

database (Wu et al., 2020), OMIM database (Kui et al., 2021), and Comparative Toxicogenomics Database (CTD) (Tianmu et al., 2021) to identify the qualified information of genes and target proteins related to eczema.

Gene Expression Omnibus (GEO)database Chip Differential Gene Verification

Based on the GEO database GSE57225 chip detection data (Liang et al., 2021), the data set included 23 patients and 17 normal control samples. The differential gene expression was analyzed using Limma software package 15 of R. The screening criteria were $|\log FC| > 1.2$ and $p < 0.05$.

Construction of the Compound Composition–Target Network

The volatile oil target, eczema target, and GEO differential gene of German chamomile were intersected by using Venny 2.1.0 (<https://bioinfogp.cnb.csic.es/tools/venny/index.html>). The active components of German chamomile volatile oil and the three overlapping genes were introduced into Cytoscape 3.7.1 (Shi et al., 2020) to construct the compound component–target network, Construction and analysis of the protein–protein interaction (PPI) 1.3.5 (Xu et al., 2020) network.

The potential targets of the active components of volatile oil, the disease targets of eczema, and the differential genes mined by GEO were integrated, intersected and introduced into the STRING database (Sang et al., 2020). The minimum interaction threshold was set to “highest confidence.” The free protein was hidden, and the protein relationship map was obtained. Results were imported into Cytoscape 3.7.1 software, and the interaction network was drawn and analyzed.

Establishment of the Weight Coefficient

The existing network pharmacology studies usually use oral bioavailability (OB) and drug-like (DL) property to screen for active ingredients in drugs. However, this method cannot be used to predict transdermal drug delivery, especially transdermal drug targets and mechanisms. To better explain the relationship between the transdermal absorption components and activity of chamomile, we introduced the log P value (an important parameter in the measurement of transdermal drug absorption) to convert the transdermal absorption rate and correlate the two to establish a relationship:

$$\begin{aligned} \log P &= \log \frac{Coil}{C_{water}} = n \\ \frac{Coil}{C_{water}} &= 10^n \\ \frac{Coil}{Coil + C_{water}} &= \frac{10^n}{10^n + 1} \end{aligned}$$

Because the drug application is percutaneous, the concentration of n-octanol (oil) indicates 100% complete absorption of the drug, and C water can indicate the part of the drug that has not been absorbed. Therefore, Coil/(Coil + C water) represents the absorption rate of volatile oil.

In order to better explain the relationship between oil–water partition coefficient, relative content, and active components in pharmacological mechanism, we correlate the three:

$$Z = \sum_{i=1}^n \left(\frac{10^{-n}}{10^{-n} + 1} \cdot w \right) i \quad (1-2)$$

$$T_i = \sum_{i=1}^n Z_i \quad (1-3)$$

$$N = T_0 + T_1 + \dots + T_n \quad (1-4)$$

In the formula, Z is the calculated score of each active component, T represents the sum of the fractions of the related active components contained in each target, and N is the sum of the target fractions contained in each pathway.

Gene Ontology–Biological Process Enrichment Analysis and Kyoto Encyclopedia of Genes and Genomes Pathway Enrichment Analysis

To further clarify the gene function of German chamomile volatile oil and the role of potential signaling pathway targets in eczema, profile in the Rstudio was used to analyze the key targets in GO–BP, the basic biological processes and pathways were analyzed by the KEGG pathway, and the results of the enrichment analysis were reordered according to their weight coefficients. The weight coefficients of each pathway were the sum of the weight coefficients of all targets in a specific pathway.

Animal Experiments

Experimental Animals Mental Animal

Male Kunming mice ($n = 42$) weighing 18–22 g were purchased from Chengdu Dashuo Experimental Animal Co., Ltd. under the experimental animal license SCXK (Sichuan) 2020–030. This study was approved by the Animal Ethics Committee of Shaanxi University of Chinese Medicine.

Establishment of the Eczema Model

To establish the eczema model, all groups, except the normal group, were sensitized on the back with 7% DNCB solution. In brief, the back hair in a 2 cm × 2 cm area was removed, and all the groups, except the normal group, were sensitized with 100 μL acetone olive oil solution containing 7% DNCB. After 5 days, all the groups, except the normal group, were challenged with 30 μL acetone olive oil solution containing 1% DNCB on the inside and outside of the right ear. The challenge was repeated three times in two consecutive days. As a control, mice in the normal group were smeared with the same amount of acetone olive oil solution on the left ear.

Experimental Grouping and Administration

The mice were adaptively fed for 3 days and randomly divided into six groups ($n = 7/\text{group}$): normal group, model group, positive drug group, low-dose chamomile group (concentration 0.15%), medium-dose group (concentration 0.3%), and high-dose group (concentration 0.5%). Each group was reared in separate cages. The aforementioned groups were treated via skin smearing on the eczema site twice a day for 14

consecutive days. The German chamomile volatile oil group was treated with 80 μL volatile oil each time in the positive drug group, and 80 μL olive oil solvent was applied in the normal group and model groups.

Mouse Skin Test and Determination of Spleen Index

After the completion of treatment, the skin water content, sebum content, and skin elasticity of the treated area were measured using an intelligent digital display multi-function skin detector (RBX-916). The mice in each group were weighed before sampling, and the spleen was removed after carefully separating the connective tissue around the spleen. After absorbing the residual blood on the organ surface with absorbent paper, the spleen mass was immediately weighed with an analytical balance. The spleen index was calculated as follows: spleen index = (spleen quality (mg))/(experimental mouse quality (g)). Each group was compared with the control group, and the difference was calculated.

Hematoxylin–Eosin Staining

Tissue specimens were fixed with 4% paraformaldehyde for 24 h gradient dehydrated with 75, 85, and 95% anhydrous ethanol until transparent and embedded in paraffin, cut into 4-μm-thick tissue sections, and then spread in water at 43°C (Zhang et al., 2020). The tissue slices were baked at a constant temperature and dried in a blast drying box at 60°C for 2–4 h. After dewaxing, the tissue sections were soaked in gradient alcohol and hydrated in distilled water for several minutes. The tissue sections were stained with hematoxylin and eosin. After dehydration, the tissue sections were sealed with xylene, and the changes were observed under a microscope.

Toluidine Blue Staining

The paraffin-embedded tissue was sliced (4 μm) (Chen et al., 2020). Each slice was stained with 0.5% toluidine blue dye solution at room temperature for 30 min and rinsed quickly with distilled water. The slices were placed in 0.5% glacial acetic acid, differentiated for several minutes and sealed via alcohol dehydration, rendered transparent with xylene, sealed with neutral gum, and observed under a microscope.

Immunohistochemistry

The slices were incubated with 3% hydrogen peroxide for 25 min and incubated with 10% normal goat serum at room temperature for 30 min. Serum was removed, the primary antibody was added, and tissues were incubated overnight at 4°C. The tissues were then washed three times with PBS for 5 min per wash. The secondary antibody was added, and tissues were incubated at room temperature for 50 min. DAB chromogenic solution was used to cover the tissues evenly, and the tissues were sliced into hematoxylin for 2 min and observed under a microscope after dehydration, transparency, and sealing.

Enzyme-Linked Immunosorbent Assay

The content of IL-6, TNF-α, and IL-17 in the serum of mice from each group was detected by ELISA, and a standard curve was drawn according to the kit instructions (Jiangsu Meimian industrial Co.,Ltd) (Šutovská et al., 2021). The cytokine content in the serum of each group was detected via the double antibody sandwich method and enzyme labeling instrument.

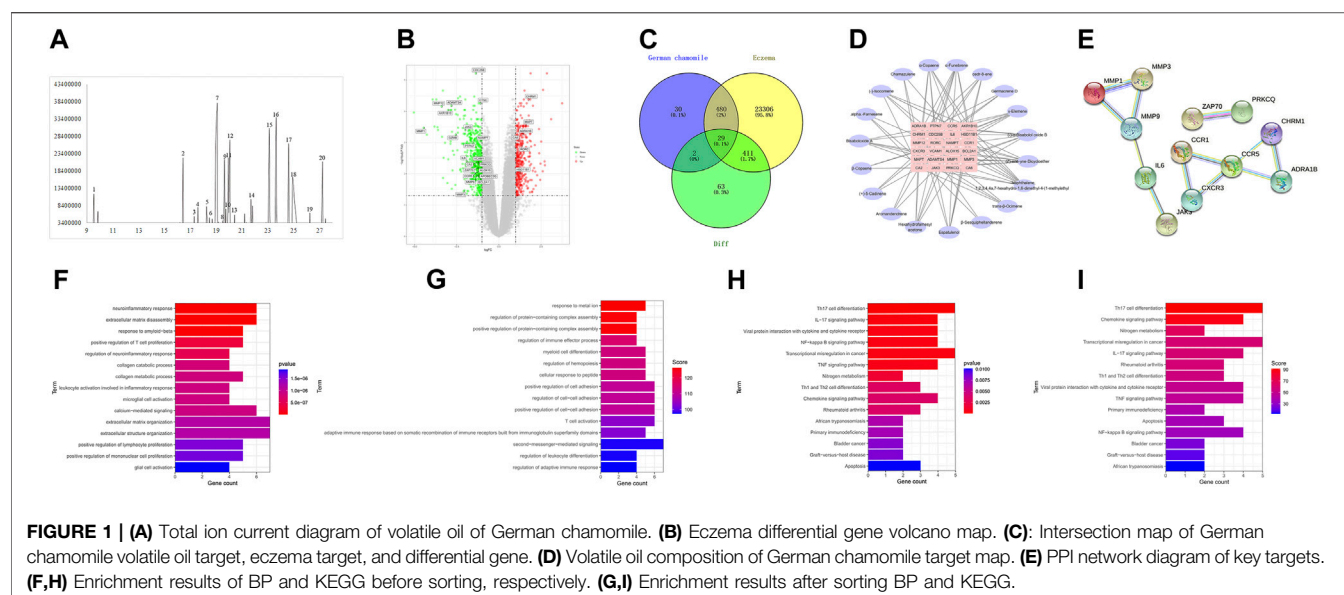


TABLE 1 | Qualitative results of volatile oil from German chamomile by GC/MS

No.	Library/ID	CAS	Pct Total	RI
1	Trans- β -ocimene	3779-61-1	2.728	1,049.212
2	γ -Elemene	29873-99-2	3.882	1,343.234
3	α -Copaene	003856-25-5	0.756	1,382.972
4	(-)-Isocomene	065372-78-3	0.943	1,396.072
5	β -Copaene	018252-44-3	2.639	1,427.655
6	Aromandendrene	000489-39-4	0.653	1,448.85
7	β -Sesquiphellandrene	020307-83-9	18.527	1,467.285
8	Naphthalene, 1,2,3,4,4a,7-hexahydro-1,6-dimethyl-4-(1-methylethyl)-	16728-99-7	0.661	1,487.56
9	Germacrene D	023986-74-5	4.835	1,494.01
10	α -Funebrene	50894-66-1	1.452	1,499.08
11	Bicyclogermacrene	100762-46-7	4.822	1,509.228
12	α -Farnesene	000502-61-4	6.573	1,515.053
13	(+)- δ -cadinene	000483-76-1	0.86	1,533.014
14	Espatulenol	006750-60-3	2.127	1,597.092
15	(-)- α -bisabolol oxide B	026184-88-3	9.46	1,672.963
16	Cedr-8-ene	000469-61-4	9.606	1,718.242
17	Chamazulene	000529-05-5	6.398	1,952.009
18	Bisabolol oxide A	022567-36-8	12.071	1,970.864
19	Hexahydrofarnesyl acetone	000502-69-2	0.888	2,043.486
20	(Z)-ene-yne-dicycloether	004575-53-5	6.074	1,906.516

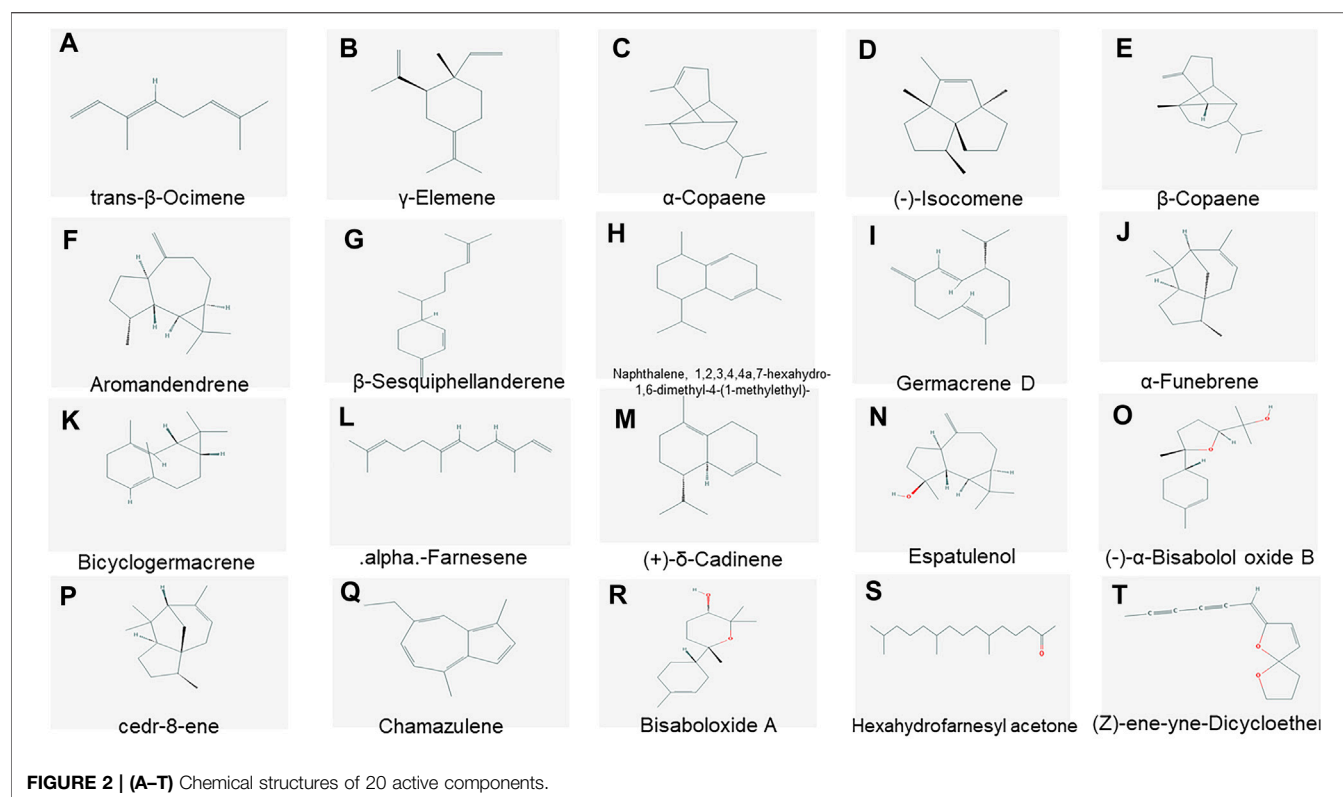
Western Blot Analysis (Gao et al., 2018).

Skin tissues from the aforementioned groups were collected and lysed with RIPA buffer, and the lysed samples were put on ice for 5 min. The supernatant was centrifuged in a cryopreserved centrifuge at 4°C, 12,000 rpm for 10 min. The supernatant was separated as the protein extract. A total of 40 μ g protein was separated *via* sodium dodecyl sulfate–polyacrylamide gel electrophoresis (SDS-PAGE) and then transferred to polyvinylidene fluoride (PVDF) membranes. The membranes were sealed with 5% skimmed milk powder and then incubated with antibodies for p38 (Wanleibio, WL00764, China), p-p38 (Wanleibio, WLP1576, China), p65 (Wanleibio, WL01980, China), and p-p65 (Wanleibio, WL02169, China). Then, the membranes were washed with Tris-buffered saline + Tween

(TBST) and incubated with the secondary antibodies. The membranes were then washed in TBST six times, sprinkled evenly with electrochemiluminescence (ECL) photoluminescence solution, and transferred to a dark box for exposure. The film was scanned, and the optical density was calculated using Gel-Pro Analyzer software. The relative expression value of the target gene (the gray value of the target gene/the internal reference gray value of β -actin) was determined using β -actin as an internal reference.

Molecular Docking

The active ingredients of German chamomile were selected as ligands, the first five proteins of the prediction pathway were



used as targets, and the area where the positive drug ligand was located was the active pocket (Jia et al., 2021). The LibDock module in the discovery studio software was used to molecularly dock the active ingredients with the target protein. After the docking was completed, the established formula was used to calculate the score of each component to screen out the key components of the target.

$$S = Z * \frac{A}{B}$$

In the formula, S represents the final score of each component, Z represents the score of each active compound, A represents the score of each component obtained by molecular docking, and B represents the score of positive drugs.

Statistical Analysis

All of the experimental data were statistically analyzed using SPSS 19.0 software. Results are expressed as mean ± standard deviations (SDs). One-way analysis of variance (ANOVA) was applied to determine the statistical significance of the differences between the groups, $p < 0.05$ and $p < 0.01$ were regarded as significantly different.

RESULTS AND ANALYSIS

Screening of Compounds and Selection of Potential Targets

The essential oil of chamomile was analyzed by gas chromatography–mass spectrometry (GC–MS), and the ion

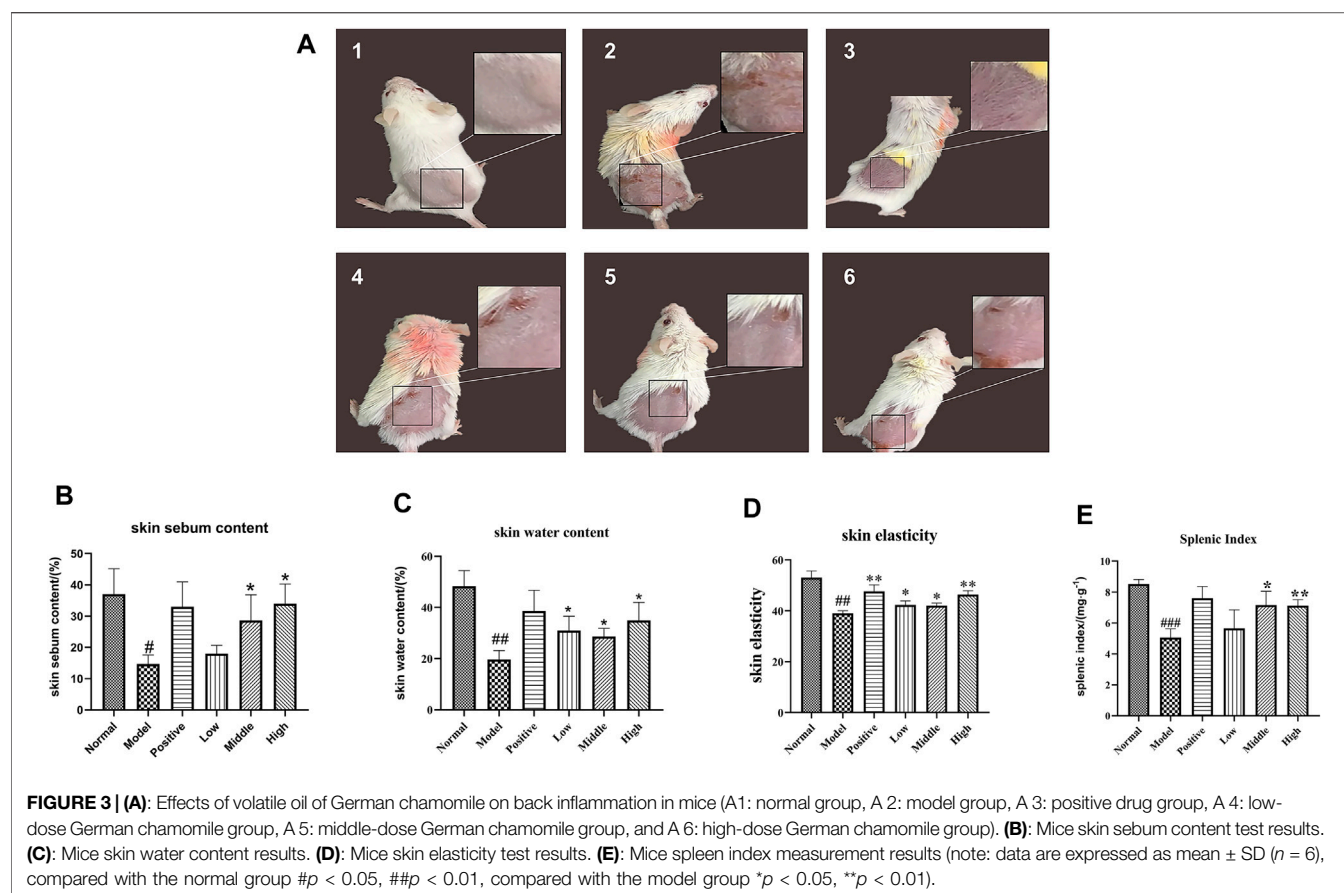
mass spectrum of the essential oil was obtained (Figure 1A). By searching the NIST database and combining with the retention index, 23 active components were obtained and 20 qualified components were identified. Specific composition information is shown in Table 1, and specific compound structures are shown in Figure 2. A total of 541 targets of German chamomile volatile oil were obtained using the PubChem database, the Swiss TargetPrediction online target screening platform, and the meta TarFisher database. Additionally, 24,226 eczema targets were obtained from the GeneCards, DisGeNet, OMIM, and CTD databases. Based on the intersection, 509 potential targets of German chamomile volatile oil for the treatment of eczema were obtained.

GEO Chip Differential Gene Verification

The GSE57225 chip and platform data were downloaded from the GEO database. A total of 62 samples were collected, including 17 normal samples and 23 eczema samples. Based on the screening conditions ($|\log_{2}FC| > 1.2$ and $p < 0.05$), 560 genes with significant differences were obtained. The upregulated gene expression (red), downregulated gene expression (green), and the volcano plot are shown in Figure 1B. The intersection between differentially expressed genes (DEG) and possible eczema targets of German chamomile volatile oil produced 29 candidate genes, as shown in Figure 1C.

Network Construction and Analysis

Network pharmacology provides a new perspective on analyzing the effects of drugs. It can analyze network characteristics



through the connections and relationships of nodes in biological networks, and further clarify the mechanism of drug action. We analyzed the relationship between the active ingredients and key targets of the volatile oil of German chamomile and then created a “component–target” map with a merge function. We then used Cytoscape 3.7.1 software to visualize the network. The results are shown in **Figure 1D**. The purple ellipse represents the key components screened out by the volatile oil, the pink rectangle represents the key target points screened out, the node represents the active ingredient, and the edge is used to connect the target to the active ingredient. The greater number of links indicates that the active ingredient or the target is more important in the network.

German Chamomile–Eczema–Differential Gene PPI Network Construction and Key Target Screening

The 29 DEGs were introduced into STRING to construct a network map, as shown in **Figure 1E**. Through the screening of the set conditions, the key targets were identified as IL-6, MMP1, MMP3, MMP9, JAK3, CCR1, CCR5, ZAP70, and PRKCQ. The network diagram had 29 nodes with an average degree of freedom of 0.828. The size of the node in the diagram

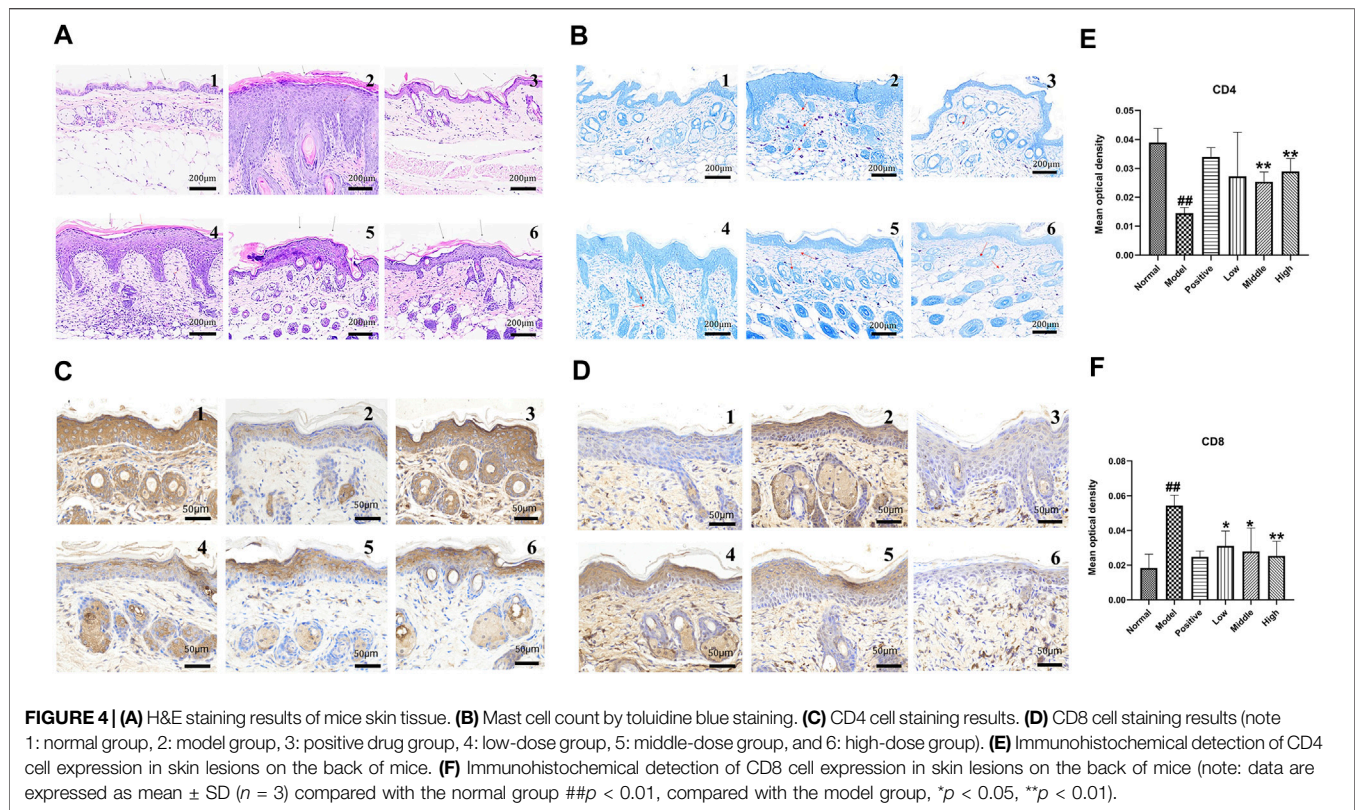
represents the size of the value. The thickness of the edge indicates that the thicker the edge, the greater the combined score value and the greater the interaction between the nodal protein and other proteins.

GO–BP and KEGG Enrichment Analysis

Through GO–BP enrichment analysis of the selected key targets, 145 biological processes and 16 signaling pathways, were identified (**Figures 1F–I**). These involved the neuroinflammatory response, extracellular matrix disassembly, response to amyloid-beta, positive regulation of T-cell proliferation chemokine signaling pathway, Th17 cell differentiation, IL-17 signaling pathway, and viral protein interaction with cytokine and cytokine receptor, among other signaling pathways. After recalculating the formula, Th17 cell differentiation was determined to be the most important one.

Animal Experiment and Efficacy Verification Comparison of the Degree of Inflammation

After DNCB induction, each group exhibited skin erythema, exudation, thickening, a rough surface, and moss-like lesions, suggesting that the model was successful. After treatment with the positive drugs and different doses of German chamomile volatile oil, the exudate, redness, and



swelling were reduced. In the positive drug and high-dose German chamomile volatile oil groups, eczema was reduced, as shown in **Figure 3A**.

Skin Test Results

Skin test results showed that when compared with the normal group, the skin sebum content (**Figure 3B**), the skin water content (**Figure 3C**), and skin elasticity (**Figure 3D**) in the model group decreased. Compared with the model group, the skin water content and sebum and skin elasticity of different dose groups increased to different degrees, with significant differences.

Comparison of Spleen Index Among Different Groups of Mice

The effect of volatile oil from German chamomile on the immune response was preliminarily evaluated by the spleen index (**Figure 3E**). The chart shows that the spleen index of the model group was lower than that in the normal group, and the spleen index of different dose groups was higher than that in the model group, with significant differences.

H&E Staining Results

The results of H&E staining (**Figure 4A**) showed that the structure of the epidermis and dermis in the normal group appeared normal, without edema, congestion, or lymphocyte infiltration. In the model group, the epidermis had proliferated, and the spinous layer was hypertrophic. The dermis showed

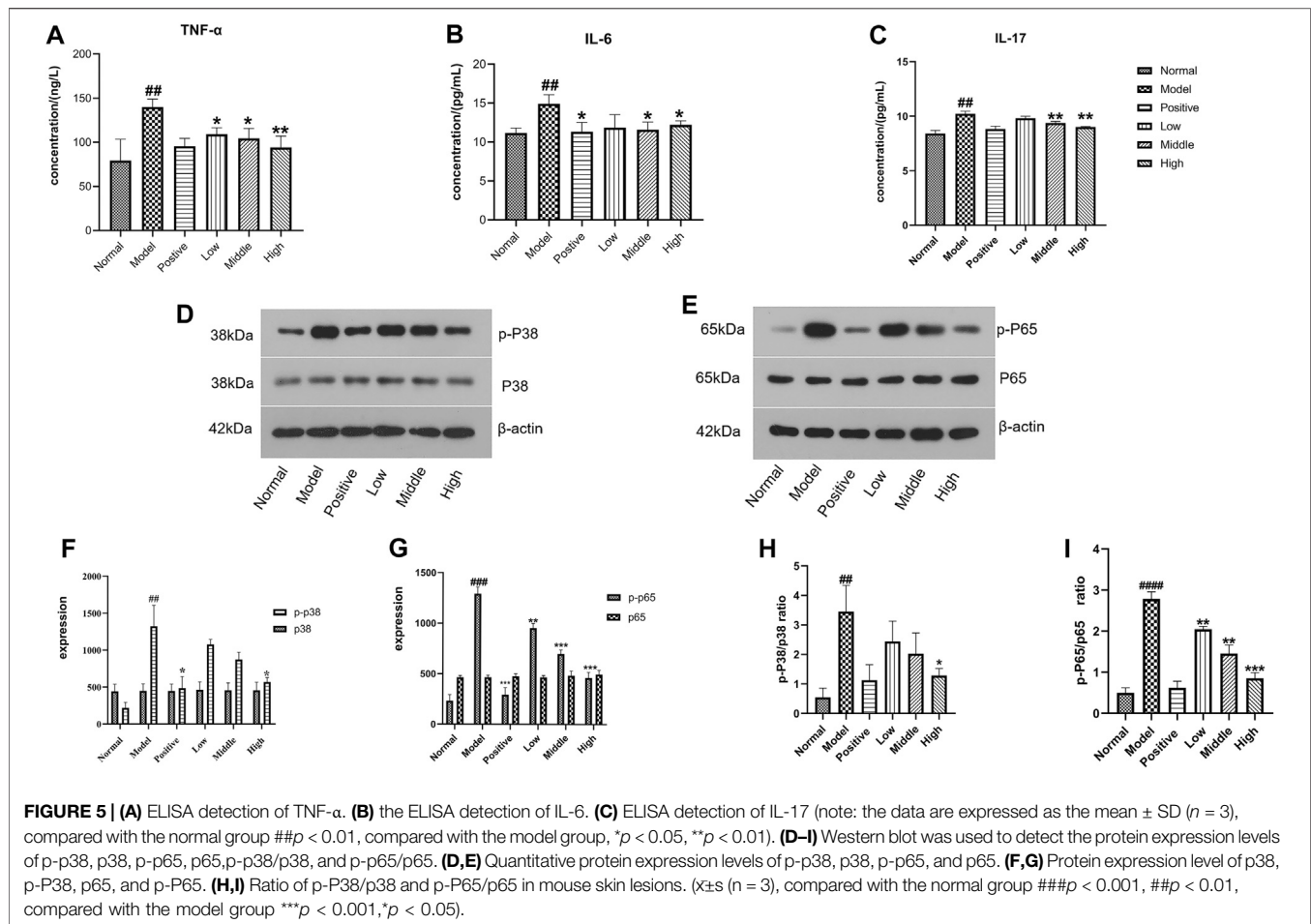
inflammatory cell infiltration accompanied by vasodilation and hyperemia. In the positive drug group, the epidermis had proliferated slightly, and most of the dermis had recovered. No edema, hyperemia, or lymphocyte infiltration was apparent. The epidermal hyperplasia and cell edema significantly decreased, with the increase in dose in the treatment group.

Toluidine Blue Staining Results

Results of toluidine blue staining are shown in **Figure 4B**. The number of mast cells was low in the normal group and high in the model group. The mast cell number was significantly reduced, in the positive drug group and decreased in a dose-dependent manner in the low, middle, and high German chamomile volatile oil groups.

CD4 and CD8 Staining Results

CD4 and CD8 cells are located in the cytoplasm and cell membrane. CD4 and CD8 cells were weakly positive in the skin tissues of the back of mice. Compared with the normal group, the distribution of CD4 cells in the cytoplasm and cell membrane of the skin lesions on the back of the eczema model group was reduced, the staining became lighter, and the positive expression of CD4 cells was reduced ($p < 0.001$, $n = 3$). Compared with the eczema model group, different doses of German chamomile volatile oil increased the expression of CD4 cells to varying degrees, and the medium and high doses were significantly different from the model group ($p < 0.001$, $n = 3$).



Compared with the normal group, CD 8 cells in the skin lesions on the back of mice in the eczema model group showed brownish-yellow particles in the cell membrane and cytoplasm, and the positive expression level of CD8 cells increased ($p < 0.001$, $n = 3$). Compared with the eczema model group, different doses of German chamomile volatile oil caused different degrees of reduction in the number of cells expressing CD8. There were significant differences between the high-dose group and the model group ($p < 0.001$, $n = 3$), as shown in **Figures 4C–F**.

Serum Levels of TNF- α , IL-6, and IL-17

Compared with the normal group, serum TNF- α , IL-6, and IL-17 in the eczema model group increased significantly ($p < 0.001$, $n = 6$). Compared with the model group, these factors were reduced in the positive drug group and the German chamomile volatile oil groups. The results are shown in **Figures 5A–C**.

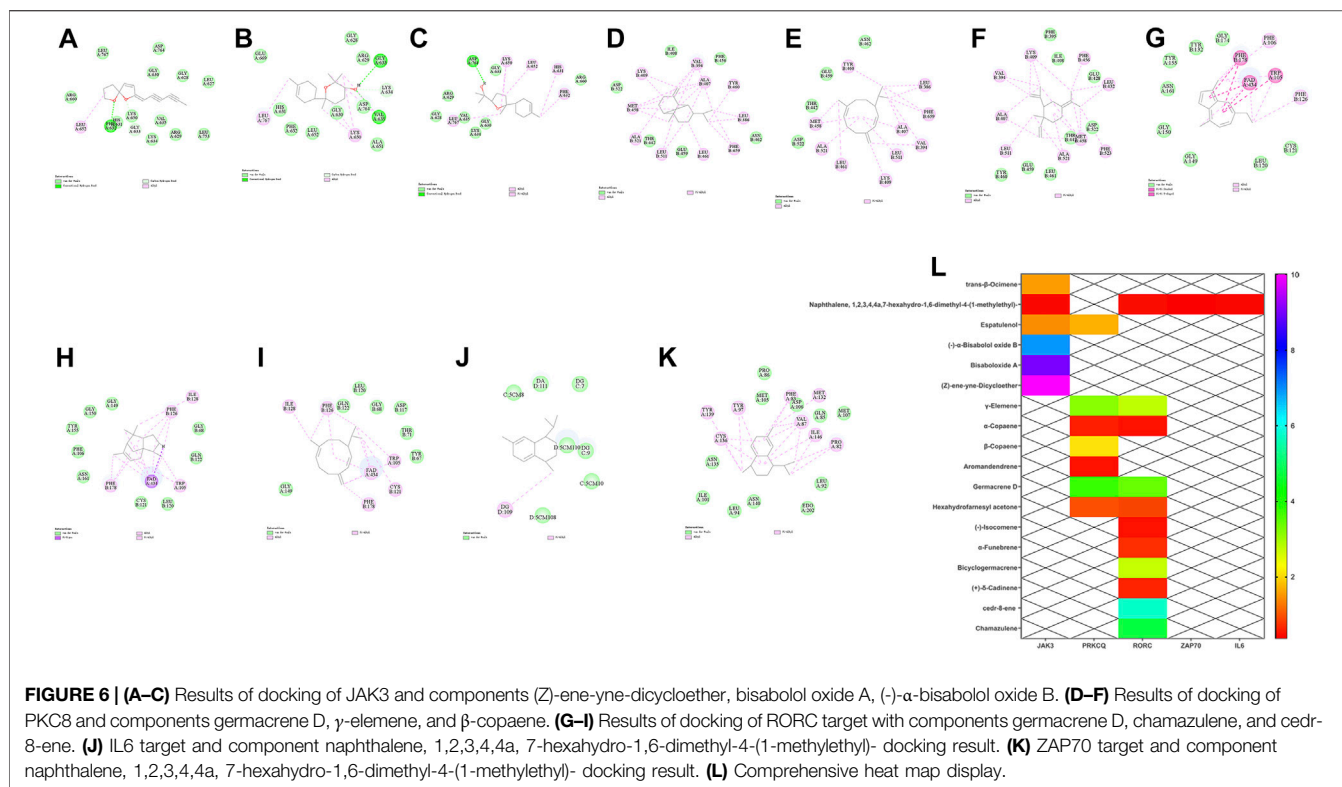
Western Blot Analysis

The expression levels of p-P38 and p-P65 proteins in the positive drug group and the treatment group were lower than those in the model group. Compared with the normal group,

the expression of p-P38/p38 and p-P65/p65 protein in the mouse eczema model group was higher than that of the mouse eczema model group ($p < 0.001$, $n = 3$). Compared with the mouse eczema model group, both the treatment group and the positive drug group had reduced protein expression of p-P38/p38 and p-P65/p65 ($p < 0.001$, $n = 3$), which indicates that German chamomile volatile oil can inhibit the MAPK and NF- κ B pathways. The results are shown in **Figures 5D–I**.

Molecular Docking Verification

The molecular docking results are shown in **Figure 6A–K**. The molecular docking of the core active component and the target was conducted using Discovery software, and the molecular docking score was calculated using the new weight formula. The higher the score of the component, the higher the importance of the component to the target and the greater the role of the component in the Th17 cell differentiation pathway. The results are shown in the heat map in **Figure 6L**. These results suggest that chamazulene, bisabolol oxide A, (-)- α -bisabolol oxide B, and γ -elemene may be key active components of German chamomile volatile oil in the treatment of eczema.



Mechanism Description

We used the dinitrochlorobenzene (DNCB) method to establish a mouse eczema model. The models were treated with low, medium, and high doses of German chamomile volatile oil. During the experiment, the mice were observed. Skin conditions include sebum content, water content, and elasticity index. The serum levels of inflammatory factors IL-6, IL-17, and TNF- α in different groups of mice were detected by ELISA, and the inflammatory cells, lymphocytes, and mast cells in the skin lesions of the mice were observed by H&E staining and toluidine blue staining. To detect the level of CD4 and CD8 cells of lymphocytes immunohistochemistry was used, and finally, to show the protein expression levels of p38, p65, p-P38, and p-P65 in the skin lesions Western blot was used. Combined with the results of each experiment, we believe that the mechanism of action of German chamomile volatile oil in the treatment of eczema may be German chamomile volatile oil can prevent the differentiation of CD4⁺ cells into Th17 cells by regulating the lymphatic subsets of T cells; inhibiting the activation of MAPK and NF- κ B pathways; reducing the secretion of inflammatory factors IL-6, IL-17, and TNF- α ; and thereby reducing the inflammatory response (Figure 7).

DISCUSSION

In the treatment of eczema, German chamomile volatile oil is administered transdermally. Therefore, our research included the

water–oil distribution coefficient (log P) and composition content as key parameters in predicting absorption into blood. We have established “weight coefficients” that can be compared with the signaling pathways enriched by traditional network pharmacology. This can be used to reassess the results of biological enrichment analysis to determine key pathways. Before and after the ranking the contribution scores of the “weight coefficient,” we found that the top five pathways enriched by traditional network pharmacology were Th17 cell differentiation, the IL-17 signaling pathway, viral protein interaction with cytokine and cytokine receptor, the NF- κ B signaling pathway, and transcriptional dysregulation in cancer. Following the calculation using the new weighting coefficient, the top five enriched pathways were the Th17 cell differentiation, chemokine signaling pathway, nitrogen metabolism, transcriptional misregulation in cancer, and IL-17 signaling pathway. Through literature review in combination with sequencing the pathways, we determined that Th17 cell differentiation is a key pathway for German chamomile volatile oil in the treatment of eczema.

Studies (Liu et al., 2019) have shown that the occurrence of dermatitis and eczema is related to an imbalance in T-cell lymphatic subsets (Th1/Th2). TNF- α secreted by Th1 cells induces the expression of ICAM-1 and L-selectin, causing T cells and macrophages to infiltrate a large number of T cells and macrophages to the inflammatory site. With inflammatory stimulation, monocytes, macrophages, and endothelial cells will release Th2 cell IL-6. The excessive secretion of Th2 type

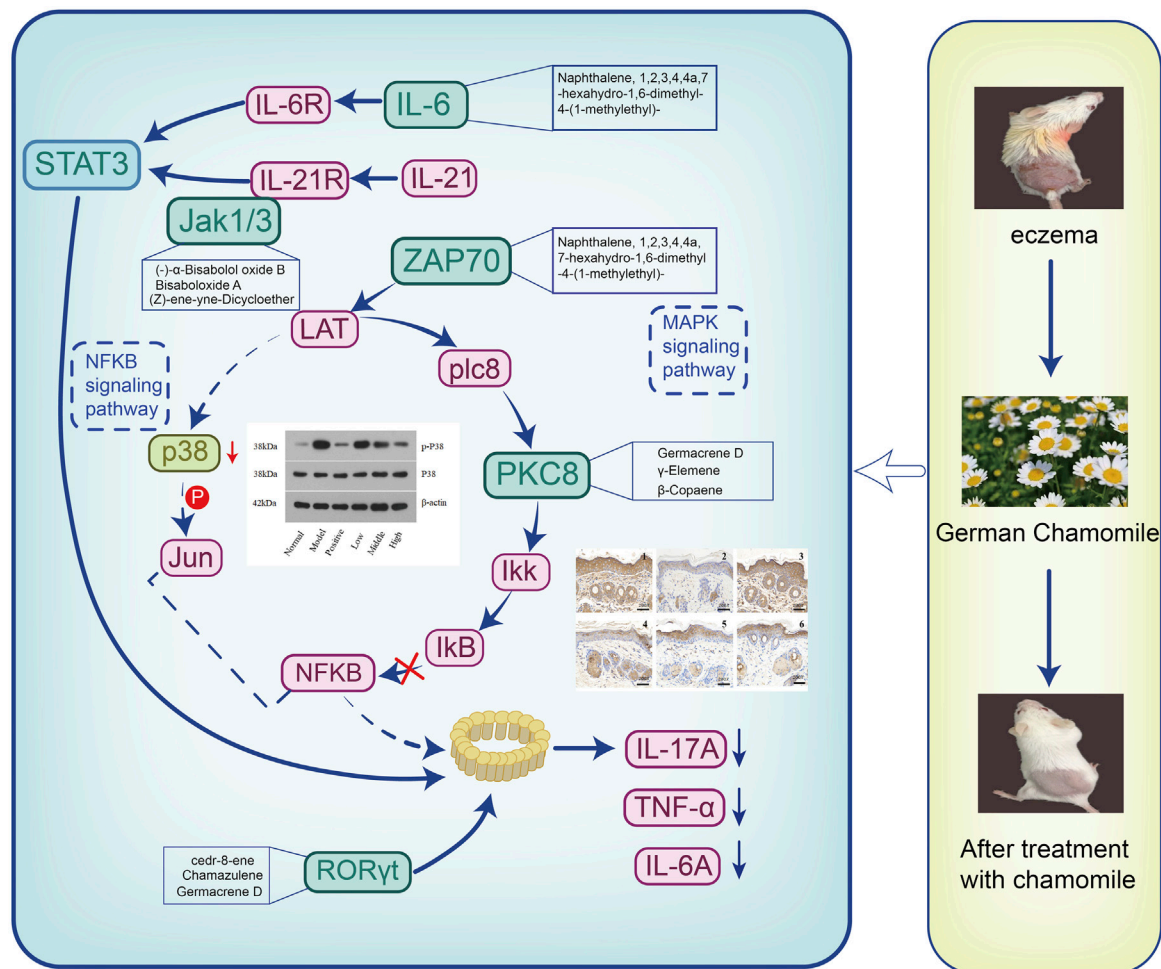


FIGURE 7 | Mechanism display.

cytokines is an important factor leading to eczema, and the excessive secretion of Th1-type cytokines aggravates the disease (Zhou et al., 2019). The level of Th17 in the peripheral blood of patients with eczema is significantly higher than that in normal people (Fan et al., 2019), and these cells secrete a large number of inflammatory cytokines that induce tissue inflammation. IL-17 secreted by Th17 cells can stimulate skin keratinocytes, increase the secretion of pre-inflammatory cytokines, and expand skin inflammation and tissue destruction (Xu and Lv, 2020). Research studies had shown that the levels of TNF- α , IL-6, and IL-17 cytokines in the serum of mice treated with German chamomile volatile oil were lower than those in the model group, indicating that the decrease in TNF- α , IL-6, and IL-17 may be one anti-inflammatory mechanism. After recognition by cell surface IL-17 receptors, IL-17 can activate downstream signaling pathways such as NF- κ B and MAPK, leading to the expression of pro-inflammatory chemokines and cytokines.

In multicellular organisms, especially mammalian cells, multiple signaling pathways often must work together to accurately complete cell functions (Yong and Xiao-Wei, 2000). The MAPK pathway is a

common intersection pathway for signal transduction pathways affecting cell proliferation, differentiation, transformation, and apoptosis (Lei et al., 2020). Some drugs participate in the activation, proliferation, and migration of immune cells via the MAPK signaling pathway to alleviate skin lesions due to AD allergic disease (Pfalzgraff et al., 2016). Oxidative damage in skin cells may be reduced via the use of a p38 inhibitor, which inhibits the downregulation of IL-6. Effective substances may attenuate the expression of NF- κ B in keratinocytes and induce thromboxane regulation, which is related to the downregulation of inflammatory cells (Chang et al., 2017; Sur et al., 2019). NF- κ B plays an important role in regulating T-cell autoimmunity and inflammation. The transcription factor p65 is a member of the NF- κ B family, which can induce the production of pro-inflammatory chemokines induced by the TNF- α /IFN- γ *in vitro* and can also induce an allergic inflammatory response. p38MAPK is the upstream kinase of NF- κ B. It is a stress-induced protein kinase. It is activated under the action of inflammatory factors and oxidative stress and enters the nucleus from the cytoplasm to further induce NF- κ B activation, which eventually leads to the production of a large number of inflammatory factors.

In this study, the model group showed hyperplasia of the damaged epidermis, hypertrophy of the spinous layer, infiltration of a large number of mast cells, infiltration of inflammatory cells in the dermis, and obvious eczema-like manifestations such as vasodilation. In the positive drug group and groups treated with different doses of German chamomile volatile oil, hyperkeratosis was inhibited and inflammatory cell infiltration in the eczema model epidermis was reduced. Also, the water content and lipid content and elasticity of the skin increased, suggesting a similar effect of volatile oil of German chamomile and positive drugs. In T lymphocytes, CD4⁺ cells assist macrophages, B lymphocytes, and killer T cells, whereas CD8⁺ cells have a direct killing effect on antigen-carrying target cells. CD4⁺ and CD8⁺ regulate each other to maintain immune balance. The immunohistochemistry results showed that after treatment with volatile oil, the positive expression of CD4⁺ in the skin lesions on the backs of mice increased, and the positive expression of CD8⁺ decreased, confirming that it can reduce inflammation and infection by improving the body's immune level. Serum levels of IL-6, TNF- α , and IL-17 in the model group were higher than in the normal group. Compared with the model group, positive drugs and German chamomile volatile oil reduced the content of inflammatory factors in the serum. Additionally, this study showed that the protein expression of P-p38/p38 p-p65/p65 increased after modeling, indicating that by activating the MAPK and NF- κ B pathways, it promotes the differentiation of CD4⁺ cells into Th17 cells to produce an inflammatory response, where treatment with the German chamomile volatile oil decreased their expression, suggesting the inhibition of the MAPK signaling pathway via the prevention of p38 phosphorylation (Shen et al., 2020). We conclude that German chamomile may reduce inflammation by regulating Th17 cell differentiation, increasing IL-17 and further affecting the MAPK and NF- κ B pathways.

To further determine the key active components in German chamomile volatile oil affecting the Th17 cell differentiation pathway, we selected the five key targets, namely, JAK3, RORC, PRKCQ, ZAP70, and IL6, and their corresponding active components and positive drugs as ligands. Molecular docking was used to verify the interaction between the main active components of German chamomile volatile oil and potential targets. Using the combination of ligand fraction, positive drug fraction, and component weight, a new formula for judging components was obtained. The results showed that chrysanthemum, red myrrh alcohol A, red myrrh alcohol B, and γ -elemene may be the key components of German chamomile volatile oil in the treatment of eczema.

REFERENCES

- Anderson, C., Lis-Balchin, M., and Kirk-Smith, M. (2000). Evaluation of Massage with Essential Oils on Childhood Atopic Eczema. *Phytother. Res.* 14 (6), 452–456. doi:10.1002/1099-1573(200009)14:6<452::aid-ptr952>3.0.co;2-4
- Arsić, I., Tadić, V., Vlaović, D., Homšek, I., Vesić, S., Isailović, G., et al. (2011). Preparation of Novel Apigenin-Enriched, Liposomal and Non-liposomal,

DATA AVAILABILITY STATEMENT

Publicly available datasets were analyzed in this study. These data can be found here: Gene Expression Omnibus database GSE57225 chip.

ETHICS STATEMENT

The animal study was reviewed and approved. This study was approved by the Animal Ethics Committee of Shaanxi University of Chinese Medicine.

AUTHOR CONTRIBUTIONS

WW, XZ, and YS participated in the design of this study, and they also performed the statistical analysis. JZ, YW, JL, CW, and YW carried out the study and collected important background information. WW, YJ, MY, JS, and DG drafted the manuscript. ZW and FW revised the manuscript for us. LW provides us with German chamomile essential oil. All authors read and approved the final manuscript.

FUNDING

This project has been supported by the National Natural Science Foundation of China (Grant No. 81703720), Discipline Innovation Team Project of Shaanxi University of Chinese Medicine (2019-YL11), Innovation talents Promotion Program of Shaanxi Province-Science and Technology Innovation team (Grant No. 2018TD005), Jiangxi University of Traditional Chinese Medicine Double First-Class Discipline Construction Project (JXSYLXK-ZHYAO008, JXSYLXK-ZHYAO083, JXSYLXK-ZHYAO084), Major Science and Technology R&D Project in Jiangxi Province (20194ABC28009), and 2017 Open Fund of the Key Laboratory of Modern Chinese Medicine Preparation by the Ministry of Education (2017003), Shaanxi Province 2021 Central Leading Local Science and Technology Innovation Special Project (2021ZY2-CG-03).

SUPPLEMENTARY MATERIAL

The Supplementary Material for this article can be found online at: <https://www.frontiersin.org/articles/10.3389/fphar.2021.706836/full#supplementary-material>

- Antiinflammatory Topical Formulations as Substitutes for Corticosteroid Therapy. *Phytother. Res.* 25 (2), 228–233. doi:10.1002/ptr.3245
- Chang, T. M., Tsen, J. H., Yen, H., Yang, T. Y., and Huang, H. C. (2017). Extract from *Periostracum Cicadae* Inhibits Oxidative Stress and Inflammation Induced by Ultraviolet B Irradiation on HaCaT Keratinocytes. *Evid. Based Complement. Alternat. Med.* 2017, 8325049. doi:10.1155/2017/8325049
- Chen, R., Ye, B., Xie, H., Huang, Y., Wu, Z., Wu, H., et al. (2020). miR-129-3p Alleviates Chondrocyte Apoptosis in Knee Joint Fracture-Induced

- Osteoarthritis through CPEB1. *J. Orthop. Surg. Res.* 15 (1), 552. doi:10.1186/s13018-020-02070-1
- El-Salamouni, N. S., Ali, M. M., Abdelhady, S. A., Kandil, L. S., Elbatouti, G. A., and Farid, R. M. (2020). Evaluation of Chamomile Oil and Nanoemulsions as a Promising Treatment Option for Atopic Dermatitis Induced in Rats. *Expert Opin. Drug Deliv.* 17 (1), 111–122. doi:10.1080/17425247.2020.1699054
- Fan, Y., Liancheng, G., Zexin, Z., Zeyu, C., Wen, L., and Zhenghui, T. (2019). Discussion on the Intervention Mechanism of Snake Huang Cream in the Skin Barrier of Eczema Based on Th17/Treg Drift. *J. Guiyang Coll. Traditional Chin. Med.* 41 (02), 41–45. doi:10.16588/j.cnki.issn1002-1108.2019.02.012
- Fu, C., Wu, D., Wang, W., Wang, Y., Zhang, L., and Li, J. (2018). GC-MS Analysis of Volatile Oil of Anthemis Nobilis from Different Areas. *J. Anhui Agric. Sci.* 46 (21), 172–174. doi:10.3969/j.issn.0517-6611.2018.21.049
- Gao, C. J., Ding, P. J., Yang, L. L., He, X. F., Chen, M. J., Wang, D. M., et al. (2018). Oxymatrine Sensitizes the HaCaT Cells to the IFN- γ Pathway and Downregulates MDC, ICAM-1, and SOCS1 by Activating P38, JNK, and Akt. *Inflammation* 41 (2), 606–613. doi:10.1007/s10753-017-0716-0
- Jia, Y., Zou, J., Wang, Y., Zhang, X., Shi, Y., Liang, Y., et al. (2021). Action Mechanism of Roman Chamomile in the Treatment of Anxiety Disorder Based on Network Pharmacology. *J. Food Biochem.* 45 (1), e13547. doi:10.1111/jfbc.13547
- Kui, F., Gu, W., Gao, F., Niu, Y., Li, W., Zhang, Y., et al. (2021). Research on Effect and Mechanism of Xuefu Zhuyu Decoction on CHD Based on Meta-Analysis and Network Pharmacology. *Evid. Based Complement. Alternat Med.* 2021, 9473531. doi:10.1155/2021/9473531
- Le-qí, W., Yun-fan, Z., Sha-sha, L., Yuan-fang, S., Jia-na, H., Xue, X., et al. (2020). Study on Component-Target-Pathway Multiple Interactive Network to Reveal Mechanism of Salvia Miltiorrhiza in Treatment of Microcirculation Disturbance. *Chin. Traditional Herbal Drugs* 51 (02), 439–450.
- Lei, L., Zhang, Y., Jian, Q., Lei, L., Lv, N., Williamson, R., et al. (2020). Resistance of Osteosarcoma Cells to the Proapoptotic Effects of Carfilzomib Involves Activation of Mitogen Activated Protein Kinase Pathways. *Exp. Physiol.* 106 (2), 438–449. doi:10.1113/ep088762
- Liang, F. Q., Gao, J. Y., and Liu, J. W. (2021). C-X-C Motif Chemokine 16, Modulated by microRNA-545, Aggravates Myocardial Damage and Affects the Inflammatory Responses in Myocardial Infarction. *Hum. Genomics* 15 (1), 15. doi:10.1186/s40246-021-00314-7
- Li, L., Zhao, J., Wang, X., Yong, T., Jiang, M., Lv, C., et al. (2013). Bioinformatics Analysis on Molecular Mechanism of Moxing Shigan Decoction in Treating H1N1 Influenza A. *Chin. J. Exp. Formulas* 19 (13), 346–350.
- Liu, T., Mou, Y., Hou, X., Liu, W., Wang, Y., and Wang, L. (2019). Identification, Immune Level and Progress Analysis of Pathogen Infection of Skin Lesions in Patients with Dermatitis and Eczema Chinese. *J. Pathog. Biol.* 14 (11), 1342–1345. doi:10.13350/j.cjpb.191123
- Liu, Y., Ma, Y., Li, Z., Yang, Y., Yu, B., Zhang, Z., et al. (2020). Investigation of Inhibition Effect of Gossypol-Acetic Acid on Gastric Cancer Cells Based on a Network Pharmacology Approach and Experimental Validation. *Drug Des. Devel Ther.* 14, 3615–3623. doi:10.2147/DDDT.S256566
- Patzelt-Wenzler, R., and Ponce-Pöschl, E. (2000). Proof of Efficacy of Kamillolan(R) Cream in Atopic Eczema. *Eur. J. Med. Res.* 5 (4), 171–175.
- Pfalzgraff, A., Heinbockel, L., Su, Q., Gutsmann, T., Brandenburg, K., and Weindl, G. (2016). Synthetic Antimicrobial and LPS-Neutralising Peptides Suppress Inflammatory and Immune Responses in Skin Cells and Promote Keratinocyte Migration. *Sci. Rep.* 6, 31577. doi:10.1038/srep31577
- Sang, L., Sun, L., Wang, A., Zhang, H., and Yuan, Y. (2020). The N6-Methyladenosine Features of mRNA and Aberrant Expression of m6A Modified Genes in Gastric Cancer and Their Potential Impact on the Risk and Prognosis. *Front. Genet.* 11, 561566. doi:10.3389/fgene.2020.561566
- Shen, Y., Feng, F., Sun, H., Li, G., and Xiang, Z. (2020). Quantitative and Network Pharmacology: A Case Study of Rhein Alleviating Pathological Progress of Renal Interstitial Fibrosis. *J. Ethnopharmacol.* 261, 113106. doi:10.1016/j.jep.2020.113106
- Shi, L., Han, X., Li, J. X., Liao, Y. T., Kou, F. S., Wang, Z. B., et al. (2020). Identification of Differentially Expressed Genes in Ulcerative Colitis and Verification in a Colitis Mouse Model by Bioinformatics Analyses. *World J. Gastroenterol.* 26 (39), 5983–5996. doi:10.3748/wjg.v26.i39.5983
- Sur, B., Kang, S., Kim, M., and Oh, S. (2019). Alleviation of Atopic Dermatitis Lesions by a Benzylideneacetophenone Derivative via the MAPK Signaling Pathway. *Inflammation* 42 (3), 1093–1102. doi:10.1007/s10753-019-00971-w
- Šutovská, M., Kocmálová, M., Kazimirová, I., Forsberg, C., Jošková, M., Adamkov, M., et al. (2021). Effects of Inhalation of STIM-Orai Antagonist SKF 96365 on Ovalbumin-Induced Airway Remodeling in Guinea Pigs. United States: Advances in experimental medicine and biology.
- Tai, Y., Hou, X., Liu, C., Sun, J., Guo, C., Su, L., et al. (2020). Phytochemical and Comparative Transcriptome Analyses Reveal Different Regulatory Mechanisms in the Terpenoid Biosynthesis Pathways between Matricaria Recutita L. And Chamaemelum Nobile L. *BMC genomics* 21 (1), 169. doi:10.1186/s12864-020-6579-z
- Tianmu, H., Qihong, C., Sha, Y., Jianyong, Z., and Xiaifei, L. (2021). Study on the Molecular Mechanism of Cantharidin-Induced Nephrotoxicity Based on Network Pharmacology. *Herald Med.* 40 (02), 180–187.
- Wu, X., Liu, J., Zhu, C., Ma, M., Chen, X., Liu, Y., et al. (2020). Identification of Potential Biomarkers of Prognosis-Related Long Non-coding RNA (lncRNA) in Pediatric Rhabdoid Tumor of the Kidney Based on ceRNA Networks. *Med. Sci. monitor: Int. Med. J. Exp. Clin. Res.* 26, e927725. doi:10.12659/msm.927725
- Xu, F., Gao, J., Munkhsaikhan, U., Li, N., Gu, Q., Pierre, J. F., et al. (2020). The Genetic Dissection of Ace2 Expression Variation in the Heart of Murine Genetic Reference Population. *Front. Cardiovasc. Med.* 7, 582949. doi:10.3389/fcvm.2020.582949
- Xu, R., and Lv, H. (2020). Expression and Clinical Significance of Th17 and Regulatory T Cells in Peripheral Blood and Skin Lesions of Patients with Eczema Shanxi. *Med. J.* 49 (05), 510–512.
- Yong, J., and Xiao-Wei, G. (2000). Regulation of Inflammatory Responses by MAPK Signal Transduction Pathways. *Acta Physiologica Sinica* 52 (4), 267–271. doi:10.3321/j.issn:0371-0874.2000.04.001
- Yuangdong, L., Xiuming, L., Juxing, J., Jianjun, X., Lizhi, D., Yanqing, D., et al. (2017). Analysis of Aroma Components in Orange Oil by GC/MS Combined with the Retention Index. *J. Food Sci. Biotechnol.* 36 (04), 438–442. doi:10.3969/j.issn.1673-1689.2017.04.018
- Zhang, W., Tang, R., Ba, G., Li, M., and Lin, H. (2020). Anti-allergic and Anti-inflammatory Effects of Resveratrol via Inhibiting TXNIP-Oxidative Stress Pathway in a Mouse Model of Allergic Rhinitis. *World Allergy Organ. J.* 13 (10), 100473. doi:10.1016/j.waojou.2020.100473
- Zhou, Y., Cao, L., and Wen, X. (2019). “Effect of Pimecrolimus Cream Treatment on Serum Inflammatory Factors and Immune Function Levels in Patients with Dermatitis and Eczema,” in *2019 National Leprosy and Skin Disease Academic Annual Conference* (Dalian, Liaoning, China: Leprosy), 7.

Conflict of Interest: Author LW was employed by Henan Feinari Aromatic Biotechnology Co., Ltd.

The remaining authors declare that the research was conducted in the absence of any commercial or financial relationships that could be construed as a potential conflict of interest.

Publisher's Note: All claims expressed in this article are solely those of the authors and do not necessarily represent those of their affiliated organizations, or those of the publisher, the editors, and the reviewers. Any product that may be evaluated in this article, or claim that may be made by its manufacturer, is not guaranteed or endorsed by the publisher.

Copyright © 2021 Wang, Wang, Zou, Jia, Wang, Li, Wang, Sun, Guo, Wang, Wu, Yang, Wu, Zhang and Shi. This is an open-access article distributed under the terms of the Creative Commons Attribution License (CC BY). The use, distribution or reproduction in other forums is permitted, provided the original author(s) and the copyright owner(s) are credited and that the original publication in this journal is cited, in accordance with accepted academic practice. No use, distribution or reproduction is permitted which does not comply with these terms.



Network Pharmacology to Explore the Molecular Mechanisms of *Prunella vulgaris* for Treating Hashimoto's Thyroiditis

OPEN ACCESS

Edited by:

Xiao Bin Zeng,
Jinan University, China

Reviewed by:

Claudio Ferrante,
University of Studies G d'Annunzio
Chieti and Pescara, Italy
Hao Li,
China Academy of Chinese Medical
Sciences, China

*Correspondence:

Bo Xu
eyboxu@scut.edu.cn
Wen-song Cai
caiweisong@163.com

[†]These authors share first authorship

*ORCID:

Bo Xu
<https://orcid.org/0000-0001-6384-6685>

Specialty section:

This article was submitted to
Inflammation Pharmacology,
a section of the journal
Frontiers in Pharmacology

Received: 27 April 2021

Accepted: 25 August 2021

Published: 06 October 2021

Citation:

Gan X-x, Zhong L-k, Shen F, Feng J-h,
Li Y-y, Li S-j, Cai W-s and Xu B (2021)
Network Pharmacology to Explore the
Molecular Mechanisms of *Prunella
vulgaris* for Treating
Hashimoto's Thyroiditis.
Front. Pharmacol. 12:700896.
doi: 10.3389/fphar.2021.700896

Xiao-xiong Gan^{1†}, Lin-kun Zhong^{2†}, Fei Shen^{1†}, Jian-hua Feng¹, Ya-yi Li¹, Si-jing Li¹,
Wen-song Cai^{1*} and Bo Xu^{1*†}

¹Department of Thyroid Surgery, Guangzhou First People's Hospital, School of Medicine, South China University of Technology, Guangzhou, China, ²Department of General Surgery, Zhongshan City People's Hospital Affiliated to Sun Yat-sen University, Zhongshan, China

Purpose: *Prunella vulgaris* (PV), a traditional Chinese medicine, has been used to treat patients with thyroid disease for centuries in China. The purpose of the present study was to investigate its bioactive ingredients and mechanisms against Hashimoto's thyroiditis (HT) using network pharmacology and molecular docking technology to provide some basis for experimental research.

Methods: Ingredients of the PV formula were retrieved from the Traditional Chinese Medicine Systems Pharmacology (TCMSP) database. Additionally, HT-related genes were retrieved from the UniProt and GeneCards databases. Cytoscape constructed networks for visualization. A protein-protein interaction (PPI) network analysis was constructed, and a PPI network was built using the Search Tool for the Retrieval of Interacting Genes (STRING) database. These key targets of PV were enriched and analyzed by molecular docking verification, Gene Ontology (GO), and Kyoto Encyclopedia of Genes and Genomes (KEGG) enrichment.

Results: The compound-target network included 11 compounds and 66 target genes. Key targets contained Jun proto-oncogene (*JUN*), hsp90aa1.1 (*AKI*), mitogen-activated protein kinase 1 (*MAPK1*), and tumor protein p53 (*TP53*). The main pathways included the AGE-RAGE signaling pathway, the TNF signaling pathway, the PI3K-Akt signaling pathway, and the mitogen-activated protein kinase signaling pathway. The molecular docking results revealed that the main compound identified in the *Prunella vulgaris* was luteolin, followed by kaempferol, which had a strong affinity for HT.

Conclusion: Molecular docking studies indicated that luteolin and kaempferol were bioactive compounds of PV and might play an essential role in treating HT by regulating multiple signaling pathways.

Keywords: *Prunella vulgaris*, Hashimoto's thyroiditis, network pharmacology, molecular docking, anti-inflammatory response

INTRODUCTION

Prunella vulgaris (PV) is a perennial herbaceous plant in the genus *Prunella*. It is a Chinese medicine widely used to treat inflammation, eye pain, and headaches (Wang et al., 2019; Chen et al., 2020). The anti-inflammatory effects of PV have been recognized during the long-term practice of traditional Chinese medicine (TCM) (hui ZRGwsbydwy, 2000). Currently, PV is combined with Western medicines, such as levothyroxine, indomethacin, or prednisone, in liquid or capsules and has been used to treat Hashimoto's thyroiditis patients. It has been shown that PV significantly reduces the antibody titers of thyroid peroxidase antibody (TPO-Ab) and thyroglobulin antibody (TG-Ab) (Yang et al., 2007; Zhang, 2014). However, the potential underlying mechanisms by which PV might exert its anti-inflammatory effects are poorly understood.

Hashimoto's thyroiditis (HT) is a genetic autoimmune disorder characterized by the destruction of thyroid cells by cell- and antibody-mediated immune responses (Hu et al., 2019). In developed countries, HT is the most common cause of hypothyroidism. The estimated incidence of HT is 3.5 per 1,000 per year in women and 0.8 per 1,000 per year in men (Ala et al., 2015). Effective treatment options for HT are limited. The main method and purpose of HT treatment is the control of hypothyroidism and consists of oral administration of a synthetic hormone, levothyroxine 4 (L-T4) (Wiersinga and Wilmar, 2001).

Additionally, the association between vitamin D deficiency, HT pathogenesis, and thyroid hypofunction has been demonstrated in several studies (Liontiris and Mazokopakis, 2017; Roehlen et al., 2018; Chao et al., 2020). Therefore, due to the low cost and minimal side effects of vitamin D, monitoring and supplementation in patients with HT may be recommended (Liontiris and Mazokopakis, 2017). Surgical therapy can be recommended for patients with HT concurrent with nodules or malignancies (Caturegli et al., 2013). However, HT patients commonly have a higher prevalence rate of postoperative complications than thyroid disorders (Gan et al., 2021).

Network pharmacology, combined with pharmacology and pharmacodynamics, is a novel research field that clarifies numerous compounds' synergistic effects and underlying mechanisms by analyzing various networks of complex and multilevel interactions (Cao et al., 2018). The study explored the potential pharmacodynamic material basis and molecular mechanism of PV against HT using network pharmacology and molecular docking technology and predicted their potential targets and signaling pathways.

MATERIALS AND METHODS

Bioactive Compound Identification Screening

The active constituents of PV were obtained from the Traditional Chinese Medicine Systems Pharmacology Database, the Analysis Platform (TCMSP, <http://tcmspw.com/>) database, and subsequent network pharmacology (Tan et al., 2017). The TCMIP database of Chinese herbal medicines is based on the

Chinese Pharmacopoeia (2015 edition), which contains 500 kinds of Chinese herbal medicines and 30,069 ingredients (Ru et al., 2014). The names and aliases of herbs and ingredients were used as keywords. Then, two parameters of ADME (the absorption, distribution, metabolism, and excretion screening method) drug-likeness (DL) and oral bioavailability (OB) were used to predict the bioactive compounds. In drug discovery and development processes, absorption, distribution, metabolism, and excretion (ADME) evaluations are necessary to predict biologically active compounds (Su et al., 2007). In this study, OB >= 30% and DL quality >= 0.18 were selected as criteria for screening the active compounds identified within the TCMSP database (Ning et al., 2017).

Identification of the Direct Protein Targets

The potential targets for the components of PV were retrieved from both TCMSP databases (<http://lsp.nwsuaf.edu.cn/tcmsp.php>), including 6,511 drug molecules and nearly 4,000 targets as well as the interaction between them (Ru et al., 2014). The UniProt Knowledgebase (UniProtKB) is a protein database partially curated by experts and contains 54, 247, 468 sequence entries (Zhang et al., 2020). Gene information, including the gene name and the gene ID, was confirmed by the UniProt database (<https://www.uniprot.org>).

Predicting the Targets of HT

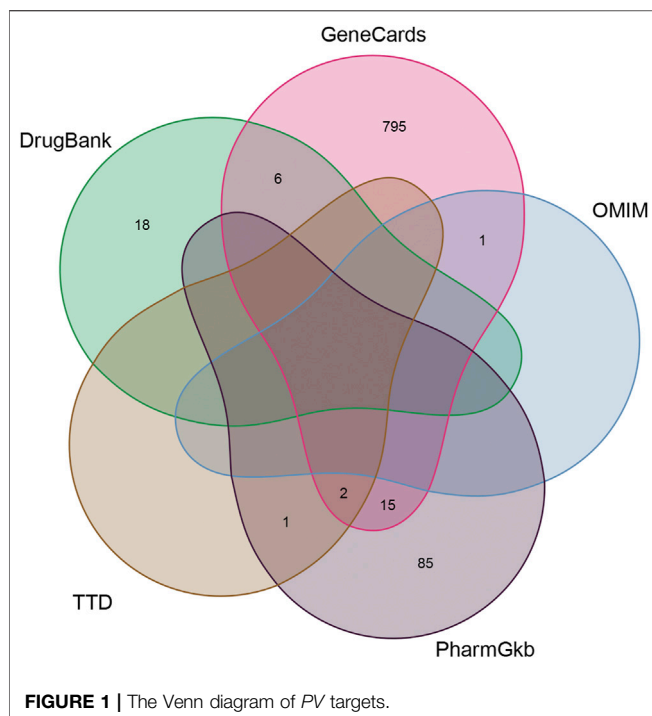
The GeneCards database (<https://www.genecards.org/>) and selection according to the criterion of RiskScore >1, the Therapeutic Target Database (TTD, <https://db.idrblab.org/ttd/>), OMIM (<https://omim.org/>), PharmGkb (<https://www.pharmgkb.org/>), and DrugBank (<https://www.drugbank.ca/>) were used to collect information on HT related to target genes. The association of PV with HT was then gathered as the core targets of PV for HT.

Construction of the Component-Target Gene Network

In this research, the network of component-target interactions was established, and the interaction between active compounds and their core target proteins was ascertained by Cytoscape 3.7.2 (<http://www.cytoscape.org/>) (Wang et al., 2011). Moreover, it was visualized by Cytoscape software, an open-source platform for visualizing complex networks (Shannon and et al., 2003). In the network, nodes represent the herbal medicines, active phytochemical compounds, targets, or signaling pathways, while edges represent the interactions between the nodes (Barabási and Oltvai, 2004). The top two compounds were chosen as the ligand for molecular docking. The degree of a node represents the number of connections (edges) that this node has with the rest of the network (Tang et al., 2020). The larger the quantitative value, the more important the node in the network, and the more likely the component is the PV of the key ingredient.

Construction of the Protein-Protein Interaction (PPI) Network

The candidate targets of PV for HT treatment were imported into the STRING database (<https://string-db.org/>) (Consortium UP,



2010) to construct a PPI network. The network analysis plug-in in Cytoscape software was used to analyze network topological features to screen the hub nodes in the PPI network (Saito et al., 2012). Degree centrality denotes several direct connections of a node to all other nodes in the network. The value of degree was used as a reference for the importance of the core target by the CytoNCA, a plug-in of Cytoscape for network centrality analysis.

GO Functional Enrichment and KEGG Pathway Analysis

Gene Ontology (GO) functional annotation and Kyoto Encyclopedia of Genes and Genomes (KEGG) pathway enrichment were performed in R using the ClusterProfiler package, and p . adjust (FDR) < 0.05 was considered statistically significant (Yu et al., 2012).

Target Screening by Molecular Docking

The three-dimensional (3D) molecular structures of hsp90aa1.1 (*AKI*) (PDB ID: P31749) (Wu et al., 2010) and mitogen-activated protein kinase 1 (*MAPK1*) (PDB ID: P28482) (Ward et al., 2017) were downloaded from the RCSB Protein Data Bank (<http://www.rcsb.org/pdb>). The protein structure was processed by AutoDock Tools (Morris et al., 2009) to remove water molecules and connect hydrogen atoms, and then Gasteiger charges were added to the ligands and the protein templates and saved as a PDBQT file. Two-dimensional (2D) structures of luteolin and kaempferol were downloaded from PubChem (available online: <https://pubchem.ncbi.nlm.nih.gov/>) as .sdf. Luteolin and kaempferol were vital active compounds, and *AKI* and *MAPK1* were considered the major targets. Molecular

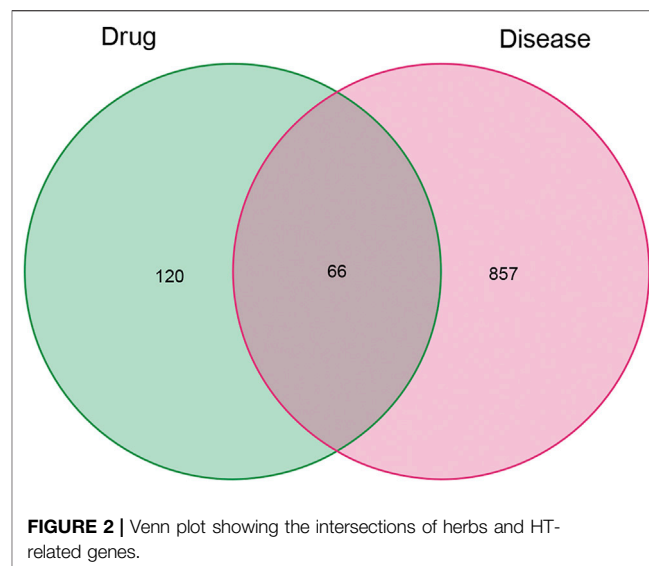


TABLE 1 | Basic information of some active components of *Prunella vulgaris*.

Mol ID	Chemical component	OB (%)	DL
MOL000006	Luteolin	36.16	0.25
MOL000098	Quercetin	46.43	0.28
MOL000358	Beta-sitosterol	36.91	0.75
MOL000422	Kaempferol	41.88	0.24
MOL000449	Stigmasterol	43.83	0.76
MOL000737	Morin	46.23	0.27
MOL004355	Spinasterol	42.98	0.76
MOL004798	Delphinidin	40.63	0.28
MOL006767	Vulgaxanthin-I	56.14	0.26
MOL006772	Poriferasterol monoglucoside_qt	43.83	0.76
MOL006774	Stigmast-7-enol	37.42	0.75

docking of the ligands luteolin and kaempferol to the *AKI* and *MAPK1* protein active sites was carried out using AutoDock Vina 1.1.2. Each docking calculation generated 20 structures, and the molecular docking output was prioritized based on the frequency of the possible ligand-binding site and a free energy score. Finally, the best possible conformations and visualized using Discovery Studio Visualizer 2.5 and PyMOL software (PyMol Molecular Graphics System, Version 1).

RESULTS

Active Compounds of *PV*

Of these, 923 were targets of the herbs comprising *PV*, and the Venn diagram of *PV* targets is shown in **Figure 1**. A Venn plot showing the intersections of herbs and HT-related genes is shown in **Figure 2**. The main active components of *PV* containing 11 compounds are shown in **Table 1**, and the structures are shown in **Table 2**. Key targets containing Jun proto-oncogene (*JUN*), *AKI*, *MAPK1*, and tumor protein p53 (*TP53*) are shown in **Table 3** and **Figure 3C**. Moreover, the scores of four centralities were calculated by CytoNCA, and details are provided in **Table 4**.

TABLE 2 | Information for candidate targets from compounds of *Prunella vulgaris*.

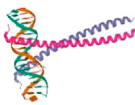
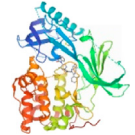

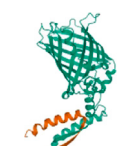
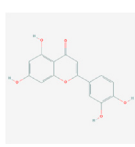
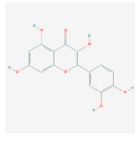
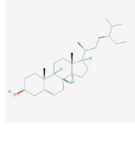
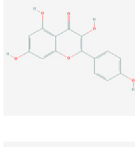
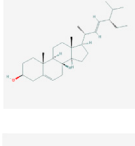
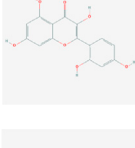
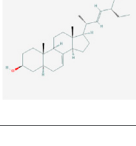
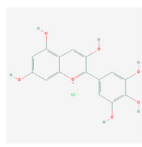
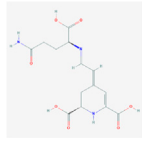
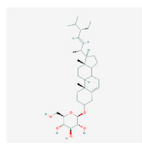
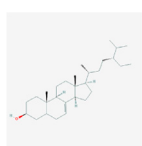
Molecule name	Structure
Luteolin	
Quercetin	
Beta-sitosterol	
Kaempferol	
Stigmasterol	
Morin	
Spinasterol	
Delphinidin	
Vulgaxanthin-I	
Poriferasterol monoglucoside_qt	
Stigmast-7-enol	

TABLE 3 | Information for targets gene from compounds of *Prunella vulgaris*.

Gene name	Code	Structure
JUN	P05412	
AKI	P31749	
MAPK1	P28482	
TP53	P04637	

The Construction of Herb-Compound-Target Network

The herb-compound-target network contained 77 nodes (11 compounds and 66 genes), as shown in **Figure 3**. The node size represents the importance of a node, and the bigger size indicates more importance. According to the degree of the compound, we finally chose the eleven more important compounds, including MOL000006 (luteolin), MOL000098 (quercetin), MOL000358 (beta-sitosterol), MOL000422 (kaempferol), MOL000449 (stigmasterol), MOL000737 (morin), MOL004355 (spinasterol), MOL004798 (delphinidin), MOL006767 (vulgaxanthin-I), MOL006772 (poriferasterol monoglucoside_qt), and MOL006774 (stigmast-7-enol), and the details are shown in **Table 1** and **Table 2**.

Prediction Results of Disease Targets and the Construction of the PPI Network

A total of 66 disease-related targets, 11 *PV*-related targets, and 17 intersection targets were identified (**Figures 3A,4**). Our study showed that targets had strong relationships in the PPI network. There were 17 nodes in the PeLBD protein interaction network, which were the core targets of *PV* in the treatment of HT (**Table 4**). *JUN*, *AKI*, *MAPK1*, and *TP53* (Aziz et al., 2018) were considered hub genes (**Figure 3B**).

GO and KEGG Enrichment Analyses

To better understand the function of intersecting genes, we conducted an enrichment analysis of Gene Ontology (GO). The top 10 biological processes mainly an inflammatory response, a cell-to-cell reaction, and a metabolic process are ranked in **Figures 5A, C**. In the enrichment analysis of GO

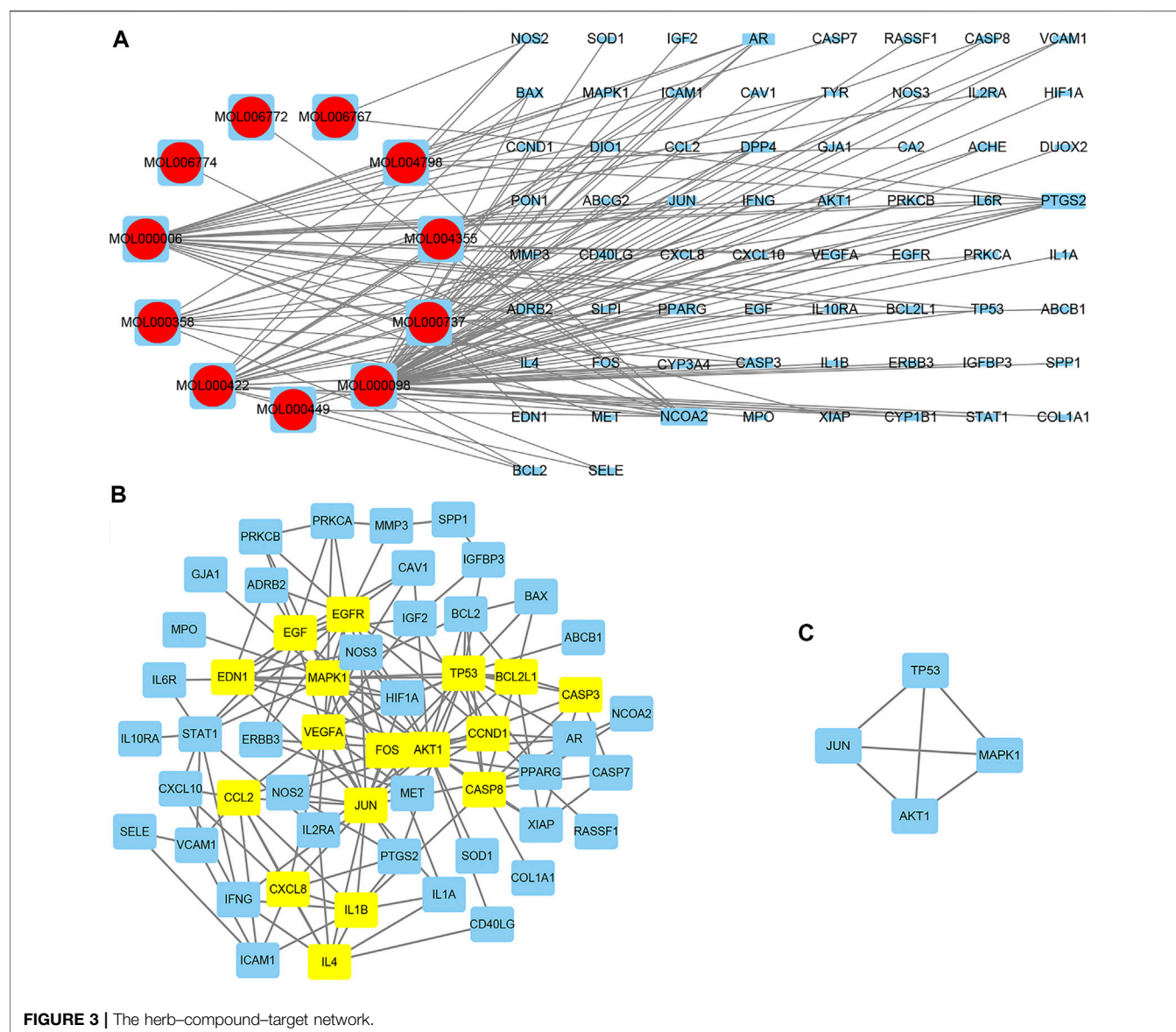


FIGURE 3 | The herb-compound-target network.

pathways, cellular components mainly contained membrane rafts, membrane microdomains, and membrane regions. Meanwhile, the GO terms enriched for a molecular function were mainly cytokine receptor binding, cytokine activity, and receptor-ligand activity. Furthermore, the KEGG pathway enrichment analysis was also conducted. A total of 30 top-ranking pathways (Figures 5B, D) were identified ($p < 0.05$). The relative enrichment analysis showed the following pathways: the AGE-RAGE signaling pathway in diabetic complications, the TNF signaling pathway, the PI3K-Akt signaling pathway, pathways in cancer, the MAPK signaling pathway, and the cancer-associated pathways, as shown in Figures 5B and Figure 6.

Results of Molecular Docking

The molecular docking assay showed that the AKI and MAPK1 proteins have a stronger affinity for HT disease molecules.

Luteolin (MOL000006) was considered as the uppermost active ingredient of PV against HT. Meanwhile, there was also a strong association between kaempferol (MOL000422) and AKI with MAPK1. The AKI and MAPK1 protein active pockets showed that the small molecules luteolin and kaempferol have a compact binding pattern (Figure 7).

DISCUSSION

The precise pathogenesis of HT remains unclear. HT is the most prevalent autoimmune thyroid disorder; currently, there is no effective means of preventing and treating HT. Hashimoto's thyroiditis (HT) is usually manageable by levothyroxine (L-T4) administration, reducing the thyroid volume and supplementing the lack of hormones. Despite thyroid hormone replacement, some euthyroid patients with HT will continue to experience

TABLE 4 | The topological parameters of hub targets.

Target	Degree	Betweenness	Closeness
JUN	11	51.61	0.76
TP53	10	28.12	0.73
AKT1	9	24.83	0.70
MAPK1	8	13.84	0.67
EGFR	7	9.07	0.59
VEGFA	7	19.16	0.64
FOS	6	6.04	0.62
CCL2	6	6.44	0.57
CXCL8	5	2.54	0.55
BCL2L1	5	1.25	0.53
CASP8	5	9.35	0.57
IL-1B	5	9.15	0.55
CCND1	5	1.57	0.59
EDN1	5	3.45	0.59
EGF	4	0.83	0.52
IL-4	4	0.00	0.50
CASP3	4	0.75	0.52

persistent symptoms that reduce their quality of life. *PV* has been empirically used to treat thyroid disorders, including HT in TCMSP, which has been applied for thousands of years. Some of its basic mechanism remains unknown. Recent studies have shown that *PV* plays an essential role in reducing the titers of

TPO-Ab, TG-Ab, and Th17 cells in autoimmune and inflammatory disorders, including HT (Wang et al., 2019; hui ZRGwsbydw, 2000; Yang et al., 2007; Zhang, 2014; Hu et al., 2019; Ala et al., 2015; Wiersinga and Wilmar, 2001). In addition, several recent studies have demonstrated that the anti-inflammatory effect of PV is related to NF- κ B in stimulated macrophages (Wu et al., 2010; Yu et al., 2012). This study demonstrates that PV has a potential therapeutic effect on HT and could explore novel anti-inflammatory therapies for its treatment.

Studies have suggested that the innate immune response in thyrocytes facilitates auto-sensitization, which may eventually lead to thyroid autoimmunity (Akira et al., 2011; Kawashima et al., 2013). In the study, eleven main active components were screened of *PV*: luteolin, quercetin, beta-sitosterol, kaempferol, stigmaterol, morin, spinasterol, delphinidin, vulgaxanthin-I, poriferasterol monoglucoside_qt, and stigmast-7-enol. Molecular docking showed that the active ingredients, including luteolin and kaempferol, had a good affinity for the hub disease proteins in clinical therapeutics (Xia et al., 2016; Habza-Kowalska et al., 2019). The results demonstrated that luteolin has a strong affinity for disease proteins of HT, and quercetin had a strong affinity for serum thyroid peroxidase (TPO). These results indicated that luteolin and kaempferol might play some important roles in the

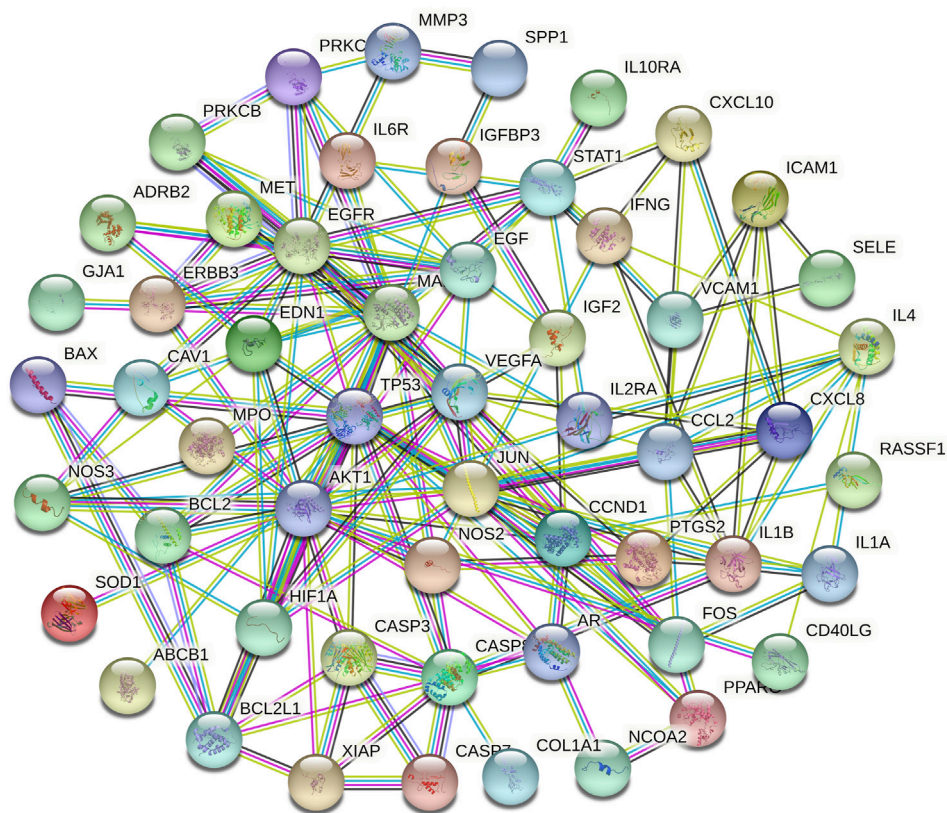


FIGURE 4 | The PPI networks of relative targets.

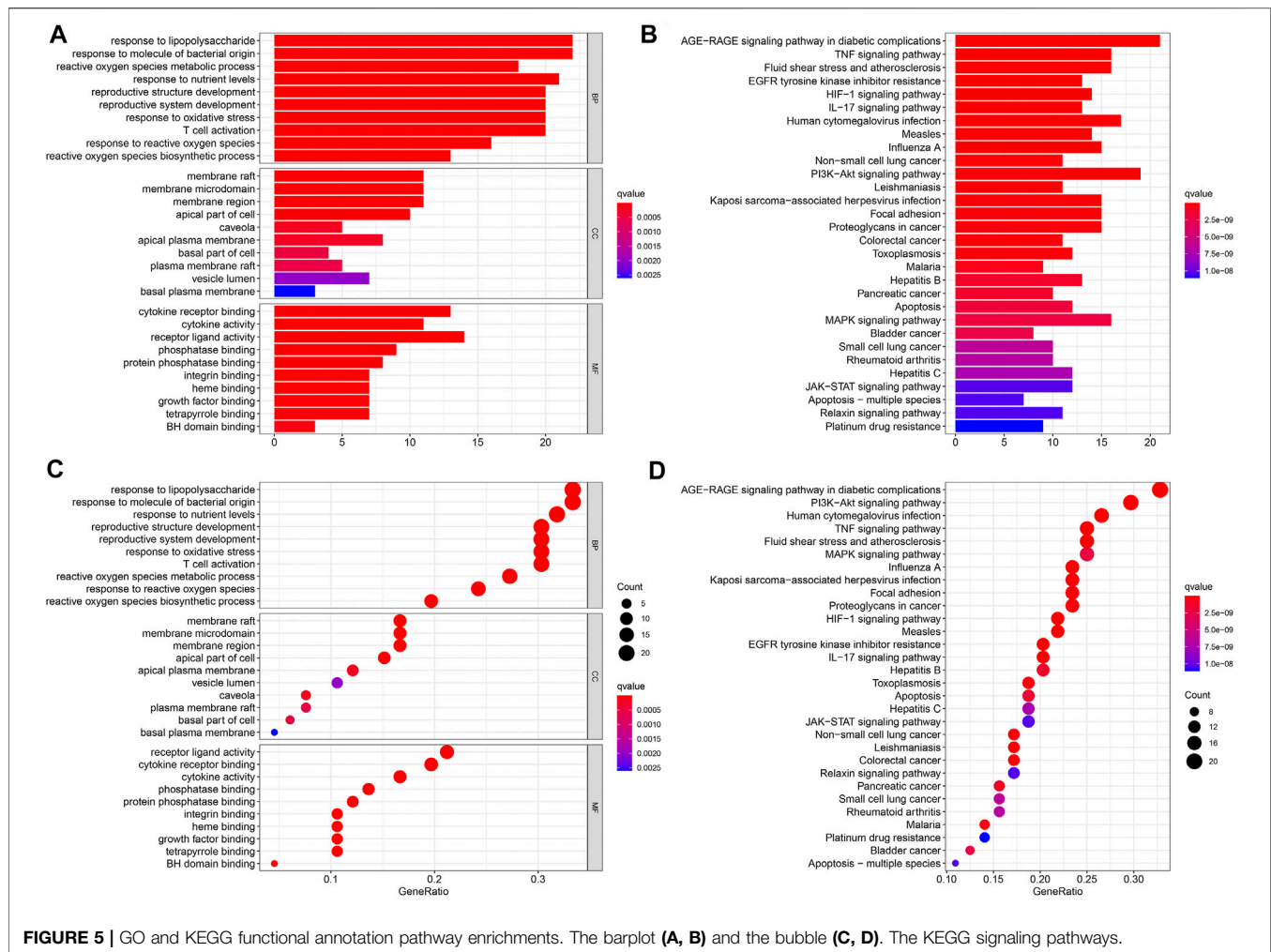


FIGURE 5 | GO and KEGG functional annotation pathway enrichments. The barplot (A, B) and the bubble (C, D). The KEGG signaling pathways.

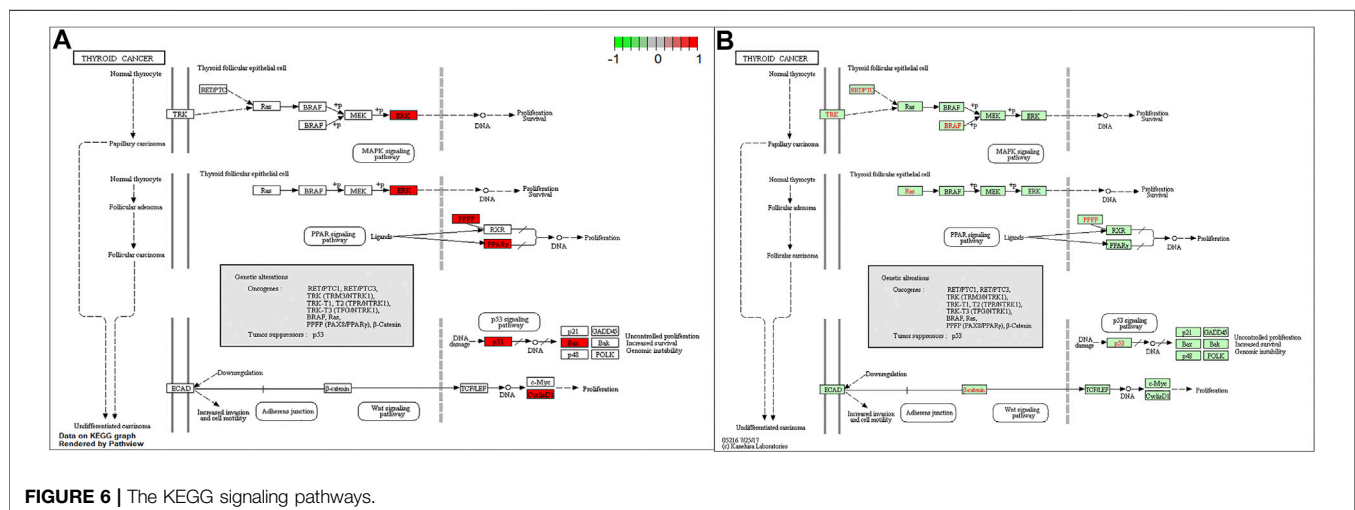


FIGURE 6 | The KEGG signaling pathways.

treatment of HT. Flavonoids are a large group of plant-derived compounds, and it is well established that certain flavonoids exhibit anti-inflammatory properties (Lee et al., 2017). Luteolin is one of

the most common flavones with antioxidant, anticancer, anti-inflammatory, and antiapoptotic properties in TCMSP (De Stefano et al., 2021). A previous study also suggests that

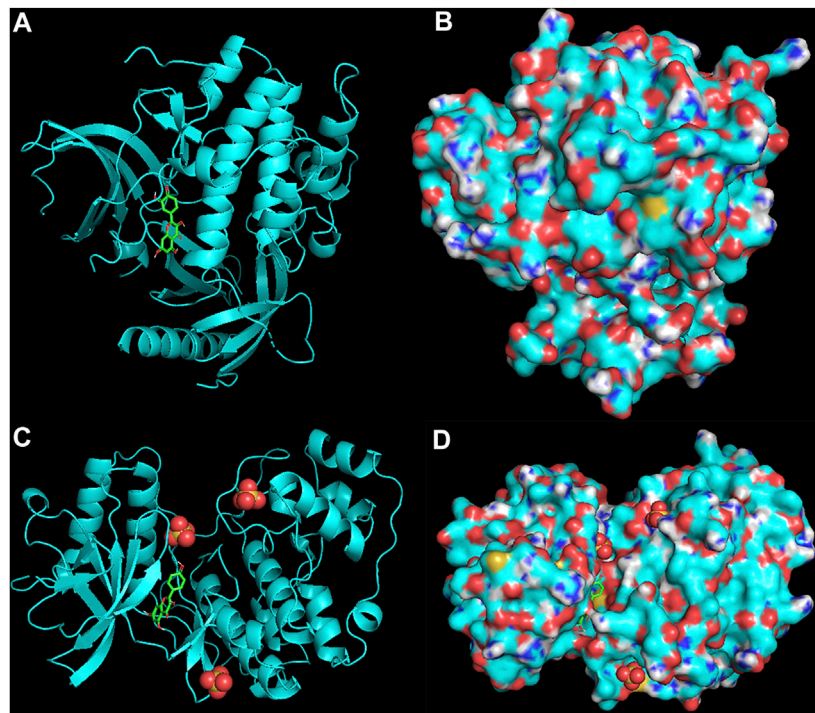


FIGURE 7 | AKI protein: luteolin (A,B) and MAPK1 protein: kaempferol (C,D).

kaempferol is a potential bioaccessible TPO activator based on effective LOX inhibitors, further indicating potentially health-promoting effects for HT (Habza-Kowalska et al., 2019). Some studies have also shown that luteolin's mechanisms showed potent anti-inflammatory activity, including the activation of NF- κ B, which leads to the expression of IL-6 and COX-2 (Xagorari et al., 2001; Ching-Chow et al., 2004). Additionally, kaempferol, a polyphenol, is a bioactive substance with antioxidative, antimutagenic, antibacterial, and antiviral activities.

The KEGG enrichment analysis revealed that the chief pathways were concentrated in the AGE-RAGE signaling pathway in the pathogenesis of diabetes and its complications, the TNF signaling pathway, the PI3K–Akt signaling pathway, pathways in cancer, the mitogen-activated protein kinase (MAPK) signaling pathway, and some related to thyroid cancer. The present study identified JUN, AKI, MAPK1, and TP53 hub genes using the PPI network analysis. These results indicated that PV affected HT through the following pathways. Furthermore, a GO functional analysis also demonstrated many biological processes, including the inflammatory response, the cell-to-cell reaction, and the metabolic process in the present study. The TNF signaling pathway plays an essential functional role in regulating the inflammatory response (Noack and Miossec, 2017). Luteolin acts as an anti-inflammatory agent by regulating the TNF signaling pathway (Zhang et al., 2018; Zhang et al., 2019). A previous study demonstrated that the MAPK signaling pathway was revealed to be correlated with the progression of HT (Luo et al., 2018). Several studies have exhibited significant anti-inflammatory activity effects by inhibiting the MAPK signaling pathways (Chen et al., 2016; Wei et al., 2016).

Luteolin is a common flavonoid that exhibits intense anti-inflammatory activity through the MAPK signaling pathway (Aziz et al., 2018). The key target gene of *MAPK1* was involved in the MAPK signaling pathway.

Meanwhile, the MAPK signaling pathway plays an important role in developing thyroid carcinoma, including cell proliferation and cell survival. The PI3K/AKT signaling pathway plays a key role in regulating the activation of inflammatory response cells and releasing inflammatory transmitters to the chronic inflammatory response in HT (Li et al., 2018). By regulating the PI3K–AKT signaling pathway, luteolin might be the critical pathway against inflammation, thus realizing the treatment of HT (Huang et al., 2020). Kaempferol-activated PI3K/AKT signaling exerts anti-inflammatory effects (Imran et al., 2019; Harikrishnan et al., 2020; Jantan et al., 2021).

The present study included some limitations. First, some further verified experiments need to be conducted. Second, their specific molecular docking methods and locations need to be verified by further experiments. A comprehensive understanding of the key gene target of PV and HT is key towards therapeutic discovery and development.

CONCLUSION

In summary, the network pharmacology and molecular docking show that luteolin and kaempferol were the main active components of PV, which indicated that they might play an essential role in treating HT. PV may act against HT mainly through the TNF signaling pathway, the MAPK signaling pathway, and the PI3K–Akt signaling pathway.

DATA AVAILABILITY STATEMENT

The raw data supporting the conclusions of this article will be made available by the authors, without undue reservation.

AUTHOR CONTRIBUTIONS

Conception: X-xG and BX. Design and revision of the manuscript: X-xG, L-kZ, and FS. Analysis and interpretation of data: X-xG, L-kZ, FS, J-h, W-sC, Y-yL, and S-jL.

REFERENCES

- Akira, K., Kazunari, T., Takeshi, A., Wu, H., Mariko, S., Aya, Y., et al. (2011). Fragments of Genomic DNA Released by Injured Cells Activate Innate Immunity and Suppress Endocrine Function in the Thyroid. *Endocrinology* 152 (4), 1702–1712. doi:10.1210/en.2010-1132
- Ala, S., Akha, O., Kashi, Z., Asgari, H., Bahar, A., and Sasanpour, N. (2015). Dose Administration Time from before Breakfast to before Dinner Affect Thyroid Hormone Levels? *Caspian J. Intern. Med.* 6, 134–140.
- Aziz, N., Kim, M. Y., and Cho, J. Y. (2018). Anti-inflammatory Effects of Luteolin: A Review of *In Vitro*, *In Vivo*, and *In Silico* Studies. *J. Ethnopharmacol.* 225, 342–358. doi:10.1016/j.jep.2018.05.019
- Barabási, A., and Oltvai, Z. N. (2004). Network Biology: Understanding the Cell's Functional Organization. *Nat. Rev. Genet.* 5 (2), 101–113. doi:10.1038/nrg1272
- Cao, H., Li, S., Xie, R., Xu, N., Qian, Y., Chen, H., et al. (2018). Exploring the Mechanism of Dangguiliuhuang Decoction against Hepatic Fibrosis by Network Pharmacology and Experimental Validation. *Front. Pharmacol.* 9, 187. doi:10.3389/fphar.2018.00187
- Caturegli, P., De Remigis, A., Chuang, K., Dembele, M., Iwama, A., Iwama, S., and Hashimoto's, H. (2013). Hashimoto's Thyroiditis: Celebrating the Centennial through the Lens of the Johns Hopkins Hospital Surgical Pathology Records. *Thyroid* 23, 142–150. doi:10.1089/thy.2012.0554
- Chao, G., Zhu, Y., and Fang, L. (2020). Correlation between Hashimoto's Thyroiditis-Related Thyroid Hormone Levels and 25-Hydroxyvitamin D. *Front. Endocrinol.* 11, 4. doi:10.3389/fendo.2020.00004
- Chen, C. C., Lin, M. W., Liang, C. J., and Wang, S. H. (2016). The Anti-inflammatory Effects and Mechanisms of Eupafolin in Lipopolysaccharide-Induced Inflammatory Responses in RAW264.7 Macrophages. *Plos One* 11, e0158662. doi:10.1371/journal.pone.0158662
- Chen, F., Kawashima, A., Luo, Y., Kiriya, M., and Suzuki, K. (2020). Innate Immune-Modulatory Activity of Prunella Vulgaris in Thyrocytes Functions as a Potential Mechanism for Treating Hashimoto's Thyroiditis. *Front. Endocrinol.* 11, 579648. doi:10.3389/fendo.2020.579648
- Ching-Chow, C., Man-Ping, C., Wei-Chien, H., Yi-Chu, L., and Ya-Jen, C. (2004). Flavonoids Inhibit Tumor Necrosis Factor- α -Induced Up-Regulation of Intercellular Adhesion Molecule-1 (ICAM-1) in Respiratory Epithelial Cells through Activator Protein-1 and Nuclear Factor-Kb: Structure-Activity Relationships. *Mol. Pharmacol.* 66 (3), 683–693. doi:10.1124/mol.66.3
- Consortium UP (2010). The Universal Protein Resource (UniProt) in 2010. *Nucleic Acids Res.* 38, D142–D148. doi:10.1093/nar/gkp846
- De Stefano, A., Caporali, S., Di Daniele, N., Rovella, V., Cardillo, C., Schinzari, F., et al. (2021). Anti-Inflammatory and Proliferative Properties of Luteolin-7-O-Glucoside. *Int. J. Mol. Sci.* 22, 1321. doi:10.3390/ijms22031321
- Gan, X., Feng, J., Deng, X., Shen, F., Lu, J., Liu, Q., et al. (2021). The Significance of Hashimoto's Thyroiditis for Postoperative Complications of Thyroid Surgery: a Systematic Review and Meta-Analysis. *Ann. R. Coll. Surg. Engl.* 103, 223–230. doi:10.1308/rcsann.2020.7013
- Habza-Kowalska, E., Gawlik-Dziki, U., and Dziki, D. (2019). Mechanism of Action and Interactions between Thyroid Peroxidase and Lipoygenase Inhibitors Derived from Plant Sources. *Biomolecules* 9, 663. doi:10.3390/biom9110663
- Harikrishnan, H., Jantan, I., Alagan, A., and Haque, M. A. (2020). Modulation of Cell Signaling Pathways by Phyllanthus Amarus and its Major Constituents: Potential Role in the Prevention and Treatment of Inflammation and Cancer. *Inflammopharmacology* 28, 1–18. doi:10.1007/s10787-019-00671-9
- Hu, Y., Zhang, L., Chen, H., Liu, X., Zheng, X., Shi, H., et al. (2019). Analysis of Regulatory T Cell Subsets and Their Expression of Helios and PD-1 in Patients with Hashimoto Thyroiditis. *Int. J. Endocrinol.* 2019, 5368473. doi:10.1155/2019/5368473
- Huang, X. F., Zhang, J. L., Huang, D. P., Huang, A. S., Huang, H. T., Liu, Q., et al. (2020). A Network Pharmacology Strategy to Investigate the Anti-inflammatory Mechanism of Luteolin Combined with *In Vitro* Transcriptomics and Proteomics. *Int. Immunopharmacol.* 86, 106727. doi:10.1016/j.intimp.2020.106727
- hui ZRGwsbydw (2000). *Pharmacopoeia of the People's Republic of China*. Beijing, China: Chemical Industry Press.
- Imran, M., Rauf, A., Shah, Z. A., Saeed, F., Imran, A., Arshad, M. U., et al. (2019). Chemo-preventive and Therapeutic Effect of the Dietary Flavonoid Kaempferol: A Comprehensive Review. *Phytother. Res.* 33, 263–275. doi:10.1002/ptr.6227
- Jantan, I., Haque, M. A., Arshad, L., Harikrishnan, H., Septama, A. W., and Mohamed-Hussein, Z. A. (2021). Dietary Polyphenols Suppress Chronic Inflammation by Modulation of Multiple Inflammation-Associated Cell Signaling Pathways. *J. Nutr. Biochem.* 93, 108634. doi:10.1016/j.jnutbio.2021.108634
- Kawashima, A., Yamazaki, K., Hara, T., Akama, T., Yoshihara, A., Sue, M., et al. (2013). Demonstration of Innate Immune Responses in the Thyroid Gland: Potential to Sense Danger and a Possible Trigger for Autoimmune Reactions. *Thyroid* 23, 477–487. doi:10.1089/thy.2011.0480
- Lee, S. B., Kang, J. W., Kim, S. J., Ahn, J., Kim, J., and Lee, S. M. (2017). Afzelin Ameliorates D-Galactosamine and Lipopolysaccharide-Induced Fulminant Hepatic Failure by Modulating Mitochondrial Quality Control and Dynamics. *Br. J. Pharmacol.* 174, 195–209. doi:10.1111/bph.13669
- Li, H., Min, J., Mao, X., Wang, X., Yang, Y., and Chen, Y. (2018). Edaravone Ameliorates Experimental Autoimmune Thyroiditis in Rats through HO-1-dependent STAT3/PI3K/Akt Pathway. *Am. J. Transl. Res.* 10, 2037–2046.
- Liontiris, M. I., and Mazokopakis, E. E. (2017). A Concise Review of Hashimoto Thyroiditis (HT) and the Importance of Iodine, Selenium, Vitamin D and Gluten on the Autoimmunity and Dietary Management of HT patients. Points that Need More Investigation. *Hell J. Nucl. Med.* 20, 51–56. doi:10.1967/s002449910507
- Luo, X., Zheng, T., Mao, C., Dong, X., Mou, X., Xu, C., et al. (2018). Aberrant MRP14 Expression in Thyroid Follicular Cells Mediates Chemokine Secretion through the IL-1 β /MAPK Pathway in Hashimoto's Thyroiditis. *Endocr. Connect.* 7, 850–858. doi:10.1530/EC-18-0019
- Morris, G. M., Huey, R., Lindstrom, W., Sanner, M. F., Belew, R. K., Goodsell, D. S., et al. (2009). AutoDock4 and AutoDockTools4: Automated Docking with Selective Receptor Flexibility. *J. Comput. Chem.* 30 (16), 2785–2791. doi:10.1002/jcc.21256
- Ning, K., Zhao, X., Ansgar, P., Chen, W. H., and Yang, J. (2017). Computational Molecular Networks and Network Pharmacology. *Biomed. Res. Int.* 2017, 7573904. doi:10.1155/2017/7573904
- Noack, M., and Miossec, P. (2017). Selected Cytokine Pathways in Rheumatoid Arthritis. *Semin. Immunopathol.* 39, 365–383. doi:10.1007/s00281-017-0619-z

FUNDING

This research was supported by Guangzhou Medicine and Health Care Technology Projects (20211A011010).

ACKNOWLEDGMENTS

Special thanks are due to Keqin Liu for support and encouragement.

- Roehlen, N., Doering, C., Hansmann, M. L., Gruenwald, F., Vorlaender, C., Bechstein, W. O., et al. (2018). Vitamin D, FOXO3a, and Sirtuin1 in Hashimoto's Thyroiditis and Differentiated Thyroid Cancer. *Front. Endocrinol. (Lausanne)* 9, 527. doi:10.3389/fendo.2018.00527
- Ru, J., Li, P., Wang, J., Zhou, W., Li, B., Huang, C., et al. (2014). TCMSP: a Database of Systems Pharmacology for Drug Discovery from Herbal Medicines. *J. Cheminform* 6, 13. doi:10.1186/1758-2946-6-13
- Saito, R., Smoot, M. E., Ono, K., Ruscheinski, J., Wang, P. L., Lotia, S., et al. (2012). A Travel Guide to Cytoscape Plugins. *Nat. Methods* 9, 1069–1076. doi:10.1038/nmeth.2212
- Shannon, P., Markiel, A., Ozier, O., Baliga, N. S., Wang, J. T., Ramage, D., et al. (2003). Cytoscape: A Software Environment for Integrated Models of Biomolecular Interaction Networks. *Genome Res.* 13: 2498–2504. doi:10.1101/gr.1239303
- Su, X., Kong, L., Lei, X., Hu, L., Ye, M., and Zou, H. (2007). Biological Fingerprinting Analysis of Traditional Chinese Medicines with Targeting ADME/Tox Property for Screening of Bioactive Compounds by Chromatographic and MS Methods. *Mini Rev. Med. Chem.* 7, 87–98. doi:10.2174/138955707779317830
- Tan, X., Zhang, X., Pan, L., Tian, X., and Dong, P. (2017). Identification of Key Pathways and Genes in Advanced Coronary Atherosclerosis Using Bioinformatics Analysis. *Biomed. Res. Int.* 2017, 1–12. doi:10.1155/2017/4323496
- Tang, S., Jing, H., Huang, Z., Huang, T., Lin, S., Liao, M., et al. (2020). Identification of Key Candidate Genes in Neuropathic Pain by Integrated Bioinformatic Analysis. *J. Cell Biochem.* 121 (2), 1635–1648. doi:10.1002/jcb.29398
- Wang, C., Jiang, W., Li, W., Lian, B., Chen, X., Hua, L., et al. (2011). Topological Properties of the Drug Targets Regulated by microRNA in Human Protein-Protein Interaction Network. *J. Drug Target.* 19, 354–364. doi:10.3109/1061186X.2010.504261
- Wang, S. J., Wang, X. H., Dai, Y. Y., Ma, M. H., and Zhang, H. (2019). Prunella Vulgaris: A Comprehensive Review of Chemical Constituents, Pharmacological Effects and Clinical Applications. *Curr. Pharm. Des.* 25 (3), 359–369. doi:10.2174/1381612825666190313121608
- Ward, R. A., Bethel, P., Cook, C., Davies, E., Debreczeni, J. E., Fairley, G., et al. (2017). Structure-Guided Discovery of Potent and Selective Inhibitors of ERK1/2 from a Modestly Active and Promiscuous Chemical Start Point. *J. Med. Chem.* 60, 3438–3450. doi:10.1021/acs.jmedchem.7b00267
- Wei, L., Jiang, H. L., Cai, L. L., Min, Y., Dong, S. J., and Bing, M. (2016). Tanreqing Injection Attenuates Lipopolysaccharide-Induced Airway Inflammation through MAPK/NF- κ B Signaling Pathways in Rats Model. *Evidence-Based Complementray Altern. Med.* 2016, 5292346. doi:10.1155/2016/5292346
- Wiersinga, W. M., and Wilmar, M. (2001). Thyroid Hormone Replacement Therapy. *Horm. Res.* 56 Suppl 1, 74–81. doi:10.1159/000048140
- Wu, W. I., Voegtli, W. C., Sturgis, H. L., Dizon, F. P., Vigers, G. P., and Brandhuber, B. J. (2010). Crystal Structure of Human AKT1 with an Allosteric Inhibitor Reveals a New Mode of Kinase Inhibition. *PloS one* 5, e12913. doi:10.1371/journal.pone.0012913
- Xagorari, A., Papapetropoulos, A., Mauromatis, A., Economou, M., Fotsis, T., and Roussos, C. (2001). Luteolin Inhibits an Endotoxin-Stimulated Phosphorylation cascade and Proinflammatory Cytokine Production in Macrophages. *J. Pharmacol. Exp. Ther.* 296, 181–187.
- Xia, N., Chen, G., Liu, M., Ye, X., Pan, Y., Ge, J., et al. (2016). Anti-inflammatory Effects of Luteolin on Experimental Autoimmune Thyroiditis in Mice. *Exp. Ther. Med.* 12 (6), 4049–4054. doi:10.3892/etm.2016.3854
- Yang, K., Guo, K. Q., and Wu, H. Y. (2007). Clinical Effect of Prunellae Oral Liquid on Goiter with Different Thyroid Function. *Zhongguo Zhong Xi Yi Jie He Za Zhi* 27, 37–39.
- Yu, G., Wang, L. G., Han, Y., and He, Q. Y. (2012). clusterProfiler: an R Package for Comparing Biological Themes Among Gene Clusters. *OMICS* 16, 284–287. doi:10.1089/omi.2011.0118
- Zhang, B. C., Li, Z., Xu, W., Xiang, C. H., and Ma, Y. F. (2018). Luteolin Alleviates NLRP3 Inflammasome Activation and Directs Macrophage Polarization in Lipopolysaccharide-Stimulated RAW264.7 Cells. *Am. J. Transl. Res.* 10, 265–273.
- Zhang, L., Wang, X., Zhang, L., Virgous, C., and Si, H. (2019). Combination of Curcumin and Luteolin Synergistically Inhibits TNF- α -Induced Vascular Inflammation in Human Vascular Cells and Mice. *J. Nutr. Biochem.* 73, 108222. doi:10.1016/j.jnutbio.2019.108222
- Zhang, M., Yuan, Y., Zhou, W., Qin, Y., Xu, K., Men, J., et al. (2020). Network Pharmacology Analysis of Chaihu Lizhong Tang Treating Non-alcoholic Fatty Liver Disease. *Comput. Biol. Chem.* 86, 107248. doi:10.1016/j.compbiolchem.2020.107248
- Zhang, X. Z. (2014). Clinical Observation of Prunella Vulgaris Oral Solution Combined with Indomethacin in the Treatment of Elderly Subacute Thyroiditis. *China Pharm. Endocrinology DO.*

Conflict of Interest: The authors declare that the research was conducted in the absence of any commercial or financial relationships that could be construed as a potential conflict of interest.

Publisher's Note: All claims expressed in this article are solely those of the authors and do not necessarily represent those of their affiliated organizations, or those of the publisher, the editors, and the reviewers. Any product that may be evaluated in this article, or claim that may be made by its manufacturer, is not guaranteed or endorsed by the publisher.

Copyright © 2021 Gan, Zhong, Shen, Feng, Li, Li, Cai and Xu. This is an open-access article distributed under the terms of the Creative Commons Attribution License (CC BY). The use, distribution or reproduction in other forums is permitted, provided the original author(s) and the copyright owner(s) are credited and that the original publication in this journal is cited, in accordance with accepted academic practice. No use, distribution or reproduction is permitted which does not comply with these terms.



Prevention of Cyclophosphamide-Induced Immunosuppression in Mice With Traditional Chinese Medicine Xuanfei Baidu Decoction

Huimin Yan^{1,2}, Jia Lu^{2,3}, Jiabao Wang^{1,2,3}, Lu Chen^{1,2,3}, Yu Wang^{1,2,3}, Lin Li^{1,2,3}, Lin Miao^{1,2,3*} and Han Zhang^{1,2,3*}

¹State Key Laboratory of Component-based Chinese Medicine, Tianjin University of Traditional Chinese Medicine, Tianjin, China, ²Institute of Traditional Chinese Medicine, Tianjin University of Traditional Chinese Medicine, Tianjin, China, ³Key Laboratory of Pharmacology of Traditional Chinese Medical Formulae, Ministry of Education, Tianjin University of Traditional Chinese Medicine, Tianjin, China

OPEN ACCESS

Edited by:

Xiaohong Tian,
McGill University, Canada

Reviewed by:

Chao-Zhan Lin,
Guangzhou University of Chinese
Medicine, China
Md. Moklesur Rahman Sarker,
State University of Bangladesh,
Bangladesh

*Correspondence:

Lin Miao
mmmlin@tjucm.edu.cn
Han Zhang
zhanghan0023@126.com

Specialty section:

This article was submitted to
Ethnopharmacology,
a section of the journal
Frontiers in Pharmacology

Received: 25 June 2021

Accepted: 13 September 2021

Published: 19 October 2021

Citation:

Yan H, Lu J, Wang J, Chen L, Wang Y,
Li L, Miao L and Zhang H (2021)
Prevention of Cyclophosphamide-
Induced Immunosuppression in Mice
With Traditional Chinese Medicine
Xuanfei Baidu Decoction.
Front. Pharmacol. 12:730567.
doi: 10.3389/fphar.2021.730567

Background and aims: Xuanfei Baidu decoction (XFBD), a traditional Chinese medicine formulation, was designed and successfully applied for COVID-19 disease treatment in China, while the mechanism is still not clear.

Methods: To evaluate the protective effect of XFBD on immunosuppression in cyclophosphamide (CY)-treated mice, XFBD was orally administrated, the body weight was measured, and the immune organ index was calculated. HE staining was performed to analyze the pathological structures of the liver, spleen, and thymus. The levels of cytokines and immunoglobulin in the serum and spleen were evaluated by ELISA and RT-PCR. Splenic lymphocytes were isolated, and LPS-stimulated cell proliferation and the number of CD4⁺ and CD8⁺ T lymphocytes were evaluated.

Results: XFBD significantly suppressed body weight loss and increased the indices of spleen and thymus. The pathological alteration was much improved after XFBD administration. The reductions of TNF- α , IFN- γ , IgG, and IgM levels in serum and IL-2, IL-4, and IL-6 expressions in the spleen were all significantly alleviated by XFBD. Splenic lymphocyte proliferation in response to LPS was further enhanced after treatment with XFBD. The reduction of CD4⁺ and CD8⁺ T lymphocytes in CY-treated mice was also highly increased in XFBD groups.

Conclusion: Our findings suggested that XFBD played a crucial role in protection against immunosuppression in CY-treated mice and could be a potential candidate for immune modification and therapy.

Keywords: Xuanfei Baidu decoction, immunosuppression, immune modification, cyclophosphamide, traditional Chinese medicine

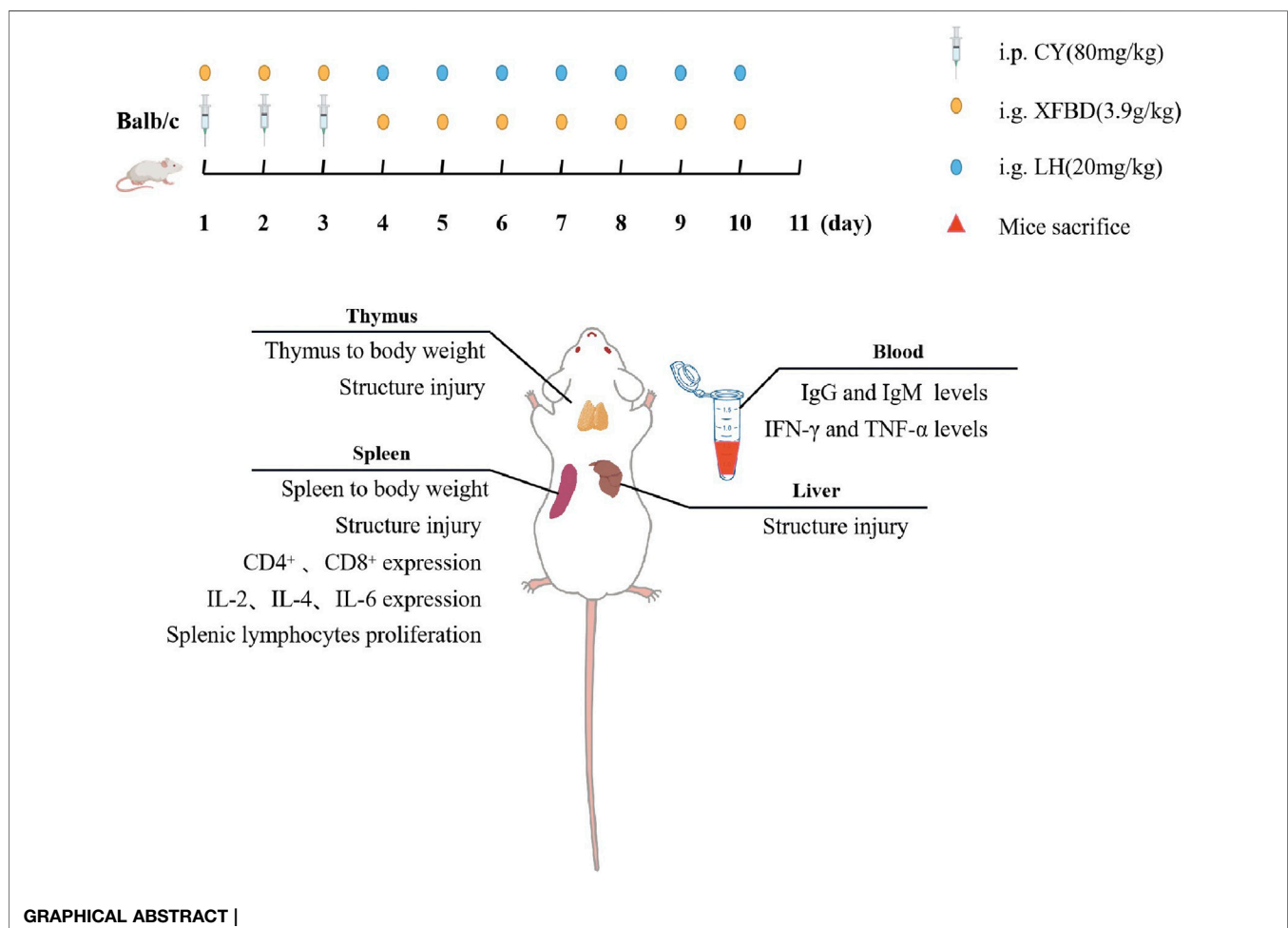
Abbreviations: XFBD, Xuanfei Baidu decoction; CY, cyclophosphamide; TCM, traditional Chinese medicine; COVID-19, coronavirus disease 2019; SARS-CoV-2, severe acute respiratory syndrome coronavirus 2; LPS, lipopolysaccharide; LH, levamisole hydrochloride; CCK-8, cell counting kit; PDA, photodiode array detector; HE, hematoxylin and eosin; GAPDH, glyceraldehyde-3-phosphate dehydrogenase; TNF- α , tumor necrosis factor- α ; IFN- γ , interferon- γ ; IgG, immunoglobulin G; IgM, immunoglobulin M; IL-2, interleukin-2; IL-4, interleukin-4; IL-6, interleukin-6.

INTRODUCTION

Cyclophosphamide (CY) is an alkylating agent that inhibits both the humoral and cellular immune responses (Emadi et al., 2009). It is widely used as a chemotherapeutic drug in the treatment of various types of diseases including cancer, autoimmune diseases, and organ transplants (Bensinger et al., 2001; Mamounas et al., 2005; Passweg and Tyndall, 2007). More importantly, the immunosuppressive state is one of the typical symptoms for a series of diseases such as coronavirus disease 2019 (COVID-19) caused by severe acute respiratory syndrome coronavirus 2 (SARS-CoV-2). It has been observed that the number of total T cells, CD4⁺, and CD8⁺ T cells was dramatically reduced in COVID-19 patients, especially in patients requiring intensive care (Diao et al., 2020). Therefore, many attempts are being made to obtain immune enhancement.

Xuanfei Baidu decoction (XFBD) was designed by Academician Boli Zhang and Professor Qingquan Liu for COVID-19 treatment as one of the clinical prescriptions, based on the recording of the famous traditional Chinese medicine book titled *Treatise on Febrile and Miscellaneous Diseases* (Pan et al., 2020). As the instruction described,

XFBD prescribes 13 herbs, including *Ephedrae Herba*, *Armeniacae Semen*, *Gypsum Fibrosum*, *Coicis Semen*, *Atractylodis Rhizoma*, *Pogostemonis Herba*, *Artemisiae Annuae Herba*, *Polygoni cuspidati Rhizoma*, *Verbenae Herba*, *Phragmitis Rhizoma*, *Lepidii/Descurainiae Semen*, *Citri grandis Exocarpium Rubrum*, and *Glycyrrhizae Radix* (Wang et al., 2020). A previous study has analyzed the chemical composition of XFBD by HPLC-MS and HPLC-DAD-ESI-MS/MS (data unpublished). It has also been reported that XFBD in combination with conventional medicine significantly improved COVID-19 patient's clinical symptoms, increased the number of white blood cells and lymphocytes, and reduced C-reactive protein and erythrocyte sedimentation rate, indicating a potential immune regulatory effect of XFBD in certain diseases (Xiong et al., 2020). Recently, our experimental data showed that XFBD ameliorated LPS-induced lung fibrosis *via* alleviating inflammatory reaction and attenuated staphylococcal protein A-induced inflammation in mice (data unpublished). However, the immunomodulatory effect of XFBD on immunosuppressed mice remains unknown. Here, we elucidated the protective effect of XFBD on immunosuppression in CY-treated mice, which may help provide evidence of XFBD for its clinical application.



MATERIALS AND METHODS

Reagents

Lipopolysaccharide (LPS) was provided by Biological Industries (Shanghai, China). Injectable cyclophosphamide was obtained from Shanxi Pude Medicine Co., Ltd (Shanxi, China). Anti-CD4⁺ (FITC) and anti-CD8⁺ (APC) antibodies were provided by Bio Legend, Inc. (San Diego, CA, United States). The IgG and IgM kits were purchased from CLOUD-CLONE Co., Ltd (Wuhan, China). ELISA kits for cytokine measurement were purchased from BoaoTuoda Biotechnology Co., Ltd (Beijing, China). The total RNA extraction kit was provided by YEASEN Co., Ltd (Shanghai, China). cDNA synthesis and qPCR kits were provided by Transgen (Beijing, China). Levamisole hydrochloride (LH) was produced from Renhe Church Pharmaceutical Co., Ltd (Shandong, China). The cell counting kit (CCK-8) was purchased from Invigentech, Inc. (Irvine, CA, United States).

Extract of XFBD

XFBD was provided by the TianJin Modern TCM Innovation Center (TRT 200302) in the form of a freeze-dried powder. To prepare the XFBD extract, the freeze-dried powder of XFBD (0.4000 g) was extracted with ultrapure water (1:25, g/mL) in an ultrasonic water bath for 30 min. The solution was diluted with 50% methanol at the ratio of 1:1 and vortex-mixed for 5 min. Then the solution was centrifuged at 14,000 rpm for 10 min before filtered with a 0.22 µm filter membrane. An aliquot (2 µL) of the supernatant solution was injected into UHPLC-PDA for analysis. A Waters Acquity UHPLC System (Waters Co., Milford, MA) equipped with a photodiode array detector (PDA) was used to separate the multiple components in XFBD. All separations were performed using a ZORBAX RRHD Eclipse XDB-C18 column (2.1 × 100 mm, 1.8 µm, Agilent Technologies). The flow rate was 0.3 ml/min. The column temperature was 40°C. The mobile phase comprised (A) aqueous formic acid (0.1%, v/v) and (B) acetonitrile using a gradient elution of 5–10% B at 0–8 min, 10–15% B at 8–13 min, 15–17% B at 13–18 min, 17–45% B at 18–30 min, and 45–95% B at 30–35 min and the re-equilibration time of gradient elution was 5 min. The detection wavelength was set at 210 and 254 nm. The components in XFBD was investigated by UPLC and the contents including 1.19 mg/g for ephedrine, 4.97 mg/g for amygdalin, 3.63 mg/g for sinapine, 5.04 mg/g for hastatoside, 4.49 mg/g for verbenalin, 8.45 mg/g for polydatin, 3.40 mg/g for liquiritin, 3.46 mg/g for acteoside, 54.91 mg/g for naringin, and 4.80 mg/g for glycyrrhizic acid in the freeze-dried powder of XFBD (data not shown).

Animals

Male BALB/c mice of 6–8 weeks old were purchased from the Charles River Laboratories (Beijing, China. License number: SCXK 2016-0006). The mice were housed under a 12 h light/dark cycle and were provided food and water. All experimental procedures were approved by the Animal Care and Use Committee of Tianjin

TABLE 1 | Primer sequences used for RT-PCR.

Gene	Forward primer (5'-3')	Reverse primer (5'-3')
<i>IL-2</i>	AGGAACCTGAAACTCCCCAG	AAATCCAGAACATGCCGCAG
<i>IL-4</i>	TCTCGAATGTACCAGGAGCC	ACCTTGGAAGCCCTACAGAC
<i>IL-6</i>	CTGCAAGAGACTTCCATCCAG	AGTGGTATAGACAGGTCTGTTGG
<i>GAPDH</i>	AGGTCGGTGTGAACGGATTG	TGTAGACCATGTAGTTGAGGTCA

University of Traditional Chinese Medicine (Animal Ethics Committee approval number: TCM-LAEC2020090).

Cyclophosphamide-Induced Immunosuppression Model

Mice were randomly assigned to four groups ($n = 6$): the normal group (Normal), the immunosuppression model group (Model), the XFBD group (XFBD), and levamisole hydrochloride group (LH) as positive control. From day 1 to 3, mice in the normal control group were treated once daily with sterile saline, mice from the other three groups were intraperitoneally administered with cyclophosphamide at 80 mg/kg. From day 4 to 10, mice were given with the following treatment by gavage: the XFBD group with XFBD at 3.9 g/kg based on the conversion from an equivalent dose for patients in clinic (Xiong et al., 2020); the LH group with LH at 20 mg/kg; and the other two groups with water. Body weights were recorded every other day.

Calculation of Immune Organ Index

Mice were sacrificed 24 h after last intragastric administration, and then the thymus and the spleen of each mouse were aseptically removed and weighed. The spleen and thymus indexes were calculated by the following formula: Spleen index or Thymus index (%) = (spleen or thymus weight/body weight) × 100%.

Hematoxylin and Eosin Staining

After isolated from mice, the spleen, liver, and thymus tissues were fixed with 4% paraformaldehyde, embedded in paraffin and cut into 4 µm sections. Then, these sections were deparaffinized and stained with hematoxylin and eosin. Finally, the slices were then observed under a light microscope.

Determination of Immunoglobulin and Cytokines in Serum by ELISA

The whole blood was obtained from mice killed by extracting eyeball under sterile conditions on the day of sacrifice. Blood samples were centrifuged at 2,500 rpm for 20 min at 4°C to obtain serum. The levels of immunoglobulin (IgG and IgM) and cytokine IFN-γ and TNF-α in the serum were measured according to the ELISA kit instructions.

Lymphocyte Proliferation

The extirpated spleens obtained from the mice were washed with cold PBS and passed through a 200-mesh filter to obtain a homogeneous splenocyte suspension. The erythrocytes were lysed and the remaining cells were centrifuged at 1,000 rpm for 8 min. After centrifugation, cells were resuspended in

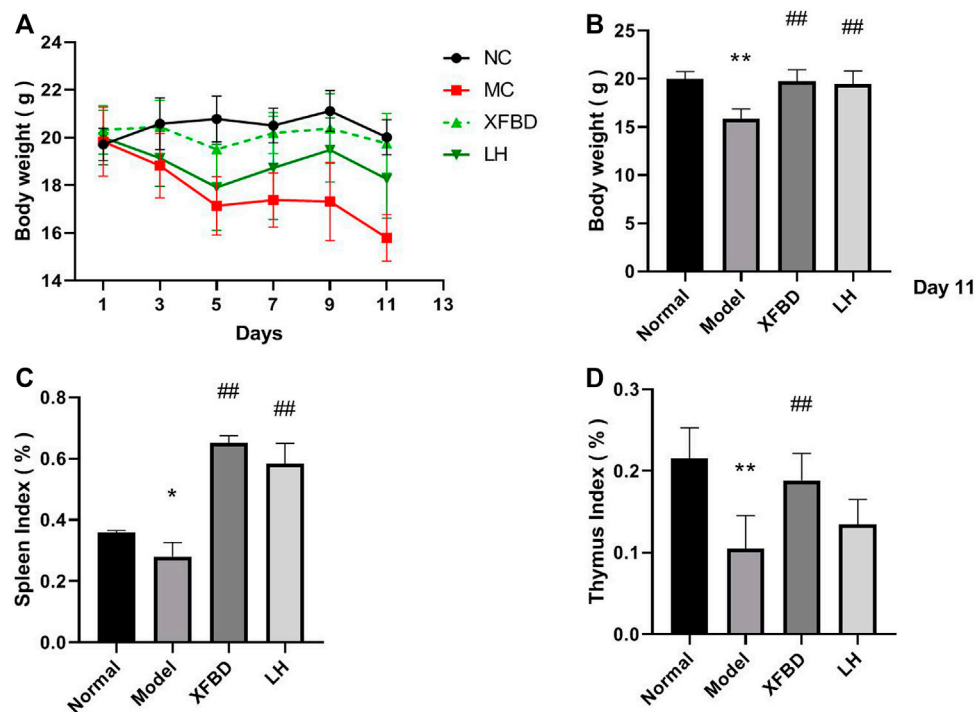


FIGURE 1 | Effect of XFBD on body weights and immune organ indices. **(A)** Body weights during treatment; **(B)** body weights after treatment; **(C)** spleen index, and **(D)** thymus index. Normal, administered with saline; Model: intraperitoneally administered with cyclophosphamide; XFBD: intraperitoneally administered with cyclophosphamide first and followed by XFBD at 3.9 g/kg/day; and LH: intraperitoneally administered with cyclophosphamide first and followed by LH at 20 mg/kg. Data are expressed as mean \pm SD ($n = 6$). * $p < 0.05$ and ** $p < 0.01$ vs. Normal group, # $p < 0.05$ and ## $p < 0.01$ vs. Model group.

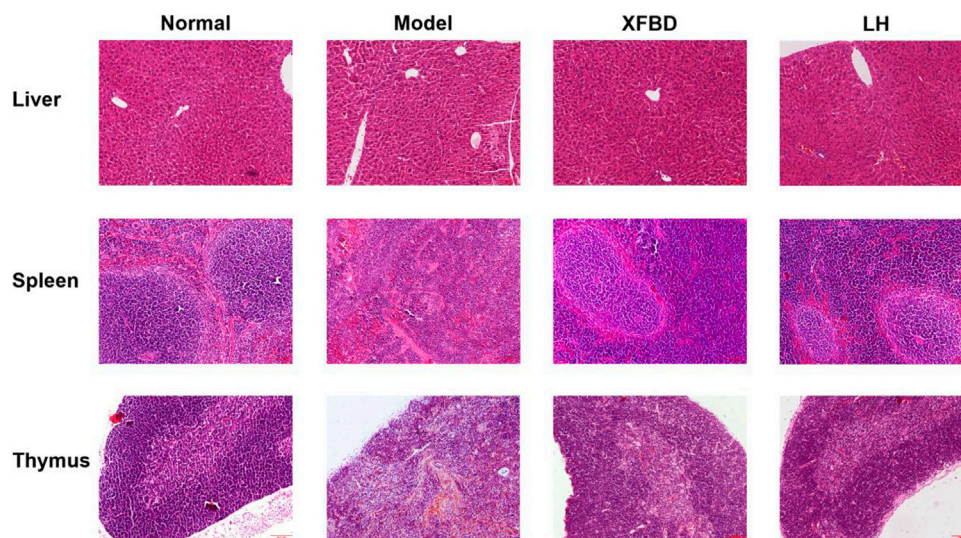


FIGURE 2 | Effects of XFBD on the morphological changes in the liver, the spleen, and the thymus in CY-treated mice. stained by H&E, 10 \times Normal, administered with saline; Model: intraperitoneally administered with cyclophosphamide; XFBD: intraperitoneally administered with cyclophosphamide first and followed by XFBD at 3.9 g/kg/day; and LH: intraperitoneally administered with cyclophosphamide first and followed by LH at 20 mg/kg.

RPMI-1640 medium with 20% FBS. Cells were placed into 96-well plates in triplicate at a density of 5×10^6 cells/ml, and LPS (2 μ g/ml) was added and followed by incubation for 48 h at 37°C

in a humidified atmosphere containing 5% CO₂. Then CCK-8 was added to each well, and after additional incubation for 2 h the absorbance at 450 nm was detected by a microplate reader.

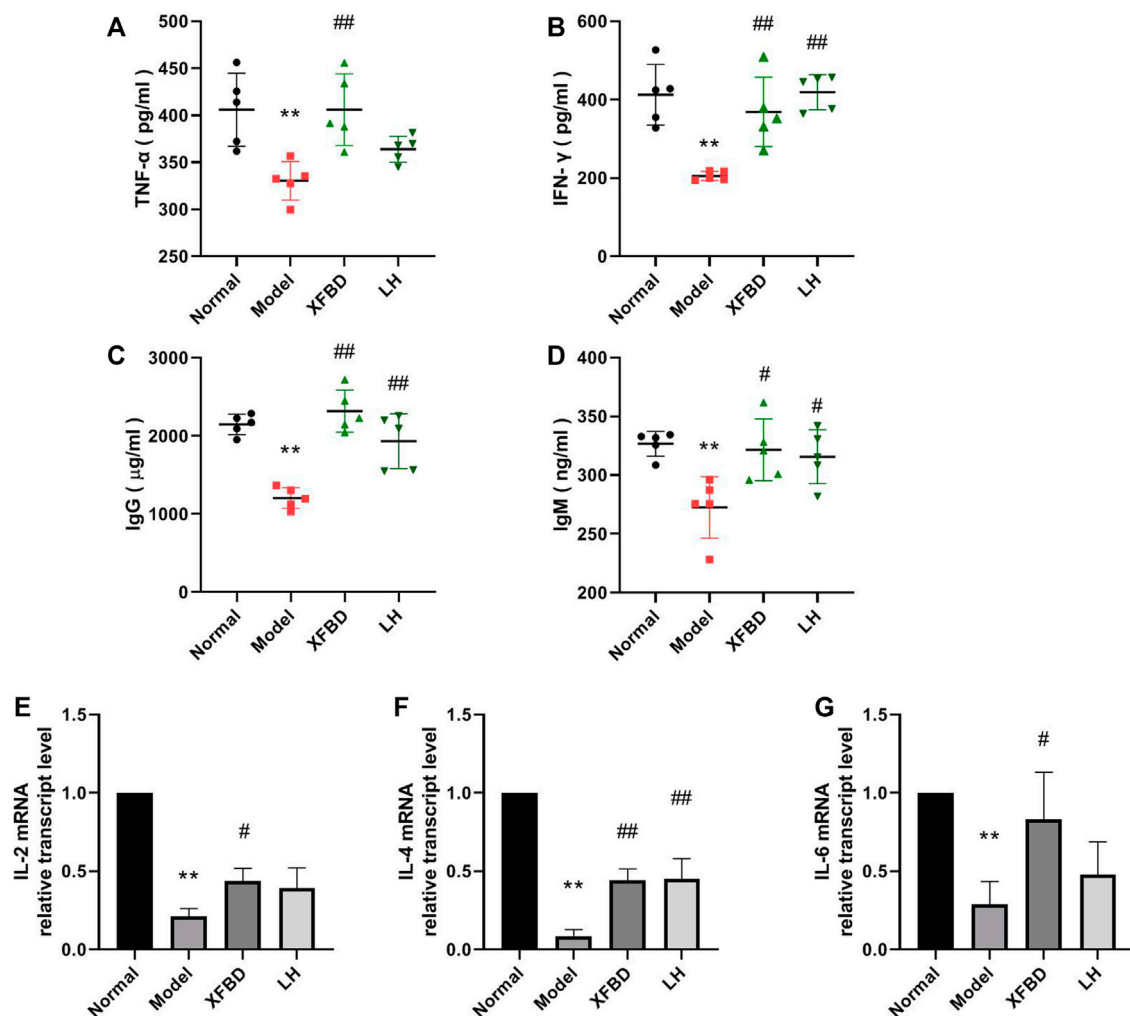


FIGURE 3 | Effect of XFBD on immunoglobulin levels and cytokines in the CY-treated mice. TNF-α (A), IFN-γ (B) IgG (C), and IgM (D) levels in serum were determined by ELISA and IL-2 (E), IL-4 (F), and IL-6 (G) expressions in the spleen were determined by RT-PCR. Normal, administered with saline; Model: intraperitoneally administered with cyclophosphamide; XFBD: intraperitoneally administered with cyclophosphamide first and followed by XFBD at 3.9 g/kg/day; and LH: intraperitoneally administered with cyclophosphamide first and followed by LH at 20 mg/kg. Data are expressed as mean \pm SD [(A–D), $n = 5$] [(E–G), $n = 3$]. * $p < 0.05$ and ** $p < 0.01$ vs. Normal group, # $p < 0.05$ and ## $p < 0.01$ vs. Model group.

Determination of CD4⁺ and CD8⁺ T Lymphocytes in the Spleen

Spleen lymphocytes were first prepared as described above and were resuspended in PBS and adjusted to 1×10^7 /ml. Cell suspensions per 100 μ L were incubated with anti-CD4⁺ (FITC) 0.5 μ L and anti-CD8⁺ (APC) 1.25 μ L for 30 min at 4°C under dark. The spleen lymphocytes were washed for two times with PBS. Then the ratio of CD4⁺ and CD8⁺ T lymphocyte subpopulations was analyzed by flow cytometry (BD FACS Calibur, United States).

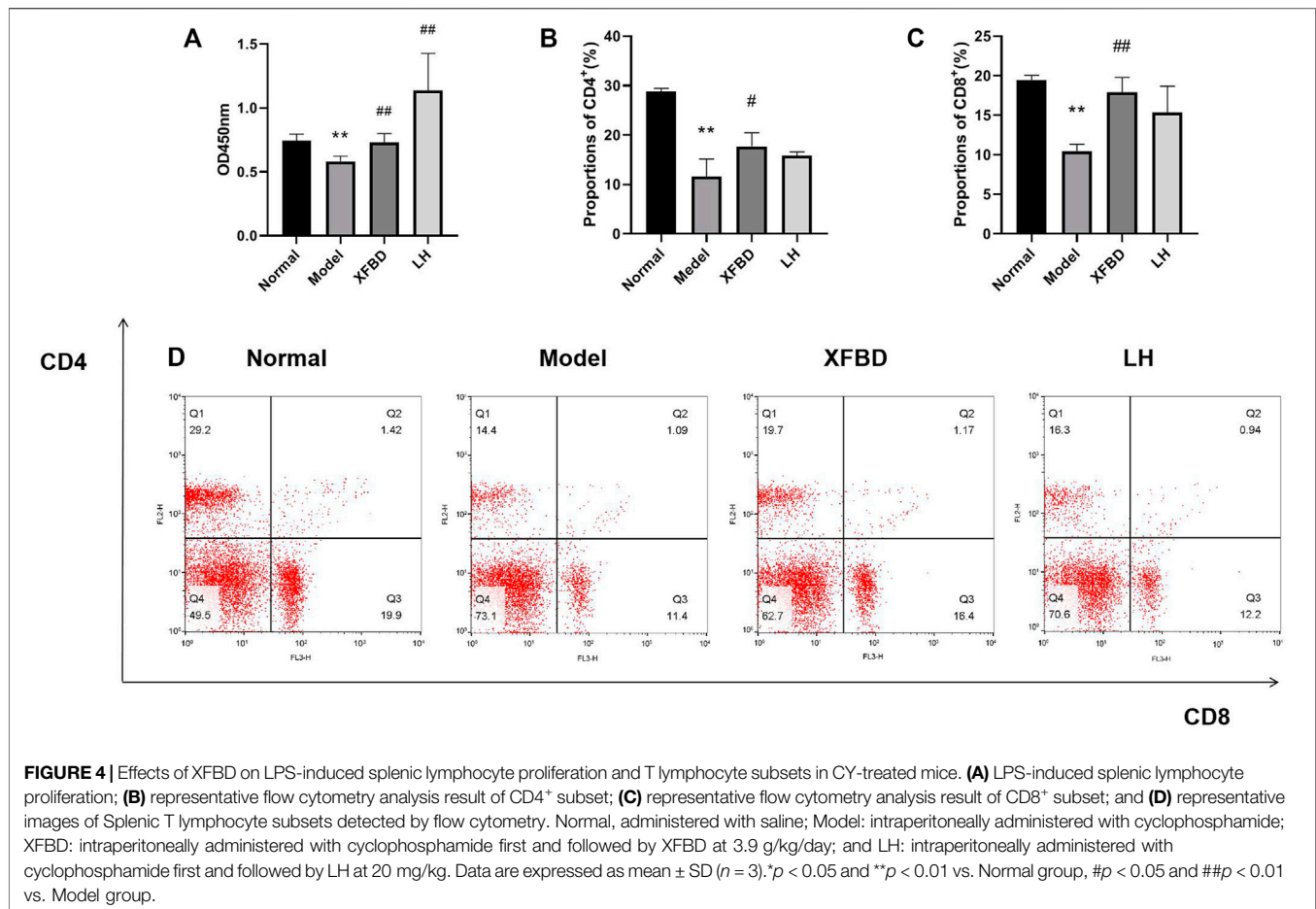
RNA Extraction and qRT-PCR Analysis

Total RNA of spleens was isolated by TRIzol (CWBIO, China). The RNA purity was detected by spectrophotometry. Then, RNA was reversely transcribed into cDNA according to a reverse

transcription kit (Transgen Biotech, China). Then 20 μ L PCR mixture containing 1 μ L cDNA, 8 μ L RNase-free water, 0.5 μ L forward, 0.5 μ L reverse primers, and 10 μ L 2x qPCR Master Mix were prepared and a PCR reaction was then conducted on a real-time PCR system (BIO-RAD, California, United States). Each sample was tested three times. The relative gene expression profiles were determined by normalizing the expression to that of the reference gene (GAPDH) using the $2^{-\Delta\Delta Ct}$ method. The primer sequences are shown in Table 1.

Statistical Analysis

Data were shown as mean \pm SD. The statistical significance of the differences between various groups was determined by an ANOVA analysis for multiple comparisons by Prism version 8.0. Differences between groups at $p < 0.05$ were considered statistically significant.



RESULTS

XFBD Suppressed the Reduction of Body Weight and Immune Organ Index in CY-Induced Immunosuppression Mice

To investigate the immune modulation of XFBD, CY-induced immunosuppression model was established in mice and there was a remarkable decrease of body weight in the Model group after injection of CY during the therapeutic 11 days. Administration with XFBD significantly rescued the weight lost (**Figure 1A**), which was most obviously observed on day 11 (**Figure 1B**). In addition, treatment with LH resulted in a similar effect as that of XFBD in body weight. Furthermore, both of the decreased spleen index and the thymus index were observed in the Model group when compared with those in the Normal group (**Figures 1C,D**) as we expected. However, after administration with XFBD, the spleen and the thymus indices were highly enhanced when compared with those in the Model group and both of which were even better than those in the LH group.

XFBD Improved the Pathological Alterations of the Liver, Spleen, and Thymus in CY-Induced Immunosuppression Mice

A pathological analysis by HE staining showed that the arrangement of liver sinusoid and hepatocyte cords in the Normal group were destroyed and massive inflammatory cells were infiltrated in CY-induced immunosuppression mice (**Figure 2**, liver). In the spleen, white pulp atrophy, hemorrhage, and necrosis were easily observed in the Model group, and red pulp and white red pulp were intermixed as well when compared with those in the Normal group (**Figure 2**, spleen). In the thymus, the clear tissue structures including cortex, medulla, and thymic corpuscle were observed in the Normal group, which were much destroyed in the Model group (**Figure 2**, thymus). However, XFBD administration significantly inhibited the pathological alterations in the mouse liver, spleen, and thymus induced by CY. Besides, as the positive control, the pathological alteration of the LH group was also much rescued, similar to those in the XFBD group (**Figure 2**).

XFBD Enhanced the Serum Levels of Cytokines and Immunoglobulin in CY-Induced Immunosuppression Mice

CY injection caused significant reduction of cytokine TNF- α and IFN- γ levels in serum, which were further rescued by XFBD (Figures 3A,B). Similarly, we found that the concentrations of IgG and IgM in serum were noticeably decreased in the Model group when compared with that in the Normal control group but highly increased in the XFBD group (Figures 3C,D). The effects of XFBD on promotion of cytokines and immunoglobulin were even better than those of LH.

XFBD Alleviated the Reduction of Cytokine Expression in Spleen Isolated From CY-Induced Immunosuppression Mice

The relative gene expressions of IL-2, IL-4, and IL-6 in the mouse spleen were determined by RT-PCR. Data showed that CY significantly decreased the expressions of IL-2, IL-4, and IL-6, which were rescued after XFBD or LH treatment (Figures 3E-G).

XFBD Promoted Proliferation of Splenic Lymphocytes Isolated From CY-Induced Immunosuppression Mice in Response to LPS

Splenic lymphocytes were isolated from different groups of mice and LPS-stimulated cell proliferation was measured. As shown in Figure 4A, LPS-induced splenic lymphocytes proliferation was significantly reduced in the Model group, when compared with that in the Normal group; however, it was further enhanced after treatment with XFBD.

XFBD Induced Splenic Lymphocytes of CD4⁺ and CD8⁺ T Cells in CY-Induced Immunosuppression Mice

The number of CD4⁺ and CD8⁺ T lymphocytes in the spleen was evaluated by flow cytometry. The percentages of CD4⁺ and CD8⁺ T lymphocytes in the Model group were significantly lower than those in the Normal group. However, the reduction of CD4⁺ and CD8⁺ T lymphocytes were then increased in XFBD groups, indicating an effect of XFBD on immune promotion, which was consistently observed in the LH group (Figures 4B-D).

DISCUSSION

Coronavirus disease 2019 (COVID-19) broke out in 2019 and spread rapidly around the world, causing a global pandemic (Li et al., 2020). Up to now, the National Health Commission of China has published eight versions of diagnosis and treatment guidelines (National Health Commission National Administration of Traditional Chinese Medicine, 2020) for COVID-19 therapy. Traditional Chinese medicine (TCM) has a history of more than 2,000 years in prevention and treatment of

epidemics and plagues (Ren et al., 2020). By the systemic diagnosis from TCM experts, it has been generally believed that COVID-19 is a pestilence in view of its epidemic and infectious nature, characterized with the external evils such as toxin evil, wet evil, and cold evil (Zheng et al., 2021), and therefore, COVID-19 is classified as “wet toxin pestilence.”

According to the previous reports, lymphopenia is a key feature of patients with COVID-19, especially in severe cases. Patients with severe COVID-19 are more likely to exhibit lymphopenia on admission, resulted in a broad immune cell reduction including CD4⁺ and CD8⁺ T cells, NK cells, and monocytes and dendritic cells. (Yang et al., 2020; Xu et al., 2020; Zhou et al., 2020). As far as we known, during SARS-CoV-2 infections, the virus appears to first immunosuppress the host and then taking advantage of the body's natural system (Jacques and Apedaile, 2020). It is well known that CY is a common chemotherapeutic drug and administration of CY leads to immunosuppression (Ahlmann and Hempel, 2016; Wang et al., 2011) such as killing immune cells, interfering with the proliferation and differentiation of B and T cells, and restraining the humoral and cellular immune response (Sistigu et al., 2011; Zhu et al., 1987; Shirani et al., 2015). Consistently, in our study, we found that CY caused weight loss of the immune organs (Figure 1), the reduction levels of cytokines in serum and the spleen (Figures 3A,B,E-G), and the imbalance of IgG and IgM production in the peripheral blood of mice (Figures 3C,D), which eventually inhibited the immune function (Noh et al., 2019). It is worthy to notice that COVID-19 links between immunosuppression and hyperinflammation (Jacques and Apedaile, 2020). The first stage is immunosuppression characterized by lymphopenia combined with T-cell exhaustion and an inadequate adaptive immune response, aimed to evade the immune system allowing for unchecked viremia. It has been found that the presence of SARS-CoV-2 virus induced T-cell lymphopenia and T-cell exhaustion (Diao et al., 2020). The second stage in severe SARS-CoV-2 infection is hyperinflammation characterized by a cytokine storm with neutrophil, monocyte/macrophage infiltration, and activation. The infected patients show increased level of cytokines, chemokines, increased numbers of neutrophils, and monocytes. In our study, we used CY-induced immunosuppressive mice as an animal model mimic the immunosuppressive state observed in COVID-19 patients. However, we did not evaluate the effect of XFBD in the second hyperinflammatory stage. Other available models such as acute lung injury and the pulmonary fibrosis model, or SARS-CoV-2-infected hACE2 mice need to be included to investigate the anti-COVID-19 effects in pneumonia, viral replication, multiple organ failure, and even death in future research.

XFBD was first created by Academician Boli Zhang and Professor Qingquan Liu, and it is highly recommended by the National Administration of Traditional Chinese Medicine concerning its definite clinical effect for COVID-19 patients as an immune modulator drug. In March 2021, XFBD got the drug approval by China Drug Administration (Zhang et al., 2020). In particular, the toxicity of XFBD has been evaluated at the dose of 142.8 g/kg. The only appearance of prone and decreased movement was observed

1–4 h after administration of XFBD, while female mice showed soft or loose stool for 1–3 days after administration of XFBD (142.8 g/kg). No other abnormality such as body weight and anatomic characteristics was found in groups. Therefore, we thought that the maximum tolerated dose of XFBD given to mice shall not be less than 142.8 g/kg.

In our study, we first found that XFBD has an immunoregulatory role in CY-induced immunosuppression mice. Data showed that compared to the Model group, the thymus and the spleen indices of XFBD-treated groups were significantly increased (**Figure 1**), the pathological alteration in the liver, the spleen, and the thymus were much improved (**Figure 2**), and splenic CD4⁺ and CD8⁺ T cells and LPS-induced lymphocyte proliferation were also highly increased (**Figure 4**). In cytokine expression, XFBD was able to significantly reverse the decline of serum TNF- α and IFN- γ and mRNA of spleen IL-2, IL-4, and IL-6 in CY-treated mice (**Figure 3**). Taken together, our results gave evidence that XFBD has multiple positive effects to enhance cellular immunity by regulating component of immune systems in CY-treated mice. For cellular assay, the anti-inflammatory effect of XFBD has also been investigated in LPS-induced THP-1 monocytes and RAW 264.7 macrophages. As we expected, XFBD significantly inhibited LPS-induced IL-6, IP-10, and TNF- α expressions in THP-1 cells (data not shown) and TNF- α , IL-6, and IL-1 β secretions in RAW 264.7 cells (data not shown), indicating an immune-modulatory effect of XFBD in a bidirectional manner.

Previously, our group employed the network strategy to predict the potential signaling pathways of XFBD which may be involved in the anti-COVID-19 effect (Wang et al., 2011). Data showed that the main biological pathways regulated by XFBD included viral infection, energy metabolism, immunity and inflammation, and parasites and bacterial infections, which indicated a multi-herb, multi-constituent, and multi-target pattern, with lung as the chief targeted organ for therapy of XFBD in COVID-19. More efforts needed to make to further uncover the mechanism of XFBD in immunomodulation.

REFERENCES

- Ahlmann, M., and Hempel, G. (2016). The Effect of Cyclophosphamide on the Immune System: Implications for Clinical Cancer Therapy. *Cancer Chemother. Pharmacol.* 78 (4), 661–671. doi:10.1007/s00280-016-3152-1
- Bensinger, W. I., Martin, P. J., Storer, B., Clift, R., Forman, S. J., Negrin, R., et al. (2001). Transplantation of Bone Marrow as Compared with Peripheral-Blood Cells from HLA-Identical Relatives in Patients with Hematologic Cancers. *N. Engl. J. Med.* 344 (3), 175–181. doi:10.1056/NEJM200101183440303
- Diao, B., Wang, C., Tan, Y., Chen, X., Liu, Y., Ning, L., et al. (2020). Reduction and Functional Exhaustion of T Cells in Patients with Coronavirus Disease 2019 (COVID-19). *Front. Immunol.* 11, 827–841. doi:10.3389/fimmu.2020.00827
- Emadi, A., Jones, R. J., and Brodsky, R. A. (2009). Cyclophosphamide and Cancer: golden Anniversary. *Nat. Rev. Clin. Oncol.* 6 (11), 638–647. doi:10.1038/nrclinonc.2009.146
- Jacques, F. H., and Apedaile, E. (2020). Immunopathogenesis of COVID-19: Summary and Possible Interventions. *Front. Immunol.* 11, 564925. doi:10.3389/fimmu.2020.564925

Taken together, our data first showed that XFBD might be involved in immunomodulatory effects *in vivo*, providing an evidence of basis use of XFBD for the prevention and treatment of immunosuppressive diseases, and also indicating the potential role of XFBD for COVID-19 treatment.

DATA AVAILABILITY STATEMENT

The original contributions presented in the study are included in the article/Supplementary Material; further inquiries can be directed to the corresponding authors.

ETHICS STATEMENT

The animal study was reviewed and approved by the Experimental Animal Ethics Committee of Tianjin University of Traditional Chinese Medicine.

AUTHOR CONTRIBUTIONS

LM and HZ initiated and designed the study; HY, JL, and JW completed the experimental research under the guidance and supervision of LM and HZ; HY and LM wrote the manuscript and draw the figures; LC, YW, LM, HZ, and LL revised the manuscript.

FUNDING

This research was funded by the National Key Research and Development Project of China (2020YFA0708004, 2020YFA0708000), Science and Technology Program of Tianjin (19ZYPTJC00060, 20ZYJDJC00070) and Scientific research project in key fields of traditional Chinese medicine of Tianjin Health Commission (202-003).

- Li, Q., Guan, X., Wu, P., Wang, X., Zhou, L., Tong, Y., et al. (2020). Early Transmission Dynamics in Wuhan, China, of Novel Coronavirus-Infected Pneumonia. *N. Engl. J. Med.* 382 (13), 1199–1207. doi:10.1056/NEJMoa2001316
- Mamounas, E. P., Bryant, J., Lembersky, B., Fehrenbacher, L., Sedlacek, S. M., Fisher, B., et al. (2005). Paclitaxel after Doxorubicin Plus Cyclophosphamide as Adjuvant Chemotherapy for Node-Positive Breast Cancer: Results from NSABP B-28. *J. Clin. Oncol.* 23 (16), 3686–3696. doi:10.1200/JCO.2005.10.517
- National Health Commission National Administration of Traditional Chinese Medicine (2020). *Guidelines for the Diagnosis and Treatment of Coronavirus Disease 2019 (trial Version Eighth)*, 10, 321–328.
- Noh, E. M., Kim, J. M., Lee, H. Y., Song, H. K., Joung, S. O., Yang, H. J., et al. (2019). Immuno-enhancement Effects of Platycodon Grandiflorum Extracts in Splenocytes and a Cyclophosphamide-Induced Immunosuppressed Rat Model. *BMC Complement. Altern. Med.* 19 (1), 322. doi:10.1186/s12906-019-2724-0
- Pan, X., Dong, L., Yang, L., Chen, D., and Peng, C. (2020). Potential Drugs for the Treatment of the Novel Coronavirus Pneumonia (COVID-19) in China. *Virus. Res.* 286, 198057. doi:10.1016/j.virusres.2020.198057

- Passweg, J., and Tyndall, A. (2007). Autologous Stem Cell Transplantation in Autoimmune Diseases. *Semin. Hematol.* 44 (4), 278–285. doi:10.1053/j.seminhematol.2007.08.001
- Ren, J.-L., Zhang, A.-H., and Wang, X.-J. (2020). Traditional Chinese Medicine for COVID-19 Treatment. *Pharmacol. Res.* 155, 104743. doi:10.1016/j.phrs.2020.104743
- Shirani, K., Hassani, F. V., Razavi-Azarkhiavi, K., Heidari, S., Zanjani, B. R., and Karimi, G. (2015). Phytotrapy of Cyclophosphamide-Induced Immunosuppression. *Environ. Toxicol. Pharmacol.* 39 (3), 1262–1275. doi:10.1016/j.etap.2015.04.012
- Sistigu, A., Viaud, S., Chaput, N., Bracci, L., Proietti, E., and Zitvogel, L. (2011). Immunomodulatory Effects of Cyclophosphamide and Implementations for Vaccine Design. *Semin. Immunopathol* 33 (4), 369–383. doi:10.1007/s00281-011-0245-0
- Wang, H., Wang, M., Chen, J., Tang, Y., Dou, J., Yu, J., et al. (2011). A Polysaccharide from Strongylocentrotus Nudus Eggs Protects against Myelosuppression and Immunosuppression in Cyclophosphamide-Treated Mice. *Int. Immunopharmacol* 11 (11), 1946–1953.
- Wang, Y., Li, X., Zhang, J. H., Xue, R., Qian, J. Y., Zhang, X. H., et al. (2020). Mechanism of Xuanfei Baidu Tang in Treatment of COVID-19 Based on Network Pharmacology. *Zhongguo Zhong Yao Za Zhi* 45 (10), 2249–2256.
- Xiong, W. Z., Wang, G., Du, J., and Ai, W. (2020). Efficacy of Herbal Medicine (Xuanfei Baidu Decoction) Combined with Conventional Drug in Treating COVID-19: A Pilot Randomized Clinical Trial. *Integr. Med. Res.* 9 (3), 100489.
- Xu, Z., Shi, L., Wang, Y., Zhang, J., Huang, L., Zhang, C., et al. (2020). Pathological Findings of COVID-19 Associated with Acute Respiratory Distress Syndrome. *Lancet Respir. Med.* 8 (4), 420–422. doi:10.1016/S2213-2600(20)30076-X
- Yang, L., Liu, S., Liu, J., Zhang, Z., Wan, X., Huang, B., et al. (2020). COVID-19: Immunopathogenesis and Immunotherapeutics. *Signal. Transduct Target. Ther.* 5 (1), 128. doi:10.1038/s41392-020-00243-2
- Zhang, X. Y., Liu, S., Sun, Y., Qiu, R. J., Chen, Z., Tang, J. Y., et al. (2020). Strategy and Thinking of the Development and Review Policies of Traditional Chinese Medicine (TCM) New Drugs Taking “Three Chinese Patent Medicines and Three TCM Prescriptions” as Examples. *Chin. J. New Drugs* 29 (16), 1818–1821.
- Zheng, Y., Jin, D., Lin, J., Zhang, Y., Tian, J., Lian, F., et al. (2021). Understanding COVID-19 in Wuhan from the Perspective of Cold-Dampness: Clinical Evidences and Mechanisms. *Front. Med. (Lausanne)* 8, 617659. doi:10.3389/fmed.2021.617659
- Zhou, R., To, K. K., Wong, Y. C., Liu, L., Zhou, B., Li, X., et al. (2020). Acute SARS-CoV-2 Infection Impairs Dendritic Cell and T Cell Responses. *Immunity* 53 (4), 864–877. doi:10.1016/j.immuni.2020.07.026
- Zhu, L. P., Cupps, T. R., Whalen, G., and Fauci, A. S. (1987). Selective Effects of Cyclophosphamide Therapy on Activation, Proliferation, and Differentiation of Human B Cells. *J. Clin. Invest.* 79 (4), 1082–1090. doi:10.1172/JCI112922

Conflict of Interest: The authors declare that the research was conducted in the absence of any commercial or financial relationships that could be construed as a potential conflict of interest.

Publisher’s Note: All claims expressed in this article are solely those of the authors and do not necessarily represent those of their affiliated organizations, or those of the publisher, the editors, and the reviewers. Any product that may be evaluated in this article, or claim that may be made by its manufacturer, is not guaranteed or endorsed by the publisher.

Copyright © 2021 Yan, Lu, Wang, Chen, Wang, Li, Miao and Zhang. This is an open-access article distributed under the terms of the Creative Commons Attribution License (CC BY). The use, distribution or reproduction in other forums is permitted, provided the original author(s) and the copyright owner(s) are credited and that the original publication in this journal is cited, in accordance with accepted academic practice. No use, distribution or reproduction is permitted which does not comply with these terms.



Ethyl 2-Succinate-Anthraquinone Attenuates Inflammatory Response and Oxidative Stress via Regulating NLRP3 Signaling Pathway

Burong Feng^{1,2}, Xiuye Zhao^{1,2}, Wei Zhao^{1,2}, Huiwei Jiang^{1,2}, Zijing Ren^{1,2}, Yingfu Chen^{1,2}, Ye Yuan^{1,2} and Zhimin Du^{1,2,3*}

¹Institute of Clinical Pharmacy, The Second Affiliated Hospital of Harbin Medical University (The University Key Laboratory of Drug Research, Heilongjiang Province), Harbin, China, ²Department of Clinical Pharmacology, College of Pharmacy, Harbin Medical University, Harbin, China, ³State Key Laboratory of Quality Research in Chinese Medicines, Macau University of Science and Technology, Macau, China

OPEN ACCESS

Edited by:

Yihai Wang,
Guangdong Pharmaceutical
University, China

Reviewed by:

George Hsiao,
Taipei Medical University, Taiwan
Jiang-Huei Jeng,
National Taiwan University, Taiwan

*Correspondence:

Zhimin Du
dzm1956@126.com

Specialty section:

This article was submitted to
Inflammation Pharmacology,
a section of the journal
Frontiers in Pharmacology

Received: 03 June 2021

Accepted: 01 October 2021

Published: 08 November 2021

Citation:

Feng B, Zhao X, Zhao W, Jiang H,
Ren Z, Chen Y, Yuan Y and Du Z (2021)
Ethyl 2-Succinate-Anthraquinone
Attenuates Inflammatory Response
and Oxidative Stress via Regulating
NLRP3 Signaling Pathway.
Front. Pharmacol. 12:719822.
doi: 10.3389/fphar.2021.719822

Aloe-emodin widely possesses antibacterial, anti-inflammatory, antioxidant, antiviral, and anti-infectious properties. This study investigated the effect of ethyl 2-succinate-anthraquinone (Luhui derivative, LHD) on inflammation. *In vitro*, a THP-1 macrophage inflammation model, made by 100 ng/ml phorbol-12-myristate-13-acetate (PMA) and 1 µg/ml LPS for 24 h, was constructed. The LHD group (6.25 µmol/L, 12.5 µmol/L, 25 µmol/L, 50 µmol/L) had no effect on THP-1 cell activity, and the expression of IL-6 mRNA was down-regulated in a concentration-dependent manner, of which the 25 µmol/L group had the best inhibitory effect. The migration of THP-1 macrophages induced by LPS was decreased by the LHD. Moreover, the LHD suppressed ROS fluorescence expression by inhibiting MDA expression and increasing SOD activity. *In vivo*, we revealed that the LHD, in different doses (6.25 mg/kg, 12.5 mg/kg, 25 mg/kg, 50 mg/kg), has a protective effect on stress physiological responses by assessing the body temperature of mice. Interestingly, acute lung injury (e.g., the structure of the alveoli disappeared and capillaries in the alveolar wall were dilated and congested) and liver damage (e.g., hepatocyte swelling, neutrophil infiltration, and hepatocyte apoptosis) were obviously improved at the same condition. Furthermore, we initially confirmed that the LHD can down-regulate the expression of NLRP3, IL-1β, and caspase-1 proteins, thereby mediating the NLRP3 inflammasome signaling pathway to produce anti-inflammatory effects. In conclusion, our results indicate that the LHD exerts anti-inflammatory activity via regulating the NLRP3 signaling pathway, inhibition of oxidative stress, and THP-1 macrophage migration.

Keywords: Luhui derivative (LHD), inflammation, oxidative stress, NLRP3, THP-1

INTRODUCTION

Inflammation, a body's response to exogenous or endogenous damage factors, is a very common and important pathological process. It has been found to mediate a wide variety of human diseases, including diabetes, cardiovascular diseases, cancer, septic shock, and sepsis. Its basic pathological changes include metamorphosis, exudation, and hyperplasia. According to the different duration, inflammation can be classified into two types: acute inflammation and chronic inflammation (Hu

et al., 2014; Furtado et al., 2016; Karim et al., 2019). In addition, the inflammatory response can remove harmful substances from the body and produce a positive protective effect through initiating tissue repair. However, it should be emphasized that the inflammatory response can release a large number of inflammatory cytokines and inflammatory mediators such as IL-6, IL-1 β , and iNOS; if they cannot disappear in time, it would be more severe. On the one hand, these inflammatory cytokines can disturb the balance of anti-inflammatory and pro-inflammatory reactions (Murray and Smale, 2012; Headland and Norling, 2015; Yang et al., 2016). On the other hand, the release of inflammatory factors can cause autoimmune and metabolic diseases, chronic nervous system diseases (Foster and Medzhitov, 2009; Headland and Norling, 2015), malignant tumors, and other diseases, which seriously threaten human health (Perez and Vago, 2014).

Lipopolysaccharide (LPS) is the component of the cell wall of Gram-negative bacteria (Widdrington et al., 2018), which could directly act on the cell membrane. Functionally, it can stimulate macrophages to polarize into M1-type macrophages and exude a large number of pro-inflammatory factors (Goodman and Brett, 2017; Skirecki and Cavaillon, 2019). However, by further amplifying the inflammatory response, these inflammatory factors could increase vascular permeability and inflammatory cell infiltration, thereby promoting systemic inflammation (Tandon et al., 2018). At the function level, LPS can cause systemic inflammatory response syndrome, including sepsis, shock, disseminated intravascular coagulation (DIC), and multiple organ failure (MOF) (Wang et al., 2015). Therefore, LPS is one of the important conditions to trigger an inflammatory response.

Macrophages, including classically activated macrophages (M1) and alternatively activated macrophages (M2) (Fuchs et al., 2016; Gao et al., 2017), are a kind of immune cells, which have functions of phagocytosis, antigen presentation, and releasing various cytokines, and play an important role in the physiological processes of inflammation, defense, repair, and metabolism (Su et al., 2015; Cullis et al., 2017). Furthermore, macrophage migration contributes directly to pathogen removal and wound healing (Yang et al., 2018; Carestia et al., 2019). Therefore, macrophages play a key role in mediating the inflammatory response.

Aloe-emodin (1,8-dihydroxyl-3-hydroxymethyl-9,10-anthraquinone) is widely found in aloe vera, rhubarb, knotweed, cassia seed, and other Chinese herbs. It is a representative anthraquinone compound of emodin type. A variety of literature studies have mentioned that emodin anthraquinone is a compound with a special structure of hydroxyl group distributed on both sides of benzene rings. Furthermore, emodin has been demonstrated to possess a series of therapeutic effects, such as antibacterial, anti-inflammatory, antioxidant, antiviral, and anti-infectious effects (Mu and Zhi-min, 2015). Arosio et al. confirmed that aloe-emodin could inhibit the inflammatory response after lipid peroxidation by reducing the expression level of TNF- α mRNA (Alshatwi and Subash-Babu, 2016). However, emodin has been reported to exert toxicity and decrease absorption, so it

has not been directly used in clinical trials. Therefore, it is necessary to optimize the structure of emodin anthraquinone compounds. In this study, we reported the finding that the Luhui derivative exhibits (Figure 1D) its anti-inflammatory effects by mediating the NLRP3 inflammasome signaling pathway and inhibits inflammatory cytokine expression in serum.

MATERIALS AND METHODS

Reagents

LPS (a surface glycolipid produced by Gram-negative bacteria) was purchased from Sigma-Aldrich (St. Louis, MO), and stock solutions of 1 mg/mL were prepared and stored at -20°C . Ethyl 2-succinate-anthraquinone (Luhui derivative, LHD) is a novel compound monomer formed by covalent binding of monomethyl succinate to the anthraquinone mother nucleus of aloe-emodin using chemical synthesis techniques in our laboratory. Kits of MDA and SOD were purchased from the Nanjing Jian Cheng Bioengineering Institute. IL-6, IL-1 β , and IL-18 ELISA kits were purchased from the Neobioscience Institute (Shenzhen, China) and Elabscience Institute (Wuhan, China). The antibodies used in this study with their working dilutions are indicated in parentheses: NLRP3 (1:500) was purchased from the Wanle Institute, IL-1 β (1:500) was purchased from the Elabscience Institute, and caspase-1 (1:500) and ASC (1:500) were purchased from Proteintech Group, Inc. (Wuhan, China).

Animal Model

C57BL/6 mice (18–22 g) were provided by the Animal Center of the Second Affiliated Hospital of Harbin Medical University. All the animals were involved in the experiment with the approval of the Ethics Committee of Harbin Medical University (SYDW2019-258), and the experimental procedures were performed in accordance with the National Institutes of Health (NIH) Guide for the Care and Use of Laboratory Animals.

After 3 days of adaptive feeding, according to the random number table method, 56 male C57BL/6 mice were randomly divided into seven groups (control group, model group, LHD 6.25 mg/kg, LHD 12.5 mg/kg, LHD 25 mg/kg, LHD 50 mg/kg, and dexamethorphan (DXM) 5 mg/kg group), and there were eight mice in each group. Then, the mice in each group were given the drug by gavage at the experimental concentration for six consecutive days (the blank control group and the model group were given the same amount of physiological salt), and the weight changes of the mice were recorded within 6 days. One hour after gavage, each group was injected with normal saline and LPS, respectively, to construct the model of inflammation *in vivo*. The body temperature of the mice in each group was measured with a frontal tester 6 h after LPS injection. Subsequently, orbital blood was taken from mice to detect the changes of IL-6, IL-1 β , and IL-18 inflammatory factors by ELISA.

Cell Culture

The human myeloid leukemia mononuclear cell line (THP-1) was obtained from the GEFAN Biotechnology company (Shanghai, China) and cultured in RPMI 1640 medium (Corning,

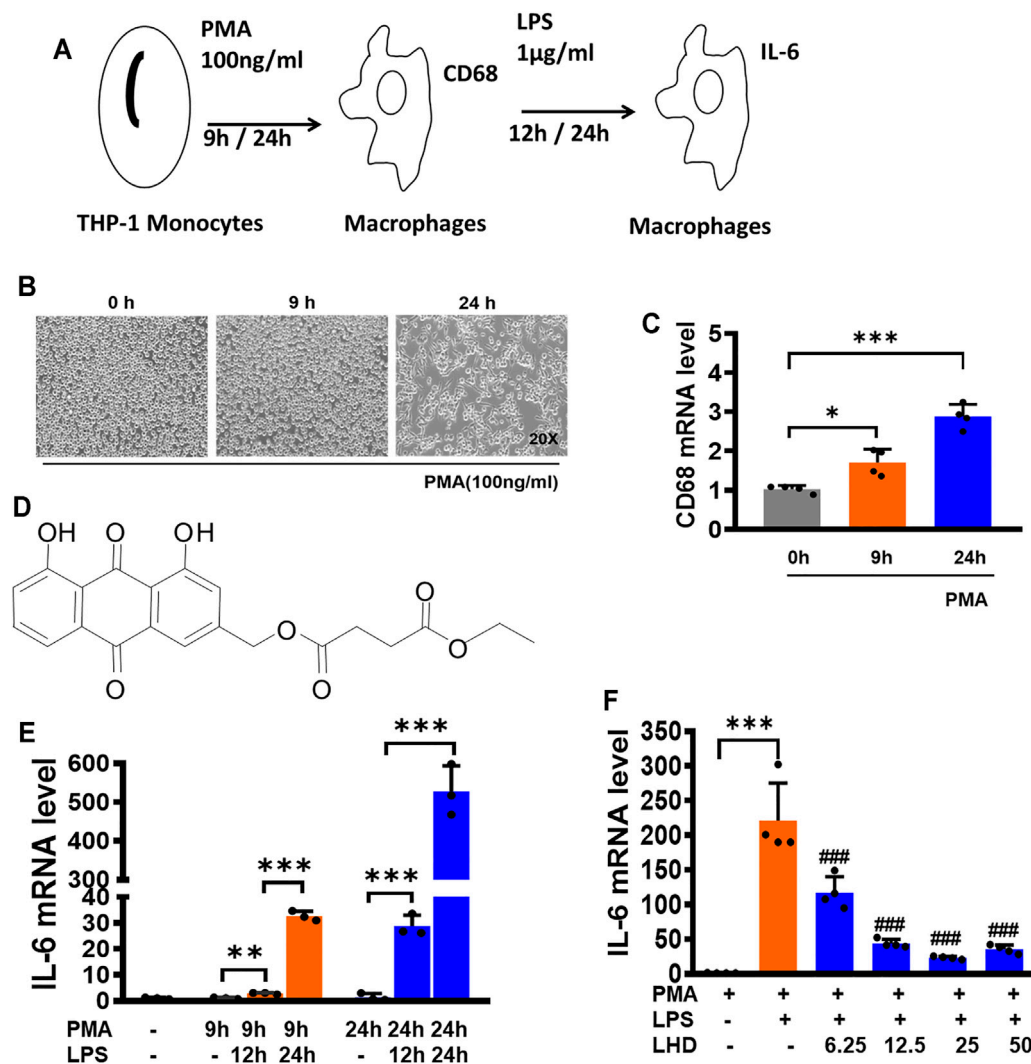


FIGURE 1 | LHD can inhibit THP-1 macrophage inflammation induced by LPS. **(A)** Construction of the macrophage inflammation model. **(B)** After 100 ng/ml PMA stimulation of THP-1 cells for 0, 9, and 24 h, the morphology of THP-1 macrophages was observed under an optical microscope (20×). **(C)** After 100 ng/ml PMA stimulation of THP-1 cells for 0, 9, and 24 h, the expression of CD68 was detected by qRT-PCR, $N = 4$. **(D)** Structures of compound LHD (1,8-dihydroxy-3-(hydroxymethyl)-anthraquinone ethyl succinate). **(E)** After 1 μg/ml LPS stimulated THP-1 macrophages for 12 and 24 h, besides 100 ng/ml PMA stimulation of THP-1 cells for 0, 9, and 24 h, the expression of IL-6 was detected by qRT-PCR, $N = 3$. **(F)** After 6.25, 12.5, 25, and 50 μmol/L LHD were co-incubated with LPS- and PMA-induced THP-1 macrophages for 24 h, and the expression of IL-6 was detected by qRT-PCR, $N = 4$ (*** $p < 0.001$, ** $p < 0.01$ vs. the PMA group; # $p < 0.05$, ## $p < 0.01$, ### $p < 0.001$ vs. the LPS group).

United States) supplemented with 10% fetal bovine serum (ExCell Bio, China). The THP-1 cells were cultured at 37°C with 5% CO₂ and 95% air after their isolation.

Histological Analyses

6 h after LPS injection, the whole lung tissue was fixed with 10% formaldehyde for 24 h, followed by gradient dehydration with sucrose and embedding in paraffin. Next, the tissue block was cut into four-bedroom slices and placed at 65°C for overnight baking. Then, xylene, anhydrous ethanol, 90% ethanol, 70% ethanol, and distilled water were used for dewaxing. Hematoxylin staining solution was used for staining, and neutral gum was used to seal

the tablet. Pathological changes of lung and liver tissues were observed and photographed under a light microscope.

Cell Counting Kit-8

THP-1 cells were adhered by 100 ng/ml PMA in a 96-well plate (1×10^4 per well) for 24 h. Then, different doses of LHD (6.25, 12.5, 25, and 50 μmol/L) were added to the 96-well plate. Finally, CCK-8 (10 μl) was added to each well and kept in an incubator for 4 h (MedChemExpress, China). The culture plates were shaken for 30 s, and the absorbance was recorded at 450 nm. The wavelength was read by an Infinite M200 microplate reader (Tecan, Salzburg, Austria).

Quantitative Real-Time Polymerase Chain Reaction

Total RNA samples were extracted from cells using Trizol reagent (Invitrogen, United States), and quantitative PCR and reverse transcription were performed following the manufacturer's protocols. RNA quantity was detected with the NanoDrop TM 8000 spectrophotometer (Thermo Scientific, France). Sequences of gene-specific PCR primers (Shanghai Generay Biotech Co., Ltd., China) used were as follows:

Human CD68	Forward: 5'-CTACATGGCGGTGGAGTACAA-3' Reverse: 5'-ATGATGAGAGGCAGCAAGATGG-3'
Human IL-6	Forward: 5'-GGTACATCCTCGACGGCATCT-3' Reverse: 5'-GTGCCTCTTTGCTTTCAC-3'
Human β -actin	Forward: 5'-AGCCTCGCCTTTGCCGA-3' Reverse: 5'-CTGGTGCCTGGGGCG-3'

Quantitative PCR was performed in 20 μ l volumes with SYBR Green PCR Master Mix (Roche, United States) at 95°C for 10 min and 40 cycles at 95°C for 15 s, 60°C for 30 s, and 72°C for 30 s with Light Cycler 480 (Roche, United States). IL-1 β , IL-6, and TNF- α levels were calculated according to the $2^{-\Delta\Delta C_t}$ method, and GAPDH mRNA was measured as an internal control.

Western Blot

Total proteins were extracted from THP-1 cells. The cells were lysed with 40 μ l of RIPA buffer (Beyotime, Jiangsu, China), and then the protein content was measured with the Bicinchoninic Acid (BCA) Protein Assay Kit (Bio-Rad, Mississauga, ON, Canada). Protein samples (60–90 μ g) were separated by sodium dodecyl sulfate–polyacrylamide gel electrophoresis (SDS-PAGE) (10–15%) at 70 V for 30 min and 100 V for 1.5 h and then transferred into nitrocellulose membranes and blocked with 5% non-fat milk for 2 h at room temperature. The membranes were incubated with primary antibodies (NLRP3, ASC, IL-1, caspase-1, and GAPDH) in a shaker at 4°C overnight. The strips were washed with PBST (PBS containing 0.1% Tween-20) and incubated with IRDye secondary antibody (LI-COR, United States) for 1 h. The protein expression was measured by the Odyssey CLx Infrared Imaging System (LI-COR Biosciences, Lincoln, NE, United States). The bands were quantified by measuring the band intensity using Odyssey CLx version 2.1.

Cell Scratch Experiment

First, each hole in the six-well plate was covered with cells (5×10^5 cells). Then, the spear head was placed perpendicular to the cell plane, and scratches were made on the cell layer along the top of the six-well plate. The scratches were kept vertical when the pipette head slid down to the bottom, and it is ensured that the width of each scratch is the same. After the scratch was completed, the cells were washed with sterile PBS three times to remove the non-adherent cells, which could ensure the gap left after the scratch could be clearly seen. Then, the fresh RPMI 1640 medium was replaced, the cells were cultured in a 37°C 5% CO₂ incubator, and the cells were taken out at 0, 24, and 48 h, respectively. The changes of

scratch width in each group were observed and recorded under an inverted microscope.

ROS Assessment

Aerobic cells produce a series of reactive oxygen species in the process of metabolism. DCFH-DA is a non-fluorescent probe that can penetrate into cells. The fluorescence intensity of DCFH-DA represents the changes in the level of reactive oxygen species in cells. THP-1 cells were incubated with 10 μ M DCFH-DA in a cell culture box of 5% CO₂ at 37°C for 20 min. Then, the cells were washed with serum-free RPMI 1640 medium three times to fully wash DCFH-DA from the cell surface in the six-well plate. Next, the cells were fixed with 4% paraformaldehyde and washed with PBS three times. Finally, DAPI was used to stain nuclei for 15 min. An FV1000 laser confocal microscope was used to detect the fluorescence intensity of reactive oxygen species at the excitation wavelength of 488 nm and the emission wavelength of 525 nm.

Malondialdehyde and Superoxide Dismutase Content Assessment

THP-1 cells were cultured in six-well plates. Then, the differentiation of THP-1 cells into macrophages was induced by addition of 100 ng/ml PMA. After 24 h, THP-1 macrophages were stimulated by 1 μ g/ml LPS to construct an inflammatory model. Finally, different doses of LHD (6.25 μ mol/L, 12.5 μ mol/L, 25 μ mol/L, 50 μ mol/L) were added to co-stimulate the culture with 1 μ g/ml LPS for 24 h. THP-1 macrophages were digested by 0.25% trypsin solution. After centrifugation, the cells were broken by sonication on ice, and the protein concentration was measured and calculated by BCA. MDA and SOD contents were determined by a commercial ELISA kit according to the manufacturer's instructions.

Inflammatory Cytokines Analyses

We used ELISA to economically detect the expression of IL-6 and other inflammation. The animals were anesthetized, and blood samples were collected via orbital puncture. Subsequently, the blood samples were maintained at room temperature for 20 min and centrifuged (3,000 rpm/min) at 4°C for 5 min. All the samples were preserved at –80°C. The ELISA kits were used to measure the level of IL-6 and other inflammation in mice serum after administering different doses of LHD (6.25 μ mol/L, 12.5 μ mol/L, 25 μ mol/L, 50 μ mol/L) according to the manufacturer's instructions.

Data Statistical Analyses

All the measurement data involved in this experiment were expressed as mean \pm SEM. One-way ANOVA was used to distinguish the data of three or more groups. * $p < 0.05$, ** $p < 0.01$, and *** $p < 0.001$ showed statistical differences. $p > 0.05$ indicated no statistical difference. The data analysis and drawing involved in this experiment were processed by GraphPad Prism version 8.0 (GraphPad Software, United States).

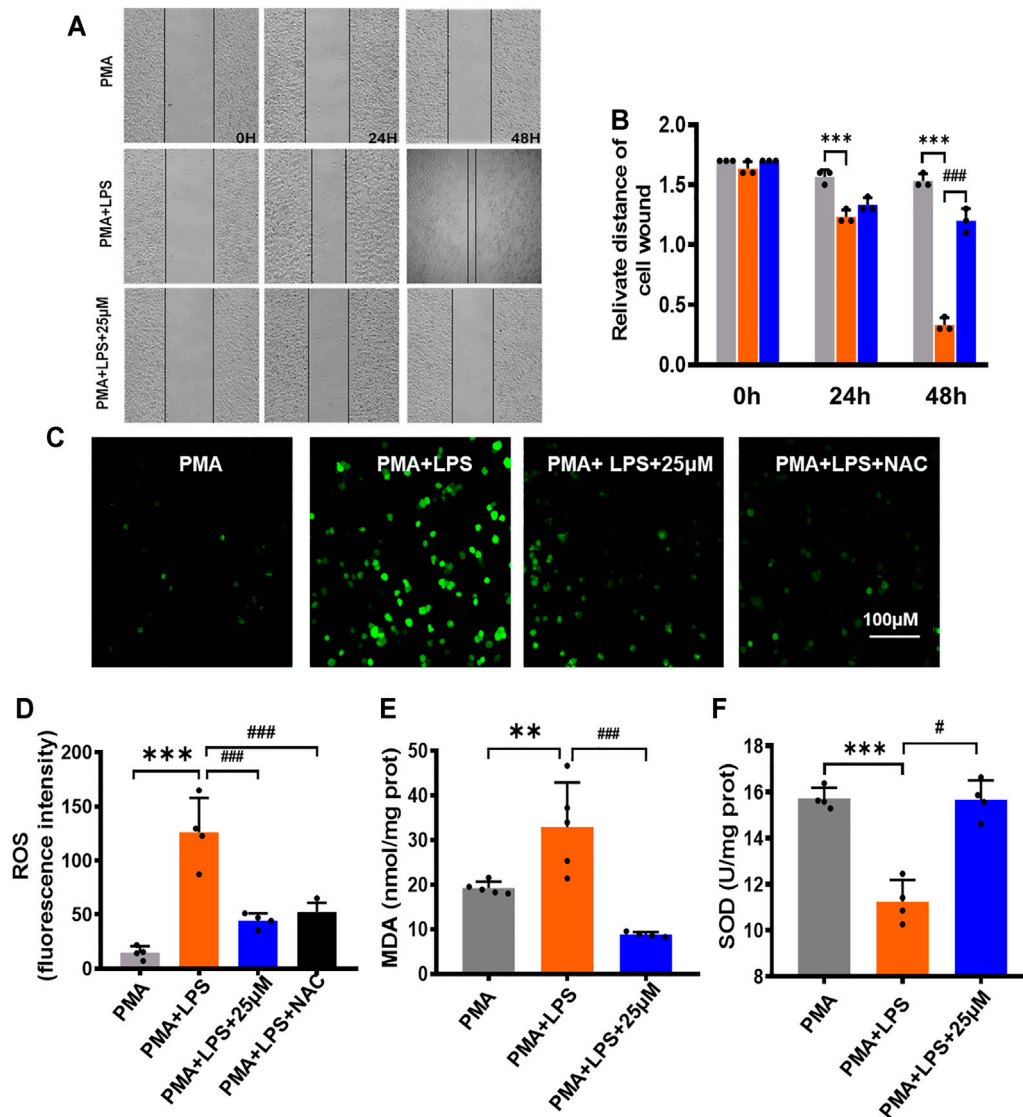


FIGURE 2 | Inhibitory effect of LHD on the oxidative stress and inflammatory cytokines in THP-1 macrophages. **(A)** 25 μ M LHD was co-incubated with LPS-induced THP-1 macrophages for 0, 24, and 48 h, and the cell migration capacity was detected by a cell scratch assay (20 \times). **(B)** Cell scratch width (cm), $N = 3$. **(C)** Representative graph of ROS levels (200 \times). Scale = 100 μ M. **(D)** Statistical graph of ROS levels, $N = 5$. **(E)** SOD activity, $N = 5$. **(F)** MDA content, $N = 4$ (** $p < 0.001$, ** $p < 0.01$ vs. the PMA group; # $p < 0.05$, ## $p < 0.01$, ### $p < 0.001$ vs. the LPS group).

RESULTS

Construction of THP-1 Macrophage Inflammation Model

THP-1 cells were induced with 100 ng/mL phorbol-12-myristate-13-acetate (PMA) for 0, 9, and 24 h (Reeves et al., 2015). At 0 h, the cells were suspended. At 9 h, some cells showed adherent state but no pseudopodia. At 24 h, the cells were all adherent to the wall, and most of them had pseudopodia sticking out, suggesting that THP-1 cells were differentiated into macrophages (Figure 1A) and the cell morphology at different time points was observed under a microscope (Figure 1B). Then,

the expression of CD68 mRNA was detected by qRT-PCR. Compared to that at 0 h, the increase of CD68 mRNA was the most obvious at 24 h, which was consistent with the observation results of cell morphology (Figure 1C). In order to detect the effect of LPS on the release of inflammatory cytokines (Ávila-Román et al., 2018), THP-1 macrophages were induced with 1 μ g/ml LPS for 12 h and 24 h and used qRT-PCR to detect the expression of IL-6 mRNA (Figure 1E). After LPS treatment for 12 and 24 h, the expression of IL-6 mRNA was significantly increased compared to that in the PMA group, and after LPS treatment for 24 h, the expression of IL-6 mRNA was nearly 500 times higher than that of the PMA

group. Therefore, we selected 1 $\mu\text{g/ml}$ LPS to stimulate the THP-1 macrophages for 24 h to conduct the following experiments.

Inhibitory Effect of Luhui Derivative on THP-1 Macrophage Release of Inflammatory Factors

We next explored whether the LHD impacted the THP-1 macrophage release of inflammatory factors. Before we assayed inflammatory factors, a CCK-8 assay was performed to reveal that the LHD had no effect on cell activity after co-incubation for 24 h at 6.25, 12.5, 25, and 50 $\mu\text{mol/L}$ (Supplementary Figure S1). Next, the effects of LHD on the release of inflammatory cytokines by THP-1 macrophages were detected by qRT-PCR. Compared to that in the LPS group, the expression of IL-6 mRNA in the groups with different doses of LHD was significantly reduced, and the three doses of 6.25, 12.5, and 25 $\mu\text{mol/L}$ showed concentration dependence, among which 25 $\mu\text{mol/L}$ showed the most obvious inhibitory effect (Figure 1F). In conclusion, 25 $\mu\text{mol/L}$ LHD could inhibit the THP-1 macrophage release of inflammatory factors.

Inhibitory Effect of Luhui Derivative on THP-1 Macrophage Migration Function

The migration of macrophages plays a positive role in pathogen clearance and wound healing. The relative migration distance of cells at each time point was observed by a scratch experiment, and the results are shown in Figures 2A,B. The inhibitory effect of the LPS+25 $\mu\text{mol/L}$ LHD group on lateral cell migration was most obvious at 48 h and showed that the LHD could inhibit the expression of the inflammatory response by inhibiting the migration of macrophages.

Inhibitory Effect of Luhui Derivative on the Oxidative Stress and Inflammatory Cytokines in THP-1 Macrophages

Inflammatory reactions can lead to an excessive increase in free radicals and superoxide anions. When THP-1 macrophages were treated with LPS for 24 h and treated with LPS+25 $\mu\text{mol/L}$ LHD for 24 h at the same time, compared to that in the PMA group, the total fluorescence expression of ROS in the LPS group increased (Figures 2C,D). However, other relevant indicators of oxidative stress were expressed as follows: MDA content increased statistically, but SOD activity decreased statistically. Compared to the LPS group, the LPS+25 $\mu\text{mol/L}$ LHD group had an inhibitory effect on the level of oxidative stress, which was reflected in the decrease of total ROS fluorescence expression, the decrease of MDA content, and the increase of SOD activity (Figures 2E,F).

Effects of Luhui Derivative on Animal Models of Myocardial Infarction

First, we assessed the average body temperature of each group of mice after treatment with different doses (6.25 mg/kg, 12.5 mg/kg, 25 mg/kg, 50 mg/kg) of LHD; compared to the normal body temperature at 37°C, it did not change much.

The average body temperature of mice in the 25 mg/kg group and the dextromethorphan (DXM) group was maintained at about 35°C, and the temperature of mice in the other concentration of the LHD group was maintained at about 34.5°C. The results showed that the LHD has a protective effect against stress physiological responses (Figure 3A). Next, we detected the changes of inflammatory cytokine IL-6 in the serum of mice in each group by ELISA (Figure 3B). It has been reported that LPS can cause multiple organ failure and even the death of the patient by triggering tissue infusion and increased release of pro-inflammatory mediators. So, in contrast with the control group, the LPS group had severe pulmonary edema by measuring the lung wet–dry weight ratio and body weight of mice (Figures 3C,D and Supplementary Figure S2). In addition, by observing lung tissue sections under the microscope, we found that the normal structure of the alveoli in the LPS group had disappeared, the capillaries in the alveolar wall were dilated and congested, and the edema of the alveolar interval was widened, accompanied by inflammatory cell infiltration, indicating that the LPS group had acute lung injury. Moreover, we revealed that the LPS group had hepatocyte swelling, neutrophil infiltration, and hepatocyte apoptosis on the liver tissue. However, when given different doses (6.25 mg/kg, 12.5 mg/kg, 25 mg/kg, 50 mg/kg) of LHD, the above-mentioned injury symptoms of lung and liver tissues in each group were significantly improved (Figure 3E).

Luhui Derivative Regulates the NLRP3 Inflammasome Signaling Pathway

According to reports in the literature, NLRP3 interacts with ASC and caspase-1 to activate the NLRP3 inflammasome and then cleaves the immature inflammatory factor pro-IL-1 β to mature and secrete it extracellularly, causing a series of inflammatory reactions. Next, we performed western blot to detect that the expression level of related protein in the LPS model group and LHD group (Figure 4A). The expression level of NLRP3 protein in the LPS model group was up-regulated, while the expression level of NLRP3 protein was significantly down-regulated after treatment with 25 $\mu\text{mol/L}$ LHD (Figure 4B). In contrast, the expression level of ASC protein did not change significantly before and after LPS or LHD administration (Figure 4C). Additionally, compared to those in the PMA group, the expression levels of IL-1 β and caspase-1 proteins in the LPS group were up-regulated, and the expression levels of IL-1 β and caspase-1 proteins were significantly down-regulated after treatment with 25 $\mu\text{mol/L}$ LHD. However, pro-caspase and pro-IL-1 β protein expression levels did not change significantly before and after LPS or LHD administration (Figures 4D,E). The results showed that the LHD down-regulated the expression of NLRP3, IL-1 β , and caspase-1 proteins, thereby mediating the NLRP3 inflammasome signaling pathway to exert anti-inflammatory effects.

Inhibitory Effect of Luhui Derivative on Inflammatory Cytokines in THP-1 Macrophages and Serum

The release of a large number of inflammatory cytokines and inflammatory mediators can lead to the occurrence of

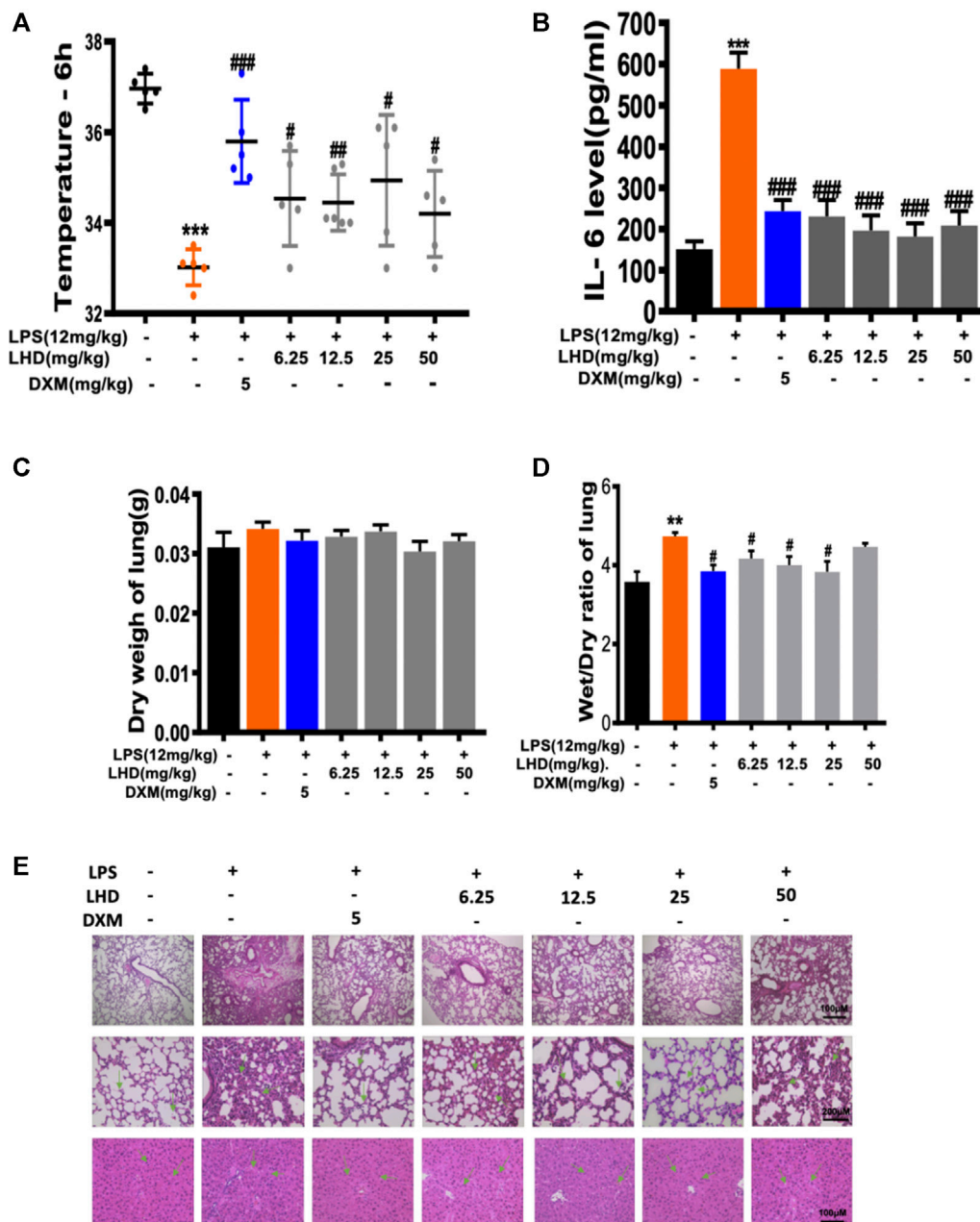


FIGURE 3 | Inhibitory effect of LHD on LPS inflammation *in vivo*. **(A)** Temperature record of mice after intraperitoneal injection of 12 mg/kg LPS for 6 h, besides the intragastric administration of different concentrations of LHD or 5 mg/kg DXM for 6 days, $N = 6$. **(B)** The IL-6 inflammatory cytokine was detected by ELISA. **(C)** Lung dry weight of mice, $N = 6$. **(D)** Lung wet-dry weight ratio of mice, $N = 6$. **(E)** H&E staining results of lung tissue and liver tissue, $N = 6$ (** $p < 0.01$, *** $p < 0.001$ vs. the PMA group; # $p < 0.05$, ## $p < 0.01$, ### $p < 0.001$ vs. the LPS group).

inflammatory diseases, such as diabetes, autoimmune diseases, and sepsis. Therefore, we investigated the changes of inflammatory cytokines (IL-6, IL-18, and IL-1 β) in THP-1 macrophages and serum of mice in each group by ELISA. The results showed that, after THP-1 macrophages were treated with LPS for 24 h, compared to that in the PMA group, the expression of inflammatory cytokines (IL-18 and IL-1 β) significantly increased. However, the IL-18 and IL-1 β expression levels were reduced when THP-1 macrophages were treated with

LPS+25 μ mol/L LHD for 24 h at the same time (**Figures 5A,B**). Next, we detected the content of inflammatory cytokines in the serum of mice. The results indicated that the LPS group was significantly higher than the control group after being infected with LPS for 6 h. On the contrary, compared to that in the LPS group, the expression of inflammatory cytokines in the serum of each group decreased significantly at different doses of LHD (6.25 mg/kg, 12.5 mg/kg, 25 mg/kg, 50 mg/kg) (**Figures 5C,D**). In conclusion, the results showed that the

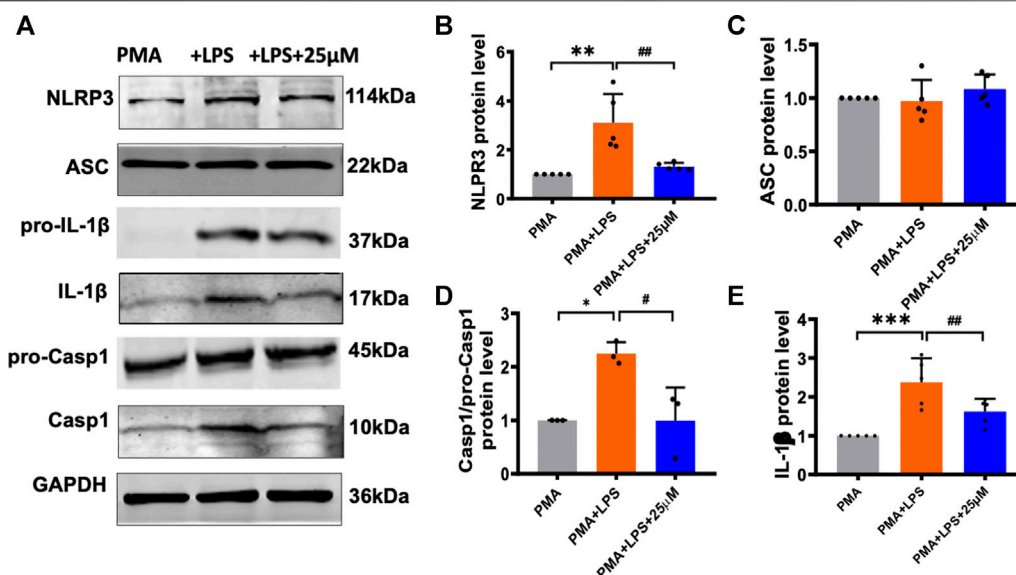


FIGURE 4 | LHD regulates the NLRP3 inflammasome signaling pathway. The THP-1 cells were pre-treated with 1 μ g/ml LPS for 24 h and subjected to 25 μ mol/L LHD for 24 h, and then the expression of NLRP3, ASC, caspase-1, and IL-1 β proteins was detected by western blot analysis. **(A)** Protein representation diagram. **(B)** Statistical map of NLRP3 protein level ($N = 5$; ** $p < 0.001$ vs. the PMA group; ## $p < 0.01$ vs. the LPS group). **(C)** Statistical graph of ASC protein. **(D)** Statistical map of caspase-1 protein level ($N = 3$; * $p < 0.05$ vs. the PMA group; # $p < 0.05$ vs. the LPS group). **(E)** Statistical map of IL-1 β protein levels ($N = 5$; *** $p < 0.001$ vs. the PMA group; ## $p < 0.01$ vs. the LPS group).

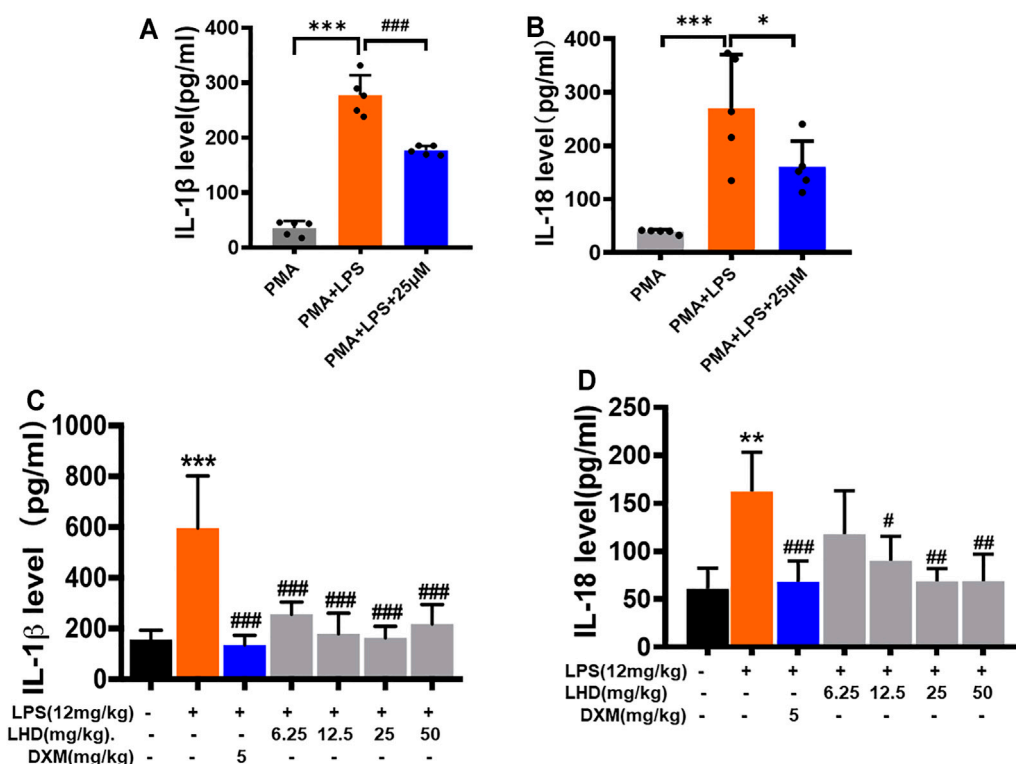


FIGURE 5 | Inhibitory effect of LHD on inflammatory cytokines in serum. **(A,B)** IL-1 β and IL-18 inflammatory cytokines were detected by ELISA, $N = 5$. **(C,D)** The different concentrations of LHD were co-incubated with LPS-induced THP-1 macrophages for 24 h, and the expression of IL-1 β and IL-18 was detected by ELISA, $N = 4$ (** $p < 0.01$, *** $p < 0.001$ vs. the PMA group; # $p < 0.05$, ## $p < 0.01$, ### $p < 0.001$ vs. the LPS group).

LHD could inhibit the high expression of inflammatory cytokines caused by LPS.

DISCUSSION

Inflammatory response is an important immune defense mechanism in the human body, which helps the body to resist pathogenic microbial infection (Medzhitov, 2008). However, the imbalance of inflammatory response can also lead to tissue and organ damage, thus promoting the occurrence of diseases. Inflammatory responses can be stimulated by a variety of sensors, for example, pathogenic microorganisms can stimulate the TLR (Toll-like receptor) family to mediate the inflammatory response (Ko et al., 2020). In addition, physical, chemical, and other harmful stimuli can also induce the secretion of inflammatory mediators and cytokines in the body via mediating pressure receptors, temperature receptors, and other signal transduction to cells, so as to induce the body to produce an inflammatory response. In this study, we uncovered a functional role of LHD inhibiting the THP-1 macrophage release of inflammatory factors via regulating the NLRP3 inflammasome signaling pathway.

It has been reported that aloe-emodin has antibacterial (Ji et al., 2020), antiviral (Xu et al., 2021), hepatoprotective (Zheng et al., 2019), anti-inflammatory (Chen et al., 2020), and anticancer (Galiardi-Campoy et al., 2021) pharmacological functions and has a broad clinical application prospect. For example, aloe-emodin inhibits the growth of A375.S2 cells by inhibiting the mRNA expression and enzyme activity of N-acetyltransferase (Lin et al., 2005). Tao et al. also found that aloe-emodin plays a neuroprotective role in Alzheimer's disease by reducing the release of NO, lactate dehydrogenase, and intracellular ROS to regulate oxidative stress response (Tao et al., 2014). However, long-term and high-dose use of aloe-emodin may result in high toxicity, poor intestinal absorption, short half-life, and low bioavailability. For example, Vath et al. showed that exposure of human skin fibroblasts to aloe-emodin and ultraviolet radiation causes significant phototoxicity (Vath et al., 2002). Zaffaroni et al. also showed that, after intraperitoneal injection of aloe-emodin at a dose of 20 mg/kg, it rapidly distributes and disappears from the plasma, when a terminal half-life of 78 min was measured (Zaffaroni et al., 2003). Therefore, further optimization is needed to improve the problem of high toxicity of emodin anthraquinone-type compounds.

NLRP3 inflammasome is a novel high-molecular-weight protein complex whose activation can promote the process of inflammation (Kelley et al., 2019). In recent years, relevant studies have shown that it is involved in the occurrence of a variety of major human diseases such as type 2 diabetes (Rovira-Llopis et al., 2018), gout (Goldberg et al., 2017), Parkinson's disease (Wang et al., 2019), and fatty liver disease (Zhang et al., 2018). Therefore, it may become a potential intervention target of the above diseases. When NLRP3 inflammasome activation is inhibited, its secretion and release of inflammatory factors such as IL-1 β and IL-18 are reduced to play an anti-inflammatory role. Therefore, activation of NLRP3 inflammasome becomes a new signaling pathway to prevent and treat inflammatory diseases. It has been reported in the

literature that knockout of NLRP3 gene not only can inhibit the activation of NLRP3 inflammasomes *in vivo* but also can reduce the septic shock caused by LPS (Xu et al., 2018). Based on the above study, we detected LPS-induced NLRP3 inflammasome activation at the macrophage level and determined that the LHD plays a role in regulating NLRP3 inflammasomes by down-regulating NLRP3, caspase-1, and IL-1 β protein expressions. At the same time, we predicted the target of LHD on NLRP3 by AutoDock software, and subsequent experiments are required to verify the specific role of its target.

On the one hand, our results showed that 25 μ M of LHD significantly inhibited cell migration and IL-1 β and IL-18 expressions *in vitro*. Thus, the LHD can play an anti-inflammatory role by inhibiting macrophage migration and inflammatory cytokine expression. On the other hand, 25 μ M LHD can also significantly inhibit ROS and MDA levels and increase SOD activity, showing the inhibitory effect of LHD on oxidative stress response, and can also inhibit the increase of IL-6 inflammatory factor expression caused by LPS in a dose-dependent manner. *In vivo*, different doses of LHD (6.25, 12.5, 25, and 50 mg/kg) can reduce the increase of IL-6, IL-1 β and IL-18 inflammatory factors in serum and the increase of lung wet-to-dry weight ratio in LPS model after preventive treatment, and the three dose groups of 6.25, 12.5, and 25 mg/kg showed a dose dependent trend, and the decrease was more significant with the increase of dose. At the same time, different doses of LHD can also significantly alleviate the pathological injury of lung and liver tissues and the physiological reaction of hypothermia. It is worth mentioning that, in this study, the low dose of LHD was observed at 6.25 μ M or 6.25 mg/kg. Again, the anti-inflammatory effects of emodin derivatives of aloe vera *in vitro* and *in vivo* are described.

The LHD is a new compound which has been chemically modified. It has better anti-inflammatory and antibacterial activity, lower toxicity, and easier absorption than aloe-emodin. However, whether the LHD can specifically inhibit the activation of NLRP3 inflammasomes remains to be further studied in subsequent experiments. Clarifying the specific relationship between the LHD and NLRP3 inflammasomes will provide new ideas for the research and development of other anti-inflammatory drugs.

DATA AVAILABILITY STATEMENT

The raw data supporting the conclusions of this article will be made available by the authors, without undue reservation.

ETHICS STATEMENT

The animal study was reviewed and approved by the Harbin Medical University.

AUTHOR CONTRIBUTIONS

BF was involved in the analysis and interpretation of data. BF, XZ, WZ, HJ, ZR, and YC were responsible for acquisition of data. YY

and ZD conceptualized and designed the study. BF, YY, and ZD wrote the manuscript. All authors read and approved the final manuscript.

FUNDING

This work was supported by the National Natural Science Fund of China (82073838) and the special funds for Scientific Research

REFERENCES

- Alshatwi, A. A., and Subash-Babu, P. (2016). Aloe-Emodin Protects RIN-5F (Pancreatic β -Cell) Cell from Glucotoxicity via Regulation of Pro-Inflammatory Cytokine and Downregulation of Bax and Caspase 3. *Biomol. Ther.* 24 (1), 346–356. doi:10.4062/biomolther.2016.346
- Ávila-Román, J., Talero, E., de Los Reyes, C., García-Mauriño, S., and Motilva, V. (2018). Microalgae-derived Oxylipins Decrease Inflammatory Mediators by Regulating the Subcellular Location of NF κ B and PPAR- γ . *Pharmacol. Res.* 128, 220–230. doi:10.1016/j.phrs.2017.10.009
- Carestia, A., Mena, H. A., Olexen, C. M., Ortiz Wilczyński, J. M., Negrotto, S., Errasti, A. E., et al. (2019). Platelets Promote Macrophage Polarization Toward Pro-Inflammatory Phenotype and Increase Survival of Septic Mice. *Cell Rep.* 28 (4), 896–905.e5. doi:10.1016/j.celrep.2019.06.062
- Chen, Y., Feng, B., Yuan, Y., Hu, J., Zhao, W., Jiang, H., et al. (2020). Aloe Emodin Reduces Cardiac Inflammation Induced by a High-Fat Diet through the TLR4 Signaling Pathway. *Mediators Inflamm.* 2020, 6318520. doi:10.1155/2020/6318520
- Cullis, J., Siolas, D., Avanzi, A., Barui, S., Maitra, A., and Bar-Sagi, D. (2017). Macropinocytosis of Nab-Paclitaxel Drives Macrophage Activation in Pancreatic Cancer. *Cancer Immunol. Res.* 5 (3), 182–190. doi:10.1158/2326-6066.CIR-16-0125
- Foster, S. L., and Medzhitov, R. (2009). Gene-specific Control of the TLR-Induced Inflammatory Response. *Clin. Immunol.* 130 (1), 7–15. doi:10.1016/j.clim.2008.08.015
- Fuchs, A. K., Syrovets, T., Haas, K. A., Loos, C., Musyanovych, A., Mäiländer, V., et al. (2016). Carboxyl- and Amino-Functionalized Polystyrene Nanoparticles Differentially Affect the Polarization Profile of M1 and M2 Macrophage Subsets. *Biomaterials* 85, 78–87. doi:10.1016/j.biomaterials.2016.01.064
- Furtado, A. A., Torres-Rêgo, M., Lima, M. C. J. S., Bitencourt, M. A. O., Estrela, A. B., Souza da Silva, N., et al. (2016). Aqueous Extract from Ipomoea Asarifolia (Convolvulaceae) Leaves and its Phenolic Compounds Have Anti-inflammatory Activity in Murine Models of Edema, Peritonitis and Air-Pouch Inflammation. *J. Ethnopharmacol.* 192, 225–235. doi:10.1016/j.jep.2016.07.048
- Galiardi-Campoy, A. E. B., Machado, F. C., Carvalho, T., Tedesco, A. C., Rahal, P., and Calmon, M. F. (2021). Effects of Photodynamic Therapy Mediated by Emodin in Cervical Carcinoma Cells. *Photodiagnosis Photodyn Ther.* 35, 102394.
- Gao, H., Liu, X., Sun, W., Kang, N., Liu, Y., Yang, S., et al. (2017). Total Tanshinones Exhibits Anti-inflammatory Effects through Blocking TLR4 Dimerization via the MyD88 Pathway. *Cell Death Dis* 8 (8), e3004. doi:10.1038/cddis.2017.389
- Goldberg, E. L., Asher, J. L., Molony, R. D., Shaw, A. C., Zeiss, C. J., Wang, C., et al. (2017). β -Hydroxybutyrate Deactivates Neutrophil NLRP3 Inflammasome to Relieve Gout Flares. *Cel Rep* 18 (9), 2077–2087. doi:10.1016/j.celrep.2017.02.004
- Goodman, C. W., and Brett, A. S. (2017). Gabapentin and Pregabalin for Pain - Is Increased Prescribing a Cause for Concern. *N. Engl. J. Med.* 377 (5), 411–414. doi:10.1056/NEJMp1704633
- Headland, S. E., and Norling, L. V. (2015). The Resolution of Inflammation: Principles and Challenges. *Semin. Immunol.* 27 (3), 149–160. doi:10.1016/j.smim.2015.03.014

Transformation of Heilongjiang Academy of Medical Sciences (CR201814).

SUPPLEMENTARY MATERIAL

The Supplementary Material for this article can be found online at: <https://www.frontiersin.org/articles/10.3389/fphar.2021.719822/full#supplementary-material>

- Hu, B., Zhang, H., Meng, X., Wang, F., and Wang, P. (2014). Aloe-emodin from Rhubarb (*Rheum rhabarbarum*) Inhibits Lipopolysaccharide-Induced Inflammatory Responses in RAW264.7 Macrophages. *J. Ethnopharmacol.* 153 (3), 846–853. doi:10.1016/j.jep.2014.03.059
- Ji, C., Xin, G., Duan, F., Huang, W., and Tan, T. (2020). Study on the Antibacterial Activities of Emodin Derivatives against Clinical Drug-Resistant Bacterial Strains and Their Interaction with Proteins. *Ann. Transl. Med.* 8 (4), 92. doi:10.21037/atm.2019.12.100
- Karim, N., Khan, I., Khan, W., Khan, I., Khan, A., Halim, S. A., et al. (2019). Anti-nociceptive and Anti-inflammatory Activities of Asparacosin A Involve Selective Cyclooxygenase 2 and Inflammatory Cytokines Inhibition: An *In-Vitro*, *In-Vivo*, and *In-Silico* Approach. *Front. Immunol.* 10, 581. doi:10.3389/fimmu.2019.00581
- Kelley, N., Jeltama, D., Duan, Y., and He, Y. (2019). The NLRP3 Inflammasome: An Overview of Mechanisms of Activation and Regulation. *Int. J. Mol. Sci.* 20 (13), 3328. doi:10.3390/ijms2013328
- Ko, H. K., Lin, A. H., Perng, D. W., Lee, T. S., and Kou, Y. R. (2020). Lung Epithelial TRPA1 Mediates Lipopolysaccharide-Induced Lung Inflammation in Bronchial Epithelial Cells and Mice. *Front. Physiol.* 11, 596314. doi:10.3389/fphys.2020.596314
- Lin, S. Y., Yang, J. H., Hsia, T. C., Lee, J. H., Chiu, T. H., Wei, Y. H., et al. (2005). Effect of Inhibition of Aloe-Emodin on N-Acetyltransferase Activity and Gene Expression in Human Malignant Melanoma Cells (A375.S2). *Melanoma Res.* 15 (6), 489–494. doi:10.1097/00008390-200512000-00002
- Medzhitov, R. (2008). Origin and Physiological Roles of Inflammation. *Nature* 454 (7203), 428–435. doi:10.1038/nature07201
- Mu, L., and Zhi-min, D. (2015). Research Progress on Pharmacological Effects of Aloe-Emodin. *Chin. J. Clin. Pharmacol.* 31 (9), 765–768. doi:10.13699/j.cnki.1001-6821.2015.09.027
- Murray, P. J., and Smale, S. T. (2012). Restraint of Inflammatory Signaling by Interdependent Strata of Negative Regulatory Pathways. *Nat. Immunol.* 13 (10), 916–924. doi:10.1038/ni.2391
- Perez, D. A., and Vago, J. P. (2014). Switching Off Key Signaling Survival Molecules to Switch on the Resolution of Inflammation. *Mediators Inflamm.* 2014, 829851. doi:10.1155/2014/829851
- Reeves, A. R., Spiller, K. L., Freytes, D. O., Vunjak-Novakovic, G., and Kaplan, D. L. (2015). Controlled Release of Cytokines Using Silk-Biomaterials for Macrophage Polarization. *Biomaterials* 73, 272–283. doi:10.1016/j.biomaterials.2015.09.027
- Rovira-Llopis, S., Apostolova, N., Bañuls, C., Muntané, J., Rocha, M., and Victor, V. M. (2018). Mitochondria, the NLRP3 Inflammasome, and Sirtuins in Type 2 Diabetes: New Therapeutic Targets. *Antioxid. Redox Signal.* 29 (8), 749–791. doi:10.1089/ars.2017.7313
- Skirecki, T., and Cavaillon, J. M. (2019). Inner Sensors of Endotoxin - Implications for Sepsis Research and Therapy. *FEMS Microbiol. Rev.* 43 (3), 239–256. doi:10.1093/femsrev/fuz004
- Su, L., Zhang, W., Wu, X., Zhang, Y., Chen, X., Liu, G., et al. (2015). Glycocalyx-Mimicking Nanoparticles for Stimulation and Polarization of Macrophages via Specific Interactions. *Small* 11 (33), 4191–4200. doi:10.1002/sml.201403838
- Tandon, A., Harioudh, M. K., Ishrat, N., Tripathi, A. K., Srivastava, S., and Ghosh, J. K. (2018). An MD2-derived Peptide Promotes LPS Aggregation, Facilitates its Internalization in THP-1 Cells, and Inhibits LPS-Induced Pro-inflammatory Responses. *Cell Mol Life Sci* 75 (13), 2431–2446. doi:10.1007/s00018-017-2735-2

- Tao, L., Xie, J., Wang, Y., Wang, S., Wu, S., Wang, Q., et al. (2014). Protective Effects of Aloe-Emodin on Scopolamine-Induced Memory Impairment in Mice and H₂O₂-induced Cytotoxicity in PC12 Cells. *Bioorg. Med. Chem. Lett.* 24 (23), 5385–5389. doi:10.1016/j.bmcl.2014.10.049
- Vath, P., Wamer, W. G., and Falvey, D. E. (2002). Photochemistry and Phototoxicity of Aloe Emodin. *Photochem. Photobiol.* 75 (4), 346–352. doi:10.1562/0031-8655(2002)075<0346:papoae>2.0.co;2
- Wang, S., Yuan, Y. H., Chen, N. H., and Wang, H. B. (2019). The Mechanisms of NLRP3 Inflammasome/pyroptosis Activation and Their Role in Parkinson's Disease. *Int. Immunopharmacol.* 67, 458–464. doi:10.1016/j.intimp.2018.12.019
- Wang, Y., Shan, X., Chen, G., Jiang, L., Wang, Z., Fang, Q., et al. (2015). MD-2 as the Target of a Novel Small Molecule, L6H21, in the Attenuation of LPS-Induced Inflammatory Response and Sepsis. *Br. J. Pharmacol.* 172 (17), 4391–4405. doi:10.1111/bph.13221
- Widdrington, J. D., Gomez-Duran, A., Pyle, A., Ruchaud-Sparagano, M. H., Scott, J., Baudouin, S. V., et al. (2018). Exposure of Monocytic Cells to Lipopolysaccharide Induces Coordinated Endotoxin Tolerance, Mitochondrial Biogenesis, Mitophagy, and Antioxidant Defenses. *Front. Immunol.* 9, 2217. doi:10.3389/fimmu.2018.02217
- Xu, C., Lu, Z., Luo, Y., Liu, Y., Cao, Z., Shen, S., et al. (2018). Targeting of NLRP3 Inflammasome with Gene Editing for the Amelioration of Inflammatory Diseases. *Nat. Commun.* 9 (1), 4092. doi:10.1038/s41467-018-06522-5
- Xu, Z., Huang, M., Xia, Y., Peng, P., Zhang, Y., Zheng, S., et al. (2021). Emodin from Aloe Inhibits Porcine Reproductive and Respiratory Syndrome Virus via Toll-Like Receptor 3 Activation. *Viruses* 13 (7), 1243. doi:10.3390/v13071243
- Yang, J. X., Hsiung, T. C., Weng, F. C., Ding, S. L., Wu, C. P., Conti, M., et al. (2018). Synergistic Effect of Phosphodiesterase 4 Inhibitor and Serum on Migration of Endotoxin-Stimulated Macrophages. *Innate Immun.* 24 (8), 501–512. doi:10.1177/1753425918809155
- Yang, Q., Pröll, M. J., Salilew-Wondim, D., Zhang, R., Tesfaye, D., Fan, H., et al. (2016). LPS-Induced Expression of CD14 in the TRIF Pathway is Epigenetically Regulated by Sulforaphane in Porcine Pulmonary Alveolar Macrophages. *Innate Immun.* 22 (8), 682–695. doi:10.1177/1753425916669418
- Zaffaroni, M., Mucignat, C., Pecere, T., Zagotto, G., Frapolli, R., D'Incalci, M., et al. (2003). High-performance Liquid Chromatographic Assay for the Determination of Aloe Emodin in Mouse Plasma. *J. Chromatogr. B Analyt. Technol. Biomed. Life Sci.* 796 (1), 113–119. doi:10.1016/j.jchromb.2003.08.012
- Zhang, B., Xu, D., She, L., Wang, Z., Yang, N., Sun, R., et al. (2018). Silybin Inhibits NLRP3 Inflammasome Assembly through the NAD⁺/SIRT2 Pathway in Mice with Nonalcoholic Fatty Liver Disease. *FASEB J.* 32 (2), 757–767. doi:10.1096/fj.201700602R
- Zheng, X. Y., Yang, S. M., Zhang, R., Wang, S. M., Li, G. B., and Zhou, S. W. (2019). Emodin-Induced Autophagy against Cell Apoptosis through the PI3K/AKT/mTOR Pathway in Human Hepatocytes. *Drug Des. Devel. Ther.* 13, 3171–3180. doi:10.2147/DDDT.S204958

Conflict of Interest: The authors declare that the research was conducted in the absence of any commercial or financial relationships that could be construed as a potential conflict of interest.

Publisher's Note: All claims expressed in this article are solely those of the authors and do not necessarily represent those of their affiliated organizations, or those of the publisher, the editors, and the reviewers. Any product that may be evaluated in this article, or claim that may be made by its manufacturer, is not guaranteed or endorsed by the publisher.

Copyright © 2021 Feng, Zhao, Zhao, Jiang, Ren, Chen, Yuan and Du. This is an open-access article distributed under the terms of the Creative Commons Attribution License (CC BY). The use, distribution or reproduction in other forums is permitted, provided the original author(s) and the copyright owner(s) are credited and that the original publication in this journal is cited, in accordance with accepted academic practice. No use, distribution or reproduction is permitted which does not comply with these terms.



Analgesic and Anti-Arthritic Activities of Polysaccharides in *Chaenomeles speciosa*

Doudou Huang^{1,2†}, Shenggui Jiang^{1†}, Zenan Du^{1†}, Yanhong Chen^{3†}, Dan Xue¹,
Xiujuan Wang¹, Mengshuang Li¹, Feng Zhang^{3*}, Wansheng Chen^{2,3*} and Lianna Sun^{1*}

¹Department of TCM Processing, Shanghai University of Traditional Chinese Medicine, Shanghai, China, ²Institute of Chinese Materia Medica, Shanghai University of Traditional Chinese Medicine, Shanghai, China, ³School of Pharmacy, Changzheng Hospital, Navy Military Medical University, Shanghai, China

OPEN ACCESS

Edited by:

Xiao Bin Zeng,
Jinan University, China

Reviewed by:

Jianxin Chen,
Beijing University of Chinese Medicine,
China
Amira Abo-Youssef,
Beni Suef University, Egypt

*Correspondence:

Feng Zhang
zhangfengky@aliyun.com
Wansheng Chen
chenwansheng@smmu.edu.cn
Lianna Sun
sssnmr@163.com

[†]These authors have contributed
equally to this work

Specialty section:

This article was submitted to
Ethnopharmacology,
a section of the journal
Frontiers in Pharmacology

Received: 21 July 2021

Accepted: 07 March 2022

Published: 24 March 2022

Citation:

Huang D, Jiang S, Du Z, Chen Y,
Xue D, Wang X, Li M, Zhang F, Chen W
and Sun L (2022) Analgesic and Anti-
Arthritic Activities of Polysaccharides in
Chaenomeles speciosa.
Front. Pharmacol. 13:744915.
doi: 10.3389/fphar.2022.744915

Chaenomeles speciosa (Sweet) Nakai has been long used as a folk medicine for rheumatic diseases treatment. This study aimed to investigate the effects and underlying mechanism of polysaccharides in *Chaenomeles speciosa* (CSP) on the pro-inflammatory cytokines and MAPK pathway in complete Freund's adjuvant (CFA)-induced arthritis and LPS-induced NR8383 cells. We used acetic acid (HAc)-induced writhing and CFA induced paw edema to determine the analgesic activity and anti-inflammatory activity, respectively. CFA rats were administered CSP (12.5, 25.0, and 50.0 mg/kg) daily for 3 weeks *via* oral gavage. The analgesic test was done using three different doses of the extract (50, 100, and 200 mg/kg). The anti-arthritic evaluation involved testing for paw swelling, swelling inhibition, and histological analysis in CFA rats. Finally, ELISA, western blot, qRT-PCR were done to determine the effect of CSP on the activation of MAPK pathway, production of pro-inflammatory cytokines in lipopolysaccharide (LPS)-stimulated NR8383 macrophage cells. In pain models, oral uptake of CSP greatly reduced pain perception. Furthermore, in CFA rats, CSP substantially decreased paw swelling as well as synovial tissue proliferation and inflammatory cell infiltration. In addition, CSP was shown to inhibit pro-inflammatory cytokines (TNF- α , IL-1 β , and COX-2) as well as JNK and ERK1/2 phosphorylation in LPS-stimulated NR8383 cells. Thus, pro-inflammatory cytokine secretion and MAPK signaling downregulation promoted the analgesic and anti-arthritic effects of CSP.

Keywords: *Chaenomeles speciosa*, polysaccharides, anti-arthritic, analgesic, MAPK

INTRODUCTION

Rheumatoid arthritis (RA) is a chronic autoimmune disease, with the pathological features of synovial tissue hyperplasia, pannus formation and cartilage erosion. The typical clinical features of RA are joint swelling, pain, and irreversible joints damage, which eventually lead to severe disability (Bang et al., 2009). Because of the characteristics of high disability rate, poor prognosis, and easy recurrence of RA, it causes heavy economic burden to the patient's family. Previous study suggested the global incidence of RA is about 0.5–1.0%, with the highest incidence in 30–50 years old (Chung et al., 2016). However, the pathogenesis of RA is still unclear, and the clinical treatment of RA is mainly chemical drugs, such as non-steroidal anti-inflammatory drugs (NSAID), anti-rheumatic drugs (ARD), glucocorticoids, etc (Smolen et al., 2016). Nevertheless, these treatments are expensive, and long-term use of chemical drugs can cause a variety of adverse reactions, such as cardiovascular

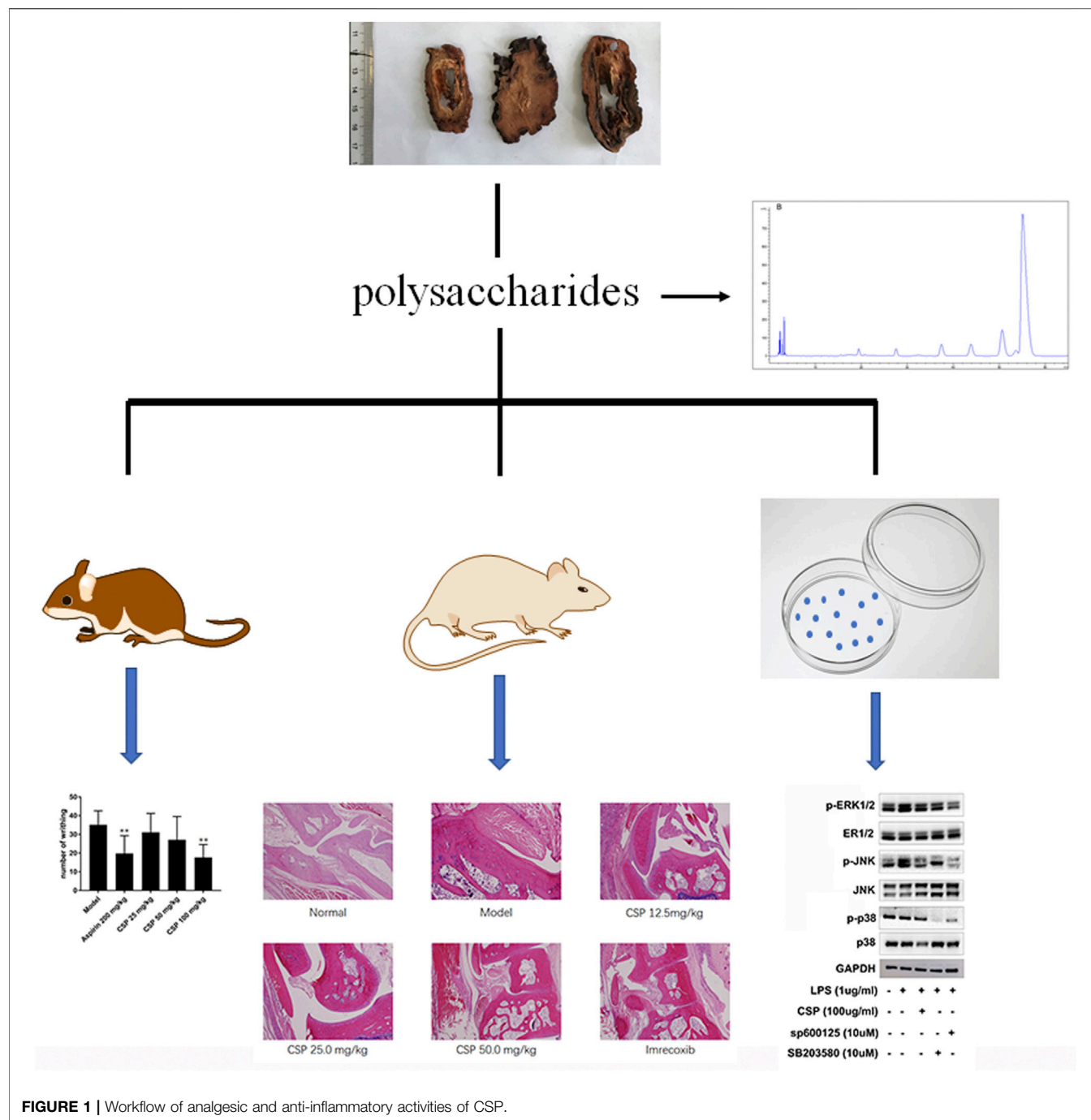


FIGURE 1 | Workflow of analgesic and anti-inflammatory activities of CSP.

disease, gastrointestinal bleeding, liver and kidney toxicity, growth inhibition, infection, and tumor risks (Urushibara et al., 2004; Andersson et al., 2008; Grosser, 2017; Chen et al., 2018).

As the number of RA patients increases year by year, people are eager to looking for alternative drugs that are inexpensive, safe and effective, and have fewer adverse reactions to treat RA. Traditional Chinese medicine has received more and more attention because of its remarkable curative effect and few adverse reactions (Newman and Cragg, 2016; Luo et al., 2019).

As a class of natural macromolecular substances, polysaccharides have obvious advantages and can exert a wide range of pharmacological effects by participating in the body's physiological reaction, such as anti-oxidation, hypoglycemic, immune regulation, anti-tumor, anti-inflammatory and other biological activities (Zou and Zhang, 2015).

Chaenomeles speciosa (Sweet) Nakai belongs to Rosaceae, mainly distributed in China and Myanmar, and it has been long used as food and medicine in China. Modern pharmacological studies have shown that *C. speciosa* has a

variety of biological activities, including immune regulation, anti-inflammatory, anti-tumor, antibacterial and antioxidant effects. As a common medicinal and edible plant, *C. speciosa* is rich in polysaccharides. At present, it has been reported that polysaccharides in *C. speciosa* have antioxidant and anti-inflammatory activities (Li and Chen, 2011; Xie et al., 2015). However, the anti-inflammatory mechanism of *C. speciosa* polysaccharide is not clear.

Here, we examined the potential medicinal effects of CSP against Complete Freund's Adjuvant (CFA)-induced inflammation in an arthritic rat model. Additionally, we used LPS-induced NR8383 cells to examine the role of CSP in inflammation. The results showed that CSP exhibited anti-RA activity by suppressing the activation of mitogen-activated protein kinase (MAPK) pathway (Figure 1).

MATERIALS AND METHODS

Preparation of CSP Extract

We collected the fruits of *C. speciosa* from Bozhou, Anhui Province, China, in October 2014 (authenticated by Prof. Hanming Zhang). A voucher specimen (No. CS20141008) for *C. speciosa* fruit was submitted to the authors' laboratory. We performed hot water extraction of the fruits of *C. speciosa* (100 kg; 1:15), followed by deproteinization using 15% trichloroacetic acid, and precipitation with 70% ethanol. After centrifugation, the precipitate was collected to obtain the crude polysaccharide. The total carbohydrate content of the polysaccharides was determined by the phenol-sulfuric acid method with glucose as standard, and determined the content was 52.97%.

Monosaccharide Compositions Assays

Mannose (B25303), rhamnose (YY91163), galacturonic acid (B21894), glucose (B21882), galactose (YY91011), and arabinose (B25845) were purchased from Shanghai Yuanye Bio-Technology Co., Ltd. PMP (1-phenyl-3-methyl-5-pyrazolone) pre-column derivatization combined with high performance liquid chromatography (HPLC) were used to determine the monosaccharide compositions of CSP (Cao et al., 2019). The polysaccharide (1.0 mg/ml) was hydrolyzed using 4 M trifluoroacetic acid (TFA) at 110°C for 6 h. The residual TFA was obtained by evaporating the residue under reduced pressure in methanol (2 ml). The hydrolysate and the hybrid standard monosaccharide solution (100 µl, glucose, D-mannose, D-galactose, xylose, maltose, L-arabinose, all 1 mg/ml) were dissolved in 200 µl water; the supernatant was mixed with PMP and 0.3 M NaOH solutions. The reaction was carried out at 70°C for 45 min before being stopped using an HCl solution. The reaction product was removed thrice with chloroform, and the upper layer was centrifuged, and filtered using a 0.22 µm membrane, followed by HPLC analysis. We used the Agilent Eclipse XDB-C18 chromatographic column (30°C), equipped with a UV-detector. The mobile phase was PBS (pH 6.8) mixed with acetonitrile (87: 13) and eluted isocratically for 60 min.

Animals and Experimental Design

We purchased the Sprague-Dawley (SD) (Male, weight: 120–140 g) rats from the Laboratory Animal Research Center at the Second Military Medical University (SCXK (hu) 2017-0010). The animal study was reviewed and approved by the Animal Ethic Committee of Second Military Medical University (No.CZ201705126) in the accordance with the National Institutes of Health guidelines for animal care. These animals were freely access to food/water and were hosted in rat cages at (24 ± 2)°C, 12 h:12 h light/dark cycle, 40–70% humidity.

Our experimental protocols followed the guidelines of the Animal Guidelines of Second Military Medical University. We followed a previously described method to establish the CFA-induced arthritis model in SD rats (Gupta et al., 2020). First, we measured the volume of the foot (reference), and then intradermally injected CFA (0.1 ml) into the foot pad and recorded as day 0. On day 7, the immunized rats were divided into five group, and then the five groups were administrated with saline (model group), 12.5 mg/kg CSP (low-dose group), 25.0 mg/kg CSP (middle-dose group), 50.0 mg/kg CSP (high-dose group), and 20.0 mg/kg imrecoxib (positive control group) via oral gavage, respectively from day 8. Another 10 non-immunized rats were treated with saline ("the control group"). Each group had 10 rats who were treated daily for 3 weeks.

Paw Edema Measurement

After treatment initiation, foot volume was measured every 3 days and each time the joints were marked based on the initial measurement. The swelling degree and swelling inhibition were calculated based on the swelling volume as follows:

Swelling degree (ΔmL) = paw volume after inflammation—paw volume before inflammation.

Swelling inhibition rate (%) = (paw volume in model group—paw volume in the treatment group)/paw volume in model group × 100%

Serum Pro-Inflammatory Cytokines Analysis

The pro-inflammatory cytokines in serum, including TNF- α , COX-2, and IL-1 β were measured by ELISA kits (Jiancheng Bioengineering, Nanjing, China) according to the manufacturer's instructions.

Histopathological Analysis

On day 29, we used isoflurane to sacrifice the rats. The legs below the knee joints (together with the feet) were simultaneously excised, fixed with 10% formalin, and treated with 5% formic acid. The paraffin-embedded tissues were sectioned, stained with H&E stain, and analyzed histopathologically.

Acetic Acid (Hac)-Induced Writhing

The KM mice (male, weight 23 ± 0.5 g) were purchased from the Laboratory Animal Research Center at the Second Military Medical University and hosted under identical conditions as the SD rats.

The KM mice were divided into five groups ($n = 10$ each): model, aspirin (positive group, 200 mg/kg), low-dose (25 mg/kg CSP), medium-dose (50 mg/kg CSP), and high-dose (100 mg/kg CSP). The animals were administered respective treatments daily for 5 days, and 1 h post-administration, each group was intraperitoneally injected with HAc (10 mg/ml) and observed and recorded for 15 min (Tadiwos et al., 2017).

The following formulas were used to calculate the number of writhing turnovers of the mice in the group, and the writhing inhibition rate:

$$\text{Writhing Inhibition Rate (\%)} = (N_1 - N_2) / N_1 \times 100\%$$

N_1 : Number of writhing in model group; N_2 : Number of writhing in CSP group.

Cell Culture

We cultured NR8383 murine macrophage cells (Institute of Biochemistry and Cell Biology, Shanghai) in high-glucose DMEM with 10% FBS and 1% antibiotics at 37°C in 5% CO₂. The CCK-8 assay was used to determine the cytotoxicity of CSP (25.0, 50.0, 100.0, and 200.0 µg/ml) (Yu et al., 2020).

Determination of mRNA Levels of Cytokines

The Total RNA Kit was used to isolate total RNA from the spleen tissues, followed by quantification via the µ Drop Plate (Thermo scientific, Finland). A Revertaid First Strand cDNA Synthesis Kit was used to synthesize cDNA, followed by qRT-PCR using a SYBR Green Master Mix using corresponding primers for cytokines. The primer sequences were as follows: TNF-α (F) 5'-GGGGCCACCACGCTCTTCTGTCTA-3'; (R) 5'-CCTCCGCTTGGTGGTTTGCTACG-3'), IL-1β (F) 5'-CCTCTGTGACTCGTGGGATGATG-3'; (R) 5'-CAGGGATTTTGTGCTTGCTTGCT-3'), COX-2 (F) 5'-CTGGTGCCGGTCTGATGATGTA-3'; (R) 5'-AGCAGGTGTGGGTGCAACTTGAG-3'), β-actin (F) 5'-CCTAAGGCCAACCGTGAAAAGATG-3'; (R) 5'-GTCCCGGCCAGCCAGGTCAG-3'). The following PCR conditions were used: pre-denaturation for 5 min at 95°C, then for 10 s at 95°C, and annealing for 20 s at 60°C for 40 cycles. The data was normalized to β-actin to estimate the relative expression of these genes.

Measurement of Cytokine Expression

NR8383 cells (1×10^5 cells/well) were cultured in 96-well plates for 24 h, followed by pretreatment with CSP (25, 50, 100, and 200.0 µg/ml) for 12 h, and p38 inhibitor (SB 203580, 10 µM) and JNK inhibitor (SP600125, 10 µM) for 5 h, followed by LPS stimulation (1 µg/ml) for another 30 min. Next, the concentrations of IL-1β, TNF-α, and COX-2 were determined in the supernatant using respective ELISA kits.

Western Blot

The samples for western blot were prepared following a previously described protocol (Xiong et al., 2019). Briefly, NR8383 cells (1×10^5 cells/well) were cultured in 96-well plates for 24 h, followed by pretreatment with CSP (25, 50, 100, and 200.0 µg/ml) for 12 h, and p38 inhibitor (SB 203580, 10 µM) and JNK inhibitor (SP600125, 10 µM) for 5 h, followed by LPS stimulation (1 µg/ml) for another 30 min. Next, the cells were washed with cold PBS and lysed in ice-

cold lysis buffer containing the Mammalian Protein Extraction Reagent. The cell lysates were centrifuged (4°C; 10,000 g; 5 min) and the supernatant was used to measure the expression of MAPKs (p-p38, p38, ERK 1/2, JNK, p-JNK) and GAPDH (Santa Cruz, United States) was used as the internal control. The BCA method was used for protein quantification. After separating the protein specimens on SDS-PAGE, they were transferred to a PVDF membrane, which was treated overnight with GAPDH (1:1,000), ERK1/2 (1:600), p-ERK1/2 (1:400), p38 (1:800), p-p38 (1:600), p-JNK (1:500), JNK (1:500) primary antibodies at 4°C. Next, the membranes were treated with HRP-conjugated secondary antibody. The protein bands were visualized using Pierce® ECL Substrate.

Statistical Analysis

All experiments were repeated at least thrice and data were represented as means ± SEM. Statistical differences were examined via GraphPad Prism 7.0 (GraphPad, La Jolla, CA, United States) by one-way ANOVA, followed by Dunnett's test.

RESULTS

The Monosaccharide Compositions of CSP

Monosaccharide content of CSP was evaluated post-PMP derivatization. HPLC chromatogram showed the presence of six peaks (19.12, 27.95, 37.98, 44.01, 51.02, and 56.89 min) (Figure 2B), and were identified as mannose, rhamnose, galacturonic acid, glucose, galactose, and arabinose, according to the references (Figure 2A), which were found to be present in a ratio of 1.66: 2.92: 4.72: 4.25: 9.42: 77.02.

CSP Attenuates the Development of CFA-Induced Inflammation

Post-immunization, CFA mice were orally administered CSP (12.5, 25, and 50 mg/kg) from days 8 to 29 to examine the inhibitory effects of CSP (Figure 3A). The swelling volume of the injured paws was used to evaluate CFA-induced disease progression. The rats in the CFA group started showing substantially enhanced paw swelling from day 7 post-injection. Pain swelling was inhibited ($p < 0.01$) after treatment with iremcoxib from day 20 (Figures 3B–C). In the high-dose and medium-dose groups, CSP considerably improved paw swelling from day 22 post-injection of CFA ($p < 0.01$, Figures 3B–C), which improved with time. Additionally, the swelling inhibition rate of the high-dose group was similar to that of the positive control (imrecoxib) from day 22 (Figure 3D).

Histopathological Analysis

The results of histopathological examination showed that the model group showed more severe pathological changes compared with normal rats not induced by CFA (Figure 4). All rats exhibited various degrees of pathological changes in the ankle joints and feet, mainly due to the proliferation of ankle synovial cells, inflammatory cell infiltration; the articular cartilage and bone tissue in the joint cavity were severely damaged, there was fibrous connective tissue proliferation on the cartilage surface, part of the periosteal fibrosis, and even joint cavity stenosis; obvious soft tissue

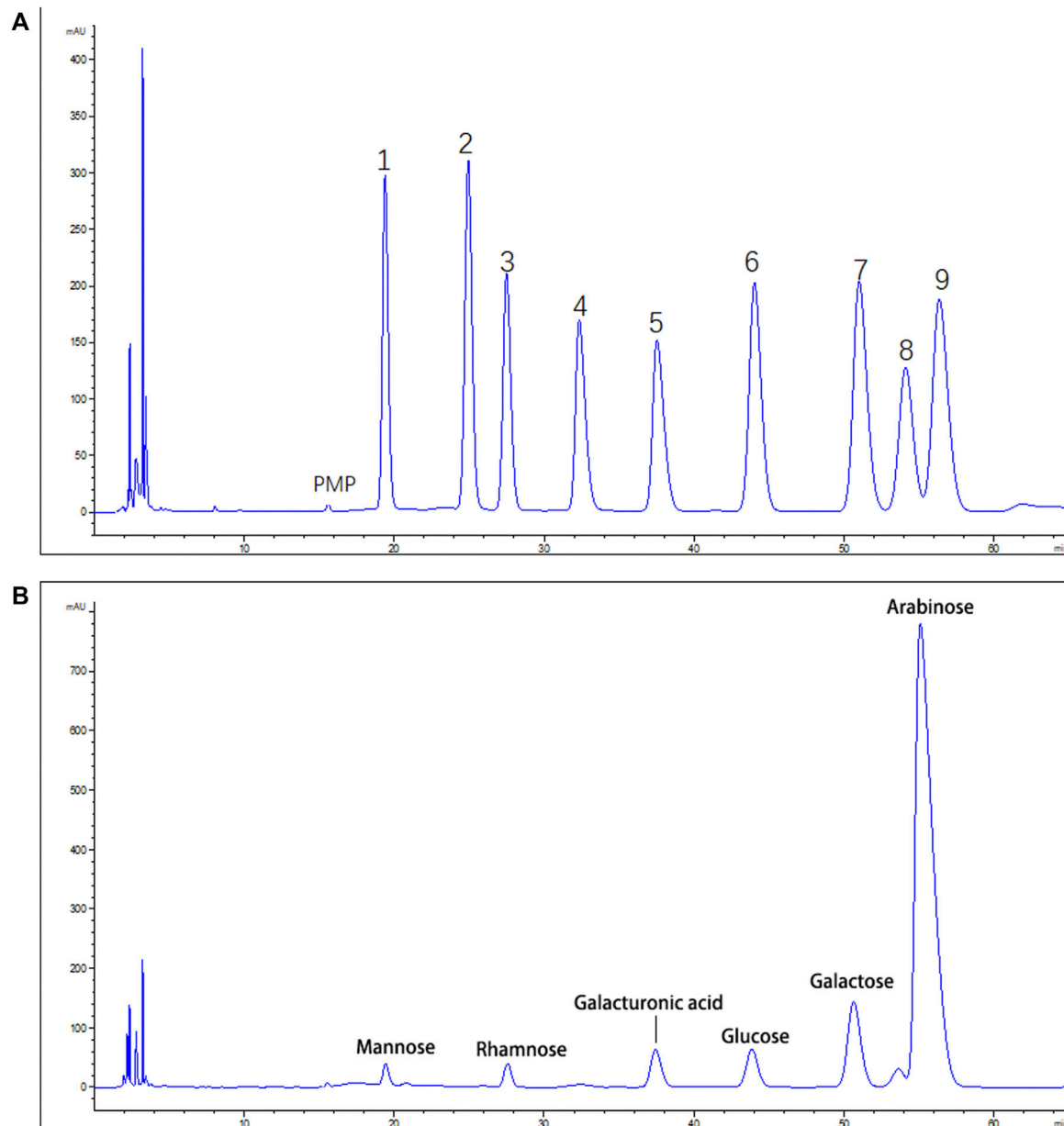


FIGURE 2 | HPLC analysis of CSP **(A)**. Standard monosaccharide mixture. 1: Mannose; 2: ribose; 3: rhamnose; 4: Glucuronic acid; 5: galacturonic acid; 6: glucose; 7: galactose; 8: xylose; 9: arabinose **(B)**. The monosaccharide compositions of CSP.

around the joint inflammation, etc., which suggested the successful establishment of the rheumatoid arthritis model in rats. There was a substantial reduction in the pathological changes in the mouse ankle joint and foot tissue. There was relatively less infiltration of inflammatory cells and proliferation of synovial cells in the ankle joint of rats. The fibrosis of articular cartilage and bone tissue was not severe, and there was no obvious articular surface stenosis. Also, adhesions and inflammation of the surrounding soft tissues were not severe. Additionally, the pathological changes in the 25.0 and 12.5 mg/kg CSP groups were slighter than that in the model group. Thus, CSP could effectively reduce the inflammatory

response of the joint synovium and prevent the destruction of cartilage tissue, bone tissue, and tissues around the joint.

Additionally, the degree of pathological changes was quantified (Table 1). The pathological changes in the synovial membrane, articular cartilage, and skin ulcer were divided into four levels, including slight (\pm), mild (+), moderate (++), and severe (+++). In this study, the number of pathological changes (moderate and severe) in the CSP (50 mg kg⁻¹) group were reduced by 33 and 67% in the synovial membrane and skin ulcer, respectively, than the model group. We observed no significant change in the articular cartilage in the CSP

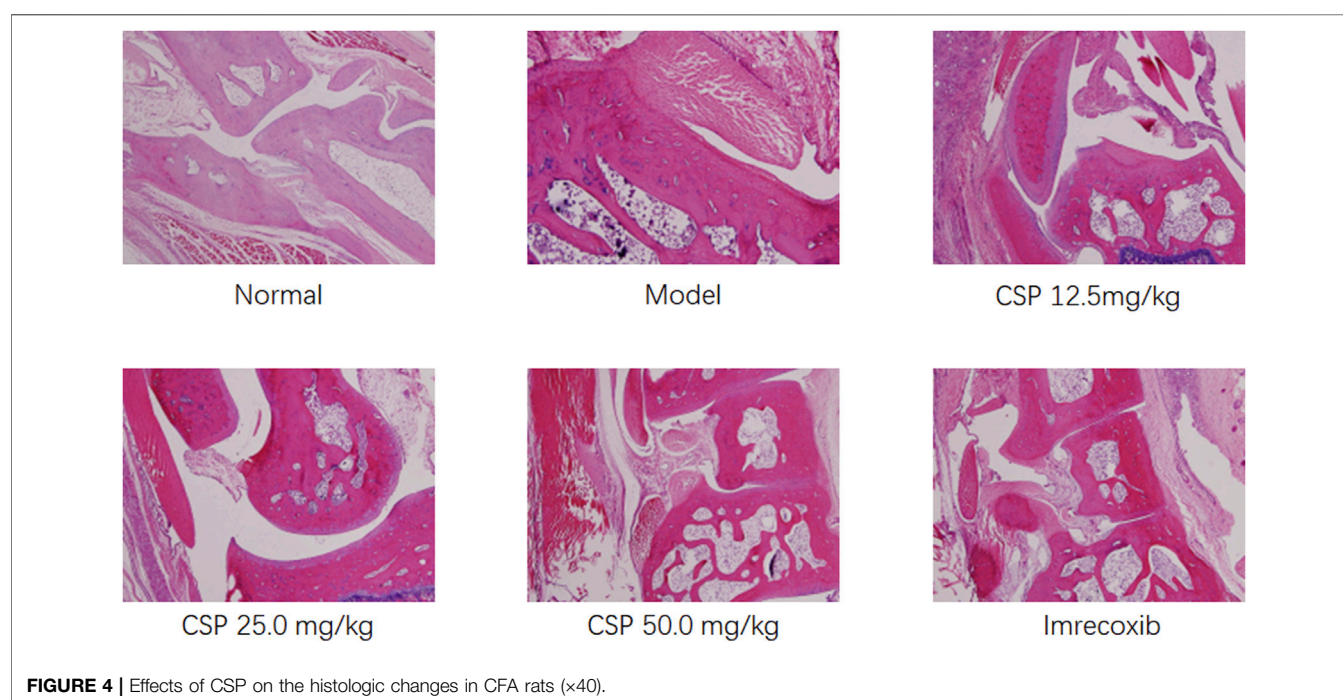
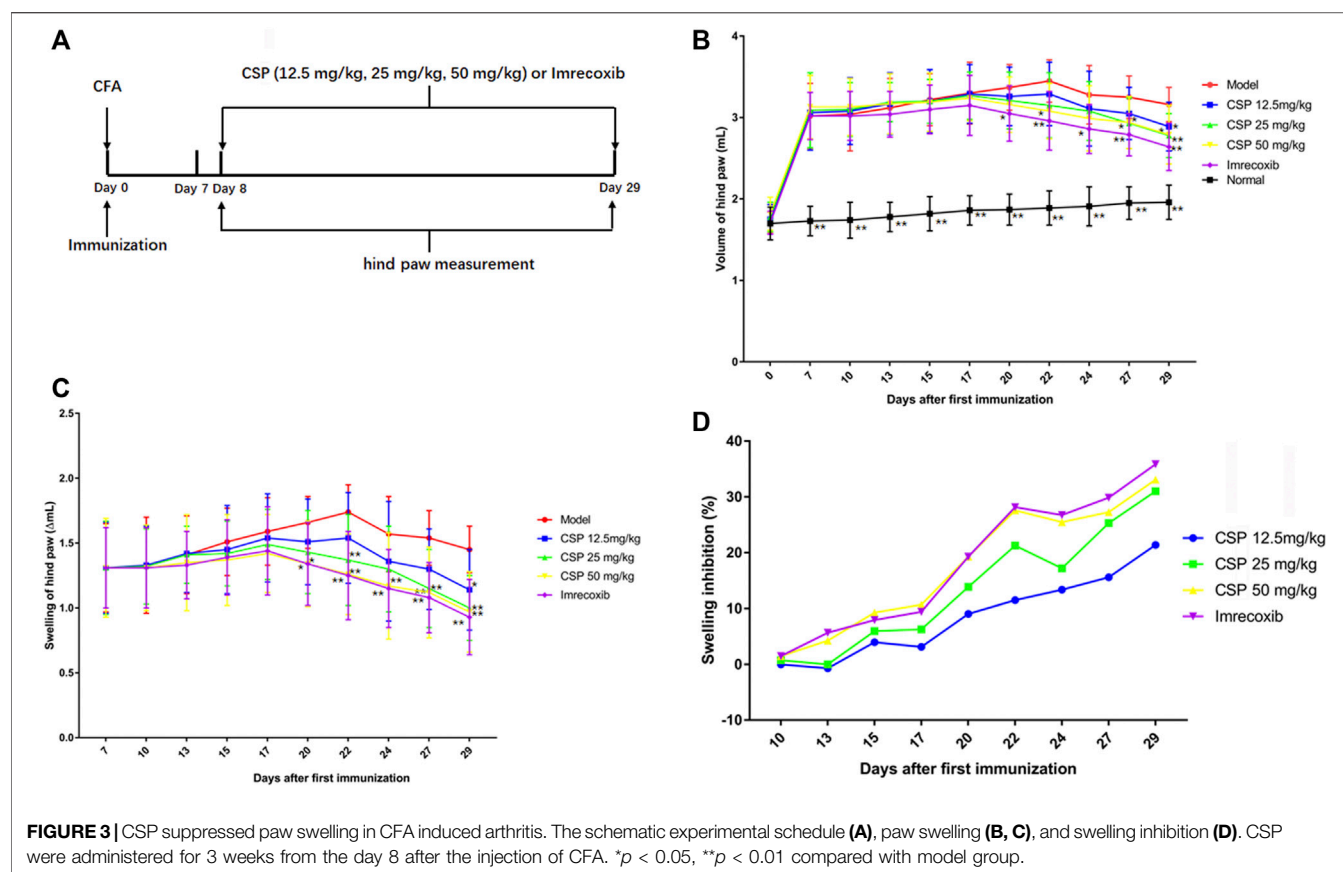
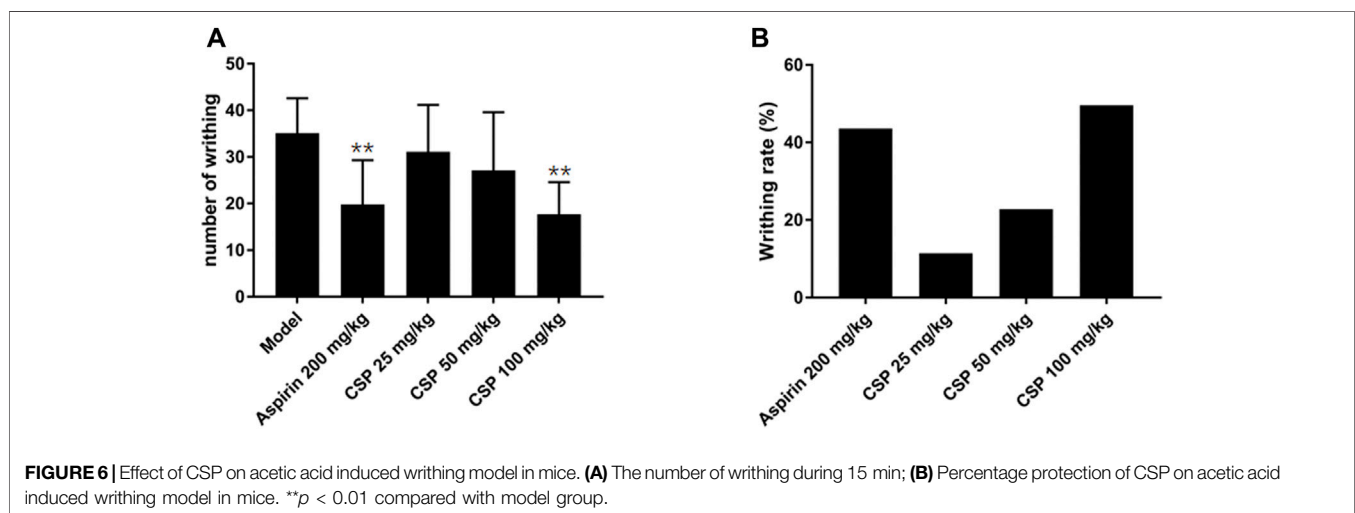
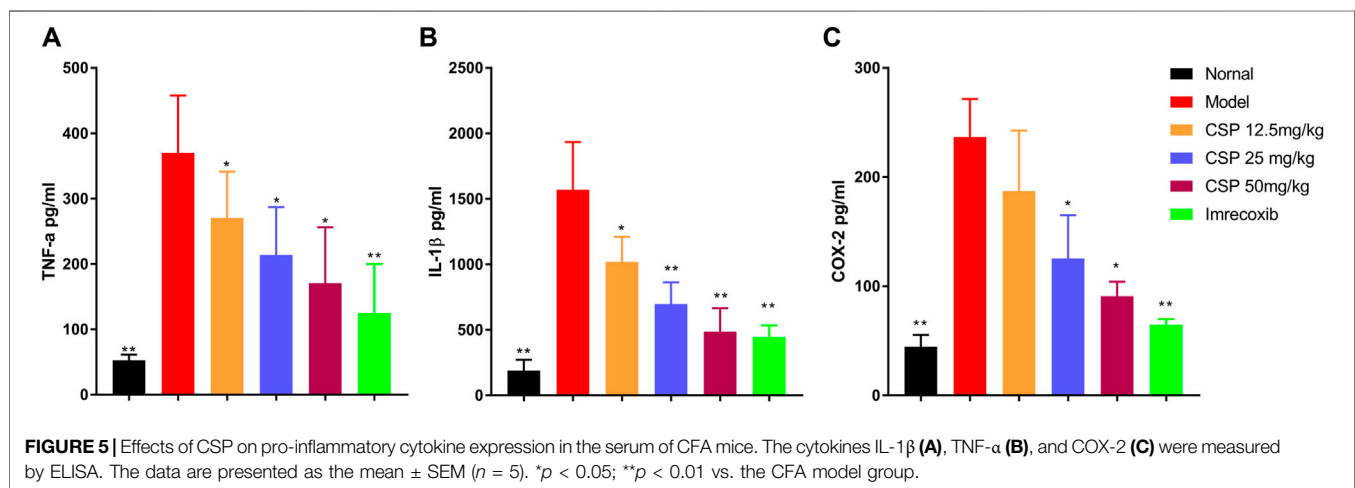


TABLE 1 | Statistical analysis of abnormal changes of hind paw in different groups.

Group	Number	Pathological changes of synovial membrane				Pathological changes of articular cartilage				Skin ulcer			
		±	+	++	+++	±	+	++	+++	±	+	++	+++
Normal	<i>n</i> = 10	0	0	0	0	0	0	0	0	0	0	0	0
Model	<i>n</i> = 10	0	7	3	0	3	4	3	0	0	1	4	5
CSP 12.5 mg/kg	<i>n</i> = 10	2	4	4	0	1	3	3	0	0	3	5	2
CSP 25 mg/kg	<i>n</i> = 10	3	4	3	0	2	5	1	0	2	1	6	1
CSP 50 mg/kg	<i>n</i> = 10	2	6	2	0	3	6	0	0	1	6	3	0
Imrecoxib	<i>n</i> = 10	2	6	2	0	5	4	0	1	1	6	1	2

Slight (±), Mild (+), Moderate (++), Severe (+++).

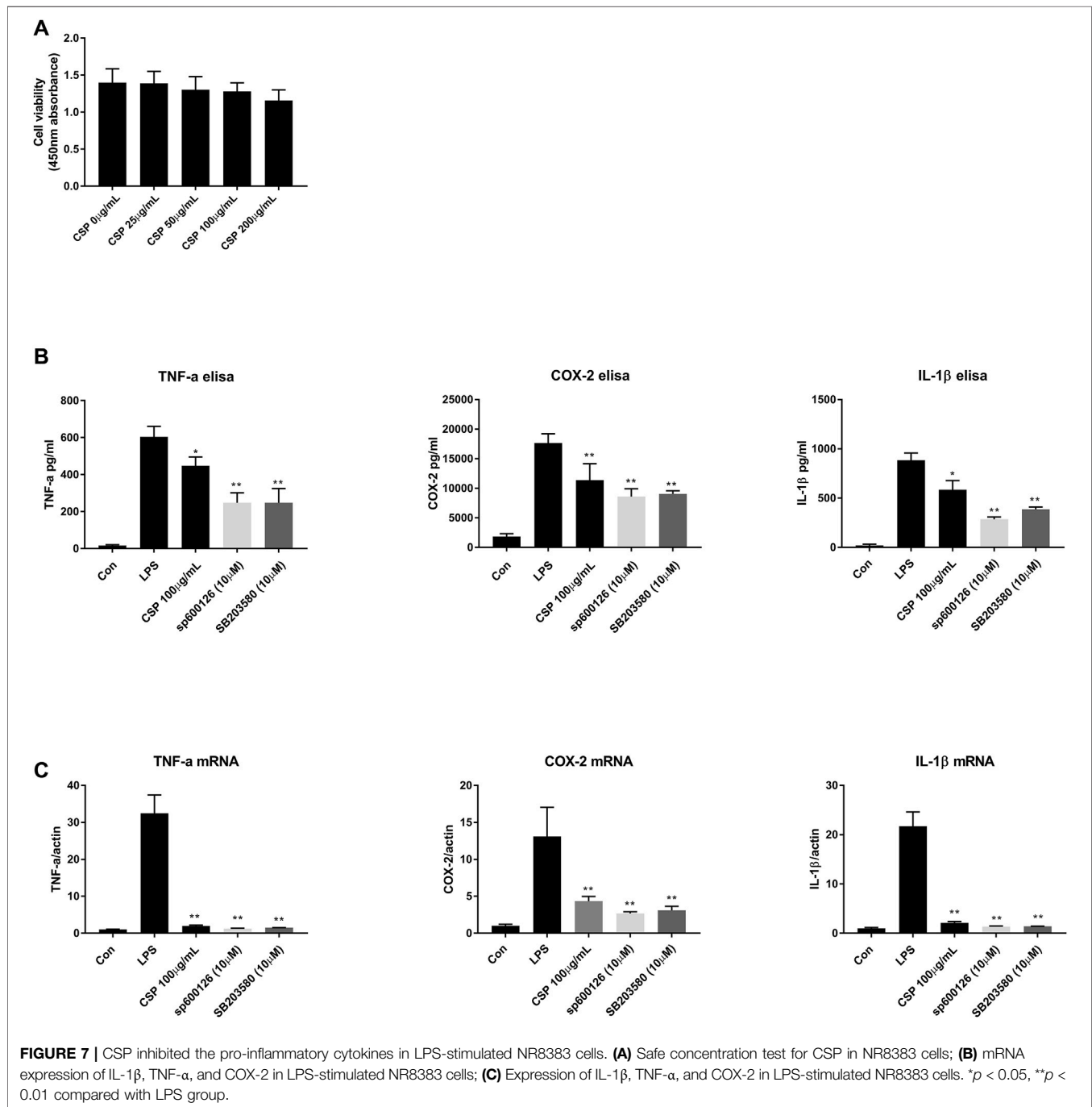


(50 mg kg⁻¹) group after 3-weeks administration, suggesting that CSP could alleviate pathological changes in CFA-induced rats.

Effect of CSP on Pro-inflammatory Cytokines in Serum

Figure 5 exhibits the production of various pro-inflammatory cytokines in the serum of CFA-induced rats. When compared to the

normal group, the model group had higher contents of TNF- α , COX-2, IL-6, and IL-1 β in the serum (*p* < 0.01), suggesting that an apparent inflammation existed in the model group (Figures 5A–C). However, the pro-inflammatory cytokines production decreased in the CSP group compared with the model group, especially for the high group with significant difference (*p* < 0.05). These findings suggested that CSP has a significant anti-inflammatory activity in CFA-induced rats.



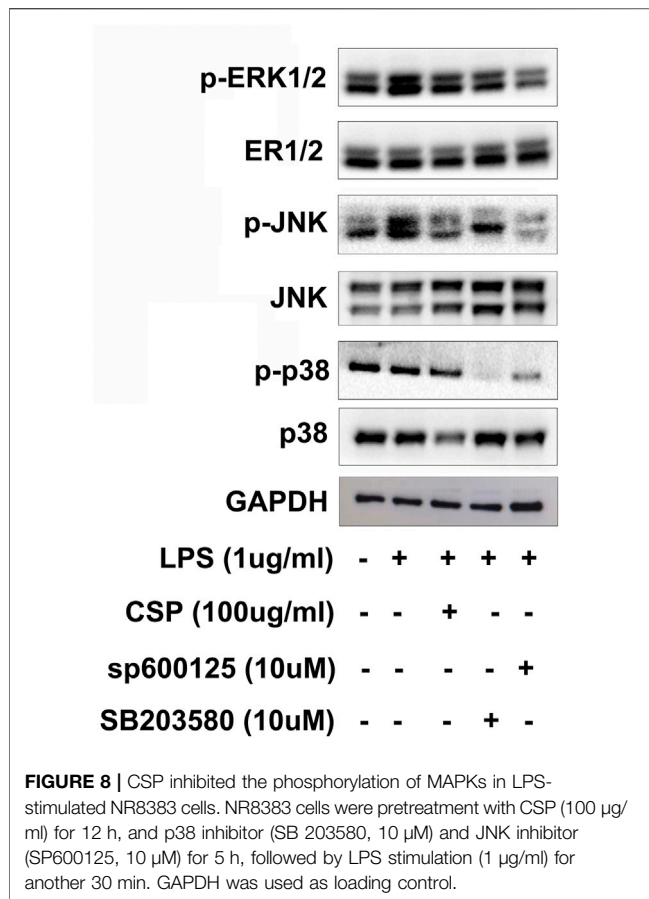
Analgesic Activity

The results of HAC-induced writhing method showed that the extract showed substantial analgesic activity. In the HAC-induced writhing method, we found that CSP dose-dependently promoted a reduction in writhing movement in mice compared with the model group; especially for the high-dose group (100 mg/kg), which showed a significant difference ($p < 0.01$) (Figure 6A). In addition, 200 mg/kg Aspirin showed significant difference in reduction in writhing movement ($p < 0.01$), compared with the model group. Moreover, the writhing inhibition rate of

CSP (100 mg/kg) was around 43.2%, which is higher than the positive control group (Aspirin 200 mg/kg).

EFFECT OF CSP ON THE PRODUCTION OF PROINFLAMMATORY CYTOKINES AND THEIR MRNA LEVELS NR8383 CELLS.

Here, we studied the effect of CSP on the production of proinflammatory cytokines *in vitro*. Firstly, CCK-8 was



used to screen the safe dosage of CSP (0–200 µg/ml), and there was no obvious cytotoxicity (Figure 7A). Thus, we chose 100 µg/ml for followed experiment. Then, qRT-PCR was done to estimate the mRNA expression of a few related cytokines in NR8383 cells after incubation with 100 µg/ml CSP. The results demonstrated a substantial increase in the mRNA expression of IL-1 β , TNF- α , and COX-2 in the LPS group ($p < 0.01$) than the normal group (Figure 7B). Additionally, CSP could downregulate the mRNA levels of IL-1 β , TNF- α , and COX-2 ($p < 0.01$), which were similar to sp600126 and SB3580. After that, ELISA was used to evaluate the contents of IL-1 β , TNF- α , and COX-2 in the supernatant of NR8383, which were decreased after CSP treatment (Figure 7C).

Effect of CSP on the MAPK Signaling Pathway

We performed western blot to test evaluate the potential mechanism involved in CSP-induced attenuation of arthritis. In order to explain whether the improvement of inflammation by CSP is related to MAPK signaling pathway, the key proteins including extracellular signal regulated kinase (ERK), p-ERK, p38 mitogen activated protein kinase (p38), p-p38, c-Jun N-terminal kinase (JNK) and p-JNK were measured (Figure 8). The results of this study demonstrated

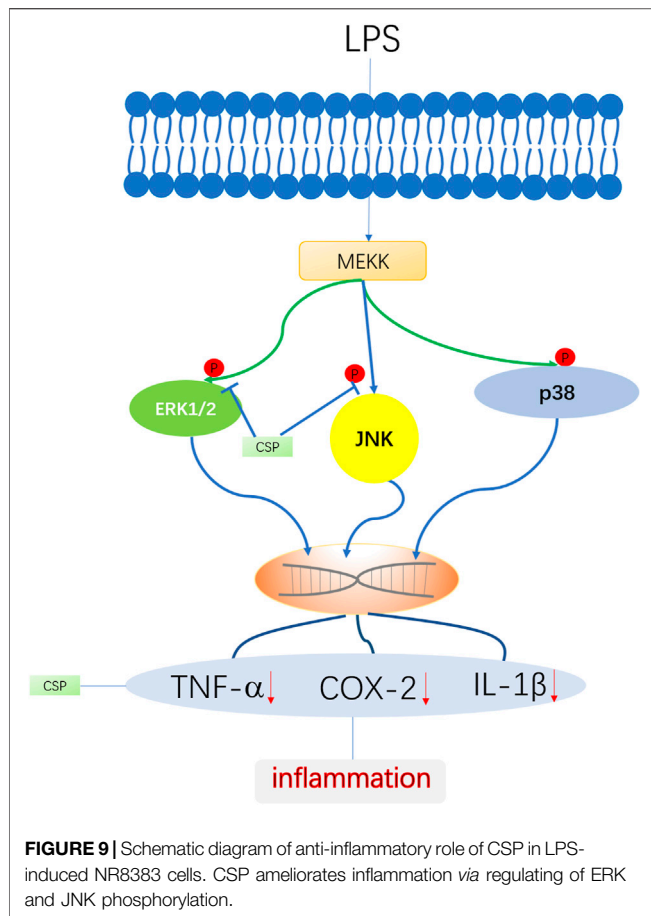
that the protein expression levels of p-ERK, p-JNK were significantly elevated in the model group. Furthermore, CSP degraded the protein expression levels of p-ERK and p-JNK, while p-p38 showed no significance after CSP treatment. Moreover, when NR8383 cells were pretreated with SP600125, a specific JNK inhibitor, this increase was markedly inhibited, which was similar to the effects of CSP treatment. Similar results were obtained when the inhibitor was replaced by SB203580, which is a broad-spectrum inhibitor of p38 (Figure 8).

DISCUSSION

C. speciosa is a TCM, which was first recorded in the book “Ming Yi Bie Lu” (名医别录). It is commonly used in the treatment of severe waist and knee joint pain. “Ben Cao Shu Jing” (本草经疏) also recorded that *C. speciosa* could dredge meridian and remove dampness. Polysaccharides, one of the main chemical components found in *C. speciosa*, are known to have various pharmacological activities, including anti-tumor potential, immunological, and anti-diabetic effect. In this study, we used CFA-induced arthritis in rats and writhing experiments in mice to investigate the medicinal effects of CSP; the LPS-induced NR8383 cell model was used to explore the effects of CSP on the MAPK signaling pathway.

Inflammation is a normal defensive response that involves the release of pro-inflammatory cytokines. Long-term and chronic inflammation, on the other hand, might be detrimental, causing fever, asthma, atherosclerosis, joint diseases, neurodegeneration, and even cancer (Palladino et al., 2003; Pu et al., 2014). Currently, anti-inflammatory medications, both steroidal and non-steroidal, are used to treat inflammation. However, steroidal anti-inflammatory drugs have the potential to cause elevated blood pressure, osteoporosis, immunosuppression, Cushing’s syndrome, etc., while non-steroidal anti-inflammatory drugs may cause hemorrhagic gastritis, liver toxicity, asthma, and other side effects. These side effects question the long-term use of steroidal and non-steroidal anti-inflammatory medications (Ma et al., 2016). Natural products are secondary metabolites synthesized in different species with distinct chemical structures, indicating their significance as candidates for drug molecules. The natural source-derived polysaccharides are composed of >10 monosaccharide molecules, with different connectivity and a complex molecular structure. Recently, polysaccharides have been used as safe, highly efficient, anti-inflammatory, immune regulators, etc. (Guo et al., 2018).

The pain sensation, as another complication of inflammation, is always accompanied by tissue disruption, and the degree of pain depends on the type of trauma, the healing process as well as the other immune factors. Analgesics are a type of drugs used for relieving pain; thus, they might be useful in the process of short-term wound healing (McHugh and McHugh, 2000; Ronchetti et al., 2017). Pain treatment includes the evaluation of the cytokines and other immune



molecules involved in the pain mechanism, which cause inflammation, mediating the formation of wounds and local pain (Widgerow and Kalaria, 2012; Aquino et al., 2013). The analgesic activity of CSP was determined using HAC-induced writhing methods. However, the HAC-induced writhing method, is commonly used to assess peripheral analgesic activity (25). During constriction, the tissue phospholipids release arachidonic acid (AA) via COX pathway (Muhammad et al., 2012; Jing et al., 2019). The nociceptive effect of HAC could be prevented using NSAIDs. Aspirin, a COX inhibitor, eliminates inflammatory mediators in the peripheral tissues, thus inhibiting HAC-induced pain. Here, high-dose CSP (100 mg kg^{-1}) substantially decreased the writhing in mice in response to intraperitoneal administration of HAC, with a greater effect compared with aspirin (15). The analgesic effect of CSP was probably mediated via the inhibition of local peritoneal receptors or COX-related AA pathways.

The CFA-induced rat foot swelling model has been commonly used for the identification of therapeutic drugs of RA in the past (Paunovic and Harnett, 2013; Saleem et al., 2020). After injecting CFA, a gradual increase in the pathological manifestations of RA was observed. Here, CSP substantially improved these pathological changes and paw swelling, indicating that CSP exhibited anti-RA effect.

The elevated levels of proinflammatory cytokines, such as IL-1 β , TNF- α , and COX-2, could aggravate the progression of RA and could contribute to synovial inflammation and cartilage damage (29). Therefore, inhibition IL-1 β , TNF- α , and COX-2 expression could be a target for RA treatment. Here, CSP declined IL-1 β , TNF- α , and COX-2 levels, indicating that the anti-RA effect of CSP was directly responsible for the inhibition of secretion of proinflammatory cytokines.

MAPK is a family of serine/threonine protein kinases involved in the inflammatory process, including ERK, JNKs, and p38 (Wu et al., 2016). Wu et al. discovered that a polysaccharide found in *Sargassum cristaefolium* inhibited iNOS expression by inhibiting p38, ERK, and JNK phosphorylation in LPS-stimulated RAW264.7 cells (Meier and McInnes, 2014). The MAPK signaling pathway molecules ERK and p38 are involved in the pathogenesis of RA (Liang et al., 2012). Our results indicated that CSP could inhibit MAPK signaling pathway activation by preventing the phosphorylation of JNK, and ERK (Figure 9). Previous studies have suggested that MAPK activation was essential for COX-2 expression in peripheral inflammation (Xu et al., 2010), thus, the MAPK signal transduction pathway is partly involved in the regulatory mechanism of this analgesic effect. In our research, we both examined the COX-2 level in CFA-induced arthritis and LPS-induced NR8383 cells, which were both decreased by CSP. Moreover, the phosphorylation of JNK and ERK1/2 were inhibited by CSP, which suggested the analgesia effect of CSP might evolved in regulation of MAPK pathway. However, the role of each MAPK component in effects of CSP on NR8383 cell remains unclear, and an activator of MAPK signaling pathway to antagonize the effects of CSP is not designed in our study. So, further investigations on the specific molecular mechanism of CSP are encouraged.

CONCLUSION

Thus, our results showed that MAPK inhibition mediated the beneficial effects of CSP on hind paw swelling and HAC-induced writhing. The anti-inflammatory effect of CSP showed its potential application for treating rheumatoid arthritis.

DATA AVAILABILITY STATEMENT

The original contributions presented in the study are included in the article/supplementary material, further inquiries can be directed to the corresponding authors.

ETHICS STATEMENT

The animal study was reviewed and approved by the Animal Ethic Committee of Second Military Medical University.

AUTHOR CONTRIBUTIONS

DH: Writing—original draft. SJ: Writing—original draft. YC, ZD, DX, XW, ML: Data analysis. WC, FZ, LS: Experiment supervision.

REFERENCES

- Andersson, A. K., Li, C., and Brennan, F. M. (2008). Recent Developments in the Immunobiology of Rheumatoid Arthritis. *Arthritis Res. Ther.* 10 (2), 204. in: Pubmed; PMID 18373887. doi:10.1186/ar2370
- Aquino, A. B., Cavalcante-Silva, L. H., Matta, C. B., Epifanio, W. A., Aquino, P. G., Santana, A. E., et al. (2013). The Antinociceptive and Anti-inflammatory Activities of *Aspidosperma Tomentosum* (Apocynaceae). *ScientificWorldJournal* 2013, 218627. in: Pubmed; PMID 23781151. doi:10.1155/2013/218627
- Bang, J. S., Oh, D. H., Choi, H. M., Sur, B. J., Lim, S. J., Kim, J. Y., et al. (2009). Anti-inflammatory and Antiarthritic Effects of Piperine in Human Interleukin 1 β -Stimulated Fibroblast-like Synoviocytes and in Rat Arthritis Models. *Arthritis Res. Ther.* 11 (2), R49. in: Pubmed; PMID 19327174. doi:10.1186/ar2662
- Cao, H., Ma, S., Guo, H., Cui, X., Wang, S., Zhong, X., et al. (2019). Comparative Study on the Monosaccharide Compositions, Antioxidant and Hypoglycemic Activities *In Vitro* of Intracellular and Extracellular Polysaccharides of Liquid Fermented *Coprinus Comatus*. *Int. J. Biol. Macromol.* 139, 543–549. Cited in: Pubmed; PMID 31381912. doi:10.1016/j.ijbiomac.2019.08.017
- Chen, Y. R., Hsieh, F. I., Chang, C. C., Chi, N. F., Wu, H. C., and Chiou, H. Y. (2018). Effect on Risk of Stroke and Acute Myocardial Infarction of Nonselective Nonsteroidal Anti-inflammatory Drugs in Patients with Rheumatoid Arthritis. *Am. J. Cardiol.* 121 (10), 1271–1277. Cited in: Pubmed; PMID 29548675. doi:10.1016/j.amjcard.2018.01.044
- Chung, I. M., Ketharnathan, S., Thiruvengadam, M., and Rajakumar, G. (2016). Rheumatoid Arthritis: The Stride from Research to Clinical Practice. *Int. J. Mol. Sci.* 17 (6). Cited in: Pubmed; PMID 27338350. doi:10.3390/ijms17060900
- Grosser, T. (2017). Cardiovascular Safety of Celecoxib, Naproxen, or Ibuprofen for Arthritis. *N. Engl. J. Med.* 376 (14), 1389. in: Pubmed; PMID 28379792. doi:10.1056/NEJMc1702534
- Guo, L., Ma, R., Sun, H., Raza, A., Tang, J., and Li, Z. (2018). Anti-Inflammatory Activities and Related Mechanism of Polysaccharides Isolated from *Sargentodoxa Cuneata*. *Chem. Biodivers* 15 (11), e1800343. Cited in: Pubmed; PMID 30153400. doi:10.1002/cbdv.201800343
- Gupta, S., Mishra, K. P., Kumar, B., Singh, S. B., and Ganju, L. (2020). Andrographolide Attenuates Complete Freund's Adjuvant Induced Arthritis via Suppression of Inflammatory Mediators and Pro-inflammatory Cytokines. *J. Ethnopharmacol.* 261, 113022. in: Pubmed; PMID 32569719. doi:10.1016/j.jep.2020.113022
- Jing, R., Ban, Y., Xu, W., Nian, H., Guo, Y., Geng, Y., et al. (2019). Therapeutic Effects of the Total Lignans from *Vitex Negundo* Seeds on Collagen-Induced Arthritis in Rats. *Phytomedicine* 58, 152825. in: Pubmed; PMID 30831463. doi:10.1016/j.phymed.2019.152825
- Li, S. G., and Chen, Y. (2011). Effect of *Chaenomeles Speciosa* Polysaccharide on Adjuvant Arthritis in Mice and its Mechanisms. *Chin. J. Exp. Traditional Med. Formulae* 12, 159–162.
- Liang, Y., Fang, J. Q., Du, J. Y., and Fang, J. F. (2012). Effect of Electroacupuncture on Activation of p38MAPK in Spinal Dorsal Horn in Rats with Complete Freund's Adjuvant-Induced Inflammatory Pain. *Evid. Based Complement. Alternat Med.* 2012, 568273. in: Pubmed; PMID 21860653. doi:10.1155/2012/568273
- Luo, C., Xu, X., Wei, X., Feng, W., Huang, H., Liu, H., et al. (2019). Natural Medicines for the Treatment of Fatigue: Bioactive Components, Pharmacology, and Mechanisms. *Pharmacol. Res.* 148, 104409. Cited in: Pubmed; PMID 31446039. doi:10.1016/j.phrs.2019.104409

ACKNOWLEDGMENTS

The authors thank the Second Military University School of Pharmacy for their aid in providing animal condition.

- Ma, L., Liu, T. W., Wallig, M. A., Dobrucki, I. T., Dobrucki, L. W., Nelson, E. R., et al. (2016). Efficient Targeting of Adipose Tissue Macrophages in Obesity with Polysaccharide Nanocarriers. *ACS Nano* 10 (7), 6952–6962. Cited in: Pubmed; PMID 27281538. doi:10.1021/acsnano.6b02878
- McHugh, J. M., and McHugh, W. B. (2000). Pain: Neuroanatomy, Chemical Mediators, and Clinical Implications. *AACN Clin. Issues* 11 (2), 168–178. Cited in: Pubmed; PMID 11235429. doi:10.1097/00044067-200005000-00003
- Meier, F. M., and McInnes, I. B. (2014). Small-molecule Therapeutics in Rheumatoid Arthritis: Scientific Rationale, Efficacy and Safety. *Best Pract. Res. Clin. Rheumatol.* 28 (4), 605–624. Cited in: Pubmed; PMID 25481553. doi:10.1016/j.berh.2014.10.017
- Muhammad, N., Saeed, M., and Khan, H. (2012). Antipyretic, Analgesic and Anti-inflammatory Activity of *Viola Betonicifolia* Whole Plant. *BMC Complement. Altern. Med.* 12:59. doi:10.1186/1472-6882-12-59
- Newman, D. J., and Cragg, G. M. (2016). Natural Products as Sources of New Drugs from 1981 to 2014. *J. Nat. Prod.* 79 (3), 629–661. Cited in: Pubmed; PMID 26852623. doi:10.1021/acs.jnatprod.5b01055
- Palladino, M. A., Bahjat, F. R., Theodorakis, E. A., and Moldawer, L. L. (2003). Anti-TNF- α Therapies: the Next Generation. *Nat. Rev. Drug Discov.* 2 (9), 736–746. Cited in: Pubmed; PMID 12951580. doi:10.1038/nrd1175
- Paunovic, V., and Harnett, M. M. (2013). Mitogen-activated Protein Kinases as Therapeutic Targets for Rheumatoid Arthritis. *Drugs* 73(2), 101–115. doi:10.1007/s40265-013-0014-6
- Pu, H. L., Chiang, W. L., Maiti, B., Liao, Z. X., Ho, Y. C., Shim, M. S., et al. (2014). Nanoparticles with Dual Responses to Oxidative Stress and Reduced pH for Drug Release and Anti-inflammatory Applications. *ACS Nano* 8 (2), 1213–1221. Cited in: Pubmed; PMID 24386907. doi:10.1021/nn4058787
- Ronchetti, S., Migliorati, G., and Delfino, D. V. (2017). Association of Inflammatory Mediators with Pain Perception. *Biomed. Pharmacother.* 96, 1445–1452. Cited in: Pubmed; PMID 29217162. doi:10.1016/j.biopha.2017.12.001
- Saleem, A., Saleem, M., Akhtar, M. F., Shahzad, M., and Jahan, S. (2020). Moringa Riva Leaf Extracts Attenuate Complete Freund's Adjuvant-Induced Arthritis in Wistar Rats via Modulation of Inflammatory and Oxidative Stress Biomarkers. *Inflammopharmacology* 28 (1), 139–151. Cited in: Pubmed; PMID 31037575. doi:10.1007/s10787-019-00596-3
- Smolen, J. S., Aletaha, D., and McInnes, I. B. (2016). Rheumatoid Arthritis. *Lancet* 388 (10055), 2023–2038. doi:10.1016/S0140-6736(16)30173-8
- Tadiwos, Y., Nedi, T., and Engidawork, E. (2017). Analgesic and Anti-inflammatory Activities of 80% Methanol Root Extract of *Jasminum Abyssinicum* Hochst. Ex. Dc. (Oleaceae) in Mice. *J. Ethnopharmacol.* 202, 281–289. Cited in: Pubmed; PMID 28242384. doi:10.1016/j.jep.2017.02.036
- Urushibara, M., Takayanagi, H., Koga, T., Kim, S., Isobe, M., Morishita, Y., et al. (2004). The Antirheumatic Drug Leflunomide Inhibits Osteoclastogenesis by Interfering with Receptor Activator of NF- κ B Ligand-Stimulated Induction of Nuclear Factor of Activated T Cells C1. *Arthritis Rheum.* 50 (3), 794–804. Cited in: Pubmed; PMID 15022321. doi:10.1002/art.20206
- Widgerow, A. D., and Kalaria, S. (2012). Pain Mediators and Wound Healing—Establishing the Connection. *Burns* 38 (7), 951–959. Cited in: Pubmed; PMID 22738827. doi:10.1016/j.burns.2012.05.024
- Wu, G.-J., Shiu, S.-M., Hsieh, M.-C., and Tsai, G.-J. (2016). Anti-inflammatory Activity of a Sulfated Polysaccharide from the Brown Alga *Sargassum Cristaeifolium*. *Food Hydrocolloids* 53, 16–23. doi:10.1016/j.foodhyd.2015.01.019
- Xie, X., Zou, G., and Li, C. (2015). Antitumor and Immunomodulatory Activities of a Water-Soluble Polysaccharide from *Chaenomeles Speciosa*. *Carbohydr. Polym.* 132, 323–329. Cited in: Pubmed; PMID 26256355. doi:10.1016/j.carbpol.2015.06.046

- Xiong, H., Ding, X., Wang, H., Jiang, H., Wu, X., Tu, C., et al. (2019). Tibetan Medicine Kuan-Jin-Teng Exerts Anti-arthritic Effects on Collagen-Induced Arthritis Rats via Inhibition the Production of Pro-inflammatory Cytokines and Down-Regulation of MAPK Signaling Pathway. *Phytomedicine* 57, 271–281. Cited in: Pubmed; PMID 30802713. doi:10.1016/j.phymed.2018.12.023
- Xu, K. D., Liang, T., Wang, K., and Tian, D. A. (2010). Effect of Pre-electroacupuncture on P38 and C-Fos Expression in the Spinal Dorsal Horn of Rats Suffering from Visceral Pain. *Chin. Med. J. (Engl)* 123 (9), 1176–1181. Cited in: Pubmed; PMID 20529559.
- Yu, L., Jia, D., Feng, K., Sun, X., Xu, W., Ding, L., et al. (2020). A Natural Compound (LCA) Isolated from Litsea Cubeba Inhibits RANKL-Induced Osteoclast Differentiation by Suppressing Akt and MAPK Pathways in Mouse Bone Marrow Macrophages. *J. Ethnopharmacol* 257, 112873. in: Pubmed; PMID 32298753. doi:10.1016/j.jep.2020.112873
- Zou, S. X. Y., and Zhang, Q. (2015). Review on Extraction and Purification Technology of Polysaccharides from Natural Plants. *Nat. Product. Res. Dev.* 27 (8), 1501–1509.

Conflict of Interest: The authors declare that the research was conducted in the absence of any commercial or financial relationships that could be construed as a potential conflict of interest.

Publisher's Note: All claims expressed in this article are solely those of the authors and do not necessarily represent those of their affiliated organizations, or those of the publisher, the editors and the reviewers. Any product that may be evaluated in this article, or claim that may be made by its manufacturer, is not guaranteed or endorsed by the publisher.

Copyright © 2022 Huang, Jiang, Du, Chen, Xue, Wang, Li, Zhang, Chen and Sun. This is an open-access article distributed under the terms of the Creative Commons Attribution License (CC BY). The use, distribution or reproduction in other forums is permitted, provided the original author(s) and the copyright owner(s) are credited and that the original publication in this journal is cited, in accordance with accepted academic practice. No use, distribution or reproduction is permitted which does not comply with these terms.

Advantages of publishing in Frontiers



OPEN ACCESS

Articles are free to read
for greatest visibility
and readership



FAST PUBLICATION

Around 90 days
from submission
to decision



HIGH QUALITY PEER-REVIEW

Rigorous, collaborative,
and constructive
peer-review



TRANSPARENT PEER-REVIEW

Editors and reviewers
acknowledged by name
on published articles

Frontiers

Avenue du Tribunal-Fédéral 34
1005 Lausanne | Switzerland

Visit us: www.frontiersin.org

Contact us: frontiersin.org/about/contact



REPRODUCIBILITY OF RESEARCH

Support open data
and methods to enhance
research reproducibility



DIGITAL PUBLISHING

Articles designed
for optimal readership
across devices



FOLLOW US

@frontiersin



IMPACT METRICS

Advanced article metrics
track visibility across
digital media



EXTENSIVE PROMOTION

Marketing
and promotion
of impactful research



LOOP RESEARCH NETWORK

Our network
increases your
article's readership